

# Standard Model Theory for the FCC-ee: The Tera-Z

**Report on the 1<sup>st</sup> Mini workshop: Precision EW and QCD calculations for the  
FCC studies: methods and tools, 12-13 January 2018, CERN, Geneva**

**<https://indico.cern.ch/event/669224/>**

A. Blondel<sup>1</sup>, J. Gluza<sup>\*,2</sup>, S. Jadach<sup>3</sup>, P. Janot<sup>4</sup>, T. Riemann<sup>2,5</sup> (editors),  
A. Akhundov<sup>6</sup>, A. Arbuzov<sup>7</sup>, R. Boels<sup>8</sup>,  
S. Bondarenko<sup>7</sup>, S. Borowka<sup>4</sup>, C.M. Carloni Calame<sup>9</sup>, I. Dubovyk<sup>8,5</sup>,  
Ya. Dydyshka<sup>10</sup>, W. Flieger<sup>2</sup>, A. Freitas<sup>11</sup>, K. Grzanka<sup>2</sup>, T. Hahn<sup>12</sup>, T. Huber<sup>13</sup>,  
L. Kalinovskaya<sup>10</sup>, R. Lee<sup>14</sup>, P. Marquard<sup>5</sup>, G. Montagna<sup>15</sup>, O. Nicrosini<sup>9</sup>,  
C. G. Papadopoulos<sup>16</sup>, F. Piccinini<sup>9</sup>, R. Pittau<sup>17</sup>, W. Placzek<sup>18</sup>, M. Prausa<sup>19</sup>,  
S. Riemann<sup>5</sup>, G. Rodrigo<sup>20</sup>, R. Sadykov<sup>10</sup>, M. Skrzypek<sup>3</sup>, D. Stöckinger<sup>21</sup>, J. Usovitsch<sup>22</sup>,  
B.F.L. Ward<sup>23,12</sup>, S. Weinzierl<sup>24</sup>, G. Yang<sup>25</sup>, S.A. Yost<sup>26</sup>

<sup>1</sup>DPNC University of Geneva, Switzerland, <sup>2</sup>Institute of Physics, University of Silesia, 40-007 Katowice, Poland, <sup>3</sup>Institute of Nuclear Physics, PAN, 31-342 Krakow, Poland, <sup>4</sup>CERN, CH-1211 Genève 23, Switzerland, <sup>5</sup>Deutsches Elektronen-Synchrotron, DESY, 15738 Zeuthen, Germany, <sup>6</sup>Departamento de Física Teórica, Universidad de València, 46100 València, Spain and Azerbaijan National Academy of Sciences, ANAS, Baku, Azerbaijan, <sup>7</sup>Bogoliubov Laboratory of Theoretical Physics, JINR, Dubna, 141980 Russia, <sup>8</sup>II. Institut für Theoretische Physik, Universität Hamburg, 22761 Hamburg, Germany, <sup>9</sup>Istituto Nazionale di Fisica Nucleare, Sezione di Pavia, Pavia, Italy, <sup>10</sup>Dzhelepov Laboratory of Nuclear Problems, JINR, Dubna, 141980 Russia, <sup>11</sup>Pittsburgh Particle physics, Astrophysics & Cosmology Center (PITT PACC) and Department of Physics & Astronomy, University of Pittsburgh, Pittsburgh, PA 15260, USA, <sup>12</sup>Max-Planck-Institut für Physik, 80805 München, Germany, <sup>13</sup>Naturwissenschaftlich-Technische Fakultät, Universität Siegen, 57068 Siegen, Germany, <sup>14</sup>The Budker Institute of Nuclear Physics, 630090, Novosibirsk, <sup>15</sup>Dipartimento di Fisica, Università di Pavia, Pavia, Italy, <sup>16</sup>Institute of Nuclear and Particle Physics, NCSR Demokritos, 15310, Greece, <sup>17</sup>Dep. de Física Teórica y del Cosmos and CAFPE, Universidad de Granada, E-18071 Granada, Spain, <sup>18</sup>Marian Smoluchowski Institute of Physics, Jagiellonian University, 30-348 Kraków, Poland, <sup>19</sup>Albert-Ludwigs-Universität, Physikalisches Institut, Freiburg, Germany, <sup>20</sup>Instituto de Física Corpuscular, Universitat de València - CSIC, 46980 Paterna, València, Spain, <sup>21</sup>Institut für Kern- und Teilchenphysik, TU Dresden, 01069 Dresden, Germany, <sup>22</sup>Trinity College Dublin - School of Mathematics, Dublin 2, Ireland, <sup>23</sup>Baylor University, Waco, TX, USA, <sup>24</sup>PRISMA Cluster of Excellence, Inst. für Physik, Johannes Gutenberg-Universität, 55099 Mainz, Germany, <sup>25</sup>CAS Key Laboratory of Theoretical Physics, Chinese Academy of Sciences, Beijing 100190, China, <sup>26</sup>The Citadel, Charleston, SC, USA

\* Corresponding editor, E-mail: janusz.gluza@cern.ch.



© owned by the authors. Copyright statement see page iii.



# Copyright Statement

"Standard Model Theory for the FCC-ee: The Tera-Z", Report on the 1<sup>st</sup> Mini workshop: Precision EW and QCD calculations for the FCC studies: methods and tools, 12-13 January 2018, CERN, Geneva, Switzerland, <https://indico.cern.ch/event/669224/>

© Copyright 2018 under the terms of the Creative Commons Attribution 4.0 International License CC BY 4.0, hold by

A. Akhundov, A. Arbuzov, A. Blondel, R. Boels, S. Bondarenko, S. Borowka, C.M. Carloni Calame, I. Dubovyk, Ya. Dydyshka, W. Flieger, A. Freitas, J. Gluza, K. Grzanka, T. Hahn, T. Huber, S. Jadach, P. Janot, L. Kalinovskaya, R. Lee, P. Marquard, G. Montagna, O. Nicrosini, C.G. Papadopoulos, F. Piccinini, R. Pittau, W. Płaczek, M. Prausa, S. Riemann, T. Riemann, G. Rodrigo, R. Sadykov, M. Skrzypek, D. Stöckinger, J. Usovitsch, B.F.L. Ward, S. Weinzierl, G. Yang, S.A. Yost.



# Executive Summary

The message of this report may be summarized as follows:

1. One of the highlights of the FCC-ee scientific programme is a comprehensive campaign of measurements of Standard Model (SM) precision observables, spanning the Z pole, the W pair threshold, Higgs production and the top quark threshold. The statistics available, up to several  $10^{12}$  visible Z decays (Tera-Z) and  $10^8$  W-pairs, leads to an experimental precision improved by one to two orders of magnitude compared to the state of the art. This increased precision opens a broad reach for discovery, but puts strong demands on the precise calculations of Standard Model and QED corrections, especially at the Z pole, on which this first report concentrates. This will require controlling perturbation theory at more than two loop levels, and constitutes in itself a novel technical and mathematical scientific undertaking. This is discussed in the Foreword and Chapters B,C and E.
2. In order to meet the experimental precision of the FCC-ee Tera-Z for ElectroWeak Pseudo-Observables (EWPOs), even 3-loop calculations of the  $Zf\bar{f}$ -vertex will be needed, comprising the loop orders  $\mathcal{O}(\alpha\alpha_s^2)$ ,  $\mathcal{O}(N_f\alpha^2\alpha_s)$ ,  $\mathcal{O}(N_f^2\alpha^3)$  and corresponding QCD 4-loop terms. This is a key problem and discussed in Chapters B and D.
3. Real photon emission is the other key problem, of a complexity that is comparable to the loop calculations. Joint treatment of electroweak and QCD loop corrections with the real photon corrections, and their interplay, is at hand. In practice, one can expect to have to tackle a variety of peculiarities as well as a huge complexity of mathematical expressions. This is discussed in Chapter B.
4. The  $Zf\bar{f}$ -vertex corrections are embedded in a structure describing the hard scattering process  $e^+e^- \rightarrow f\bar{f}$ , based on matrix elements in form of Laurent series around the Z pole. Here, additional non-trivial contributions like 2-loop weak box diagrams show up. This is discussed in Chapter C.
5. Full 2-loop corrections to the  $Zf\bar{f}$ -vertex have been completed recently. We estimate that future calculations of the above-mentioned higher order terms would meet the experimental FCC-ee-Z demands if they are performed with a 10 percent accuracy, corresponding to 2 significant digits. A specific issue is the treatment of the electroweak  $\gamma_5$  problem. This is discussed in Chapters B and D.
6. The central techniques for the electroweak loop calculations will be numerical. This is due to the large number of scales involved. In order to achieve the accuracy goals, we have identified and discussed these and several additional exploratory strategies, methods and tools in Chapters C, D and E.
7. The treatment of four fermion processes will be required for the W mass and width measurements and will be addressed with as much synergy as possible in future work. Special treatment will be required for the Higgs and top physics, but the experimental precision is less demanding. The high precision Z pole work will provide a strong basis for these further studies.

The techniques for higher order SM corrections are basically understood, but not easily worked out or extended. We are confident that the community knows how to tackle the described problems. We anticipate that at the beginning of the FCC-ee campaign of precision measurements, the theory will be precise enough not to limit their physics interpretation. This statement is however conditional to sufficiently strong support by the physics community and the funding agencies, including strong training programs.

Cooperation of experimentalists and theorists will be highly beneficial, as well as the blend of experienced and younger colleagues; the workshop gained considerably from joining the experience from LEP/SLC with the most advanced theoretical developments. We hope that the meeting was a starting event for forming an active SM@FCC-ee community.



# Editors' Note

We should think big. And the FCC-ee project is a big chance to step up in our case for understanding the physical world at the smallest scales. We were surprised by the enthusiasm of the participants of the workshop on the theoretical backing of the FCC-ee Tera-Z stage and by the following commitment. The present report documents this. The contributions by the participants of the workshop, with several additional invited submissions and accomplished with approximately 800 detailed references, prove that the theory community needs and enjoys such demanding long-term projects like the FCC, including the FCC-ee mode running at the  $Z$  peak. They push particle physics research into most advanced challenges which stand ahead of the XXI century science.

A quote from the report's body:

*The huge improvements will allow the FCC-ee Tera-Z stage to test the Standard Model at an unprecedented precision level. The step in precision corresponds to the step which was represented by LEP/SLC at their time; they tested the SM at a precision which needed “complete” one-loop corrections, plus leading higher order terms. The FCC-ee at the  $Z$  peak needs “complete” two-loop corrections, plus leading higher order terms. Even without a reference to New Physics, the FCC-ee Tera-Z stage lets us expect exciting, qualitatively new results.*

We hope that the workshop was a good starting point for further regular workshops on FCC-ee physics and international collaboration in future. Innovations, endorsement and stability on a long-term scale give us a unique chance to accomplish the big FCC-ee vision.

We thank all authors for their excellent work.





# Contents

<b>Abstract</b>	<b>5</b>
<b>Foreword. Precision measurements at the FCC-ee: the wish-list to theory</b>	<b>5</b>
<b>A Introduction and Overview</b>	<b>13</b>
1 Introduction . . . . .	13
2 Electroweak observables (EWPOs) . . . . .	14
3 QED issues . . . . .	15
4 Methods and tools . . . . .	17
<b>B Theory status of Z-boson physics</b>	<b>19</b>
<b>C Theory meets experiment</b>	<b>27</b>
1 Introduction . . . . .	27
2 Loops, matrix elements, EWPOs . . . . .	33
2.1 Renormalization in a nutshell . . . . .	34
2.2 The $2 \rightarrow 2$ matrix elements . . . . .	35
2.3 The Z resonance as Laurent series . . . . .	38
2.4 Electroweak pseudo-observables . . . . .	40
2.5 Loops in the $2 \rightarrow 2$ matrix element . . . . .	44
2.6 A coexistence of photon and $Z$ exchange . . . . .	46
2.7 Electroweak and QED corrections in the CEEX scheme of KKMC . . . . .	47
2.8 Radiative loops: 5-point functions . . . . .	49
2.9 Bhabha scattering: Massive loops at NNLO . . . . .	49
3 QED deconvolution and pseudo-observables at FCC-ee precision . . . . .	51
3.1 EWPOs in the LEP era . . . . .	52
3.2 Potential problems with LEP deconvolution at FCC-ee precision . . . . .	53
3.3 Electroweak pseudo-observables at FCC-ee . . . . .	55
3.4 More on QED and EW separation beyond 1st order . . . . .	57
4 The ZFITTER project . . . . .	61
4.1 Introduction . . . . .	61
4.2 The form factors $\rho, v_e, v_f, v_{ef}$ . . . . .	62
4.3 Fortran versus C++. Modernity and modularity . . . . .	63
4.4 Prospects of QED flux functions . . . . .	64
4.5 The SMATASY interface . . . . .	66
4.6 Conclusions . . . . .	70
4.7 Appendix. QED flux functions . . . . .	70
5 The event generator BABAYAGA . . . . .	77
5.1 Introduction . . . . .	77
5.2 The event generator BABAYAGA and BABAYAGA@NLO . . . . .	77

5.3	Results and estimate of the theoretical error at flavour factories . . . . .	79
5.4	Exploratory results at FCC-ee . . . . .	81
5.5	Conclusions . . . . .	82
6	BHLUMI: The path to 0.01% theoretical luminosity precision . . . . .	83
6.1	Introduction . . . . .	83
6.2	Theoretical uncertainty in LEP luminometry, A.D. 1999 . . . . .	83
6.3	Present status (2018) . . . . .	84
6.4	Path to 0.01% precision for FCC-ee . . . . .	84
6.5	Summary . . . . .	91
7	The SANC project . . . . .	93
<b>D</b>	<b>Towards 3- and 4-loop form factors</b>	<b>99</b>
1	Form factors and $\gamma_5$ . . . . .	99
1.1	Introduction . . . . .	99
1.2	Massive Form factor . . . . .	99
1.3	Massless form factor . . . . .	100
1.4	Remarks on regularization and $\gamma_5$ . . . . .	101
2	Four-loop form factor in N=4 super Yang-Mills theory . . . . .	103
2.1	General motivation: N=4 SYM as a toy model . . . . .	103
2.2	Concrete motivation: the non-planar cusp anomalous dimension at four loops . . . . .	103
2.3	Constructing the integrand, briefly . . . . .	104
2.4	Maximally transcendental integrals from a conjecture . . . . .	105
2.5	Putting the pieces together: results . . . . .	107
2.6	Discussion and conclusion . . . . .	108
<b>E</b>	<b>Methods and Tools</b>	<b>111</b>
1	Introduction . . . . .	111
2	The MBnumerics project . . . . .	113
2.1	Introduction . . . . .	113
2.2	Mellin-Barnes integral . . . . .	114
2.3	Minkowskian kinematics . . . . .	115
3	Pragmatic evaluation of Feynman integrals with pySecDec and TayInt – Loopedia . . . . .	119
3.1	Introduction . . . . .	119
3.2	Preliminaries . . . . .	119
3.3	Loopedia - a database for loop integrals . . . . .	120
3.4	Numerical evaluation with the program pySecDec . . . . .	120
3.5	Accurate approximation using the TayInt approach . . . . .	122
3.6	Summary and outlook . . . . .	123
4	AMBRE - Construction of Mellin-Barnes integrals for 2- and 3-loop $Z$ -boson vertices . . . . .	125
4.1	Introduction . . . . .	125
4.2	AMBRE how to: present status . . . . .	125
4.3	3-loop AMBRE representations . . . . .	127

4.4	Conclusions and Outlook . . . . .	129
5	Mellin-Barnes meets Method of Brackets . . . . .	133
5.1	Introduction . . . . .	133
5.2	The Method of Brackets . . . . .	133
5.3	The example . . . . .	134
5.4	Optimization . . . . .	135
5.5	The rules . . . . .	135
5.6	Conclusion . . . . .	137
6	New approach to Mellin-Barnes integrals for massive one-loop Feynman integrals . . . . .	139
6.1	Introduction . . . . .	139
6.2	The MB-iterations for the massive oneloop integrals . . . . .	142
6.3	The cases of vanishing Cayley determinant and vanishing Gram determinant . . . . .	143
6.4	Example: A massive 4-point function with vanishing Gram determinant . . . . .	144
7	MB thimbles . . . . .	147
7.1	Introduction . . . . .	147
7.2	One dimension . . . . .	148
7.3	Extension to higher dimensions . . . . .	149
7.4	Application to physics and MB trials . . . . .	151
7.5	Summary . . . . .	152
8	Differential equations for multiloop integrals . . . . .	153
8.1	Obtaining differential equations . . . . .	153
8.2	$\epsilon$ -expansion of differential equations . . . . .	155
8.3	$\epsilon$ -form of the differential systems . . . . .	155
8.4	Reducing differential systems to $\epsilon$ -form . . . . .	157
9	About Cuts of Feynman integrals and differential equations . . . . .	165
9.1	Introduction . . . . .	165
9.2	The Simplified Differential Equations Approach . . . . .	166
9.3	Massless pentabox MI with up to one off-shell leg . . . . .	167
9.4	The Baikov representation . . . . .	168
9.5	Cutting Feynman Integrals . . . . .	170
9.6	Discussion and Outlook . . . . .	171
10	Exploring the function space of Feynman integrals . . . . .	173
10.1	Introduction: Precision calculations for the FCC-ee . . . . .	173
10.2	Differential equations and multiple polylogarithms . . . . .	173
10.3	Beyond multiple polylogarithms: Single scale integrals . . . . .	175
10.4	Towards multi-scale integrals beyond multiple polylogarithms . . . . .	177
10.5	Conclusions . . . . .	178
11	Direct calculation of multi-loop integrals in $d = 4$ with FDR . . . . .	179
11.1	UV divergent loop integrals . . . . .	179
11.2	Keeping unitarity . . . . .	181
11.3	Infrared singularities . . . . .	181

11.4	Scaleless integrals . . . . .	183
11.5	Renormalization . . . . .	183
11.6	Making contact with other methods . . . . .	184
11.7	Results . . . . .	184
11.8	Outlook . . . . .	187
12	Subtractions versus unsubtractions . . . . .	189
13	Numerical Integration with the Cuba Library . . . . .	193
13.1	Overview . . . . .	193
13.2	Concepts . . . . .	193
13.3	Algorithms . . . . .	196
13.4	Mathematica interface . . . . .	197
13.5	Parallelization . . . . .	198
13.6	Summary . . . . .	200
<b>Acknowledgements</b>		<b>201</b>
<b>Bibliography</b>		<b>201</b>

# Abstract

The future 100-km circular collider FCC at CERN is planned to operate in one of its modes as an electron-positron FCC-ee machine. We give an overview of the theoretical status compared to the experimental demands of one of four foreseen FCC-ee operating stages, which is  $Z$ -boson resonance energy physics, FCC-ee Tera-Z stage for short. The FCC-ee Tera-Z will deliver the highest integrated luminosities as well as very small systematic errors for a study the Standard Model (SM) with unprecedented precision. In fact, the FCC-ee Tera-Z will allow to study at least one more quantum field theoretical perturbative order compared to the LEP/SLC precision. This is a new quality by itself, independent of specific New Physics searches. The real problem is that the present precision of theoretical calculations of the various observables within the SM does not match that of the anticipated experimental measurements. To overcome this situation, the bottle-neck problems are specified. In particular, the issues of precise QED unfolding and of the correct calculation of SM pseudo-observables are critically reviewed. In an *Executive Summary* we specify which basic theoretical calculations are needed to meet the strong experimental expectations at the FCC-ee Tera-Z. Finally, several methods, techniques and tools needed for higher order multi-loop calculations are presented. By inspection of the  $Z$ -boson partial and total decay widths analysis, arguments are given that at the beginnig of operation of the FCC-ee Tera-Z, the theory predictions may be tuned to be precise enough not to limit the physics interpretation of the measurements. This statement is based on the anticipated progress in analytical and numerical calculations of multi-loop and multi-scale Feynman integrals and on the completion of two-loop electroweak radiative corrections to the SM pseudo-observables this year. However, the above statement on a time perspective over one or two decades is conditional, because the theoretical issues demand a very dedicated and focused investment by the community in order to get developed to the necessary level.



# Foreword. Precision measurements at the FCC-ee: the wish-list to theory

**Authors:** Alain Blondel [Alain.Blondel@cern.ch] and Patrick Janot [Patrick.Janot@cern.ch].  
Physics co-coordinators of the FCC-ee design study and members of the FCC coordination group.

Particle Physics has arrived at an important moment of its history. The discovery of the Higgs boson at the LHC, with a mass of 125 GeV, completes the matrix of particles and interactions that has constituted the "Standard Model" for now several decades. The Standard Model is a very consistent and predictive theory, which has proven extraordinarily successful at describing the vast majority of phenomena accessible to experiment. The observed masses of the top quark and the Higgs boson are found to agree well with the values that could be predicted, before their direct observation, from a wealth of precision measurements collected at  $e^+e^-$  colliders LEP and SLC, at the Tevatron and from other precise low energy experimental input. Given the top and Higgs masses, the Standard Model can even be extrapolated to the Planck scale without encountering a breakdown of the stability of the Universe.

At the same time, we know that the story is not over. Several experimental facts require extension of the Standard Model, in particular: i) in the composition of the observable Universe, matter largely dominates antimatter; ii) the well known evidence for dark matter from astronomical and cosmological observations; and, iii) more closely to particle physics, not only neutrinos have masses, but these masses are about  $10^{-7}$  times smaller than that of the electron. To these experimental facts can be added a number of theoretical issues of the Standard Model, including the hierarchy problem, the neutrality of the Universe and the stability of the Higgs boson mass upon radiative corrections, the strong CP problem, to name a few. The problem faced by Particle Physics is that the possible solutions to these questions seem to require the existence of new particles or phenomena that can occur over an immense range of mass scales and coupling strengths. To make things more challenging, it is worth recalling that the predictions of the top quark and Higgs boson masses from precision measurements were made within the Standard Model framework, assuming that no other new physics exists, which would modify the loop corrections upon which the predictions were made.

The observation of new particles or phenomena may happen by luck, by increasing energy. The past history has shown however that e.g. the existence of the W and Z, of the top and of the Higgs, as well as their properties, were predicted before their actual observations, from a long history of experiments and theoretical maturation.

In this context, a decisive improvement in precision measurements of electroweak observables (EWPO) could play a crucial role, by integrating sensitivity to a large range of new physics possibilities. The observation of a significant deviation from the Standard Model predictions will definitely be a discovery. It will require not only a considerable improvement in precision, but also a large set of measured observables in order to i) eliminate spurious deviations and ii) possibly reveal a pattern of deviations allowing to guide the theoretical interpretation. **Improved precision equates discovery potential.**

For these quantum effects to be measurable, however, the precision of theoretical calculations of the various observables within the standard model will have to match that of the experiment, i.e., to improve by up to two orders of magnitude with respect to current achievements. This tour-de-force will require complete two- and three-loop corrections to be calculated. Probably, this will lead to the development of breakthrough computation techniques to keep the time needed for these numerical calculations within reasonable limits.

The 2013 European Strategy for Particle Physics, ESPP [1], stated in a first bullet: "To stay at the forefront of particle physics, Europe needs to be in a position to propose an ambitious post-LHC accelerator project at CERN by the time of the next Strategy update, when physics results from the LHC running at 14 TeV will be available. CERN should undertake design studies for accelerator projects in a global context, with emphasis on proton-proton and electron-positron high-energy frontier machines (...)".

Table 1: Run plan for FCC-ee in its baseline configuration with two experiments. The WW event numbers are given for the entirety of the FCC-ee running at and above the WW threshold.

Phase	Run duration (years)	Center-of-mass Energies ( GeV )	Integrated Luminosity ( $\text{ab}^{-1}$ )	Event Statistics
FCC-ee-Z	4	88-95	150	$3.10^{12}$ visible Z decays
FCC-ee-W	2	158-162	12	$10^8$ WW events
FCC-ee-H	3	240	5	$10^6$ ZH events
FCC-ee-tt	5	345-365	1.5	$10^6$ $t\bar{t}$ events

The importance of precision was not forgotten by the ESPP however, and the next bullet states: "There is a strong scientific case for an electron-positron collider, complementary to the LHC, that can study properties of Higgs boson and other particles with unprecedented precision and whose energy can be upgraded (...)" .

The FCC international collaboration [2] has thus undertaken the study of a future 100-km circular infrastructure, designed with the capability to host, as ultimate goal, a 100 TeV pp collider (FCC-hh). Within the study a considerable effort is going into the design of a high-luminosity, high precision  $e^+e^-$  collider, FCC-ee, that would serve as a first step in a way similar to the LEP/LHC success story. The study established that FCC-ee is feasible with high expected performance, has a strong physics case [3] in its own right and could technically be built within a timescale so as to start seamlessly at the end of the HL-LHC program. Thus, with a combination of synergy and complementarity, both in the infrastructure and for the physics, the FCC program fulfills both recommendations of the ESPP.

The FCC-ee is designed to deliver  $e^+e^-$  collisions to study the Z, W, and Higgs bosons, and the top quark, but also the b and c quarks, and the tau lepton. The run plan spanning 15 years including commissioning is shown in table 1. The number of Z bosons planned to be produced by FCC-ee (up to  $5.10^{12}$ ), for example, is more than five orders of magnitude larger than the number of Z bosons collected at LEP ( $2.10^7$ ), and three orders of magnitude larger than that envisioned with a linear collider (a few  $10^9$ ). Furthermore, the exquisite determination of the centre-of-mass energy by resonant depolarization available in the storage rings will allow measurements of the W and Z masses and widths with a precision of a few hundred keV. The high-precision measurements and the observation of rare processes that will be made possible by these large data samples will open opportunities for new physics discoveries, from very weakly-coupled light particles that could explain the yet unobserved dark matter or neutrino masses, to quantum effects of weakly coupled new particles up to masses up to the better part of 100 TeV.

Apart from FCC-ee, other options are considered internationally for future electron colliders. Linear colliders ILC (International Linear Collider) [3, 4] and CLIC (Compact Linear Collider) [5] offer high energy reach and are to a large extent complementary to the FCC-ee. The ILC proposal is presently in the final stage of negotiations in Japan. It is planned with a first step at a center-of-mass of 250 GeV, and could be extended to possibly 500 GeV. While the present plan does not foresee intense running at the Z, a 'GigaZ' run has been discussed. The CLIC (Compact Linear Collider) studied at CERN based on high gradient room-temperature acceleration system, would cover the energies between 0.5 TeV and 3 TeV. Finally, the CEPC (Circular Electron Positron Collider) [6] in China, similar to the FCC-ee, is designed for collisions from the Z to the ZH production maximum at 250 GeV. Among these projects FCC-ee is the most ambitious for precision measurements; we will concentrate on this project here. Precision calculations suitable for FCC-ee will by definition suit the other projects.

Table 2 summarizes a some of the most significant FCC-ee experimental accuracies and compares them to those of the present measurements.



Table 2: Measurement of Electroweak quantities at the FCC-ee, compared with the present precisions.

Observable	Present value	$\pm$ error	FCC-ee Stat.	FCC-ee Syst.	Source and dominant exp. error
$m_Z$ (keV/c <sup>2</sup> )	91186700	$\pm$ 2200	5	100	Z line shape scan Beam energy calibration
$\Gamma_Z$ (keV)	2495200	$\pm$ 2300	8	100	Z line shape scan Beam energy calibration
$R_\ell^Z (\times 10^3)$	20767	$\pm$ 25	0.06	1	Ratio of hadrons to leptons Acceptance for leptons
$\alpha_s(m_Z) (\times 10^4)$	1196	$\pm$ 30	0.1	1.6	$R_\ell^Z$ above
$R_b (\times 10^6)$	216290	$\pm$ 660	0.3	<60	Ratio of $b\bar{b}$ to hadrons Stat. extrapol. from SLD [7]
$\sigma_{\text{had}}^0 (\times 10^3)$ (nb)	41541	$\pm$ 37	0.1	4	Peak hadronic cross-section Luminosity measurement
$N_\nu (\times 10^3)$	2991	$\pm$ 7	0.005	1	Z peak cross sections Luminosity measurement
$\sin^2\theta_W^{\text{eff}} (\times 10^6)$	231480	$\pm$ 160	3	2 - 5	$A_{\text{FB}}^{\mu\mu}$ at Z peak Beam energy calibration
$1/\alpha_{\text{QED}}(m_Z)(\times 10^3)$	128952	$\pm$ 14	4	small	$A_{\text{FB}}^{\mu\mu}$ off peak
$A_{\text{FB}}^{b,0} (\times 10^4)$	992	$\pm$ 16	0.02	<1	b-quark asymmetry at Z pole Jet charge
$A_{\text{FB}}^{\text{pol},\tau} (\times 10^4)$	1498	$\pm$ 49	0.15	<2	$\tau$ polar. and charge asymm. $\tau$ decay physics
$m_W$ (keV/c <sup>2</sup> )	803500	$\pm$ 15000	600	300	WW threshold scan Beam energy calibration
$\Gamma_W$ (keV)	208500	$\pm$ 42000	1500	300	WW threshold scan Beam energy calibration
$\alpha_s(m_W)(\times 10^4)$	NA	NA	3	small	$R_\ell^W$
$N_\nu (\times 10^3)$	2920	$\pm$ 50	0.8	small	Ratio of invis. to leptonic in radiative Z returns
$m_{\text{top}}$ (MeV/c <sup>2</sup> )	172740	$\pm$ 500	20	small	$t\bar{t}$ threshold scan QCD errors dominate
$\Gamma_{\text{top}}$ (MeV/c <sup>2</sup> )	1410	$\pm$ 190	40	small	$t\bar{t}$ threshold scan QCD errors dominate
$\lambda_{\text{top}}/\lambda_{\text{top}}^{\text{SM}}$	$m = 1.2$	$\pm$ 0.3	0.08	small	$t\bar{t}$ threshold scan QCD errors dominate
$t\bar{t}Z$ couplings		$\pm$ 30%	<2%	small	$E_{\text{CM}} = 365\text{GeV}$ run

Some important comments are in order:

- FCC-ee will provide a set of ground breaking measurements of a large number of new-physics sensitive observables, with improvement with respect to the present status by a factor of 20-50 or even more; moreover it will improve input parameters,  $m_Z$  of course, but also  $m_{\text{top}}$ ,  $\alpha_s(m_Z)$  and, for the first time a direct and precise measurement of  $\alpha_{\text{QED}}(m_Z)$ , with a precision that will reduce considerably the parametric uncertainties in the electroweak predictions.
- The table 2 is only a first sample of the accessible observables. Work on the future projections of experimental and theory requirements are subject of intensive studies within the FCC-ee design study groups. Important contributions are expected from b, c and tau physics at the Z pole, such as Forward-Backward and Polarization asymmetries. Also the tau lepton branching fraction and life time measurements, especially if a more precise tau mass becomes available, will provide another dimension of precision measurements.
- While statistical precisions follow straightforwardly from the integrated luminosities, the systematic uncertainties do not. It is quite clear that for the Z and W mass and width the center-of-mass energy uncertainty will dominate, and that for the total cross-sections (thus the number of neutrino determination) the luminosity measurement error will dominate. These have been the subject of considerable work already. However there is no obvious limit in the experimental precision reachable for such observables as  $R_\ell^Z$  or  $R_b$  or the top quark pair cross-section measurements.
- While we have indicated a possible experimental error level for  $R_\ell^Z$  or  $R_b$ , these should be considered **indicative** and might improve with closer investigation. It is likely however that the interpretation of these measurements in terms of e.g. the b weak couplings, the strong coupling constant, or the top mass, width and its weak and Yukawa couplings, will be limited by questions related to the precise definition of these quantities, or to issues such as "what is the b-quark mass?".

The table clearly sets the requirements for theoretical work: the aim should be to either provide the tools to compare experiment and theory at a level of precision better than the experimental errors, or identify which additional calculation or experimental input would be required to achieve it. Another precious line of research to be done jointly by theorists and experimenters should be to try to find observables or ratios of observables for which theoretical uncertainties are reduced.

The theoretical work that experiment requires from the theoretical community can be separated in a few classes.

- QED (mostly) and QCD corrections to cross-sections and angular distributions that are needed to convert experimentally measured cross-sections back to 'pseudo-observables': couplings, masses, partial widths, asymmetries, etc. that are close to the experimental measurement (i.e. the relation between measurements and these quantities does not alter the possible 'new physics' content). Appropriate event generators are essential for the implementation of these effects in the experimental procedures.
- Calculation of the pseudo-observables with the precision required in the framework of the Standard Model with the required precision so as to take full advantage of the experimental precision.
- Identify the limiting issues and in particular the questions related to the definition of parameters, in particular the treatment of quark masses and more generally QCD objects.
- An investigation of the sensitivity of the proposed experimental observables (or new ones) to the effect of new physics in a number of important scenarios. This is an essential work to be done early, before the project is fully designed, since it potentially affects the detector design and potentially the running plan.

The workshop at CERN *Precision EW and QCD calculations for the FCC studies: methods and tools* was the start of a process that will be both exciting and challenging. The precision calculations might look like a high mountain to climb but may contain the gold nugget: the discovery of the signals pointing the Particle Physics community towards the solution of some of our deep questions about the Universe.

It is a pleasure to thank Janusz Gluza, Staszek Jadach and Tord Riemann for their competence and enthusiasm in organizing the workshop and the write-up, and all the participants for their contributions. We look forward to this adventure together.



# Chapter A

## Introduction and Overview

**Authors:** Janusz Gluza, Stanisław Jadach, Tord Riemann

Corresponding Author: Stanisław Jadach [stanislaw.jadach@cern.ch]

### 1 Introduction

This report includes a collection of material devoted to a discussion of the status of theoretical efforts towards the calculation of higher order Standard Model (SM) corrections needed for the FCC-ee. It originates from presentations at the FCC-ee mini workshop *Precision EW and QCD calculations for the FCC studies: Methods and tools*, 12-13 January 2018, CERN, Geneva, Switzerland [8]. Both at the workshop and in this survey we have deliberately focused on the FCC-ee Tera-Z mode, see Tab.1. It will be the first operational stage of FCC-ee. The mini-workshop was intended to initiate a discussion on several topics:

- (i) What are the necessary precision improvements of theoretical calculations in the Standard Model, such that they match the needs of the experiments at the planned FCC-ee collider in the Z peak mode?
- (ii) A focus is on the calculation of Feynman diagrams in terms of Feynman integrals. Which calculational techniques are available and/or have to be developed in order to attain the necessary precision level?
- (iii) Besides the high-loop vertex corrections, the realistic QED contributions are highly nontrivial.
- (iv) What else has to be calculated and put together for a data analysis? Respecting thereby gauge invariance, analyticity, unitarity.

Although the theoretical calculations are universal and will be crucial for the success of any future high-luminosity collider, we will focus on the FCC-ee Tera-Z study as the most precise facility. Its precision would be useless without the corresponding higher order Standard Model predictions.

To get an imagination of the unprecedented accuracy of the FCC-ee Tera-Z project, let us look at the electron asymmetry parameter  $A_e$ . The most precise theory prediction in the SM is [9, 10]. The actual LEP/SLC based value is  $\sin^2 \theta_{\text{eff}}^{\text{lept}} = 0.23152 \pm 16 \times 10^{-5}$  [11], see also Tab. 2. Interestingly, also the LHC can play a role for electroweak precision measurements. The presently claimed ATLAS measurement is  $\sin^2 \theta_{\text{eff}}^{\text{lept}} = 0.23140 \pm 36 \times 10^{-5}$  [12]. It is planned to get improved. The FCC-ee Tera-Z will measure the leptonic effective weak mixing angle with highest precision from the muon charge asymmetry, namely  $\delta \sin^2 \theta_{\text{eff}}^{\text{lept}} = \pm 0.3 \times 10^{-5}$ , see Tab. 2 in the Foreword. This may be compared to the so-called Giga-Z option of the ILC [13], which might have a certain degree of polarization. Presently, the option is not at the priority list of the ILC. For Giga-Z, a relative uncertainty  $\delta \sin^2 \theta_{\text{eff}}^{\text{lept}} = \pm 1.3 \times 10^{-5}$  is expected [14]. In sum, the FCC-ee -Z will improve the  $A_e$  measurement by at least one order of magnitude.

Similarly, the values of mass and width of the Z boson will get improved by factors of 20.

The meeting and the report presented here are based on two complementary sources of knowledge. First, the knowledge base accumulated by physicists who have worked for many years at LEP/SLC. Their expertise is accelerating the FCC-ee studies during all their steps. A second equally important source is the huge progress made in the last two decades in the area of analytical and numerical methods and practical tools for multi-loop calculations in perturbative field theory. These two strong pillars are manifest in this document; see chapters C

and B for the first one and chapter D and E for the second one. The report reflects also another component for the success of such a complicated long term project – the many contributions by young, talented mathematically oriented colleagues, who are contributing bold and new ideas to this study. Further, a certain degree of coherence of the community is needed and the workshop has shown that we may reach it.

As pronounced already in the Foreword, the FCC-ee claims a dramatically improved experimental accuracy compared to that of LEP/SLC for practically all electroweak measurements.

In the following sections we introduce the issues of importance from the perspective of FCC-ee Tera-Z theoretical studies.

## 2 Electroweak observables (EWPOs)

The so called electroweak pseudo observables, or EWPOs in short, are quantities like  $Z$  mass and width, the various  $2 \rightarrow 2$   $Z$  peak cross sections, and all kinds of  $2 \rightarrow 2$  charge and spin asymmetries at the  $Z$  peak; one may also add the equivalent effective electroweak mixing angles. They are derived directly from experimental data such that QED contributions and kinematic cut-off effects are removed. For a more detailed definition of EWPOs see Section C.3.

For the  $Z$  width, the experimental error will go down to about  $\pm 0.1$  MeV, which is about 1/20 of the LEP/SLC accuracy. For the measurement of the effective electroweak mixing angles from asymmetries, an improvement by a factor of up to about 50 is envisaged, see Tab. 2 in the Foreword.

*Such huge improvements will allow the FCC-ee Tera-Z to test the Standard Model at an unprecedented precision level. The step in precision corresponds to the step which was represented by LEP/SLC at their time; they tested the SM at a precision which needed “complete” one-loop corrections, plus leading higher order terms. The FCC-ee Tera-Z needs “complete” two-loop corrections, plus leading higher order terms. Even without a reference to New Physics, the FCC-ee Tera-Z lets us expect exciting, qualitatively new results.*

Consequently, the tremendous precision of the FCC-ee will require serious efforts in the area of 3-loop electroweak calculations. We would like to mention that only recently the electro-weak 2-loop calculations for  $Z$ -physics were completed [15, 16]. In the QCD sector of the SM some additional 4-loop calculations seem to be necessary as well. Discussing the status and prospects of 3-loop weak and of 4-loop QCD calculations is a main subject of chapter B. The questions why and how SM calculations must improve is elaborated there and summarized; it was also discussed recently on several occasions [17–19].

Very briefly, for SM calculations of the  $Z$  boson width, the complete EW 2-loop and some leading partial QCD/mixed 3-loop terms are known. The present so called “intrinsic” theoretical (TH) error due to uncontrolled higher order terms is estimated to be  $\delta\Gamma_Z \sim \pm 0.4$  MeV in [16]; see also Tab. B.5 in Chapter B. The value is below the experimental accuracy of LEP, but it is bigger than the anticipated accuracy of the FCC-ee Tera-Z. Here, a new round of calculations is indispensable. For other quantities the situation is similar, see Tab. B.7.

The essential question is: How difficult is the calculation of EW 3-loop and QCD 4-loop contributions? Do we know how to do this? This issue is addressed in more details in Chapters B and D.

Let us also note the following aspect of higher order SM corrections for the FCC-ee. At LEP it was a standard procedure that QED was extracted such that only the first and higher EW effects have remained in EWPOs. The elimination of QED from EWPOs was a natural task at LEP, because since the 1970s QED theory and higher order techniques were already fully established. Hence, in the LEP data analysis physicists were interested only in the exploration of the QCD and EW effects. Thanks to LHC, QCD is presently treated in high energy studies similarly as QED. It is quite likely that in future FCC-ee Tera-Z searches for new physics the EW higher order effects will be treated the same way, namely as known, calculable effects to be removed from data. But at least at the 2-loop level! Notably, particles like  $W, Z, H$  bosons as well as the top quark are considered to be heavy from the present perspective. In future, they will be regarded as light particles compared to the 20-50 TeV mass scales of the effective theories used to analyze FCC data. Such a change of perspective poses a non-trivial practical question for the future strategy of the data analysis: How to treat EW

higher order corrections? Should we keep them in the EWPOs or extract them like QED effects? This kind of questions is natural in the context of Chapter C. Generally, we propose to start from what was done at LEP, but keep an eye on potential modifications, in particular on possible new definitions of EWPOs. Accordingly, in chapter C the use of Laurent series around the  $Z$ -pole and an S-matrix inspired framework for  $2 \rightarrow 2$  scattering are discussed in more detail. It might also happen that a consistent description of real processes and the extraction of effective couplings at the FCC-ee Tera-Z will demand to change from analyzing differential, squared amplitudes to analyzing spin amplitudes, merged properly with a Monte Carlo analysis. In this respect a possible modification of the language with EWPOs into a language with EWPPs (EW "pseudo-parameters") is discussed in C.3. See also further remarks connected with these issues in the QED section A.3.

Another non-trivial issue is how to test non-standard (BSM) physics. As discussed in [20], the structure of higher order corrections can be quite different when comparing the SM with extensions. This is actually the case for all models with  $\rho_{\text{tree}} \equiv M_W^2/(M_Z^2 \cos^2 \theta_W) \neq 1$ . In the Standard Model Effective Field Theory (SMEFT) approach, EWPOs with dimension-6 operators are considered in the "Warsaw" basis [21] or in the "SILH" basis [22, 23]. For some recent 1-loop SMEFT analysis, see [24]. In [25] SMEFT corrections to  $Z$ -boson decays are considered. For a present SMEFT global analysis, see e.g. [26]. It seems that the SMEFT framework is also the most practical way for parameterizing new physics at other FCC-ee stages, namely the FCC-ee-W, FCC-ee-H and FCC-ee- $t\bar{t}$  stages (Foreword, Tab. 1.)

### 3 QED issues

The problem of a better control of the sizeable QED effects at the FCC-ee Tera-Z is vital. The theoretical precision of QED calculations has to be better by a factor of 20-100 in comparison to the LEP era. This is more than one perturbative order, hence not trivial: There are subtle problems due to high-order infrared singularities, many-particle final states in the real cross sections, and higher- $n$ -point functions. We need a theoretically well justified, clear and clean recipe of disentangling the QED component of the SM from the electroweak/QCD part working at the 2-4 loop level. This includes for instance massless and massive double box diagrams with internal photons, and also initial-final state interference radiative effects; as is well-known, both are related. The general answer is known in principle. But one has to define and implement an efficient methodology of subtracting and resumming QED corrections due to universal, process-independent soft and collinear parts of the perturbative series, known to infinite order, while process-dependent small non-soft and non-collinear remnants may remain together with the "pure" EW corrections. Once the above problem is fixed, practical methods of removing QED effects from data, the so-called "QED deconvolution", at a much higher precision level than at LEP has also to be elaborated. Especially for those observables measured near the  $Z$  peak, where the boost of experimental precision will be biggest.

There are three groups of observables near the  $Z$  peak where the QED issues look differently:

- (i) Observables related to resonance phenomena: the  $Z$  line-shape as a function of  $s$ , i.e. the various total cross sections at the peak, as well as the  $Z$  mass and total and partial decay widths and branching ratios.
- (ii) Charge and spin asymmetries at the  $Z$  peak, related to angular distributions of the final fermion pairs, including also wide angle Bhabha scattering.
- (iii) Small angle Bhabha scattering, photon pair production, the  $Z$  radiative return above the  $Z$  peak,  $WW$ ,  $ZH$ ,  $t\bar{t}$  production and other processes with multiparticle final states over some range in  $s$ .

For the first group the so-called flux function approach was used in the LEP analyses [27]. There is a chance that it may still be sufficiently precise at the FCC-ee. In this approach the integrated cross sections could be formulated with sufficient accuracy by using a one-dimensional residual integration, describing the folding of the hard scattering kernels due to weak interactions (or effective Born terms) with flux functions representing the loss of center of mass energy due to single initial (and/or final) state photon emission plus exponentiated soft photon emission. The  $Z$  resonance is, mathematically seen, a Laurent series in the center of mass energy

squared  $s$ . This fact could be sufficiently well described as a Breit-Wigner resonance, interfering with the “background” of photon exchange. It is known how to include weak loop effects into this approach. Accordingly, EWPOs were defined in the LEP data analysis and related to the hard kernels due to weak interactions (i.e. the effective Born cross sections with effective coupling constants) with relatively simple relations, practically neglecting any factorization problems or imaginary parts. The above methodology worked well due to the limited precision of LEP data: The non-factorizable QED corrections (initial-final state interferences) and other effects like those due to imaginary parts of the effective  $Z$  couplings could be neglected. This was numerically controlled with tools like ZFITTER and TOPAZ0. It is not proved yet that a similar approach will work at FCC-ee Tera-Z precision for the  $Z$  lineshape related EWPOs, but a chance exists and should be explored. The gain would be a relatively simple and fast analysis methodology.

For the second group of observables like the leptonic charge asymmetry and the tau spin asymmetry the QED issue is much more serious. For instance the muon charge asymmetry will be measured  $\sim 50$  times more precisely than at LEP, see Tab. 2 in the Foreword. The non-factorizable initial-final state QED interference (IFI), which was about 0.1% and could be just neglected at LEP, will have to be calculated at the FCC-ee Tera-Z with a two-digits precision and then explicitly removed from the data. Moreover, there is, at LEP accuracy, a set of simple formulae for the IFI with a 1-dimensional convolution over some flux functions and hard effective Born terms at the next-to-leading order. This is implemented in ZFITTER [28]. There is no such simple formula beyond the next-to-leading order. The well known formula of this kind for the charge asymmetry, based on soft photon approximation, involves a 4-dimensional convolution. In addition, IFI-type corrections mix up with electroweak corrections; for the FCC-ee Tera-Z at the 3-4 loop level. Fortunately, the methodology of disentangling pure QED corrections from pure electroweak corrections at the amplitude level, summing up soft photon effects to infinite order (exponentiation) and adding QED collinear non-soft corrections order by order (independently of the EW part) is well known and numerically implemented in the KKMC program [29]. This program includes so far QED non-soft corrections to second order and pure EW corrections up to first order (with some 2nd order EW improvements, QCD etc.) using the weak library DIZET [30] of ZFITTER [27]. The calculational scheme of KKMC can be extended to 2-4 loops in a natural way. The interrelations of hard kernels due to weak interactions and QED folding is understood since long, at the level of sophistication which is needed for FCC-ee studies. A correct treatment of the  $Z$  resonance as a Laurent series in the hard kernel, namely using the S-matrix approach [31, 32], which was formulated already in the nineteen nineties, fits very well in the above scheme. It is basically clear how to do this in principle and in practice, also going beyond the flux function approach. All of that is described in several sections of this report in chapter C.

The above describes a scenario in which the QED and EW parts are separated in a systematic, clean manner at the amplitude level, and where the hard kernels due to weak interactions are encapsulating all 2-4 loop EW/QCD corrections. However, in the construction of EWPOs at LEP, the above hard kernel was replaced by effective Born cross sections (i.e. squared amplitudes) with effective couplings, which on one hand were fit to data and on the other hand could be compared to the best knowledge of SM predictions. The muon charge asymmetry without QED effects was with sufficient precision just a one-to-one representation of the effective couplings of the  $Z$  boson, neglecting s-channel photon exchange, a non-factorizing component, and all QED effects. It is not excluded that a similar method will work at FCC-ee precision. The important difference is that instead of the primitive flux method a Monte Carlo approach with sophisticated matrix elements would take care of all QED effects, including non-factorizable parts.

Note that including loop corrections to the hard kernel and its formal simplification in terms of an effective Born cross section will generate a need of the calculation of additional, more complicated contributions like additional massive 2-loop box terms. Some general formulations in this direction at the amplitude level are given in chapter C for the effective Born. The above approach is elaborated in section C.3; see also section C.2.

Finally, few remarks on the QED effects in the third group of observables like luminosity measurements using small angle Bhabha scattering, or photon pair production, or for neutrino counting the radiative return above the  $Z$  peak. They are so strongly dependent on the experimental event selection and the cut-offs, that



the only way to take them into account is the direct comparison of experimental data with the results of the Monte Carlo programs with sophisticated QED matrix elements. These QED matrix elements have to cover the relevant weak effects, too.

Having all the above in mind, we try to describe how a theoretical treatment of the measurements of the  $Z$  peak parameters might be formulated for the FCC-ee Tera-Z or for similar projects. We will not answer all immediate questions, will not work out all ideas completely, nor will we be able to perform the necessary detailed numerical calculations. Here the QED expertise of the Cracow group and the formalism of the S-matrix language worked out in Zeuthen with support of other groups should meet together in the exploration of unsolved problems.

These issues are defined in Chapter C. If needed, they may be treated in a more detail. But due to the amount of necessary resources and research work, such a project definition would not be unconditional concerning any kind of support.

The JINR/Dubna SANC/ZFITTER group has expressed interest to cooperate in creating a new tool like SANC/ZFITTER/SMATASY. Altogether with the BabaYaga and BHLUMI groups they close properly the Chapter C, treating there mainly luminosity problems in future colliders.

Certainly, on a larger time-scale, it would be a highly welcome situation if other, independent groups would constitute and start to work on the above issues.

## 4 Methods and tools

Our general conclusion from the discussions during and after the workshop is that the techniques and software available today would be not sufficient for an appropriate FCC-ee Tera-Z data analysis. The issues of methods, techniques and tools for the calculation of Feynman integrals and higher order loop effects are discussed in chapter E. Moreover, it is quite probable that approaches which were developed for higher loop effects in other areas of research, and which are not discussed here, can be also used in future for the calculation of EWPOs of the FCC-ee Tera-Z. Let us mention only the case of the decay  $B \rightarrow X_s \gamma$  [33,34], where the  $Z$ -propagator with unitary cut at the 4-loop level level is equivalent to 3-loop EWPOs of the  $Z$ -boson decay studies.

The chapter E on methods and tools includes the description of both analytical and numerical methods for the calculation of higher order corrections. Five contributions – E.2, E.4, E.5, E.6, and E.7 – deal completely or partly with the Mellin-Barnes (MB) method. In one contribution, E.3, the purely numerical sector decomposition (SD) method is described. Both methods are used heavily in present studies and are supposed to be crucial for FCC-ee Tera-Z calculations.

The reasons for a preference of the two numerical methods mentioned, MB and SD, are two-fold: Integrals depend on  $M_Z, M_W, M_H, m_t$  plus  $s$  for vertices – and for box integrals additionally also on  $t$  –, i.e. on up to four or five dimensionless ratios of the parameters. We have no analytical tools to cover that. Further, the integrals contain infrared singularities. The MB- and the SD-methods are the only known numerical methods with algorithms to deal with these singularities systematically at all loop orders.

*It is consensus in the community that for achieving the goals of precision it will be most crucial to have the numerical integrations efficiently implemented for Feynman integrals in Minkowskian kinematics.*

This is discussed in sections E.3 and E.2.

Sections E.8 and E.9 deal with different approaches to differential equations, including a discussion of cut Feynman integrals. In E.10 first steps are discussed towards solutions for multi-scale, multi-loop Feynman integrals. Special functions are introduced which go into the topics of elliptic functions. Some sections deal with still exploratory new ideas. E.g. MB thimbles are discussed in E.7. A new low-dimensional, numerically efficient approach to MB representations at the 1-loop level is introduced in E.6, which might be generalized to multi-loop cases as well. In sections E.11 and E.12, direct numerical calculations of Feynman integrals in  $d = 4$  are explored. Further, to achieve the goals of precision, we are interested also in methods and tools

used for the calculation of extensions of the Standard Model. In fact, extensions of the SM are in general more complex in structure. A representative example is studied in section E.2. We cannot exclude that some of the methods covered here will become standard or complementary tools in precision calculations in future.

Finally, in section E.13 the Cuba library for numerical integrations is described, exhibiting some features of importance for multi-dimensional integral calculations.

## Chapter B

### Theory status of Z-boson physics

**Authors:** Ievgen Dubovyk, Ayres Freitas, Janusz Gluza, Krzysztof Grzanka, Stanisław Jadach, Tord Riemann, Johann Usovitsch

Corresponding author: Ayres M. Freitas [afreitas@pitt.edu]

The number of Z bosons collected at LEP, approximately 17 millions in total, made it possible to determine a large amount of electroweak observables with very high precision through measurements of the Z lineshape and of cross section asymmetries, joined by high-precision parity-violating asymmetries measured at the SLC

These measurements are typically expressed through the following set of quantities: The cross-section  $e^+e^- \rightarrow f\bar{f}$  at the Z pole,  $\sigma_f^0 \equiv \sigma_f(s = M_Z^2)$ , for different final states  $f\bar{f}$ , the total width of the Z boson,  $\Gamma_Z$ , determined from the shape of  $\sigma_f(s)$ , and branching ratios of various final states:

$$\sigma_{\text{had}}^0 = \sigma[e^+e^- \rightarrow \text{hadrons}]_{s=M_Z^2}, \quad (\text{B.1})$$

$$\Gamma_Z = \sum_f \Gamma[Z \rightarrow f\bar{f}], \quad (\text{B.2})$$

$$R_\ell = \frac{\Gamma[Z \rightarrow \text{hadrons}]}{\Gamma[Z \rightarrow \ell^+\ell^-]}, \quad \ell = e, \mu, \tau, \quad (\text{B.3})$$

$$R_q = \frac{\Gamma[Z \rightarrow q\bar{q}]}{\Gamma[Z \rightarrow \text{hadrons}]}, \quad q = u, d, s, c, b. \quad (\text{B.4})$$

In the definition of these quantities, contributions from s-channel photon exchange, virtual box contributions and initial-state as well as initial–final state interference QED radiation are understood to be already subtracted; see *e. g.* Refs. [11, 35].

*The precise calculation of the terms to be subtracted, at variable cms energy  $\sqrt{s}$  around the Z peak, will be a substantial part of the theoretical analysis for the FCC-ee-Z. Further, for a determination of  $M_Z$  and  $\Gamma_Z$  we will have to confront cross section data and predictions around the Z peak position as part of the analysis.* Correspondingly, section C of this report contains an updated discussion of QED unfolding in the context of the demanding FCC-ee needs is given. To clarify this fact, the parameters (B.1)–(B.4) have become known as so-called electroweak pseudoobservables (EWPOs), rather than true observables. However, (B.1)–(B.4) still include the effect of final-state QED and QCD radiation. Fortunately, the final-state radiation effects factorize from the massive electroweak corrections almost perfectly; see *e. g.* Refs. [36, 37]. Therefore it is possible to compute the latter, as well as potential contributions from new physics, without worrying about effects from soft and collinear real radiation.

The remaining basic pseudoobservables are cross section asymmetries, measured at the Z pole. The forward-backward asymmetry is defined as

$$A_{\text{FB}}^f = \frac{\sigma_f[\theta < \frac{\pi}{2}] - \sigma_f[\theta > \frac{\pi}{2}]}{\sigma_f[\theta < \frac{\pi}{2}] + \sigma_f[\theta > \frac{\pi}{2}]}, \quad (\text{B.5})$$

where  $\theta$  is the scattering angle between the incoming  $e^-$  and the outgoing  $f$ . It can be approximately written as a product of two terms (for more precise discussion, see C.2.4)

$$A_{\text{FB}}^f = \frac{3}{4} \mathcal{A}_e \mathcal{A}_f, \quad (\text{B.6})$$

with

$$\mathcal{A}_f = \frac{1 - 4|Q_f| \sin^2 \theta_{\text{eff}}^f}{1 - 4|Q_f| \sin^2 \theta_{\text{eff}}^f + 8(Q_f \sin^2 \theta_{\text{eff}}^f)^2}. \quad (\text{B.7})$$

The  $\sin^2 \theta_{\text{eff}}^f$  is called the effective weak mixing angle, which contains the net contributions from all the radiative corrections. The most precise measurements of  $A_{\text{FB}}^f$  have been obtained for leptonic and bottom-quark final states ( $f = \ell, b$ ). In the presence of polarized electron beams, one can also measure the parity-violating left-right asymmetry

$$A_{\text{LR}}^f = \frac{\sigma_f [P_e < 0] - \sigma_f [P_e > 0]}{\sigma_f [P_e < 0] + \sigma_f [P_e > 0]} = \mathcal{A}_e |P_e|. \quad (\text{B.8})$$

Here  $P_e$  denotes the polarization degree of the incident electrons where  $P_e < 0$  ( $P_e > 0$ ) refers to left-handed (right-handed) polarizations, respectively. Since  $A_{\text{FB}}^f$  and  $A_{\text{LR}}^f$  are defined as normalized asymmetries, they do not depend on (parity conserving) initial- and final-state QED and QCD radiation effects<sup>1</sup>.

The present and predicted future experimental values for the most relevant EWPOs are given in the Wishlist Tab. 1 in the Foreword. In the following, we will compare these numbers with the present theoretical situation and with estimates for future precision calculations. In this context, a discussion of theoretical errors connected with these calculations is crucial.

	$\delta\Gamma_Z$ [MeV]	$\delta R_l$ [ $10^{-4}$ ]	$\delta R_b$ [ $10^{-5}$ ]	$\delta \sin^2 \theta_{\text{eff}}^l$ [ $10^{-6}$ ]	$\delta \sin^2 \theta_{\text{eff}}^b$ [ $10^{-5}$ ]
Present EWPO errors					
EXP1 [11]	2.3	250	66	160	1600
TH1 [9, 38, 39]	0.5	50	15	45	5
FCC-ee-Z EWPO error estimations					
EXP2 [40] & Tab. 2	0.1	10	$2 \div 6$	6	70

Table B.1: Present total experimental errors EXP1 and, estimated in 2014 [9, 38, 39], theoretical intrinsic errors TH1 for selected EW observables. EXP2 gives corresponding error estimations for the FCC-ee Z-resonance mode, see Foreword.

Tab. B.1 shows the FCC-ee experimental goals for the basic EWPOs. As is evident from the table, the theoretical intrinsic uncertainties of the current results TH1 are safely below the current experimental errors EXP1. However, they are not sufficiently small in view of the FCC-ee experimental precision targets EXP2.

This situation, as seen from the perspective of 2014, underlines the goals and strategic plan for improvements in the theoretical calculation of radiative SM corrections defined here. Historically, the complete one-loop corrections to the Z-pole EWPOs were calculated for the first time in Ref. [41]. Over the next 32 years many groups with many methods determined partial 2- and 3-loop corrections to EWPOs. A more detailed list of the relevant types of radiative corrections will be given below.

In the last two years, as discussed in Ref. [17], substantial progress in numerical calculations of multiloop and multiscale Feynman integrals was made and the calculation of the last piece of 2-loop corrections, of order  $\mathcal{O}(\alpha_{\text{bos}}^2)$ , to all Z-pole EWPOs [15, 16] became possible. Here “bos” denotes diagrams without closed fermion loops.

All the numerical results discussed below are based on the input parameters gathered in Tab. B.2.

<sup>1</sup>Here it is assumed that any issues related to the determination of the experimental acceptance have been evaluated and unfolded using Monte-Carlo methods.

Parameter	Value
$M_Z$	91.1876 GeV
$\Gamma_Z$	2.4952 GeV
$M_W$	80.385 GeV
$\Gamma_W$	2.085 GeV
$M_H$	125.1 GeV
$m_t$	173.2 GeV
$m_b^{\overline{\text{MS}}}$	4.20 GeV
$m_c^{\overline{\text{MS}}}$	1.275 GeV
$m_\tau$	1.777 GeV
$m_e, m_\mu, m_u, m_d, m_s$	0
$\Delta\alpha$	0.05900
$\alpha_s(M_Z)$	0.1184
$G_\mu$	$1.16638 \times 10^{-5} \text{ GeV}^{-2}$

Table B.2: Input parameters used in the numerical analysis, from Refs. [42–44].

As a concrete example, let us discuss the different higher-order contributions to the Standard Model prediction for the bottom-quark effective weak mixing in more detail. It can be written as

$$\sin^2 \theta_{\text{eff}}^b = \left(1 - \frac{M_W^2}{M_Z^2}\right)(1 + \Delta\kappa_b), \quad (\text{B.9})$$

where  $\Delta\kappa_b$  contains the contributions from radiative corrections. Numerical results from loop corrections of different order are shown in Table B.3. Altogether, the corrections included in the table are: electroweak  $\mathcal{O}(\alpha)$  [41] and  $\mathcal{O}(\alpha^2)$  – fermionic  $\alpha_{\text{ferm}}^2$  [38, 45–48] and bosonic  $\alpha_{\text{bos}}^2$  [15] EW contributions;  $\mathcal{O}(\alpha\alpha_s)$  corrections to internal gauge-boson self-energies [49–53]; leading three- and four-loop corrections in the large- $m_t$  limit, of order  $\mathcal{O}(\alpha_t\alpha_s^2)$  [54, 55],  $\mathcal{O}(\alpha_t^2\alpha_s)$ ,  $\mathcal{O}(\alpha_t^3)$  [56, 57], and  $\mathcal{O}(\alpha_t\alpha_s^3)$  [58–60], where  $\alpha_t \equiv \alpha(m_t^2)$ ; and non-factorizable vertex contributions  $\mathcal{O}(\alpha\alpha_s)$  [61–66] which account for the fact that the factorization between virtual EW corrections and final-state radiation effects is not exact.

The most recently determined piece, the  $\mathcal{O}(\alpha_{\text{bos}}^2)$  electroweak two-loop corrections amount to  $\Delta\kappa_b^{(\alpha^2, \text{bos})} = -0.9855 \times 10^{-4}$ , which is comparable in magnitude to the fermionic corrections. Taking into account this new result, an updated error estimation due to missing higher order terms will be discussed later on, see Tab. B.3.

Order	Value [ $10^{-4}$ ]	Order	Value [ $10^{-4}$ ]
$\alpha$	468.945	$\alpha_t^2\alpha_s$	1.362
$\alpha\alpha_s$	−42.655	$\alpha_t^3$	0.123
$\alpha_t\alpha_s^2$	−7.074	$\alpha_{\text{ferm}}^2$	3.866
$\alpha_t\alpha_s^3$	−1.196	$\alpha_{\text{bos}}^2$	−0.986

 Table B.3: Comparison of different kinds of radiative corrections to  $\Delta\kappa_b$  [15], using the input parameters in Tab. B.2. Here  $\alpha_t = y_t^2/(4\pi)$ , where  $y_t$  is the top Yukawa coupling.

Table B.4 summarizes the known contributions to  $Z$  boson production and decay vertices, order by order. The technically challenging *bosonic* two-loop calculation was completed very recently [16]. This result has

been achieved through a combination of different methods: (a) numerical integration of Mellin-Barnes (MB) representations with contour rotations and contour shifts for a substantial improvement of the convergence; (b) sector decomposition (SD) with numerical integration over Feynman parameters; (c) dispersion relations for sub-loop insertions. The MB and SD methods were discussed intensively at the workshop [67, 68]; see Chapter E for details.

As is evident from Tab. B.4, the two-loop electroweak corrections to the  $Z$ -boson partial decay widths are sizeable, of the same order as the  $\mathcal{O}(\alpha\alpha_s)$  terms. The bosonic corrections  $\mathcal{O}(\alpha_{\text{bos}}^2)$  are smaller than the fermionic ones, but larger than previously estimated in Ref. [39]. This underlines that theory error evaluations are always to be taken with a grain of salt.

For the total width  $\Gamma_Z$ , the corrections are also significantly larger than the projected future experimental error EXP2 given in Tab. B.1.

$\Gamma_i$ [MeV]	$\Gamma_e$	$\Gamma_\nu$	$\Gamma_d$	$\Gamma_u$	$\Gamma_b$	$\Gamma_Z$
$\mathcal{O}(\alpha)$	2.273	6.174	9.717	5.799	3.857	60.22
$\mathcal{O}(\alpha\alpha_s)$	0.288	0.458	1.276	1.156	2.006	9.11
$\mathcal{O}(\alpha_t\alpha_s^2, \alpha_t\alpha_s^3, \alpha_t^2\alpha_s, \alpha_t^3)$	0.038	0.059	0.191	0.170	0.190	1.20
$\mathcal{O}(N_f^2\alpha^2)$	0.244	0.416	0.698	0.528	0.694	5.13
$\mathcal{O}(N_f\alpha^2)$	0.120	0.185	0.493	0.494	0.144	3.04
$\mathcal{O}(\alpha_{\text{bos}}^2)$	0.017	0.019	0.059	0.058	0.167	0.51

Table B.4: Loop contributions, in units of MeV, to the partial and total  $Z$  widths with fixed  $M_W$  as input parameter. Here  $N_f$  and  $N_f^2$  refer to corrections with one and two closed fermion loops, respectively, whereas  $\alpha_{\text{bos}}^2$  denotes contributions without closed fermion loops. Furthermore,  $\alpha_t = y_t^2/(4\pi)$ , where  $y_t$  is the top Yukawa coupling. Table taken from Ref. [16].

These numerical examples demonstrate that radiative electroweak corrections beyond the two-loop level must be calculated for future high-luminosity  $e^+e^-$  experiments. In B.4 corrections are calculated using  $M_W$  as an input. By calculating  $M_W$  obtained from  $G_\mu$ , we get for  $\mathcal{O}(\alpha_{\text{bos}}^2)$  instead 0.51 MeV a value 0.34 MeV [16].

Let us discuss impact of radiative corrections in more detail by estimating their potential values.

On one hand, a source of uncertainty for the Standard Model prediction for any EWPO is their dependence on input parameters, as listed in Tab. B.2. The impact of input parameters is best evaluated through a global fit, as shown *e.g.* in Refs. [26, 42]. On the other hand, a separate source of uncertainty is the missing knowledge of theoretical higher-order corrections.

To estimate the latter, one can take different approaches, each of which has its own advantages and disadvantages [69]:

1. Determination of relevant prefactors of a class of higher-order corrections such as couplings, group factors, particle multiplicities, mass ratios, *etc.* and assuming the remainder of the loop amplitude to be order  $\mathcal{O}(1)$ .
2. Extrapolation under the assumption that higher order radiative corrections can be approximated by a geometric series.
3. Testing the scale dependence of a given fixed-order result in the  $\overline{\text{MS}}$  renormalization scheme in order to estimate the size of the missing higher orders; used more often in QCD.
4. Comparing results in the on-shell and  $\overline{\text{MS}}$  schemes, where the differences are of the next order in the perturbative expansion.

In Tab. B.5, the intrinsic errors are shown for the  $Z$ -boson decay width. TH1 gives numerical estimates that are mainly based on the geometric series extrapolation, but corroborated by some of the other methods. In [16] the  $\alpha_{\text{bos}}^2$  contribution has been calculated to be +0.505 MeV with a net numerical precision of about four digits, which eliminates the uncertainty associated with that term completely. It also shifts some of the geometric series extrapolations, such as

$$\mathcal{O}(\alpha^3) - \mathcal{O}(\alpha_t^3) \sim \frac{\mathcal{O}(\alpha^2) - \mathcal{O}(\alpha_t^2)}{\mathcal{O}(\alpha)} \mathcal{O}(\alpha^2) \sim 0.2 \text{ MeV}, \quad (\text{B.10})$$

where the full  $\mathcal{O}(\alpha^2)$  term was previously not available. The new error estimate TH-new is  $\pm 0.4$  MeV. As we can see, the estimated theoretical error is still much larger than what is needed for the projected EXP2 goals in Tab. B.1, which is for the  $Z$ -boson decay width  $\lesssim \pm 0.1$  MeV. The dominant remaining uncertainty stems from unknown three-loop contributions with either QCD loops,  $\mathcal{O}(\alpha\alpha_s^2)$  and  $\mathcal{O}(\alpha^2\alpha_s)$ , or from electroweak fermionic loops,  $\mathcal{O}(N_f^2\alpha^3)$ , where  $N_f^2$  refers to diagrams with at least two closed fermion loops.

Once these corrections become available, with a robust intrinsic numerical precision of at least two digits, the remaining theory error will become dominated by missing four-loop terms. Estimating these future errors is rather unreliable at this time using geometric series of perturbation, since it requires two orders of extrapolation. Nevertheless, a rough guess can be obtained by using the following experience-based scaling relations: each order of  $N_f\alpha$  and  $\alpha_{\text{bos}}$  generate corrections of about 0.1 and 0.01, respectively, and  $n$  orders of  $\alpha_s$  produce a correction of roughly  $n! \times (0.1)^n$ , where the  $n!$  factor accounts for the combinatorics of the SU(3) algebra. In this fashion one arrives at the TH2 scenario in Tab. B.5<sup>2</sup>.

For a safe interpretation of Fcc-ee- $Z$  measurements, the theory error must be subdominant relative to the experimental uncertainties. Comparing the TH2 scenario with the EXP2 numbers, one can see that it does not yet fit this bill. This implies that calculation of 4-loop corrections, or at least the leading parts thereof, will be necessary to fully match the planned precision of the FCC-ee experiments. Since estimates of future theory errors are highly uncertain, and 4-loop contributions are two orders beyond the current state of the art, we do not attempt to make a quantitative estimate of the achievable precision, but it seems plausible that the remaining uncertainty will be well below the EXP2 targets.

Let us now come back to the prospects for computing the missing three-loop contributions. There are two basic factors which play a role: the number of Feynman diagrams (or, correspondingly, the number of Feynman integrals) and the precision with which single Feynman integrals can be calculated. Some basic bookkeeping concerning the number of diagram topologies and different types of diagrams is given in Tab. B.6. First, let us compare the known number of diagram topologies and individual diagrams at two loops and three loops. Comparing the genuine three-loop fermionic diagrams, which are simpler than the bosonic ones, to the already known two-loop bosonic diagrams, there is about an order of magnitude difference in their number: 17580 diagrams for  $Z \rightarrow b\bar{b}$  (and 13104 diagrams for  $Z \rightarrow e^+e^-$ ) at  $\mathcal{O}(\alpha_{\text{ferm}}^3)$  versus 964 (766) diagrams at  $\mathcal{O}(\alpha_{\text{bos}}^2)$ . In general, however, the number of diagrams is of course not equivalent to the number of integrals to be calculated. At  $\mathcal{O}(\alpha_{\text{ferm}}^3)$  we expect  $\mathcal{O}(10^3) - \mathcal{O}(10^4)$  distinct three-loop Feynman integrals before a reduction to a basis, because different classes of diagrams often share parts of their integral basis.

Second, the accuracy with which three-loop diagrams can be calculated must be estimated. For the two-loop bosonic vertex integrals, results have been obtained with a high level of accuracy, which was 8 digits in most cases and at least 6 digits for the few worst integrals; with some room for improvements. The final accuracy of the complete results for the bosonic two-loop corrections to the EWPOs was at the level of at least four digits [15, 16]. To achieve this goal, the Feynman integrals have been calculated numerically, directly in the Minkowskian region, with two main approaches: (i) SD as implemented in the packages FIESTA 3 [70] and SecDec 3 [71], and (ii) MB integrals as implemented in the package MBsuite [72–77]. Because fermionic three-loop diagrams are technically not much more complicated than two-loop bosonic integrals

<sup>2</sup> Accounting for “everything else” besides the specific orders listed in Tab. B.5, one may assign a more conservative future theory error estimate of  $\delta\Gamma_Z \sim 0.2$  MeV, see also Ref. [69].

$\delta_1 :$	$\delta_2 :$	$\delta_3 :$	$\delta_4 :$	$\delta_5 :$	$\delta\Gamma_Z$ [MeV]
$\mathcal{O}(\alpha^3)$	$\mathcal{O}(\alpha^2\alpha_s)$	$\mathcal{O}(\alpha\alpha_s^2)$	$\mathcal{O}(\alpha\alpha_s^3)$	$\mathcal{O}(\alpha_{bos}^2)$	$= \sqrt{\sum_{i=1}^5 \delta_i^2}$
TH1 (estimated error limits from geometric series of perturbation)					
0.26	0.3	0.23	0.035	0.1	0.5
TH1-new (estimated error limits from geometric series of perturbation)					
0.2	0.21	0.23	0.035	$< 10^{-4}$	0.4

$\delta'_1 :$	$\delta'_2 :$	$\delta'_3 :$	$\delta_4 :$		$\delta\Gamma_Z$ [MeV]
$\mathcal{O}(N_f^{\leq 1}\alpha^3)$	$\mathcal{O}(\alpha^3\alpha_s)$	$\mathcal{O}(\alpha^2\alpha_s^2)$	$\mathcal{O}(\alpha\alpha_s^3)$		$\sqrt{\delta_1'^2 + \delta_2'^2 + \delta_2'^3 + \delta_4'^2}$
TH2 (extrapolation through prefactor scaling)					
0.04	0.1	0.1	0.035	$10^{-4}$	0.15

Table B.5: The intrinsic theoretical error estimates TH1 for  $\Gamma_Z$ , as given in [39, 69], and updates taking into account the newly completed  $\mathcal{O}(\alpha_{bos}^2)$  corrections TH1-new [16]. TH2 is a projection into the future, assuming  $\delta_{2,3}$  and the fermionic parts of  $\delta_1$  to be known.

(*e. g.* in the case of self-energy insertions the dimensionality of MB integrals increases by only one), an overall two-digit precision for the final phenomenological results appears within reach. This estimate is based on present knowledge and available methods and tools.

Two further remarks are in order. First, the previously estimated value of the bosonic two-loop correction to  $\Gamma_Z$  based on the geometric series (TH1) was at the level of 0.1 MeV, which is much smaller than its actual calculated value [16, 69]. This is partly based on the fact that all final-state flavors sum up because they contribute to  $\Gamma_Z(\alpha_{bos}^2)$  with the same sign, which was not foreseen in the previous estimate. Thus care should be taken in interpreting any theory error estimates. Nonetheless, due to lack of a better strategy, we *assume* that the values TH1-new in Tab. B.5 are representative of the actual size of the currently unknown three-loop corrections. Second, the achievement of at least 2 digits intrinsic net numerical precision for the three-loop electroweak corrections will likely require the evaluation of single Feynman integrals with much higher precision than in two-loop case, since the larger number of diagrams leads to more numerical cancellations, and each new diagram topology poses new challenges for the numerical convergence.

Thus, besides straightforward improvements in numerical calculations based on SD and MB methods, work on new innovative numerical and analytical techniques (and combinations thereof) should continue and may lead to accelerated progress. There are many other places for future improvements, *e.g.* optimizations at the 3-loop and 4-loop level of the minimal number of MB-integral dimensions (see Section 3.6 in this report), IBP reductions to master integrals, reliable practical prescriptions for the  $\gamma_5$  issue at 3 loops and beyond. The numerical methods will certainly be complemented by progress in analytical and semi-analytical approaches (both in methods and tools), to which Chapter E is devoted. Similarly, other EWPOs can be discussed. Table B.7 gathers all present and expected theoretical intrinsic error estimations (see *e. g.* Ref. [69]).

To summarize, FCC-ee-Z imposes very strong demands on future theoretical calculations of currently unknown higher-order quantum EW and QCD corrections. As shown here, different estimations lead to predictions for EWPO error bands which are at the level or of the order of future experimental demands. Then, actual calculations may shift the values and diminish the errors of EWPOs substantially, as it has been shown



$Z \rightarrow b\bar{b}$			
Number of topologies	1 loop	2 loops	3 loops
	1	$14 \xrightarrow{(A)} 7 \xrightarrow{(B)} 5$	$211 \xrightarrow{(A)} 84 \xrightarrow{(B)} 51$
Number of diagrams	15	$2383 \xrightarrow{(A,B)} 1074$	$490387 \xrightarrow{(A,B)} 120472$
Fermionic loops	0	150	17580
Bosonic loops	15	924	102892
Planar / Non-planar	15 / 0	981/133	84059/36413
QCD / EW	1 / 14	98 / 1016	10386/110086
$Z \rightarrow e^+e^-, \dots$			
Number of topologies	1 loop	2 loops	3 loops
	1	$14 \xrightarrow{(A)} 7 \xrightarrow{(B)} 5$	$211 \xrightarrow{(A)} 84 \xrightarrow{(B)} 51$
Number of diagrams	14	$2012 \xrightarrow{(A,B)} 880$	$397690 \xrightarrow{(A,B)} 91472$
Fermionic loops	0	114	13104
Bosonic loops	14	766	78368
Planar / Non-planar	14 / 0	782/98	65487/25985
QCD / EW	0 / 14	0 / 880	144/91328

Table B.6: Number of topologies and diagrams for  $Z \rightarrow f\bar{f}$  decays in the Feynman gauge. Statistics for planarity, QCD and EW type diagrams is also given. Label (A) denotes statistics after elimination of tadpoles and wavefunction corrections, and label (B) denotes statistics after elimination of topological symmetries of diagrams.

FCC-ee-Z EWPO error estimations				
	$\delta\Gamma_Z$ [MeV]	$\delta R_l$ [ $10^{-4}$ ]	$\delta R_b$ [ $10^{-5}$ ]	$\delta \sin^2 \theta_{\text{eff}}^l$ [ $10^{-5}$ ]
EXP2 [40]	0.1	10	$2 \div 6$	6
TH1-new	0.4	60	10	45
TH2	0.15	15	5	15
TH3	$< 0.07$	$< 7$	$< 3$	$< 7$

Table B.7: Comparison of experimental FCC-ee precision goals for selected EWPOs (EXP2, from Table B.1) to various scenarios for theory error estimations. TH1-new is the current theory error based on extrapolations through geometric series. TH2 is an estimate of the theory error (using prefactor scalings), assuming that electroweak 3-loop corrections are known. TH3 denotes a scenario where also the dominant 4-loop corrections are available. Since reliable quantitative estimates of TH3 are not possible at this point, only conservative upper bounds on the theory error are given.

recently in the case of the Z-boson decay width [16]. Here the result of the bosonic two-loop corrections was found to be larger than the previous estimate by a factor 3–5, depending on the chosen input parametrization. One of the most promising avenues for addressing the challenges of these future calculations are numerical

integration methods. These are more flexible than analytical techniques, but are limited by the achievable numerical precision. Our estimations bring us to the conclusion that at least two digits accuracy in future 3- and 4-loop calculations of EWPOs is needed. Therefore, dedicated and increased efforts by the theory community will be important to meet the experimental demands of the FCC-ee-Z or other lepton collider projects in the  $Z$  line shape mode and not limit the physical interpretation of the corresponding precision measurements.

Let us stress that apart from the problems mentioned here, there is also the issue of extracting EWPOs from real processes, including the QED unfolding. This is the subject of Chapter C, see also [35] and [78].

# Chapter C

## Theory meets experiment

### 1 Introduction

**Authors:** Janusz Gluza, Stanisław Jadach, Tord Riemann

Corresponding author: Tord Riemann [Tord.Riemann@cern.ch]

The interpretation of real cross sections at the  $Z$  peak is a delicate problem for the FCC-ee, due to its incredible precision. We consider here exclusively fermion pair production. The real cross section describes the reaction

$$e^+e^- \rightarrow f^+f^- + \text{invisible } (n \gamma + e^+e^- \text{ pairs} + \dots), \quad (\text{C.1})$$

i.e. fermion pair production including those additional final state configurations which stay invisible in the detector. It is well-known that one may describe such a reaction with multi-dimensional generic ansatzes like e.g.:

$$\sigma^{e^+e^- \rightarrow f^+f^- + \dots}(s) = \int dx_1 dx_2 g(x_1) g(x_2) \sigma^{e^+e^- \rightarrow f^+f^-}(s') \delta(s' - x_1 x_2 s). \quad (\text{C.2})$$

In the one-loop approximation with soft photon exponentiation, or the flux function approach, it is  $x_2 = 1 - x_1$ , resulting in the generic ansatz

$$\sigma^{e^+e^- \rightarrow f^+f^- + \dots}(s) = \int dx f(x) \sigma^{e^+e^- \rightarrow f^+f^-}(s') \delta(x - s'/s). \quad (\text{C.3})$$

The  $\sigma^{e^+e^- \rightarrow f^+f^-}$  is called the underlying hard scattering cross section or the effective Born cross section. The kernel functions  $g(x)$  and  $f(x)$  depend on the process, the observable to be described, and on the experimental conditions like choice of variables and cuts. Further, if initial-final state radiation interferences are considered, combined with box diagram contributions, then the hard scattering basic Born function in the flux function approach has a more general structure, see [27, 30, 79–85]:

$$\sigma^{e^+e^- \rightarrow f^+f^-}(s') \rightarrow \sigma^{e^+e^- \rightarrow f^+f^-}(s, s'). \quad (\text{C.4})$$

An example from [85] is reproduced in (C.20).

Concerning the extraction of physical parameters from real cross sections, one may follow two different strategies:

1. Direct fits of  $\sigma^{real}$  in terms of quantities like  $M_Z, \Gamma_Z$  and other parameters. The other parameters are called *ElectroWeak Pseudo Observables*, or short EWPOs.
2. Extraction of the various hard 2to2 scattering cross sections  $\sigma_{tot, FB, \dots}^{(0)}$  from the real cross sections  $\sigma^{real}$  and the a subsequent analysis of the hard cross sections in terms of quantities like  $M_Z, \Gamma_Z$  and other parameters like  $A_f$ .

In practice, at LEP the second approach was chosen by all experimental collaborations [11].

For a  $Z$  line shape analysis the structure functions or flux functions are assumed to be known from theoretical calculations with a sufficient accuracy in order to match the experimental demands. Before the unfolding, data have to be prepared with Monte Carlo programs like KKMC [29] in order to match the simplified

unfolding conditions of the analysis programs like ZFITTER [27, 36, 84, 86, 87].

*To determine the structure function or flux function kernels for data preparation or for unfolding is one of the challenges of FCC-ee-Z physics.*

At LEP, the  $Z$  line shape analysis was performed with the ZFITTER package. ZFITTER relies completely on the flux function approach, which is sufficiently accurate. If the photonic next to leading order (NLO) corrections plus soft photon exponentiation dominate the invisible terms in C.1. This is in accordance with the condition  $x_2 = 1 - x_1$ . ZFITTER contains a variety of flux functions  $f(x)$  which have been determined in a series of theoretical papers; see below. Details may also be found in the ZFITTER descriptions quoted above.

The crucial point in the unfolding procedure is the following: The result of the unfolding depends on the ansatz chosen. This sounds trivial. But the statement reflects the need of knowing sufficiently many details of the analytical structure of the hard scattering process, as a function of the chosen physical parameters.

Be it a so-called model-independent (MI) approach or the Standard Model (SM) ansatz, parameters like  $M_Z$  and  $\Gamma_Z$  have to be introduced in a proper way, respecting e.g. their universality (channel independence etc.) and also the quantum field theoretical structure of the underlying theory; see for a discussion [79].

*To determine the correct hard scattering ansatz in an MI- or SM-based ansatz is another challenge of FCC-ee-Z physics.*

At LEP it was possible to determine the mass and width of the  $Z$  boson with experimental errors of 2 MeV each [11, 88]. The experimental challenges are many-fold, including high event statistics, good apparatus systematics, good knowledge of the beam energy. In all these respects, FCC-ee claims to be much better, resulting in unprecedented error estimates. Several of the anticipated experimental errors are reproduced in the FCC-ee-Z wishlist, reproduced in the Foreword. We mention here as challenging experimental aims:

$$\frac{\delta M_Z}{M_Z} \approx \frac{0.1 \text{ MeV}}{93 \text{ GeV}} \approx 10^{-6}, \quad (\text{C.5})$$

$$\frac{\delta \Gamma_Z}{\Gamma_Z} \approx \frac{0.1 \text{ MeV}}{2 \text{ GeV}} \approx 5 \times 10^{-5}. \quad (\text{C.6})$$

Certain asymmetry errors are also anticipated to be smaller than at LEP by orders of magnitude, e.g.:

$$\delta A_{FB}^{\bar{b}b} \approx 10^{-5}, \quad (\text{C.7})$$

which is about two orders of magnitude better than at LEP [89, 90],  $A_{FB}^{\bar{b}b} = 0.0992 \pm 160 \times 10^{-5}$ , corresponding to  $A_b = 0.923 \pm 200 \times 10^{-4}$ . Similarly, the planned improvements of net experimental accuracies compared to LEP amount to a factor of 20 for  $M_Z, \Gamma_Z$  and are so high that the unfolding of real observables has to be re-analyzed compared to LEP physics. Such a demand was first worked out in some detail in an article predicting the complete leptonic weak mixing in the SM at two loops [10]. It has been argued there that the structure of the ansatz in ZFITTER contradicts, beginning at 2-loop accuracy, the structure predicted by perturbative quantum field theory around a resonance like the  $Z$  boson.

In the following two sections, the authors will describe the state of the art by now and the needed progress in order to meet the demands from FCC-ee measurements on the issues of unfolding in an MI- and the SM-based approaches. Concerning the proper unfolding ansatzes of hard scattering, both in some MI- and the SM-ansatz, see section 2. Concerning the determination of the structure functions at three loop orders combined with appropriate exponentiations of larger higher order terms see section 3.

*To summarize, packages like KKMC and ZFITTER have to be improved in two qualitatively different respects, namely: (i) Consider the necessary higher orders in perturbation theory; and (ii) respect hereby the correct structure of the hard scattering ansatz. What this means in detail will be the subject of the next two sections.*

The relevant  $2 \rightarrow 2$  hard scattering matrix elements to be used in Monte Carlo programs will be discussed at length in the next section. The  $2 \rightarrow 2$  total cross section  $\sigma_{tot}^{(0)}(s)$  and the various asymmetries, based on these

matrix elements, are defined as follows:

$$\sigma_{tot}^{(0)}(s) = \int_{-1}^{+1} d\cos\theta \frac{d\sigma^{(0)}}{d\cos\theta}, \quad (C.8)$$

$$A_{FB}^{(0)}(s) = \frac{\sigma_{FB}^{(0)}(s)}{\sigma_{tot}^{(0)}(s)} = \frac{1}{\sigma_{tot}^{(0)}(s)} \left( \int_0^{+1} - \int_{-1}^0 \right) d\cos\theta \frac{d\sigma^{(0)}}{d\cos\theta}, \quad (C.9)$$

$$A_{LR}^{(0)}(s) = \frac{\sigma_{LR}^{(0)}(s)}{\sigma_{tot}^{(0)}(s)} = \frac{1}{\sigma_{tot}^{(0)}(s)} \int_{-1}^{+1} d\cos\theta \left( \frac{d\sigma_{e_L^-}^{(0)}}{d\cos\theta} - \frac{d\sigma_{e_R^-}^{(0)}}{d\cos\theta} \right), \quad (C.10)$$

$$A_{pol}^{(0)}(s) = \frac{\sigma_{pol}^{(0)}(s)}{\sigma_{tot}^{(0)}(s)} = \frac{1}{\sigma_{tot}^{(0)}(s)} \int_{-1}^{+1} d\cos\theta \left( \frac{d\sigma_{f_R^-}^{(0)}}{d\cos\theta} - \frac{d\sigma_{f_L^-}^{(0)}}{d\cos\theta} \right), \quad (C.11)$$

$$\begin{aligned} A_{LR,pol}^{(0)}(s) &= \frac{\sigma_{LR,pol}^{(0)}(s)}{\sigma_{tot}^{(0)}(s)} \\ &= \frac{1}{\sigma_{tot}^{(0)}(s)} \int_{-1}^{+1} d\cos\theta \left( \frac{d\sigma_{e_L^-,f_R^-}^{(0)}}{d\cos\theta} - \frac{d\sigma_{e_L^-,f_L^-}^{(0)}}{d\cos\theta} - \frac{d\sigma_{e_R^-,f_R^-}^{(0)}}{d\cos\theta} + \frac{d\sigma_{e_R^-,f_L^-}^{(0)}}{d\cos\theta} \right), \end{aligned} \quad (C.12)$$

$$\begin{aligned} A_{LR,FB}^{(0)}(s) &= \frac{\sigma_{LR,FB}^{(0)}(s)}{\sigma_{tot}^{(0)}(s)} \\ &= \frac{1}{\sigma_{tot}^{(0)}(s)} \left( \int_0^{+1} - \int_{-1}^0 \right) d\cos\theta \left( \frac{d\sigma_{e_L^-}^{(0)}}{d\cos\theta} - \frac{d\sigma_{e_R^-}^{(0)}}{d\cos\theta} \right), \end{aligned} \quad (C.13)$$

$$A_{pol,FB}^{(0)}(s) = \frac{\sigma_{FB,pol}^{(0)}(s)}{\sigma_{tot}^{(0)}(s)} = \frac{1}{\sigma_{tot}^{(0)}(s)} \left( \int_0^{+1} - \int_{-1}^0 \right) d\cos\theta \left( \frac{d\sigma_{f_R^-}^{(0)}}{d\cos\theta} - \frac{d\sigma_{f_L^-}^{(0)}}{d\cos\theta} \right) \quad (C.14)$$

$$\begin{aligned} A_{LR,pol,FB}^{(0)}(s) &= \frac{\sigma_{LR,pol,FB}^{(0)}(s)}{\sigma_{tot}^{(0)}(s)} \\ &= \frac{1}{\sigma_{tot}^{(0)}(s)} \left( \int_0^{+1} - \int_{-1}^0 \right) d\cos\theta \\ &\quad \left( \frac{d\sigma_{e_L^-,f_R^-}^{(0)}}{d\cos\theta} - \frac{d\sigma_{e_L^-,f_L^-}^{(0)}}{d\cos\theta} - \frac{d\sigma_{e_R^-,f_R^-}^{(0)}}{d\cos\theta} + \frac{d\sigma_{e_R^-,f_L^-}^{(0)}}{d\cos\theta} \right). \end{aligned} \quad (C.15)$$

Here,  $L$  and  $R$  are helicities of the massless external particles. For unpolarized scattering, initial state helicities are assumed to be averaged, and final helicities combine incoherently to the final state polarization  $A_{pol}^{(0)}(s)$ .

Let us assume that an unbiased unfolding is possible from real cross sections to the  $2 \rightarrow 2$  processes. Here, we understand under real cross sections those cross sections and also cross section asymmetries which may be measured in the detector. The experiments determine numbers with dimension of e.g.  $\text{cm}^2$  or nanobarns. Theory, on the other hand, either works with matrix elements or integrated squared matrix elements.

In order to be definite and to shorten notations, let us work first with squared matrix elements and use the flux function approximation. This is how the analysis tool ZFITTER is composed. And we will have to improve that for the FCC-ee applications considerably.

The total cross section and asymmetries are defined generically through

$$\sigma_A^{real}(s) = \int \frac{ds'}{s} \rho_{tot}(s'/s) \sigma_A^{(0)}(s'), \quad A = tot, LR, pol, LRpol, \quad (C.16)$$

$$\sigma_A^{real}(s) = \int \frac{ds'}{s} \rho_{FB}(s'/s) \sigma_A^{(0)}(s'), \quad A = FB, LRFB, polFB, LRpolFB. \quad (C.17)$$

using the notations

$$s' \equiv s_{f+f-} = s \left( 1 - \frac{E_\gamma}{\sqrt{s}} \right), \quad (C.18)$$

$$R \equiv 1 - v = \frac{s'}{s}. \quad (C.19)$$

Here,  $s$  is the center of mass energy squared,  $s'$  the invariant mass squared of the final fermion pair, and  $E_\gamma$  the photon energy. As indicated in the equations above, the flux functions  $\rho_{T,FB}$  for  $\cos \theta$ -even and for  $\cos \theta$ -odd integrals differ. They depend also on the other experimental cuts. Only four of the seven observables shown are independent because the  $2 \rightarrow 2$  scattering of (practically) massless external spin-1/2 particles has only four helicity degrees of freedom.

When taking the complete photonic  $O(\alpha)$  corrections into account, including initial and final state radiations and their interferences, the cross section foldings have the following general structure:

$$\begin{aligned} \sigma_A^{real}(s) &= \sigma_A^{(0)}(s) + \sigma_A^{real,ini}(s) + \sigma_A^{real,fin}(s) + \sigma_A^{real,int}(s) \\ &= \sigma_A^{(0)}(s) + \int dR \sigma_A^{(0)}(s') \rho_A^{ini}(R) + \sigma_A^{(0)}(s) \int dR \rho_A^{fin}(R) \\ &\quad + \int dR \sum_{V_i, V_j=\gamma, Z} \sigma_A^{(0)}(s, s', i, j) \rho_A^{int}(R, i, j). \end{aligned} \quad (C.20)$$

In the initial-final state interferences, the effective Born cross-sections depend on both  $s$  and  $s'$  as well as on the type of exchanged vector particles  $V_i$  (e.g. photon and or  $Z$ ). Additionally, one has to be aware in the interference that for  $A = tot, LR, pol$  one needs  $\bar{A} = FB$  and for  $A = FB, LRFB$  one needs  $\bar{A} = tot$ . The composition of real cross sections gets modified when contributions are exponentiated, e.g. for initial state soft photon exponentiation of  $\sigma_{tot}$  [80, 91]:

$$\sigma_{tot}^{(0)}(s) + \sigma_{tot}^{real,ini}(s) \rightarrow \int dR \sigma_{tot}^{(0)}(s') \rho_{tot}^{ini}(R), \quad (C.21)$$

$$\rho_{tot}^{ini}(R) = (1 + \bar{S}) \beta (1 - R)^{\beta-1} + \bar{H}_{tot}^{ini}(R), \quad (C.22)$$

$$\bar{S} = \frac{3}{4} \beta + \frac{\alpha}{\pi} Q_e^2 \left( \frac{\pi^2}{3} - \frac{1}{2} \right) + h.o., \quad (C.23)$$

$$\beta = \frac{2\alpha}{\pi} Q_e^2 L_e, \quad (C.24)$$

$$L_e = \left( \ln \frac{s}{m_e^2} - 1 \right), \quad (C.25)$$

$$\bar{H}_T^{ini}(R) = \left[ H_{BM}(R) - \frac{\beta}{1-R} \right] + h.o., \quad (C.26)$$

where  $h.o.$  stands for higher orders, and  $H_{BM}(R)$  is the Bonneau-Martin kernel [92]:

$$H_{BM}(R) = \frac{1}{2} \frac{1+R^2}{1-R} \beta. \quad (C.27)$$

The radiator function for the forward-backward antisymmetric cross section differs, due to the different integration over the scattering angle. To show the simplest term, we reproduce here the  $\mathcal{O}(\alpha)$  approximated initial state radiation hard scattering part for  $\sigma_{FB}$  [80]:

$$\rho_{FB}^{ini}\left(\frac{s'}{s}\right) \sim h_e(v) = Q_e^2 \frac{\alpha}{\pi} \left( L_e - 1 - \ln \frac{1-v}{(1-\frac{v}{2})^2} \right) \frac{1+(1-v)^2}{v} \frac{1-v}{(1-\frac{v}{2})^2}. \quad (\text{C.28})$$

The  $v$  vanishes in the soft photon limit with  $s' \rightarrow s$ , and then  $\rho_{FB}$  approaches  $\rho_{tot}$ .

*In the above formulae we assume that we can consider  $\gamma$  exchange and  $Z$  exchange as independently defined. In subsection 2.6, we will discuss that such an assumption is the result of careful considerations, starting with one and only one  $Z$  amplitude as a Laurent series in  $s$ .*

The unfolding of realistic observables can be performed with the analysis tools TOPAZ0 [93–95] and ZFITTER. The latter one relies on the work quoted above for  $\rho_{tot}$  and  $\rho_{FB}$ . Evidently, the result of unfolding depends on the model chosen for the hard process  $\sigma_{tot}^0(s')$  or  $\sigma_{FB}^0(s')$ . This fact is reflected by the various model-dependent so-called *interfaces* of ZFITTER.

The parameter  $s'$  is distinguished when soft photon emission gets exponentiated, which runs in this variable.

The complications in the derivation of flux functions arise from (i) higher order corrections and (ii) more sophisticated cuts, and (iii) the resonance character of the  $Z$  peak.

In the simplest case, with no cuts at all, and to order  $\mathcal{O}(\alpha)$ , one has extremely simple expressions for the photonic corrections which may be completely integrated out, see [80]. With soft photon exponentiation, this gets modified as discussed in [80, 91]. Flux functions being differential in the scattering angle, with and without soft photon exponentiation, are derived in [82, 83]. Additional common exponentiation of initial and final state radiation may be found in [27, 36, 84], where also many properties of two-particle scattering at the  $Z$  peak are discussed. The introduction of an additional acollinearity cut between the two final state fermions is treated in [80, 85, 96, 97]. Whenever any unfolding of real cross sections is discussed, one has to have in mind that a real cross section is, seen by theory, a relatively complicated aggregation of terms.

For massive final states (e.g. top-pair production, opening kinematically much above the  $Z$  peak region), one has two additional degrees of freedom [98, 99].

The real asymmetries from the experiment are pure numbers with errors and defined typically as follows:

$$A_{FB}^{real}(s) = \frac{\sigma_{FB}^{real}(s)}{\sigma_{tot}^{real}(s)}, \quad (\text{C.29})$$

$$A_{LR}^{real}(s) = \frac{\sigma_{LR}^{real}(s)}{\sigma_{tot}^{real}(s)}, \quad (\text{C.30})$$

$$A_{pol}^{real}(s) = \frac{\sigma_{pol}^{real}(s)}{\sigma_{tot}^{real}(s)}. \quad (\text{C.31})$$

Here, the indices  $tot, FB, LR, pol$  refer to definitions introduced in (C.8) to (C.17). As mentioned, only three of the asymmetries are independent quantities besides  $\sigma_{tot}^{real}$ .

At this stage, there is no difference between an MI or SM based data analysis. In the next section, we will introduce explicit expressions for the effective Born cross sections and discuss their relevance for an exact analysis of the data. The notion of pseudo-observables (POs), or electroweak pseudo-observables (EWPOs), will be introduced there. They all are defined at  $s = M_Z^2$ . It will also be shown how the notations used for the analysis of cross section formulae can be taken over to the modelling with MC programs, which rely not on cross-sections but on effective Born matrix elements.





## 2 Loops, matrix elements, EWPOs

**Authors:** Ayres Freitas, Janusz Gluza, Stanisław Jadach, Tord Riemann

Corresponding author: Tord Riemann [Tord.Riemann@cern.ch]

In this section, we will consider the  $2 \rightarrow 2$  reaction

$$e^+ e^- \rightarrow f \bar{f}. \quad (\text{C.32})$$

At the  $Z$  peak, we may neglect the initial and final state fermion masses at many places. Assuming the planned FCC-ee accuracy, one may expect that at least for  $b\bar{b}$  production the Born and one-loop contributions have to be described with full account of the  $b$ -quark mass. This part of the predictions is available in several software packages, see e.g. [99–102, 102–107] and will not be discussed here in more detail.

People often analyze a set of so-called pseudo-observables in a chosen theory frame, e.g. a “measured” forward-backward asymmetry. The exact expression will be given in (C.89). Usually, the following approximated ansatz has been sufficiently correct:

$$A_{FB}^{\text{meas}} = \frac{3}{4} A_e^{\text{th}} A_f^{\text{th}}, \quad (\text{C.33})$$

where  $A_e, A_f$  are simple expressions in terms of the effective weak mixing angle. In fact,  $A_{FB}^{\text{meas}}$  has to be extracted with the anticipated accuracy from an experimentally measured cross section. The  $A_f^{\text{th}}$  has a simple definition:

$$A_f^{\text{th}} = 2 \frac{\frac{v_f^2}{a_f^2}}{1 + \frac{v_f^2}{a_f^2}}, \quad (\text{C.34})$$

$$\frac{v_f}{a_f} = 1 - 4|Q_f| \sin^2 \theta_{\text{eff}}^f \equiv 1 - 4|Q_f| \Re(\kappa_f) \sin^2 \theta_W. \quad (\text{C.35})$$

The right-hand side has to be calculated with the necessary precision from some theory, here the Standard Model at some loop order. For massless final state fermions, there are only two form factors, the vector and the axial vector couplings, taken at  $q^2 = M_Z^2$ . At an FCC-ee Tera-Z, the precisions are of typically  $10^{-5}$  or better and so one should bear in mind that the relation (C.33) is approximate and its validity has to be checked before use. Further, as we will discuss later, in addition to the weak mixing angle  $\sin^2 \theta_{\text{eff}}^f$ , which is defined in terms of the vector and axial-vector couplings of the  $Z f \bar{f}$  vertex, there are two other often-used definitions of the weak mixing angle. The various definitions are not identical but agree approximately.

In this section we are explaining in detail the definitions of and the relations between the following quantities:

- (i) The matrix element for the vertex  $Z \rightarrow f \bar{f}$ ;
- (ii) The exact matrix element for  $2 \rightarrow 2$  scattering with loop corrections;
- (iii) The  $2 \rightarrow 2$  effective Born cross sections.

The relations of  $2 \rightarrow 2$  Born cross sections (iii) with real observables was discussed in section 1.

*Here, in this section, we introduce the most general massless  $2 \rightarrow 2$  matrix element which is characterized by four form factors.*

These form factors have to be determined by theory, be it the Standard Model with  $n$  loops, be it supersymmetry in Born approximation, or something else. In principle, these four form factors would be what in

an experiment should be measured.<sup>1</sup> In practice, it is more comfortable to measure some derived quantities, called electroweak pseudo observables (EWPOs). A better name would SMPOs, for Standard Model pseudo observables, thus including the QCD part in the abbreviation.

At FCC-ee it might be even better to measure some other building blocks instead of the EWPOs, but for our didactic purposes it is fine to deal here with EWPOs. Some ideas on alternative strategies are introduced in section 3.

We try to describe the  $Z$  resonance near its pole position with highest numerical precision. Consequently, special attention is given to a correct treatment of the  $2 \rightarrow 2$  matrix elements in several respects:

- (i) Treat the  $2 \rightarrow 2$  matrix elements strictly in its most general form with four complex kinematics-dependent form factors in order to cover, in principle, all aspects of physics and in all needed orders of perturbation theory. The form factors may be chosen to be e.g.  $\rho_{ef}, \kappa_e, \kappa_f, \kappa_{ef}$  or, alternatively,  $\rho_{ef}, v_e, v_f, v_{ef}$ . While the axial couplings are fixed to some real number, e.g.  $a_f = I_{3,L}(f) = \pm \frac{1}{2}$ .
- (ii) Respect unitarity, analyticity, gauge-invariance for quantum field theoretic perturbative corrections close to the resonance peak; this is fulfilled by the so-called pole renormalization scheme, combined with using a Laurent series representation for the matrix element (i.e. for the four form factors), with one single first order pole in the  $s$ -plane located at  $s_0 = M_Z^2 - iM_Z\Gamma_Z$ .
- (iii) Besides the  $Z$  boson exchange, there are substantial contributions from photon exchange. A correct treatment of the coexistence of  $Z$  boson and  $\gamma$  exchange and of their interferences deserves a careful discussion.
- (iv) The theoretical treatment of real observables has to respect items (i) to (iii), and a careful re-analysis of its structural aspects is needed.

People who were active in LEP analyses and who have some knowledge in using the ZFITTER package will notice that many features of the ZFITTER approach might be taken over from the 1980s/90s. Both several conceptual changes and a questioning of approximations are necessary when going from LEP accuracy to FCC-ee accuracy. In the Standard Model, ZFITTER covers  $2 \rightarrow 2$  scattering with an accuracy corresponding to one electroweak loop (and two loops with QCD), plus certain leading two-loop terms (and three-loop terms with QCD). Let us call this  $1+1/2$  loops. Real scattering has to cope with that, and flux functions basically do this job. For the FCC-ee, the theory has to include  $2+1/2$  loops, in the sense that complete electroweak 2-loop calculations are needed (and exist by today), accompanied by selected 3-loop and 4-loop terms, to be determined yet. This concerns vertex corrections. Weak box diagrams are needed at one loop-order less than vertices, i.e. at 2-loop order. Here we have to mention that the 2-loop weak box terms are unknown so far.

We try to cover the whole calculational scheme in a language which allows experimentalists to understand much of the conceptual details. Evidently, we can work out here the principal ideas, but an analysis of their numerical relevance for real observations at the FCC-ee- $Z$  has to be left for future studies.

## 2.1 Renormalization in a nutshell

We want to give a short introduction to few of the most important definitions used.

The weak mixing angle  $s_W^2 \equiv \sin^2 \theta_W$  has three potential different meanings or functions in the model-building:

- (i) It describes the ratio of the two gauge couplings,

$$g'/g = c_W/s_W, \tag{C.36}$$

usually in the  $\overline{\text{MS}}$  scheme.

---

<sup>1</sup>We mention that for the production of massive top-quarks six form factors are needed for a general ansatz [98, 99].

(ii) It describes the ratio of two gauge boson (on-shell) masses,

$$s_W^2 = 1 - \frac{M_W^2}{M_Z^2}. \quad (\text{C.37})$$

(iii) It describes the ratio of the vector and axial-vector couplings of an (on-shell)  $Z$  boson to fermions,

$$\frac{v_f}{a_f} = 1 - 4|Q_f|s_W^2. \quad (\text{C.38})$$

This definition is called the *effective weak mixing angle*, henceforth denoted as  $\sin^2 \theta_W^{f,\text{eff}}$ .

At the Born level of the Standard Model, all these definitions agree, with  $a_f^B = \pm 1/2$ <sup>2</sup>

At orders in perturbation theory one has to define a renormalization scheme. In the on-shell scheme according to Alberto Sirlin [108], one uses the following renormalization conditions: all particle masses are fixed, and additionally one coupling constant  $\alpha$ :  $e^2 = 4\pi\alpha$ . The weak mixing angle is not an independent quantity in this scheme.

There are several variations of this renormalization scheme. For example, one may use a renormalization condition for the Fermi constant  $G_F$  instead of  $M_W$ .  $G_F$  is related to other SM parameters via

$$\frac{G_F}{\sqrt{2}} = \frac{\pi\alpha_{em}}{2\sin^2 \theta_W \cos^2 \theta_W M_Z^2} (1 + \Delta r), \quad (\text{C.39})$$

where  $\Delta r$  contains the contributions from radiative corrections.

These choices are fully equivalent and are mostly a matter of convenience. Some renormalization schemes lead to smaller one-loop corrections, but arguments like these become more complicated beyond the one-loop level.

Due to certain approximations, which we describe in the present section of this report, the EWPOs are related to the effective vector and axial-vector couplings of the  $Z$  boson to a fermion type  $f$ ,  $v_f$  and  $a_f$ .<sup>3</sup> These, in turn, are related to the weak mixing angle according to

$$\frac{v_f}{a_f} = 1 - 4|Q_f| \sin^2 \theta_W^{f,\text{eff}} \equiv 1 - 4|Q_f| s_W^2 \kappa_f^Z, \quad (\text{C.40})$$

where from now on (C.37) holds. The  $s_W^2 = 1 - M_W^2/M_Z^2$  is the on-shell weak mixing angle, and  $\kappa_f^Z$  captures the effect of radiative corrections (in Born approximation,  $\kappa_f^B = 1$ ). The form factor  $\kappa_f^Z$  was introduced by A. Sirlin [108, 110]. Even though  $s_W^2$  is not a (pseudo-)observable in itself, it is a useful quantity for discussions of the EWPOs with higher order corrections.

## 2.2 The 2→2 matrix elements

We now consider the definitions of the hard scattering kernels used in (C.8) to (C.14). All momenta are assumed to be incoming. The scattering of massless fermions,

$$e^-(p_1) + e^+(p_2) \rightarrow f^-(p_3) + f^+(p_4), \quad (\text{C.41})$$

depends on two invariants, chosen here to be the squared center of mass energy  $s$  and the 4-momentum transfer  $t$ :

$$s = (p_1 + p_2)^2 = 4E_{\text{beam}}^2, \quad (\text{C.42})$$

<sup>2</sup>In ZFITTER and related literature, it is used universally  $a_f = 1$ . This is convenient but contradicts the by now generally accepted conventions.

<sup>3</sup> It needs to be checked if at FCC-ee-Z accuracy these approximations are still valid. This is relatively "easy" but necessary and deserves a dedicated study a la [109].

$$T = -t = -(p_2 + p_3)^2 = \frac{s}{2}(1 - \cos \theta), \quad (\text{C.43})$$

where  $\cos \theta$  is the scattering angle in the center of mass system. We further will use

$$U = -u = -(p_2 + p_4)^2 = \frac{s}{2}(1 + \cos \theta). \quad (\text{C.44})$$

Often, the matrix element is split into contributions from  $s$ -channel photon exchange and the remaining contributions, which include  $s$ -channel  $Z$ -boson exchange:

$$\mathcal{M}^{(0)}(e^-e^+ \rightarrow f^-f^+) = \mathcal{M}_\gamma^{(0)}(e^-e^+ \rightarrow f^-f^+) + \mathcal{M}_Z^{(0)}(e^-e^+ \rightarrow f^-f^+). \quad (\text{C.45})$$

At Born level one has

$$\mathcal{M}_Z^{(0,B)}(e^-e^+ \rightarrow f^-f^+) = 4ie^2 \frac{\chi_Z(s)}{s} (v_e^B - a_e^B \gamma_5) \gamma_\alpha \otimes (v_f^B - a_f^B \gamma_5) \gamma^\alpha, \quad (\text{C.46})$$

$$\mathcal{M}_\gamma^{(0,B)}(e^-e^+ \rightarrow f^-f^+) = \frac{ie^2}{s} Q_e Q_f \gamma_\alpha \otimes \gamma^\alpha, \quad (\text{C.47})$$

where we have used the short-hand notation

$$\Gamma_1 \otimes \Gamma_2 \equiv (\bar{v}_e \Gamma_1 u_e)(\bar{u}_f \Gamma_2 v_f). \quad (\text{C.48})$$

Furthermore,

$$\chi_Z(s) = \frac{G_F M_Z^2}{\sqrt{2} 8\pi \alpha_{em}} K_Z(s) \approx 0.37393 K_Z(s). \quad (\text{C.49})$$

In the *pole scheme*, where  $\bar{M}_Z$  is defined as the real part of the pole of the S matrix, one has

$$K_Z(s) = (1 + i\bar{\Gamma}_Z/\bar{M}_Z)^{-1} \frac{s}{s - \bar{M}_Z^2 + i\bar{M}_Z\bar{\Gamma}_Z}. \quad (\text{C.50})$$

In many analyses of the LEP era, it was assumed that the  $Z$  width is  $s$ -dependent, because it is a result of renormalizing the  $Z$  boson self energy, which depends on  $s$ . Due to the absence of production thresholds around the  $Z$  peak, one finds to a very good level of precision:

$$K_Z(s) = \frac{s}{s - M_Z^2 + iM_Z\Gamma_Z(s)}, \quad \Gamma_Z(s) = \frac{s}{M_Z^2} \Gamma_Z. \quad (\text{C.51})$$

Both definitions are related [79]:

$$\bar{M}_Z \approx M_Z - \frac{1}{2} \frac{\Gamma_Z^2}{M_Z} \approx M_Z - 34 \text{ MeV}, \quad (\text{C.52})$$

$$\bar{\Gamma}_Z \approx \Gamma_Z - \frac{1}{2} \frac{\Gamma_Z^3}{M_Z^2} \approx \Gamma_Z - 0.9 \text{ MeV}. \quad (\text{C.53})$$

The Born couplings are:

$$Q_e = -1, \quad (\text{C.54})$$

$$a_f^B = \pm \frac{1}{2}, \quad (\text{C.55})$$

$$v_f^B = a_f^B (1 - 4|Q_f| \sin^2 \theta_W), \quad (\text{C.56})$$

with

$$\sin^2 \theta_W = 1 - \frac{M_W^2}{M_Z^2}.$$

Beyond Born level, one can write

$$\mathcal{M}_\gamma^{(0)}(e^-e^+ \rightarrow f^-f^+) = \frac{4\pi i \alpha_{em}(s)}{s} Q_e Q_f \gamma_\alpha \otimes \gamma^\alpha, \quad (\text{C.57})$$

$$\begin{aligned} \mathcal{M}_Z^{(0)}(e^-e^+ \rightarrow f^-f^+) &= 4ie^2 \frac{\chi_Z(s)}{s} [M_{vv}^{ef} \gamma_\alpha \otimes \gamma^\alpha - M_{av}^{ef} \gamma_\alpha \gamma_5 \otimes \gamma^\alpha \\ &\quad - M_{va}^{ef} \gamma_\alpha \otimes \gamma^\alpha \gamma_5 + M_{aa}^{ef} \gamma_\alpha \gamma_5 \otimes \gamma^\alpha \gamma_5]. \end{aligned} \quad (\text{C.58})$$

Here  $\alpha_{em}(s)$  is the running electromagnetic coupling in the Standard Model, whose value is extracted from  $e^+e^-$  data and theory [43, 111–114]. The complex coefficients  $M_{vv}, M_{va}, M_{av}, M_{aa}$  are by construction gauge invariant and contain all contributions of a given perturbative order. It is important to note that they contain not only  $Z$ -boson vertex and self-energy corrections, but also corrections to the  $s$ -channel photon exchange contribution (beyond the running of  $\alpha$ ) and box contributions. Therefore, the general matrix element (C.58) does not factorize into initial-state and final-state form factors of the  $Z$  boson.

From comparing with the Born matrix element  $\mathcal{M}_Z^{(0,B)}$  (C.46) we see the correspondences:

$$M_{vv}^{ef,B} = v_e^B v_f^B, \quad M_{va}^{ef,B} = v_e^B a_f^B, \quad M_{av}^{ef,B} = a_e^B v_f^B, \quad M_{aa}^{ef,B} = a_e^B a_f^B. \quad (\text{C.59})$$

Beyond Born level, there exists in general no set of couplings  $v_e, a_e, v_f, a_f$  allowing to write the matrix element like (C.59). Of course, if the non-factorizing part of radiative corrections in the SM, e.g. from weak insertions to the photon self-energy or from 1-loop box diagrams at the  $Z$  peak, or in New Physics models is small, then factorization is approximately fulfilled.

An alternative language, in terms of the weak vertex form factors  $\rho_f$  and  $\kappa_f$ , was first introduced in [108, 110] for  $Z$  boson decay. In [30, 84, 115], based on [116], the concept was generalized to  $2 \rightarrow 2$  scattering by splitting the effective weak mixing angle into three of them. This goes as follows:

$$M_{aa}^{ef} = I_e I_f \rho_Z = \pm \frac{1}{4} \rho_Z a_e^{ZF} a_f^{ZF}, \quad (\text{C.60})$$

$$\frac{M_{av}^{ef}}{M_{aa}^{ef}} \equiv 1 - 4|Q_f| \kappa_f \sin^2 \theta_W = \frac{v_f^{ZF}}{a_f^{ZF}}, \quad (\text{C.61})$$

$$\frac{M_{va}^{ef}}{M_{aa}^{ef}} \equiv 1 - 4|Q_e| \kappa_e \sin^2 \theta_W = \frac{v_e^{ZF}}{a_e^{ZF}}, \quad (\text{C.62})$$

$$\frac{M_{vv}^{ef}}{M_{aa}^{ef}} \equiv 1 - 4(|Q_e| \kappa_e + |Q_f| \kappa_f) \sin^2 \theta_W + 16|Q_e Q_f|^2 \sin^4 \theta_W \kappa_{ef} = \frac{v_{ef}^{ZF}}{a_e^{ZF} a_f^{ZF}}, \quad (\text{C.63})$$

where  $I_f = \pm \frac{1}{2}$  is the weak isospin of fermion  $f$ . We indicate here the relation to ZFITTER notions by introducing the effective couplings  $v_e^{ZF}, v_f^{ZF}, v_{ef}^{ZF}$ , while  $a_e^{ZF} = a_f^{ZF} = 1$ . Note the different normalization compared to the symbols without superscript “ZF”. Further,

$$v_{ef}^{ZF} = v_e^{ZF} v_f^{ZF} + \Delta_{ef}, \quad (\text{C.64})$$

$$\Delta_{ef} = 16|Q_e Q_f| \sin^4 \theta_W (\kappa_{ef} - \kappa_e \kappa_f). \quad (\text{C.65})$$

In terms of  $\rho_Z$  and  $\kappa_i$ , the  $Z$  exchange matrix element may be again rewritten into a simple form. We quote from [27], eq. (3.3.1):

$$\begin{aligned} \mathcal{M}_Z^{(0)}(s, t) &\sim 4ie^2 \frac{\chi_Z(s)}{s} I_e I_f \rho_Z(s, t) \{ \gamma_\alpha (1 - \gamma_5) \otimes \gamma^\alpha (1 - \gamma_5) \\ &\quad - 4|Q_e| \sin^2 \theta_W \kappa_e(s, t) \gamma_\alpha \otimes \gamma^\alpha (1 - \gamma_5) \\ &\quad - 4|Q_f| \sin^2 \theta_W \kappa_f(s, t) \gamma_\alpha (1 - \gamma_5) \otimes \gamma^\alpha \\ &\quad + 16|Q_e Q_f| \sin^4 \theta_W \kappa_{ef}(s, t) \gamma_\alpha \otimes \gamma^\alpha \}. \end{aligned} \quad (\text{C.66})$$

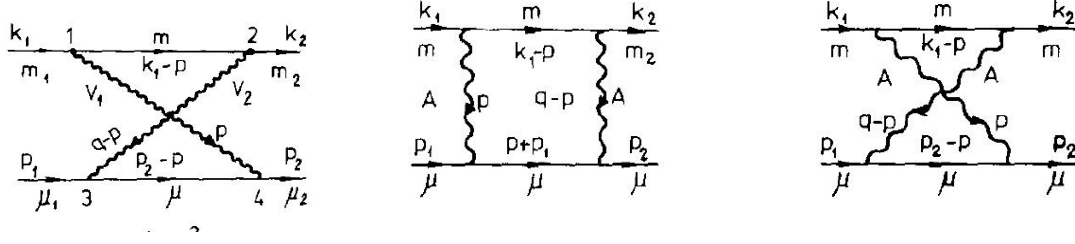


Fig. C.1: Figure 4.11 from [117], showing a generic massive crossed one-loop box diagram of the  $ZZ$  and  $WW$  box type and Fig. 4.20 with the two photon box diagrams. The latter two diagrams have to be combined with initial-final state interference soft photon bremsstrahlung in order to get a finite result.

Here the matrix element is not written in terms of vector and axial-vector components as in (C.58), but in terms of left-handed and vector components.

As examples, we reproduce in Fig. C.2 two equations from [117]. They express the contributions of crossed  $ZZ$  and  $WW$  box diagrams of Fig. C.1, left, and of the sum of the two photon box diagrams, Fig. C.1, right, in the unitary gauge. It is exhibited how the box diagrams contribute to the form factors introduced in (C.58). For detailed definitions we refer to the original. External fermion masses are taken into account only in the pole terms, in order to allow the exact cancellation of these pole terms in observable quantities. From the QED boxes, there are divergent contributions only to the structure  $\gamma_\alpha \otimes \gamma^\alpha$ , while finite terms contribute to the two combinations  $\gamma_\alpha \otimes \gamma^\alpha \pm \gamma_\alpha \gamma_5 \otimes \gamma^\alpha \gamma_5$ . So the photon box terms go exclusively into  $M_{aeaf} = a_e a_f \rho_Z$  and  $M_{vef} = \rho_Z v_{ef}$ , while the  $ZZ$  and  $WW$  boxes contribute to the various form factors quite differently. Evidently, all box diagrams violate the factorization of the Born matrix element (C.46). From a closer inspection of the analytical representations, one may easily read off the contributions to residues  $R$  and background terms  $B^{(n)}$  of the corresponding Laurent series, introduced in the next subsection.

$$\begin{aligned}
 B(q) = & i \frac{f_1^{\gamma\gamma} f_2^{\gamma\gamma} f_3^{\gamma\gamma} f_4^{\gamma\gamma}}{16\pi^2} \left\{ \left[ -u + v - \frac{1}{3} \frac{m_2 \mu_2}{M_1^2 M_2^2} (A_1 + B_1 \gamma_5) \otimes (A_3 + B_3 \gamma_5) \right. \right. \\
 & - \frac{2}{3} \frac{m_3 \mu_2}{M_1^2 M_2^2} (A_1 - B_1 \gamma_5) \otimes (A_3 + B_3 \gamma_5) - \frac{2}{3} \frac{m_2 \mu_1}{M_1^2 M_2^2} (A_1 + B_1 \gamma_5) \otimes (A_3 - B_3 \gamma_5) \\
 & \left. - \frac{1}{3} \frac{m_1 \mu_1}{M_1^2 M_2^2} (A_1 - B_1 \gamma_5) \otimes (A_3 - B_3 \gamma_5) \right] P + [\omega(q^2, M_1^2, M_2^2) \\
 & + 2(S - q^2) B(q^2, q^2 - S; M_1^2, M_2^2)] \gamma_\alpha (A_1 + B_1 \gamma_5) \otimes \gamma_\alpha (A_3 + B_3 \gamma_5) \\
 & + \frac{1}{S} [A(q^2, q^2 - S; M_1^2, M_2^2) + C(q^2, q^2 - S; M_1^2, M_2^2) - D(q^2 - S, S)] \\
 & \times [\gamma_\alpha (A_1 + B_1 \gamma_5) \otimes \gamma_\alpha (A_3 + B_3 \gamma_5) \\
 & + \gamma_\alpha \gamma_5 (A_1 + B_1 \gamma_5) \otimes \gamma_\alpha \gamma_5 (A_3 + B_3 \gamma_5)] \Big\}. \quad (4.12)
 \end{aligned}$$

$$\begin{aligned}
 B(q) = & i \frac{e^4 (f^q)^2 (\mathcal{F}^q)^2}{16\pi^2} \left\{ \left[ 4 \frac{S - m^2 - \mu^2}{q^2} \mathcal{J}(-S, m^2, \mu^2) P_{\text{IR}} \right. \right. \\
 & + 4 \frac{S - q^2 + m^2 + \mu^2}{q^2} \mathcal{J}(S - q^2, m^2, \mu^2) P_{\text{IR}} \\
 & + 4 \frac{1}{q^2} \ln \left| \frac{S - q^2}{S} \right| \ln \left| \frac{q^2}{M_W^2} \right| \gamma_\alpha \otimes \gamma_\alpha \\
 & + \frac{1}{S - q^2} \left[ -\ln \left| \frac{S}{q^2} \right| + \left( 1 + \frac{1}{2} \frac{q^2}{S - q^2} \right) \ln^2 \left| \frac{q^2}{S} \right| \right] (\gamma_\alpha \otimes \gamma_\alpha - \gamma_\alpha \gamma_5 \otimes \gamma_\alpha \gamma_5) \\
 & + \frac{1}{S} \left[ -\ln \left| \frac{S - q^2}{q^2} \right| + \left( 1 - \frac{1}{2} \frac{q^2}{S} \right) \left( \ln^2 \left| \frac{q^2}{S - q^2} \right| + \epsilon \pi^2 \right) \right] \\
 & \left. \times (\gamma_\alpha \otimes \gamma_\alpha + \gamma_\alpha \gamma_5 \otimes \gamma_\alpha \gamma_5) \right\}, \quad (4.21)
 \end{aligned}$$

with  $\epsilon = 1$  for  $q^2 > 0$ ,  $S > 0$ , and  $\epsilon = 0$  for  $q^2 \leftrightarrow -S$ .

Fig. C.2: Eqns. 4.12 and 4.21 from [117] with the contributions of Figs. 4.11 and 4.20 to the general  $2 \rightarrow 2$  matrix element in the unitary gauge.

### 2.3 The Z resonance as Laurent series

So far we have kept the c.m. energy arbitrary. However, the most sensitive  $e^+e^-$  measurements have been performed near the  $Z$  pole, so that we aim for a precise description for  $s \approx M_Z^2$ ; let us mention [118] for a MI approach and [119, 120] for a discussion in the SM. The completely model-independent S-matrix approach, ignoring the notion of loop corrections, was advocated in [31, 32, 121, 122]. Near a resonance the perturbative

series can be considered as a meromorphic function in  $s$  with a simple pole, and close to the pole it may be represented by a Laurent series. This introduces the pole position  $s_0 = s - \bar{M}_Z^2 + i\bar{M}_Z\bar{\Gamma}_Z$  as an additional parameter, and when  $s - \bar{M}_Z^2$  becomes small, the  $Z$  boson width gets important, which itself is a higher order term in perturbative QFT. The width appears in the Breit-Wigner resonance term  $1/(s - \bar{M}_Z^2 + i\bar{M}_Z\bar{\Gamma}_Z)$ , see (C.50). Further, one has to respect gauge invariance and unitarity. These conditions are fulfilled by the “pole scheme”, where the matrix element is constructed as a Laurent expansion in the  $s$ -plane with a single, simple pole and a Taylor series called “background” [31, 119, 120, 123–128]:

$$\mathcal{M} = \frac{R}{s - s_0} + \sum_{n=0}^{\infty} (s - s_0)^n B^{(n)}, \quad (\text{C.67})$$

where

$$s_0 = \bar{M}_Z^2 + i\bar{M}_Z\bar{\Gamma}_Z. \quad (\text{C.68})$$

The derivation of a scheme for realistic analyses from this ansatz is called the S-matrix approach [31, 32, 121, 129]. A mini review with a rather complete collection of experimental applications is given in [122].

The residue  $R$  and the coefficients  $B^{(n)}$  are complex numbers characteristic of the process, and  $\bar{M}_Z$  and  $\bar{\Gamma}_Z$  are the universal mass and width of the  $Z$  particle. The full process can be represented by introducing the four independent helicity matrix elements which describe the  $2 \rightarrow 2$  scattering of massless fermions. We follow [130], and we will use the notion

$$i = [1, 2, 3, 4] = [(LR)(LR), (LR)(RL), (RL)(LR), (RL)(RL)]. \quad (\text{C.69})$$

The matrix element with photon exchange is helicity blind:

$$\mathcal{M}_{1,\gamma} = \mathcal{M}_{4,\gamma} = 4\pi\alpha_{em}(s) Q_e Q_f \frac{U}{s}, \quad (\text{C.70})$$

$$\mathcal{M}_{2,\gamma} = \mathcal{M}_{3,\gamma} = 4\pi\alpha_{em}(s) Q_e Q_f \frac{T}{s}. \quad (\text{C.71})$$

We remind the reader that the definitions of  $U$  and  $T$  are given in (C.43) and (C.44). For the weak amplitudes  $\mathcal{M}_{i,Z}$  one finds

$$\mathcal{M}_{1,Z} = \mathcal{M}_Z(e_L^- e_R^+ \rightarrow f_L^- f_R^+) = C \left[ M_{aa}^{ef} + M_{av}^{ef} + M_{va}^{ef} + M_{vv}^{ef} \right] \frac{U}{s - s_0}, \quad (\text{C.72})$$

$$\mathcal{M}_{2,Z} = \mathcal{M}_Z(e_L^- e_R^+ \rightarrow f_R^- f_L^+) = C \left[ -M_{aa}^{ef} + M_{av}^{ef} - M_{va}^{ef} + M_{vv}^{ef} \right] \frac{T}{s - s_0}, \quad (\text{C.73})$$

$$\mathcal{M}_{3,Z} = \mathcal{M}_Z(e_R^- e_L^+ \rightarrow f_L^- f_R^+) = C \left[ -M_{aa}^{ef} - M_{av}^{ef} + M_{va}^{ef} + M_{vv}^{ef} \right] \frac{T}{s - s_0}, \quad (\text{C.74})$$

$$\mathcal{M}_{4,Z} = \mathcal{M}_Z(e_R^- e_L^+ \rightarrow f_R^- f_L^+) = C \left[ M_{aa}^{ef} - M_{av}^{ef} - M_{va}^{ef} + M_{vv}^{ef} \right] \frac{U}{s - s_0}, \quad (\text{C.75})$$

$$C = 2 \frac{G_F}{\sqrt{2}} \frac{\bar{M}_Z^2}{1 + i\bar{\Gamma}_Z/\bar{M}_Z}. \quad (\text{C.76})$$

In Born approximation, using (C.59) and  $\bar{\Gamma}_Z \rightarrow 0$ , we recover the helicity amplitudes of [130].<sup>4</sup>

We mention here that the introduction of a photon exchange amplitude may be formally avoided by putting the corresponding terms into the  $Z$  amplitude with the replacement

$$M_{vv}^{ef} \rightarrow M_{vv}^{ef} + \frac{s - s_0}{s} Q_e Q_f \frac{4\pi\alpha}{C}. \quad (\text{C.77})$$

<sup>4</sup>Here, one has to observe a sign convention difference for the axial couplings. In [130], it is  $Q_L \sim Q_V - Q_A$ . Intuitively, in a left-handed or  $(V - A)$  theory, there is only a left-handed coupling, and the vector and axial couplings are equal,  $V = +A$ , and so it would be  $Q_L = V - A = 0$ . Due to a sign change of  $Q_A$  in [130], the combination  $V + A$  becomes  $Q_V - Q_A$  etc.

This is a consequence of the above definitions, where both  $v_{ef}$  and the  $\gamma$  exchange go together with the matrix element structure  $\gamma \otimes \gamma$ . See also subsection 2.6.

Each of the helicity matrix elements (C.72)–(C.75) may then be expanded in a Laurent series according to (C.67). As a result the four helicity matrix elements

$$\mathcal{M}_i(e^+e^- \rightarrow f\bar{f}) = \mathcal{M}_{i,\gamma}^f + \mathcal{M}_{i,Z}^f \quad (\text{C.78})$$

have the generic form

$$\mathcal{M}_i(e^+e^- \rightarrow f\bar{f}) = \frac{s(1 \pm \cos \theta)}{2} \left( Q_e Q_f \frac{4\pi\alpha_{em}(s)}{s} + \frac{R_f^{(i)}}{s - s_0} + \sum_{n=0}^{\infty} B_{f,n}^{(i)} (s - s_0)^n \right). \quad (\text{C.79})$$

The last equation is the central element of a phenomenological analysis. Their form results from the demand of a correct determination of the loop corrections in accordance with unitarity, analyticity, gauge invariance. A phenomenological ansatz which is expected not to contradict perturbation theory should respect this form as well.

We allow for an explicit account of  $s$ -channel photon exchange besides the  $Z$  as it was discussed above. Because a Laurent series has only one pole term, the ansatz (C.78) seems to contradict a consistent mathematical structure by also introducing the photon pole  $1/s$ . In section 2.6 we will show that in fact this treatment can be put on solid theoretical footing [122].

The residues  $R_f^{(i)}$ , the universal pole location  $s_0$ , and the coefficients  $B_{f,n}^{(i)}$  can be computed in the Standard Model or some other model, or in a model-independent parameterization of new physics. They are the basic building blocks for any experimental analysis. For the phenomenologically most important residue terms, one gets for the four helicity matrix elements:

$$R_f^{(i)} = C[\pm M_{aa}^{ef} \pm M_{av}^{ef} \pm M_{va}^{ef} + M_{vv}^{ef}]_{s=s_0}. \quad (\text{C.80})$$

The sign conventions are introduced in (C.69). In Born approximation, the background terms vanish. They arise only from radiative corrections or from New Physics, if not the photon is formally made part of background, see section 2.6.

In Monte Carlo approaches which rely on the use of helicity matrix elements instead of using squared matrix elements, the above considerations may be used for constructing the radiatively corrected matrix elements which have to replace the Born matrix elements in the codes.

In Monte Carlo programs which already contain matrix elements with weak corrections like KKMC [29] where the original weak library DIZET [30] of the ZFITTER project is implemented, one has to check if the higher order contributions in these matrix elements respect the origin from the pole renormalization scheme with Laurent series.

## 2.4 Electroweak pseudo-observables

Let us now calculate the basic  $2 \rightarrow 2$  observables (C.8) to (C.14) without specific assumptions on the underlying matrix elements. The starting point are the differential cross sections, composed out of the incoherent sums of squared helicity matrix elements (C.72) to (C.75):

$$\begin{aligned} \frac{d\sigma_A^{(0)}}{d\cos\theta} &= \frac{\pi\alpha^2}{2s} |\chi_Z(s)|^2 [(1 + \cos^2\theta) k_A + (2\cos\theta) k_{A,FB}] \\ &= \frac{N_c}{32\pi s} (c_{A,1} |\mathcal{M}_1|^2 + c_{A,2} |\mathcal{M}_2|^2 + c_{A,3} |\mathcal{M}_3|^2 + c_{A,4} |\mathcal{M}_4|^2), \quad A = T, LR, pol, LRpol. \end{aligned} \quad (\text{C.81})$$



The subscripts stand for:  $T$  – total cross section,  $LR$  – electron’s left-right asymmetry,  $pol$  – the final state polarization,  $LRpol$  – the combination of the last two asymmetries. The coefficients are:

$$c_{T,i} = [+1, +1, +1, +1], \quad (C.82)$$

$$c_{LR,i} = [+1, +1, -1, -1], \quad (C.83)$$

$$c_{pol,i} = [-1, +1, -1, +1], \quad (C.84)$$

$$c_{LRpol,i} = [-1, +1, +1, -1]. \quad (C.85)$$

The terms in (C.81) with proportionality to  $(1 + \cos^2 \theta)$  will contribute to the total cross sections:

$$\begin{aligned} \sigma_T^{(0)}(s) &= \int_{-1}^{+1} d \cos \theta \frac{d\sigma_T^{(0)}}{d \cos \theta}, \\ &= \frac{64\pi\alpha^2 N_c}{3s} |\chi_Z|^2 (|M_{aa}^{ef}|^2 + |M_{va}^{ef}|^2 + |M_{av}^{ef}|^2 + |M_{vv}^{ef}|^2) \\ &= \frac{4\pi\alpha^2}{3s} |\chi_Z|^2 [|a_e^{ZF} a_f^{ZF}|^2 + |v_e^{ZF} a_f^{ZF}|^2 + |a_e^{ZF} v_f^{ZF}|^2 + |v_e^{ZF} v_f^{ZF}|^2] \\ &\stackrel{Z \text{ only}}{=} \frac{64\pi\alpha^2 N_c}{3s} |\chi_Z|^2 (|a_e|^2 + |v_e|^2) (|a_f|^2 + |v_f|^2), \end{aligned} \quad (C.86)$$

Here and in the following, we don’t show the photon exchange terms explicitly. Further, the notion  $Z$  only restricts kinematics to  $s = M_Z^2$ , and the non-factorizing parts are neglected. The  $\chi_Z(s)$  is defined in (C.49). In the above, the terms  $M_{aa}^{ef}$  etc. are assumed to cover both photon and  $Z$  exchange contributions. The approximated last line indicates the result after removal of the photon-exchange and box contributions, where the remaining terms  $a_f$  and  $v_f$  are the higher-loop generalizations of the  $Z f^+ f^-$  vertex couplings as introduced in (C.55), (C.56). They are related to the vertex form factor  $\kappa_f^Z$  introduced in (C.40).

The forward-backward asymmetric cross section stems from the  $(2 \cos \theta)$  term:

$$\begin{aligned} \sigma_{T,FB}^{(0)}(s) &= \left[ \int_0^{+1} - \int_{-1}^0 \right] d \cos \theta \frac{d\sigma_T^{(0)}}{d \cos \theta}, \\ &= \frac{16\pi\alpha^2}{s} |\chi_Z|^2 2\Re\{M_{av}^{ef}(M_{va}^{ef})^* + M_{aa}^{ef}(M_{vv}^{ef})^*\} \\ &= \frac{16\pi\alpha^2}{s} |\chi_Z|^2 |\rho_Z|^2 2\Re(a_e^{ZF*} a_f^{ZF*} v_{ef}^{ZF} + a_e^{ZF*} a_f^{ZF} v_e^{ZF} v_f^{ZF*}) \\ &\stackrel{Z \text{ only}}{=} \frac{16\pi\alpha^2}{s} |\chi_Z|^2 \Re\{(a_e v_e^* + v_e a_e^*)(a_f v_f^* + v_f a_f^*)\}. \end{aligned} \quad (C.87)$$

The forward-backward asymmetry can be evaluated as follows:

$$\begin{aligned} A_{T,FB}^{(0)}(s) &= \frac{\sigma_{T,FB}^{(0)}(s)}{\sigma_T^{(0)}(s)} \\ &= \frac{\left[ \int_0^{+1} - \int_{-1}^0 \right] d \cos \theta (|\mathcal{M}_1|^2 + |\mathcal{M}_2|^2 + |\mathcal{M}_3|^2 + |\mathcal{M}_4|^2)}{\int_{-1}^{+1} d \cos \theta (|\mathcal{M}_1|^2 + |\mathcal{M}_2|^2 + |\mathcal{M}_3|^2 + |\mathcal{M}_4|^2)} \\ &= \frac{3}{4} \frac{2\Re\{M_{av}^{ef}(M_{va}^{ef})^* + M_{aa}^{ef}(M_{vv}^{ef})^*\}}{|M_{aa}^{ef}|^2 + |M_{va}^{ef}|^2 + |M_{av}^{ef}|^2 + |M_{vv}^{ef}|^2} \\ &= \frac{3}{4} \frac{2\Re\{a_e^{ZF} v_e^{ZF*} a_f^{ZF*} v_f^{ZF} + a_e^{ZF} a_f^{ZF} v_{ef}^{ZF*}\}}{|a_e^{ZF} a_f^{ZF}|^2 + |v_e^{ZF} a_f^{ZF}|^2 + |a_e^{ZF} v_f^{ZF}|^2 + |v_e^{ZF} v_f^{ZF}|^2} \\ &= \frac{3}{4} \frac{(a_e v_e^* + v_e a_e^*)(a_f v_f^* + v_f a_f^*) + \Delta_{FB}}{(|a_e|^2 + |v_e|^2)(|a_f|^2 + |v_f|^2) + \Delta_T} \end{aligned} \quad (C.89)$$

$$\begin{aligned}
&\simeq \frac{3}{4} \left[ \frac{(a_e v_e^* + v_e a_e^*)(a_f v_f^* + v_f a_f^*)}{(|a_e|^2 + |v_e|^2)(|a_f|^2 + |v_f|^2)} + \frac{\Delta_{FB}}{(|a_e|^2 + |v_e|^2)(|a_f|^2 + |v_f|^2)} \right. \\
&\quad \left. - \frac{(2 \Re\{a_e v_e\})(2 \Re\{a_f v_f\})}{[ (|a_e|^2 + |v_e|^2)(|a_f|^2 + |v_f|^2) ]^2} \Delta_T \right] \\
&\equiv \frac{3}{4} A_e A_f + c_{FB} \Delta_{FB} - c_T \Delta_T
\end{aligned}$$

Here, we use the abbreviations:

$$\Delta_T = |\Delta v_{ef}|^2 + 2 \Re \left( \frac{v_e}{a_e} \frac{v_f}{a_f} \Delta v_{ef}^* \right), \quad (\text{C.90})$$

$$\Delta_{FB} = 2 \Re \Delta v_{ef}. \quad (\text{C.91})$$

The  $\Delta v_{ef}$  is defined in (C.65). Assuming factorization, which is the case for the  $s$ -channel  $Z$ -boson contribution, one has  $\Delta_T = \Delta_{FB} = 0$ . The  $\Delta_T$  and  $\Delta_{FB}$  capture sub-leading contributions from photon-exchange and box contributions that are suppressed by  $(s - s_0)/s$  (these include the non-factorizing term  $\Delta M_{vv}$ , introduced in the previous sub-section).

In the last line of (C.89) we identify the asymmetry parameters  $A_e, A_f$ :

$$A_f = \frac{2 \Re\{a_f v_f\}}{a_f^2 + |v_f|^2} \equiv \frac{1 - 4|Q_f| \sin^2 \theta_f^{\text{eff}}}{1 - 4|Q_f| \sin^2 \theta_f^{\text{eff}} + 8|Q_f|^2 \sin^4 \theta_f^{\text{eff}}}. \quad (\text{C.92})$$

The effective weak mixing angle is defined as

$$\sin^2 \theta_f^{\text{eff}} \equiv \Re\{\kappa_Z^f\} \sin^2 \theta_W, \quad (\text{C.93})$$

where  $\kappa_Z^f$  is the  $Z$ -exchange contribution of the vertex form factor  $\kappa_f$ , see eq. (C.61).

$A_f$  has a very weak dependence on the cms energy  $s$ , resulting from the loop corrections in  $\kappa_Z^f$ , or equivalently in  $v_f/a_f$ .  $\Delta_T$  and  $\Delta_{FB}$  depend more significantly on  $s$ .

The assumption that the form factors are independent of the scattering angle is correct for self-energies and vertices, but not for box diagrams. See the Eqns. in Figure (C.2) as examples. There, the scalar 1-loop functions like  $A(q^2, q^2 - S, M_1^2, M_2^2), B(q^2, q^2 - S, M_1^2, M_2^2), C(q^2, q^2 - S, M_1^2, M_2^2), D(q^2 - S, S)$  of the spin structures  $\gamma_\alpha \otimes \gamma^\alpha$  etc. in the  $ZZ, WW$  box functions have additional angular dependences; they depend on both  $S = s$  and  $q^2 = t$ , where the latter contains the scattering angle. Similarly for the other box diagrams.

In a precision study, one has to determine by explicit calculations if the angular dependences of the 4-point functions may be neglected or not when studying angular-integrated observables.

The remaining asymmetries are:

$$\begin{aligned}
A_{LR}^{(0)}(s) &= \frac{\sigma_{eL} - \sigma_{eR}}{\sigma_{eL} + \sigma_{eR}} \\
&= \frac{\int_{-1}^1 d \cos \theta (|\mathcal{M}_1|^2 + |\mathcal{M}_2|^2 - |\mathcal{M}_3|^2 - |\mathcal{M}_4|^2)}{\int_{-1}^1 d \cos \theta (|\mathcal{M}_1|^2 + |\mathcal{M}_2|^2 + |\mathcal{M}_3|^2 + |\mathcal{M}_4|^2)} \\
&= \frac{2 \Re\{M_{aa}^{ef}(M_{va}^{ef})^* + M_{av}^{ef}(M_{vv}^{ef})^*\}}{|M_{aa}^{ef}|^2 + |M_{va}^{ef}|^2 + |M_{av}^{ef}|^2 + |M_{vv}^{ef}|^2} \\
&\stackrel{Z \text{ only}}{=} A_e, \\
\lambda_f &\equiv A_{pol}^{(0)}(s) = \frac{\sigma_{fR} - \sigma_{fL}}{\sigma_{fR} + \sigma_{fL}}
\end{aligned} \quad (\text{C.94})$$

$$\begin{aligned}
 &= \frac{\int_{-1}^1 d\cos\theta(-|\mathcal{M}_1|^2 + |\mathcal{M}_2|^2 - |\mathcal{M}_3|^2 + |\mathcal{M}_4|^2)}{\int_{-1}^1 d\cos\theta(|\mathcal{M}_1|^2 + |\mathcal{M}_2|^2 + |\mathcal{M}_3|^2 + |\mathcal{M}_4|^2)} \\
 &= -\frac{2\Re\{M_{aa}^{ef}(M_{av}^{ef})^* + M_{va}^{ef}(M_{vv}^{ef})^*\}}{|M_{aa}^{ef}|^2 + |M_{va}^{ef}|^2 + |M_{av}^{ef}|^2 + |M_{vv}^{ef}|^2} \quad (C.95)
 \end{aligned}$$

$$\stackrel{Z \text{ only}}{=} -A_f,$$

$$\begin{aligned}
 A_{LRpol}^{(0)}(s) &= \frac{\int_{-1}^1 d\cos\theta(-|\mathcal{M}_1|^2 + |\mathcal{M}_2|^2 + |\mathcal{M}_3|^2 - |\mathcal{M}_4|^2)}{\int_{-1}^1 d\cos\theta(|\mathcal{M}_1|^2 + |\mathcal{M}_2|^2 + |\mathcal{M}_3|^2 + |\mathcal{M}_4|^2)} \\
 &= -\frac{2\Re\{M_{av}^{ef}(M_{va}^{ef})^* + M_{aa}^{ef}(M_{vv}^{ef})^*\}}{|M_{aa}^{ef}|^2 + |M_{va}^{ef}|^2 + |M_{av}^{ef}|^2 + |M_{vv}^{ef}|^2} \quad (C.96)
 \end{aligned}$$

$$\stackrel{Z \text{ only}}{=} -A_e A_f,$$

$$\begin{aligned}
 A_{polFB}^{(0)}(s) &= \frac{\left[\int_0^{+1} - \int_{-1}^0\right] d\cos\theta(-|\mathcal{M}_1|^2 + |\mathcal{M}_2|^2 - |\mathcal{M}_3|^2 + |\mathcal{M}_4|^2)}{\int_{-1}^1 d\cos\theta(|\mathcal{M}_1|^2 + |\mathcal{M}_2|^2 + |\mathcal{M}_3|^2 + |\mathcal{M}_4|^2)} \quad (C.97) \\
 &= -\frac{3}{4} \frac{2\Re\{M_{aa}^{ef}(M_{va}^{ef})^* + M_{av}^{ef}(M_{vv}^{ef})^*\}}{|M_{aa}^{ef}|^2 + |M_{va}^{ef}|^2 + |M_{av}^{ef}|^2 + |M_{vv}^{ef}|^2} \\
 &\stackrel{Z \text{ only}}{=} -\frac{3}{4} A_e
 \end{aligned}$$

$$\begin{aligned}
 A_{LRFB}^{(0)}(s) &= \frac{3}{4} \frac{2\Re\{M_{aa}^{ef}(M_{av}^{ef})^* + M_{va}^{ef}(M_{vv}^{ef})^*\}}{|M_{aa}^{ef}|^2 + |M_{va}^{ef}|^2 + |M_{av}^{ef}|^2 + |M_{vv}^{ef}|^2} \quad (C.98) \\
 &\stackrel{Z \text{ only}}{=} \frac{3}{4} A_f,
 \end{aligned}$$

$$\begin{aligned}
 A_{LRpolFB,Z}^{(0)}(s) &= -\frac{3}{4} \frac{(a_e^{ZF})^2(a_f^{ZF})^2 + (a_e^{ZF})^2|v_f^{ZF}|^2 + |v_e^{ZF}|^2(a_f^{ZF})^2 + |v_e^{ZF}|^2|v_f^{ZF}|^2}{(|a_e^{ZF}a_f^{ZF}|^2 + |v_e^{ZF}a_f^{ZF}|^2 + |a_e^{ZF}v_f^{ZF}|^2 + |v_e^{ZF}|^2|v_f^{ZF}|^2)} \quad (C.99) \\
 &= -\frac{3}{4}.
 \end{aligned}$$

At the  $Z$  peak,  $s = M_Z^2$ , the photon and box terms become suppressed by their proportionality to  $(s - s_0)/s \rightarrow i\Gamma_Z/M_Z$ . The photon term and the  $\gamma Z$  interference are generally numerically important for experimental analyses.

For definition and measurement of  $A_{polFB,Z}^{(0)}$  and other asymmetries see [131]. We follow the definitions used in [132], where most of the asymmetries are defined and calculated in Born approximation. Further,  $\lambda_f$  is the polarization of  $f^-$ .

All the above considerations were independent of assuming the Standard Model or any other underlying model. They are introduced at this length in order to show that the hard scattering process around the  $Z$  peak contains exactly four form factors per final state fermion  $f$ , which suffice to describe any observable:

$$M_{aa}^{ef} = a_e a_f, \quad M_{av}^{ef} = a_e v_f, \quad M_{va}^{ef} = v_e a_f, \quad M_{vv}^{ef} = v_e v_f, \quad (C.100)$$

or

$$\rho_z, \kappa_e, \kappa_f, \kappa_{ef}, \quad (C.101)$$

or

$$\rho_z, \sin^2 \theta_W^{e,\text{eff}}, \sin^2 \theta_W^{f,\text{eff}}, \sin^2 \theta_W^{ef,\text{eff}}. \quad (C.102)$$

If we further restrict ourselves to the  $Z$ -exchange amplitude only and neglect non-factorizing terms, then they reduce to three independent quantities  $M_{aa}^{ef,Z}$ ,  $M_{av}^{ef,Z}$ ,  $M_{va}^{ef,Z}$ . Since then  $M_{vv}^{ef,Z} = M_{av}^{ef,Z} M_{va}^{ef,Z} / M_{aa}^{ef,Z}$  and  $\kappa_Z^{ef} = \kappa_Z^e \kappa_Z^f$ . Another choice for these three quantities is, in this restricted sense:

$$\rho_Z, \sin^2 \theta_W^{e,\text{eff}}, \sin^2 \theta_W^{f,\text{eff}}. \quad (\text{C.103})$$

Similarly, quantities like  $A_f$  are only defined for the  $Z$ -exchange amplitude, and thus additional steps are needed to extract them from the observables. The art of a  $Z$  line shape analysis relies on the ability to reduce the many degrees of freedom from experiment to a sufficiently small set of intermediate variables, which are easily described by theory. With one loop accuracy (and a bit beyond) this was prepared in the ZFITTER package [27, 36, 84, 86] and studied at many occasions, notably in [11, 88, 109] and references therein.

## 2.5 Loops in the $2 \rightarrow 2$ matrix element

We now address the question of how to compute the  $2 \rightarrow 2$  pseudo-observables in the Standard Model or any extended models, up to some desired loop order. For concreteness, we show explicit expressions for the example of an evaluation to two-loop order in this subsection, but they can be straightforwardly extended to higher loop orders. This was studied notably in [119, 120, 125] and [10] and the many references therein.

To proceed, one has to expand the four independent quantities, e.g.  $M_{aa}^{ef}$ ,  $M_{av}^{ef}$ ,  $M_{va}^{ef}$ ,  $M_{vv}^{ef}$ , in a Laurent series about the complex pole  $s_0 = \bar{M}_Z^2 + i\bar{M}_Z\bar{\Gamma}_Z$ . The most relevant pseudo-observables are defined for  $s = \bar{M}_Z^2$ , so that the expansion parameter becomes  $s - s_0 = -i\bar{M}_Z\bar{\Gamma}_Z$ . Since  $\bar{\Gamma}_Z/\bar{M}_Z \sim \mathcal{O}(g^2)$ , where  $g$  is the weak coupling, one has to perform the expansion *simultaneously* in  $s - s_0$  and in the loop order of the form factors. For example, if the residue term  $R$  in (C.67) is expanded to 2-loop order, then  $B^{(0)}$  and  $B^{(1)}$  should be expanded to 1-loop and tree-level order, respectively, while all higher  $B^{(n)}$  can be neglected. Specifically, the residue contribution of  $M_{vv}^{ef}$  at two-loop order is given by [10, 125]

$$\begin{aligned} R_{vv} = & v_e^{(0)} R_{ZZ} v_f^{(0)} + \left[ v_e^{(1)}(M_Z^2) v_f^{(0)} + v_e^{(0)} v_f^{(1)}(M_Z^2) \right] \left[ 1 + \Sigma_{ZZ}^{(1)'}(M_Z^2) \right] \\ & + v_e^{(2)}(M_Z^2) v_f^{(0)} + v_e^{(0)} v_f^{(2)}(M_Z^2) + v_e^{(1)}(M_Z^2) v_f^{(1)}(M_Z^2) \\ & - iM_Z \Gamma_Z \left[ v_e^{(1)'}(M_Z^2) v_f^{(0)} + v_e^{(0)} v_f^{(1)'}(M_Z^2) \right], \end{aligned} \quad (\text{C.104})$$

$$\begin{aligned} R_{ZZ} = & 1 - \Sigma_{ZZ}^{(1)'}(M_Z^2) \\ & - \Sigma_{ZZ}^{(2)'}(M_Z^2) + \left( \Sigma_{ZZ}^{(1)'}(M_Z^2) \right)^2 + iM_Z \Gamma_Z \Sigma_{ZZ}^{(1)''}(M_Z^2) \\ & - \frac{1}{M_Z^4} \left( \Sigma_{\gamma Z}^{(1)}(M_Z^2) \right)^2 + \frac{2}{M_Z^2} \Sigma_{\gamma Z}^{(1)}(M_Z^2) \Sigma_{\gamma Z}^{(1)'}(M_Z^2). \end{aligned} \quad (\text{C.105})$$

Here the superscript  $(n)$  indicates the loop order and a prime denotes the derivative with respect to  $s$ . The  $\Sigma_{V_1 V_2}$ ,  $V_i = Z, \gamma$  stand for transverse gauge-boson self-energies, whereas  $v_f(s)$  is the vector form factor used in (C.86) ff. Note that  $v_f^{(n)}(s)$  and  $a_f^{(n)}(s)$  are understood to include the effects of  $\gamma$ - $Z$  mixing, see [10] for more details. Similar expressions for  $M_{va}^{ef}$ ,  $M_{av}^{ef}$ ,  $M_{aa}^{ef}$  can be obtained in an obvious way.

The residue  $R$  is essentially factorizing into the product of the two renormalized vertex functions  $v_e(M_Z^2)$  and  $v_f(M_Z^2)$ , sandwiching  $R_{ZZ}$ . The  $R_{ZZ}$  subsumes the self-energy contributions. The subsequent terms,  $B_v v^{(n)}$  in the Laurent expansion contain contributions from the  $Z$ -exchange amplitude as well as the photon-exchange and box amplitudes [125].

Using these expressions, one can derive explicit formulae for the pertinent pseudo-observables. Since the latter are defined solely for the  $Z$ -exchange, we assume that the photon-exchange and box contributions have been removed. Thus the expressions below are given solely in terms of  $Z$ -amplitude form factors.

When computing the asymmetries, one can explicitly verify that terms involving self-energies and derivatives cancel, leading to the naively expected result [10]

$$\begin{aligned} \sin^2 \theta_{\text{eff}}^f &\equiv \left(1 - \frac{\bar{M}_W^2}{M_Z^2}\right) \Re \left\{1 + \Delta \bar{\kappa}_Z^f(M_Z^2)\right\} \\ &= \left(1 - \frac{\bar{M}_W^2}{M_Z^2}\right) \Re \left\{1 + \frac{a_f^{(1)} v_f^{(0)} - v_f^{(1)} a_f^{(0)}}{a_f^{(0)} (a_f^{(0)} - v_f^{(0)})} \Big|_{k^2=M_Z^2} \right. \\ &\quad \left. + \frac{a_f^{(2)} v_f^{(0)} a_f^{(0)} - v_f^{(2)} (a_f^{(0)})^2 - (a_f^{(1)})^2 v_f^{(0)} + a_f^{(1)} v_f^{(1)} a_f^{(0)}}{(a_f^{(0)})^2 (a_f^{(0)} - v_f^{(0)})} \Big|_{s=M_Z^2} \right\}, \end{aligned} \quad (\text{C.106})$$

which is compatible with

$$\bar{\kappa}_Z^f(s) = \frac{1}{4|Q_f| \sin^2 \theta_W} \left(1 - \frac{v_f(s)}{a_f(s)}\right), \quad (\text{C.107})$$

As before, the barred quantities refer to the pole scheme, see subsection 2.2. At 2-loop accuracy, it is not necessary to distinguish between barred and un-barred masses in the radiative corrections, since  $\bar{M}_Z^2 - M_Z^2 = \mathcal{O}(\alpha^2)$ . For further details of notations, we refer to [10].

For the cross-section one also needs the form factor  $\bar{\rho}_{ef}$  in addition to  $\bar{\kappa}_f$ , see eq. (C.67). Again assuming that photon-exchange and box contributions have been removed, the result for the  $Z$ -exchange contribution can be written as [39, 133]

$$\bar{\rho}_Z^{ef} = F_A^e F_A^f (1 + \delta X), \quad (\text{C.108})$$

$$\begin{aligned} F_A^f &= \left[ (a_f^{(0)})^2 \left[ 1 - \Re e \Sigma_{ZZ}^{(1)'} - \Re e \Sigma_{ZZ}^{(2)'} + (\Re e \Sigma_{ZZ}^{(1)'})^2 \right] + 2 \Re e \{a_f^{(0)} a_f^{(1)}\} \left[ 1 - \Re e \Sigma_{ZZ}^{(1)'} \right] \right. \\ &\quad \left. + 2 \Re e \{a_f^{(0)} a_f^{(2)}\} + |a_f^{(1)}|^2 - \frac{1}{2} M_Z \Gamma_Z (a_f^{(0)})^2 \Im m \Sigma_{ZZ}^{(1)''} \right]_{s=M_Z^2}. \end{aligned} \quad (\text{C.109})$$

Note that  $F_A^f$  is also the contribution from the axial-vector form factor to the partial decay width  $\Gamma(Z \rightarrow f \bar{f})$ . There is an additional factor  $\delta X$ , which stems from  $Z$ -propagator correction terms that are present in the cross-section for  $e^+ e^- \rightarrow f \bar{f}$ , but not in the partial widths [39, 133]. It first occurs at two-loop order, where it is given by

$$\delta X^{(2)} = -(\Im m \Sigma_{ZZ}^{(1)''})^2 - 2 M_Z \Gamma_Z \Im m \Sigma_{ZZ}^{(1)''}. \quad (\text{C.110})$$

The effective vector and axial-vector  $Z$  vertex couplings,  $v_f$  and  $a_f$  have been computed at one loop in [41, 134–136] and at two loops in [9, 10, 15, 16, 38, 39, 50–53, 61, 62, 133, 137, 138]. In addition, some leading higher-order corrections at three- and four-loop level are known [54–60].

The quantity  $\bar{\kappa}_{ef}$  has a non-factorizing part from photon exchange and from (1-loop)  $ZZ$ ,  $WW$  boxes, as expected from the general considerations of subsection 2.6. We refer also to Fig. C.2 where explicit expressions for  $ZZ$  and  $WW$  boxes are reproduced from [117]. But one should be aware that [117] and the ZFITTER project use the unitary gauge, while [10] uses the 't Hooft-Feynman gauge, and only the complete form factors (and residues) are gauge invariant.

When focusing on  $Z$ -exchange amplitudes only, however, factorization is recovered, one can write  $\bar{\kappa}_Z^{ef} = \bar{\kappa}_Z^e \bar{\kappa}_Z^f$ .

From  $\bar{\rho}_Z^{ef}$ ,  $\bar{\kappa}_Z^e$  and  $\bar{\kappa}_Z^f$  one can straightforwardly obtain the hadronic peak cross-section,  $\sigma_{\text{had}}^0$ , while the (partial)  $Z \rightarrow f \bar{f}$  width is a function of  $F_A^f$  and  $\bar{\kappa}_Z^f$ .

## 2.6 A coexistence of photon and $Z$ exchange

In this overview, it is not intended to cover the common treatment of  $Z$  boson and  $\gamma$  exchange in detail. One may consult many documents for that, e.g. [30, 31, 84, 88] and C.6.4.5. In this subsection, we concentrate us on the interplay of the loop-corrected propagators under the assumption that they were, after renormalization, finite and well-defined objects.

There are two integrating notations. They may be applied if one does not want to use photonic and weak Born amplitudes in parallel, or if one wants to use a factorizing weak Born amplitude. In order to construct the latter, one rewrites the two matrix elements with the structure  $\gamma_\alpha \otimes \gamma_\alpha$  as follows:

$$\begin{aligned} & \frac{M_\gamma}{s} \gamma_\alpha \otimes \gamma^\alpha + \frac{M_{vv}}{s - s_0} \gamma_\alpha \otimes \gamma^\alpha \\ & \rightarrow \left[ \frac{M_\gamma}{s} + \frac{1}{s - s_0} \left( M_{vv} - \frac{M_{va} M_{av}}{M_{aa}} \right) \right] \gamma_\alpha \otimes \gamma^\alpha + \frac{1}{s - s_0} \frac{M_{va} M_{av}}{M_{aa}} \gamma_\alpha \otimes \gamma^\alpha. \end{aligned} \quad (\text{C.111})$$

This construction results in a photon term that is corrected by the non-factorizing weak part, plus a weak structure that has a Born-like factorized form (although the terms  $M_{va,av,aa}$  receive contributions from initial- and final-state vertex corrections and box corrections).

Introducing the measure for the degree of non-factorization  $\Delta M_{vv} = M_{vv} - M_{va} M_{av} / M_{aa}$  one may rewrite the sum of the general matrix elements for  $Z$  and  $\gamma$  exchange (C.46)–(C.47) as follows:

$$\mathcal{M}^{(0)}(e^- e^+ \rightarrow f^- f^+) = \mathcal{M}_Z^{(0,mod)}(e^- e^+ \rightarrow f^- f^+) + \mathcal{M}_\gamma^{(0,mod)}(e^- e^+ \rightarrow f^- f^+), \quad (\text{C.112})$$

$$\mathcal{M}_Z^{(0,mod)}(e^- e^+ \rightarrow f^- f^+) \sim \frac{M_{aa}^{ef}}{s - s_0} [-M_{v/a}^e \gamma_\alpha + \gamma_\alpha \gamma_5] \otimes [-M_{v/a}^f \gamma_\alpha + \gamma_\alpha \gamma_5], \quad (\text{C.113})$$

$$\mathcal{M}_\gamma^{(0,mod)}(e^- e^+ \rightarrow f^- f^+) \sim (Q_e Q_f + c_{fact} \Delta M_{vv}) \gamma_\alpha \otimes \gamma^\alpha. \quad (\text{C.114})$$

Here

$$M_{v/a}^f = M_{av}^{ef} / M_{aa}^{ef}, \quad M_{v/a}^e = M_{va}^{ef} / M_{aa}^{ef}, \quad (\text{C.115})$$

$$c_{fact} = \frac{s}{s - s_0} \times \frac{C}{8\pi\alpha}. \quad (\text{C.116})$$

This ansatz looks trivial, but it has a similar *factorized* form for the  $Z$ -exchange amplitude as the Born matrix element – without any loss of generality. The price is that the photon amplitude undergoes a finite renormalization. Such an ansatz is a useful starting point for writing Monte Carlo programs based on non-squared matrix elements. Note, however, that  $M_{v/a}^f$  and  $M_{v/a}^e$  are not identical to the loop corrected  $Z$  couplings, since they still include contributions from photon vertex corrections and box diagrams.

Alternatively, the general amplitude  $\mathcal{M}(e^+ e^- \rightarrow f^+ f^-)$  may also be written as *one* amplitude, by using the replacement in (C.77). We see in that approach that the photon will become inevitably a part of the  $Z$  resonance background.

This ansatz is natural when describing the  $Z$  resonance matrix element as a Laurent series in the complex  $s$  plane with a single pole at  $s = s_0$ . The photon exchange contribution, as well as its radiative corrections, to the cross section at the  $Z$  peak are non-negligible. However, assuming four helicity matrix elements of the form

$$\mathcal{M}^i(s) = \frac{R_\gamma^i}{s} + \frac{R_Z^i}{s - s_0} + F^i(s), \quad i = 1, \dots, 4, \quad (\text{C.117})$$

with *two poles*, would be mathematically inconsistent with the very idea a Laurent series; this is discussed already in e.g. [119, 139]. The critics is well-founded, but the entire amplitudes (C.117) are not yet Laurent

series. They are physical ansatzes where the  $Z$  parts have already the correct form. When expanding them around the pole at  $s_0$ , the photon contribution looks as follows [122]:

$$\begin{aligned} \frac{R_\gamma^i(s)}{s} &= \frac{\sum_{n=0}^{\infty} B_n^i(s-s_0)^n}{s} = \frac{\sum_{n=0}^{\infty} B_n^i(s-s_0)^n}{s_0 - (s_0 - s)} = \sum_{n=0}^{\infty} B_n^i(s-s_0)^n \frac{1}{s_0} \frac{1}{1 - \frac{s_0-s}{s_0}} \\ &= \sum_{n=0}^{\infty} B_n^i(s-s_0)^n \frac{1}{s_0} \left[ 1 + \frac{s_0-s}{s_0} + \left( \frac{s_0-s}{s_0} \right)^2 \dots \right]. \end{aligned} \quad (\text{C.118})$$

The  $R_\gamma^i(s)$  are defined in (C.57). The message of (C.118) is: The photon exchange term  $R_\gamma^i(s)/s$  may be understood as part of the background term  $B(s)$  of  $\mathcal{M}_Z$ . It depends on the phenomenological application whether (C.112) or (C.118) is the more appropriate description.

We see that there are several opportunities to include photon exchange into a formally correct Laurent series ansatz: Either treating the photon sub-series of background terms additively as a separate matrix element interfering with the  $Z$  exchange amplitude, leading to the well-known form

$$M_\gamma \sim \frac{\alpha_{em}(s)}{s}, \quad (\text{C.119})$$

or as a part of the  $v_{ef}$  term of the  $Z$  amplitude itself as indicated in (C.77). Both approaches are exactly equivalent. Normally, in  $Z$  peak phenomenology one prefers the intuitive first approach of the two.

The considerations of this and the following subsections apply in all cases of finite matrix elements, after renormalization. This is assumed here. Unfortunately, nature is of some complexity and, normally, the matrix elements are *not finite* after renormalization. This is due to the infrared (IR) singularities arising from soft and collinear situations with massless particles. An elimination of the IR singularities is a complex procedure and needs the combination of several matrix elements of different nature, e.g.  $2 \rightarrow 2$  matrix elements with  $2 \rightarrow 3$  matrix elements of some (different) loop order. Further, one has to regularize the singularities, usually by dimensional regularization. At one loop, the infrared problem is solved; see e.g. the formulae in subsection C.4. An isolation is difficult in multi-loop situations. Analytical solutions are preferred, but in the most difficult cases one has to use numerical tools like sector decomposition and Mellin-Barnes representations for the IR-divergent Feynman integrals. For short introductions to these methods, see sections E.3 and E.4 of this report and the references cited therein. The systematic treatment of IR singularities in presence of a resonance has not been solved in full generality<sup>5</sup> and with the accuracy needed for the FCC-ee Tera-Z. Although, there are several approaches in specific cases. One of them is the exact 2-loop renormalization of small angle QED Bhabha scattering for small electron mass [140–142]. A systematic approach to the solution of the QED infrared problem in  $e^+e^-$  annihilation including resummation and proper treatment of the narrow neutral resonances like  $Z$  was worked out by the Krakow group [29, 143, 144], and is shortly introduced in the following subsection C.2.7.

The understanding and safe numerical handling of the higher-order IR structure of cross sections around the  $Z$  peak is of course an old topic of research, see refs. [29, 143–154]. The IR-problem is certainly one of the most demanding theoretical issues of future FCC-ee Tera-Z studies.

## 2.7 Electroweak and QED corrections in the CEEX scheme of KKMC

Let us explain briefly in the following short overview how the EW part of the SM corrections to fermion pair production in electron-positron annihilation are actually embedded in the most sophisticated scheme CEEX<sup>6</sup> of the QED calculations with soft photon resummation of refs. [143, 144], as implemented in the KKMC Monte Carlo event generator [29]. We are going to follow the notations of ref. [144], suppressing spin and/or spinor

<sup>5</sup>Systematic treatment of IR divergences in QED to infinite order for charged narrow resonances ( $W^\pm$ ) is still missing in the literature.

<sup>6</sup>CEEX stands for *Coherent Exclusive EXponentiation*.

indices for simplicity. It will be also shown that it is rather easy to modify the existing implementation of the EW part in CEEX of KKMC, such that it follows precisely the S-matrix approach advocated in the present Section, i.e. following in practice what is described around eq. (C.116).

In the CEEX *factorization scheme* cross section for the process

$$e^-(p_a) + e^+(p_b) \rightarrow f(p_c) + \bar{f}(p_d) + \gamma(k_1), \dots, \gamma(k_n)$$

with complete perturbative corrections up to  $\mathcal{O}(\alpha^r)$  and soft photon resummation reads as follows:

$$\sigma^{(r)} = \sum_{n=0}^{\infty} \frac{1}{n!} \int d\tau_n(p_1 + p_2; p_3, p_4, k_1, \dots, k_n) e^{2\alpha\Re B_4(p_a, \dots, p_d)} \frac{1}{4} \sum_{\text{spin}} \left| \mathfrak{M}_n^{(r)}(p, k_1, k_2, \dots, k_n) \right|^2, \quad (\text{C.120})$$

where the virtual formfactor  $B_4$  is factorized (exponentiated) and real emission factors  $\mathfrak{s}$  are also factorized out<sup>7</sup>:

$$\mathfrak{M}_n^{(r)}(p, k_1, k_2, k_3, \dots, k_n) = \prod_{s=1}^n \mathfrak{s}(k_s) \left\{ \hat{\beta}_0^{(r)}(p) + \sum_{j=1}^n \frac{\hat{\beta}_1^{(r)}(p, k_j)}{\mathfrak{s}(k_j)} + \sum_{j_1 < j_2} \frac{\hat{\beta}_2^{(r)}(p, k_{j_1}, k_{j_2})}{\mathfrak{s}(k_{j_1})\mathfrak{s}(k_{j_2})} + \dots \right\}, \quad (\text{C.121})$$

such that the subtracted amplitudes  $\hat{\beta}_j^{(r)}$  are IR-finite. Resummation, that is spin summing/averaging of the squared amplitudes and the phase space integration  $\int d\tau_n$  is performed numerically in a separate Monte Carlo module of the KKMC, independent from the other part of KKMC where spin amplitudes  $\mathfrak{M}_n^{(r)}(p, k_1, k_2, k_3, \dots, k_n)$  are constructed and evaluated. The S-matrix methodology of eqs.(C.111)-(C.116) is relevant for the  $2 \rightarrow 2$  Born like object  $\hat{\beta}_0^{(r)}$ . In the  $\mathcal{O}(\alpha^2)$  ( $r = 2$ ) implementation of KKMC, this object reads:

$$\hat{\beta}_0^{(2)}(p) = \mathfrak{M}_0^{(2)}(p) = \left[ e^{-\alpha B_4(p)} \mathcal{M}_0^{(2)}(p) \right] \Big|_{\mathcal{O}(\alpha^2)}, \quad (\text{C.122})$$

where  $\mathcal{M}_0^{(2)}(p)$  represents Born spin amplitudes corrected up to 2-loops, derived directly from Feynman diagrams. In practice, the non-soft parts of the QED corrections are complete in  $\hat{\beta}_0^{(2)}(p)$  up to 2-loops, while the EW corrections are taken from DIZET 6.21 [27] (i.e. they are at 1+1/2 loops), exactly according to the prescription shown in eqs. C.124; see also eqs. (21-24) in ref. [29]. This implementation of the EW corrections in KKMC can be easily modified to be compatible with the S-matrix approach, following the prescription of eqs. (C.125-C.129).

Concerning the EW corrections to the  $2 \rightarrow 3$  process, they would enter into

$$\hat{\beta}_1^{(2)}(p, k_1) = \mathfrak{M}_1^{(2)}(p, k_1) - \hat{\beta}_0^{(1)}(p) \mathfrak{s}(p, k_1), \quad \mathfrak{M}_1^{(2)}(p, k_1) = \left[ e^{-\alpha B_4(p)} \mathcal{M}_1^{(2)}(p, k_1) \right] \Big|_{\mathcal{O}(\alpha^2)}. \quad (\text{C.123})$$

In the KKMC implementation 1-loop complete QED corrections are included in  $\hat{\beta}_1^{(2)}$ , mandatory for the completeness of the  $\mathcal{O}(\alpha^2)$  QED<sup>8</sup>, neglecting the 1-loop EW part. For the future FCC-ee applications it will be necessary to include also 1-loop (5-point) EW corrections, see the discussion in subsection 2.8. However, it should be stressed that in order to be useful in the CEEX scheme, they will have to be properly subtracted at the amplitude level, instead of combining them with real emission for the differential cross sections á la Bloch-Nordsieck.

In subsection 3.4 we are also discussing two examples of proper treatment of EW and non-soft QED corrections in the CEEX scheme at the amplitude level for 3-loop corrections in  $\hat{\beta}_0^{(3)}(p)$  and 2-loop corrections in  $\hat{\beta}_1^{(2)}(p, k_1)$ .

Summarizing, it is straightforward to insert into an existing, sophisticated QED calculation based on the CEEX factorization scheme arbitrary EW and QED loop corrections, following the S-matrix approach. For test purposes it is mandatory to look at the numerical effects, if not even for realistic calculations for the FCC-ee Tera-Z stage.

<sup>7</sup>Momenta of all fermions  $p_a, p_b, p_c, p_d$  are denoted collectively as  $p$ .

<sup>8</sup>Except of numerically small 5-point graphs in Fig.5 of ref. [29].



## 2.8 Radiative loops: 5-point functions

An isolated topics are the contributions from so-called radiative loop diagrams. The simplest case are 5-point functions which result from one-loop box diagrams with an additional emission of a (soft) photon. This is a  $2 \rightarrow 3$  process and will interfere with other  $2 \rightarrow 3$  processes, and is thus a NNLO contribution to  $2 \rightarrow 2$  scattering. In principle, it is well-know how to calculate such processes and there are several 1-loop packages which can deal with tensor five-point functions, for instance FeynArts/FormCalc [155, 156], CutTools [157], Blackhat [158], Helac-1loop [159, 160], Samurai [161], Madloop [162], GoSam [163], OpenLoops [164], RECOLA [165] and PJFry [166–171], as well as COLLIER [172]. In precision analysis, the numerically stable treatment of tensor reduction is very important, and we advocate especially the recent developments the latter two approaches. See also the mini-review [173], but we are not aware of dedicated studies for  $e^+e^-$ -scattering, with the notable exclusion of PJFry [174–177]. The numerical impact of these  $2 \rightarrow 3$  processes, including fermion pair emission, is very small at meson factories with their typical precision [174–178]. In view of the extra-ordinary precision of the FCC-ee-Z one has to reconsider corresponding studies.

## 2.9 Bhabha scattering: Massive loops at NNLO

Bhabha scattering is a basic process for theoretical luminosity precision determination. It will be discussed in more detail in section C.6 where the present status of BHLUMI is given with a path to better precision needed at FCC-ee compared to LEP. There it is also discussed the uncertainty due to photonic higher-order corrections, the hadronic vacuum polarization and light fermion pair emissions. These issues at the level of accuracy needed at the FCC-ee should be confronted in future Monte Carlo FCC-ee studies with fixed two-loop corrections, including QED insertions with massive fermions. These issues are also discussed in section C.5.

For Bhabha scattering, the results for 2-loop Feynman diagrams have been determined by at least two independent groups, relying on different methods:

- (i) *Photonic corrections*: computed in [140, 141] and recalculated in [179];
- (ii) *Electron  $N_f = 1$  corrections*: computed in [180] and cross-checked in [181] (with full  $m_e$  dependence) and in [179] (small electron mass limit);
- (iii) *Heavy-fermion  $N_f = 2$  contributions*: determined with two independent methods in the limit  $m_f^2 \ll s, t$  in [179, 181] and for any mass  $m_f$  in [182, 183] (dispersive approach) and in [184, 185] (analytical result).
- (iv) *Virtual hadronic NNLO contributions*, including both reducible self-energy insertions and irreducible vertex and box corrections [183, 186, 187].

## Acknowledgements

We thank A. Blondel, S. Heinemeyer, P. Janot, F. Piccinini, R. Tenchini, S. Riemann, M. Zralek and many other colleagues for encouragement, fruitful discussions and support.



### 3 QED deconvolution and pseudo-observables at FCC-ee precision

**Authors:** Ayres Freitas, Janusz Gluza and Stanisław Jadach

Corresponding author: Stanisław Jadach [Stanislaw.Jadach@cern.ch]

The concept of the electroweak *pseudo-observables* was essential in the final analysis of the LEP1 data of ref. [11]. Electroweak pseudo-observables, EWPOs, were instrumental in (a) combining data from four LEP collaboration and SLD experiments and (b) organizing conveniently the procedure of fitting the Standard Model to experimental data. The EWPOs used in the final analysis of LEP data [11] near Z resonance were defined and thoroughly tested in ref. [109]. Both works have exploited ZFITTER [36] and TOPAZ0 [93, 94] programs.

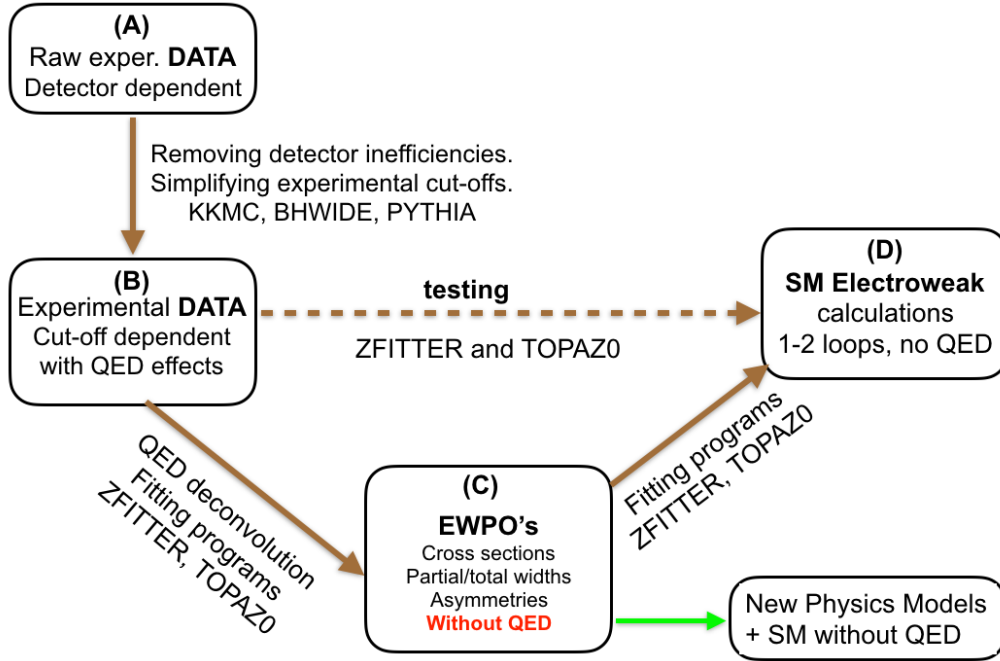


Fig. C.3: Scheme of construction of the EWPOs in data analysis of LEP

The effects of QED in data, even if large, are in principle perfectly calculable with arbitrary precision. Once they are removed, the remaining EWPOs of LEP include smaller pure electroweak corrections and possibly signals of a New Physics beyond the SM (BSM). The procedure of removing deformation of the data by QED effects, commonly referred as *QED deconvolution*<sup>9</sup> is essential part of the definition/construction of the EWPOs. Separating QED part from the higher order EW part consistently and systematically is an important and delicate issue, especially at higher orders, and we shall come back to it later on.

Note that for some processes the of low angle Bhabha process used for the measurement of luminosity,  $Z\gamma$  production for  $s^{1/2} > M_Z$  (radiative return) above Z peak or production of W pairs, the technique of EWPOs including QED deconvolution could not be used and data were compared directly with the Monte Carlo programs (BHLUMI, KORALW etc.), mainly because of more complicated dependence of QED effects on the event selection criteria (experimental cut-offs).

Before addressing the challenge of constructing EWPOs at the very high precision level of FCC-ee, we are going to summarize briefly on the definition and the use of the EWPOs in LEP data analysis.

<sup>9</sup>"Deconvolution" name is not quite adequate – operationally it is just fitting procedure, but it is kept for historical reasons.

### 3.1 EWPOs in the LEP era

The entire procedure of constructing testing and using EWPOs in the final analysis of LEP/SLC data [11] is schematically illustrated in Fig. C.3.

In the first step, from (A) to (B) in the above scheme, raw data are transformed such that they are corrected for inefficiencies of the detector and kinematic cut-offs are rounded up to a simpler shape, which can be dealt with semianalytical non-MC "fitter" programs based on ZFITTER and TOPAZ0. The transition (A)→(B) was done with sophisticated Monte Carlo event generators like KORALZ, KKMC, BHWIDE, PYTHIA etc. Data of stage (B) were obtained separately for each LEP collaboration. The important point is that the choice of the type/shape of simplified cut-offs was dictated by the limited capabilities of the fitter programs of dealing with realistic experimental cuts<sup>10</sup>.

The aim of next most important transformation of data from (B) to (C) in Fig. C.3, using fitter programs based on ZFITTER and TOPAZ0, was to remove QED effects and cut-off dependence, such that resulting "pseudo-data", that is EWPOs, do not depend on specific details of the individual experiments and are not "polluted" by QED. It is important to keep in mind that this step is introducing certain well known loss of the data precision, which was tolerable at LEP precision, but may be not tolerable at FCC-ee. This procedure introduces some small, hopefully negligible, dependence on the SM parameters and the details of the QED calculations used.

The fitter programs based on ZFITTER and TOPAZ0 were able to calculate cross sections and asymmetries for some class of simplified kinematic cut-offs (minimum mass of fermion pair, acollinearity, angular range of one of fermions) combining inclusive ISR electron structure function of ref. [188],  $\mathcal{O}(\alpha^1)$  QED analytical calculations, and the effective Born amplitudes of the EWPO scheme. As already noticed and strongly underlined in ref. [109], the sticky point was that the above scenarios could be invalidated by the initial-final state interference (IFI) contributions for various reasons, For instance the convolution of the ISR SF involves integration over the effective mass  $\sqrt{s'}$  after ISR and before final state radiation (FSR). If IFI is switched on, this variable loses its physical meaning. The way out was to introduce acollinearity cut, which was approximately limiting  $s'$ , accompanied with the cut-off on angle one of the final fermions, leaving angle of the other one uncontrolled.

In the (B)→(C) transition in Fig. C.3 an effective Born is used in the fitter programs instead of complete EW corrections. The differential distribution of the effective Born is obtained from spin amplitudes of the  $e^-e^+ \rightarrow f\bar{f}$  process, with the carefully defined (real) effective coupling constants of  $\gamma$  and  $Z$  bosons to electron and other fermion  $f = e, \mu, \tau, u, d, s, c, b$ . In fact, the differential distribution of the effective Born in eq. (1.34) of ref. [11] is in one-to-one correspondence with the spin amplitudes of eq. C.45, or Born version eqs. (C.70-C.71) and (C.72-C.75), with adjustable parameters being  $M_Z, \Gamma_Z, \alpha_{em}(M_Z)$  and  $Z$  couplings for each fermion type  $a_f$  and  $v_f$ .

The above one-to-one correspondence of the parameters of the effective Born at the amplitude level, that is four couplings per one fermion, mass and width of  $Z$  – which will be referred to as EW "pseudo-parameters", EWPPs in short<sup>11</sup>, means in practice that from their values one obtains easily partial widths proportional to  $a_f^2 + v_f^2$ , hadronic peak cross section, and all possible charge and spin asymmetries being simple functions of  $v_f/a_f$  (eqs. (1.37), (1.45) and (1.51-54) in ref. [11]), either during the data fitting procedure or for obtaining final/fitted EWPOs for each experiment.

The list of EWPOs in ref. [11] representing LEP/SLC data consists of  $M_Z, \Gamma_Z, \sigma_{had}^{(0)}, R_f^{(0)}, A_{FB}^{(0),f}$ ,  $f = e, \mu, \tau, c, b$  see Tables (2.5), (2.13) (5.10) therein. The EWPOs created at stage (C) separately for each LEP and SLD collaboration were then combined into common EWPOs, with experimental error reduced by factor two roughly<sup>12</sup>. The number of the combined EWPOs was still much larger than the number of independent parameters of the SM Lagrangian. For instance there were several values of  $\sin^2\theta_{eff}^2$  derived from various types

<sup>10</sup>For the same type of experimental cuts the values of the cut-off parameters could be different among experiments

<sup>11</sup>The prefix "*pseudo*-" underlines the fact that they are different from the SM Lagrangian parameters.

<sup>12</sup>In principle EWPPs can be re-derived from EWPOs after combining over experiments.

of asymmetries for different species of final fermions.

The peculiarity of the LEP EWPOs is that final state radiation (FSR) effects are included in the partial  $Z$  widths<sup>13</sup>, see section 3.5.3 in ref. [11], including non-factorizable  $\mathcal{O}(\alpha\alpha_s)$  FSR corrections of ref. [61] That means that these corrections are removed from data when fitting EWPPs and later on reinstalled in the EWPOs related to partial widths.

The EWPOs at stage (C) in Fig. C.3 in principle know nothing about parameters in the SM Lagrangian<sup>14</sup>. The fitting procedure of the SM Lagrangian parameters to EWPOs, (C)→(D) in Fig. C.3, is done with QED effects switched off.

For a given LEP experiment, one could fit the SM directly to data from stage (B), as illustrated in (B)→(D) in Fig. C.3. In such a fit, without the use of EWPOs, one avoids introduction of an additional bias present in the two step fitting (A)→(C)→(D). It was an important crosscheck on the size of this kind of bias. In ref. [109] it was estimated to be smaller than LEP experimental errors. Such a crosscheck was also done using separately data of each LEP collaboration in Sect 2.5.4 of ref. [11], see also Table 2.12 therein.

The disadvantage of the direct fitting (C)→(D) is that it consumes more CPU time (due to QED component) and makes combining data from several experiments more difficult. Note that the effective Born in the above LEP construction of EWPOs was chosen such that it encapsulates in most effective way one loop and higher order loop pure EW corrections, thus minimizing the bias introduced in the two-step variant of fitting SM parameters using EWPOs of the intermediate step (C), but there is no guarantee that such a bias is below FCC-ee precision level.

In the above procedure QED effects are taken into account in (A)→(B) step, thanks to the sophistication of the MC programs, in most a complete form, up to  $\mathcal{O}(\alpha^2)$  with soft photon resummation, also for non-factorisable IFI, and collinear logs up to  $\mathcal{O}(\alpha^3)$ . Fitter programs used in (B)→(C) use simplified representation of QED, typically with ISR integrated over photons to the level of the so-called radiator (flux) function convoluted in a single dimension with the effective Born. Other non-ISR QED effects (including IFI) were taken in the  $\mathcal{O}(\alpha^1)$  and combined with ISR additively. The above treatment of QED in (B)→(C) was carefully proven in Ref. [109] to be precise enough for EWPOs near  $Z$  peak as compared to precision of LEP data, but most likely requires a lot of improvement to be compatible with the FCC-ee precision, as discussed below.

### 3.2 Potential problems with LEP deconvolution at FCC-ee precision

Generally, one may still hope that for the lineshape related group of EWPO's like mass of  $Z$  boson, peak cross section, total and partial  $Z$  width, one can still employ in FCC-ee data analysis the same LEP scheme using QED-independent (experiment-independent) EWPOs in the intermediate step on the way between experimental data and SM or SM+BSM, as depicted in Fig. C.3.

In the LEP EWPOs scheme, there were some solvable problems, compared to LEP data precision. However, they may get much worse due to higher precision of FCC-ee:

- (a) The errors introduced in the transition (A)→(B), adjusting true experimental cut-off to unrealistic cut-offs required by the non-MC fitter programs, may be too big and not tolerable. It is the matter of the future data analysis to check on them.
- (b) The non-factorisable IFI contribution, which could be neglected at LEP near the  $Z$  resonance, will be to difficult to control at the factor  $\sim 50$  better precision level. In particular, reliable extension of the simple 1-dimensional convolution formula used for ISR incorporating also IFI contribution does not exist<sup>15</sup>.

---

<sup>13</sup>This is to preserve that partial widths sum up to total  $Z$  width.

<sup>14</sup>In practice a residual dependence of EWPOs on EW/QED details remains in fitted EWPOs.

<sup>15</sup>It is possible to integrate analytically over soft photons energies and angles keeping IFI in the game, even for energies comparable with the resonance width  $\Gamma_Z$ , as was shown in refs. [91, 145] and more recently developed further in ref. [189]. However, the remaining four-dimensional convolution integral over photon energies cannot be reduced to one-dimension.

- (c) The methodology of the separation of QED and EW parts in perturbative SM calculations, which was conceptually and practically relatively simple in LEP era due to  $\mathcal{O}(\alpha^1)$  restriction, will require an update in order to work for 2-3 loop EW corrections decorated with extra photon insertions.

The issue of item (a) is discussed later on in the following. Let us only indicate that the restriction in stage (B) to cut-offs that are manageable by the fitter programs are going to be removed.

Concerning IFI contribution to the lineshape and all related EWPOs, it is rather small due to suppression by the  $\Gamma_Z/M_Z$  factor – in ref. [190] it was estimated near the Z resonance to be at the level of  $\delta\sigma/\sigma = 10^{-4}$  for the integrated cross section. Lineshape experimental precision at FCC-ee will improve by about factor  $\sim 7$  for  $\sigma_{tot}(M_Z)$  and  $\sim 20$  for  $M_Z$  and  $\Gamma_Z$ , see Table 2 in the Foreword, hence the LEP scheme with ISR radiator function neglecting IFI may still work, at least for these observables, although its precision will have to be reexamined, especially for energies up to  $\pm 3.5\text{GeV}$  away from  $M_Z$ , where IFI suppression deteriorates significantly, see for instance ref. [189].

The situation will be worse for the angular distribution related EWPO's, where experimental precision at FCC-ee will improve for charge asymmetry by factor  $\sim 50$ . Again, the IFI effect near Z resonance for cut-offs on photon energies not too strong is suppressed by the  $\Gamma_Z/M_Z$  factor and in the LEP experiment IFI effect was compatible with the LEP experimental error, which for muon charge asymmetry was  $\delta A_{FB} \sim 0.1\%$  near Z resonance and  $\delta A_{FB} \sim 1\%$  further away. In the rare cases when IFI was coming to the level of LEP experimental precision, it was taken into account (subtracted from data) in the construction of EWPOs in the  $\mathcal{O}(\alpha^1)$  approximation, additively, without any resummation, using LEP era ZFITTER and TOPAZ0, in the (A)→(B) step using Monte Carlo programs like KORALZ.

The above LEP era approach to IFI problem is inherently limited to a rather loose experimental cut-offs on the total photon energy, hence the treatment of IFI in the LEP era fitter programs is definitely not adequate for the FCC-ee purpose, where  $A_{FB}$  will be measured at FCC-ee down to  $\delta A_{FB} \sim 10^{-5}$  precision, which means that IFI contribution  $\sim 0.1\%$  will have to be controlled with two-digit precision or better. NB. It will be also possible to eliminate IFI in the earlier step, in the transition (A)→(B), with help of the sophisticated MC program of the KKMC class [29, 144].

Summarizing on item (b), the methodology of the QED deconvolution of LEP, and the resulting construction of EWPOs, see Fig. C.3, may not work for important observables at much higher experimental precision of FCC-ee, especially for asymmetries. This is why we are motivated to think already now about alternative solutions, which do not suffer from the above problems, and in addition have several advantages. This is what we are going to do in the following.

Before we present new alternative scenarios of removing cut-off dependent QED effects from data, let us first comment on the fundamental question of the existence of theoretically clean methodology of separating in the perturbative calculations, beyond 1st order, QED effects from the remaining pure EW part, as indicated in item (c). In fact, the methodology of disentangling pure QED corrections from pure electroweak corrections *at the amplitude level*, resumming up soft photon effects to infinite order (exponentiation) and adding QED collinear non-soft corrections order by order, independently of EW part, is well known. Multiphoton spin amplitudes of the KKMC program [29, 144] are constructed according to the such a scheme, the coherent exclusive exponentiation (CEEX) scheme formulated in ref. [191].

It should be stressed immediately, that the above CEEX factorization of the scattering matrix element into universal part encapsulating all leading QED corrections and the remaining part (EW connections and IR finite QED remnants, without collinear mass logs) works at any order and for arbitrary precision.

CEEX scheme is the complete scheme of QED infrared factorization/resummation and matching consistently finite non-IR contribution with the resummed parts, working also for narrow resonances like Z resonance. The role of the Monte Carlo is merely to square CEEX matrix element, sum up over spins of photons and fermions, integrate over the soft+hard photon phase space and sum up over photon multiplicities, numerically and without any approximation. All that was implemented for the  $e^-e^+ \rightarrow f\bar{f}$  process in the KKMC event generator [29] but the CEEX technique is universal and can be used for any other process. The IFI contributions

due to real photons are just resulting from squaring and spin summing of the scattering matrix element, hence are automatically and fully taken into account (virtual ones has to be worked out separately).

More precisely, spin amplitudes in KKMC include QED non-soft corrections to second order and pure EW correction up to first order (with some 2nd order EW improvements, QCD etc.) using DIZET library [30]. The CEEX calculation scheme of KKMC can be extended in a natural way to higher orders, including EW corrections up to 2-3 loops. More details on CEEX scheme will be given in the following section 3.4.

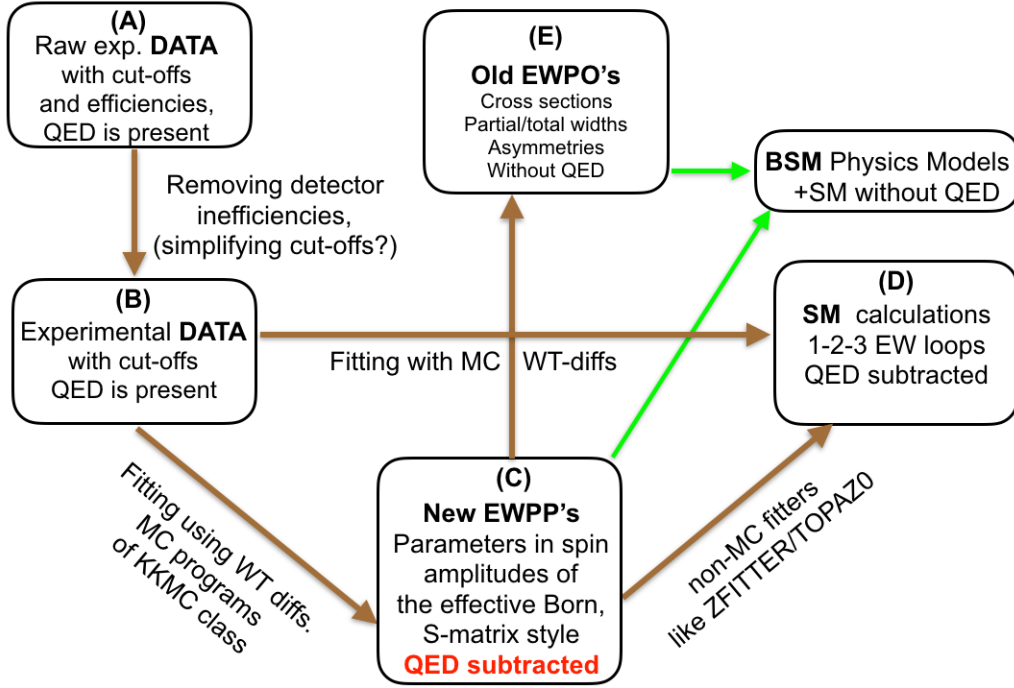


Fig. C.4: Possible scheme of construction of the EWPPs in data analysis of FCC-ee

### 3.3 Electroweak pseudo-observables at FCC-ee

With all these introductory remarks in mind, let us present an alternative scheme of QED deconvolution, which should work at the FCC-ee precision and is free of the indicated problems of the LEP EWPO scheme. This new scheme is illustrated in Fig. C.4.

In the 1st step (A)→(B) detector inefficiencies are removed. Kinematic boundaries of the detectors can be also replaced by simpler phase space boundaries in terms of some kinematic cuts, without any loss of the precision, using MC event generators with sophisticated QED matrix element and full phase space coverage, interfaced with the detector simulation programs. Contrary to LEP procedure, here we are not limited to the limited choice of the semi-realistic cut-offs of the non-MC programs, which may be far away from the true experimental cut-offs, due to more use of the Monte Carlo programs in the following steps.

In the new scheme of Fig. C.4 the role of the direct fitting of the SM internal parameters in single step (B)→(D) will grow. Contrary to former LEP scenario, this step is now implemented using sophisticated Monte Carlo program, because only this kind of tool is capable to calculate QED effects for arbitrary cut-offs and properly combine IR-resummed QED and 2-3 loop EW corrections with arbitrary precision. The use of MC programs in the fitting cannot be done in a straightforward way due to slowness of the MC event generators (even without detector simulation). But according to more detailed discussion in the following, it will be possible using weight difference methodology, WT-diff in short.

Of course, the two-step scenario  $(B) \rightarrow (C) \rightarrow (D)$  in Fig. C.4, with some kind of EW pseudo-observables at the intermediate stage (C) will be preferred. However, similarly as in the older LEP scheme, the single step  $(B) \rightarrow (C)$  will be more precise and will be used to crosscheck biases introduced in the two-step scenario  $(B) \rightarrow (C) \rightarrow (D)$ . If these biases are acceptable in view of the FCC-ee experimental precision then two-step  $(B) \rightarrow (C) \rightarrow (D)$  will be preferred, otherwise  $(B) \rightarrow (D)$  scenario will be the principal one, and pseudo-observables of the intermediate stage (C) will lose a lot of its attractiveness.

Let us now concentrate on the transformation of data in  $(B) \rightarrow (C)$  of Fig. C.4. The principal aim of removing large QED effects and the dependence on the kinematic cut-off specific to a given detector remains the same, and the use MC programs (for arbitrary experimental cut-offs) instead on non-MC fitters is again envisaged.

*The key strategic point is now whether in the transition  $(B) \rightarrow (C)$  we intend to remove only all QED effects, as in LEP, or we decide courageously to remove in addition to QED part or most of pure EW higher order corrections as well?* In any case, all of available EW+QED corrections will be included in the two steps  $(B) \rightarrow (C) \rightarrow (D)$ , from data to SM (or to SM+BSM). The question is only whether pure EW effects are located in  $(B) \rightarrow (C)$  or in  $(C) \rightarrow (D)$  or distributed among them in a clever way, such that most of convenient features of the LEP EWPOs are preserved.

Operationally, in  $(B) \rightarrow (C)$  we would use the same MC tool as in  $(B) \rightarrow (D)$ , but with the hard process part of the multi-photon spin amplitudes in the MC program simplified to an effective Born with mass and width of Z-boson and some couplings or formfactors, possibly for each fermion type, fitted to data of the stage (B). All higher order QED corrections including IFI will be kept, of course. Non-factorizable QED corrections to 1-loop EW corrections (2-loop in SM sense) will be neglected and will have to be restored in the  $(C) \rightarrow (D)$  step towards SM or SM+BSM. If the validation using direct fitting in  $(B) \rightarrow (D)$  proves that the additional bias in two-step scenario is below FCC-ee precision, then this kind of LEP-like solution will be considered as acceptable. Similarly as in LEP case EWPPs will be  $M_Z$ ,  $\Gamma_Z$  and two  $Z$  couplings for each fermion type. Derived EWPOs following  $(C) \rightarrow (E)$  will be again peak cross section partial widths and various asymmetries (calculated without QED). For instance charge asymmetry can be calculated from EWPPs using eq. (C.89).

A new interesting option to be considered is to include in the effective Born spin amplitudes (to be decorated according to CEEX scheme also with multiphoton QED real and virtual (resummed) contributions), not only Born type couplings of  $Z$ , but also some additional factors representing h.o. EW corrections, see for instance amplitudes of eqs. (C.70-C.71) and (C.72-C.75), following S-matrix approach. As advocated in Section C.2.5 this kind of spin amplitudes encapsulate efficiently 2-3 loop EW corrections, and are not in contradiction with gauge invariance, unitarity etc. In such an approach, two well defined additional parameters, for instance  $\rho_z$  and  $\kappa_{ev}$  per each final state  $f$  of eq. C.101. These  $\rho_z$  and  $\kappa_{ev}$  will be calculated in the SM and will depend slightly on the SM input parameters. This dependence will have to be well controlled and recorded, along with the remaining coupling constants  $a_f$  and  $v_f$ . Altogether,  $M_Z$ ,  $\Gamma_Z$ ,  $a_f$  and  $v_f$  will form again EW pseudo-parameters, EWPPs, as in case of LEP, and will be fitted to data using  $\rho_z$  and  $\kappa_{ev}$  calculated from the SM for some well known SM input parameters. The advantage will be that in the next step of fitting SM in step  $(C) \rightarrow (D)$  only very subtle missing 2-3 loop corrections will have to be included. The same in case of fitting SM+BSM.

Can we include in our new scheme FSR corrections to partial widths the same way as in LEP scenario? For hadronic final states due to almost perfect 100% acceptance we may proceed the same way as in LEP, also for  $\mathcal{O}(\alpha_s)$  corrections [39, 61], i.e. using multiplicative overall factor. For leptonic final states one may worry about dependence on the cut-off<sup>16</sup> on the real photons emitted from EW 1-loop vertex. Since we envisage in the  $(B) \rightarrow (C)$  construction of EWPPs the use of MC with sophisticated CEEX type spin amplitudes, it will be also possible to include at this step 2-loop and 1-real 1-virtual non-factorisable EW+QED corrections without any approximations<sup>17</sup>. For more details see next section.

<sup>16</sup>Lepton separation from beams indirectly cuts on FSR.

<sup>17</sup>This would also streamline the use of fitted EWPPs in comparisons with the SM+BSM predictions.



Finally, let us come back to the problem that MC programs were always regarded as too slow for fitting procedure, if used in a straightforward way. For instance, recent calculation of the cross sections and  $A_{FB}$  with five digit precision using KKMC in ref. [189], have required generating  $\sim 10^{10}$  events, which was taking 3 days of CPU time on the 100-processor farm. The use of the MC in the fitting procedure is, however, not so hopeless, because such a long MC run to get high precision is needed only once, for central values of a few parameters in the effective Born of the EWPP construction. Small deviations  $\sim 0.1\%$  away from the central value can be calculated very quickly with  $< 10^{-4}$  precision using small differences of the MC weights corresponding to EWPP deviations from the central values, needed for the fitting procedure. Moreover, the dependence of the realistic observable on these small variations of EWPPs are ideally linear, hence linear extrapolation using only 2-3 points in each variable will work with sufficient precision over the entire interesting range of all EWPPs in the matrix element of the effective Born required in the fits. In addition, modern methods of calculating 2-3 loop EW corrections numerically, see Chapter E in the present report, consume also much of CPU time per phase space point, then look-up tables and interpolation over space of input parameters and phase space of external legs, will be mandatory anyway. This kind of pre-calculated EW higher order corrections will also speed-up considerably fitting procedures using MC programs.

Summarizing, the Monte Carlo integration/simulation will always be the ultimate tool for implementing perfect factorization into QED and pure electroweak parts at any order, at any needed precision level. In principle, it could be used to extract/fit EWPPs corresponding to a well defined effective Born matrix element (before squaring it), for any kind of experimental cut-off, without any problems due to presence of the non-factorisable QED corrections like IFI. This would come at a price of some effort. In particular, the simplified effective Born matrix element will have to be implemented in the MC optionally, in parallel with the full SM matrix element and subprograms providing weight differences due to variation of the EWPPs has to be added. For implementing scenario (B)→(D) better 2-3 loop corrections (with subtracted QED and interpolation over input parameters) have to be added in the MC event generator of the KKMC class, along with the most sophisticated QED matrix element.

### 3.4 More on QED and EW separation beyond 1st order

The essential feature the LEP EWPOs was that they were defined using  $2 \rightarrow 2$  process and it would be desirable to keep this feature in the FCC-ee extension proposed above. For LEP EWPOs construction was based essentially on  $\mathcal{O}(\alpha^1)$  SM calculations (including QED), so it was easy to justify such a restriction, because EW and QED loops combine additively and single real photon of  $\mathcal{O}(\alpha^1)$  was attached to tree level  $2 \rightarrow 2$  process. In the FCC-ee environment where 2-3 loop EW calculation will be the standard ones, one has to consider 2 loops with mixed EW and QED content and EW corrections  $2 \rightarrow 3$  process with extra real photons attached to EW loops. In the following we shall discuss how to separate QED and EW parts in a consistent and practical way in the calculations beyond 1-st order and how it should be done in the scheme of Fig. C.4.

The methodology formulated in refs. [144, 191] of separating (resummed) EQD component from SM (or SM+BSM) amplitudes we are going to illustrate with help of a representative examples of the  $WW$  box diagram and of FSR  $\mathcal{O}(\alpha^2)$  "non-factorisable" EW+QED contributions. The above technique is referred to as the coherent exclusive exponentiation (CEEX) factorization/resummation technique.

Before coming to more complicated 2-loop case, let us recall briefly how  $\gamma - Z$  box is treated in the CEEX scheme. In this scheme  $\gamma - Z$  box is split at the amplitude level into IR part, which is combined later on with the corresponding real emission part, in the resummation over photons in the soft approximation to infinite order. (MC does all the numerics of that, executing also IR cancellations). The remaining non-soft, non-collinear, pure  $\mathcal{O}(\alpha^1)$  part is not included in the resummation and is treated the same way as all other EW corrections. i.e. is included in the Born-like spin amplitudes of the  $2 \rightarrow 2$  process. Note that in CEEX implementation one never deals analytically with the differential cross section, all that is done numerically: squaring, spin summing, integrating over phase space. In addition, specific part of  $\gamma - Z$  box involved in the IFI suppression near the  $Z$  resonance of the class  $\ln(\Gamma_Z/M_Z)$  is isolated and also properly resummed to infinite order.

Let us now elaborate on the 2-loop example of the  $WW$  box diagram, with  $W^+$  and  $W^-$  lines connecting incoming electron line and outgoing muon line, and with insertion of an additional photon line attached to all 6 internal and external lines of charged fermions and bosons, forming gauge invariant (in QED) 2-loop spin amplitude. According to well known analysis of Yennie-Frautschi-Suura [192] (YFS) infrared (IR) divergences reside in  $6+4=10$  diagrams, where one or both photons are attached to external legs. The actual decomposition of the IR terms among these diagrams depends on the choice of the gauge, but the sum is unique and gauge independent.

One is, of course, tempted to apply the classic method of dealing with IR cancellations by Bloch-Nordsieck (BN) method, that is to take interference of the above amplitude with Born  $2 \rightarrow 2$  process and combine it with the squared amplitude where 1-real photon is attached to all charged external and internal particles in the basic 1-loop  $WW$  diagram, integrated up to some photon energy limit. *It is however wrong way to proceed, in case when experimental acceptance affects the real photon phase space and the use of CEEX scheme is the only practical method to apply.* The results of BN method are completely useless for construction of the CEEX matrix element implemented in the MC like KKMC, simply because MC is managing all IR cancellations by itself, so doing it with BN method is counterproductive. Instead, the construction of the  $\text{QED} \times \text{EW}$  matrix element in CEEX requires subtraction of the IR part from the above two loop matrix element, using well known 4-point YFS virtual formfactor. Similarly, one should subtract from the corresponding 1-real photon spin amplitude well known soft factor<sup>18</sup> times  $WW$  box amplitude. These two IR-finite objects are then used as building blocks in the construction of the CEEX matrix element<sup>19</sup>.

Another group of diagrams with mixed  $\text{QED} \times \text{EW}$  content can be obtained by means of inserting virtual or real photon line attached to all internal and external line of the 1-st order diagram with final or initial EW vertex corrections. These corrections are non-factorisable in a sense of ref. [61], simply because of non-planar diagrams<sup>20</sup> As already said, within FCC-ee precision, one may worry for these corrections about the dependence on cut-off on real photon, for leptonic final states. Similarly as in the previous  $WW$  box case, the CEEX scheme allows to treat these issues without any approximation. First of all, in the CEEX scheme as implemented in KKMC, the above  $\mathcal{O}(\alpha\alpha_{em})$  class effects are already taken into account in the soft photon approximation. What remains, is to calculate and add to spin amplitudes non-soft IR-finite parts. They are obtained by means of IR subtraction from spin amplitudes of the YFS formfactor from 2-loop diagrams and subtraction of the soft factor (electromagnetic current) from the diagrams with real photon insertion to diagram with EW loop. All additional comments made in case of  $WW$  box diagram apply here as well.

Similarly, one may also insert one photon to any other 2-loop pure EW diagram, creating family of 3-loop diagram, for which the same procedure of CEEX subtractions will work – 1-real photon insertion to 2-loop diagram would then enter into the game.

The above CEEX subtraction scheme of IR singularities at the amplitude level extends to higher orders, with arbitrary number of photons inserted into basic diagram with pure EW content. For instance, insertion of two photons in the 1-loop  $WW$  box diagram creates family of 3-loop diagrams.

In other words, in all 2-loop and 3-loop corrections in the SM one can isolate groups gauge invariant subsets like in the above examples, that is obtained by means of one or two photon insertions to basic 1- or 2-loop pure EW diagram. For each group CEEX subtraction at the amplitude level can be done independently. Also, for EW diagrams with 1 or 2 real photon insertions similar CEEX subtraction procedure at the amplitude level is done *independently* in parallel.

IR regulation for the real-photon subtracted object is obviously not necessary. On the other hand, since YSF form factor has simple integral representation, in principle, for each gauge invariant group of diagrams

---

<sup>18</sup>A kind of square root of eikonal factor.

<sup>19</sup>They will still include non-soft collinear mass logs, which would be also subtracted in case when collinear resummation was done in the basic QED matrix element in the KKMC. So far collinear resummation is not done in the CEEX matrix element of KKMC, but it could be done.

<sup>20</sup>For FSR the relevant diagrams are the same as in ref. [61], modulo replacement of gluons by photons.

obtained with the virtual photon insertions it is also possible to do subtraction before the loop virtual phase space integration, thus avoiding the need of IR regulation whatsoever. In practice it may be more convenient to use some IR regulator in the intermediate steps. Contrary to Bloch-Nordsieck approach, this regulator may be chosen differently for each group of IR-entangled diagrams and YFS formfactor.

Summarizing, the CEEX scheme described above briefly, already tested in practice KKMC, provides for a well defined, clear and clean methodology of the separation of QED and EW parts in the 1-3 loop perturbative calculation. This scheme covers also 1-2 real photon emission attached to diagrams with EW loops. More details on the CEEX subtraction/resummation scheme may be found in Refs. [29, 144, 191]

In this way, one of the main obstacles, towards the establishing new scheme of the QED-independent EWPOs or rather EWPPs compatible with the high precision of FCC-ee can be viewed as solved.

In the practice of the scheme illustrated in Fig. C.4 it means that the IR-subtracted remnants of the diagrams with EW loops decorated with photon insertions will be taken into account exactly in the MC programs used in the data fitting  $(B) \rightarrow (C)$  and/or  $(B) \rightarrow (D)$ . These contributions are expected to be small and by means of switching them on/off one will be able to test how strongly they influence the bias of the two step  $(B) \rightarrow (C) \rightarrow (D)$  procedure with respect to single step path  $(B) \rightarrow (D)$ .

## Acknowledgements

We thank Tord Riemann for useful feedback concerning issues discussed in this section.



## 4 The ZFITTER project

**Authors:** Arif Akhundov, Andrej Arbuzov, Lida Kalinovskaya, Sabine Riemann, Tord Riemann

Corresponding Author: Tord Riemann [tordriemann@gmail.com]

*Dedicated to Dima Bardin 19.4.1945 – 30.6.2017*



© Foto: Wikipedia

### 4.1 Introduction

In the foregoing sections it was mentioned at several occasions that the ZFITTER project was the preferred theoretical basis for the physics analyses at LEP1/SLC. Features behind are:

- (0) ZFITTER calculates cross sections for the reaction  $e^+e^- \rightarrow f\bar{f}$  at energies around the  $Z$  peak. It is not a fitting program, and it is no Monte Carlo program. The efficient modeling of  $Z$  peak phenomena, combining exact weak loops and one-dimensional representations of the photonic corrections, are the basis for a preferred use of ZFITTER in data fitting. The last released version is ZFITTER 6.43.<sup>21</sup> ZFITTER contains two related parts. One is the Standard Model library (or also called: weak library), whose central part is DIZET. The other part are QED corrections from (mainly) additional photon emission.
- (i) The Standard Model library DIZET of ZFITTER was in its first published 1989 version accurate at 1 loop, later at 1+1/2 loops. This means that the 1-loop corrections are complete and supplemented by selected higher order loop terms. For EWPOs higher orders are implemented a la [10], which is by far sufficient for LEP1/SLC physics accuracy.
- (ii) The QED corrections in ZFITTER are available in several calculational "chains". They are result of analytical phase space integrations, so that only a few simple cuts on the final state kinematics are possible. All versions include complete QED NLO corrections plus soft photon exponentiation, plus few higher order terms. Roughly speaking, they also comprise 1+1/2 perturbative orders.
- (iii) The user can select quite different "interfaces" and flags, allowing to adapt ZFITTER to the description of certain EWPOs, or just to some  $Z$  line shape ansatz. Be it defined in the Standard Model, or be it model-independent. The strict modularity of ZFITTER was an important feature for this, but got unnecessarily restricted due to later implementations of higher order corrections.
- (iv) ZFITTER is open-source from the beginning. A careful user support is being delivered permanently, supplemented by more than 300 pages of program descriptions. Until 2011, many program versions were available for anonymous download from a webpage and a CERN AFS account.

All this is described in much detail in the published program versions [27, 30, 36, 84] and in the theoretical papers quoted therein. See also the 2013 ZFITTER review [86] with plots from version 6.43, the ZFITTER webpages [87, 194, 195], and the talks on the *Dima Day* at the conference CALC2018 [196].

<sup>21</sup>The last documented version is ZFITTER 6.42 [36]. Version 6.43 contains additional h.o. QCD corrections to the  $Z$  width of no numerical relevance for LEP1/SLC physics, see [193].

*An interesting question is that on the future of the ZFITTER package.*

There was a prediction by Lew Okun in 2000 [197]. He wrote the following in his review on the ZFITTER project for the JINR scientific prize 2000:

*In the long term, with the advent of more precise experiments, ZFITTER will allow to take into account all two-loop electroweak corrections.*

...

*The series of theoretical articles on precision tests of the Standard Model at electron-positron colliders certainly deserves the award of the JINR prize 2000.*

In the following subsections, we will present our vision of the future package for the analysis of FCC-ee Tera-Z precision data. We will show that there are many promising features of ZFITTER. But in a perspective of about 20 years from now, it is evident that a new generation of physicists should create their own, modern tool.

## 4.2 The form factors $\rho$ , $v_e$ , $v_f$ , $v_{ef}$

The effective Born approximation of ZFITTER, i.e. its  $2 \rightarrow 2$  cross section ansatz is:

$$\begin{aligned} \mathcal{A}[e^+e^- \rightarrow f\bar{f}] &= 4\pi i \alpha_{em}(s) \frac{Q_e Q_f}{s} \gamma_\mu \otimes \gamma^\mu \\ &+ i \frac{\sqrt{2} G_\mu M_Z^2}{1 + i\Gamma_Z/M_Z} I_e^{(3)} I_f^{(3)} \frac{1}{s - \overline{M}_Z^2 + i\overline{M}_Z \Gamma_Z} \\ &\times \rho_{ef} \left[ \gamma_\mu (1 + \gamma_5) \otimes \gamma^\mu (1 + \gamma_5) - 4|Q_e| s_W^2 \kappa_e \gamma_\mu \otimes \gamma^\mu (1 + \gamma_5) \right. \\ &\left. - 4|Q_f| s_W^2 \kappa_f \gamma_\mu (1 + \gamma_5) \otimes \gamma^\mu + 16|Q_e Q_f| s_W^4 \kappa_{ef} \gamma_\mu \otimes \gamma^\mu \right]. \end{aligned} \quad (\text{C.124})$$

This implementation depends on the form factors  $\alpha_{em}(s)$  and  $\rho_{ef}(s, t)$ ,  $\kappa_e(s, t)$ ,  $\kappa_f(s, t)$ ,  $\kappa_{ef}(s, t)$ . These parameterizations were invented to  $Z$  peak physics in [81] in 1989, following the implementation [115], where deep inelastic scattering was investigated. The original calculations [117, 198] used form factors  $F_{Z,i}$  and were defined close to  $M_{vv}^{ef}$  to  $M_{aa}^{ef}$ , see C.58. The introduction of  $\rho_Z$  and  $\kappa_e, \kappa_f, \kappa_{ef}$  intended an intuitive generalization of the form factors invented by A. Sirlin for the  $Z$  vertex [108]. They correspond to a renormalization of  $G_\mu$  by  $\rho_Z$  and three generalized weak vector couplings  $v_e, v_f, v_{ef}$ . The relations between the various parameters are given in (C.60) to (C.63).

Having these remarks in mind, the weak library of ZFITTER is operable also in future. Present restrictions arise from broken modularity due to too pragmatic implementations of higher order corrections. Further, ZFITTER does not rely on Laurent expansions of the loop corrections as introduced in subsection 2.3. This leads to small deviations of derived quantities. In [10], it is shown that e.g. the weak mixing angle of a strict pole renormalization differs from the ZFITTER default. The difference of  $\sin^2 \theta_{\text{eff}}^f$  between ZFITTER and the pole scheme is found to be, expressed in terms of notations of [10]:

$$\begin{aligned} \sin^2 \theta_{\text{eff}, \text{ZFITTER}}^f &= s_W^2 \Re \left\{ \kappa_Z^f(M_Z^2) \right\}, \\ \sin^2 \theta_{\text{eff}, \text{pole}}^f &= \overline{s}_W^2 \Re \left\{ \overline{\kappa}_Z^f(M_Z^2) \right\} \\ &= \sin^2 \theta_{\text{eff}, \text{ZFITTER}}^f - \frac{\Gamma_Z}{M_Z} \frac{q_f^{(0)}}{a_e^{(0)}(a_f^{(0)} - v_f^{(0)})} \Im \left\{ p_e^{(1)} \right\}, \end{aligned}$$

with the component

$$\overline{s}_W^2 = \left( 1 - \frac{\overline{M}_W^2}{M_Z^2} \right) = s_W^2 \left[ 1 + \frac{c_W^2}{s_W^2} \left( \frac{\Gamma_W^2}{M_W^2} - \frac{\Gamma_Z^2}{M_Z^2} \right) \right]^{-1}.$$

As a result, the ZFITTER value of  $\sin^2 \theta_{\text{eff}}^f$ ,  $_{\text{ZFITTER}}$  has to be corrected by a shift:

$$s_W^2 \delta \kappa_f = -\frac{\Gamma_Z}{M_Z} \frac{q_f^{(0)}}{a_e^{(0)}(a_f^{(0)} - v_f^{(0)})} \Im m \left\{ p_e^{(1)} \right\} \approx 1.5 \times 10^{-6}. \quad (\text{C.125})$$

To be compared with the actual accuracy of not better than  $170 \times 10^{-6}$  [11], or the planned accuracy at FCC-ee, Tera-Z of  $3 \times 10^{-6}$ . Here, this difference will become relevant.

An additional difference between the ZFITTER renormalization and the pole scheme arises from the Laurent expansions of weak loop contributions. Look at the  $ZZ$  and  $WW$  box diagrams, which are included in ZFITTER at the one-loop level, being sufficient for the next-to-next-to-leading order calculation in the pole scheme. Look at the  $v_e$  term, being related to the asymmetry parameter  $A_e$ . The  $v_e$  arises from the ratio of two Laurent series, where we introduce here in the background series only the box contributions,  $b_{a_e a_f}$ ,  $b_{v_e a_f}$ :

$$M_{a_e a_f}^{ef} = \frac{r_{a_e a_f}}{s - s_0} + \epsilon b_{a_e a_f}, \quad (\text{C.126})$$

$$M_{v_e a_f}^{ef} = \frac{r_{v_e a_f}}{s - s_0} + \epsilon b_{v_e a_f}, \quad (\text{C.127})$$

$$v_e = \frac{M_{v_e a_f}^{ef}}{M_{a_e a_f}^{ef}}, \quad (\text{C.128})$$

$$\begin{aligned} \kappa_e &= -\frac{v_e/a_e - 1}{4|Q_e| \sin^2 \theta_W} \\ &= \frac{r_{a_e a_f} - r_{v_e a_f}}{4r_{a_e a_f} \sin^2 \theta_W} - \epsilon (s - s_0) \frac{b_{v_e a_f} r_{a_e a_f} - b_{a_e a_f} r_{v_e a_f}}{4r_{a_e a_f}^2 \sin^2 \theta_W} + \mathcal{O}[(s - s_0), \epsilon^2]. \end{aligned} \quad (\text{C.129})$$

Setting for simplicity (as is done in ZFITTER)  $a_e = a_f = 1$ , and setting  $\epsilon$  a coupling constant, typically  $\alpha_{em}/(4\pi)$ , we see that the 1-loop box terms  $b_{a_e a_f}$  and  $b_{v_e a_f}$  are suppressed compared to the pole term as expected. In  $\kappa_e$  an extra term arises from the box contributions, which is proportional to  $iM_Z \Gamma_Z$ . The term is due to the difference of  $(s - s_0)$  (pole scheme) compared to  $(s - M_Z^2)$  (ZFITTER scheme). However, it does not contribute to the squared matrix element because weak box diagrams are real at  $s = M_Z^2$ ; they are here below the production threshold of  $Z$  or  $W$  pairs and thus have no absorptive part.<sup>22</sup>

To conclude, the Standard Model loop library of ZFITTER should undergo several adaptations and improvements in order to make it fit for FCC-ee applications at the  $Z$  peak. Its general structure would allow this, although a complete new programming seems to be preferable.

### 4.3 Fortran versus C++. Modernity and modularity

ZFITTER is written in Fortran. At the time, this was the only natural choice. The history of ZFITTER began with the central subroutine ZRATE, then ZWRATE (calculating  $\Gamma_W$  and  $\Gamma_Z$ , based on appendix F of [116] with  $m_t = 0$  and on [41, 199] with the exact top mass dependences) in about 1981 to 1986.

If Fortran is a sufficiently “modern” programming language is an open question. Maybe no more in 20 years, when FCC will get into operation! To beat Fortran in calculational speed with C++ is possible only with a very good optimization of C++ programming.<sup>23</sup> At the other hand, young colleagues don’t learn Fortran programming any more. And it is easier to perform structured, modular programming with an object-oriented language like C++. So the answer might be: For the user the choice plays no role as long as compilers exist, but for the source programmers C++ will be the choice. Although, programming in C++ has its own essential drawbacks, so maybe the language C, or some other alternative is a better choice?<sup>24</sup>

<sup>22</sup>A special case is Bhabha scattering,  $f = e$ , where additional box and t-channel diagrams contribute.

<sup>23</sup>V. Yundin, private communication to TR.

<sup>24</sup>J. Vermaseren, private communication to TR.

The authors' team M. Goebel, J. Haller, A. Hoecker, K. Mönig et al. of the early Gfitter project (see `cern.ch/gfitter` and references therein) summarizes in the introduction of EPJ C69 (2009) 543:

*Several theoretical libraries within and beyond the SM have been developed in the past, which, tied to a multi-parameter minimisation program, allowed to constrain the unbound parameters of the SM [5-8]. However, most of these programs are relatively old, were implemented in outdated programming languages, and are difficult to maintain in ... progress. It is unsatisfactory to rely on them during the forthcoming era ...*

...

*None of the previous programs were modular enough to ... allow ... to be extended ... beyond the SM, and they are usually tied to a particular minimisation package. These considerations led to the development of the generic fitting package Gfitter [9], designed to provide a framework for model testing in high-energy physics. Gfitter is implemented in C++ ...*

*Ref. [5-8] = ZFITTER (Bardin et al.), TOPAZ0 (Passarino et al.), DAPP (Erler)*

*Ref. [9] = <http://cern.ch/Gfitter>*

To comment this in short: All these statements on ZFITTER, TOPAZ0, DAPP are wrong with the notable exclusion that the programs are really “old”.

Ironically, all early versions of the Gfitter code are, to this day, non-declared one-to-one copies of large parts of ZFITTER 6.42, translated from Fortran to a very simple, Fortran-like C++ [200]. A motivation for the copy-paste actions was, due to the Gfitter authors, to retain ZFITTER for the future.

In any case, we need to build a suitable theory framework. ZFITTER/DIZET will not be a useful basis for FCC-ee, since it is structured to achieve consistent  $(1+1/2)$ -loop precision, but not beyond. No Laurent series approach is foreseen in the kernel ZFITTER; but see subsection C.4.5 on the SMATASY project and its applications to data. Further, later versions of the code lost modularity due to too lazy additions, concerning this item. We will have to begin developing a new program framework – likely object-oriented, e.g. C++ – that is general enough to be extended to any loop order and to different assumptions about QED and inputs. All the future calculations, covering up to weak 3 loops and QCD 4 loops should be performed to fit into this new framework.

#### 4.4 Prospects of QED flux functions

We discussed several reasons to plan with a newly written package, substituting ZFITTER. In view of the high precision demands of the FCC-ee Tera-Z on the QED descriptions, one might assume that the flux function approach of ZFITTER is outdated; see for some introduction to that approach in the appendix 4.7. In fact, this is not clear.

It is true that the flux function approach has a limited accuracy. At the other hand, it is relatively close to the real data, depending on the experimental situation with a precision of about roughly 0.5%. Additionally, the account of experimental cuts is limited. Already at LEP, ZFITTER's QED part was not precise enough for fits in accordance with the experimental accuracy. At the other hand, ZFITTER is fast and flexible in many other respects. So, experimentalists prepared data such that they correspond to ZFITTER's layout with a Monte Carlo program, preferably the KKMC [201]. It is of some importance here that KKMC uses for the data simulation the weak library of ZFITTER, so that in this respect there is sufficient coherence of the tools.<sup>25</sup>

As a result of combining KKMC and ZFITTER, the limited accuracy of ZFITTER's QED ansatz and its limited cut structure are *not limiting* the accuracy of the net fitting environment. Of course, the high *technical* precision of both packages is understood on default.

---

<sup>25</sup>In subsection 4.5 we demonstrate that the data simulation may be performed without use of a weak library. This is then a strict model-independent approach.



Let us now look at FCC-ee Tera-Z data. They demand a higher accuracy than LEP data. Let us assume that the higher loop terms are implemented properly. Applying again the combination KKMC/ZFITTER, the reduction of data to the ZFITTER model can proceed in exactly the same way as at LEP. The crucial difference to LEP analyses would be that KKMC has to model the additionally needed higher order QED corrections properly before that reduction. But the procedure could basically remain unchanged.

*The somewhat unexpected conclusion is that a ZFITTER successor package might well be suited to FCC-ee Tera-Z demands, concerning the QED part.*

There are subtleties to be considered carefully. To mention one example, the higher order terms of the initial-final state interferences have a specific dependence on the weak form factors (in Born approximation: the weak couplings). Another example is the potential importance of the usually neglected dependence of the weak couplings on  $s$  and  $\cos \theta$ . The influence of all that has to be studied.

Another interesting future application of ZFITTER might happen at meson factories.<sup>26</sup> The Belle II physics program foresees to measure the  $A_{FB}(e^+e^- \rightarrow \mu^+\mu^-)$  at  $\sqrt{s} = 10.58$  GeV. See section 5.14 of [202]. The authors estimate: “With a statistical error of  $\sigma(A_{FB}) = \pm 1 \times 10^{-5}$  on the charge asymmetry the corresponding error on  $\sin^2 \theta_W$  is  $\sigma(\sin^2 \theta_W) = 5 \times 10^{-4}$ .” The expected systematic errors are not discussed there, for that see [203, 204].

The point of interest here is the statement in [202] that Belle II will detect about  $10^9 \mu^+\mu^-$  pairs at  $\sqrt{s} = 10.58$  GeV, with a need of theoretical precision of about  $10^{-3}$  or even better. Evidently, one has to check if the account of the final state muon mass is needed,  $m_\mu^2/s \approx 10^{-4}$ .

*The physical analysis of the high statistics of  $\mu$ -pair events at BELLE II with such a high precision seems to be feasible only with one combination of tools: KKMC+ZFITTER.<sup>27</sup> ZFITTER 6.42 would deserve a test if the  $\mu$  mass has to be considered in the weak library a la [98, 106], while for KKMC one would have to check if the necessary higher orders in QED are available.*

In fact, from the formulas of appendix C.4.7 (see also [205]), it is evident which contributions dominate the analysis, from the point of view of weak physics: It is the  $\gamma Z$  interference. The forward-backward asymmetry is, in notations of [202]:

$$A_{FB} \approx \frac{3c_2}{8c_1} = \frac{3}{8} \frac{-4Q_e Q_\mu a_e a_\mu \chi + 8a_e a_\mu v_e v_\mu \chi^2}{Q_e^2 Q_\mu^2 + 2Q_e Q_\mu v_e v_\mu + (a_e^2 + v_e^2)(a_\mu^2 + v_\mu^2)\chi^2} \quad (\text{C.130})$$

$$\approx -\frac{3}{2} a_e a_\mu \chi,$$

$$\chi|_{s=10\text{GeV}} = \frac{G_F M_Z^2}{\sqrt{2} 8\pi \alpha_{em}} K(s)|_{s=10\text{GeV}} \approx -6.49 \times 10^{-3}, \quad (\text{C.131})$$

with  $a_e = a_\mu = -1$  and  $v_e = v_\mu = -1 + 4s_W^2$ , and

$$K(s) = \frac{s}{s - M_Z^2 + iM_Z \Gamma_Z}. \quad (\text{C.132})$$

Combining (C.130) and (C.131), we see that the weak library will be needed for  $\Delta A_{FB} \sim 10^{-5}$  at only one-loop accuracy, since the factor  $\chi \sim 10^{-3}$  suppresses its numerical influence.

The definitions are very close to those in (C.49). An alternative notion of  $\chi(s)$  is  $\chi_2(s)$ :

$$\chi_2(s) = \frac{1}{16s_W^2 c_W^2} K(s). \quad (\text{C.133})$$

The difference of the two definitions of  $\chi$  arises from renormalization; see subsection 2.1. In [202], a factor  $\rho$  is introduced and set  $\rho = 1$  for the Standard Model. In fact, with radiative corrections, the only change of

<sup>26</sup>This was pointed out by Torben Ferber, private communication.

<sup>27</sup>Torben Ferber, private communication.

(C.130) is the replacement  $a_e a_\mu \rightarrow \rho_Z a_e a_\mu$ , as discussed in detail in this section. Evidently, a measurement of the running of the leptonic weak mixing angle, as it arises from an  $s$ -dependence of  $v_e(s)$  is not possible from (C.130) because  $A_{FB}$  is independent of the vector couplings.

*Contrary, a measurement of  $A_{FB}$  at  $\sqrt{s} = 10.56 \text{ GeV}$  allows a measurement of the radiative corrections to the Fermi constant  $G_\mu$ . It will be a true single parameter measurement with a high precision.*

If one uses instead  $A_{FB}$  via the definition (C.133) for a determination of  $s_W^2$ , the meaning of that is not clear, at least not in the context presented in [202]. It is impossible to interpret fine-tuned measurements without the account of the weak corrections and without using a well-defined renormalization scheme.

## 4.5 The SMATASY interface

The correct quantum field theoretical treatment of higher order loop contributions to a resonance like the  $Z$  boson in  $e^+e^- \rightarrow f\bar{f}$ , i.e. in  $2 \rightarrow 2$  scattering, was studied since 1991 by several authors, see [119, 120, 206–208] and [125]. The essential finding was that one has to interpret the loop corrections as Laurent series around a single pole at  $s_0 = \bar{M}_Z^2 - i\bar{M}_Z\bar{\Gamma}_Z$  in the complex  $s$  plane. This corresponds to the understanding of the weak amplitudes as meromorphic functions with simple poles originating from particle resonances. Another name for the approach was S-matrix approach.

The approach lead to the idea to try a fitting of the  $Z$  resonance by Laurent series, where only the residues and the pole position are fitted. In that way, the underlying theory gets no interpretation, while mass and width of the  $Z$  boson get measured [31]. This worked quite well. Of course, one has to adopt the effects from bremsstrahlung, a 2to3 or even 2ton reactions, and also the interference of the  $Z$ -exchange amplitude with the photon-exchange amplitude. This goes beyond the S-matrix model, so that one should call the resulting formalism more accurately to be "S-matrix inspired".

An unpublished *stand-alone* software ZPOLE was used first, with a simplified treatment of the QED corrections. An observed systematic shift of the central value of the S-matrix  $Z$  mass determination, compared to ZFITTER fits, was not understood (and not documented) see [31]. In order to clarify this, an SMATRIX interface for ZFITTER was written, so that the S-matrix fits have the same QED environment like conventional ZFITTER fits.<sup>28</sup> A careful investigation showed that the observed systematic shift of the S-matrix  $Z$  mass was due to an internal (not documented) fixing of the hadronic  $\gamma Z$  interference term in ZFITTER with some input for the quark couplings. When this was done, the numerical effect on fits was considered to be negligible, but in the meantime the accuracy was improved. Further, the measured values for the quark couplings were shifted. In sum, an artificial  $Z$  mass shift in ZFITTER resulted from that programming. After repairing, the S-matrix  $Z$  mass determination agreed with its central value with the conventional ZFITTER fit, as it should be. A new, corrected ZFITTER version was released.

Why this episode is mentioned? It demonstrates how subtleties of the fitting libraries may influence the fitting in a completely unexpected manner.

The S-matrix (inspired) approach was extended to the fit of asymmetries, with account of QED corrections, in [32], and finally the interface package SMATASY (1991-2005) to ZFITTER 6.42 was written [121, 129]. Its release allowed the experimental groups to perform S-matrix (inspired) fits to their data from LEP and TRISTAN. The first application of the S-matrix (inspired) approach to LEP data was made by the L3 collaboration [209]. Later, ALEPH used the approach to study the  $\gamma Z$  interference at the  $Z$  peak [210]. Further experimental analyses followed [211–213], also at TRISTAN [214, 215]. A rather complete mini review on the SMATASY approach and various experimental applications may be found in [122]. See also the recent discussion related to FCC-ee physics in [90].

Today, when facing the immense accuracy of the FCC-ee Tera-Z data, it looks natural to combine the potential of ZFITTER for describing QED contributions with SMATASY as interface to the language of Laurent series. And to introduce into the latter an interface to a weak library with 2-4 loop accuracy. Such an approach

---

<sup>28</sup>This was initiated by S. Riemann, unpublished.

would constitute a prototype of a fit library for the EWPOs with FCC-ee Tera-Z accuracy.

Instead of describing in detail how SMATASY works, let us only quote few important facts. We will reproduce a short introduction to the essentials of the SMASY approach, and start from the generic matrix elements (C.79). Calculating from them the integrated cross sections, we arrive at generic forms, which now are understood to include also the contributions from photon exchange and from the  $\gamma Z$  interference [31]. The self-explanatory notation of [121] is used:

$$\begin{aligned}
 \sigma_A^0(s) &= \frac{4}{3}\pi\alpha^2 \left[ \frac{r_A^{\gamma f}}{s} + \frac{sr_A^f + (s - \bar{m}_Z^2)j_A^f}{(s - \bar{m}_Z^2)^2 + \bar{m}_Z^2\bar{\Gamma}_Z^2} + \frac{r_A^{f0}}{\bar{m}_Z^2} + \text{further background} \right], \\
 &\rightarrow \frac{4}{3}\pi\alpha^2 \left[ \frac{r_A^{\gamma f}}{s} + \frac{sr_A^f + (s - \bar{m}_Z^2)j_A^f}{(s - \bar{m}_Z^2)^2 + \bar{m}_Z^2\bar{\Gamma}_Z^2} + \frac{r_A^{f0}}{\bar{m}_Z^2} \right], \quad A = T, FB, pol, polFB, \dots \\
 &\approx \frac{4}{3}\pi\alpha^2 \left[ \frac{r_A^{\gamma f}}{s} + \frac{sr_A^f + (s - \bar{m}_Z^2)j_A^f}{(s - \bar{m}_Z^2)^2 + \bar{m}_Z^2\bar{\Gamma}_Z^2} \right].
 \end{aligned} \tag{C.134}$$

The  $r_A^{\gamma f}$  is the photon exchange term,

$$r_A^{\gamma f} = \frac{1}{4}c_f \sum_{i=1}^4 \{\pm 1\} |R_\gamma^f|^2 R_{QCD}. \tag{C.135}$$

For a better precision one may use  $\alpha_{em}(s)$  instead of the constant parameter  $r_A^{\gamma f}$ ; bu assuming a resummation of background parts, as it was discussed in subsection 2.6. This term vanishes for all asymmetric cross-section combinations, i.e. for  $A \neq T$ . It is  $c_f = 1, 3$  for leptons and quarks, respectively. QCD corrections for quarks are taken into account by the factor  $R_{QCD}$  of [27]. The  $Z$ -exchange residues  $r_A^f$  and the  $\gamma Z$ -interference terms  $j_A^f$  are:

$$\begin{aligned}
 r_A^f &= c_f \left\{ \frac{1}{4} \sum_{i=1}^4 \{\pm 1\} |R_Z^{fi}|^2 + 2 \frac{\bar{\Gamma}_Z}{\bar{m}_Z} \Im m C_A^f \right\} R_{QCD}, \\
 j_A^f &= c_f \left\{ 2 \Re C_A^f - 2 \frac{\bar{\Gamma}_Z}{\bar{m}_Z} \Im m C_A^f \right\} R_{QCD},
 \end{aligned} \tag{C.136}$$

and the  $C_A^f$  are the complex-valued interferences of the residues  $R_f^{(i)}$  of (C.79) with  $\alpha_{em}(s)$ .

$$C_A^f = (R_\gamma^f)^* \left( \frac{1}{4} \sum_{i=1}^4 \{\pm 1\} R_Z^{fi} \right). \tag{C.137}$$

The factors  $\{\pm 1\}$  in (C.135) and (C.136) indicate that the signs of  $|R_\gamma^f|$ ,  $|R_Z^{fi}|^2$ , and of  $R_Z^{fi}$  correspond to the signs of  $\sigma_i$  in (C.72) to (C.75). Explicit expressions for the background contributions may well become of numerical importance in the FCC-ee Tera-Z era. We refer for explicit expressions to the literature quoted.

When measuring the  $Z$  line shape, the independent parameters of a pseudo observable are  $M_Z, \Gamma_Z$  as well as the residue term  $r_A$  and the  $\gamma Z$  interference term  $j_A$ , and potentially more parameters arising from the background. So each of the observables depends on a least four parameters.

*For an adequate fit of the  $Z$  line shape one needs, consequently, at least five independent data points taken at different  $s$ . When fitting also background, one needs more data points.*

From the correlation tables not shown here one derives that  $M_Z$  and  $j_T$  are strongly correlated, as well as  $\Gamma_Z$  and  $r_T$  are. In fact, there is a simple, but very accurate relation between an uncertainty (or shift) of the  $Z$  peak position  $s_{\max}$  (the center of gravity of the  $Z$  peak is defined by the  $Z$  mass) and the  $\gamma Z$  term  $j_T$  [216]:

$$\Delta M_Z \sim \Delta(\sqrt{s_{\max}}) = \frac{1}{4} \frac{\Gamma_Z^2}{M_Z} \times \frac{j_T}{r_T} \approx 17 \text{ MeV} \times \frac{j_T}{r_T}. \quad (\text{C.138})$$

The mass and width of the  $Z$  boson are best determined from the hadronic cross section  $\sigma_{had}$ , so that we may set:  $j_T \rightarrow j_{T,had}$  and  $r_T \rightarrow r_{T,had}$ . A conclusion for fitting is the following:

*For an adequate fit of  $M_Z$ , one has to control the correlation with the  $\gamma Z$  interference term  $j_{T,had}$ . A fixing of the latter produces a smaller error of  $M_Z$ , but in a model-independent understanding this is not correct. For the FCC-ee Tera- $Z$  applications, one has to study the interplay of all the components of fitting carefully. Similar statements apply to the correlation of  $\Gamma_Z$  and  $r_{T,had}$ .*

A further remark concerns the asymmetries [32]. They all are ratios of Laurent series, thus becoming themselves Taylor expansions in  $s$  around  $s_0$ . If there would be no contributions from photon exchange, the asymmetries would be at first approximation independent of  $s$ , if no other background contributes considerable.

How do such observations change if we do not consider the  $2 \rightarrow 2$  cross sections and observables, but the real cross sections? This has been studied, assuming the applicability of a flux function approach with sufficient accuracy, in [31, 122] and can be further studied using ZFITTER/SMATASY [121, 129]. If QED is described by some Mont Carlo code, all the conclusions remain unchanged because the formulae are truly generic concerning QED.

The main results on the influence of QED corrections are the following.

*One has to distinguish helicity asymmetries and angular asymmetries due to their different QED corrections.*

The former undergo the same photonic corrections as the total cross section, and the latter go with the forward-backward ( $FB$ ) anti-symmetric cross sections. Both differ from each other, and they differ more, if more hard radiation happens. See for details on that issue subsection 4.7.

In fact one may derive very elegant and universal formulae for the real asymmetries in the S-matrix (inspired) approach. This was done in [32]. They exhibit explicitly the accessible EWPOs, but here in the S-matrix (inspired) language.

The  $2 \rightarrow 2$  forward-backward asymmetry is

$$A_{0,FB}(s) = A_0 + A_1(s - s_0) + A_2(s - s_0)^2 + \dots \quad (\text{C.139})$$

Here,

$$A_0 = \frac{r_{FB}}{r_T}, \quad (\text{C.140})$$

$$A_1 = \frac{j_{FB}}{r_{FB}} - \frac{j_T}{r_T}, \quad (\text{C.141})$$

etc. One may show that the QED corrected asymmetries are quite similar to the Born asymmetries. They are modified by certain factors  $c_n$ , which are smooth functions of the kinematics. The real forward-backward asymmetry is:

$$A_{FB}(s) = c_{0,FB}(s)A_0 + c_{1,FB}(s)A_1(s - s_0) + c_{2,FB}(s)A_2(s - s_0)^2 + \dots \quad (\text{C.142})$$

The QED functions  $c_{i,FB}(s)$  are independent of the underlying model. While

$$c_{0,T}(s) = 1, \quad (\text{C.143})$$

it is

$$c_{0,FB}(s) = \frac{C_{FB}^R(s)}{C_T^R(s)}, \quad (\text{C.144})$$

$$c_{1,FB}(s) = c_{0,FB}(s) \frac{C_T^J(s)}{C_T^R(s)}, \quad (\text{C.145})$$

etc. The functions  $c_{i,A}(s)$  depend on the QED treatment. For the account of initial state radiation a la ZFITTER:

$$C_{T,FB}^R = \int d\frac{s'}{s} \rho_{T,FB}^{ini}(s') \frac{s'}{s} \frac{|s - s_0|^2}{|s' - s_0|^2}, \quad (\text{C.146})$$

$$C_{T,FB}^J = \int d\frac{s'}{s} \rho_{T,FB}^{ini}(s') \frac{s' - M_Z^2}{s - M_Z^2} \frac{|s - s_0|^2}{|s' - s_0|^2}, \quad (\text{C.147})$$

etc. Evidently,  $C_T^{R,J}$  and  $C_{FB}^{R,J}$  are smooth in  $s$  and independent of the weak interactions model.

In case of another treatment of the QED corrections, the QED factors will get modified by a necessary replacement of the flux functions  $\rho_{T,FB}^{ini}(s')$ , while the QED "kernels"  $s'/s |s - s_0|^2/|s' - s_0|^2$  and  $s' - M_Z^2/s - M_Z^2 |s - s_0|^2/|s' - s_0|^2$  etc. will stay unchanged.

The figure C.5 shows a typical forward backward asymmetry around the  $Z$  peak, here for muon pair production. The non-vanishing  $\gamma Z$  interference close to the  $Z$  peak makes the asymmetry not staying constant, a 2to2 effect. Because the photonic corrections differ for  $\sigma_T$  and  $\sigma_{FB}$ , the real asymmetry does not agree with the Born asymmetry at  $s = M_Z^2$ ; see (C.144). If there would be no hard photons emitted, the real asymmetry would be equal to the Born approximation because in that case the QED corrections would cancel out, see 4.7; this is very good fulfilled at  $s = M_Z^2$  where hard photon emission is suppressed. The rise of  $A_{FB}$  around the  $Z$  peak is due to the  $\gamma Z$  interference. Further, the behavior right of the peak is markedly due to the radiative corrections. The curve with QED and no cuts gets strongly damped at larger  $s$  because the  $\sigma_T$  develops a resonating behavior (resonance tail due to radiative return), but the  $\sigma_{FB}$  does not; see the formulas and their comments in 4.7. If one cuts the maximal allowed energy of the photon emission, the radiative return is suppressed and we see a QED corrected line shape close to the Born shape - as it appears left of the  $Z$  peak.

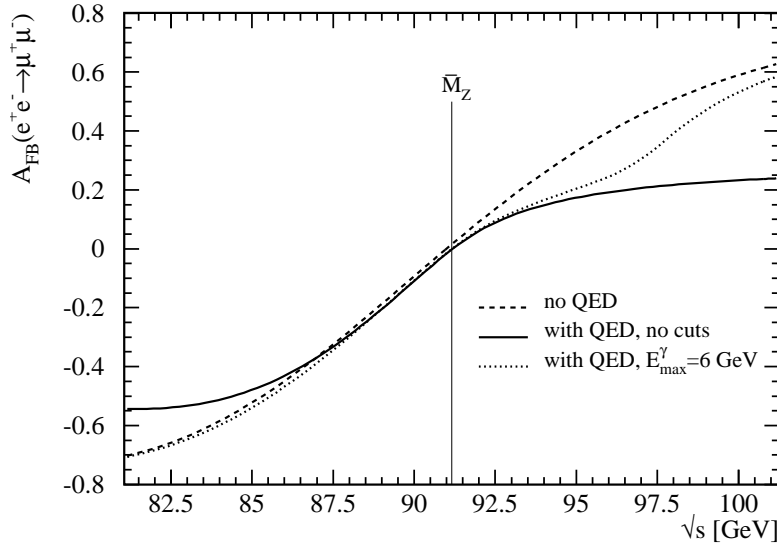


Fig. C.5: Figure from [121]. The forward-backward asymmetry for the process  $e^+e^- \rightarrow \mu^+\mu^-$  near the  $Z$  peak.

## 4.6 Conclusions

ZFITTER is a mighty tool for all its applications at precision goals like those at LEP1/SLC. For true precision, the Monte Carlo tool used for preparing the measurements (e.g. KKMC) should rely on the same weak library as ZFITTER. The combination ZFITTER/SMATASY is a role model for applying the S-matrix (inspired) ansatz, using Laurent series. If interpreted in the Standard Model, it would be fit for multi-loop FCC-ee Tera-Z applications. Preferable is the development of a new package. The SANC collaboration made already steps in this direction, see section 7. It is fair to say that a completely numerical Monte Carlo approach might also be appropriate for FCC-ee Tera-Z applications. One has to study the pros and the cons of the semi-analytical and the pure numerical approaches. In any case, the weak library of the unfolding and that of the fitting procedures have to be the same, in order to be consistent and accurate in a controlled way.

A completely model-independent fit is possible, when based on the residues and background coefficients of the Laurent series of the matrix elements, not interpreting them in terms of the Standard Model. The correlations of fit parameters have to be very carefully studied.

## 4.7 Appendix. QED flux functions

The origin of ZFITTER is two-fold. At one hand, the seminal articles with the one-loop weak form factors, together with the Fortran code BCF (in Euklidean metrics), became the basis of the weak library DIZET of ZFITTER [116, 117], after translation to the Minkowskian metrics. The other basis was the analytical calculation of the integrated, complete  $\mathcal{O}(\alpha)$  photonic corrections to  $e^+e^- \rightarrow \mu^+\mu^-$  scattering around the  $Z$  peak without a cut. The original work remained unpublished, because the referee of Nuclear Physics B estimated the contents too far from true physics – because no cuts were included. As a compensation, the preprint appeared twice [217, 218]. For didactic purposes, we reproduce the main results. The formulae are exact, have no kinematical cuts, and can be useful for basic tests of MC programs. They are extremely compact. The corresponding Fortran program is presumably lost. It had been very carefully checked in 1988 against the 1982 Monte Carlo code MUSTRAAL [219, 220] which did basically the same calculation, but numerically. The explicit expressions are:

$$\sigma_T = \sigma_0 \left\{ Q_e^2 Q_f^2 \left[ 1 + \frac{\alpha}{\pi} (Q_e^2 F_0^T + Q_f^2 F_2^T) \right] + \frac{\alpha}{\pi} Q_{e,a} Q_{f,a} Q_e^2 Q_f^2 \Re(F_4^T) \right. \quad (\text{C.148})$$

$$+ 2|Q_e Q_f| v_e v_f \Re \left[ \chi + \frac{\alpha}{\pi} \chi (Q_e^2 G_0^T + Q_f^2 G_2^T) \right] + 2|Q_e Q_f| a_e a_f \frac{\alpha}{\pi} Q_e Q_f \Re(\chi G_4^T) \\ + (v_e^2 + a_e^2)(v_f^2 + a_f^2) |\chi|^2 \left[ 1 + \frac{\alpha}{\pi} \Re(Q_e^2 H_0^T + Q_f^2 H_2^T) \right] \quad (\text{C.149}) \\ + 4v_e a_e v_f a_f |\chi|^2 \frac{\alpha}{\pi} Q_e Q_f \Re(H_4^T) \left. \right\},$$

$$A_{FB} = \frac{\sigma_0}{\sigma_T} \left\{ Q_e Q_f \frac{\alpha}{\pi} \left[ Q_e^2 Q_f^2 \Re(F_1^T) + 4Q_{e,a} Q_{f,a} Q_e Q_f \Re(Q_e^2 F_3^T + Q_f^2 F_5^T) \right] \right. \\ + 2|Q_e Q_f| v_e v_f \frac{\alpha}{\pi} Q_e Q_f \Re(\chi G_1^T) + 2|Q_e Q_f| a_e a_f \Re \left[ \frac{3}{4} \chi + \frac{\alpha}{\pi} \chi (Q_e^2 G_3^T + Q_f^2 G_5^T) \right] \\ + (v_e^2 + a_e^2)(v_f^2 + a_f^2) |\chi|^2 \frac{\alpha}{\pi} Q_e Q_f \Re(H_1^T) \\ \left. + 4v_e a_e v_f a_f |\chi|^2 \left[ \frac{3}{4} + \frac{\alpha}{\pi} \Re(Q_e^2 H_3^T + Q_f^2 H_5^T) \right] \right\},$$

with

$$\chi = \frac{G_\mu M_Z^2}{\sqrt{28\pi\alpha_{em}}} \frac{s}{s - M^2}. \quad (\text{C.150})$$

In the following, the suffixes *br* stand for bremsstrahlung and *box* for 1-loop QED  $\gamma\gamma$  and  $\gamma Z$  box terms.

The initial-state one-loop contributions to  $\sigma_T$  are:

$$F_0^T = A + B \left[ L_f - \frac{7}{6} \right], \quad (\text{C.151})$$

$$G_0^T = A + B \left[ R + \frac{1}{2} + (1 + R^2)L_R \right], \quad (\text{C.152})$$

$$H_0^T = A + B \left[ 2R + \frac{1}{2} - |R|^2 + \frac{i}{g}(1 - R^*)R(1 + R^2)L_R \right], \quad (\text{C.153})$$

with

$$A = \frac{\pi^2}{3} - \frac{1}{2}, \quad (\text{C.154})$$

$$B = L_e - 1. \quad (\text{C.155})$$

The well-known global enhancement  $L_e = \ln(s/m_e^2)$  appears only in the initial state contributions. The enhancement  $L_f = \ln(s/m_f^2)$  in the pure photonic part disappears with cuts. A logarithmic term is related to the  $Z$  boson:

$$L_R = \ln \left( 1 - \frac{1}{R} \right), \quad (\text{C.156})$$

$$R = \frac{M^2}{s}, \quad (\text{C.157})$$

$$M^2 = M_Z^2 - iM_Z\Gamma_Z. \quad (\text{C.158})$$

A trace of the  $Z$  propagator treatment, enabling the analytical integrations,

$$\frac{1}{|s - M^2|^2} = \frac{i}{2M_Z\Gamma_Z} \left( \frac{1}{s - M^2} - \frac{1}{s - M^{*2}} \right), \quad (\text{C.159})$$

is seen in  $H_0^T$ , and only there: The pure  $Z$  exchange initial state radiation term develops at energies above  $s = M_Z^2$  the so-called radiative tail. This is a huge enhancement, proportional to  $M_Z/\Gamma_Z$ , of the cross section,

$$\begin{aligned} \Re \left( \frac{i}{g} L_R \right) &= \Re \left[ \frac{i}{\Gamma_Z} \frac{s}{M_Z} \ln \left( 1 - \frac{s}{M^2} \right) \right] \\ &\equiv \frac{M_Z}{\Gamma_Z} \frac{s}{M_Z^2} \Re [i \times \ln(1 - s/M_Z^2 - is\Gamma_Z/M_Z^3)] \\ &= 0 \quad \text{if } s < M_Z^2, \quad (\text{the } \ln\text{-function is real there}). \end{aligned} \quad (\text{C.160})$$

The enhancement is possible due to the prefactor  $i/g$ . If  $M_Z/\Gamma_Z$  is small, then

$$\begin{aligned} \Re \left( \frac{i}{g} L_R \right) &= \frac{M_Z}{\Gamma_Z} \frac{s}{M_Z^2} \Re [i [\ln(1 - s/M_Z^2) - i\pi]] \\ &\sim -\frac{s}{M_Z^2} \frac{M_Z}{\Gamma_Z} \quad \text{if } s > M_Z^2. \end{aligned} \quad (\text{C.161})$$

The same tail function as in  $H_0^T$  will appear also in the  $Z$  squared initial state part  $H_3^T$  of  $\sigma_{FB}$ .

The final state photonic corrections are known to be small and universal:

$$F_2^T = G_2^T = H_2^T = \frac{3}{4}. \quad (\text{C.162})$$

Finally, we come to the initial-final state interferences, combined with box contributions. The initial-final state interferences fulfill the relation [221]:

$$G_i = \frac{1}{2}(F_i + H_i), \quad (\text{C.163})$$

so that only the pure photonic and the pure  $Z$  exchange functions are to be determined:

$$F_{4\ br}^T = 6\bar{P}_{IR} - 9, \quad (C.164)$$

$$H_{4\ br}^T = 6\bar{P}_{IR} - 9 + 3R[1 + (1 + R)L_R], \quad (C.165)$$

$$F_{4\ box}^T = -6\bar{P}_{IR} + \frac{9}{2}, \quad (C.166)$$

$$H_{4\ box}^T = -6\bar{P}_{IR} + 9 - 3R[1 + (1 + R)L_R] - 3L_Z, \quad (C.167)$$

with

$$L_Z = -\ln R, \quad (C.168)$$

$$\bar{P}_{IR} = P_{IR} + \frac{1}{2} \ln \frac{s}{M_W^2} = \ln \frac{2E}{\lambda}, \quad (C.169)$$

$$P_{IR} = \frac{1}{n-4} + \frac{1}{2} \gamma_E - \ln(2\sqrt{\pi}) = \ln \frac{M_W}{\lambda}. \quad (C.170)$$

The  $\lambda$  is a small regularizing photon mass. As in  $H_0^T$  and  $H_3^T$ , also in  $H_4^T$  we meet the  $L_R$  of (C.156), but here it is not in connection with a factor  $i/\Gamma_Z$ , so that no tail property will arise. The total interference contributions to  $\sigma_T$  are:

$$F_4^T = -\frac{9}{2}, \quad (C.171)$$

$$G_4^T = \frac{1}{2}(F_4^T + H_4^T), \quad (C.172)$$

$$H_4^T = -3L_Z. \quad (C.173)$$

The function  $F_4^T$  does not appear in  $\sigma_T$ , because the axial couplings of the photon vanish, see (C.150). It will appear when sufficiently many of the scattering particles are polarized; see the modifications of the coupling constants due to spin effects as given e.g. in (19) of [218]. For a polarized electron, among others the changes  $v_e v_f \rightarrow (v_e - \lambda a_e) v_f$  and  $a_e a_f \rightarrow (a_e - \lambda v_e) a_f$  appear. For the electric charges (vector couplings) this means additional mixing terms. If now both beam particles are polarized, then the combination  $Q_{e,a} Q_{f,a}$  produces vector couplings in the cross section expressions and so contributions of  $F_1^T$  and  $F_4^T$  will appear. For a coexistence not only of photon and  $Z$  boson, but also a second  $Z'$  boson, the terms  $F_3$  and  $F_4$  are needed also in unpolarized scattering [222].

We come now to the contributions to the forward-backward asymmetry  $A_{FB}$ , initial state corrections:  $F_3^T, G_3^T, H_3^T$ , initial-final interferences:  $F_1^T, G_1^T, H_1^T$ , and final state corrections:

$$F_5^T = G_5^T = H_5^T = 0. \quad (C.174)$$

The initial state contributions are:

$$\begin{aligned} \frac{1}{3} G_3^T &= -\frac{1}{8} + \frac{1-R}{1+R} (1 - \ln 2) + (1-R) \ln^2 2 + \frac{1}{4} (1+2R) \text{Li}_2(1) \\ &+ \frac{1}{2} \frac{1-R}{1+R} \left[ -\frac{1+3R}{1+R} \ln 2 + \frac{7-R}{4(1-R)} \right] (L_e - 1) + R \frac{1+R^2}{(1+R)^2} D_3, \end{aligned} \quad (C.175)$$

$$\begin{aligned} \frac{1}{3} H_3^T &= -\frac{2R}{|1+R|^2} - \left| \frac{1-R}{1+R} \right|^2 \ln 2 + |1-R|^2 \ln^2 2 + \frac{1}{4} (1+4R-2|R|^2) \text{Li}_2(1) \\ &+ \left( \frac{7}{8} - 2 \frac{R}{|1+R|^2} \right) L_e + \left( -\frac{5}{2} + 2 \frac{6R-1}{|1+R|^2} + 4 \frac{1-R^2}{|1+R|^4} \right) (L_e - 1) \ln 2 \\ &+ R^2 \frac{1+R^2}{(1+R)^2} \left[ 2 + \frac{i}{g} (1-R) \right] D_3. \end{aligned} \quad (C.176)$$



The QED function  $F_3^T$  was implemented in ZFITTER later, so we refer to the code for this term. With  $F_4^T$  the situation is simpler because it may be reconstructed from  $G_4^T$  and  $H_4^T$ , which were determined explicitly. The function  $D_3$  introduces through its  $L_R$  the term  $\frac{i}{g} \ln(1-1/R)$ , producing the radiative tail of  $H_0^T$  also into  $H_3^T$ .

The photonic part  $F_1^T$  from the initial-final state interference is a constant:

$$F_{1\ br}^T = (1 + 8 \ln 2) \bar{P}_{IR} + \frac{3}{4} [1 - 16 \ln 2 - \text{Li}_2(1)], \quad (\text{C.177})$$

$$F_{1\ box}^T = -(1 + 8 \ln 2) \bar{P}_{IR} + \frac{3}{4} (1 + 6 \ln 2 + \ln^2 2) - \frac{i\pi}{2} (2 - 5 \ln 2). \quad (\text{C.178})$$

The sum of the two  $F_1^T$  in C.150 contributes to  $A_{FB}$ :

$$\Re e(F_1^T) = -\frac{3}{4} \text{Li}_2(1) + \frac{3}{4} \ln^2 2 - \frac{15}{2} \ln 2 + \frac{3}{2} = -4.572. \quad (\text{C.179})$$

This value agrees with equation (25) of [205].

The initial-final state interference function due to pure  $Z$ -boson exchange and the two  $\gamma Z$  box diagrams is  $H_1^T$ :

$$\begin{aligned} H_{1\ br}^T &= (1 + 8 \ln 2) \bar{P}_{IR} - \frac{1}{4} (5R - 3) - \frac{3}{4} (1 + R - 2R^2) \text{Li}_2(1) \\ &\quad + \frac{1}{1+R} (-12 + 3R + 8R^2 + 5R^3) \ln 2 \\ &\quad + \frac{1}{2} (1 - R) (5 - R + R^2) \text{Li}_2\left(\frac{1}{R}\right) - \frac{R}{1+R} (1 - 4R + R^2) L_R + \frac{1}{2} (5 - 3R + 6R^2) D_1 \\ &\quad + \frac{R}{2} (6 - 3R + 5R^2) D_2, \end{aligned} \quad (\text{C.180})$$

$$\begin{aligned} H_{1\ box}^T &= -(1 + 8 \ln 2) \bar{P}_{IR} + \frac{3}{2} - R + (9 - 4R - 4R^2) \ln 2 + 2 \ln^2 2 + \frac{1}{2} (-5 + 4R) L_Z \\ &\quad + 4R^3 \left[ \text{Li}_2(1) - \text{Li}_2\left(1 - \frac{1}{R}\right) \right] \\ &\quad + \frac{1}{2} [4 - 9R + 3R^2 + 2(-5 + 3R - 6R^2) \ln 2] L_R \\ &\quad + (1 - 3R + 6R^2 - 8R^3) \left[ \text{Li}_2\left(1 - \frac{1}{2R}\right) - \text{Li}_2\left(1 - \frac{1}{R}\right) \right]. \end{aligned} \quad (\text{C.181})$$

It is

$$D_{0,1} = \text{Li} \left( \pm \frac{1+R}{1-R} \right) + \frac{1}{2} L_R^2, \quad (\text{C.182})$$

$$D_2 = D_0 + \text{Li}_2 \left( -\frac{1}{R} \right) - \text{Li}_2(1) + \ln \left( \frac{R+1}{R-1} \right) \ln \left( -\frac{1}{R} \right), \quad (\text{C.183})$$

$$D_3 = D_1 + D_2 + \ln^2(2) + (L_e - 1 - 2 \ln(2)) L_R \quad (\text{C.184})$$

The initial-final interference,  $\gamma Z$  term in the asymmetry  $A_{FB}$  contains the sum of two,

$$G_1^T = F_1^T + H_1^T. \quad (\text{C.185})$$

The phase space to be integrated was the following:

$$\int d\Gamma = \frac{\pi^2}{4s} \int_{-1}^1 d \cos \theta \int_0^1 x dx \frac{1-x}{1-x+m_f^2/s} \frac{1}{4\pi} \int_{-1}^1 d\phi_\gamma \int_0^{2\pi} d \cos \theta_\gamma, \quad (\text{C.186})$$

where  $x = 2E_{f^+}/\sqrt{s}$  and the photon variables are defined in the rest system of fermion+photon [223]. The problematic feature of the above results is the lack of variable  $s'$ , the invariant mass of the final state fermion pair, related the photon energy by  $s'/s = 1 - 2E_\gamma/\sqrt{s}$ . Due to that lack, soft photon exponentiation may not be implemented, and it was decided to change to other variable.

As a consequence, a new parameterization of QED corrections was published in a series of three papers from May 1989 to October 1990 [80, 82, 83] and implemented in ZFITTER: integrated cross-sections with no cut, differential in the scattering angle  $\cos\theta$  cross-sections, and cross-sections integrated with cut on  $\cos\theta$ . Additionally, cuts on  $s'$  are possible. Later, this was accomplished with the account of an alternative  $f^+f^-$ -collinearity cut  $\zeta$ , 1989 to 1999 [85, 96, 97], using techniques developed in [224–226].

The phase space was now chosen to allow for a cut on the photon energy:

$$\int d\Gamma = \frac{\pi^2}{4s} \int_{-c_m}^{c_m} d\cos\theta \int_0^{v_m} dv \int_{v_{2,min}}^{v_{2,max}} dv_2 \frac{1}{2\pi} \int_0^{2\pi} d\varphi_\gamma, \quad (\text{C.187})$$

with

$$v_{2,max(min)} = \frac{1}{2}v \left[ 1 \pm v_m(s')^{1/2} \right], \quad (\text{C.188})$$

$$v_m(s) = 1 - 4m_f^2/s. \quad (\text{C.189})$$

In (C.187),  $\varphi_\gamma$  is the azimuthal angle of the photon in the cms and

$$v_2 = -\frac{2}{s}p_{f^+}p_\gamma = 1 - 2E_{f^-}/\sqrt{s}. \quad (\text{C.190})$$

The integration boundaries for  $\cos\theta$  are chosen:

$$c_m = 1 - 2m_e^2/s. \quad (\text{C.191})$$

Finally,  $x$  is the momentum fraction of  $f^+$  in the cms in units of the beam energy:

$$x = -2p_{f^+}(p_{e^+} + p_{e^-})/s = 2E_{f^+}/\sqrt{s}. \quad (\text{C.192})$$

The corresponding formulas are published, so we need not to reproduce them here. For didactic reasons, we show some initial-final interference formulas for the totally integrated cross sections with numerical integration over  $s'/s = 1 - 2E_\gamma/\sqrt{s}$ , taken from [218]. They are reproduced in C.193 to C.202. It is

$$A_{FB}(s) = \frac{\sigma_{FB}}{\sigma_T}, \quad (\text{C.193})$$

and the corresponding cross sections are

$$\sigma_T = \sum_{\substack{a=e,i,f \\ k,l=1,2}} \text{Re} \int_0^1 dv \sigma_T^{a,0}(s, s'; B_k, B_l) r_{T,a}(v; B_k, B_l), \quad (\text{C.194})$$

and

$$\sigma_{FB} = \sum_{\substack{a=e,i,f \\ k,l=1,2}} \text{Re} \int_0^1 dv \sigma_{FB}^{a,0}(s, s'; B_k, B_l) r_{FB,a}(v; B_k, B_l), \quad (\text{C.195})$$

with  $B_1 = Z, B_2 = \gamma$  and

$$\sigma_{FB}^{i,0}(s, s'; B_k, B_l) = \frac{3}{4} \sigma_T^0(s, s'; B_k, B_l), \quad (\text{C.196})$$

$$\sigma_A^0(s, s'; B_k, B_l) = \frac{4\pi\alpha^2}{3s'} C_A(B_k, B_l) \times \frac{1}{2} [\kappa_k(s') \kappa_l^*(s) + \kappa_k(s) \kappa_l^*(s')], \quad A = T, FB \quad (\text{C.197})$$

$$\kappa_l(s) = \frac{s}{s - m_l^2}; \quad (\text{C.198})$$

$$m_l^2 = M_l^2 - i M_l \Gamma_l(s), \quad (\text{C.199})$$

$$\Gamma_l(s) = \frac{s}{M_l^2} \Gamma_l, \quad (\text{C.200})$$

where  $C_A(B_k, B_l)$  are corresponding coupling constant combinations, of the kind used in the one-loop formulas; see any ZFITTER reference.

The point of relevance here are the convolution weights for  $\sigma_T$  and  $A_{FB}$ :

$$r_{A,a}(v; B_k, B_l) = \delta(v) s_a(B_k, B_l) + \theta(v - \epsilon) H_{A,a}(v), \quad A = T, FB, \quad a = e, i, f, \quad (\text{C.201})$$

where

$$B(Z, Z) = H_{1box}^T, \quad B(\gamma, \gamma) = F_{1box}^T, \quad B(Z, \gamma) = \frac{1}{2} [B^*(\gamma, \gamma) + B(Z, Z)]. \quad (\text{C.202})$$

The soft functions are:

$$S_a = s_a, \quad a = e, f, \quad (\text{C.203})$$

$$s_a = Q_a^2 \frac{\alpha}{\pi} \left[ (L_a - 1) [2 \ln(\epsilon) + \frac{3}{2}] + \frac{\pi^2}{3} - \frac{1}{2} \right], \quad a = e, f, \quad (\text{C.204})$$

$$S_i(B_k, B_l) = s_i(B_k, B_l), \quad (\text{C.205})$$

$$s_i(B_k, B_l) = Q_e Q_f \frac{\alpha}{\pi} \left( -(1 + 8 \ln 2) \ln \frac{2\epsilon}{\lambda} + 4 \ln^2 2 + \ln 2 + \frac{1}{2} + \frac{1}{3} \pi^2 - B(B_k, B_l) \right). \quad (\text{C.206})$$

The hard functions for  $\sigma_T$  are  $H_{T,a}(v) \equiv H_a(v)$ :

$$H_e(v) = Q_e^2 \frac{\alpha}{\pi} (L_e - 1) \frac{1 + (1 - v)^2}{v}, \quad (\text{C.207})$$

$$H_i(v) = Q_e Q_f \frac{\alpha}{\pi} \frac{3}{v} (1 - v)(v - 2), \quad (\text{C.208})$$

$$H_f(v) = Q_f^2 \frac{\alpha}{\pi} \frac{1}{v} [1 + (1 - v)^2] [(L_e - 1) + \ln(1 - v)]. \quad (\text{C.209})$$

The hard  $FB$  functions are  $H_{FB,a}(v) \equiv h_a(v)$ :

$$h_e(v) = Q_e^2 \frac{\alpha}{\pi} \frac{1 + (1 - v)^2}{v} \frac{1 - v}{(1 - v/2)^2} \left[ L_e - 1 - \ln \frac{1 - v}{(1 - v/2)^2} \right], \quad (\text{C.210})$$

$$h_i(v) = Q_e Q_f \frac{\alpha}{\pi} \frac{2}{3v} [2(1 - v)(v^2 + 2v - 2) + (1 - v)(5v^2 - 10v + 8) \ln(1 - v) + (5v^3 - 18v^2 + 24v - 16) \ln(2 - v)], \quad (\text{C.211})$$

$$h_f(v) = Q_f^2 \frac{\alpha}{\pi} \frac{2}{v} \left[ (1 - v)(L_f - 1) + \ln(1 - v) + \frac{1}{2} v^2 L_f \right]. \quad (\text{C.212})$$

Soft photon exponentiation is described by the following replacements for the initial state terms:

$$\bar{s}_e = \bar{S}_e = Q_e^2 \frac{\alpha}{\pi} \left[ \frac{3}{2}(L_e - 1) + \frac{1}{3}\pi^2 - \frac{1}{2} \right], \quad (\text{C.213})$$

$$\bar{h}_e(v) = h_e(v) - \frac{\beta_e}{v}, \quad (\text{C.214})$$

$$\bar{H}_e(v) = H_e(v) - \frac{\beta_e}{v}. \quad (\text{C.215})$$

The soft cross sections become modified:

$$\int_0^1 dv \sigma_{T,FB}(s') [\delta(v)(1 + S_e) + \theta(v - \epsilon) \frac{\beta_e}{v}] \rightarrow (1 + \bar{S}_e) \int_0^1 dv \sigma_{T,FB}(s') [\beta_e v^{\beta_e - 1}]. \quad (\text{C.216})$$

The term  $\theta(v - \epsilon) \frac{\beta_e}{v}$  comes from the hard parts, so that these have to be modified as in (C.214) and (C.215).

An important phenomenological remark is the following. It is known that, at the  $Z$  peak, soft photon emission dominates hard photon emission. This is because the emission of hard photons moves the  $\sigma(s')$  away from the peak, making it thus rapidly smaller. Further, for soft emission  $v$  is being small. For small  $v$ , the hard initial state kernels  $H_e(v)$  and  $h_e(v)$  approach each other, see C.207 and C.210. The consequence is that at the  $Z$  peak the radiation due to  $\sigma_T$  and due to  $\sigma_{FB}$  are much alike. This explains that the  $A_{FB}$  has small radiative corrections at the  $Z$  peak; a well-known phenomenon. Further, helicity asymmetries have same-type QED corrections in numerator and denominator, and thus get practically no photonic corrections; also a well-known fact.

## Acknowledgement

We would like to thank Janusz Gluza for his contribution in an early stage of the write-up.

## 5 The event generator BABAYAGA

**Authors:** C.M. Carloni Calame, G. Montagna, O. Nicrosini, F. Piccinini

**Corresponding Author:** F. Piccinini [fulvio.piccinini@pv.infn.it]

The Monte Carlo event generator `BabaYaga` has been developed for high precision simulation of QED processes ( $e^+e^- \rightarrow e^+e^-$ ,  $e^+e^- \rightarrow \mu^+\mu^-$  and  $e^+e^- \rightarrow \gamma\gamma$ ) at flavour factories, chiefly for luminometry purposes, with an estimated theoretical accuracy at the 0.1% level or better. QED radiative corrections are included by means of a Parton Shower in QED matched with exact next-to-leading order corrections to reach the required accuracy. The latter is assessed by means of consistent comparisons to independent calculations and an estimate of the size of missing higher-order corrections. The main theoretical framework is overviewed and the status of the generator is summarized. Some possible developments of the generator for FCC-ee physics are addressed and considered.

### 5.1 Introduction

The knowledge of the luminosity  $\mathcal{L}$  is an important ingredient for any measurement at  $e^+e^-$  machines. The common strategy is to calculate it through the relation  $\mathcal{L} = N_{obs}/\sigma_{th}$ , where  $\sigma_{th}$  is the theoretical cross section of a QED process, namely  $e^+e^- \rightarrow e^+e^-$  (Bhabha),  $e^+e^- \rightarrow \mu^+\mu^-$  or  $e^+e^- \rightarrow \gamma\gamma$ , and  $N_{obs}$  is the number of observed events. QED processes are the best choice because of their clean signal, low background and the possibility to push the theoretical accuracy up to the 0.1% level or better. The latter requires the inclusion of the relevant radiative corrections (RCs) in the cross sections calculation and their implementation into Monte Carlo (MC) event generators (EGs) in order to easily account for realistic event selection criteria.

Modern EGs used for luminometry simulate QED processes by including the exact next-to-leading order (NLO) QED corrections and/or a leading-logarithmic (LL) approximation of higher-order (h.o.) effects [227–235]. The consistent inclusion and matching of NLO and h.o. LL contributions is mandatory in view of the required theoretical accuracy. In the following, it is discussed how this is achieved and implemented in the `BabaYaga` EG.

### 5.2 The event generator BABAYAGA and BABAYAGA@NLO

The EG `BabaYaga` was originally developed for the precise simulation of large-angle Bhabha scattering at low energy  $e^+e^-$  colliders, with center of mass energy up to 10 GeV. It was later extended to simulate also  $\mu^+\mu^-$  and  $\gamma\gamma$  final states in the same energy regime. For the sake of clarity, in this section we focus on Bhabha scattering as reference process to discuss the theoretical framework of the generator.

In its first version [227, 228], the generator relied upon a QED Parton Shower (PS) to account for the LL photonic corrections, resummed up to all orders in perturbation theory. The PS is a MC algorithm which gives an exact iterative solution of the Dokshitzer-Gribov-Lipatov-Altarelli-Parisi (DGLAP) equation in QED for the non-singlet QED structure function (SF)  $D(x, Q^2)$ , which reads

$$\begin{aligned} Q^2 \frac{\partial}{\partial Q^2} D(x, Q^2) &= \frac{\alpha}{2\pi} \int_x^1 \frac{dy}{y} P_+(y) D\left(\frac{x}{y}, Q^2\right) \\ P_+(x) &= \frac{1+x^2}{1-x} - \delta(1-x) \int_0^1 dt P(t), \end{aligned} \quad (\text{C.217})$$

where  $P_+(x)$  is the regularized Altarelli-Parisi vertex,  $x$  is the fraction of energy lost because of radiation and  $Q^2$  is the scale of the process. The QED SFs account for photon radiation emitted by both initial-state and final-state fermions and allow to include the universal virtual and real photonic corrections, resummed up to all orders of perturbation theory. The advantage of the PS solution is that the kinematics of the emitted photons can be recovered (within some approximation) and hence an exclusive event generation can be performed, *i.e.* all the momenta of the final state particles (fermions and an indefinite number of photons) can be reconstructed.

Within the SF approach the corrected cross section can be written as

$$\sigma(s) = \int dx_1 dx_2 dy_1 dy_2 \int d\Omega \times D(x_1, Q^2) D(x_2, Q^2) D(y_1, Q^2) D(y_2, Q^2) \times \frac{d\sigma_0(x_1 x_2 s)}{d\Omega} \Theta(cuts). \quad (\text{C.218})$$

Despite its advantages, the PS is intrinsically accurate at the LL level and a precision better than 0.5-1% can not be expected in the calculation of the cross section (C.218). In order to improve the accuracy, a matching with the exact NLO RCs is mandatory, in such a way that the features of the PS are preserved (*i.e.* exclusive event generation and resummation of LL corrections up to all orders) while avoiding the double counting of the  $\mathcal{O}(\alpha)$  LL corrections, present both in the PS approach and in the NLO calculation.

An original matching algorithm has been implemented in the latest version of BabaYaga [229–231] (BabaYaga@NLO), which includes exact NLO corrections into a PS framework and achieves an accuracy at the 0.1% level in the calculation of the cross sections.

Without spelling out the details, the fully differential PS cross section implicit in Eq. (C.218) can be recast in the form

$$d\sigma_{PS}^\infty = \Pi(Q^2, \varepsilon) \sum_{n=0}^{\infty} \frac{1}{n!} |\mathcal{M}_{n,PS}|^2 d\Phi_n, \quad (\text{C.219})$$

where  $\Pi(Q^2, \varepsilon)$  is the Sudakov form factor accounting for virtual and soft (up to  $x = \varepsilon$ ) radiation,  $\mathcal{M}_{n,PS}$  is the amplitude for the emission of  $n$  real photons in the PS approximation and  $d\Phi_n$  is the exact phase space for the emission of  $n$  real photons (with  $x \geq \varepsilon$ ), divided by the incoming flux factor. Eq. (C.219) can be improved to include the missing NLO contributions by defining the following correction factors

$$\begin{aligned} F_{SV} &= 1 + \frac{d\sigma_{SV}^{NLO} - d\sigma_{SV}^{[\alpha, PS]}}{d\sigma_0} \\ F_{i,H} &= 1 + \frac{d\sigma_{i,H}^{NLO} - d\sigma_{i,H}^{[\alpha, PS]}}{d\sigma_{i,H}^{[\alpha, PS]}}, \end{aligned} \quad (\text{C.220})$$

where  $SV$  stands for soft and virtual photon corrections,  $H$  for non-soft real photon corrections,  $[\alpha, PS]$  stands for the  $\mathcal{O}(\alpha)$  expansion of the PS contribution,  $i$  runs over the emitted photons and  $d\sigma_0$  is the lowest-order differential cross section. With these definitions, the matched differential cross section can be written in the form

$$d\sigma_{matched}^\infty = \Pi(Q^2, \varepsilon) F_{SV} \sum_{n=0}^{\infty} \frac{1}{n!} |\mathcal{M}_{n,PS}|^2 F_{n,H} d\Phi_n, \quad (\text{C.221})$$

which is the master formula according to which event generation and cross section calculation are performed in BabaYaga@NLO.

A few comment are in order with respect to the master formula (C.221):

1. by construction, the factors in Eq. (C.220) are infrared and collinear safe quantities and they let the  $\mathcal{O}(\alpha)$  expansion of  $d\sigma_{matched}^\infty$  in Eq. (C.221) coincide with the exact NLO result;
2. the resummation of h.o. LL corrections is preserved;
3. the correction factors (C.220) tend to be larger in those phase space regions where the PS is more unreliable, typically in phase space regions where the photon is hard and not collinear to one of the charged particles;
4. Eq. (C.221) is cast in a completely differential form, so that events can be generated exclusively as in the pure PS approach;

5. the theoretical error is shifted to corrections of order  $\alpha^2$ , *i.e.* at the next-to-next-to-leading-order (NNLO) level.

Eq. (C.221) is used in `BabaYaga@NLO` to generate events for Bhabha,  $e^+e^- \rightarrow \mu^+\mu^-$  and  $e^+e^- \rightarrow \gamma\gamma$  [231] processes, with an indefinite number of extra photons to account for NLO and h.o. QED radiative corrections. Some numerical results and the estimate of the theoretical accuracy of the approach are sketched in the next sections.

### 5.3 Results and estimate of the theoretical error at flavour factories

Table (C.1) shows the impact of different classes of QED RCs in the determination of large-angle Bhabha cross section within typical event selection criteria used for luminometry at flavour factories. Setups *a-b* correspond to  $\sqrt{s} = 1.02$  GeV and *c-d* to  $\sqrt{s} = 10$  GeV, for large (*a-c*) and narrower (*b-d*) angular acceptance cuts. In Ref. [230] the detailed description of the setups, which tend to select elastic events, is reported.

setup	<i>a</i>	<i>b</i>	<i>c</i>	<i>d</i>
$\sigma_0$	6855.74	529.463	71.333	5.502
$\sigma_{0,VP}$	6976.5	542.66	74.763	5.8552
$\sigma_{NLO}$	6060.1	451.523	59.90	4.425
$\sigma_{PS}^\alpha$	6083.6	454.50	60.14	4.456
$\sigma_{PS}^\infty$	6107.6	458.44	60.62	4.530
$\sigma_{matched}^\infty$	6086.7	455.86	60.42	4.504

Table C.1: Bhabha cross section (in nb) according to different precision levels. The table is taken from Ref. [230], where also the experimental setups are detailed.

The first row of table (C.1) is the lowest order cross section, the second includes the effects of vacuum polarization (VP), the third one is the exact NLO result, the fourth is the  $\mathcal{O}(\alpha)$  expansion of Eq. (C.219) (*i.e.*, the PS approximation of the NLO result), the fifth is Eq. (C.219) and the last one corresponds to the most accurate matched formula of Eq. (C.221). By comparing the cross sections calculated at different theoretical accuracies, it can be inferred that VP affects the cross section at some per-cent level, fixed  $\mathcal{O}(\alpha)$  QED corrections at the 10-20% level and h.o. QED corrections have an impact of 0.5-1.5%: all these classes of corrections are important to achieve the theoretical precision required by the experiments and are consistently included and simulated in `BabaYaga@NLO` by means of the master formula (C.221).

In order to assess the theoretical accuracy of the approach implemented in `BabaYaga@NLO`, an important step is performing tuned comparisons to independent MC EGs.

As an example, in Figs. (C.6) and (C.7), the acollinearity and final-state invariant mass distributions obtained by `BabaYaga@NLO` and the independent EG `Bhwide` [232] are compared for setup *a*. While the difference on the integrated cross sections is below the 0.01% level, some differences at the 1% level appear (see the insets in the figures) in the differential distributions and are due to the different theoretical frameworks on which the two EGs are based. However, it is worth noticing that such differences appear where the differential cross section drops by several order of magnitude with respect to the elastic region and where the different treatment of hard radiation beyond NLO can have an impact.

A further step to estimate the theoretical accuracy is to compare with existing calculations of the NNLO corrections to Bhabha scattering, which have been published over the years [140, 141, 180, 236–242] (see also Ref. [174] and references therein). The dominant part of such corrections are already included in the master formula (C.221), which can be expanded up to NNLO and whose NNLO terms can be unambiguously compared to analytical exact results: any difference should be considered as a theoretical error in the formulation of `BabaYaga@NLO`. A detailed and non-trivial comparison has been carried out in Ref. [230], finding that the

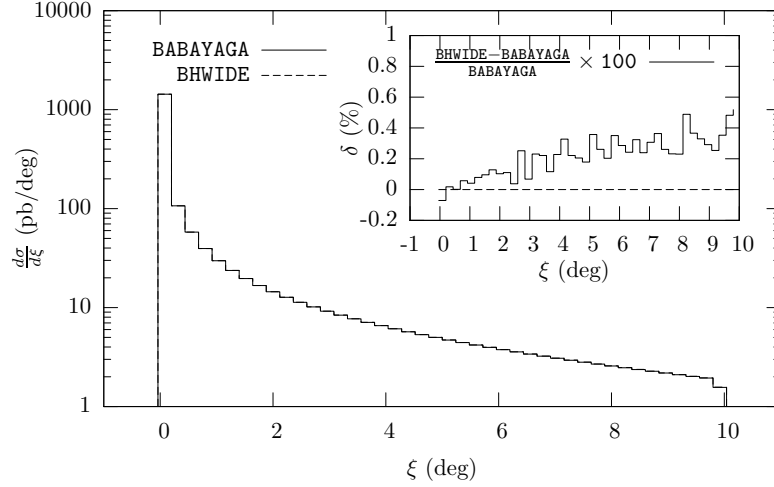


Fig. C.6: Comparison between BabaYaga@NLO and Bhwide on the acollinearity distribution.

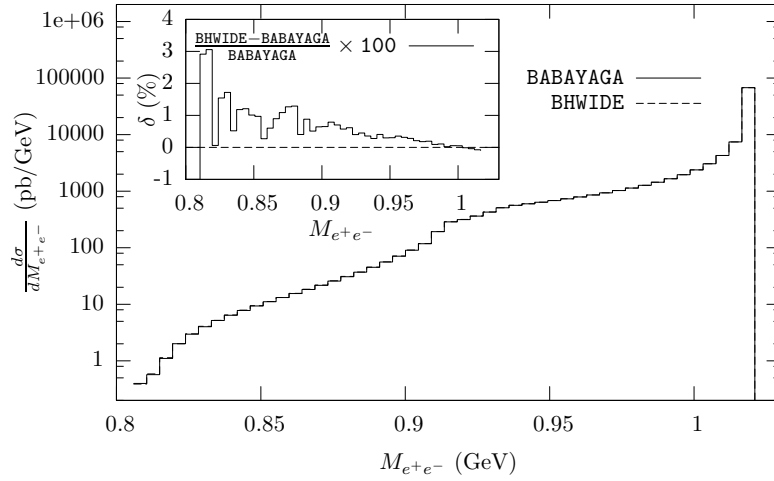


Fig. C.7: Comparison between BabaYaga@NLO and Bhwide on the final-state invariant mass distribution.

NNLO corrections not included in Eq. (C.221) impact the cross section at the level of few units in  $10^{-4}$ , when typical event selection criteria are taken into account.

In the Luminosity section of Ref. [174], also other sources of theoretical uncertainties were considered, such as the uncertainty on the hadronic contribution to VP and extra light-pair emission (for which see also Refs. [175, 176]). The main conclusion of that section is that a sound estimate of the present theoretical error on the luminosity determination via Bhabha scattering at flavour factories lies in the region of 0.1% or slightly below, which is enough for the present experimental requirements. Any further improvement would require the inclusion of the full exact NNLO RCs into MC EGs for Bhabha scattering, matched with LL h.o. contributions. This should be considered a feasible, although not trivial, task.

In a similar way, the matching algorithm of Eq. (C.221) has been also applied to the  $e^+e^- \rightarrow \gamma\gamma$  process and a phenomenological study at flavour factories has been presented in Ref. [231].

As an example, in table (C.2) the impact of different classes of radiative corrections for typical event selection criteria at flavour factories is shown, in analogy with table (C.1) for Bhabha scattering. In the  $e^+e^- \rightarrow \gamma\gamma$  case, the impact of NLO RC is in the 5-10% range while h.o. corrections change the cross sections by 0.1-0.5%: both effects must be accounted for to reach a theoretical accuracy at the 0.1% level. To the best of our



$\sqrt{s}$ (GeV)	1	3	10
$\sigma_0$	137.53	15.281	1.3753
$\sigma_{PS}^\alpha$	128.55	14.111	1.2529
$\sigma_{NLO}$	129.45	14.211	1.2620
$\sigma_{PS}^\infty$	128.92	14.169	1.2597
$\sigma_{matched}$	129.77	14.263	1.2685

Table C.2: Photon pair production cross sections (in nb) to different accuracy levels (from Ref. [231], see there for details).

knowledge, `BabaYaga@NLO` is the only MC EG implementing a matching of NLO and h.o. corrections in a PS approach for the  $\gamma\gamma$  final state, being able to reach such a theoretical accuracy.

It is worth also mentioning that an extension of `BabaYaga` has been developed for dark photon searches at low energy via the radiative return method [243] and has been extensively used by the KLOE-2 collaboration to set limits on the dark photon couplings and mass [244, 245].

Furthermore, it is planned to exploit the same theoretical framework described above for the development of a high-precision EG for the QED process  $\mu e \rightarrow \mu e$ , which is needed for the measurement of the hadronic contribution to the running of  $\alpha_{QED}$  in the space-like region and, in turn, for an independent determination of the leading order hadronic corrections to the muon anomalous magnetic moment. The proposed experiment ( $\mu one e$ ) and the underlying ideas are discussed in Refs. [246, 247].

#### 5.4 Exploratory results at FCC-ee

In this section we present some exploratory and preliminary results obtained with `BabaYaga@NLO` at FCC-ee, considering different scenarios for its center-of-mass energy, namely  $Z$  peak ( $\sqrt{s} = 91$  GeV),  $WW$  threshold ( $\sqrt{s} = 160$  GeV), above  $ZH$  threshold ( $\sqrt{s} = 240$  GeV) and  $t\bar{t}$  threshold ( $\sqrt{s} = 350$  GeV). The aim is to show some phenomenological results in view of a luminosity monitoring with Bhabha scattering at small angles or with the  $e^+e^- \rightarrow \gamma\gamma$  process at large angles. At this stage, we refrain from firmly assessing the achievable theoretical precision in the calculation of the cross-section. From past experience, it is beyond dispute that going below the 0.1-0.05% accuracy will require the inclusion of the complete set of NNLO QED corrections, together with the resummation of higher-orders.

$\sqrt{s}$ (GeV)	91	160	240	350
$\sigma_0^{VP}$ (nb)	36.0030	11.8062	5.28998	2.50709
+ $Z$	+0.064%	−0.062%	−0.044%	−0.030%
+ QED NLO	−17.41%	−18.73%	−19.57%	−20.35%
+ QED h.o.	+0.54%	+0.66%	+0.71%	+0.77%
$VP$	+5.17%	+6.27%	+7.14%	+7.99%
$\pm\delta\Delta\alpha_h(q^2)$	$\pm 0.021\%$	$\pm 0.027\%$	$\pm 0.030\%$	$\pm 0.032\%$

Table C.3: Small-angle Bhabha cross section at FCC-ee for different center-of-mass energies.

In table (C.3), the Bhabha cross section (in nb) is reported for different energies, calculated by requiring that the final state  $e^-$  lies between  $3^\circ$  and  $6^\circ$ , the final state  $e^+$  lies between  $174^\circ$  and  $176^\circ$  and the product of their energies  $E^+ E^-$  is larger than  $0.2 \times s$ . The first row is the QED tree-level cross section (improved with VP effects), the second row shows the impact of the inclusion of the  $Z$ -exchange tree-level diagrams, the third one the impact of QED NLO RCs and the fourth represents the higher-order QED corrections, as implemented in

BabaYaga@NLO. It can be seen that  $Z$  contributions are at some 0.01% level, that NLO QED RCs change the cross section by 15-20% and the size of higher-orders is at the 0.5-1% level. The last two rows at the bottom of the table show the effect of VP (which first enters at NLO in Bhabha process) and the uncertainty induced on the integrated cross section by the error on the hadronic contribution to VP<sup>29</sup>. We stress that the error in the hadronic part of VP induces by itself an uncertainty at some  $10^{-4}$  level, which can become a limiting factor in the knowledge of the theoretical cross section in view of a very precise luminosity determination. Since the hadronic contribution on VP relies through dispersion relations and the optical theorem on the measurement of  $e^+e^- \rightarrow \text{hadrons}$  cross sections at low energies, any future improvement on this respect is of critical importance.

Alternatively, the luminosity could be monitored with the  $e^+e^- \rightarrow \gamma\gamma$  process, which is not affected, at least up to NNLO, by VP hadronic errors (nor by  $Z$  “contamination”) and in BabaYaga@NLO is simulated with the same theoretical accuracy as the Bhabha scattering, as far as photonic RCs are concerned [231].

$\sqrt{s}$ (GeV)	91	160	240	350
$\sigma_0$ (pb)	60.962	19.785	8.793	4.135
+ QED NLO	−8.61%	−9.06%	−9.40%	−9.71%
+ QED h.o.	−0.37%	−0.41%	−0.42%	−0.44%

Table C.4: Large-angle  $e^+e^- \rightarrow \gamma\gamma$  cross section at FCC-ee for different center-of-mass energies.

In table (C.4) the cross section for the  $e^+e^- \rightarrow \gamma\gamma$  process at large angles is shown as a function of the collider energy, where we consider events with at least two photons between  $10^\circ$  and  $170^\circ$  and requiring the product of the energies of the two most energetic ones (falling in the angular range)  $E_1 E_2$  to be larger than  $0.2 \times s$ . We notice that the cross section is a factor  $\sim 500$  smaller than the small-angle Bhabha process considered above and that the impact of different classes of radiative corrections is roughly a factor of two smaller than in the previous case. From these preliminary considerations on  $\gamma\gamma$  final state, we remark that it is a promising and complementary alternative to Bhabha scattering as luminosity monitor and it is worth being studied in more detail [250, 251].

## 5.5 Conclusions

The theoretical framework of the BabaYaga and BabaYaga@NLO event generators has been overviewed and summarized. BabaYaga@NLO is a Monte Carlo event generator developed for high-precision simulation of QED processes (Bhabha scattering,  $e^+e^- \rightarrow \mu^+\mu^-$  and  $e^+e^- \rightarrow \gamma\gamma$ ) at flavour factories, mainly for luminometry purposes, and it is based on an original algorithm to match exact NLO with higher-order QED radiative corrections in a Parton Shower approach. Within typical event selection criteria for luminometry at flavour factories, the cross sections can be calculated with an overall theoretical error at the level of 0.1% or better. The assessment and the scrutiny of the theoretical error are based on consistent and detailed comparisons with independent generators and existing exact NNLO calculations of the relevant radiative corrections.

The generator can be used also to study QED processes at FCC-ee, and we showed some exploratory results for small-angle Bhabha scattering and large-angle  $e^+e^- \rightarrow \gamma\gamma$  process. We notice that the error on the hadronic part of VP, as known in the present parameterizations, could become a limiting factor on the precise knowledge of the Bhabha cross section with an accuracy at the  $10^{-4}$  level. We thus advocate the study of the large-angle  $e^+e^- \rightarrow \gamma\gamma$  process as an alternative way to monitor the FCC-ee collider luminosity.

An assessment of the theoretical accuracy of BabaYaga/BabaYaga@NLO for FCC-ee predictions at the sub per mille level would require the inclusion in the code of pure weak and QED NNLO corrections.

<sup>29</sup>We used the routine (2012 version) developed by Prof. Fred Jegerlehner to evaluate the hadronic contribution to VP and its errors [248, 249].

## 6 BHLUMI: The path to 0.01% theoretical luminosity precision

**Authors:** S. Jadach, W. Placzek, M. Skrzypek, B.F.L. Ward, S.A. Yost

Corresponding Author: Stanisław Jadach [Stanislaw.Jadach@cern.ch]

### 6.1 Introduction

The current status of the theoretical precision for the Bhabha luminometry is critically reviewed and pathways are outlined to the requirement targeted by the FCC-ee precision studies. Various components of the pertinent error budget are discussed in detail – starting from the context of the LEP experiments, through their current updates, up to prospects of their improvements for the sake of the FCC-ee. It is argued that with an appropriate upgrade of the Monte Carlo event generator `BHLUMI` and/or other similar MC programs calculating QED effects in the low angle Bhabha (LABH) process  $e^-e^+ \rightarrow e^-e^+$ , the total theoretical error of 0.01% for the luminometry at the high luminosity FCCee machine [252] can be reached. Possible ways of this upgrade are also discussed.

In Section 6.2 we recap the main aspects of the theoretical precision in the LEP luminosity measurement and present important components of the corresponding error budget. In Section 6.3 we present current improvements on some of the above components. In Section 6.4 we discuss in detail prospects on reaching the 0.01% theory precision for the FCCee luminometry and outline ways of upgrading the main Monte Carlo program for this purpose, `BHLUMI`, in this respect. Finally, in Section 6.5 we briefly summarize our work.

### 6.2 Theoretical uncertainty in LEP luminometry, A.D. 1999

Let us recapitulate the essential aspects of the theory (mainly QED) uncertainty in the LEP luminometry, as seen A.D. 1999. Luminosity measurements of all four LEP collaborations at CERN and also of SLD at SLAC relied on theoretical predictions for the low-angle Bhabha process obtained using the `BHLUMI` Monte Carlo multiphoton event generator featuring a sophisticated QED matrix element with soft photon resummation. Its version 2.01 was published in 1992 (see ref. [253]) and the upgraded version 4.04 was published in ref [254].

Type of correction/error	LEP1		LEP2	
	1996	1999	1996	1999
(a) Missing photonic $\mathcal{O}(\alpha^2)$ [255, 256]	0.10%	0.027%	0.20%	0.04%
(b) Missing photonic $\mathcal{O}(\alpha^3 L_e^3)$ [257]	0.015%	0.015%	0.03%	0.03%
(c) Vacuum polarization [248, 258]	0.04%	0.04%	0.10%	0.10%
(d) Light pairs [259, 260]	0.03%	0.03%	0.05%	0.05%
(e) $Z$ and $s$ -channel $\gamma$ [261, 262]	0.015%	0.015%	0.0%	0.0%
Total	0.11% [262]	0.061% [263]	0.25% [262]	0.12% [263]

Table C.5: Summary of the total (physical+technical) theoretical uncertainty for a typical calorimetric detector. For LEP1, the above estimate is valid for a generic angular range within  $1^\circ$ – $3^\circ$  (18–52 mrad), and for LEP2 energies up to 176 GeV and an angular range within  $3^\circ$ – $6^\circ$ . Total uncertainty is taken in quadrature. Technical precision included in (a).

The theoretical uncertainty of the `BHLUMI` Bhabha prediction, initially rated at 0.25% [264], was re-evaluated in 1996 after extensive tests and debugging to be 0.16% [265]. From that time, the code of `BHLUMI` version 4.04 used by all LEP collaborations in their data analysis remains frozen. The following re-evaluation of its precision came from investigations using external calculations outside the `BHLUMI` code. For instance, the 0.11% estimate of ref. [262], was based on better estimations of the QED corrections missing in `BHLUMI` and on improved knowledge of the vacuum polarization contribution. The detailed composition of the final estimate of the theoretical uncertainty  $\delta\sigma/\sigma \simeq 0.061\%$  of the `BHLUMI` 4.04 prediction, based on published

works, is shown in Table C.5, following ref. [263]. This value was used in the final LEP1 data analysis in ref. [11]. On the other hand, at LEP2 the experimental error was substantially larger than the QED uncertainty of the Bhabha process listed in Table C.5, where we define  $L_e = \ln(|t|/m_e^2)$ .

All four LEP collaborations were quoting the experimental luminosity errors for LEP1 data below 0.05%, that is below the theoretical error. The best experimental luminosity error 0.034% was quoted by the OPAL collaboration<sup>30</sup> – they also quoted a slightly smaller theory error, 0.054%, thanks to use of improved light-fermion-pair calculations of refs. [267, 268]; see also the review article [269] and workshop presentations [270, 271].

### 6.3 Present status (2018)

From the end of LEP until the present time there has been limited progress on practical calculations for low-angle Bhabha scattering at energies around and above the  $Z$  resonance<sup>31</sup>. A new Monte Carlo generator *BabaYaga* based on the parton shower algorithm was developed [227, 228, 230, 269]. It was intended mainly for low energy electron–positron colliders with  $\sqrt{s} \leq 10$  GeV, claiming precision at 0.1%, but was not validated for energies near the  $Z$  peak.

There was, however, a steady improvement in the precision of the vacuum polarization in the  $t$ -channel photon propagator; see the recent review in the FCCee workshop [272]. Using the uncertainty  $\delta\Delta_{had.}^{(5)} = 0.63 \cdot 10^{-4}$  at  $\sqrt{-t} = 2$  GeV quoted in Ref. [113] one obtains  $\delta\sigma/\sigma = 1.3 \cdot 10^{-4}$ . It is shown in the second column in Table C.6, marked "Update 2018". The improvement of the light-pair corrections of refs. [267, 268] is also taken into account there.

Type of correction / Error	1999	Update 2018
(a) Photonic $\mathcal{O}(L_e\alpha^2)$	0.027% [256]	0.027%
(b) Photonic $\mathcal{O}(L_e^3\alpha^3)$	0.015% [257]	0.015%
(c) Vacuum polariz.	0.040% [248, 258]	0.013% [272]
(d) Light pairs	0.030% [260]	0.010% [267, 268]
(e) $Z$ and $s$ -channel $\gamma$ exchange	0.015% [261, 262]	0.015%
(f) Up-down interference	0.0014% [273]	0.0014%
(f) Technical Precision	–	(0.027)%
Total	0.061% [263]	0.038%

Table C.6: Summary of the total (physical+technical) theoretical uncertainty for a typical calorimetric LEP luminosity detector within the generic angular range of 18–52 mrad. Total error is summed in quadrature.

The important point is that the technical precision, which is marked in parentheses as 0.027%, is not included in the sum, because according to ref. [262] it is included in the uncertainty of the photonic corrections. Future reduction of the photonic correction error will require a clear separation of the technical precision from other uncertainties and it may turn out to be a dominant one.

### 6.4 Path to 0.01% precision for FCC-ee

In the following we shall describe what steps are needed on the path to the  $\leq 0.01\%$  precision required for the low-angle Bhabha (LABH) luminometry at the FCC-ee experiments. The last column in Table C.7 summarizes

<sup>30</sup>The OPAL collaboration has found all their experimental distributions for low-angle Bhabha data to be in a striking agreement with the *BHLUMI* Monte Carlo simulation [266].

<sup>31</sup> This is in spite of a considerable effort on the  $\mathcal{O}(\alpha^2)$  so-called "fixed-order" (without resummation) QED calculations for the Bhabha process; see below for more discussion.

this goal component-by-component in the precision forecast for the FCC-ee luminometry. We will also specify all improvements in the next version BHLUMI which could bring us to the FCC-ee precision level.

Type of correction / Error	Update 2018	FCC-ee forecast
(a) Photonic $\mathcal{O}(L_e^4 \alpha^4)$	0.027%	$0.6 \times 10^{-5}$
(b) Photonic $\mathcal{O}(L_e^2 \alpha^3)$	0.015%	$0.1 \times 10^{-4}$
(c) Vacuum polariz.	0.014% [272]	$0.6 \times 10^{-4}$
(d) Light pairs	0.010% [267, 268]	$0.5 \times 10^{-4}$
(e) $Z$ and $s$ -channel $\gamma$ exchange	0.090% [261]	$0.1 \times 10^{-4}$
(f) Up-down interference	0.009% [273]	$0.1 \times 10^{-4}$
(f) Technical Precision	(0.027)%	$0.1 \times 10^{-4}$
Total	0.097%	$1.0 \times 10^{-4}$

Table C.7: Anticipated total (physical+technical) theoretical uncertainty for a FCC-ee luminosity calorimetric detector with the angular range being 64–86 mrad (narrow), near the  $Z$  peak. The total error is summed in quadrature.

Before coming to the details of the envisaged improvements in QED calculations for the LABH process, let us recapitulate briefly basic features of the LABH luminometry which have to be kept in mind in QED perturbative calculations for FCC-ee. First of all, the largest photonic QED effects due to multiple real and virtual photon emission are strongly cut-off dependent. Event acceptance of the LABH luminometer is quite complicated, and cannot be dealt with analytically, hence a Monte Carlo implementation of QED perturbative results is mandatory. The LABH detector at FCC-ee will be similar to that of LEP, with calorimetric detection of electrons and photon (not distinguishing them) within the angular range  $(\theta_{\min}, \theta_{\max})$  on opposite sides of the collision point [250]. The detection rings are divided into small cells and the angular range on both sides is slightly different in order to minimize QED effects. The angular range at FCCee is planned to be 64–86 mrad (narrow) [250] while at LEP it was typically 28–50 mrad (narrow range, ALEPH/OPAL silicon detector); see Fig. 2 in ref. [265] (also Fig. 16 in ref. [274]) for an idealized detection algorithm of the generic LEP silicon detector. The average  $t$ -channel transfer near the  $Z$  resonance will be  $|\bar{t}|^{1/2} = \langle |t| \rangle^{1/2} \simeq 3.25$  GeV at FCC-ee instead of 1.75 GeV at LEP.<sup>32</sup> The important scale factor controlling photonic QED effects,  $\gamma = \frac{\alpha}{\pi} \ln \frac{|\bar{t}|}{m_e^2} = 0.042$  for FCC-ee, that is only slightly greater than 0.039 for LEP. On the other hand, the factor  $x = |t|/s$  suppressing  $s$ -channel contributions will be  $1.27 \times 10^{-3}$ , significantly larger than  $0.37 \times 10^{-3}$  for LEP.

Finally, let us remark that the process  $e^+e^- \rightarrow 2\gamma$  is also considered for FCC-ee luminometry, see refs. [231, 269] for more discussion on the QED radiative corrections to this process.

#### 6.4.1 Photonic higher-order and subleading corrections

Photonic corrections (items (a) and (b) in Table C.6) are large but they are mainly due to collinear and soft singularities which are known in QED at any perturbative order, hence can be resummed. The cross section of the LABH luminometer is highly sensitive to emission of real soft and collinear photons. Even relatively soft collinear photon emission in the initial state (ISR) may pull final electrons outside the acceptance angular range, while final-state photons can easily change the shape of the final state “calorimetric cluster”. This is why resummation of the multiple photon effects has to be implemented in an exclusive way, using the method of exclusive exponentiation (EEX), as in BHLUMI [254], or using the parton shower (PS) method as in BabaYaga [227]. It was shown [275] that, for instance, the so-called “fixed-order”  $\mathcal{O}(\alpha^2)$  calculations without resummation<sup>33</sup> are completely inadequate for the LABH luminometry, leaving out uncontrolled QED effects of the order  $\sim 0.5\%$  in the angular distribution, and even a few percent in some other important distributions.

<sup>32</sup> At 350 GeV, the FCC-ee luminometer will have  $|\bar{t}| = 12.5$  GeV.

<sup>33</sup>For instance, the calculations of refs. [141, 276].

Assuming that the technical precision is dealt with separately (see the discussion in the following Section 6.4.6), item (a) in Table C.6, missing in BHLUMI v. 4.04, scales like  $L_e = \ln(|t|/m_e^2)$ , where  $t$  is the relevant squared momentum transfer. However, this item will disappear from the error budget completely once the EEX matrix element of BHLUMI is upgraded to include  $\mathcal{O}(L_e\alpha^2)$  contributions, which are already known and published. In fact, these  $\mathcal{O}(L_e\alpha^2)$  corrections consist of 2-real photon contributions, 1-loop corrections to 1-real emission and 2-loop corrections. Efficient numerical and analytical methods of calculating the exact  $\mathcal{O}(\alpha^2)$  matrix element (spin amplitudes) for 2 real photons, keeping fermion masses, have been known for decades; see refs. [277, 278]. In ref. [279] exact 2-photon amplitudes were compared with the matrix element of BHLUMI.

Truly pioneering work on  $\mathcal{O}(L_e\alpha^2, L_e^0\alpha^2)$  virtual corrections to 1-photon distributions was done in ref. [255]. These were calculated neglecting interference terms between  $e^+$  and  $e^-$  lines, which near the  $Z$  peak are of the order of  $(\frac{\alpha}{\pi})^2 \frac{|t|}{s} L_e \sim 10^{-7}$  times some logarithm of the cut-off. Let us note in passing that we know from the  $s$ -channel analog in [280] that the pure  $\mathcal{O}(L_e\alpha^2)$  correction of this class (neglecting the  $\mathcal{O}(L_e^0\alpha^2)$  term) is amazingly compact – it consists of merely a 3-line formula at the amplitude level. Let us add for completeness that the above correction was also calculated numerically in ref. [281].

Finally, in ref. [263], the two-loop  $\mathcal{O}(L_e\alpha^2)$   $t$ -channel photon form-factor relevant for the LABH process (keeping in mind  $|t|/s$  suppression) continued analytically from the known  $s$ -channel result of ref. [282] was added, thus accounting for the complete  $\mathcal{O}(L_e\alpha^2)$  photonic correction, known but not included in the MC BHLUMI v4.04. Once the above well-known photonic  $\mathcal{O}(L_e\alpha^2)$  part is added in the future upgrade of the EEX matrix element in BHLUMI, the corresponding item will disappear from the list of the projected FCC-ee luminometry uncertainties in Table. C.7.

In view of the above discussion, it is clear that the major effort of calculating the complete  $\mathcal{O}(\alpha^2)$  QED correction to low and wide-angle Bhabha processes in refs. [141, 240, 276, 283], see also [181, 186, 187, 284], is of rather limited practical importance for the LABH luminometry at FCC-ee<sup>34</sup>. All these works essentially add previously unknown  $\mathcal{O}(L_e^0\alpha^2)$  corrections, which are of order  $\sim 10^{-5}$ . Their size should be checked<sup>35</sup> using auxiliary programs outside the BHLUMI Monte Carlo, in order to be listed among QED uncertainties in the uncertainty budget as in our Table. C.7. In any case, we expect corrections of this class to stay well below  $10^{-4}$ , and most likely there will be no need to add the complete  $\mathcal{O}(L_e^0\alpha^2)$  corrections to the matrix element of any MC for the LABH process.

Another important photonic correction listed as item (b) in Table C.5 as an uncertainty of BHLUMI is the  $\mathcal{O}(\alpha^3 L_e^3)$  correction (third order LO). It is already known from Ref. [257, 285] and is currently omitted from v. 4.04 of BHLUMI, although already included in the LUMLOG part of BHLUMI. Given its already known size, we would need to implement this third order leading-order result into the EEX matrix element of BHLUMI, and it will disappear from the uncertainty list. Once it is done, the uncertainty due to  $\mathcal{O}(\alpha^4 L_e^4)$  and  $\mathcal{O}(\alpha^3 L_e^2)$  should be estimated and included in the list of photonic uncertainties of BHLUMI with the upgraded EEX matrix element. We can use the scaling rules indicated in the previous discussion to estimate an error due to missing  $\mathcal{O}(\alpha^4 L_e^4)$  as  $0.015\% \times \gamma = 0.6 \times 10^{-5}$  near the  $Z$  peak. The scale of the missing  $\mathcal{O}(\alpha^3 L_e^2)$  is also of a similar order,  $\gamma^2 \alpha / \pi \simeq 10^{-5}$ , and its actual estimate is currently highly uncertain.

The so called up-down interference between photon emission from  $e^+$  and  $e^-$  lines was calculated in ref. [273] at  $\mathcal{O}(\alpha^1)$  to be roughly  $\delta\sigma/\sigma \simeq 0.07 |t|/s$ . At LEP1 its contribution is negligible, see Table C.6, but at the FCCee luminometer it will be the factor of 10 larger and has to be included in the matrix element of the upgraded BHLUMI. Once it is done, its uncertainty should be again negligible, as indicated in Table C.7, where we used  $2\gamma \times 0.07 |t|/s$  as a crude estimator of its future uncertainty.

<sup>34</sup>They are more relevant for the wide-angle Bhabha, provided they are included in the MC with soft-photon resummation. However, this is rather problematic, because in all these works soft-real-photon contributions are added to loop corrections *à la* Bloch–Nordsieck, instead of subtracting the well-known virtual form-factor from virtual loop results already at the amplitude level, before squaring them.

<sup>35</sup>This kind of correction is often enhanced by  $\pi^2$  factors.

### 6.4.2 EEX versus CEEX matrix element

BHLUMI multi-photon distributions obey a clear separation into exact Lorentz invariant phase space and squared matrix element. The matrix element is an independent part of the program and is currently built according to exclusive exponentiation (EEX) based on the Yennie–Frautshi–Suura [192] (YFS) soft photon factorization and resummation performed on the spin-summed squared amplitude. It includes complete  $\mathcal{O}(\alpha^1)$  and  $\mathcal{O}(L_e^2\alpha^2)$  corrections, neglecting interference terms between electron and positron lines, suppressed by a  $|t|/s$  factor.

Let us underline that the above EEX-style matrix element in BHLUMI has not been changed in the upgrades since version 2.01 [253]. As already said, we may continue this practice and introduce the results from Refs. [255, 257, 263, 285] into the EEX matrix element, that is  $\mathcal{O}(\alpha^2 L_e)$  and  $\mathcal{O}(\alpha^3 L_e^3)$ , neglecting again some  $\sim |t|/s$  terms.

On the other hand, using the same underlying multi-photon phase space MC generator of BHLUMI and exploiting the results from Refs. [255, 257, 263, 285], one could implement a more sophisticated matrix element of the CEEX [144] type, where CEEX stands for coherent exclusive exponentiation. In the CEEX resummation methodology, soft photon factors are factorized at the amplitude level and the matching with fixed order results is also done at the amplitude level (before squaring and spin-summing). The big advantage of CEEX over EEX is that the separation of the infrared (IR) parts and matching with the fixed-order result are much simpler and more transparent when done at the amplitude level – all IR cancellations for complicated interferences are managed automatically and numerically. The inclusion of the  $s$ -channel  $Z$  and photon exchange and  $t$ -channel  $Z$  exchange including  $\mathcal{O}(\alpha)$  corrections, soft photon interference between electron and positron lines, and all that would be much easier to take into account for CEEX than in the case of EEX. However, the inclusion of  $\mathcal{O}(\alpha^3 L_e^3)$  in CEEX will have to be worked out and implemented.

Summarizing, the CEEX version would allow a more systematic further development of the program as we move forward with the FCC-ee project. From this perspective, the CEEX version is preferable, although the improvement of the EEX matrix element should be also pursued. See some additional discussion in Sect. 6.4.6.

### 6.4.3 Error on hadronic vacuum-polarization contribution

The uncertainty of the low-angle Bhabha cross section due to imprecise knowledge of the QED running coupling constant of the  $t$ -channel photon exchange is simply  $\frac{\delta_{VP}\sigma}{\sigma} = 2\frac{\delta\alpha_{eff}(\bar{t})}{\alpha_{eff}(\bar{t})}$ , where  $\bar{t}$  is the average transfer of the  $t$ -channel photon. For the FCCee luminometer, it will be  $|\bar{t}|^{1/2} \simeq 3.5 \text{ GeV}$  near the  $Z$  peak and  $|\bar{t}|^{1/2} \simeq 13 \text{ GeV}$  at 350 GeV.

The uncertainty of  $\alpha_{eff}(t)$  is mainly due to the use of the experimental cross section  $\sigma_{had}$  for  $e^-e^+ \rightarrow \text{hadrons}$  below 10 GeV as an input to the (subtracted) dispersion relations. A comprehensive review of the corresponding methodology and the latest update of the results can be found in refs. [286, 287], see also the FCC-ee workshop presentation [272].

In the above works, the hadronic contribution to  $\alpha_{eff}$  from the dispersion relation is encapsulated in  $\Delta\alpha^{(5)}(-s_0)$ , where  $2 \text{ GeV} \leq s_0^{1/2} \leq 10 \text{ GeV}$  in order to minimize the dependence on  $\sigma_{had}(s)$ , such that the main contribution comes from  $s^{1/2} \leq 2 \text{ GeV}$ . Moreover, prospects of improving experimental data on  $\sigma_{had}(s)$  in this energy range are very good also, because the main contribution to the error in the measurement of the muon  $g - 2$  comes from the same cross section range [286].

The above works are focusing on the parameter range  $2 \text{ GeV} \leq s_0^{1/2} \leq 10 \text{ GeV}$ , which is accidentally of paramount interest for the FCC-ee luminometry, are part of a wider strategy in refs. [286, 287] of obtaining  $\alpha_{eff}(M_Z^2)$  in two steps, where  $\Delta\alpha^{(5)}(-s_0)$  is obtained from dispersion relations and the difference  $\Delta\alpha^{(5)}(M_Z^2) - \Delta\alpha^{(5)}(-s_0)$  is calculated using the perturbative QCD technique of the Adler function [288]. The error of the above difference due to limited knowledge of  $\alpha_s$ , the  $c$  and  $b$  quark masses and higher-order perturbative QCD effects is small enough, such that the overall uncertainty of  $\alpha_{eff}(M_Z^2)$  is smaller than that from the direct use of the dispersion relation.

Taking  $s_0^{1/2} = 2.0 \text{ GeV}$  and the value  $\Delta\alpha^{(5)}(-s_0) = (64.09 \pm 0.63) \times 10^{-4}$ , of ref. [113] as a bench-

mark, in Table C.6 we quote  $(\delta_{VP}\sigma)/\sigma = 1.3 \times 10^{-4}$ . Thanks to anticipated improvements of data for  $\sigma_{\text{had}}(s)$ ,  $s^{1/2} \leq 2.5$  GeV, one may expect the factor of 2 improvement by the time of the FCC-ee experiments, that is  $\delta_{VP}\sigma/\sigma = 0.65 \times 10^{-4}$  near the  $Z$  peak, see Table C.7.

At the high-energy end of FCC-ee, 350 GeV, due to the increase of the average transfer  $|\bar{t}| = 12.5$  GeV, one obtains presently from the dispersion relation  $\delta\alpha_{\text{eff}}/\alpha_{\text{eff}} = 1.190 \times 10^{-4}$  and  $\delta_{VP}\sigma/\sigma \simeq 2.4 \times 10^{-4}$ , and again with the possible improvement of the factor of 2, so that the FCC-ee expectation<sup>36</sup> is  $(\delta_{VP}\sigma)/\sigma \simeq 1.2 \times 10^{-4}$ .

There are also alternative proposals for the measurement of  $\alpha_{\text{eff}}(t)$  not relying (or relying less) on dispersion relations; see refs. [246, 289]. Ref. [289] proposed a method for the direct measurement of  $\alpha_{\text{eff}}(M_Z^2)$  using charge asymmetry in  $e^-e^+ \rightarrow \mu^-\mu^+$  near the  $Z$  resonance. One may ask whether its precise value can also be used to predict very precisely  $\alpha_{\text{eff}}(t)$  in the FCC-ee luminometer range  $2 \text{ GeV} \leq |t|^{1/2} \leq 10 \text{ GeV}$ ? It turns out that the uncertainty due to the use of pQCD [272] in the transition from the  $M_Z$  scale down to below 10 GeV is about the same as in the traditional methods. However, a direct measurement of  $\alpha_{\text{eff}}(M_Z^2)$  may serve as an important crosscheck. The other proposal, in ref. [246], of the direct measurement of  $\alpha_{\text{eff}}(t)$ ,  $t \sim -1 \text{ GeV}^2$ , from the elastic scattering of energetic muons on atomic electrons sounds interesting, but requires more studies.

#### 6.4.4 The uncertainty due to light fermion pairs

Three groups of calculations are available for the light-fermion-pair effect in the low angle Bhabha process: [259, 260], [267, 268] and [290–294].

The biggest correction, due to additional electron pair production, was calculated in Ref. [267], where process  $e^+e^- \rightarrow e^+e^-e^+e^-$  calculated with the help of the ALPHA algorithm [295] was combined with virtual/soft corrections of Refs. [28, 296, 297], resulting in the theoretical error on pair correction to be 0.01%.<sup>37</sup> This value is quoted in Table C.6 as the present state of the art for the uncertainty of corrections due to light fermion pair production.

In Refs. [291, 292]  $e^+e^-$  pair corrections were calculated in a semi-analytical way at NLO accuracy, omitting non-logarithmic corrections and taking virtual corrections from [296, 297]. The third order LO correction due to simultaneous emission of the additional  $e^+e^-$  pair (Non-Singlet and Singlet) and additional photon were also evaluated. The overall precision of the Bhabha scattering formula of Refs. [291, 292] was estimated there to be 0.006%, mainly due to omission of the heavier lepton pairs ( $\mu^+\mu^-$ ,  $\tau^+\tau^-$ ) and quark pairs (0.005%). One can assume conservatively the same 0.006% as the total error on additional pair correction.

In the Ref. [259] the complete LO semi-analytical calculations based on the electron structure functions were presented up to the third order for the Non-Singlet<sup>38</sup> and Singlet structure functions. Contrary to Ref. [291], results are provided also for the asymmetric acceptances.

The approach of [260] was based on the extension of the YFS [192] scheme of the soft photon resummation to the case of soft  $e^+e^-$  pair emission, with relevant real and virtual soft ingredients calculated in [298] (omitting up-down interference, multi-peripheral graphs *etc.*). The calculation is implemented in the unpublished BHLUMI v. 2.30 MC code. The accuracy of results was estimated to be 0.02% for the asymmetric angular acceptance, i.e.  $3.3^\circ - 6.3^\circ$  and  $2.7^\circ - 7.0^\circ$ , with the energy cut  $1 - s'/s < z_{\text{cut}} = 0.5$ . Ref. [267] has concluded that this precision is even better,  $6 \times 10^{-5}$  for  $z_{\text{cut}} \leq 0.5$ , while for hard emission,  $z_{\text{cut}} > 0.5$ , with significant multi-peripheral component, the precision deteriorates to 0.01%.

*What should be done in order to consolidate the above, mostly LEP era, calculations of the fermion pair contribution and to reach even better precision level needed for FCCee?*

As in ref. [267], for the additional real  $e^+e^-$  pair radiation the complete matrix element should be used,

<sup>36</sup>We thank F. Jegerlehner for elucidating private communications on the above predictions.

<sup>37</sup>The emission of a  $\mu$ -pair is also discussed in Ref. [267]

<sup>38</sup>This is contrary to the incorrect statement in Ref. [291]. Third order NS  $e^+e^-\gamma$  corrections are realized in Ref. [259] by second order structure function with the running coupling.



because non-bremsstrahlung-type graphs can contribute as much as 0.01% for the cut-off  $z_{cut} \sim 0.7$ . There is a number MC generators for the  $e^+e^- \rightarrow 4f$  process, developed for the LEP2 physics to be exploited for that purpose<sup>39</sup>.

In order to improve on 0.005% uncertainty of Ref. [291], due to the emission of the  $\mu^+\mu^-$ ,  $\tau^+\tau^-$ , and quark pairs, one may use LO calculation of ref. [259], incorporating lepton pair contributions by means of the modification of the running coupling. A naive rescaling of the electron logarithm (due to the mass of the muon) gives  $\ln \frac{|t|}{m_e^2} = 17.5$  and  $\ln \frac{|t|}{m_\mu^2} = 6.9$  i.e. for muon pairs we find a suppression factor of  $\ln^2 \frac{|t|}{m_\mu^2} / \ln^2 \frac{|t|}{m_e^2} = 0.4^2 = 0.16$  relative to the electron pair. Rescaling additional  $e^+e^-$  pair contribution of 0.05% one obtains an estimate of the muon pair contribution of 0.008%.<sup>40</sup> For the tau lepton logarithm  $\ln \frac{|t|}{m_\tau^2} = 1.2$  we obtain  $\ln^2 \frac{|t|}{m_\tau^2} / \ln^2 \frac{|t|}{m_e^2} = 0.07^2 = 0.005$  suppression factor relative to the electron pair, hence this contribution can be neglected. Adding  $\mu^+\mu^-$  pairs to the BHLUMI v. 2.30 code of Ref. [298] would be straightforward. Also in the approach of ref. [267, 268] this should be possible<sup>41</sup>. The contribution of light quark pairs ( $\pi$  pairs etc.) can be roughly estimated using quantity  $R_{had} = \sigma_{had} / \sigma_\mu \simeq 3$  for the effective hadronic production threshold of the order of 1 GeV. One obtains  $R_{had} \ln^2 \frac{|t|}{0.5^2 \text{ GeV}^2} / \ln^2 \frac{|t|}{m_\mu^2} = 0.9$ , i.e. this contribution is of the size of the muon pair contribution, that is of the order of 0.008%.<sup>42</sup>

The third group of corrections are the higher order terms. The emission of two (or more) electron pairs is suppressed by another factor  $(\frac{\alpha}{\pi} \ln \frac{|t|}{m_e^2})^2 \sim 10^{-3}$  and is negligible. The additional  $e^+e^- + n\gamma$  correction is non-negligible. Its evaluation was based either on LO structure functions ([291] (Table 1), [267] (Fig. 8), [259]) or on the YFS [192] soft approximation [260] (Fig. 4), resulting in quite different results and their comparison is rather inconclusive. They are at most of the order of 0.5 to 0.75 of the additional  $e^+e^-$  correction (without  $\gamma$ ). The remaining non-leading, non-soft additional  $e^+e^- + n\gamma$  corrections are suppressed by another  $1 / \ln \frac{|t|}{m_e^2} \sim 0.06$  and should be negligible ( $\sim 0.003\%$ ). It would be also possible to calculate the additional  $e^+e^- + \gamma$  real emission in a way similar to the existing code for LEP2 physics, [301]

The above improvements can be implemented either directly in the upgraded BHLUMI or using a separate calculation, such as BHLUMI 2.30 [260] code, or external MC programs like these of Refs. [267, 268]. To summarize, the proposed future error budget is the following: (1) The contribution of light quark pairs must be calculated with the accuracy of 25%, i.e. 0.0027%. (2) The contribution of the muon pairs will be known to 10%, i.e. to 0.0008%. (3) The non-leading, non-soft additional  $e^+e^- + n\gamma$  corrections will be treated as an error of 0.003%. Adding (1)–(3) in quadrature we obtain 0.004%. Applying safety factor of 1.5 we end up with 0.006% possible pair production uncertainty forecast for the FCC-ee, quoted in Table C.7.

#### 6.4.5 Z exchange and s-channel photon exchange

In the Bhabha scattering process, in addition to  $\gamma$  exchange in the  $t$  channel  $\gamma_t$ , there are also contributions from  $\gamma$  exchange in the  $s$  channel  $\gamma_s$  and  $Z$  exchange in both  $t$  and  $s$  channels,  $Z_t$  and  $Z_s$ . In fact, they all should be added at the amplitude level (Feynman diagram) and then squared to obtain the differential cross section for the Bhabha process, giving rise to several interference contributions. Numerically the most important for the low angle Bhabha (LABH) luminometry, apart from the pure  $t$ -channel  $\gamma$  exchange,  $\gamma_t \otimes \gamma_t$ , are interferences of other contributions with the  $\gamma_t$  amplitude, due to the enhancement factor  $\sim s/|t|$ . Among these, near the  $Z$  peak, the most sizable is the interference  $\gamma_t \otimes Z_s$ , because of the resonant enhancement. In the context of LEP luminometry it was studied in detail in ref. [261] for two types of detectors: SICAL with an angular coverage of

<sup>39</sup> One needs to be sure that the collinear configurations of outgoing four electrons are covered, like for example KoralW [299] which in addition, in its latest version 1.53 [300], accounts for t-channel-type photonic radiation as well.

<sup>40</sup> This is less optimistic than the estimate in Ref. [291].

<sup>41</sup> The other option is to use the above described general purpose LEP2  $4f$  codes, including also the discussed earlier corresponding virtual corrections.

<sup>42</sup> This is less optimistic than the estimate in Ref. [291]. Adding in quadrature errors due to muon and light quark pairs one obtains 0.011% rather than 0.006% of Ref. [291]. 0.011% is consistent with the estimate of Ref. [267].

$\sim 1.5^\circ\text{--}3^\circ$  and LCAL with an angular coverage of  $\sim 3^\circ\text{--}6^\circ$ . Based on this work, the  $\gamma_t \otimes Z_s$  contribution was implemented in BHLUMI 4.02 and its theoretical precision for the LEP luminosity measurement was assessed. We are going to exploit these results and estimate theoretical errors of all other contributions beyond the dominant  $\gamma_t \otimes \gamma_t$ . Since the angular coverage of the planned FCC-ee luminometer [250] is close to the LCAL one, we shall use the results of ref. [261] obtained for this type of the detector.

The Born-level  $\gamma_t \otimes Z_s$  contribution is up to  $\sim 1\%$  and changes from being positive below the  $Z$  peak to negative above, reaching the maximal absolute value at about  $\pm 1$  GeV from the peak. Radiative corrections, dominated by QED, are sizable, up to  $\sim 0.5\%$  (up to  $\sim 50\%$  of the Born-level contribution) and change in the opposite way, i.e. from negative to positive values when going from below to above the  $Z$  peak. BHLUMI includes the QED corrections and running-coupling effects for this contribution within the  $\mathcal{O}(\alpha)$  YFS exclusive exponentiation. The theoretical uncertainty for this calculation was estimated at 0.090% for LCAL and is used as an initial estimate of the theoretical error for the FCCee luminometry concerning the  $\gamma_t \otimes Z_s$  contribution in Table C.7.

The other contributions will be estimated by means of relating them to the  $\gamma_t \otimes Z_s$  or  $\gamma_t \otimes \gamma_t$ , using rescaling factors,  $|t|/s \approx 1.3 \times 10^{-3}$  and  $\tilde{\gamma}_Z = \Gamma_Z/M_Z \approx 2.7 \times 10^{-2}$ .

The next most sizable contribution comes from the interference  $\gamma_t \otimes \gamma_s$ . At the Born level, near the  $Z$  peak, it is smaller than the  $\gamma_t \otimes Z_s$  contribution by the factor<sup>43</sup>  $\sim 4\tilde{\gamma}_Z \approx 0.1$ . Taking  $\sim 1\%$  for the Born-level  $\gamma_t \otimes Z_s$ , we get  $\sim 0.1\%$  for  $\gamma_t \otimes \gamma_s$ . It is included in BHLUMI, so we need to estimate the missing radiative corrections. Since this is smooth near the  $Z$  peak, the photonic QED corrections should stay within 10%, for not too tight cuts on radiative photons. The resulting estimate of the theoretical precision of  $\gamma_t \otimes \gamma_s$  contribution in BHLUMI for the FCC-ee luminometry is  $\sim 0.01\%$ .

The resonant pure  $s$ -channel  $Z$  contribution,  $Z_s \otimes Z_s$ , at the Born level, is multiplied with respect to the  $\gamma_t \otimes Z_s$  term by the factor  $\sim |t|/s \times 1/(4\tilde{\gamma}_Z) \approx 1.3 \times 10^{-2}$ , thus its size is  $\sim 0.01\%$ . It is omitted in the current version of BHLUMI, hence it enters into theoretical error as a whole. However, it can be included rather easily, such that only the missing radiative corrections will matter. Due to the  $Z$ -resonance effect, they can reach even  $\sim 50\%$  of the Born-level contribution, hence the corresponding theoretical error would be  $\sim 0.005\%$ .

The  $t$ -channel interference  $\gamma_t \otimes Z_t$  we estimate multiplying the  $\gamma_t \otimes Z_s$  contribution by the  $\sim |t|/s \times \tilde{\gamma}_Z \approx 3.5 \times 10^{-5}$  factor. It can be easily implemented in BHLUMI, with the theoretical error due to the missing photonic corrections being below  $10^{-5}$ .

The pure  $s$ -channel  $\gamma_s \otimes \gamma_s$  contribution is much smaller in the  $Z$ -peak region than the resonant  $Z$  exchange. It is suppressed by the factor  $\sim (4\tilde{\gamma}_Z)^2 \approx 0.01$  with respect to  $Z_s \otimes Z_s$  (which is worth  $\sim 0.01\%$ ), so is of the order of  $10^{-6}$ .

Finally, the  $Z_t \otimes Z_t$  contribution is smaller than the dominant  $\gamma_t \otimes \gamma_t$  one by the factor  $\sim (|t|/s/4)^2 < 10^{-6}$ , thus it is completely negligible.

Adding the above theoretical errors in the quadrature, we obtain the total uncertainty (contributions omitted in BHLUMI) due to the  $Z$  exchanges and  $\gamma_s$  exchange for the FCC-ee luminometer near the  $Z$  peak at the level of 0.090%, quoted as present state of the art in Table C.7.

The above uncertainty is completely dominated by the uncertainty of the  $\gamma_t \otimes Z_s$  contribution which comes from a rather conservative estimate in ref. [261] based on comparisons of BHLUMI with the MC generator BABAMC [302] and the semi-analytical program ALIBABA [303, 304], the latter including higher-order leading-log QED effects. Later on, the new MC event generator BHWIDE [232] was developed for the wide-angle Bhabha scattering including all Born-level contributions for Bhabha process and  $\mathcal{O}(\alpha)$  YFS exponentiated EW radiative corrections. The comparison of BHLUMI with BHWIDE for FCC-ee luminometer would help to reduce all the above theoretical errors. In principle, the Born-level but also  $\mathcal{O}(\alpha)$  QED matrix elements of BHWIDE could be implemented in BHLUMI. This would reduce the theoretical error for the above group of contributions below 0.01%, as indicated in Table C.7.

<sup>43</sup>The factor of 4 comes from the ratio of the corresponding coupling constants.

In ref. [305] it was shown that for  $\sqrt{s} \gg M_Z$  all the above contributions are below 0.01% – they then can be neglected in the FCC-ee luminometry at energies above the  $Z$  peak.

The best method to reduce the uncertainty of the above contributions practically to zero would be to include these  $Z$  exchanges and  $s$ -channel photon exchange into the CEEX matrix element at  $\mathcal{O}(\alpha^1)$  in BHLUMI. Most likely, it would be enough to add the EW corrections to the LABH process in the form of effective couplings in the Born amplitudes. On the other hand, such a CEEX matrix element with the  $Z$  exchanges in BHLUMI would serve as a starting point for a better wide-angle Bhabha MC generator, much as BHLUMI v. 4.04 served as a starting point for BHWIDE [232].

#### 6.4.6 Technical precision

The question of the technical precision is quite nontrivial and difficult. The evaluation of the technical precision of BHLUMI v.4.04 with YFS soft-photon resummation and complete  $\mathcal{O}(\alpha^1)$  relies on two pillars: the comparison with semi-analytical calculations done in ref. [285] and comparisons with two hybrid MC programs LUMLOG+OLDBIS and SABSPV, reported in ref. [274]. This precision was established to be 0.27% (together with missing photonic corrections). Note that this was not an ideal solution, because the above two hybrid MCs did not feature complete soft photon resummation and disagreed with BHLUMI by more than 0.17% for sharp cut-offs on the total photon energy.

In fact, after the LEP era, another MC program BabaYaga [227, 228, 230], with soft-photon resummation has been developed using a parton shower (PS) technique, and in principle could be used for better validation of the technical precision of both BHLUMI and BabaYaga. In fact, such a comparison with BHWIDE MC [232] was done for  $s^{1/2} \leq 10$  GeV and the 0.1% agreement was found. It is quite likely that such an agreement persists near  $s^{1/2} = M_Z$ .

Let us note in passing that the inclusion of the complete  $\mathcal{O}(\alpha^1)$  into BabaYaga was done before three technologies of matching fixed-order NLO calculations with a parton shower (PS) algorithm were unambiguously established: MC@NLO [306], POWHEG [307] and KrkNLO [308]. The algorithm of NLO matching in BabaYaga is quite similar to that of KrkNLO<sup>44</sup>

Ideally, in the future validation of the upgraded BHLUMI, in order to get its technical precision at the level  $10^{-5}$  for the total cross section and  $10^{-4}$  for single differential distributions, one would need to compare it with another MC program developed independently, which properly implements the soft-photon resummation, LO corrections up to  $\mathcal{O}(\alpha^3 L_e^3)$ , and the second-order corrections with the complete  $\mathcal{O}(\alpha^2 L_e)$ .

In principle, an extension of a program like BabaYaga to the level of NNLO for the hard process, keeping the correct soft-photon resummation, would be the best partner for the upgraded BHLUMI to establish the technical precision of both programs at the  $10^{-5}$  precision level<sup>45</sup>. In the meantime, the comparison between the upgraded BHLUMI with EEX and CEEX matrix elements would also offer a very good test of its technical precision, since the basic multi-photon phase space integration module of BHLUMI was already well tested in ref. [285] and such a test can be repeated at an even higher-precision level.

### 6.5 Summary

Summarizing, we conclude that an upgraded new version of BHLUMI with the error budget of 0.01% shown in Table C.7 is perfectly feasible. With appropriate resources, such a version of BHLUMI with the  $\mathcal{O}(\alpha^2)$  CEEX matrix element and with the precision tag of 0.01%, needed for the FCC-ee physics, could be realized. Keeping in mind that the best experimental error of luminosity error achieved at LEP was 0.034% [266], it would be

---

<sup>44</sup>Single MC weight is introducing NLO correction in both methods, but in KrkNLO it sums over real photons, while in BabaYaga it takes product over them. However, it is the same when truncated to  $\mathcal{O}(\alpha^1)$ . We are grateful to authors of BabaYaga for clarification on this point.

<sup>45</sup> The upgrade of the BHLUMI distributions will be relatively straightforward because its multi-photon phase space is exact [29] for any number of photons.

interesting to study whether systematic error of the designed FCC-ee luminosity detector [250] can match the above anticipated theory precision.

## 7 The SANC project

**Authors:** A. Arbuzov, S. Bondarenko, Ya. Dydyshka, L. Kalinovskaya, R. Sadykov

**Corresponding Author:** Lidia Kalinovskaya [lidia.kalinovskaya@cern.ch]

In this section we present a plan of studies that will be performed in the framework of the new stage of the SANC project aimed at the preparation of the electron-positron collider (EPC) research program on precision tests of the Standard Model. The accuracy of the corresponding experimental studies improves continuously with increased luminosity, novel detector technologies, elaboration of new analysis techniques, etc. All that leads to new requirements on the accuracy of theoretical predictions challenged by the experimental data.

The particular goal of our project is the development of a Monte-Carlo event generator for processes that will be studied at electron-positron colliders. QED, QCD, and electroweak (EW) effects will be treated in the complete one-loop accuracy level within the Standard Model. Numerically relevant higher order radiative corrections will be implemented into the generator upon availability. In particular, we will include the known higher-order corrections through the  $\Delta\rho$  parameter (all calculations for the EW and QCD sectors that exist today). Possible polarization of electron and positron beams will be allowed. In creation of the new Monte Carlo event generator we will use the experience of our group accumulated in similar projects such as (Pol)HECTOR [309], ZFITTER [27, 36], and SANC [310, 311].

We will concentrate on the processes which are most relevant for the verification of the electroweak sector of the SM including  $W$  and  $Z$  gauge bosons, the Higgs boson, and the top quark. In particular, future high-energy  $e^+e^-$  colliders will provide an experimental environment to study with excellent precision the following processes and ingredients of the SM:

- Bhabha scattering process  $e^+e^- \rightarrow e^+e^-$ , since it will be used for luminosity measurements, detector calibration etc.;
- the top quark mass, width, and coupling constants in  $e^+e^- \rightarrow t\bar{t}$ ;
- the sine of the effective weak mixing angle  $\sin\vartheta_W^{eff}$ ;
- the Higgs boson properties via the Higgsstrahlung process  $e^+e^- \rightarrow ZH$ ;
- the  $WW$ -fusion process  $e^+e^- \rightarrow H\nu_e\bar{\nu}_e$ .

Special attention will be devoted to the processes of electron-positron annihilation into a fermion pair at the  $Z$  resonance center-of-mass energy. We are going to describe those processes by means of a Monte Carlo generator which will include the complete set of one-loop corrections supplemented with the most important higher-order contributions. A new feature of our generator will be inclusion of the effects due to beam polarization.

The general plan of the project is:

- Development of a Monte Carlo (MC) event generator at the level of the complete one-loop and leading multi-loop radiative corrections and taking into account longitudinal or transverse beam polarization for the processes  $e^+e^- \rightarrow e^+e^-$  ( $\mu^+\mu^-$ ,  $\tau^+\tau^-$ ,  $t\bar{t}$ ,  $HZ$ ,  $H\gamma$ ,  $Z\gamma$ ,  $ZZ$ ,  $H\nu\bar{\nu}$ ,  $H\mu^+\mu^-$ ,  $f\bar{f}\gamma$ ,  $\gamma\gamma$ ).
- Creating an interface to supplement electroweak RC to PYTHIA. The possible implementation of "the best we have" is: the first stage (PHYTIA + PHOTOS) is to account the lowest order plus QCD and/or QED parton showers (LO+PS) in the final state; the second stage MCSANC is to account the NLO EW and higher order EW and QCD corrections via the  $\Delta\rho$  parameter. The possibility to construct such an interface has been demonstrated in Ref. [312] where events generated by our MCSANC code were transferred to (PHYTIA + PHOTOS) or (HERWIG + PHOTOS) to simulate QCD and QED parton showers.
- Implementation of the single-resonance approach to describe complex cascade processes.
- Elaboration of the standard SANC procedure for calculating helicity amplitudes for processes  $2 \rightarrow 3, 4$ .

- Creation of additional SANC building blocks to include the complete weak 2-loop (EW) and 3-loop (QCD) calculations, and the leading 3-loop (EW) and 4-loop (QCD) ones.

The helicity amplitude (HA) formalism will be applied. It allows to get a cross-section by summing up the squares of helicity amplitudes (instead of squaring the sum of amplitudes in the conventional approach), see e.g. [313]. Therefore we have the basement for implementation of both transverse and longitudinal beam polarizations.

The active environment of the existing SANC system allows to obtain analytic results for scalar form factors (FF), helicity amplitudes (HA), and Bremsstrahlung (BR) contributions. For the calculation of HA's, the Vega-Wudka [314] and the Kleiss-Stirling [277] methods are used. All calculations of HA's are implemented in a single thread computing. The advantage of the calculation of one-loop corrections using the helicity amplitude method is the possibility to take into account the polarization effects in a simple way.

The SANC system contains programs in the language of symbolic computation FORM [315] to calculate SM processes of the following types:  $4f \rightarrow 0$ ,  $4b \rightarrow 0$  and  $2f2b \rightarrow 0$ . These programs compute one-loop ultraviolet-finite scalar form factors and amplitudes. To verify the correctness of the results, first of all, we check the Ward identities and the independence of scalar form factors on the gauge parameters, and secondly, we perform extensive numerical comparisons of our results with independent calculations known in the literature: with ZFITTER [27, 36], FeynArts [316], the GRACE system [317], the topfit program [100], etc.

The first steps for the basement for the future MC generator are: a) the library for the parameter  $\Delta\rho$  (in preparation) and b) the recent experience with the description of polarized Bhabha scattering at the one-loop level [318].

#### a) Higher-order radiative corrections for massless four-fermion processes

A large group of the dominant radiative corrections can be absorbed into the shift of the  $\rho$  parameter from its lowest order value  $\rho_{Born} = 1$ . These groups of radiative corrections are:

$$\Delta\rho = \Delta\rho_{X_t} + \Delta\rho_{\alpha\alpha_s} + \Delta\rho_{X_t\alpha_s^2} + \Delta\rho_{(X_t^3+X_t^2\alpha_s)} + \Delta\rho_{X_t\alpha_s^2} + \Delta\rho_{\alpha_t^2} + \Delta\rho_{X_t\alpha_s^3} + \Delta\rho_{X_t^2(bos)} + \Delta\rho_{X_t^3}. \quad (C.222)$$

#### b) Bhabha scattering

Theoretical description of Bhabha scattering with radiative corrections taken into account is crucial for high-precision measurements of this process and thus for luminosity monitoring at future  $e^+e^-$  colliders. The Bhabha scattering cross section with the one-loop QED contribution including transverse and longitudinal polarizations of the incoming beams was presented in [319, 320].

Our first attempt to estimate the theoretical uncertainty for this process at one-loop level by MC was performed in [310]. We describe this process by means of a Monte Carlo generator which includes now the complete set of one-loop corrections [318]. The most relevant higher-order contributions will be supplemented. A new feature of our results is taking into account the beam polarization.

We have shown that the complete  $\mathcal{O}(\alpha)$  electroweak radiative corrections provide a considerable impact on the differential cross section and the left-right asymmetry. Moreover, the corrections themselves are rather sensitive to polarization degrees of the initial beams.

Below we present the analytic expressions for the helicity amplitudes of Bhabha scattering. There are six non-zero HA's, however, since for Bhabha scattering  $\mathcal{F}_{LQ}^Z = \mathcal{F}_{QL}^Z$ , the number of independent HA's is actually reduced to four.

We obtained the compact expression for the Born level ( $\mathcal{F}_{QL,LL,QQ}^Z = 1$ ) and the virtual (loop) contributions to the cross section in the HA approach:

$$\mathcal{H}_{++++} = \mathcal{H}_{-----} = -2e^2 \frac{s}{t} \left[ \mathcal{F}_{QQ}^{(\gamma,Z)}(t, s, u) - \chi_Z(t) \delta_e \mathcal{F}_{QL}^Z(t, s, u) \right], \quad (C.223)$$

$$\mathcal{H}_{+--+} = \mathcal{H}_{-++-} = -2e^2 \frac{t}{s} \left[ \mathcal{F}_{QQ}^{(\gamma,Z)}(s, t, u) - \chi_Z(s) \delta_e \mathcal{F}_{LQ}^Z(s, t, u) \right], \quad (C.224)$$

$$\mathcal{H}_{+--+} = 2e^2 \frac{u}{s} \left( \left[ \mathcal{F}_{QQ}^{(\gamma,Z)}(s, t, u) + \chi_Z(s) (\mathcal{F}_{LL}^Z(s, t, u) - 2\delta_e \mathcal{F}_{LQ}^Z(s, t, u)) \right] + \frac{s}{t} [s \leftrightarrow t] \right), \quad (\text{C.225})$$

$$\mathcal{H}_{-++-} = 2e^2 \frac{u}{s} \left( \left[ \mathcal{F}_{QQ}^{(\gamma,Z)}(s, t, u) \right] + \frac{s}{t} [s \leftrightarrow t] \right), \quad (\text{C.226})$$

where

$$\mathcal{F}_{QQ}^{(\gamma,Z)}(a, b, c) = \mathcal{F}_{QQ}^{(\gamma)}(a, b, c) + \chi_Z(a) \delta_e^2 \mathcal{F}_{QQ}^{(Z)}(a, b, c) \quad (\text{C.227})$$

To study the case of the longitudinal polarization, we produce the helicity amplitudes and make a formal application of Eq. (1.15) from [313]:

$$\begin{aligned} \frac{d\sigma(P_{e-}, P_{e+})}{d\cos\vartheta} = & \frac{1}{128\pi s} \left[ (1 + P_{e-})(1 + P_{e+}) \sum_{ij} |\mathcal{H}_{++ij}|^2 + (1 + P_{e+})(1 - P_{e-}) \sum_{ij} |\mathcal{H}_{+-ij}|^2 \right. \\ & \left. + (1 - P_{e+})(1 + P_{e-}) \sum_{ij} |\mathcal{H}_{-+ij}|^2 + (1 - P_{e+})(1 - P_{e-}) \sum_{ij} |\mathcal{H}_{--ij}|^2 \right]. \end{aligned} \quad (\text{C.228})$$

For the cross check we got analytic zero for the difference between the square of the covariant amplitude (we introduced the spin density matrix into our procedures) and Eq. (C.228).

The left-right asymmetry  $A_{LR}$  and the relative correction  $\delta$  are defined as

$$\begin{aligned} A_{LR} &= \frac{d\sigma(-1, 1) - d\sigma(1, -1)}{d\sigma(-1, 1) + d\sigma(1, -1)}, \\ \delta &= \frac{d\sigma^{1\text{-loop}}(P_{e-}, P_{e+})}{d\sigma^{\text{Born}}(P_{e-}, P_{e+})} - 1, \end{aligned} \quad (\text{C.229})$$

where we omitted  $d\cos\vartheta$  for shortness.

All numerical results are obtained for the set of energies  $E_{cm} = 250, 500$ , and  $1000$  GeV for the following magnitudes of the electron ( $P_{e-}$ ) and positron ( $P_{e+}$ ) beam polarizations:  $(0, 0)$ ,  $(-0.8, 0)$ ,  $(-0.8, -0.6)$ , and  $(-0.8, 0.6)$ .

Table C.8: The Born and 1-loop cross sections of Bhabha scattering and the corresponding relative corrections  $\delta$  for  $\sqrt{s} = 250, 500$ , and  $1000$  GeV.

$P_{e-}, P_{e+}$	0, 0	-0.8, 0	-0.8, -0.6	-0.8, 0.6
$\sqrt{s} = 250$ GeV				
$\sigma_{e^+e^-}^{\text{Born}}, \text{pb}$	56.6763(1)	57.7738(1)	56.2725(4)	59.2753(5)
$\sigma_{e^+e^-}^{1\text{-loop}}, \text{pb}$	61.731(6)	62.587(6)	61.878(6)	63.287(7)
$\delta, \%$	8.92(1)	8.33(1)	9.96(1)	6.77(1)
$\sqrt{s} = 500$ GeV				
$\sigma_{e^+e^-}^{\text{Born}}, \text{pb}$	14.3789(1)	15.0305(1)	12.7061(1)	17.3550(2)
$\sigma_{e^+e^-}^{1\text{-loop}}, \text{pb}$	15.465(2)	15.870(2)	13.861(1)	17.884(2)
$\delta, \%$	7.56(1)	5.59(1)	9.09(1)	3.05(1)
$\sqrt{s} = 1000$ GeV				
$\sigma_{e^+e^-}^{\text{Born}}, \text{pb}$	3.67921(1)	3.90568(1)	3.03577(3)	4.77562(5)
$\sigma_{e^+e^-}^{1\text{-loop}}, \text{pb}$	3.8637(4)	3.9445(4)	3.2332(3)	4.6542(7)
$\delta, \%$	5.02(1)	0.99(1)	6.50(1)	-2.54(1)

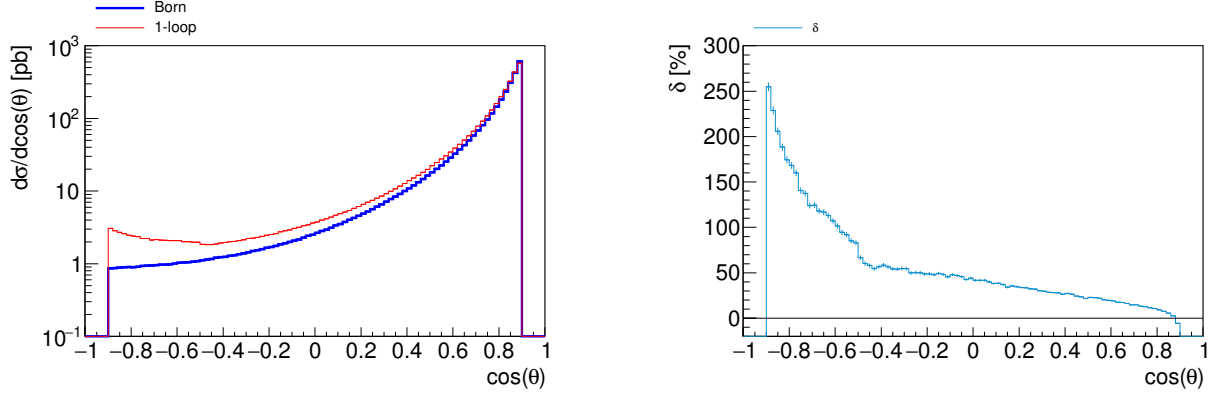


Fig. C.8: The differential cross section (left) [in pb] and the relative correction  $\delta$  (right) [in %] vs. the cosine of the electron scattering angle for  $\sqrt{s} = 250$  GeV.

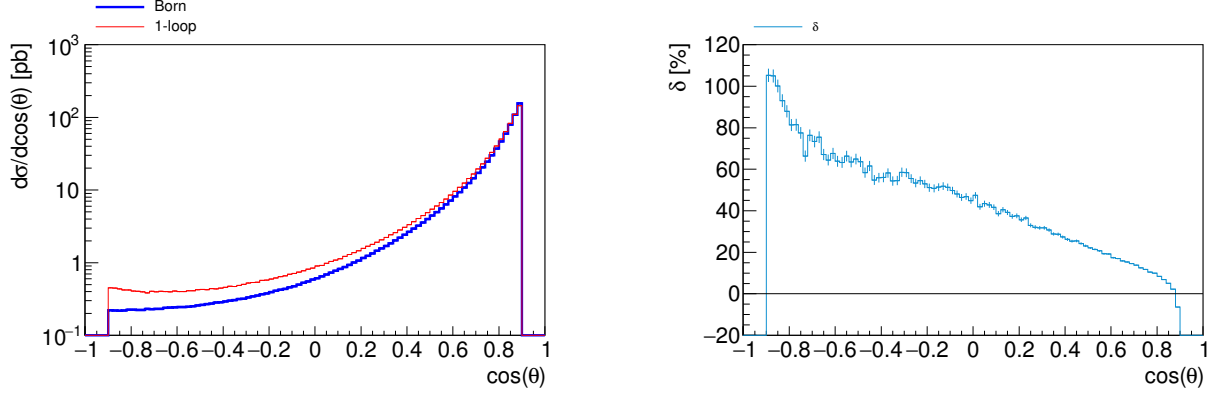


Fig. C.9: The differential cross section (left) [in pb] and the relative correction  $\delta$  (right) [in %] vs. the cosine of the electron scattering angle for  $\sqrt{s} = 500$  GeV.

The unpolarized differential cross section of Bhabha scattering and the corresponding relative  $\mathcal{O}(\alpha)$  correction  $\delta$  (in percent) as a function of the electron scattering angle are shown in Figs. C.8, C.9, and C.10 for  $|\cos \theta| < 0.9$  and different center-of-mass energies. The huge relative radiative corrections for the backward scattering angles are due to the smallness of the Born cross section in this domain, that does not mean any problem with the perturbation theory.

The integrated cross section of the Bhabha scattering and the relative correction  $\delta$  are given in the Table C.8 for various energies and beam polarization degrees.

The  $A_{LR}$  asymmetry at  $\sqrt{s} = 250, 500$ , and 1000 GeV is shown in Figs. C.11-C.12. One can see that the EW radiative corrections affect the asymmetry very strongly.

One can see that the one-loop EW radiative corrections are quite large and should be certainly taken into account. But to satisfy the precision requirements of the future experiments, one should include necessarily also higher order effects. Only a part of the latter effects can be introduced as oblique or factorizable corrections, while many other corrections are process and kinematics dependent. That is why, creation of a Monte Carlo generator with explicit treatment of various contributions is of great importance.



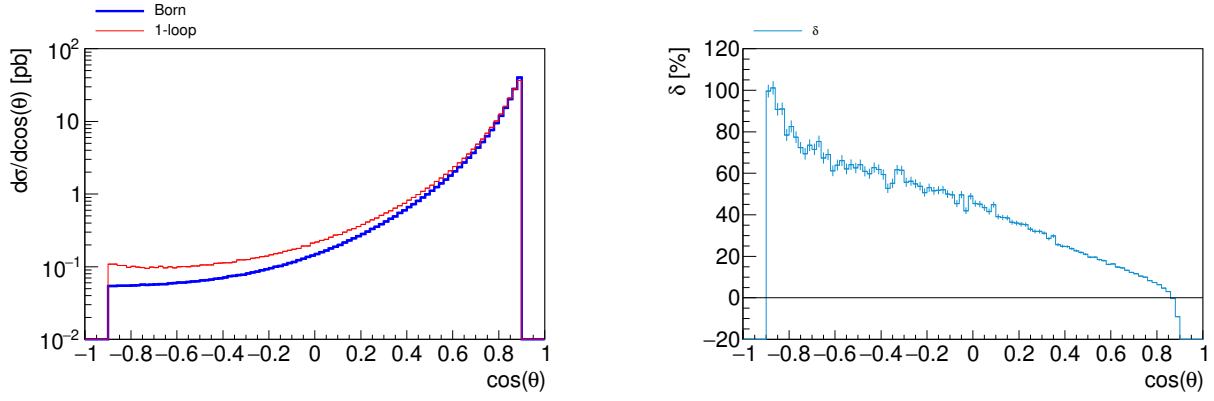


Fig. C.10: The differential cross section (left) [in pb] and the relative correction  $\delta$  (right) [in %] vs. the cosine of the electron scattering angle for  $\sqrt{s} = 1000$  GeV.

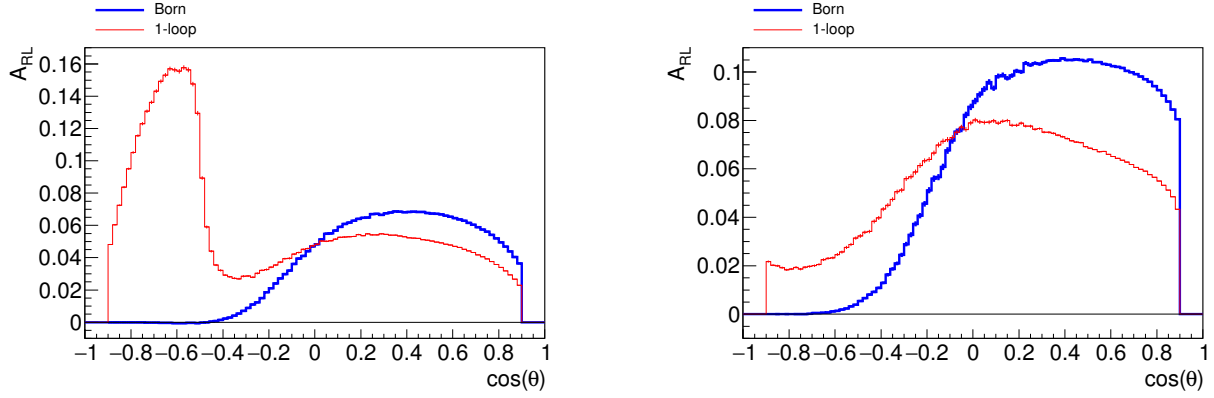


Fig. C.11: The left-right asymmetry  $A_{LR}$  as a function of the cosine of the electron scattering angle at  $\sqrt{s} = 250$  GeV (left) and at  $\sqrt{s} = 500$  GeV (right).

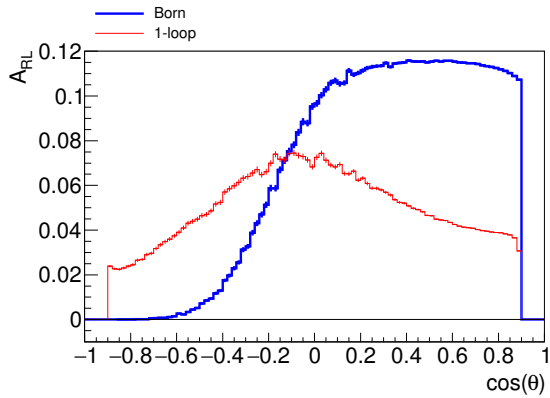


Fig. C.12: The left-right asymmetry  $A_{LR}$  as a function of the cosine of the electron scattering angle at  $\sqrt{s} = 1000$  GeV.



# Chapter D

## Towards 3- and 4-loop form factors

### 1 Form factors and $\gamma_5$

**Authors:** Peter Marquard, Dominik Stöckinger

Corresponding Author: Peter Marquard [peter.marquard@desy.de]

#### 1.1 Introduction

As discussed in Chapter C, the key objects in the deconvolution of observables in FCC-ee-Z are  $2 \rightarrow 2$  processes. The leading, residuum terms are besides self-energies products of vertices. So vertices are central objects which can be calculated systematically order by order in radiative corrections. They constitute in form of form factors the hard, pure virtual, part of the calculation and allow for the study of the pointlike nature of the involved particles. Their poles correspond to universal anomalous dimensions which govern the infrared behaviour of QCD. In this chapter we explore it in details by discussing present status and perspective as, see Chapter B, 3- and 4-loop vertex corrections to the Z-boson decay will be needed. Some important technicalities like  $\gamma_5$  issue or beyond SM frameworks are also discussed, see section D.2.

In general we have to distinguish the two cases of heavy, massive, or light, massless quarks or gluons. We need to keep the mass of the quark if the centre of mass energy is comparable to the mass of the quark in question. If the centre of mass energy is well above the production threshold we can safely neglect the quark mass in higher order calculations. Thus, at a future electron-positron collider the quarks up to the bottom quark will be in general considered massless while the mass of the top quark is kept.

We will summarize status and prospects for the two cases in the following sections.

#### 1.2 Massive Form factor

In the case of massive-quark form factor we have to consider couplings of a pair of heavy quarks to an external current through a scalar, pseudo-scalar, vector or axial-vector coupling. All of these coupling, but the pseudo-scalar one, are realized within the Standard Model through the couplings of quarks to the gauge bosons and the Higgs boson. Thus we will consider the following general coupling structure of a pair of massive quarks with momenta  $q_1$  and  $q_2$

$$\begin{aligned}\Gamma^\mu &= \Gamma_V^\mu + \Gamma_A^\mu \\ &= -i \left[ v_Q \left( \gamma^\mu F_{V,1} + \frac{i}{2m_Q} \sigma^{\mu\nu} q_\nu F_{V,2} \right) + a_Q \left( \gamma^\mu \gamma_5 F_{A,1} + \frac{1}{2m_Q} q^\mu \gamma_5 F_{A,2} \right) \right],\end{aligned}\quad (\text{D.1})$$

where  $\sigma^{\mu\nu} = \frac{i}{2}[\gamma^\mu, \gamma^\nu]$ ,  $q = q_1 + q_2$ , and  $v_Q$  and  $a_Q$  are the SM vector and axial-vector coupling constants as defined by

$$v_Q = \frac{e}{\sin \theta_w \cos \theta_w} \left( \frac{T_3^Q}{2} - \sin^2 \theta_w Q_Q \right), \quad a_Q = -\frac{e}{\sin \theta_w \cos \theta_w} \frac{T_3^Q}{2}.\quad (\text{D.2})$$

$e$  denotes the elementary charge,  $\theta_w$  the weak mixing angle,  $T_3^Q$  the third component of the weak isospin, and  $Q_Q$  the charge of the heavy quark. Here,  $F_{V,1}$  and  $F_{V,2}$  correspond to the electric and magnetic form factor, respectively.

In the case of a (pseudo-)scalar coupling we have

$$\Gamma = \Gamma_S + \Gamma_P = -\frac{m}{v} \left[ s_Q F_S + i p_Q \gamma_5 F_P \right], \quad (\text{D.3})$$

where  $s_Q$  and  $p_Q$  are the scalar and pseudo-scalar coupling, respectively.

Higher-order QCD corrections to all form factors corresponding to the different currents have been studied extensively in the past decades. The results are in general too lengthy to reproduce here and we refer to the literature for the explicit expressions. The form factors have first been studied at one-loop order in [321, 322]. At two loops they have, together with the required master integrals, first been calculated in [323–327]. These calculation have later been extended to include more orders in  $\epsilon$  for the vector current in [328] and all other currents in [329]. At three-loop order there is up to now no complete calculation available. Only partial results, the color-planar, i.e. leading color, contributions and the full light-fermionic contributions exist [330–333]. The corresponding master integrals have been calculated in [334] and independently also for [329]. For a review about general strategies for the calculation of master integrals see, e.g., [335]. At three-loop these calculations successfully reproduce the universal cusp anomalous dimensions obtained in [336, 337]. The universal infrared structure in general and in particular for the heavy quark form factors has been studied in [338, 339].

The massive form factors depend on the ratio  $q^2/m_Q^2$  and it proved favourable to express them through the variable  $x$  defined via  $q^2/m_Q^2 = -(1-x)^2/x$ . Expressed through the variable  $x$  the available results for the massive form factors at three-loop order only contain normal harmonic polylogarithms (HPLs) with letters  $1/x, 1/(1-x), 1/(1+x)$ , and cyclotomic HPLs with letters  $1/(1-x+x^2), x/(1-x+x^2)$  or their corresponding linearized sixth-root-of-unity counterparts. Beyond the color-planar contributions elliptic structures are expected to appear, a topic which currently attracts a lot of attention.

The axial and pseudoscalar form factors suffer from the general problem of an ill-defined  $\gamma_5$  in dimensional regularization. While for the non-singlet contributions we can safely use a naive anticommuting  $\gamma_5$ , this is no longer possible for the singlet contributions. We discuss general aspects of this issue and possible solutions in 1.4.

### 1.3 Massless form factor

The form factors where all quarks are considered massless also play an important role. In the context of massless form factors the scalar  $h \rightarrow gg$  and vector  $\gamma \rightarrow q\bar{q}$  form factor, but also the axialvector form factor contributing to  $Z \rightarrow q\bar{q}$ , have received the most attention. The scalar form factor constitutes the virtual correction for Higgs production through gluon fusion in the Higgs effective theory.  $e^+e^- \rightarrow 2$  jets is governed purely by the vector form factor, while for Z-boson production and decay we need both vector and axialvector form factors. If only QCD corrections are considered, the vector and axialvector form factors agree.

Considering only pure QCD corrections a plethora of results for the form factors is available. They have been calculated at the two-loop level in [340–345]. At three-loop order they have been obtained in [346, 347]. These result have later been extended to higher orders in the dimensional regulator in [347, 348]. The relevant master integrals have been calculated in [349–351]. The infrared structure of massless form factors is again universal and has been studied in [344, 352–355].

At four-loop order again only partial result exist. For the quark form factor, the color-planar, i.e. leading color, contributions have been obtained first for the fermionic contributions in [356] and later for the purely bosonic ones in [357]. The complete result for contributions containing at least 2 fermion loops, i.e.  $n_f^2$ , has been calculated in [358]. For the gluon form factor only the  $n_f^3$  contributions are available from [359]. While in the massive case the main difficulty lies in the calculation of the master integrals, in the massless one, even the reduction to master integrals poses a major challenge.

The massless form factor has also been considered in  $N = 4$  SYM. For recent progress see section D.2.

#### 1.4 Remarks on regularization and $\gamma_5$

One technical step in quantum field theoretical higher-order calculations is the regularization of loop and phase space integrals. Here we point out that the regularization of multi-loop electroweak calculations is particularly non-trivial and progress needs to be made for the desired computations.

Generally the topic of regularization has already received increasing attention in recent years. On the one hand existing schemes such as dimensional regularization, dimensional reduction, or the four-dimensional helicity scheme have been investigated in more detail and relations between them have been better understood. On the other hand novel reformulations of dimensional schemes and also purely 4-dimensional schemes have been developed. These developments have been summarized in the recent review [360]. A major driving force of those developments was the need for highly non-trivial higher-order calculations for the LHC — clearly further progress will have to be made for higher-order calculations for the physics at Fccee.

An issue of particular importance for electroweak calculations is the regularization of  $\gamma_5$ , which is notoriously problematic in dimensional schemes. In 4 dimensions, three properties hold:

$$\{\gamma_5, \gamma^\mu\} = 0, \quad (D.4)$$

$$\text{Tr}(\gamma_5 \gamma^\mu \gamma^\nu \gamma^\rho \gamma^\sigma) = 4i\epsilon^{\mu\nu\rho\sigma}, \quad (D.5)$$

$$\text{Tr}(\Gamma_1 \Gamma_2) = \text{Tr}(\Gamma_2 \Gamma_1). \quad (D.6)$$

The last equality means that traces are cyclic. In  $D = 4 - 2\epsilon$  dimensions, it is inconsistent to require these properties simultaneously, and one has to give up one of them. As a result there is a plethora of proposals how to treat  $\gamma_5$ . The standard one, which is known to be mathematically well-defined and consistent, is the so-called HVBM scheme [361, 362]. This scheme gives up the anticommutation property of  $\gamma_5$ ; it is consistent in the sense that it is compatible with unitarity and causality of quantum field theory, but it does not manifestly lead to the correct conservation/non-conservation properties of currents — these have to be ensured by hand.

A variant of the HVBM scheme has been developed by Larin [363], and Larin's scheme has been applied regularly in multiloop QCD calculations involving the axial current. In this context, the vector current is manifestly preserved. The anomalous non-conservation of the axial current is restored by adding a certain finite counterterm. The determination of this counterterm is difficult. Ref. [363] used an anomalous Ward identity to determine the two-loop counterterm via a three-loop calculation. Recently, Ref. [364] suggested a simplification which could allow the determination of the  $n$ -loop counterterm via only an  $n$ -loop calculation.

It is important to realize that applying the HVBM scheme to electroweak physics is significantly more complicated. In this case, neither the vector- nor the axial-vector currents are conserved, but the left-handed SU(2) gauge current must be conserved in order to preserve gauge invariance of the theory. This is not manifestly the case. Hence the HVBM scheme breaks electroweak gauge invariance, i.e. the regularized Green functions do not satisfy the Ward/Slavnov-Taylor identities for the electroweak Standard Model and gauge invariance-restoring counterterms are required which do not arise from the usual renormalization transformation. The form of these counterterms is unknown at the  $\geq 2$ -loop level.

As an alternative to HVBM, recipes have been proposed which promise to preserve electroweak gauge invariance either completely or to a larger extent than HVBM. To exemplify the set of problems we describe here three existing electroweak multi-loop calculations where the  $\gamma_5$ -problem was relevant:

- In the evaluation of the two-loop electroweak contributions to  $g - 2$  of the muon [365], a simplified treatment was possible where  $\gamma_5$  was treated as anticommuting but the trace formula (D.5) was used in its 4-dimensional form by hand. It was shown that because of the particular structure of diagrams the inconsistency did not lead to incorrect results; rather, gauge invariance was manifestly preserved, simplifying the computation.
- In the evaluation of two-loop electroweak contributions to muon decay [366], the fermionic one-loop subdiagrams were first evaluated in the HVBM scheme and gauge invariance-restoring counterterms were added. Then the result was inserted into the second loop, which could be evaluated in 4 dimensions.

- In Refs. [367, 368] the four-loop  $\beta$ -function for  $\alpha_s$  in the full Standard Model has been computed using various prescriptions involving anticommuting  $\gamma_5$  and the reading-point prescription of Ref. [369] were used, with conflicting results.

These examples show that no established practical procedure exists which could be applied to e.g. 3-loop calculations in the electroweak Standard Model, but progress can be made in several directions.

One avenue for improvement is to further study the recipes used in Refs. [365, 367, 368] and to clarify when simplified prescriptions are possible. Refs. [369, 370] have provided arguments that such simpler prescriptions, based e.g. on reading points for  $\gamma_5$  and traces, should exist.

Apart from dimensional regularization schemes, a variety of non-dimensional regularization schemes, which stay in the physical 4-dimensional space, has been developed in recent years, see the review [360]. These schemes might offer practical advantages with respect to the treatment of  $\gamma_5$ . Ref. [371] has considered a wide class of 4-dimensional regularization schemes, which have the important property of momentum-routing invariance and do not break gauge invariance as immediately as e.g. the Pauli-Villars scheme. This reference showed clearly that all these schemes have very similar problems for  $\gamma_5$  as dimensional schemes. The reason is that in those schemes the regularization is essentially done by replacement rules, and those replacement rules do not necessarily commute with applying e.g. cyclicity of traces. Nevertheless, these 4-dimensional schemes offer promising alternative avenues for future progress in developing practical treatments of  $\gamma_5$ .

Within dimensional schemes, Ref. [364] has recently shown that one particular recent reformulation, the so-called FDF approach [372] offers a simpler way to treat  $\gamma_5$ . So far, the FDF approach exists only at the one-loop level; it is clearly motivated to study its extension to the multi-loop level.

Finally, it remains of course a viable possibility to use the HVBM scheme. In this case, it is important to determine the required gauge invariance-restoring step by step at the 2- and 3-loop level. A systematic procedure to achieve this has been put forward in Ref. [373] based on the quantum action principle and Ref. [374] based on the quantum action principle and the background field method. These methods should be worked out and applied to the multi-loop level.

## 2 Four-loop form factor in N=4 super Yang-Mills theory

Authors: Rutger H. Boels, Tobias Huber, Gang Yang

Corresponding Author: Tobias Huber [huber@physik.uni-siegen.de]

### 2.1 General motivation: N=4 SYM as a toy model

In preparing for an order of magnitude increase in computational capabilities, it is important to track progress at the cutting edge of what is currently possible. A common approach in physics is to first trial tools and techniques in toy-models, which are still general enough to capture all essential details of more physical computations. The most common approach to compute quantities such as form factors and scattering amplitudes in high-energy physics beyond the trivial tree level for instance involves a number of steps:

1. generate an integrand for the quantity under study, for instance through Feynman graphs or by employing unitarity methods. This integrand still has to be integrated over unobserved loop momenta,
2. simplify the integrand by solving integration-by-parts identities. The result is now given in terms of a basis of remaining so-called master integrals,
3. compute the master integrals analytically or numerically, typically as an expansion in terms of the dimensional regularisation parameter  $\epsilon$ .

The interest in this report is ultimately collider physics, so the goal is to implement these steps in QCD or even the full-fledged standard model. It is known, however, that this is algebraically a complicated problem even at step one, while the output generated is also complex. For any new tools and techniques it is therefore a good idea to study a less physical but more symmetric theory where the initial inputs are simpler and there is more control over the expected output. In the context of gauge theories, a prime candidate toy model is the  $\mathcal{N} = 4$  maximally supersymmetric gauge theory in dimensional regularisation, i.e. in  $4 - 2\epsilon$  dimensions.

The  $\mathcal{N} = 4$  super Yang-Mills (SYM) theory plays a prime role in many branches of formal high-energy physics, for instance in the AdS/CFT correspondence [375]. For the purposes of this report it serves two purposes. First, it leads to technically much simpler integrands. Second, it is known through many examples that results in this theory typically obey a special number theory property known as the maximal transcendentality principle. Very roughly speaking the latter means that the hardest part of the integration of the master integrals appearing in physical theories such as QCD is the same as that in  $\mathcal{N} = 4$ , making the latter an ideal toy model to explore concrete simplification and integration techniques. The current subsection is an application of this philosophy. In general we expect that  $\mathcal{N} = 4$  super Yang-Mills theory can play a lighthouse role in the push for the precision required for the FCC-ee-Z experimental program. For this to work it is important that the focus remains squarely on tools and techniques which at least in principle apply directly to physical theories. This is the route followed here. The results listed below include work first reported in [376] [377].

### 2.2 Concrete motivation: the non-planar cusp anomalous dimension at four loops

In this subsection we study the Sudakov form factor of  $\mathcal{N} = 4$  SYM, which consists of one off-shell member of the stress-tensor multiplet, and two on-shell supersymmetric massless gluon multiplets, in dimensional regularisation in the four-dimensional helicity scheme in momentum space. Supersymmetry determines the form factor to be proportional to the tree form factor. Kinematically this is a single-scale problem which can be expressed at the  $l$ -loop order as

$$\mathcal{F}^{(l)} = \mathcal{F}^{\text{tree}} g_{\text{ym}}^{2l} (-q^2)^{-l\epsilon} F^{(l)}(C_i), \quad (\text{D.7})$$

where  $q^2 = (p_1 + p_2)^2$  with  $p_1^2 = p_2^2 = 0$  the on-shell gluon multiplet momenta,  $C_i$  stands for all possible Casimir invariants of the underlying gauge group and  $g_{\text{ym}}$  is the Yang-Mills coupling constant. Up to three loops only the quadratic Casimir invariant  $C_A$  – defined via  $f^{acd} f^{bcd} = C_A \delta^{ab}$  – appears, raised to the  $l$ -th

power. Four-loop order is the first place a new, quartic Casimir invariant can appear, see e.g. [378], defined through  $d_{44} = d_A^{abcd} d_A^{abcd} / N_A$  with

$$d_A^{abcd} = \frac{1}{6} [f^{\alpha a}_{\beta} f^{\beta b}_{\gamma} f^{\gamma c}_{\delta} f^{\delta d}_{\alpha} + \text{perms.}(b, c, d)] . \quad (\text{D.8})$$

For gauge group  $SU(N_c)$  the values of the Casimir invariants are  $N_A = N_c^2 - 1$ ,  $C_A = N_c$  and  $d_{44} = N_c^2 / 24 (N_c^2 + 36)$ . Hence, four loops is the first loop-order for which the form factor acquires a color sub-leading, non-planar, correction in 't Hooft's large  $N_c$  limit [379]. Since  $\mathcal{N} = 4$  SYM has no ultraviolet divergences famously, the form of the form factor is determined by powerful infrared exponentiation theorems [380–384], which relate it to two universal functions, the cusp ( $\gamma_{\text{cusp}}^{(l)}$ ) and collinear ( $\mathcal{G}_{\text{coll}}^{(l)}$ ) anomalous dimension at  $l$  loops through

$$(\log F)^{(l)} = - \left[ \frac{\gamma_{\text{cusp}}^{(l)}}{(2l\epsilon)^2} + \frac{\mathcal{G}_{\text{coll}}^{(l)}}{2l\epsilon} + \text{Fin}^{(l)} \right] + \mathcal{O}(\epsilon) . \quad (\text{D.9})$$

These two functions are common to many situations which involve soft and/or collinear divergences and are fixed by the theory under study. Their universal nature leads to a plethora of possible calculational approaches and potential applications, see e.g. [385], [386] and [387]. In maximal super Yang-Mills theory the leading term in the large  $N_c$  limit, referred to as the planar contribution, of the cusp anomalous dimension (CAD) is known to be captured by a universal equation at any value of the coupling [388]. Direct computations of the four-loop planar cusp anomalous dimension can be found in [389–391]. The first numerical result for the first non-planar correction to the cusp anomalous dimension at four loops in any theory appeared in [376], see also [392–396]. Previous work on the Sudakov form factor integrals includes [397] at two loops and [346–348, 398, 399] at three loops, see also [356–359, 400–403] for progress on four-loop integrals.

Apart from the general high interest in high loop computations as evidenced in the many contributions to this document a particular motivation to compute the non-planar correction to the cusp anomalous dimension was a conjecture based on naive extrapolation of results through three loops in [404] that quite generically the cusp anomalous dimension in perturbation theory was proportional to an appropriate power of the quadratic Casimir invariant only, see also [385]. This would require the non-planar correction to the CAD at four loops to vanish, in any theory. By the results in [376] this conjecture is now known to be false, see also [377, 392–396, 405]. The activity the conjecture has sparked has however yielded a veritable treasure trove of insight into gauge theory and its IR divergences, for instance in [339, 355, 404, 406–409].

### 2.3 Constructing the integrand, briefly

In principle the integrand for the problem at hand can be constructed using textbook Feynman graphs. This leads to two problems: one is the prohibitive intermediate expression swell that is to be expected in a Feynman graph computation of this size. The second problem is less immediate but more serious: there is no off-shell, Lorentz-covariant formulation of a theory with maximal supersymmetry. Hence, the resulting expression will have either apparent UV singularities or unphysical poles such as those that arise in the light-cone gauge. Bad apparent UV behaviour translates directly into integrals which are much harder to reduce to an integral basis by integration-by-parts identities due to high numerator count.

To circumvent these problems we have applied in [378] a conjectural idea for the form of the integrand: that of color-kinematic duality [410, 411], see e.g. the lecture [412] for a pedagogical introduction. In essence, color-kinematic duality poses that the integrand of quite general observables in gauge theories can be written in a form where not only do the color factors obey a color-Jacobi identity, but the kinematic, loop-dependent parts do as well. Although there is no known way in general to generate such a representation in field theory, even the suspicion of this duality is enough as an Ansatz generator. With the Ansatz in hand, one fixes coefficients from unitarity cuts. In fact, up until [378] it was thought this approach only applied to scattering amplitudes; we extended it to a variety of form factors [378], while in subsequent work it was extended even to the five-loop



level [413]. The appearing integrals generically can be written as

$$I = (-q^2)^{2+4\epsilon} e^{4\epsilon\gamma_E} \int \frac{d^D l_1}{i\pi^{D/2}} \cdots \frac{d^D l_4}{i\pi^{D/2}} \frac{N(l_i, p_j)}{\prod_{k=1}^{12} D_k}, \quad (\text{D.10})$$

where  $D_i$  are twelve propagators and  $N(l_i, p_j)$  are dimension-four numerators in terms of inner products of the four independent loop and two independent external on-shell momenta.

Having obtained the integrand for the quantity under study (it can be found in [378]) the next step as outlined above is IBP reduction. Integration-by-parts (IBP) identities [414, 415] follow from

$$\int d^D l_1 \dots d^D l_L \frac{\partial}{\partial l_i^\mu} (\text{integrand}) = 0, \quad (\text{D.11})$$

which is the observation that the value of the integrals over loop momenta are invariant under linear transformations of the momenta. For the case at hand a reduction of the integrals obtained in [378] was eventually obtained in [416] using the Reduze code [417]<sup>1</sup>. The output is expressions in terms of a relatively small basis of master integrals. The problem with this is that one can *choose* a set of basis integrals. Since the basis integrals obtained in [416] evaded direct integration methods (see below), a new criterion was needed to select a natural integral basis. For this we turn to number theory.

## 2.4 Maximally transcendental integrals from a conjecture

In general the Feynman integrals that appear in high-energy physics, including those in equation (D.10), have a special property when computed as an expansion in the dimensional regularisation parameter: there is a notion of transcendental weight which functions as the number-theory version of mass-dimension. Assigning weight  $-1$  to  $\epsilon$ , at each order only a sum of rational multiples of certain constants appears, where the constants all have positive, integer-valued weight. Generically at fixed order all terms have transcendental weight less than or equal to a maximum. These constants are mostly multiple zeta values (MZVs), which also obey several algebraic relations. A basis for these constants for low weights is given by (see e.g. [426])

$$\{1\}_0, \{ \}_1, \{\pi^2\}_2, \{\zeta_3\}_3, \{\pi^4\}_4, \{\pi^2\zeta_3, \zeta_5\}_5, \dots \quad (\text{D.12})$$

with increasing weight denoted by the subscripts. Although more general numbers such as Euler sums (which also have well-defined transcendental weight) could appear, it is known through three loops that for the Sudakov form factor only MZVs appear in the component integrals.

The notion of transcendental weight appears in a natural mathematical question: in a given class of integrals such as those in equation (D.10) for a given integral topology, can one find special linear combinations such that the  $\epsilon$  expansion is maximally transcendental? That is, the expansion at each order only contains maximal weight terms, not the sub-leading ones. These integrals will be called Uniformly Transcendental (UT). This notion is important since it is known in examples that for the maximally supersymmetric Yang-Mills theory observables such as the planar cusp anomalous dimension are typically maximally transcendental. Even better, a general conjecture known as the “maximal transcendental principle” [427, 428] states that the maximal transcendental terms appearing in QCD are directly related to the  $\mathcal{N} = 4$  SYM. Just on this basis alone it is already interesting to explore the transcendental properties of Feynman integrals, especially for observables in maximally supersymmetric Yang-Mills theory. Even better, the three-loop form factor in  $\mathcal{N} = 4$  SYM was written in terms of UT integrals in [429]. Hence a natural expectation for the four-loop form factor is that its expansion is maximally transcendental. This property would be guaranteed if it can be expressed in terms of UT master integrals with rational number coefficients.

This leads to the question how UT integrals may be identified other than by the prohibitively complicated direct integration. There are three known criteria

<sup>1</sup>There are various private and public implementations of IBP reduction, such as AIR [418], FIRE [419–421] and Reduze [417, 422]. These are all variants based on the Laporta algorithm [423]. LiteRed [424, 425] implements a somewhat different approach to IBP reduction.

- If an integral can be written in so-called  $d\text{Log}$  form it is UT [430, 431].
- A full set of UT integrals will allow differential equations to be written in so-called  $\epsilon$ -form [432].
- Conjecturally, the residues at all possible poles of a UT integral's integrand (also known as the leading singularities) must always be a constant [356, 431, 433].

The differential equations in Mandelstam invariants mentioned in the second point are not directly applicable to the Sudakov form factor at hand since it is a single-scale problem. See, however, [356, 434] for a way around this problem, which introduces a more complicated class of integrals with an additional off-shell leg in a first step, and later takes the limit of this leg going on-shell. The first criterion requires one to find a special and typically highly non-linear transformation of variables. Although we succeeded to derive a  $d\text{Log}$  form for some integrals, this currently falls more into the art category. The last criterion, however, enables the construction of an algorithm.

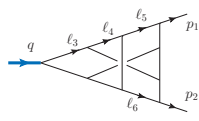
To compute the residues, one first parametrises all loop momenta in a four-dimensional basis of momenta,

$$l_i = \sum_{j=1}^4 \alpha_{i,j} v^j \quad (\text{D.13})$$

In the case at hand there is a preferential choice for the  $v^j$  vectors due to the special kinematics: the set  $\{p_1, p_2, e_1, e_2\}$ . Here  $e_i$  are massless momenta spanning the plane orthogonal to that spanned by  $p_1$  and  $p_2$ . As a result, the only inner products which do not vanish are  $p_1 \cdot p_2$  and  $e_1 \cdot e_2$ , which can be taken to be equal. Then, by mass dimension homogeneity the remaining scale factors out of all integrands, and we are left with a pure function of the 16  $\alpha_{i,j}$  parameters. The criterion introduced above states that an integral is UT if and only if all of the possible poles taken consecutively are single. In principle, this leads to more than  $16!$  possible orders of taking single poles to check – an un-doable task in practice. In our experience, however, if an integral is not UT it will fail the criterion rather quickly, typically within a 100 attempts with randomly chosen pole orders. Hence, given an integral one can relatively quickly check if it is potentially a UT integral.

Given standard, mass-dimension two propagators in a topology with 12 different propagators in the denominator, the criterion requires a generic mass-dimension four numerator. For a fixed integral topology this class of numerators can be parametrised as a linear combination of 191 basis elements. Given the simple-pole criterion one can now derive linear constraints on this set by requiring absence of higher-order poles. Solving these constraints then leads to a smaller Ansatz. This process can be iterated until no further constraints are found in a large number of random residue checks (typically several thousand). Then, the remaining class of integrals is a set of candidate UT integrals.

For the next step one should realise that most numerical integration algorithms greatly prefer to have input numerators given as products of propagators (mass-dimension two Lorentz invariants involving loop momenta). Hence, one should find linear combinations of the candidate UT integrals to obey this criterion. Given the form of the integrand as derived above, we have performed this task by a combination of brute-force equation solving and inspired guesswork. In several cases which involved the full twelve-line integrals it turned out to be impossible to find good product-form UT candidates. In these cases a linear combination was obtained with one or several ten-line integrals added which consequently possess unit numerator. As an example, consider

$$I_6^{(26)} = \text{Diagram} \times \left\{ [(\ell_3 - \ell_4 - \ell_5)^2 - (\ell_3 - \ell_4 - p_1)^2 - (\ell_6 - p_2)^2 - \ell_5^2] \right. \\ \left. \times [\ell_5^2 - \ell_4^2 - \ell_6^2 + (\ell_4 - \ell_6)^2] \right\}$$


$$+4\ell_5^2(\ell_6 - p_2)^2 + (\ell_4 - \ell_5)^2(\ell_3 - \ell_4 + \ell_6 - p_2)^2\} \quad (\text{D.14})$$

where the entries on the last line are ten-line remnants, see [377] (where the same picture appears) for more details.

## 2.5 Putting the pieces together: results

For all 34 different integral topologies of the Sudakov form factor [378] a list of UT candidate integrals in product form (sometimes with ten-line corrections) was obtained. For both planar as well as non-planar form factor we have related the result in [378] to a rational sum over UT candidate integrals. This is non-trivial since a subset of the general IBP identities which can be derived from equation (D.11) consists of IBP relations without dependence on  $\epsilon$ . This subset will be referred to as rational IBP identities, see [435] for an explanation of how to derive them from a full reduction. The rational IBP identities induce relations between UT candidate integrals. Solving them requires a basis choice. We have found a choice of 32 and 23 UT integrals works for planar and non-planar cases respectively, consistently at minimising the number of different UT integrals in the problem. The fact that the Sudakov form factor found in [378] can be expressed in terms of UT candidate integrals with only rational coefficients is quite non-trivial and requires intricate cancellations between the different integral topologies. Having settled on a list of UT candidate integrals we have performed more than 10000 random pole checks to make sure they are UT. This provides strong evidence that the four-loop form factor in  $\mathcal{N} = 4$  super Yang-Mills theory, including its non-planar correction is indeed maximally transcendental. For several integrals a d-log form was found.

Considering the physical motivations, the next step is integration of the integrals especially in the non-planar sector. Due to the conjecture of [404], the physically relevant question is to what extent the result is in tension with a vanishing cusp and collinear anomalous dimensions. The problem is that while the form factor in total in the non-planar sector diverges as  $\frac{1}{\epsilon^2}$ , the individual integrals diverge as  $\frac{1}{\epsilon^8}$ . This requires the integrals to be expanded up to 6 and 7 orders in the epsilon expansion to obtain information on the cusp and collinear anomalous dimensions respectively. Checking vanishing of the sums up to and including  $\frac{1}{\epsilon^3}$  provides a useful sanity check on the performance of any integration method.

For the problem at hand we have employed a mix of two integration methods: Mellin-Barnes representations [436–438] as well as sector decomposition [439, 440]. Both methods are discussed in more detail in other contributions to this report, so the focus here will be on salient details of our applications. Public packages written in several different languages exist for either method, e.g. for sector decomposition FIESTA [70, 441–443] and SecDec [71, 444, 445] and for MB representations [438, 446–449]. If possible, MB representations tend to yield faster and more accurate results. The problem is that efficient MB representations that are valid (integrable) for non-planar integrals are hard to derive automatically. Hence, for the cases where we have succeeded, these representations were obtained by a mix of methods, while we are still lacking a straightforward strategy to obtain low-dimensional MB representations for non-planar integral topologies. This is an obvious area of potential improvement, see other contributions to this report. For the remaining integrals we have mainly used FIESTA, with cross-checks for simpler integrals using SecDec. To speed up and simplify FIESTA, it pays to implement as much as possible sector symmetries. These are graph symmetries of the parent topology. If the integrand has a manifest graph symmetry, then one can reduce the number of independent sectors. What remains is however still a very hard computation, which we have eventually solved using brute force.

Since numerical methods are employed, a thorough discussion of numerical integration errors is called for. The precision on MB integrals is many orders of magnitude higher than sector decomposition and therefore MB integrals can safely be ignored for this discussion. Where possible we did cross-check FIESTA and MB results. FIESTA employs the CUBA integration library [450], used here in VEGAS mode. VEGAS reports an error which, given enough evaluation points, approaches asymptotically the standard deviation of a Gaussian error. There have been reports in the literature, e.g. in [451], that this reported error underestimates the real error. To guard for this we have for each integral carefully evaluated consistency of central value and error while increasing the number of evaluation points, finding no significant instabilities.

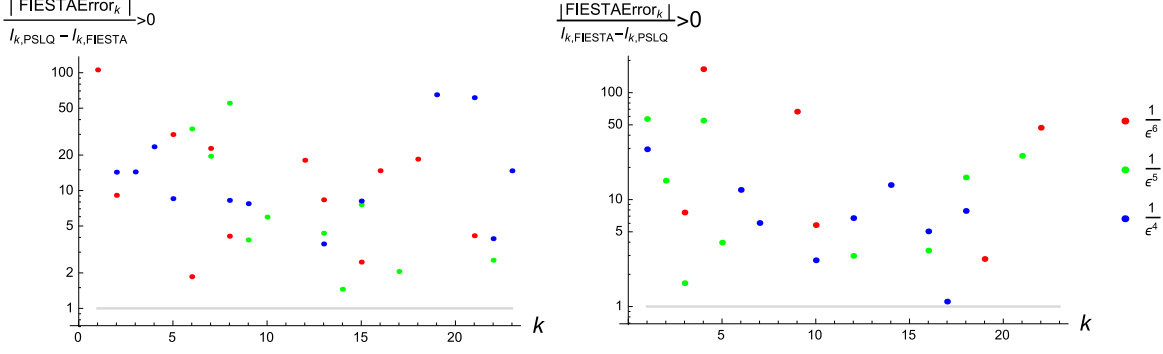


Fig. D.1: Scatterplot of the relative error of FIESTA results compared to PSLQ results for the  $\epsilon^{\{-6,-5,-4\}}$  coefficients. (Left) Plot of cases  $\frac{FIESTA\ error}{I_{PSLQ} - I_{FIESTA}} > 0$ . (Right) Plot of cases  $\frac{FIESTA\ error}{I_{FIESTA} - I_{PSLQ}} > 0$ . A logarithmic scale appears on the vertical axis, and all ratios larger than 200 are not shown in the figures. All ratios are larger than unity, which clearly indicates that the FIESTA errors are conservative estimates. Deviations of FIESTA results from PSLQ results show no tilt to the positive or negative, which supports the conclusion that there is no source of systematic errors.

Since the integrals are expected to be UT, their epsilon expansion is governed by multiple zeta values. From the list in equation (D.12) one can see that for the first five orders of expansion one would expect the coefficients to be a single MZV times a rational. Given a numerical result with a precision of at least a few digits, one can guess which rational number this is through the PSLQ algorithm [452], which is implemented even in Mathematica (`FindIntegerNullVector`). If we take this to be the exact answer, then this gives a platform to relate the true error to the FIESTA-reported error. Hence we can use the number-theoretic properties of integrals to evaluate a numerical integration algorithm. The outcome of this is summarised in the figure D.1, which is taken from [377]. Basically, there is ample evidence that the FIESTA-reported error overestimates the true error by a considerable margin.

Pushing through the computation then gives the following results for the non-planar, light-like cusp and collinear anomalous dimensions in  $\mathcal{N} = 4$  super Yang-Mills theory,

$$\gamma_{\text{cusp, NP}}^{(4)} = -3072 \times (1.60 \pm 0.19) \frac{1}{N_c^2} \quad \text{and} \quad \mathcal{G}_{\text{coll, NP}}^{(4)} = -384 \times (-17.98 \pm 3.25) \frac{1}{N_c^2}. \quad (\text{D.15})$$

These numbers emerge from the  $1/\epsilon^2$  and  $1/\epsilon$ -pole of the non-planar part of the four-loop form factor, respectively. Both of them are statistically significantly different from zero, while all the higher-order poles from  $1/\epsilon^8$  through  $1/\epsilon^3$  vanish within error bars.

## 2.6 Discussion and conclusion

This contribution has discussed the steps needed to compute for the first time the non-planar part of the Sudakov form factor in  $\mathcal{N} = 4$  SYM, which appears first at four loops. The result shows that contrary to a conjecture the cusp and collinear anomalous dimensions do not vanish in the non-planar sector, for this particular theory. This implies that the structure of IR divergences for general gauge theories is more complicated than (perhaps naively) expected. The computation at various places involves educated guess-work and manual labor. In the context of the FCC this should be taken as direct motivation for the development of automated tools and techniques. The UT finding algorithm described here is especially ripe for much more general applications. There has also been quite some encouraging development of automated tools for MB representations, some of which was reported at the workshop. The integrals treated in this contribution are however beyond the current round of development and will need further improvements. As always, having explicit results for specific integrals greatly benefits development of code of this type.

One interesting direction is to investigate two-point form factors like the Sudakov one beyond the confines of  $\mathcal{N} = 4$  SYM, probably first in massless QCD. This will pave the way to more intricate computations in the electroweak sector. The ease of integration for UT integrals we have encountered here alone is sufficient motivation. Furthermore, in massless QCD for the four-loop Sudakov form factor for instance, one could seek for an expansion in terms of UT integrals which have a genuine Taylor expansion around  $\epsilon = 0$ , see [453] for progress in this direction.

Perhaps the most immediately important observation made in the execution of the project is that UT integrals are much simpler to integrate using sector decomposition than generic integrals in the same class. This applies both to integration timing as well as to accuracy. In fact, we have observed that the expansion coefficients of UT integrals typically grow by one decade per expansion order, where for generic integrals these can grow by several decades per expansion order. Whereas the first behaviour leads to a numerical precision which is just enough to obtain the physical result, with the latter it would have been out of the question. This offers an immediate advantage to be exploited for explicit computations beyond the scope of the present project, for instance for self-energy computations at high loop orders. For integrals which have more complicated kinematics it would be interesting to explore UT finding methods, perhaps as a help along the way of finding so-called  $\epsilon$ -form differential equations, see the talk of Johannes Henn [454] and the section E.8 by Roman Lee.



# Chapter E

## Methods and Tools

### 1 Introduction

**Authors:** Janusz Gluza, Stanisław Jadach, Tord Riemann

There are two frontiers of theoretical research. One is the quest for new basic concepts. The other one is the quest for higher precision. Both together are the fundamental of physics since centuries, and they will so also in future. Both need special methods and tools to explore, though this is especially important in case of precision studies and theoretical calculations where frontier knowledge from mathematics and computational physics must be used. Very often studies there have an interrogative character, going into so-called exploratory mathematics [455,456].

In this chapter we try cover all relevant from today's perspective available methods and tools, which are needed in higher order radiative corrections calculations and specifically at FCC-ee-Z. Among them there are already well established methods like differential equation method, sector decomposition numerical method and Mellin-Barnes analytical and numerical method. They are already widely in use in particle physics. There are also some emerging methods which we will discuss. Usually methods must be accompanied by suitable tools, here it means that specific software must be developed. It is also discussed in this chapter. The calculations which are ahead as seen from the FCC-ee-Z perspective are very challenging and have to be more precise than the experimental accuracy to be reached. In many sections of this chapter accuracy, limitations and ways out to reach the goal which is ahead of us are discussed.

Of course, though basically all relevant methods and tools are represented in this chapter, it is not possible to explore them on the same footing, concerning the computational complexity and the different theoretical, mathematical and computer algebraic details.

Here we explore especially sector decomposition and Mellin-Barnes methods as they bring us lately to completion of the 2-loop weak corrections to the Z-boson decay [16, 76], as EWPOs are actually the main issues of this report explored in previous chapters. Our estimation is that these methods can be used for next step which is needed, namely 3-loop electroweak calculations. However, there are also there many places for improvements in existing packages.

Some more materials related to the issue of loop calculations for FCC-ee-Z can be found in talks [8], which are not included in this report. Namely for unitarity approach see Harald Ita [457], for bootstrapping at NNLO see Johannes Henn [454], for IBP methods and difference equations see Vladimir Smirnov [458], and finally, for tools on canonical form of differential equations see Oleksandr Gituliar [459]. Other useful talks can be found in web pages of recent conferences: "Loops and Legs in QFT" [460] and "LoopFest" [461]. In addition to the advanced material we are presenting here, we recommend some excellent works and textbooks in addition. For analytical methods of multiloop calculations, see [462–464], for numerical and general computation methods, see [69].





## 2 The MBnumerics project

**Authors:** Johann Usovitsch, Ievgen Dubovyk, Tord Riemann

Corresponding Author: Johann Usovitsch [jusovitsch@googlemail.com]

### 2.1 Introduction

Our starting point will be the loop-momenta integral representation of a scalar Feynman integral:

$$G_L = \int \prod_{j=1}^L \frac{d^D k_j}{i\pi^{D/2}} \frac{1}{P_1^{\nu_1} \dots P_N^{\nu_N}}. \quad (\text{E.1})$$

The functions  $P_i^{\nu_i}$  in the denominator are expressed in terms of the  $L$  loop-momenta  $k_l$  which are not fixed through momentum conservation at each vertex and the  $E$  linearly independent external momenta  $p_e$ :

$$P_i = \left( \sum_{l=1}^L a_{il} k_l + \sum_{e=1}^E b_{ie} p_e \right)^2 - m_i^2 + i\delta, \quad a_{il}, b_{ie} \in \{-1, 0, 1\}, \quad (\text{E.2})$$

where the  $m_i$  denote the masses of the corresponding virtual particles. The  $i\delta$  is the Feynman prescription. In the most general case the  $P_i$  are a linear combination of  $N$  linearly independent scalar products depending on the loop-momenta  $k_l$ . The propagator exponents  $\nu_i$  are complex variables if not stated otherwise. Within dimensional regularization,  $D = 4 - 2\epsilon$  denotes the dimension of space-time. As usual  $D \neq 4$  is used to regularize infrared or ultraviolet divergences.

Before evaluating these integrals one often applies the Feynman trick:

$$\frac{(-1)^\nu}{\prod_{j=1}^N (-P_j^{\nu_j})} = \frac{(-1)^\nu \Gamma(\nu) \left( \prod_{j=1}^N \tilde{n}_j \right) \delta(1 - \sum_{j=1}^{N_G} x_j)}{(-k_l^\mu M_{ll'} k_{l'\mu} + 2k_l^\mu Q_{l\mu} + J - i\delta)^\nu}, \quad \nu = \sum_{j=1}^N \nu_j, \quad (\text{E.3})$$

where

$$M_{ll'} = \sum_{j=1}^N a_{jl} a_{jl'} x_j \quad (\text{E.4})$$

is an  $L \times L$  symmetric matrix,

$$Q_l^\nu = - \sum_{j=1}^N x_j a_{jl} \sum_{e=1}^E b_{je} p_e^\nu \quad (\text{E.5})$$

is a vector with  $L$  components and

$$J = - \sum_{j=1}^N x_j \left( \sum_{e=1}^E b_{je} p_e^\mu \sum_{e'=1}^E p_{e'}^\nu b_{je'} g_{\mu\nu} - m_j^2 \right), \quad (\text{E.6})$$

where  $x_j$  are the Feynman parameters introduced with the Feynman trick. The set of Feynman parameters  $\{x_1, \dots, x_{N_G}\}$  corresponds to the set of functions  $\{P_1, \dots, P_{N_G}\}$  with positive  $\{\nu_1, \dots, \nu_{N_G}\}$  in Eq.(E.1). The metric tensor is  $g_{\mu\nu} = \text{diag}(1, -1, \dots, -1)$ . The  $\tilde{n}_j$  is defined as:

$$\tilde{n}_j \phi(\vec{x}) = \begin{cases} \int_{\{x_j \geq 0\}} \frac{dx_j x_j^{\nu_j-1}}{\Gamma(\nu_j)} \phi(\vec{x}), & \nu_j \neq -m, \\ (-1)^{\nu_j} \phi^{(-\nu_j)}(0, x_{i \neq j}), & \nu_j = -m, \end{cases} \quad m \in \mathbb{N}_0, \quad (\text{E.7})$$

where  $\phi^{(-\nu_j)}(0, x_{i \neq j})$  means to take  $(-\nu_j)$  derivative in  $x_j$  and then set  $x_j$  to zero.

The Feynman integral can now be written in the Feynman parameter integral representation:

$$G_L = (-1)^\nu \Gamma(\nu - LD/2) \left( \prod_{j=1}^N \tilde{n}_j \right) \delta(1 - \sum_{j=1}^{N_G} x_j) \frac{\mathcal{U}(x)^{\nu - (L+1)D/2}}{\mathcal{F}(x)^{\nu - LD/2}}, \quad (\text{E.8})$$

where

$$\mathcal{U}(x) = \det M, \quad (\text{E.9})$$

$$\mathcal{F}(x) = \mathcal{U}(x)(Q_l^\mu M_{ll'}^{-1} Q_{l'\mu} + J - i\delta). \quad (\text{E.10})$$

From these definitions it follows that the functions  $\mathcal{F}(x)$  and  $\mathcal{U}(x)$  are homogeneous in the Feynman parameters  $x_i$ . The function  $\mathcal{U}(x)$  is of degree  $L$  and the function  $\mathcal{F}(x)$  is of degree  $L + 1$ . The functions  $\mathcal{U}(x)$  and  $\mathcal{F}(x)$  are also known as Symanzik polynomials.

## 2.2 Mellin-Barnes integral

Feynman integrals may be infrared and ultraviolet divergent. To treat these integrals in a consistent and automated way two methods are known: The Mellin-Barnes integral approach [436–438, 448, 465] and the sector decomposition approach [439, 440, 466–469].

To derive a Mellin-Barnes integral one will use either the loop-by-loop approach [72] or the global approach [75]. Both techniques apply in their core to the  $\mathcal{F}(x)$  and  $\mathcal{U}(x)$  functions in Eq. (E.8) the Mellin-Barnes integral master formula:

$$\frac{1}{(a+b)^\nu} = \int_{-i\infty}^{i\infty} \frac{dz}{2\pi i} \frac{a^z b^{-z-\nu} \Gamma(-z) \Gamma(\nu+z)}{\Gamma(\nu)}, \quad |\arg a - \arg b| < \pi, \quad (\text{E.11})$$

until the integrations over the Feynman parameters can be all carried out in terms of Euler's Beta-functions:

$$B(\xi, \chi) = \int_0^\infty \frac{x^{\xi-1}}{(1+x)^{\xi+\chi}} dx = \frac{\Gamma(\xi) \Gamma(\chi)}{\Gamma(\xi+\chi)}, \quad \Re \xi > 0, \Re \chi > 0. \quad (\text{E.12})$$

These steps lead to Mellin-Barnes integrands depending on a ratio of Euler's Gamma-functions  $\Gamma$  depending on the integration variables  $z_i$  and some kinematics raised to the powers of  $z_i$ .

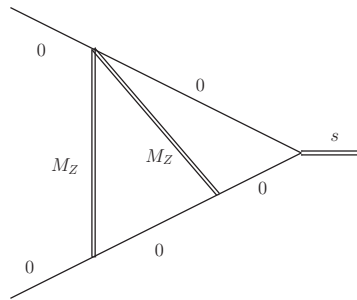


Fig. E.1: Two-loop vertex Feynman integral with two internal massive lines and the kinematics are  $p_{1,2}^2 = 0$  and  $2p_1 p_2 = s$ . The  $Z$ -boson mass  $M_Z$  indicates massive propagators.

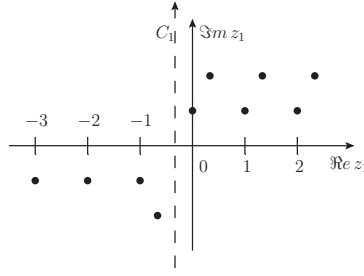


Fig. E.2: The black dots are the poles of the integrand in Eq. (E.18) in the  $z_1$  complex plane. The dashed line is the integration contour parallel to the imaginary axis.

As an example we study the Feynman integral in Fig. E.1, whose loop-momenta integral representation contains one nontrivial numerator  $k_1 p_1$ :

$$I_{0h0w14r} = \int \frac{d^D k_1}{i\pi^{D/2}} \frac{d^D k_2}{i\pi^{D/2}} \frac{k_1 p_1}{k_1^2((k_1 - k_2)^2 - M_Z^2)k_2^2((k_2 + p_1)^2 - M_Z^2)(k_1 + p_1 + p_2)^2}, \quad (\text{E.13})$$

and its Mellin-Barnes integral representation is:

$$I_{0h0w14r} = \int_{-\frac{1}{3}-i\infty}^{-\frac{1}{3}+i\infty} \frac{dz_1}{2\pi i} \int_{-\frac{1}{3}-i\infty}^{-\frac{1}{3}+i\infty} \frac{dz_2}{2\pi i} \frac{\Gamma(-z_1)\Gamma(-z_2)\Gamma(z_2+1)\Gamma(-\epsilon-z_1)\Gamma(2\epsilon+z_1+1)\left(-\frac{M_Z^2}{s}\right)^{z_1}}{2\Gamma(1-z_2)\Gamma(-3\epsilon-z_1+2)\Gamma(-2\epsilon-2z_1-z_2)} \times (-s)^{-2\epsilon} \Gamma(-2\epsilon-z_1-z_2)^2 \Gamma(-\epsilon-z_1-z_2) \Gamma(\epsilon+z_1+z_2+1), \quad (\text{E.14})$$

where  $\epsilon = (4-D)/2$ . A straight integration contour parallel to the imaginary axis is chosen, such that all poles are well separated, see Fig. E.2 for  $z_{1,2} = -1/3 + it$ ,  $t \in [-\infty, \infty]$ . The expansion around  $\epsilon = 0$  in Eq. (E.14) leads to a finite contribution in the lowest order:

$$I_{0h0w14r} = - \int_{-\frac{1}{3}-i\infty}^{-\frac{1}{3}+i\infty} \frac{dz_1}{2\pi i} \int_{-\frac{1}{3}-i\infty}^{-\frac{1}{3}+i\infty} \frac{dz_2}{2\pi i} \frac{\Gamma(-z_1)^2 \Gamma(z_1+1) \Gamma(-z_2) \Gamma(z_2+1) \left(-\frac{M_Z^2}{s}\right)^{z_1} \Gamma(-z_1-z_2)^3}{2\Gamma(2-z_1)\Gamma(1-z_2)\Gamma(-2z_1-z_2)} \times \Gamma(z_1+z_2+1) + \mathcal{O}(\epsilon). \quad (\text{E.15})$$

### 2.3 Minkowskian kinematics

Whether we derive the Mellin-Barnes integrals with the loop-by-loop or the global approach, we face problems in the numerical treatment of these integrals in Minkowskian kinematics. To illustrate this we apply the well known Stirling approximation formula

$$\Gamma(z) \underset{|z| \rightarrow \infty}{\approx} z^{z-1/2} e^{-z} \sqrt{2\pi}, \quad |\arg z| < \pi, \quad (\text{E.16})$$

to the integrand in Eq. (E.15) and examine the asymptotic behavior for  $z_1 = -\frac{1}{3} + it_1$ , and  $z_2 = -\frac{1}{3} + it_2$ ,  $t_1 \rightarrow -t$  and  $t_2 \rightarrow t$ :

$$\mathcal{I}_{0h0w14r} \underset{t \rightarrow \infty}{\approx} t^{-2+2x_1+2x_2} \Big|_{x_1=x_2=-1/3}. \quad (\text{E.17})$$

In comparison to the Euclidean kinematics, where the asymptotic behavior is everywhere exponentially damped, we see that for Minkowskian kinematics the asymptotic behavior is polynomial. In the case of a Mellin-Barnes integral this polynomial asymptotic behavior leads to numerous numerical instabilities, some of which are:

- Oscillations are less damped compared to the Euclidean case.

- Integrals may be not absolutely convergent if the asymptotic behavior is worse than  $1/t^a$ , with  $a < 2$ .
- At any level of accuracy, we need to evaluate the integrands for bigger values  $t_i$  than in the case of Euclidean kinematics.
- In particular, if we are interested in high accuracy results, we have to evaluate the  $\Gamma$  functions for very big arguments and this leads again to numerical instabilities.

We assume that the treatment of one-dimensional Mellin-Barnes integrals is a solved problem by means of contour deformation. We describe techniques which are applied to multi-dimensional Mellin-Barnes integrals. These techniques are automatized in the Mathematica package MBnumerics, which was developed to treat numerically Feynman integrals appearing in the calculation of the electroweak two-loop corrections to the pseudo observables at the Z-boson resonance [15], [16].

In the case of the Mellin-Barnes integral the linear transformation of integration variables may lead to improvements of the numerical integration. If we apply the variable change  $z_2 \rightarrow z_2 - z_1$  to the example integral in Eq. (E.15) we get

$$I_{0h0w14} = - \int_{-\frac{1}{3}-i\infty}^{-\frac{1}{3}+i\infty} \frac{dz_1}{2\pi i} \int_{-\frac{2}{3}-i\infty}^{-\frac{2}{3}+i\infty} \frac{dz_2}{2\pi i} \frac{(-\frac{M_Z^2}{s})^{z_1} \Gamma(-z_1)^2 \Gamma(1+z_1) \Gamma(z_1-z_2) \Gamma(-z_2)^3}{2\Gamma(2-z_1) \Gamma(-z_1-z_2) \Gamma(1+z_1-z_2)} \times \Gamma(1+z_2) \Gamma(1-z_1+z_2). \quad (E.18)$$

After this simple change of variable the asymptotic behavior of the Mellin-Barnes integrand has been changed. If we apply again the Stirling formula in Eq. (E.16) to the integrand in Eq. (E.18), and study the asymptotic behavior for  $z_1 = -\frac{1}{3} + it_1$ ,  $z_2 = -\frac{2}{3} + it_2$ ,  $t_1 \rightarrow -t$  and  $t_2 \rightarrow 0$ , we find

$$\mathcal{I}_{0h0w14} \underset{t \rightarrow \infty}{\approx} t^{-2+2x_2} \big|_{x_2=-2/3}, \quad (E.19)$$

i.e. the polynomial asymptotic behavior depends only on  $x_2$ . Linear integration variable transformations give a possibility for a nontrivial cross check of the numerical evaluation of the Mellin-Barnes integrals, since the integrands have different asymptotic behavior before and after the linear transformation.

An obvious improvement is the application of the cotangent mapping  $t = \frac{1}{\tan(-\pi d)}$ , which maps the integration boundaries from  $t \in [-\infty, \infty]$  to  $d \in [0, 1]$ . We apply this mapping to a polynomial function, which gives

$$\frac{1}{t^a} = \tan(-\pi d)^a, \quad (E.20)$$

and the Jacobian is:

$$\frac{\pi}{\sin(\pi d)^2}, \quad (E.21)$$

where the limits of the integrand at the boundaries of the new integration domain are:

$$\lim_{d \rightarrow 0, d \rightarrow 1} \frac{\pi \tan(-\pi d)^a}{\sin(\pi d)^2} = \begin{cases} \frac{1}{0}, & a < 2, \\ \pi, & a = 2, \\ 0, & a > 2. \end{cases} \quad (E.22)$$

Compared to the cotangent mapping, a logarithmic mapping, as it is advocated in the program MB.m [448], always leads to infinities at the new integration boundaries, which would lead to numerical instabilities.

Since we use the cotangent mapping it is mandatory to transform the integrand as follows:

$$\prod_i \Gamma_i \rightarrow \exp \left( \sum_i \log \Gamma_i \right), \quad (E.23)$$

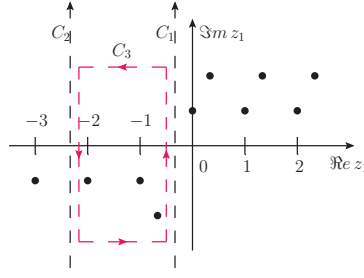


Fig. E.3: The original contour  $C_1$  is shifted by  $n_1 = -2$  to a contour  $C_2$ . The third contour  $C_3$  encircles the poles to correct the shift.

where the key idea is that the  $\log \Gamma(z_i)$  functions grow slower than the  $\Gamma(z_i)$  functions for large values of  $|z_i|$ .

If we shift the Mellin-Barnes integration variables according to

$$z_i = x_i + it_i + n_i, \quad n_i \in \mathbb{R}, \quad (\text{E.24})$$

the asymptotic behavior of a given Mellin-Barnes integrand may depend explicitly on the shifts  $n_i$ :

$$\mathcal{I}_{0h0w14} \underset{t \rightarrow \infty}{\approx} t^{-2+2x_2+2n_2} \big|_{x_2=-2/3}. \quad (\text{E.25})$$

It is then possible to improve the polynomial asymptotic behavior by tuning the shifts  $n_i$ . If, by changing the values of  $n_i$ , the contour crosses some poles of the Mellin-Barnes integrand, we have to collect their residues.

The shifts may also be used as a method to evaluate Mellin-Barnes integrals in Minkowskian regions due to one more observation: the integral along a shifted contour may be numerically smaller by orders of magnitude compared to the original integral.

For example, the original integral in Eq. (E.18), with  $M_Z = \sqrt{s} = 1$ , evaluated along the contour  $C_1$ , see Fig. E.3, gives  $0.392382858857 + 0.7456388536613i$ . The shifted integral with  $n_1 = -2$ , evaluated along the contour  $C_2$  gives  $-0.00974965823202$ . In addition the following equation holds:

$$\int \frac{dz_2}{2\pi i} \int_{C_1} \frac{dz_1}{2\pi i} \mathcal{I}_{0h0w14} = \int \frac{dz_2}{2\pi i} \int_{C_2} \frac{dz_1}{2\pi i} \mathcal{I}_{0h0w14} + \overbrace{\int \frac{dz_2}{2\pi i} \left( \sum_{z_0} \text{Res}_{z_0} \mathcal{I}_{0h0w14} \right)}^{\text{1 dim integrals}}. \quad (\text{E.26})$$

We have corrected the result of the integral along the shifted contour by calculating three residues, corresponding to the three poles enclosed by the contour  $C_3$ . Upon integrating them over  $z_2$ , their sum is  $0.402132517117807 + 0.745638853661318i$ . In general, shifting the contour of an  $n$ -fold Mellin-Barnes integral will yield residue terms, which will be  $(n-1)$ -fold Mellin-Barnes integrals and hence simpler to evaluate.

Authors' note:

The present report on the MBnumerics project has been presented in similar forms at the Conferences LL2018 and Loopfest2018, and at the FCC-ee-Z Theory Miniworkshop at CERN, January 2018. The present contribution is shortend compared to the contribution to the proceedings of LL2018.



### 3 Mini-review on the pragmatic evaluation of multi-loop multi-scale integrals using Feynman parameters

Author: Sophia Borowka [sophia.borowka@cern.ch]

#### 3.1 Introduction

The numerical evaluation of multi-loop multi-scale integrals has become a vital pillar for phenomenological predictions at high energies. In particular at current and future colliders like the proposed FCC-ee, the masses of heavy quarks, vector bosons and the Higgs boson can be resolved. To arrive at the desired accuracy for predictions of exclusive processes, these need to be taken into account exactly. A particularly prominent example is Higgs-boson pair production at NLO in gluon fusion, where naive approximations assuming an infinitely large top-quark mass fail dramatically [470, 471].<sup>1</sup> As a result of the additional non-negligible scales, the Feynman integrals involved in the computation of perturbative predictions become harder to compute. In particular, the virtual contributions beyond the one-loop level contain massive propagators, which can lead to the appearance of elliptic structures, see e.g., [473–475]. However, these can just as well appear in fully massless integrals, as was shown in Ref. [476] for the two-loop hexagon integral in  $N = 4$  supersymmetric Yang-Mills theory. Since the analytical treatment of these structures is still under way, see e.g. [477] and references therein, other methods to compute these types of integrals become highly attractive. Two of these methods are reviewed in this contribution, see Secs. 3.4 and 3.5. The first approach [71, 444, 445, 478, 479] is highly algorithmic and allows for a full numerical evaluation of multi-loop multi-scale integrals. While the second method [480] is based on Taylor series expansions and of similar algorithmic nature, the generation of a library for one integral result takes considerably more time. Yet once the library is generated, the results for arbitrary kinematic values can be evaluated instantaneously and to very high accuracy, see for more details.

Before considering explicit calculations of (multi-)loop integrals, it is advisable to check if analytic results are already available in the literature. A growing subset of these is listed on the community driven database Loopedia [481], introduced in Sec. 3.3.

#### 3.2 Preliminaries

A general Feynman loop integral  $G$  at  $L$  loops with  $N$  propagators, where the propagators  $P_j$  can have in principle arbitrary powers  $\nu_j$  and mass  $m_j$ , has the following representation in momentum space

$$G_{l_1 \dots l_R}^{\mu_1 \dots \mu_R}(\{p\}, \{m\}) = \prod_{l=1}^L \int d^D \kappa_l \frac{k_{l_1}^{\mu_1} \dots k_{l_R}^{\mu_R}}{\prod_{j=1}^N P_j^{\nu_j}(\{k\}, \{p\}, m_j^2)} \quad (\text{E.27})$$

$$d^D \kappa_l = \frac{\mu_r^{4-D}}{i\pi^{\frac{D}{2}}} d^D k_l, \quad P_j(\{k\}, \{p\}, m_j^2) = q_j^2 - m_j^2 + i\delta, \quad (\text{E.28})$$

where the  $q_j$  are linear combinations of external momenta  $p_i$  and loop momenta  $k_l$ . The integral is of rank  $R$ , the indices  $l_i$  indicate the loop momentum associated with Lorentz index  $\mu_i$ . In what follows, the renormalization scale  $\mu_r$  is set to one by default.

After rewriting the integral in terms of Feynman parametrization and integration of the angular component, a scalar integral reads

$$G = \frac{(-1)^{N_\nu}}{\prod_{j=1}^N \Gamma(\nu_j)} \prod_{j=1}^N \int_0^\infty dt_j t_j^{\nu_j-1} \delta(1 - \sum_{l=1}^N t_l) \frac{\mathcal{U}^{N_\nu-(L+1)D/2}}{\mathcal{F}^{N_\nu-LD/2}}, \quad (\text{E.29})$$

<sup>1</sup>It should be noted that an approximation supplemented by the appropriate threshold expansion performs very well, see [472].

where  $\mathcal{U}$  and  $\mathcal{F}$  denote the first and second Symanzik polynomial. They are homogeneous in the Feynman parameters and of degree  $L$  and  $L + 1$ , respectively.

An integral in Feynman parametrization can possess physical singularities in the ultraviolet or infrared limit that need to be regulated dimensionally. Their proper factorization can be performed using sector decomposition [439, 440, 466, 482]. The integration of the  $\delta$ -distribution in Eq. (E.29) can either be done by splitting the integral into  $N$  primary sectors before performing an iterated factorization of the poles. This has the advantage of moving the integration boundaries of the remaining Feynman parameters to zero and one. Alternatively, the Cheng-Wu theorem [447, 483] can be utilized. In this case, the resulting integration boundaries of the remaining Feynman parameters can only be mapped to zero and one, when the factorization of the poles is performed with a deterministic sector decomposition strategy based on algebraic geometry, first introduced in Refs. [484, 485]. The resulting decomposition strategy [71, 486] has proven most efficient in terms of the number of generated sectors and the complexity of the resulting functions. For completeness, other strategies are presented and compared in Refs. [441, 442, 487–489].

### 3.3 Loopedia - a database for loop integrals

Before embarking on the computation of (multi-)loop integrals, it is preferable to have a database of loop integrals, where already existing results are listed and linked to the associated literature reference. Until recently, such a database did not exist. LOOPEDIA [481] attempts to fill this gap, though it is not limited to bibliographic information. The description field of each record can hold any kind of textual information (e.g. links to software). In addition, arbitrary files can be uploaded, for example Fortran programs or Maple worksheets. The database can not only be searched, but new entries can also be submitted and are then reviewed by the LOOPEDIA administrators.

Integrals in the database are generally associated with their underlying graph. In the case of non-trivial numerators, linear combinations, or a set of integrals in a topology, the reference is indexed by the scalar integral of the topology. In this context, a topology is defined as a fixed set of propagators and external lines with fixed mass assignments. Tensor integrals are intentionally not covered. In legitimate cases, they can be added as an additional entry for the scalar integral of the same topology by providing the additional information in the description box of the submission.

LOOPEDIA is located at `loopedia.org`. Its landing page is depicted in Fig. E.4.

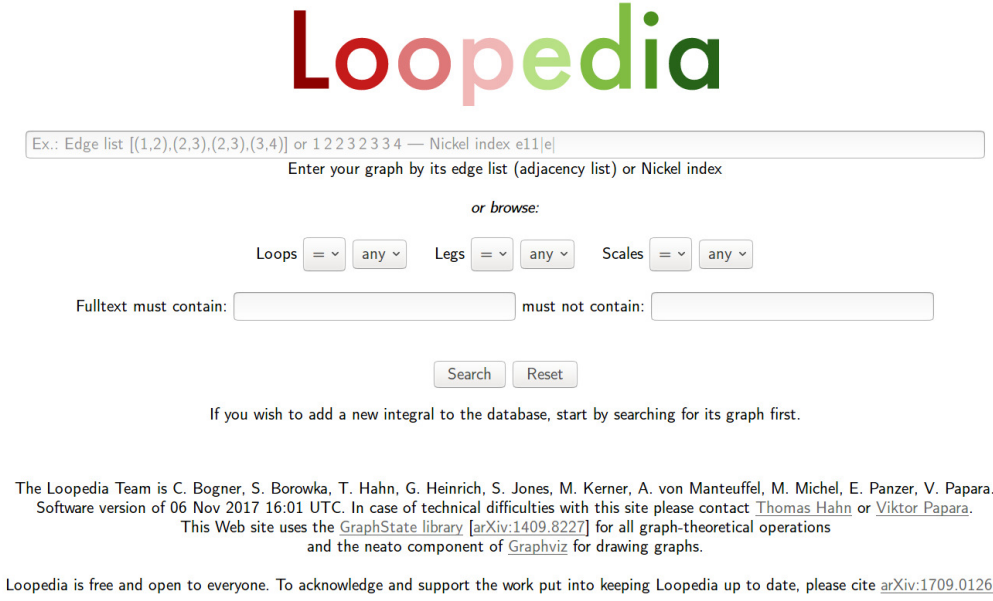
### 3.4 Numerical evaluation with the program pySecDec

For a highly automated and user-friendly calculation of multi-loop and multi-scale Feynman integrals the publicly available program PYSECDEC [479] is introduced. PYSECDEC is the direct successor of the program SECDEC [71, 444, 445, 478]. It is based on the method of sector decomposition and is one out of several publicly available programs [70, 73, 441–443, 487] to perform the integration of multi-loop integrals numerically. While SECTOR\_DECOMPOSITION [73, 487] is restricted to the Euclidean region or single-scale integrals, (PY)SECDEC and FIESTA [70, 441–443] allow for an evaluation in the physical region of in principle arbitrary multi-loop multi-scale integrals.

Unlike previous versions of SECDEC, PYSECDEC relies on open-source software only. It performs the automated factorization of dimensionally regulated poles in Feynman and more general parametric integrals and the subsequent numerical evaluation of the finite coefficients.

The algebraic part of the program is written in the form of python modules allowing for a very flexible usage. An optimized C++ code is generated using the program FORM [490, 491], leading to a faster numerical convergence with respect to previous versions of the program. To facilitate the integration itself, the program is linked to the publicly available CUBA library [450, 492, 493]. For one-dimensional integrals, the integrator CQUAD contained in the GNU scientific library [494] can be used. An overview of the operational sequence is depicted in Fig. E.5. The generated files can be used as an integral library which can be interfaced with user-specific codes, e.g., for the evaluation of matrix elements.





Ex.: Edge list [(1,2),(2,3),(2,3),(3,4)] or 1 2 2 3 2 3 3 4 — Nickel index e11[e]

Enter your graph by its edge list (adjacency list) or Nickel index

or browse:

Loops  any  Legs  any  Scales  any

Fulltext must contain:  must not contain:

If you wish to add a new integral to the database, start by searching for its graph first.

The Loopedia Team is C. Bogner, S. Borowka, T. Hahn, G. Heinrich, S. Jones, M. Kerner, A. von Manteuffel, M. Michel, E. Panzer, V. Papara.  
 Software version of 06 Nov 2017 16:01 UTC. In case of technical difficulties with this site please contact [Thomas Hahn](#) or [Viktor Papara](#).  
 This Web site uses the [GraphState library](#) [arXiv:1409.8227] for all graph-theoretical operations  
 and the neato component of [Graphviz](#) for drawing graphs.

Loopedia is free and open to everyone. To acknowledge and support the work put into keeping Loopedia up to date, please cite [arXiv:1709.01266](#).

Fig. E.4: LOOPEDIA's landing page.

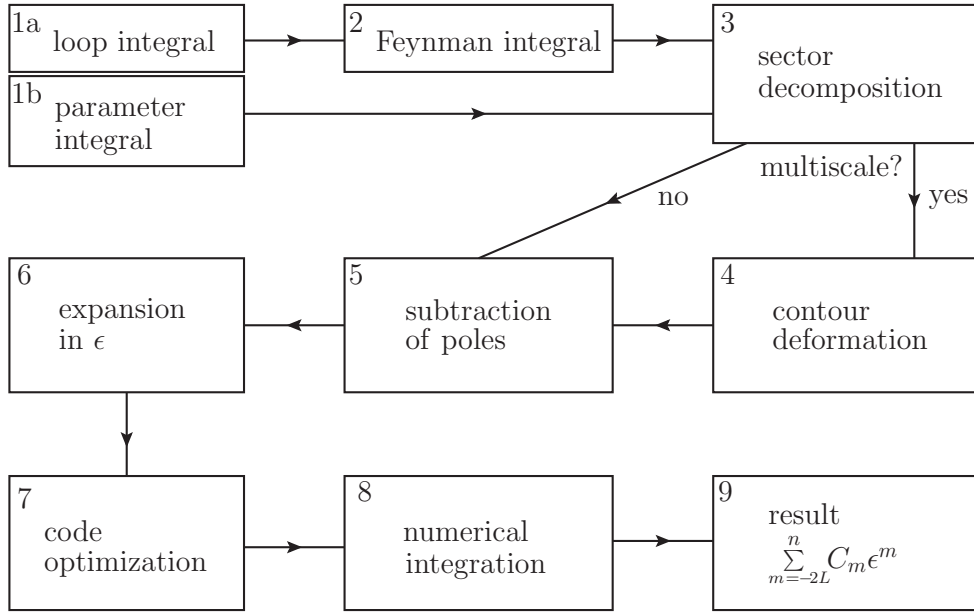


Fig. E.5: Flowchart showing the main building blocks of PYSECDEC. Steps 1 to 6 are executed in python. FORM is used in step 7 to produce optimized C++ code.

Further new features in PYSECDEC:

- The evaluation of multiple integrals or even amplitudes is now possible, using the generated C++ library.
- The treatment of numerators of loop integrals is more flexible. Numerators can be defined in terms of contracted Lorentz vectors or inverse propagators or a combination of both.

- The functions can have any number of regulators for endpoint singularities, not only the dimensional regulator  $\epsilon$ .
- The inclusion of additional functions which do not enter the decomposition has been facilitated and extended.
- A symmetry finder [495] has been implemented which can detect isomorphisms between sectors.
- A procedure has been implemented to detect and remap singularities at  $x_i = 1$  which result from special kinematic configurations.
- The treatment of poles which are higher than logarithmic has been improved.
- If the propagators are given in terms of an edge list, the resulting loop diagram can be drawn using neato [496]. This functionality is optional and the program runs normally if neato is not installed.
- The distinction between "general functions" and "loop integrands" is removed in the sense that all features are available for both, loop integrals and general polynomial functions (as far as they make sense outside the loop context).
- complete re-structuring and usage of open source software only

More details on the usage are found in Ref. [479] and [497].

### 3.5 Accurate approximation using the TayInt approach

To shorten the evaluation times with respect to a fully numerical evaluation, the results have to be algebraic in the kinematical parameters (Mandelstam invariants, external and internal particle masses). Then the evaluation at each kinematic point takes just as much as the time needed for the insertion of their numerical values. Algebraic results can be obtained if the integrands are Taylor expanded in the Feynman parameters. To ensure that the approximation is fastly-converging in all regions of parameter space, each integrand must be manipulated so that it is in a form optimized for a Taylor expansion. This task and the expansion itself is performed by TAYINT [480], a program to analytically approximate loop integrals. Its algorithm can be summarized as follows:

1. Input an integral.
2. Reduce the integral to a quasi-finite basis introduced in Refs. [498,499], such that the divergences are in the coefficient of the simplest integrals. An automated script using the libraries of the publicly available program REDUZE [417,499,500] performs this.
3. For those basis integrals that are not known in analytic form, carry out a decomposition into subsectors with smoother integrands. These are obtained using the publicly available program SECDEC 3 [71, 444,445,479], without its contour deformation option. The subsector integrands are analytic within the integration region, but may contain integrable singularities over thresholds and at end points.
4. Use a conformal mapping to move the singularities outside of the region of integration as far away as is possible. This is done in MATHEMATICA [501].
5. (a) To produce a result valid below the kinematic thresholds, the integrand is Taylor expanded, and integrated over the Feynman parameters. This is all done in FORM [490,491].  
 (b) To produce a result valid above thresholds, there is a separate algorithm implemented in MATHEMATICA. The subsectors are first mapped onto the complex half plane. The algorithm then determines which configuration to use for each sector, that is, which contour orientation to use for the multiple variable integration and how to partition the subsequent region into smaller pieces. The Taylor expansion and integration are then performed on the new integrands specified by TAYINT.

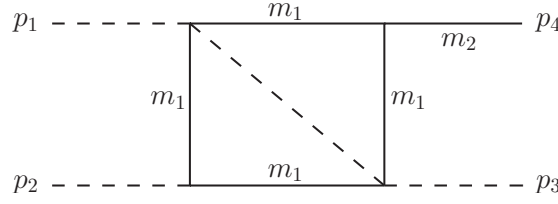


Fig. E.6: The box-type integral I39 is so far unknown analytically. Dashed lines indicate massless and solid lines massive propagators.

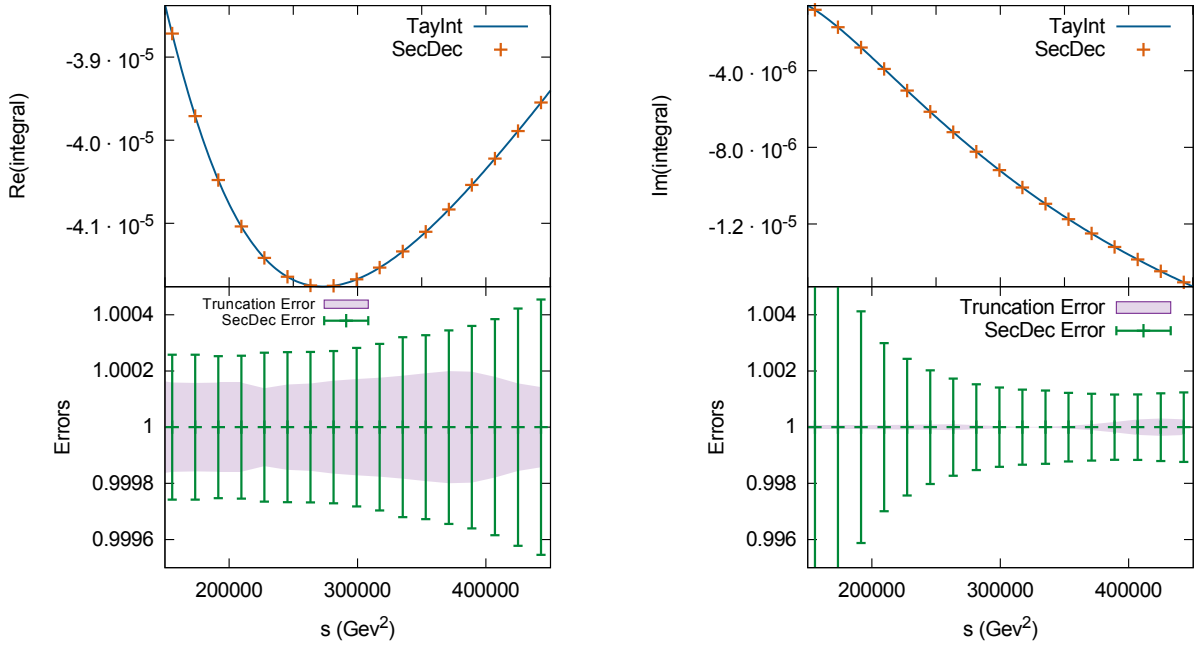


Fig. E.7: The I39 Integral calculated at  $\mathcal{O}(\epsilon^0)$  with a fourth order series expansion. The scale  $s$  is over the  $4m_1^2$  threshold, with  $u = -59858\text{GeV}^2$ ,  $m_2 = \frac{1}{\sqrt{2}}m_1$  and  $m_1 = 173 \text{ GeV}$ . The lower plots show the relative TAYINT and SECDEC uncertainties, respectively.

The method and its applications are described in comprehensive detail in Ref. [480]. Among the applications is the prediction of results for the finite I39 integral, see Fig. E.6, which is so far not available in the literature and contributes, e.g., to Higgs+jet production at NLO. Its coefficient at finite order is reprinted in Fig. E.7. Results for higher orders in the dimensional regulator  $\epsilon$  are found in Ref. [480].

### 3.6 Summary and outlook

First, the community-driven public online database for loop integrals, LOOPEDIA, was introduced. Next, a mini-review on the pragmatic evaluation of multi-loop multi-scale integrals using Feynman parameters was presented, introducing two different methods that do not rely on the analytical evaluation when dealing with highly complicated integrals. As both approaches are highly algorithmic, the computation of multi-loop multi-scale integrals entering predictions for the FCC-ee can be further automated.

## **Acknowledgements**

I want to thank my collaborators, C. Bogner, T. Gehrmann, T. Hahn, G. Heinrich, D. Hulme, S. Jahn, S.P. Jones, M. Kerner, A. von Manteuffel, M. Michel, E. Panzer, J. Schlenk and V. Papara, for the fruitful collaboration.

## 4 AMBRE - Construction of Mellin-Barnes integrals for two- and three-loop $Z$ -boson decays

Authors: Ievgen Dubovyk, Janusz Gluza, Tord Riemann

Corresponding Author: Ievgen Dubovyk [e.a.dubovyk@gmail.com]

### 4.1 Introduction

AMBRE is a project devoted to the representation of Feynman integrals by a finite number of Mellin-Barnes integrals (MB-integrals) in  $d = n - 2\epsilon$  dimensions,  $n \in \mathbb{Z}$ . It includes (i) Automatic construction of planar and non-planar diagrams with up to three loops; (ii) Treatment of tensor integrals.

Descriptions of the AMBRE project with details and examples can be found in [72, 73, 76, 502–506]. Two basic strategies are realized in the construction of MB which we call loop-by-loop (LA) and global (GA) approaches.

In practice, a choice between LA and GA strategies for a given integral aiming at the lowest MB dimensionality of integrals seems not to be unique. For instance, in the case of a massless non-planar two-loop vertex, a minimal fourfold MB representation was derived starting from the global Feynman parameter representation in [437]. On the other hand, in the massive case, it appears that the LA approach is more efficient; an eightfold MB representation can be obtained [465]. In this case, a most optimal tenfold MB representation can be obtained if we start from global Feynman parameters [465]. As discussed there and in [507], those representations may differ also concerning the regularization of singularities. This is another subtlety which shows up when constructing MB representations in real applications.

Taking into account the above examples, it is clear why it is not easy to get a general and efficient program for the construction of a broad class of MB representations. Below we give a short overview on the how to.

### 4.2 AMBRE how to: present status

In Fig. E.8 the flow of operations is shown and the present versions of the corresponding software for the generation of MB integrals and the numerical solutions are indicated.

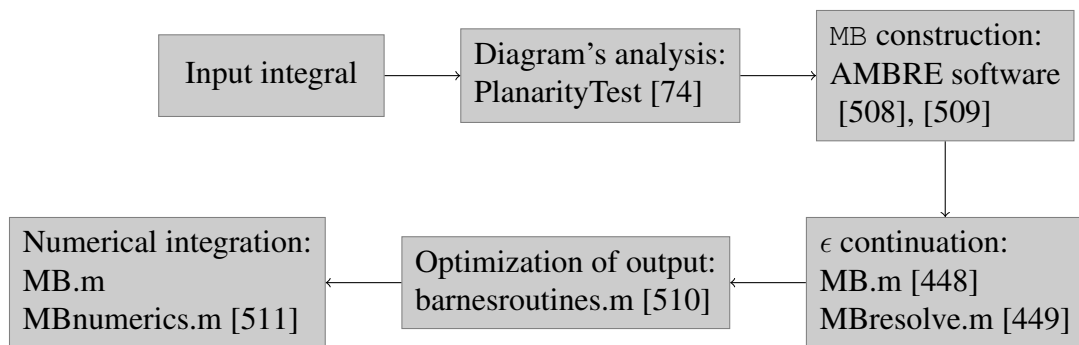


Fig. E.8: The operational sequence of the MB-suite. The flowchart shows the main steps and the corresponding software for producing a Mellin-Barnes representation for a Feynman integral and for performing its numerical evaluation.

The procedure starts from the diagram's topology identification. Based on that a proper version of the AMBRE program is used. Drawing and topology identification of the diagrams is based on the knowledge of propagators (masses and momenta flow) and can be made using `PlanarityTest` [74]. This seems to be trivial, but in case of more loops sometimes it is not easy to determine planarity of the diagram by eye and

an automation is desired. An example is given in Fig. E.9. It is planar though it was identified as non-planar in [443].

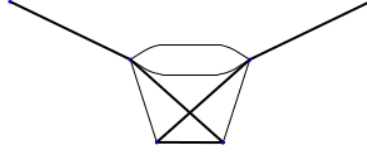


Fig. E.9: Example of a planar four-loop diagram.

After MB construction, an analytic  $\epsilon$  continuation in  $d = 4 - 2\epsilon$  dimensions can be made using `MB.m` or `MBresolve.m` [448, 449]. Then a further optimization beyond what is already done by `AMBRE` can be made using the `barnesroutines` from the `MBtools` web page [512]. Finally, numerical calculations can be made with `MB.m` or `MBnumerics`.

For planar diagrams, the LA method is kept, independent of the number of loops involved. However, we would like to make clear that in general the construction of MB integrals beyond three loops results in high dimensional MB integrals. This is a natural limitation of the MB method as it is used in the `AMBRE` project.<sup>2</sup> On top of that, both methods are not necessarily optimal, if more masses and legs are involved. This is a bottleneck of the present automatic method. In special cases the final choice may depend on the particular physical problem to be solved. That is why the user has in addition an opportunity to improve the factorization of the  $U$  and  $F$  polynomials manually and can continue either with LA (using `AMBREv1.3.1`) or GA. For 2-loop non-planar instances we proceed in a fully automatic way by the GA approach. In this case, independent of the diagram types, the  $U$  polynomials are unique. In 3-loop cases, we divided the procedure depending on the subgraphs involved.

In summary, we are using the following methods and corresponding `AMBRE` software:

- Iteratively to each subloop – LA approach (`AMBREv1.3.1` & `AMBREv2.1.1`)
- In one step to the complete  $U$  and  $F$  polynomials – GA approach (`AMBREv3.1.1`)
- Combination of the above methods – hybrid approach (under development - `AMBREv4`)

Examples, descriptions, and links to basic tools and literature can be found in [502]. Let us refer to other recent approaches, being presented in section 2 and the method of brackets in section 5.

We would like to mention some important facts, which were already described on few occasions in `AMBRE` `www` [502], in publications and in a series of talks:

- for LA the momentum flow really matters;
- The 1st and 2nd Barnes lemmas are key ingredients. For instance,  $-sx_1x_2 - sx_1x_4 + \dots = -sx_1(x_2 + x_4) + \dots$  is equivalent to the 1st Barnes lemma [72];
- LA may work also for non-planar diagrams. For instance, for the diagram in Fig. E.10 `AMBREv2.1.1` gives a 6-dim MB integral while `AMBREv3.1.1` gives a 13-dim MB integral. However, the problem here is that even in Euklidean kinematics highly oscillatory factors may appear, e.g.  $(-s)^z s^z$ .
- GA works for both planar and non-planar diagrams. Though, often less dimensional MB integrals are expected when using `AMBRE` packages tuned for LA approach.

---

<sup>2</sup>For one-loop integrals, a way to reduce the number of MB-dimensions was found in [513, 514], see section E.6.

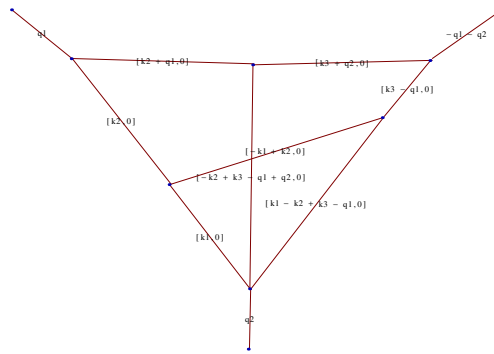


Fig. E.10: Example of a 3-loop non-planar integral where  $\text{LA}$  gives a less dimensional MB integral than  $\text{GA}$ , though its numerical stability can be worse due to more complicated kinematical factors; even in Euklidean kinematical regions.

### 4.3 3-loop AMBRE representations

To be able to use `MB` method efficiently for FCC-ee calculations of EWPOs at 3 loops, a further tuning of the packages is necessary. It appears that at the 3-loop level there are only two basic topologies from which all physical diagrams can be obtained [515]. They are shown in Fig. E.11. To get any 3-loop diagram one has to attach a corresponding amount of external legs to lines and/or vertices of the skeleton diagram.

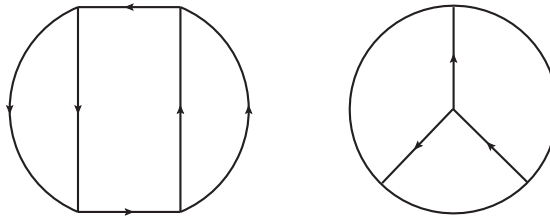


Fig. E.11: Basic skeleton generating diagrams for 3-loop topologies [515].

What we need in the first instance in the FCC-ee case are 3-loop vertex diagrams. The diagram at the left side in Fig. E.11 and all its derivatives can be divided into two one loop pieces, see Fig. E.12. Vertex diagrams of this type have a planar sub-loop and can be treated using the hybrid approach, see next section.

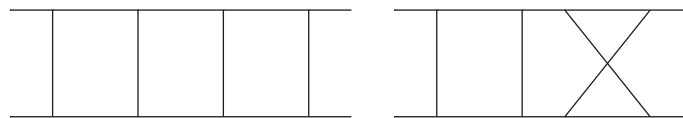


Fig. E.12: 3-loop topologies generated from the left skeleton diagram in Fig. E.11.

The skeleton diagram on the right side in Fig. E.11 generates the most complicated non-planar topologies, see Fig. E.13. Here the more advanced GA is needed. As in the two loop case, after a proper transformation of variables all child diagrams have the same  $U$  function of the form

$$U = v_1v_2v_3 + v_1v_2v_4 + v_1v_3v_4 + v_1v_2v_5 + v_1v_3v_5 + v_2v_3v_5 + v_2v_4v_5 + v_3v_4v_5$$

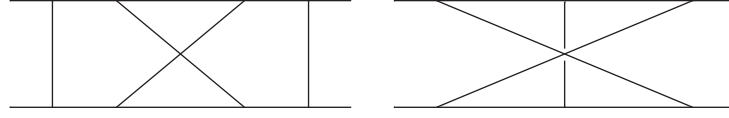


Fig. E.13: 3-loop topologies generated from the right skeleton diagram in Fig. E.11.

$$+ v_1 v_2 v_6 + v_2 v_3 v_6 + v_1 v_4 v_6 + v_2 v_4 v_6 + v_3 v_4 v_6 + v_1 v_5 v_6 + v_3 v_5 v_6 + v_4 v_5 v_6. \quad (\text{E.30})$$

In the next step E.30 can be simplified using the Cheng-Wu theorem [483], [75, 516, 517], keeping in the common  $\delta$ -function 3 variables:

$$\int_0^\infty dv_2 dv_3 dv_4 \int_0^1 dv_1 dv_5 dv_6 \delta(1 - v_1 - v_5 - v_6) \quad (\text{E.31})$$

which gives

$$U_{CW} = v_2 v_3 + v_2 v_4 + v_3 v_4 + v_1 v_2 v_5 + v_1 v_3 v_5 + v_1 v_2 v_6 + v_1 v_4 v_6 + v_1 v_5 v_6 + v_3 v_5 v_6 + v_4 v_5 v_6. \quad (\text{E.32})$$

This form is not unique, the variables in the common  $\delta$ -function can be chosen in 4 different ways. One of the possibilities to perform an integration from 0 to  $\infty$  is to use the following factorization trick:

$$U_{CW} = v_2(v_3 + v_4 + v_1 v_5) + v_3(v_4 + v_1 v_5) + v_1 v_6(v_2 + v_5) + v_4 v_6(v_1 + v_5) + v_3 v_5 v_6. \quad (\text{E.33})$$

There are 6 different ways to get 4 terms in  $U$ , altogether we have 24 variants to apply the Cheng-Wu theorem and to factorize  $U$ . The final choice is based first on the minimization of the amount of terms in  $F$  and second on the presence of the same factorization patterns as in Eq. E.33 for  $U$ , also in  $F$ . Finally, the  $U$  polynomial can be reduced to 4 MB terms. As a rule of thumb, the GA approach usually gives optimal representations if from the beginning  $\text{Length}(U) \leq \text{Length}(F)$ .

#### 4.3.1 The mixed 3-loop approach: an example

At 3 loops we can also approach propagators and sub-loops combining the LA and GA approaches. This depends on whether or not a given topology includes a planar sub-topology which can be disconnected or not. In the first case, Fig. E.14, propagators connected with a planar sub-topology in the form of the one-loop box are transformed into an MB form in a first step, defining a new effective propagator. In this way an effective two-loop diagram is created. In the second case, Fig. E.15, a non-planar disconnected sub-graph can be identified. In this case the first step is to take five propagators of the 2-loop connected propagators, leading in a straightforward way to an effective one-loop topology.

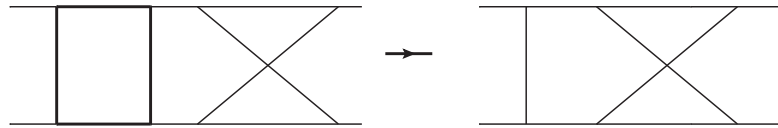


Fig. E.14: Transforming propagators of the one-loop box at the left side into an effective propagator which changes the whole diagram into a two-loop topology.

These strategies are realized in the new AMBRE 4.0 package which is yet under development. Below, as an example it is shown the AMBRE output for the momenta flow as given in Fig. E.16. Some parts of the output are omitted for simplicity.



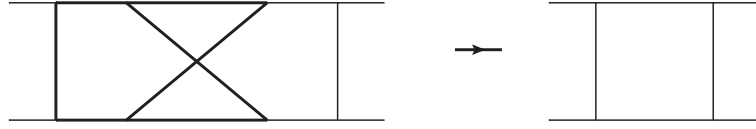


Fig. E.15: Transforming five propagators of the chosen 2-loop sub-diagram into an effective propagator leading directly to the one-loop topology.

```
MBrepr[{{1}}, {PR[k1, 0, n1] PR[-k1 + k2, 0, n2] PR[k2, 0, n3]
PR[k2 + q1, 0, n4] PR[k3 + q2, 0, n5] PR[k3 - q1, 0, n6]
PR[-k2 + k3 - q1 + q2, 0, n7] PR[k1 - k2 + k3 - q1, 0, n8]},
{k1, {k2, k3}}];
```

First, the integration is performed over the  $k_1$  subloop. In Fig. E.16 this is shown by the thick line:

```
--iteration nr: 1 with momentum: k1

--integral: PR[k1, 0, n1] PR[-k1 + k2, 0, n2] PR[k1 - k2 + k3 - q1, 0, n8]
```

Coefficients in the  $F$  polynomial can be represented in form of propagators, as in the case of the LA approach:

```
F polynomial during this iteration
-PR[k2, 0] X[1] X[2] -PR[k2 - k3 + q1, 0] X[1] X[3] -PR[k3 - q1, 0] X[2] X[3]
```

In the next step, the integration is performed over the remaining two loop momenta  $k_2$  and  $k_3$  using GA approach

```
--iteration nr: 2 with momentum: k2, k3

--integral: PR[k2, 0, n3 + z1]
PR[k3 - q1, 0, n6 - z1 - z2 - n1 - n2 - n8 + d/2]
PR[k2 + q1, 0, n4] PR[k3 + q2, 0, n5]
PR[-k2 + k3 - q1 + q2, 0, n7] PR[k2 - k3 + q1, 0, z2]
```

Propagators which remain after the first integration, together with those appearing in  $F$ , form the 2-loop non-planar vertex. Now it is easily seen that the final MB representation is 4-dimensional.

### 4.3.2 Comparisons with the method of brackets

Recently a very interesting new approach to the construction of MB representations was introduced in [518]. Here we compare some basic results from this method of brackets (see Section 5 for details) with results by AMBRE 4.0, in which the above discussed 3-loop non-planar cases were optimized.

From Tab. E.1 it is clear that the new version of AMBRE is much better optimized towards 3-loop  $Z$ -boson studies than the previous public version AMBRE 3, which was discussed in [518].

## 4.4 Conclusions and Outlook

1. The dimensionality of MB representations strongly depends on topology, number of legs and loops, internal and external masses.

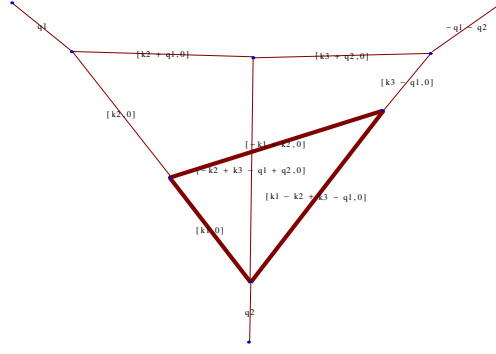
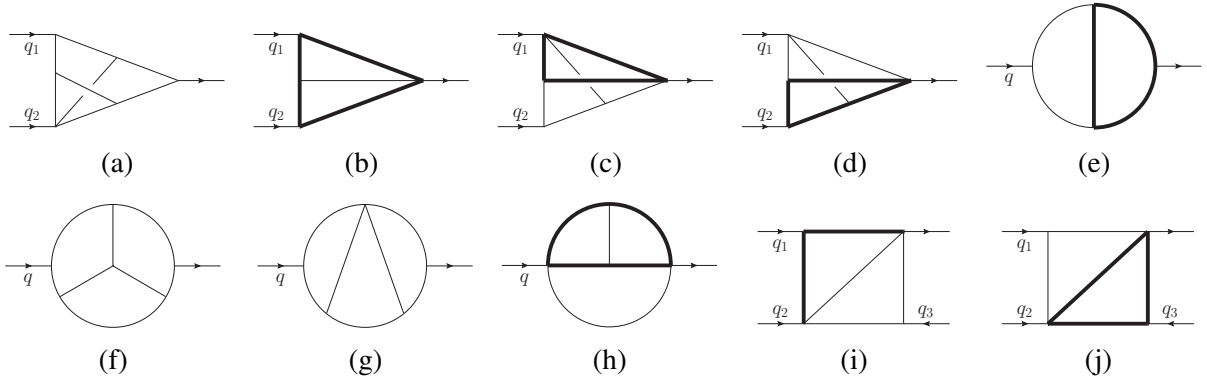

 Fig. E.16: First integration over momentum  $k_1$  in the 3-loop diagram.


Fig. E.17: Examples of two- and three-loop diagrams. Bold (thin) lines represent massive (massless) propagators. Taken from [518] and discussed in Tab. E.1

diagram	Method of Brackets	AMBRE	planarity	AMBRE 4*
fig.5.1(a)	<b>7</b>	13	NP	<b>4</b>
fig.5.1(b)	<b>1</b>	2	P	<b>1</b>
fig.5.1(c)	<b>7</b>	9	NP	<b>5</b>
fig.5.1(d)	<b>7</b>	8	NP	8
fig.5.1(e)	5	<b>3</b>	P	<b>3</b>
fig.5.1(f)	9	<b>4</b>	P	<b>4</b>
fig.5.1(g)	7	<b>4</b>	P	<b>4</b>
fig.5.1(h)	5	<b>4</b>	P	<b>4</b>
fig.5.1(i)	<b>2</b>	<b>2</b>	P	<b>2</b>
fig.5.1(j)	<b>2</b>	<b>2</b>	P	<b>2</b>

Table E.1: The number of MB integrations of the representation constructed by the Method of Brackets compared to the previous AMBRE versions [72,73,76,517] and the last version AMBRE 4. P (NP) stands for planarity (non-planarity) of the diagram.

2. The AMBRE software is based on two different approaches:
  - LA – general planar and some non-planar diagrams
  - GA – 2-loop planar and non-planar, 3-loop non-planar diagrams with massless external legs.

3. The new AMBRE 4, which is not yet public, combines all advantages of the methods above; it has been constructed and tested preliminary. It is optimized for FCC-ee precision 3-loop  $Z$ -boson studies.



## 5 Mellin-Barnes meets Method of Brackets

Author: Mario Prausa [prausa@physik.rwth-aachen.de]

### 5.1 Introduction

The evaluation of Feynman integrals by means of Mellin-Barnes (MB) representation is one of the most successful techniques in the field of multiloop computation. Over the years a large collection of public tools was developed for the numerical as well as analytical calculation of MB representations [448, 449, 519, 520]. An important criterion for the applicability of all of these tools is a rather small dimensionality of the MB representation.

The construction of a MB representation for a Feynman integral is a highly non-trivial task. The public tool `AMBRE` [72, 73, 76, 517] offers two powerful approaches to face this problem. The loop-by-loop approach [72, 73] is the preferable method for planar Feynman integrals, which, in most cases, leads to a very small dimensionality of the MB representation. Non-planar Feynman integrals can be treated by the global approach [76, 517]. A hybrid approach applicable for non-planar Feynman integrals with planar sub-graphs combining the two previously mentioned methods was presented in the previous section E.4.

While the loop-by-loop approach is a well developed method for purely planar Feynman integrals, the treatment of non-planar integrals might still have room for improvements. In this contribution, a different method for the construction of MB representations of Feynman integrals, published in Ref. [518], is explained with a non-planar two-loop example. This technique is applicable for both planar and non-planar topologies and leads in some cases (especially non-planar ones) to a smaller dimensionality than the `AMBRE`-package. Our approach is based on the ‘Method of Brackets’ introduced in Ref. [521–523], which is a technique for the construction of multi-fold sums starting directly from a Schwinger-parameterized Feynman integral.

### 5.2 The Method of Brackets

In this section we introduce the Method of Brackets developed by Gonzalez in Ref. [521–523] and motivate our modifications (see Ref. [518]) in order to obtain MB representations instead of multi-fold sums.

If a function  $g(x)$  has a formal power series

$$g(x) = \sum_{n=0}^{\infty} G(n) \frac{(-x)^n}{n!},$$

the integral

$$\int_0^{\infty} dx x^{\alpha-1} g(x) = \Gamma(\alpha) G(-\alpha)$$

holds true. This is known as Ramanujan’s master theorem, which is the basis for the Method of Brackets formulated in Ref. [521–523]. In these references a special notation

$$\langle \alpha \rangle \equiv \int_0^{\infty} dx x^{\alpha-1}, \quad (\text{E.34})$$

denoted the ‘bracket’, is introduced in order to write this theorem in the more compact way

$$\sum_{n=0}^{\infty} \frac{(-1)^n}{n!} G(n) \langle n + \alpha \rangle = \Gamma(\alpha) G(-\alpha). \quad (\text{E.35})$$

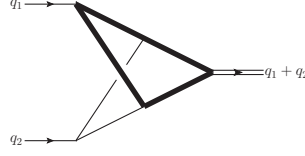


Fig. E.18: Two-loop non-planar vertex-type Feynman integral.

In particular, this notation is useful to express the generalization of Ramanujan's theorem to multi-fold sums

$$\sum_{n_1=0}^{\infty} \cdots \sum_{n_K=0}^{\infty} \frac{(-1)^{n_1+\cdots+n_K}}{n_1! \cdots n_K!} G(\vec{n}) \langle \beta_1 + \vec{\alpha}_1 \cdot \vec{n} \rangle \cdots \langle \beta_K + \vec{\alpha}_K \cdot \vec{n} \rangle = \frac{1}{|\det(A)|} \Gamma(-n_1^*) \cdots \Gamma(-n_K^*) G(\vec{n}^*),$$

where  $A = (\vec{\alpha}_1, \dots, \vec{\alpha}_K)^T$ ,  $\vec{n} = (n_1, \dots, n_K)^T$ ,  $\vec{n}^* = -A^{-1}\vec{\beta}$  and  $\vec{\beta} = (\beta_1, \dots, \beta_K)^T$ . This is the master formula for the original Method of Brackets.

The idea behind the original Method of Brackets is that the integrand of a Schwinger-parameterized Feynman integral can be formally Taylor expanded in the Schwinger parameters. The Schwinger parameter integrals can then be written as *brackets*, which makes the master formula applicable to some of the sums that originate from the Taylor expansion.

The first step to modify the Method of Brackets so that it yields MB representations instead of multi-fold sums is to find a new master formula in which the sums are replaced by contour integrals. Mellin's inversion theorem provides exactly what is needed for this step. Using the bracket notation the inversion theorem can be written as

$$\int \frac{dz}{2\pi i} F(z) \langle z + \alpha \rangle = F(-\alpha),$$

which resembles Ramanujan's theorem (E.35). The generalization to multi-dimensional MB integrals, which will be the master formula for our modified Method of Brackets, reads

$$\int \frac{dz_1}{2\pi i} \cdots \int \frac{dz_K}{2\pi i} F(\vec{z}) \langle \beta_1 + \vec{\alpha}_1 \cdot \vec{z} \rangle \cdots \langle \beta_K + \vec{\alpha}_K \cdot \vec{z} \rangle = \frac{1}{|\det A|} F(-A^{-1}\vec{\beta}), \quad (\text{E.36})$$

where  $\vec{z} = (z_1, \dots, z_K)^T$ .

The Method of Brackets consists of a small set of simple rules on how to rewrite a Schwinger-parameterized integral into a form to which this master formula can be applied. Instead of describing these rules in their most general form (as it was done in Ref. [518]), we follow a more didactic way in this contribution, i.e. we will apply the method immediately to a non-trivial two-loop example.

### 5.3 The example

Throughout this contribution, we consider the example in fig. E.18, where the thin lines are massless propagators and the bold lines carry mass  $m$ . The kinematics is given by

$$q_1^2 = q_2^2 = 0, \quad (q_1 + q_2)^2 = M^2.$$

The Schwinger parametrization of this two-scale integral is given by

$$\frac{1}{\Gamma(a_1) \cdots \Gamma(a_6)} \int_0^\infty dx_1 x_1^{a_1-1} \cdots \int_0^\infty dx_6 x_6^{a_6-1} \frac{e^{-F/U - \sum_i x_i m_i^2}}{U^{d/2}}, \quad (\text{E.37})$$

where the Symanzik polynomials  $U$  and  $F$ , and the sum over the squared internal masses are

$$\begin{aligned} U &= x_2 x_5 + x_1 x_2 + x_4 x_5 + x_2 x_4 + x_2 x_6 + x_3 x_6 + x_1 x_5 + x_1 x_6 + x_3 x_5 + x_1 x_3 + x_4 x_6 + x_3 x_4, \\ F &= -M^2 [x_2 x_3 x_5 + x_1 x_3 x_6 + x_1 x_2 x_3 + x_2 x_4 x_5 + x_2 x_3 x_4 + x_2 x_3 x_6], \\ \sum_i m_i^2 x_i &= m^2 [x_1 + x_2 + x_3 + x_4]. \end{aligned}$$

Our example has a  $U$  polynomial with 12 terms, an  $F$  polynomial with 6 terms, 4 massive lines and 6 propagators. A naive application of the Method of Brackets would lead to a  $12 + 6 + 4 - 6 - 1 = 15$  dimensional MB representation. This number can be easily derived from the set of rules given in Ref. [518]. Such a high number of dimensions is most certainly very inconvenient.

## 5.4 Optimization

In the context of the original Method of Brackets, Ref. [521] suggests an optimization procedure to be applied to the graph polynomials, which drastically reduces the multiplicity of the sums in the final result. The same procedure can be used to reduce the dimensionality of the final MB representations in the modified Method of Brackets.

The optimization consists of *recursively* identifying common subexpressions in  $U$ ,  $F$  and  $\sum_i m_i^2 x_i$ . The common subexpressions are then replaced by auxiliary variables. If a common subexpression with  $N$  terms is found to appear  $J$  times, this leads to a reduction of the dimensionality by  $(J - 1)(N - 1)$ .

In the example, such an optimization leads to

$$\begin{aligned} r_1 &= x_1 + x_4, \\ r_2 &= x_2 + x_3, \\ r_3 &= r_1 + r_2, \\ r_4 &= x_5 + x_6, \\ U &= r_4 r_3 + r_2 r_1, \\ F &= -M^2 [r_4 x_2 x_3 + x_1 x_3 x_6 + r_1 x_2 x_3 + x_2 x_4 x_5], \\ \sum_i m_i^2 x_i &= m^2 r_3, \end{aligned}$$

where the auxiliary variables are denoted by  $r_i$ . Here, the recursive nature of the factorization becomes clear since the auxiliary variable  $r_3$  depends on further auxiliary variables  $r_1$  and  $r_2$ . We will see later on that this optimized form leads to only four MB integrals in the final result.

## 5.5 The rules

In this section, we apply a set of four simple rules, derived in Ref. [518], to the Schwinger-parameterized Feynman integral (E.37) in order to rewrite it as a MB representation.

### Rule A

Inserting  $F$  and  $\sum_i m_i^2 x_i$  in optimized form into (E.37) leads to

$$\frac{1}{\Gamma(a_1) \cdots \Gamma(a_6)} \int_0^\infty dx_1 x_1^{a_1-1} \cdots \int_0^\infty dx_6 x_6^{a_6-1} \frac{e^{M^2[r_4 x_2 x_3 + x_1 x_3 x_6 + r_1 x_2 x_3 + x_2 x_4 x_5]/U - m^2 r_3}}{U^{d/2}}.$$

The exponential function in the integrand has now to be split into factors using  $e^{-\sum_i A_i} = \prod_i e^{-A_i}$ , so that  $A_i$  consists only of a monomial or a monomial divided by  $U$ ,

$$\frac{1}{\Gamma(a_1) \cdots \Gamma(a_6)} \int_0^\infty dx_1 x_1^{a_1-1} \cdots \int_0^\infty dx_6 x_6^{a_6-1} \frac{e^{M^2 r_4 x_2 x_3 / U} e^{M^2 x_1 x_3 x_6 / U} e^{M^2 r_1 x_2 x_3 / U} e^{M^2 x_2 x_4 x_5 / U} e^{-m^2 r_3}}{U^{d/2}}.$$

To each exponential function the Cahen-Mellin formula

$$e^{-A_i} = \int \frac{dz_i}{2\pi i} A_i^{z_i} \Gamma(-z_i)$$

can be applied, which introduces a MB integral. This yields

$$\int_0^\infty dx_1 x_1^{a_1-1} \cdots \int_0^\infty dx_6 x_6^{a_6-1} \int \frac{dz_1}{2\pi i} \cdots \int \frac{dz_5}{2\pi i} (-M^2)^{z_{1234}} (m^2)^{z_5} \frac{\Gamma(-z_1) \cdots \Gamma(-z_5)}{\Gamma(a_1) \cdots \Gamma(a_6)} \\ \times r_1^{z_3} r_3^{z_5} r_4^{z_1} U^{-z_{1234}-d/2} x_1^{z_2} x_2^{z_{134}} x_3^{z_{123}} x_4^{z_4} x_5^{z_4} x_6^{z_2},$$

with the widely used index notation  $z_{ijk\dots} = z_i + z_j + z_k + \dots$ . Note that all powers are arranged in a way, that every base appears only once, which is important for later steps.

### Rule B

Now the Symanzik polynomial  $U$ , as well as the auxiliary variables  $r_4$ ,  $r_3$ ,  $r_2$  and  $r_1$  have to be reinserted in that order. This requires a rule to rewrite multinomials raised to some power in terms of MB integrals and brackets. Such a rule is given by

$$(A_1 + \cdots + A_J)^\alpha = \frac{1}{\Gamma(-\alpha)} \int \frac{dz_1}{2\pi i} \cdots \int \frac{dz_J}{2\pi i} \langle z_1 + \cdots + z_J - \alpha \rangle A_1^{z_1} \cdots A_J^{z_J} \Gamma(-z_1) \cdots \Gamma(-z_J).$$

Inserting  $U$  and applying the formula leads to

$$\int_0^\infty dx_1 x_1^{a_1-1} \cdots \int_0^\infty dx_6 x_6^{a_6-1} \int \frac{dz_1}{2\pi i} \cdots \int \frac{dz_7}{2\pi i} (-M^2)^{z_{1234}} (m^2)^{z_5} \langle z_{123467} + d/2 \rangle \\ \times \frac{\Gamma(-z_1) \cdots \Gamma(-z_7)}{\Gamma(a_1) \cdots \Gamma(a_6) \Gamma(z_{1234} + d/2)} r_1^{z_{37}} r_2^{z_7} r_3^{z_{56}} r_4^{z_{16}} x_1^{z_2} x_2^{z_{134}} x_3^{z_{123}} x_4^{z_4} x_5^{z_4} x_6^{z_2}.$$

Note that the powers had to be arranged properly in the same way as in Rule A.

Repeating this step for  $r_4$ ,  $r_3$ ,  $r_2$  and  $r_1$  yields.

$$\int_0^\infty dx_1 \cdots \int_0^\infty dx_6 \int \frac{dz_1}{2\pi i} \cdots \int \frac{dz_f}{2\pi i} (-M^2)^{z_{1234}} (m^2)^{z_5} \langle z_{123467} + d/2 \rangle \langle z_{89} - z_{16} \rangle \langle z_{ab} - z_{56} \rangle \langle z_{cd} - z_{7b} \rangle \langle z_{ef} - z_{37a} \rangle \\ \times x_1^{a_1+z_{2e}-1} x_2^{a_2+z_{134c}-1} x_3^{a_3+z_{123d}-1} x_4^{a_4+z_{4f}-1} x_5^{a_5+z_{48}-1} x_6^{a_6+z_{29}-1} \\ \times \frac{\Gamma(-z_1) \cdots \Gamma(-z_f)}{\Gamma(a_1) \cdots \Gamma(a_6) \Gamma(z_{1234} + d/2) \Gamma(-z_{16}) \Gamma(-z_{56}) \Gamma(-z_{7b}) \Gamma(-z_{37a})},$$

where the integration variables are counted alphabetically after  $z_9$ .

### Rule C

Since at this point all auxiliary variables are eliminated, the  $x_i$ -integrals are all of the form of the right-hand side of (E.34) such that they can be rewritten in terms of brackets. This yields

$$\int \frac{dz_1}{2\pi i} \cdots \int \frac{dz_f}{2\pi i} (-M^2)^{z_{1234}} (m^2)^{z_5} \langle z_{123467} + d/2 \rangle \langle z_{89} - z_{16} \rangle \langle z_{ab} - z_{56} \rangle \langle z_{cd} - z_{7b} \rangle \langle z_{ef} - z_{37a} \rangle \\ \times \langle a_1 + z_{2e} \rangle \langle a_2 + z_{134c} \rangle \langle a_3 + z_{123d} \rangle \langle a_4 + z_{4f} \rangle \langle a_5 + z_{48} \rangle \langle a_6 + z_{29} \rangle \\ \times \frac{\Gamma(-z_1) \cdots \Gamma(-z_f)}{\Gamma(a_1) \cdots \Gamma(a_6) \Gamma(z_{1234} + d/2) \Gamma(-z_{16}) \Gamma(-z_{56}) \Gamma(-z_{7b}) \Gamma(-z_{37a})}, \quad (\text{E.38})$$

which is called the *presolution* of the Feynman integral.



### Rule D

In the final step, the master formula (E.36) will be applied to the presolution (E.38). Since (E.38) has 15 MB integrals but only 11 brackets, not all integrals can be solved with the master formula. It is a matter of choice which MB integrals should remain. Out of the  $\binom{15}{11} = 1365$  possibilities, 868 lead to a singular matrix  $A$  in (E.36) and must be rejected. The remaining 497 choices all lead to possible MB representations.

Let us arrange the integration variables for which we want to apply the master formula into a vector  $\vec{z}_1$  and the remaining ones into a vector  $\vec{z}_2$ . With these definitions, the master formula reads

$$\begin{aligned} & \int \frac{dz_1}{2\pi i} \cdots \int \frac{dz_J}{2\pi i} \langle \beta_1 + \vec{\alpha}_1 \cdot \vec{z}_1 + \vec{\gamma}_1 \cdot \vec{z}_2 \rangle \cdots \langle \beta_K + \vec{\alpha}_K \cdot \vec{z}_1 + \vec{\gamma}_K \cdot \vec{z}_2 \rangle f(\vec{z}_1, \vec{z}_2) \\ &= \frac{1}{|\det A|} \int \frac{dz_{K+1}}{2\pi i} \cdots \int \frac{dz_J}{2\pi i} f(-A^{-1}\vec{\beta} - A^{-1}C\vec{z}_2, \vec{z}_2), \end{aligned} \quad (\text{E.39})$$

where  $A = (\vec{\alpha}_1, \dots, \vec{\alpha}_K)^T$  and  $C = (\vec{\gamma}_1, \dots, \vec{\gamma}_K)^T$ .

For the example we choose the integrals over  $z_2, z_4, z_6$  and  $z_d$  to remain. This choice leads to

$$\begin{aligned} \vec{z}_1 &= (z_1, z_3, z_5, z_7, z_8, z_9, z_a, z_b, z_c, z_e, z_f)^T, \quad \vec{z}_2 = (z_2, z_4, z_6, z_d)^T, \\ f(\vec{z}_1, \vec{z}_2) &= \frac{(-M^2)^{z_{1234}} (m^2)^{z_5} \Gamma(-z_1) \cdots \Gamma(-z_f)}{\Gamma(a_1) \cdots \Gamma(a_6) \Gamma(z_{1234} + d/2) \Gamma(-z_{16}) \Gamma(-z_{56}) \Gamma(-z_{7b}) \Gamma(-z_{37a})}, \\ \vec{\beta} &= (d/2, 0, 0, 0, 0, a_1, a_2, a_3, a_4, a_5, a_6)^T, \end{aligned}$$

$$A = \begin{pmatrix} 1 & 1 & 0 & 1 & 0 & 0 & 0 & 0 & 0 & 0 & 0 \\ -1 & 0 & 0 & 0 & 1 & 1 & 0 & 0 & 0 & 0 & 0 \\ 0 & 0 & -1 & 0 & 0 & 0 & 1 & 1 & 0 & 0 & 0 \\ 0 & 0 & 0 & -1 & 0 & 0 & 0 & -1 & 1 & 0 & 0 \\ 0 & -1 & 0 & -1 & 0 & 0 & -1 & 0 & 0 & 1 & 1 \\ 0 & 0 & 0 & 0 & 0 & 0 & 0 & 0 & 0 & 1 & 0 \\ 1 & 1 & 0 & 0 & 0 & 0 & 0 & 0 & 1 & 0 & 0 \\ 1 & 1 & 0 & 0 & 0 & 0 & 0 & 0 & 0 & 0 & 0 \\ 0 & 0 & 0 & 0 & 0 & 0 & 0 & 0 & 0 & 0 & 1 \\ 0 & 0 & 0 & 0 & 1 & 0 & 0 & 0 & 0 & 0 & 0 \\ 0 & 0 & 0 & 0 & 0 & 1 & 0 & 0 & 0 & 0 & 0 \end{pmatrix}, \quad C = \begin{pmatrix} 1 & 1 & 1 & 0 \\ 0 & 0 & -1 & 0 \\ 0 & 0 & -1 & 0 \\ 0 & 0 & 0 & 1 \\ 0 & 0 & 0 & 0 \\ 1 & 0 & 0 & 0 \\ 0 & 1 & 0 & 0 \\ 1 & 0 & 0 & 1 \\ 0 & 1 & 0 & 0 \\ 0 & 1 & 0 & 0 \\ 1 & 0 & 0 & 0 \end{pmatrix}.$$

Plugging these into the right-hand side of (E.39) yields the final four-dimensional MB representation

$$\begin{aligned} & (m^2)^{-a_{12456}+d} (-M^2)^{-a_3} \int \frac{dz_2}{2\pi i} \int \frac{dz_4}{2\pi i} \int \frac{dz_6}{2\pi i} \int \frac{dz_d}{2\pi i} \left( -\frac{m^2}{M^2} \right)^{-z_4+z_d} \frac{\Gamma(-z_2)\Gamma(-z_4)\Gamma(-z_6)\Gamma(-z_d)}{\Gamma(a_1) \cdots \Gamma(a_6)} \\ & \times \frac{\Gamma(a_1 + z_2)\Gamma(a_4 + z_4)\Gamma(a_5 + z_4)\Gamma(a_6 + z_2)\Gamma(a_{1456} - d/2 + z_{24})\Gamma(a_{12456} - d + z_4 - z_d)}{\Gamma(a_{14} + z_{24})\Gamma(a_{56} + z_{24})} \\ & \times \frac{\Gamma(a_3 - a_{56} - z_{46} + z_d)\Gamma(a_2 - a_3 - z_{2d} + z_4)\Gamma(a_2 - d/2 - z_{26d})\Gamma(-a_3 + d/2 + z_{46} - z_d)\Gamma(a_{56} + z_{246})}{\Gamma(a_2 - a_3 - z_2 + z_4 - 2z_d)\Gamma(-a_3 + d/2 + z_4 - z_d)\Gamma(a_{12456} - d + z_4 - z_{6d})}, \end{aligned}$$

for the Feynman integral in fig. E.18.

## 5.6 Conclusion

In this contribution we explained a new technique to construct MB representations with a non-trivial example. The approach is based on a reformulation of the Method of Brackets. Our modified Method of Brackets yields not only one but many possible MB representations where every single one is a valid representation of the full Feynman integral.

A crucial part of the method is the optimization procedure. Here, one has to analyze the graph polynomials for common sub-expressions. With this optimization, the method is able to produce low-dimensional MB representations.



## 6 New approach to Mellin-Barnes integrals for massive one-loop Feynman integrals

**Authors:** Johann Usovitsch, Tord Riemann

Corresponding Author: Johann Usovitsch [jusovitsch@googlemail.com]

### Abstract

Two methods are known for the infrared safe calculation of potentially arbitrary Feynman integrals (FI): Sector decomposition (SD) and Mellin-Barnes (MB) representations. In recent years, in both approaches mighty, complementary tools have been developed for the numerical solution of Feynman integrals in arbitrary kinematics. Unfortunately, the dimensionality of MB integrals is often growing quadratically with the number of scales, so that an evaluation becomes difficult or even impossible. For the case of one-loop integrals, a dedicated choice of invariants leads to a linear growth of dimensionality. The most complicated term in a general one-loop FI basis is the scalar box integral. Its dimensionality gets reduced from nine to three with the new variables, in agreement with the dimensionality in the SD method. Further, Minkowskian kinematics shows no specific convergence problems compared to the Euklidean case. A generalization of the approach to higher loop cases would be extremely desirable.

### 6.1 Introduction

In [524], the  $d$ -dependent recurrence relation for one-loop  $n$ -point Feynman integrals  $J_n(d)$ , Eqn. (13), is used to derive solutions for the integrals  $J_n(d)$  in terms of infinite sums of simpler functions  $J_n(d-2)$ ,  $J_{n-1}(d-2)$ , and in turn in terms of generalized hypergeometric functions:

$$(d-1-n) G_n J_n(d) = \left[ 2\lambda_n + \sum_{k=1}^n (\partial_k \lambda_n) \mathbf{k}^- \right] J_n(d-2). \quad (\text{E.40})$$

The relation was derived in [525, 526] for the case of canonical powers of propagators,  $\nu_i = 1$ . The  $G_n$  is the Gram determinant, the  $\lambda_n$  the Cayley determinant, and further notations will be explained below. In [513, 514, 527], another recurrence relation for  $J_n(d)$ , namely in terms of Mellin-Barnes integrals over dimensional shifts  $s$  of simpler functions  $J_{n-1}(d+2s)$  was derived and also solved. Both methods give partially identical results, and the evaluation of the latter approach in terms of generalized hypergeometric functions has been described elsewhere.

Here, we will use an intermediate result of [513] in order to derive new compact Mellin-Barnes relations for one-loop  $n$ -point Feynman integrals  $J_n(d)$ , which extend the applicability of the MB-method considerably.

We start the derivations from the well-known Feynman parameter representation for scalar one-loop  $N$ -point Feynman integrals:

$$J_n \equiv J_n(d; \{p_i p_j\}, \{m_i^2\}) = \int \frac{d^d k}{i\pi^{d/2}} \frac{1}{D_1^{\nu_1} D_2^{\nu_2} \dots D_n^{\nu_n}}, \quad (\text{E.41})$$

with inverse propagators

$$D_i = (k + q_i)^2 - m_i^2 + i\varepsilon. \quad (\text{E.42})$$

In the following, we assume  $d = 4 + 2n - 2\epsilon$  with integer  $n \geq 0$ , momentum conservation and all momenta to be incoming,  $\sum_i^n p_i = 0$ . The  $q_i$  are loop momenta shifts and will be expressed for applications by the external momenta  $p_i$ . Following [528], general tensor integrals with  $n$  legs may be reduced to scalar integrals with up to four legs, but introducing higher space-time dimension  $d \geq 4$  and higher propagator powers  $D_i^{\nu_i}$ . Indices  $\nu_i > 1$  may be reduced by recursion relations given in [529] or buy a general-purpose implementation

like [530]. If we would reduce in addition the space-time dimension to  $d = 4 - 2\epsilon$ , we would introduce inverse powers of potentially vanishing Gram determinants, see [168, 529] and references quoted therein. For our derivations, this feature is unwanted and we allow for a general space-time  $d$ . In sum, by solving (E.41) one covers arbitrary one-loop Feynman integrals.

We use the Feynman parameter representation for the evaluation of (E.41):

$$J_n = (-1)^n \Gamma(n - d/2) \int_0^1 \prod_{j=1}^n dx_j \delta\left(1 - \sum_{i=1}^n x_i\right) \frac{1}{F_n(x)^{n-d/2}}. \quad (\text{E.43})$$

Here, the  $F$ -function is the second Symanzik polynomial. It is derived from the propagators,  $M^2 \equiv x_1 D_1 + \dots + x_n D_n = 2Qk + J$ . Using further the  $\delta(1 - \sum x_i)$  under the integral in order to transform in  $F$  the linear terms in  $x_i$  into bilinear ones, one obtains:

$$F_n(x) = Q^2 - J \times \left(\sum_{i=1}^n x_i\right) = \frac{1}{2} \sum_{i,j} x_i Y_{ij} x_j - i\varepsilon. \quad (\text{E.44})$$

This representation of  $F$  relies on the elements of the Cayley matrix  $Y$ , which was introduced in [531]:

$$\lambda = \begin{pmatrix} Y_{11} & Y_{12} & \dots & Y_{1n} \\ Y_{12} & Y_{22} & \dots & Y_{2n} \\ \vdots & \vdots & \ddots & \vdots \\ Y_{1n} & Y_{2n} & \dots & Y_{nn} \end{pmatrix}, \quad (\text{E.45})$$

with elements

$$Y_{ij} = Y_{ji} = m_i^2 + m_j^2 - (q_i - q_j)^2. \quad (\text{E.46})$$

In a second preparational step after the elimination of linear terms in  $x$ , the  $\delta$ -function in (E.41) gets eliminated by integrating over, e.g.,  $x_n$ ; this re-introduces linear terms in  $x$ , and also an inhomogeneity. For later use, we split the expression into two pieces as follows:

$$F_n(x) = (x - y)^T G(x - y) + r_n - i\varepsilon \equiv \Lambda_n(x) + R_n. \quad (\text{E.47})$$

The Gram matrix  $G$  is  $(n - 1)$  dimensional. It is independent of the propagator masses and depends in a symmetrical way on the internal momenta  $q_1$  to  $q_n$ :

$$G = - \begin{pmatrix} (q_1 - q_n)^2 & \dots & (q_1 - q_n)(q_{n-1} - q_n) \\ (q_1 - q_n)(q_2 - q_n) & \dots & (q_2 - q_n)(q_{n-1} - q_n) \\ \vdots & \ddots & \vdots \\ (q_1 - q_n)(q_{n-1} - q_n) & \dots & (q_{n-1} - q_n)^2 \end{pmatrix}. \quad (\text{E.48})$$

Due to relations like  $q_i = p_{i+1} - p_i$  one may also write it in terms of the external momenta  $p_i$ . At this stage it is easy to prove that the isolated inhomogeneity part of  $F(x)$  depends on two determinants:

$$R_n \equiv r_n - i\varepsilon = - \frac{\lambda_n}{G_n} - i\varepsilon, \quad (\text{E.49})$$

where

$$\lambda_n = \det(\lambda), \quad G_n = \det(G). \quad (\text{E.50})$$

The  $(n - 1)$  coefficients of the linear terms in (E.47) depend on the same determinants:

$$y_i = \frac{\partial r_n}{\partial m_i^2} = - \frac{1}{G_n} \frac{\partial \lambda_n}{\partial m_i^2} \equiv - \frac{1}{G_n} \partial_i \lambda_n, \quad i = 1 \dots n. \quad (\text{E.51})$$

The auxiliary condition  $\sum_i^n y_i = 1$  is fulfilled. The notations for the  $F$ -function are finally independent of the choice of variable which was eliminated by use of the  $\delta$ -function in the integrand of the  $x$ -integral. The inhomogeneity  $R_n$  is the only variable carrying the causal  $i\varepsilon$ -prescription, while the matrices  $\lambda$  and  $G$ , as well as  $\Lambda(x)$  and the  $y_i$  are by definition real quantities – as long as we consider real masses and momenta.

Representations like (E.47) for the  $F$ -polynomial may be found in the literature. Here (E.47) is the starting point for integrating out the  $x$ -variables and introduction of a generic Mellin-Barnes integral. This has been derived in [513].

The use of Mellin-Barnes representations for solving Feynman integrals in form of Feynman representations was advocated in [436] and is being systematically worked out in the Mathematica package MBsuite with the basic tools AMBRE/MB/MBnumerics [72, 73, 75, 448, 511, 532]. The idea is to replace sums by products [533],

$$\frac{1}{(A+B)^k} = \frac{B^{-k}}{2\pi i} \int_{-i\infty}^{+i\infty} ds \frac{\Gamma(-s) \Gamma(k+s)}{\Gamma(k)} \left[ \frac{A}{B} \right]^s, \quad (\text{E.52})$$

where the integration path separates the poles of  $\Gamma(-s)$  from the poles of  $\Gamma(k+s)$ . Further, the condition  $|\text{Arg}(A/B)| < \pi$  has to be fulfilled. Applying (E.52) to the  $F$ -function (E.44) in (E.43),  $(x^T Y x)^{d/2-n}$ , leads for our most general case of one-loop box functions with up to 4 masses, 4 virtualities plus  $s$  and  $t$  to MB-representations of dimensionality  $D = 9$ , which are rather unsolvable. One has to compare this with the one other robust method to treat arbitrary infrared Feynman integrals: sector decomposition [440, 466, 534]. Here, the dimensionality  $D$  of (direct  $x$ -) integrations is just  $(n-1)$ ; being  $D = 3$  for the box integral discussed. For higher loop-orders the difference in dimensionality may become even more drastic.

Let us now follow [513] and apply an MB-integration to the integrand of the  $x$ -integral, thus separating the  $x$ -dependent part from the isolated inhomogeneity:

$$\frac{1}{[\Lambda_n(x) + R_n]^{n-\frac{d}{2}}} = \frac{R_n^{\frac{d}{2}-n}}{2\pi i} \int_{-i\infty}^{+i\infty} ds \frac{\Gamma(-s) \Gamma(n-\frac{d}{2}+s)}{\Gamma(n-\frac{d}{2})} \left[ \frac{\Lambda_n(x)}{R_n} \right]^s. \quad (\text{E.53})$$

In order to solve the  $x$ -integral, the differential operator  $\hat{P}_n$  [535, 536],

$$\frac{\hat{P}_n}{s} \left[ \frac{\Lambda_n(x)}{R_n} \right]^s \equiv \sum_{i=1}^{n-1} \frac{1}{2s} (x_i - y_i) \frac{\partial}{\partial x_i} \left[ \frac{\Lambda_n(x)}{R_n} \right]^s = \left[ \frac{\Lambda_n(x)}{R_n} \right]^s, \quad (\text{E.54})$$

is introduced into the integrand of the  $x$ -integral:

$$K_n = \frac{1}{s} \int dS_{n-1} \hat{P}_n \left[ \frac{\Lambda_n(x)}{R_n} \right]^s = \frac{1}{2s} \sum_{i=1}^{n-1} \prod_{k=1}^{n-1} \int_0^{u_k} dx'_k (x_i - y_i) \frac{\partial}{\partial x_i} \left[ \frac{\Lambda_n(x)}{R_n} \right]^s.$$

This trick allows to rewrite, after application of a Barnes-transformation, the  $n$ -point integral in  $d$  space-time dimensions as an MB-integral of an  $(n-1)$ -point integral in  $d+2$  space-time dimensions:

$$\begin{aligned} J_n(d, \{q_i, m_i^2\}) &= \frac{-1}{4\pi i} \frac{1}{\Gamma(\frac{d-n+1}{2})} \int_{-i\infty}^{+i\infty} ds \Gamma(-s) \Gamma(s+1) \Gamma(s + \frac{d-n+1}{2}) R_n^{-s} \\ &\quad \times \sum_{k=1}^n \left( \frac{1}{r_n} \frac{\partial r_n}{\partial m_k^2} \right) \mathbf{k}^- J_n(d+2s; \{q_i, m_i^2\}). \end{aligned} \quad (\text{E.55})$$

The operator  $\mathbf{k}^-$  reduces notationally an  $n$ -point Feynman integral  $J_n$  to an  $(n - 1)$ -point integral  $J_{n-1}$  by shrinking the  $k^{th}$  propagator,  $1/D_k$ :

$$\mathbf{k}^- J_n = \mathbf{k}^- \int \frac{d^d k}{i\pi^{d/2}} \frac{1}{\prod_{j=1}^n D_j} = \int \frac{d^d k}{i\pi^{d/2}} \frac{1}{\prod_{j \neq k, j=1}^n D_j}. \quad (\text{E.56})$$

Eq. (E.55) is the starting point for our numerical approach. It is an analogue to a similar relation derived in [513], where a difference equation in  $d$  was derived and solved for  $J_n(d; \{p_i p_j\}, \{m_i^2\})$  iteratively.

## 6.2 The MB-iterations for the massive oneloop integrals

In deriving (E.55), it was assumed that  $\Lambda_n(x)$  and  $R_n$  are finite, and we will not discuss here the many special cases otherwise appearing.

The simplest case of a massive one-loop scalar Feynman integral is the one-point function or tadpole,

$$J_1(d; m^2) = \int \frac{d^d k}{i\pi^{d/2}} \frac{1}{k^2 - m^2 + i\varepsilon} = \frac{-1}{4\pi i} \frac{\Gamma(1 - d/2)}{(m^2)^{1-d/2}}. \quad (\text{E.57})$$

For  $m^2 = 0$ , the tadpole vanishes,  $J_1(d; 0) = 0$ . The two-point integral is:

$$\begin{aligned} J_2(d; p^2, m_1^2, m_2^2) &= \left( \frac{-1}{4\pi i} \right)^2 \frac{1}{\Gamma(\frac{d-1}{2})} \sum_{k_1, k_2=1}^2 (1 - \delta_{k_1 k_2}) \left( \frac{1}{r_2} \frac{\partial r_2}{\partial m_{k_2}^2} \right) (m_{k_1}^2)^{d/2-1} \\ &\quad \int_{-i\infty}^{+i\infty} dz_2 \left( \frac{m_{k_1}^2}{R_2} \right)^{z_2} \Gamma(-z_2) \Gamma(z_2 + 1) \Gamma(-z_2 - \frac{d-2}{2}) \Gamma(z_2 + \frac{d-1}{2}). \end{aligned} \quad (\text{E.58})$$

The 2-point function depends on the masses  $m_1, m_2$  (due to the tadpole basis) and on the ratio

$$r_2 \equiv r_{12} \equiv r_2(p^2, m_1^2, m_2^2) = -\frac{\lambda_2}{g_2} = \frac{\lambda(p^2, m_1^2, m_2^2)}{4p^2}, \quad (\text{E.59})$$

where  $\lambda(a, b, c)$  is the Källen function. The vertex depends on the internal masses and the virtualities  $p_i^2$ . A generic argument list, corresponding to  $\{d, p_1^2, p_2^2, p_3^2, m_1^2, m_2^2, m_3^2\}$ , is  $\{d, q_1, m_1^2, q_2, m_2^2, q_3, m_3^2\}$ :

$$\begin{aligned} J_3(d; \{p_i^2\}, \{m_i^2\}) &= \left( \frac{-1}{4\pi i} \right)^3 \frac{1}{\Gamma(\frac{d-2}{2})} \sum_{k_1, k_2, k_3=1}^3 D_{k_1 k_2 k_3} \left( \frac{1}{r_3} \frac{\partial r_3}{\partial m_{k_3}^2} \right) \left( \frac{1}{r_{k_2 k_1}} \frac{\partial r_{k_2 k_1}}{\partial m_{k_2}^2} \right) \\ &\quad (m_{k_1}^2)^{d/2-1} \int_{-i\infty}^{+i\infty} dz_3 \int_{-i\infty}^{+i\infty} dz_2 \left( \frac{m_{k_1}^2}{R_3} \right)^{z_3} \left( \frac{m_{k_2 k_1}^2}{R_{k_2 k_1}} \right)^{z_2} \Gamma(-z_3) \Gamma(z_3 + 1) \\ &\quad \times \Gamma(z_2 + z_3 + \frac{d-1}{2}) \Gamma(-z_2 - z_3 - \frac{d+2}{2}) \Gamma(-z_2) \Gamma(z_2 + 1) \\ &\quad \times \frac{\Gamma(z_3 + \frac{d-2}{2})}{\Gamma(z_3 + \frac{d-1}{2})}, \end{aligned} \quad (\text{E.60})$$

with the condition  $k_1 \neq k_2 \neq k_3$ :

$$D_{k_1 \dots k_n} = \prod_{\substack{i,j=1 \\ i \neq j}}^n (1 - \delta_{k_i k_j}). \quad (\text{E.61})$$

Here,  $r_3 \equiv r_{123}$  and  $r_{ij\dots} = r_{\dots j \dots i \dots}$ . One has to choose some conventions, e.g. (E.42) with additionally setting  $q_1 = 0, q_2 = -p_2, q_3 = p_1$ . Often one selects  $p_3^2 = s$ . We have to use besides the three internal masses  $m_k^2$  and the three parameters  $r_2(p_i^2, m_j^2, m_k^2)$  the additional variable

$$r_3(p_1^2, p_2^2, p_3^2, m_1^2, m_2^2, m_3^2) \equiv -\frac{\lambda_3}{g_3}. \quad (\text{E.62})$$

For the chosen conventions, it is

$$\begin{aligned} \lambda_3 = & 2(m_1^2 m_2^2 p_1^2 - m_2^4 p_1^2 - m_1^2 m_3^2 p_1^2 2m_2^2 m_3^2 p_1^2 - m_2^2 p_1^4 - m_1^2 m_2^2 p_2^2 + m_1^2 m_3^2 p_2^2 + m_2^2 m_3^2 p_2^2 \\ & - m_3^4 p_2^2 + m_2^2 p_1^2 p_2^2 + m_3^2 p_1^2 p_2^2 - m_3^2 p_2^4 - m_1^4 p_3^2 + 2m_1^2 m_2^2 p_3^2 + m_1^2 m_3^2 p_3^2 \\ & - m_2^2 m_3^2 p_3^2 + m_1^2 p_1^2 p_3^2 + m_2^2 p_1^2 p_3^2 + m_1^2 p_2^2 p_3^2 + m_3^2 p_2^2 p_3^2 - p_1^2 p_2^2 p_3^2 - m_1^2 p_3^4), \end{aligned} \quad (\text{E.63})$$

$$g_3 = 2\lambda(p_1^2, p_2^2, p_3^2). \quad (\text{E.64})$$

Specifying to a massive on-shell QED vertex with  $p_3^2 = s, p_1^2 = p_2^2 = M^2$  and  $m_1 = 0, m_2 = m_3 = M$ , one gets  $\lambda_3 = 0$  and  $g_3 = -6M^2$ . This simple example is not covered by (E.55). It demonstrates that the various special cases of the approach have to be worked out in order to cover all the frequently met physical situations. We do not go into details here because e.g. the massive on-shell QED vertex and box cases in the usual MB-approach of AMBRE will be represented by 1- and 2-dimensional MB-integrals, so that there is no need to apply the present approach.

And finally we reproduce the box integral, dependent on  $d$  and the internal variables  $\{d, q_1, m_1^2, \dots, q_4, m_4^2\}$  or, equivalently, on a set of external variables, e.g.  $\{d, \{p_i^2\}, \{m_i^2\}, s, t\}$ :

$$\begin{aligned} J_4(d; \{p_i^2\}, s, t, \{m_i^2\}) = & \left(\frac{-1}{4\pi i}\right)^4 \frac{1}{\Gamma(\frac{d-3}{2})} \sum_{k_1, k_2, k_3, k_4=1}^4 D_{k_1 k_2 k_3 k_4} \left(\frac{1}{r_4} \frac{\partial r_4}{\partial m_{k_4}^2}\right) \\ & \left(\frac{1}{r_{k_3 k_2 k_1}} \frac{\partial r_{k_3 k_2 k_1}}{\partial m_{k_3}^2}\right) \left(\frac{1}{r_{k_2 k_1}} \frac{\partial r_{k_2 k_1}}{\partial m_{k_2}^2}\right) (m_{k_1}^2)^{d/2-1} \\ & \int_{-i\infty}^{+i\infty} dz_4 \int_{-i\infty}^{+i\infty} dz_3 \int_{-i\infty}^{+i\infty} dz_2 \left(\frac{m_{k_1}^2}{R_4}\right)^{z_4} \left(\frac{m_{k_1}^2}{R_{k_3 k_2 k_1}}\right)^{z_3} \left(\frac{m_{k_1}^2}{R_{k_2 k_1}}\right)^{z_2} \\ & \Gamma(-z_4) \Gamma(z_4 + 1) \frac{\Gamma(z_4 + \frac{d-3}{2})}{\Gamma(z_4 + \frac{d-2}{2})} \Gamma(-z_3) \Gamma(z_3 + 1) \frac{\Gamma(z_3 + z_4 + \frac{d-2}{2})}{\Gamma(z_3 + z_4 + \frac{d-1}{2})} \\ & \Gamma(z_2 + z_3 + z_4 + \frac{d-1}{2}) \Gamma(-z_2 - z_3 - z_4 - \frac{d+2}{2}) \Gamma(-z_2) \Gamma(z_2 + 1). \end{aligned} \quad (\text{E.65})$$

The representations (E.58) to (E.65) can be treated by the Mathematica packages MB and MBnumerics of the MBsuite, replacing AMBRE by a derivative of MBnumerics [527].

### 6.3 The cases of vanishing Cayley determinant and vanishing Gram determinant

We refer to two important special cases, where the general derivations cannot be applied.

In the case of a vanishing Cayley determinant,  $\lambda_n = 0$ , we cannot introduce the inhomogeneity  $R_n = -\lambda_n/G_n$  into the Symanzik polynomial  $F_2$ , see (E.47). Let us assume that it is  $G_n \neq 0$ , so that  $r_n = 0$ . A useful alternative representation to (E.55) is known from the literature see e.g. Eqn. (3) in [524]:

$$J_n(d) = \frac{1}{d-n-1} \sum_{k=1}^n \frac{\partial_k \lambda_n}{G_n} \mathbf{k}^- J_n(d-2). \quad (\text{E.66})$$

Another special case is a vanishing Gram determinant,  $G_n = 0$ . Here, again one may use Eqn. (3) of [524] and the result is (for  $\lambda_n \neq 0$ ):

$$J_n(d) = - \sum_{k=1}^n \frac{\partial_k \lambda_n}{2\lambda_n} \mathbf{k}^- J_n(d). \quad (\text{E.67})$$

The representation was, for the special case of the vertex function, also given in Eqn. (46) of [537].

#### 6.4 Example: A massive 4-point function with vanishing Gram determinant

As a very interesting, non-trivial example we study the numerics of a massive 4-point function with a small or vanishing Gram determinant. The example has been taken from Appendix C of [168]. The kinematics is:

$$\begin{aligned} p_1^2 = p_2^2 &= m_1^2 = m_3^2 = m_4^2 = 0, \\ m_2^2 &= (911876/10000)^2, \\ p_3^2 &= s_3 = s_{\nu u} = 10000, \\ p_4^2 &= t_{ed} = -60000(1+x), \\ s &= (p_1 + p_2)^2 = s_{12} = t_{e\mu} = -40000, \\ t &= (p_2 + p_3)^2 = s_{23} = s_{\mu\nu u} = 20000. \end{aligned} \quad (\text{E.68})$$

The resulting Gram determinant is

$$G_4 = -2t_{e\mu}[s_{\mu\nu u}^2 + s_{\nu u}t_{ed} - s_{\mu\nu u}(s_{\nu u} + t_{ed} - t_{e\mu})]. \quad (\text{E.69})$$

The Gram determinant vanishes if

$$t_{ed} \rightarrow t_{ed,crit} = \frac{s_{\mu\nu u}(s_{\mu\nu u} - s_{\nu u} + t_{e\mu})}{s_{\mu\nu u} - s_{\nu u}}. \quad (\text{E.70})$$

Introducing a parameter  $x$ , we can describe the vanishing of  $G_4$  by the limiting process  $x \rightarrow 0$ :

$$t_{ed} = (1+x)t_{ed,crit}, \quad (\text{E.71})$$

$$G_4 = -2xs_{\mu\nu u}t_{e\mu}(s_{\mu\nu u} - s_{\nu u} + t_{e\mu}). \quad (\text{E.72})$$

For  $x = 0$ , the Gram determinant vanishes. Further, it is simple to calculate e.g. the value at  $x = 1$ :  $G_4(x = 1) = -4.8 \times 10^{13} \text{ GeV}^3$ . Further, if the Gram determinant vanishes exactly, a reduction of  $J_4$  according to (E.41) is possible and allows a simple and very precise calculation. For small  $x$ , the calculations become with usual reductions a la Passarino/Veltman [538] unstable due to the occurrence of inverse Gram determinants. Several solutions were worked out; we refer to the review



[539]. Here we will use the solution which was worked out in [168] and has been implemented in the C++ program PJFry [169, 170, 540, 541].

In the new approach presented here, a calculation of  $J_4$  is possible as follows. First reduce the indices  $\nu_i$  of the propagators, if any, to the canonical value  $\nu_i = 1$ , and then apply the MB-formula directly. This has been done with the C++ package KIRA [530], without generating inverse powers of Gram determinants. In fact, the procedure introduces for a  $J_4(d)$  a basis of functions  $J_4(d + 2n)$ , where  $n \geq 0$  is related to the indices  $\nu_i \geq 1$ . We use here the short notation

$$J_4(D, \nu_1, \nu_2, \nu_3, \nu_4) = I_4(D, p_1^2, p_2^2, p_3^2, p_4^2, s, t, m_1^2, m_2^2, m_3^2, m_4^2)[\nu_1, \nu_2, \nu_3, \nu_4]. \quad (\text{E.73})$$

The numerical solution of (E.55) is stable also in the Minkowskian case. This contrasts the usual MB-representations derived with AMBRE. A reason is that the instabilities in the AMBRE-approach origin from  $\Gamma$ -functions from Beta-functions which do not appear here.

The tables contain our numerical result, for two different cases which were also studied in [168]. In LoopTools notations, they correspond to the tensor coefficients  $D_{2222}$  and  $D_{222}$ . The former one is numerically less stable then the second. In both cases, we have a numerical agreement of more than 10 digits, although we performed here no expansion in the small parameter  $x$ . Such an expansion would improve calculations considerably. Our results give an impression on the accuracy of the small Gram expansion in [168], where an error propagation of the Pade approach was not done: In all cases, [168] had at least 10 reliable digits.

$x$	value for $4! \times J_4(12 - 2\epsilon, 1, 5, 1, 1)$	
0	$(2.05969289730 + 1.55594910118i)10^{-10}$	[J. Fleischer, T. Riemann, 2010]
0	$(2.05969289730 + 1.55594910118i)10^{-10}$	MBOneLoop + Kira + MBnumerics
$10^{-8}$	$(2.05969289342 + 1.55594909187i)10^{-10}$	[J. Fleischer, T. Riemann, 2010]
$10^{-8}$	$(2.05969289363 + 1.55594909187i)10^{-10}$	MBOneLoop + Kira + MBnumerics
$10^{-4}$	$(2.05965609497 + 1.55585605343i)10^{-10}$	[J. Fleischer, T. Riemann, 2010]
$10^{-4}$	$(2.05965609489 + 1.55585605343i)10^{-10}$	MBOneLoop + Kira + MBnumerics

Table E.2: The Feynman integral  $J_4(12 - 2\epsilon, 1, 5, 1, 1)$  compared to numbers from [168]. The  $I_{4,2222}^{[d+]}^4$  is the scalar integral where propagator 2 has index  $\nu_2 = 1 + (1 + 1 + 1 + 1) = 5$ , the others have index 1. The integral corresponds to  $D_{1111}$  in notations of LoopTools [542]. For  $x = 0$ , the Gram determinant vanishes. We see an agreement of about 10 to 11 relevant digits. The deviations of the two calculations seem to stem from a limited accuracy of the Pade approximations used in [168].

$x$	value for $3! \times J_4(10 - 2\epsilon, 1, 4, 1, 1)$	
0	$-(3.15407250453 + 3.31837792634i)10^{-10}$	[J. Fleischer, T. Riemann, 2010]
0	$-(3.15407250453 + 3.31837792634i)10^{-10}$	MBOneLoop + Kira + MBnumerics
$10^{-8}$	$-(3.15407250057 + 3.31837790700i)10^{-10}$	[J. Fleischer, T. Riemann, 2010]
$10^{-8}$	$-(3.15407250055 + 3.31837790700i)10^{-10}$	MBOneLoop + Kira + MBnumerics
$10^{-4}$	$-(3.15403282194 + 3.31818461838i)10^{-10}$	[J. Fleischer, T. Riemann, 2010]
$10^{-4}$	$-(3.15403282195 + 3.31818461838i)10^{-10}$	MBOneLoop + Kira + MBnumerics

Table E.3: Same as Table E.2, for the Feynman integral  $J_4(10 - 2\epsilon, 1, 4, 1, 1)$  compared to numbers from [168]. The  $I_{4,222}^{[d+]}^3$  is the scalar integral where propagator 2 has index  $\nu_2 = 1 + (1 + 1 + 1) = 4$ , the others have index 1. The integral corresponds to  $D_{111}$  in notations of LoopTools [542]. We see an agreement of about 11 to 12 relevant digits. The deviations of the two calculations seem to stem from a limited accuracy of the Pade approximations used in [168].

## 7 In search of the optimal contour of integration in Mellin-Barnes integrals

**Author: Wojciech Flieger** [woj.flieger@gmail.com]

### 7.1 Introduction

As is evident from a couple of contributions to this report, Mellin-Barnes integrals (MB) are widely used in computation of higher order radiative corrections where more and more loops and scales are involved.

Here we will focus on the numerical computation of MB integrals. We aim at numerical calculations as the complexity of considered Feynman integrals increases with number of loops and masses involved so it is much harder to find analytical solutions. There is a substantial progress in recent years in numerical treatment of MB integrals, mostly due to better understanding of complex contours over which integrals are computed in the multidimensional complex plane. The main problem is the oscillatory character of the MB integrals in physical kinematic regions of calculations. It is not a problem in Euclidean region and in fact there is a public package `MB.m` [448] which works in this region by calculation of integrals over straight complex lines with fixed real values of integrands. A kind of real breakthrough brought an idea [534] to rotate contours of integration which can damp oscillatory character of integrands in the Minkowskian region. Other ideas like shifted contours [72, 73, 76] made it possible to build up finally a set of procedures and packages [74, 448–450, 502, 511, 543, 544] where at least two-loop vertex Feynman diagrams represented by multidimensional MB integrals can be calculated in an efficient way with high precision of several digits [15].

However, there is always room for improvement. We would like to explore the geometrical aspect of MB integrals, i.e., consider the optimal contour of integration. The biggest obstacle from the numerical point of view in the computation of Feynman integrals in the MB representation is their bad convergence due to their highly oscillatory behaviour. Thus, it would be a big improvement if we could find a contour on which that oscillatory behaviour would be alleviated. In order to do this, we will adopt a concept originated in asymptotic analysis [545, 546] called method of steepest descent.

This method extends the idea of Laplace's method to the domain of complex numbers. Therefore, we consider integrals of the form

$$J(\lambda) = \int_{\mathcal{C}} g(z) e^{\lambda f(z)} dz, \quad (\text{E.74})$$

where  $\mathcal{C}$  is a contour in the complex plane,  $f(z)$ ,  $g(z)$  are analytic functions of the complex variable  $z$  and  $\lambda$  is a real positive parameter. In this method we take advantage of Cauchy integral theorem to deform the contour of integration into a new contour  $\mathcal{C}'$  that makes integration as easy as possible. If we can do this in such a way that the imaginary part of the function  $f(z)$  remains constant  $\text{Im}(f(z)) = \text{Im}(f(z_0)) = \text{const}$  along the new contour, our integral will take the form

$$J(\lambda) = e^{i\lambda \text{Im}(f(z_0))} \int_{\mathcal{C}'} g(z) e^{\lambda \text{Re}(f(z))} dz. \quad (\text{E.75})$$

Thus, on this new contour we are left with the Laplace's type of integral for which well established methods exist. It is known that the oscillatory behaviour of the exponential function is mainly contained in the complex part of such integrand. Therefore, if we will be able to find a contour of integration in the MB representation along which an imaginary part is constant, the convergence problem can be reduced. This problem has been investigated recently for one-dimensional cases in [547, 548] but going beyond is nontrivial and our present status has an exploratory character.

## 7.2 One dimension

To present the idea of the optimal contour of integration and its most important properties we will start the discussion by considering a one dimensional scenario. In this case, our integral has the form of the integral given by (E.74). We will say that a contour of integration is a contour of steepest descent  $\mathcal{J}$  if it possesses the following three properties

1. it goes through one or more critical points  $z_\alpha$  of  $f(z)$ ,
2. the imaginary part of  $f(z)$  is constant along  $\mathcal{J}$ ,
3. the real part of  $f(z)$  decreases moving away from critical points.

In the one dimensional case, the contour of steepest descent is completely determined by the above properties. Before we move on and try to generalize this idea to higher dimensions, let us look at the behaviour of the integrand  $f(z)$  in the neighbourhood of its critical points. Since it is a holomorphic function its imaginary and real part are harmonic functions. Thus by virtue of the maximum principle none of them attains extremal values inside the domain of analyticity [549]. However, the imaginary part of  $f(z)$  along the contour of steepest descent remains constant, therefore we will look at a contour that goes from one valley into another on the landscape of the real part of  $f(z)$  crossing the critical point that in this case is a saddle point, see Fig. E.19. Moreover, assuming that the function  $f(z)$  has

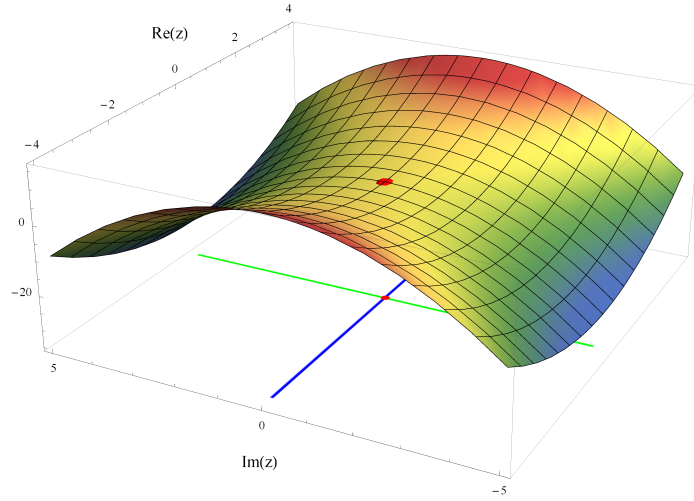


Fig. E.19: The real part of the function  $f(z) = z^2$  with a marked critical value  $f(z_0) = 0$  at the critical point  $z_0 = (0, 0)$ . Below the surface of  $Re(z^2)$  you can see the level set curves of  $Im(f(z)) = Im(f(z_0))$  which correspond to the contour of steepest descent (green) and steepest ascent (blue).

only non-degenerate critical points  $z_\alpha$ , i.e.,

$$\frac{d^2 f}{dz^2} \Big|_{z_\alpha} \neq 0, \quad (\text{E.76})$$

the behaviour of  $f(z)$  near the critical point  $z_0$  is mostly controlled by its second derivative

$$f(z) = f(z_0) + \frac{1}{2} \frac{d^2 f}{dz^2} \Big|_{z_0} (z - z_0)^2 + \dots \Rightarrow f(z) - f(z_0) \approx \frac{1}{2} \frac{d^2 f}{dz^2} \Big|_{z_0} (z - z_0)^2 \quad (\text{E.77})$$

Let us write the right-hand side of the second equation as follows

$$\begin{aligned}\frac{d^2 f}{dz^2}|_{z_0} &= r e^{i\theta}, \\ (z - z_0)^2 &= R e^{i\varphi}.\end{aligned}\tag{E.78}$$

This gives us

$$\frac{d^2 f}{dz^2}|_{z(0)}(z - z_0)^2 = r R^2 e^{i(\theta+2\varphi)}.\tag{E.79}$$

The direction of steepest descent is given when the value of  $Re[f(z) - f(z_0)]$  is negative and the imaginary part of this difference is equal to zero. This occurs when

$$\varphi = -\frac{\theta}{2} + \frac{\pi}{2}.\tag{E.80}$$

However, since the critical point is a saddle point, there is also a direction of steepest ascent that is perpendicular to the direction of steepest descent. In this case  $Re[f(z) - f(z_0)]$  is positive and we have

$$\varphi = -\frac{\theta}{2}.\tag{E.81}$$

We can see that the direction of steepest descent is determined by the argument of  $\frac{d^2 f}{dz^2}|_{z_0}$ . If it happens so that the second derivative vanishes, we have to look at higher derivatives.

### 7.3 Extension to higher dimensions

Let us extend the idea of the contour of steepest descent to an arbitrary  $n$ -complex dimensional space where the integrand takes the form  $f(z) = f(z_1, \dots, z_n)$ . We are looking for an universal parametrization of integration surfaces. Learning from the one-dimensional case we know that along the contour of steepest descent the imaginary part of the integrand is constant and that this contour goes through saddle points of  $f(z)$ . This is sufficient information in the one-dimensional scenario. However, the first condition

$$Im(f(z)) - Im(f(z_0)) = 0,\tag{E.82}$$

is not sufficient in higher dimensions since in the general  $n$ -complex space  $\mathbb{C}^n$  this condition constrains only one real dimension. Thus, we are left with a  $2n - 1$  real dimensional variety. Therefore either we find additional constraints or we find a way to parametrize the surface of steepest descent. We will discuss the second option and try to use the one dimensional definition and adapt it to higher dimensions. At the beginning let us define the set of curves of steepest descent as the solution of the flow equation

$$\left(\frac{dx_1}{dt}, \frac{dy_1}{dt}, \dots, \frac{dx_n}{dt}, \frac{dy_n}{dt}\right) = -\nabla Re[f(x_1, y_1, \dots, x_n, y_n)]\tag{E.83}$$

where  $z_k = x_k + iy_k$  for  $k = 1, 2, \dots, n$ . Taking  $t$  as a nonnegative real parameter. This equation ensures that the real part of  $f(z)$  decreases along these curves and that the imaginary part remains constant. The approach involving the above flow equation as the parametrization of the surface of steepest descent as a whole is considered in [550]. However, instead of looking for the whole surface of integration, we can use the idea of geometrical objects called Lefschetz thimbles  $\mathcal{J}$ , each associated with one critical point of  $f(z)$ . The system (E.83) can be written in the following form

$$\frac{dz_i}{dt} = -\left(\frac{\partial f}{\partial z_i}\right)^*, \quad i = 1, \dots, n.\tag{E.84}$$

This allows us to define Lefschetz thimbles associated with a given critical point as

$$\mathcal{J}_\alpha = \{z \in \mathbb{C}^n : \lim_{t \rightarrow \infty} z(t) = z_\alpha\}, \quad (\text{E.85})$$

where  $z(t)$  is the solution of the flow equation (E.84). Thus, the Lefschetz thimble is a collection of all curves flowing into the direction of steepest descent that asymptotically reach the corresponding critical point. Note that the real part of the integrand for critical points are in the same time saddle points. There exists an alternative direction, in which real part changes the most, i.e., direction of steepest ascent. With this direction are associated geometrical structures similar to the Lefschetz thimbles, called anti-thimbles, which satisfy the system of upward flow differential equations

$$\mathcal{K}_\alpha = \{z \in \mathbb{C}^n : \lim_{t \rightarrow \infty} \bar{z}(t) = z_\alpha\}, \quad (\text{E.86})$$

where  $\bar{z}(t)$  are curves that satisfy the following system of upward flow equations

$$\frac{dz_i}{dt} = \left( \frac{\partial f}{\partial z_i} \right)^*, \quad i = 1, \dots, n. \quad (\text{E.87})$$

The idea of thimbles as a surface of steepest descent appeared in [551, 552]. It has been shown there that within homology theory an initial contour of integration  $\mathcal{C}$  can be changed into a finite sum of thimbles, each associated with one critical point

$$\mathcal{C} = \sum_{\alpha} N_{\alpha} \mathcal{J}_{\alpha}. \quad (\text{E.88})$$

The sum in the above equation goes over critical points and  $N_{\alpha} \in \mathbb{Z}$ . In this way, we can change the integration over one surface into the sum of integrals over thimbles. In practical implementations of the thimble method it is convenient to take as the initial point a point near the critical point since none of the points on a thimble are known in the beginning besides the critical point. Then instead of solving downward flow equations that in this situation will result in a short line segment connecting the initial point to the critical one, we move in the reverse direction, i.e., we solve upward flow equations. For the initial condition, it is also important to set a proper initial direction towards the steepest descent path. To do this we mimic the method from one dimensional case. Therefore, we look at the behaviour of the  $f(z)$  in the neighbourhood of the critical point. In the general  $n$ -dimensional space this behaviour is governed by the Hessian matrix  $\mathcal{H}$  evaluated at the critical point, i.e., the matrix of partial second derivatives of  $f(z)$

$$f(z) = f(z_0) + \frac{1}{2}(z - z_0)^T \mathcal{H}|_{z_0} (z - z_0) + \dots \quad (\text{E.89})$$

with

$$\mathcal{H} = \begin{pmatrix} \frac{\partial^2 f}{\partial z_1^2} & \frac{\partial^2 f}{\partial z_1 \partial z_2} & \dots & \frac{\partial^2 f}{\partial z_1 \partial z_n} \\ \frac{\partial^2 f}{\partial z_2 \partial z_1} & \frac{\partial^2 f}{\partial z_2^2} & \dots & \frac{\partial^2 f}{\partial z_2 \partial z_n} \\ \vdots & \vdots & \ddots & \vdots \\ \frac{\partial^2 f}{\partial z_n \partial z_1} & \frac{\partial^2 f}{\partial z_n \partial z_2} & \dots & \frac{\partial^2 f}{\partial z_n^2} \end{pmatrix}. \quad (\text{E.90})$$

The direction of steepest ascent or descent is determined then by eigenvectors of this matrix.

There exists also another approach of the Lefschetz thimbles parametrization. This approach appeared in [551] and is based on cuts  $L_\alpha$ , i.e., half-lines attached to the value of  $f(z)$  at the critical points and going towards infinity into the direction of the positive real axis

$$L_\alpha = (f(\alpha), t_0), \quad (\text{E.91})$$

where  $t_0 = f(\alpha) + r_0 e^{i\phi}$  with  $\phi$  being the phase of  $\lambda$  parameter and  $r_0$  denotes a small radius of the neighbourhood of a given critical point. The relation between thimbles and cuts follows from the behaviour of the function  $f(z)$  near the critical point which tells us that thimbles are mapped by  $f(z)$  into cuts

$$\mathcal{J}_\alpha \xrightarrow{f} L_\alpha. \quad (\text{E.92})$$

Thus, to find thimbles starting from cuts, we have to consider inverse function  $f^{-1}$

$$L_\alpha \xrightarrow{f^{-1}} \mathcal{J}_\alpha. \quad (\text{E.93})$$

The detailed discussion of this method with an example can be found in [553].

#### 7.4 Application to physics and MB trials

The idea of choosing the initial contour of integration as the contour of steepest descent was considered in the study of the evolution of parton distribution in QCD [554]. Recently Witten used geometrical and topological properties of the Lefschetz thimbles to prove analytic continuation of the Chern-Simons theory [555, 556]. These works contain also a nice introduction to Morse theory and Lefschetz thimbles in the context of physics. The methods of Lefschetz thimbles and contours of steepest descent are used also in calculations in the context of the sign problem in QCD which is connected with cancelations occurring in oscillatory lattice integrals. Here both theoretical and practical aspects of thimbles are studied. A big effort is put on the development of Monte-Carlo algorithms to compute system dynamics on thimbles [557–563]. In the case of Mellin-Barnes integrals, both exact contours of steepest descent as a solution of flow equations and some useful approximations were studied [547, 548].

Despite the fact that thimbles are described by well established mathematical theory [564], a practical parametrization of them is a very challenging task. In the case of MB integrals we have to face the following issues:

- since the gamma function has infinitely many critical points we have to consider how many of them is necessary to match the assumed numerical precision;
- the parametrization of thimbles by solving flow equations for each relevant critical point. This stage requires also calculation of the Hessian matrix and the associated eigensystem;
- the knowledge of singularities of the MB integrand is necessary to avoid them by thimbles;
- the determination of the inverse function for the cuts approach;
- the summation of thimbles with suitable coefficients in (E.88) to reconstruct the whole integral.

Therefore work done so far concerned on one-dimensional problems with very few exceptions like the two-dimensional case discussed recently in [565].

## 7.5 Summary

The Mellin-Barnes representation is one of the methods for the Feynman integrals computation. The main problem with numerical integration of these integrals is bad convergence due to highly oscillatory behaviour of integrands. Fortunately, since they are defined in the complex domain, we can change the contour of integration and find the optimal contour of integration along which the imaginary part of the function is constant defining the contour of steepest descent. In the one dimensional case, the condition that the imaginary part of the integrand must be constant together with a requirement that the contour must go through the critical point is sufficient to parametrize it. The extension of this idea to higher dimensions can be done with help of geometric structures called Lefschetz thimbles where each thimble is associated with one critical point of the integrand. However, practical implementation of this idea to a particular problem is a very difficult task. We discussed two known approaches to this issue. Namely, thimbles can be parametrized as the union of curves given by the solution of flow differential equations. Or, a correspondence between thimbles and half-lines connected to the value of a function at the critical point can be used. Both approaches require analytical knowledge of the integrand all its critical points. Moreover, the singularity structure of the function is very important since the new contour cannot cross any singularity. Knowledge of singularities is needed also in the second approach where the inverse function is required. A numerical solution of the flow equations requires calculation of all critical point, the Hessian matrix and its eigensystem to make the construction of thimbles efficient. Currently, the methods of Lefschetz thimbles is developed in the lattice QCD and in the context of Mellin-Barnes integrals. However, only simple one-dimensional problems are solved. Multidimensional cases are still in the exploratory stage and more work is needed. Though we are aiming in numerical applications, the method of Lefschetz thimbles and homology theory, singularity theory or multidimensional complex analysis required to study complex contours can be helpful in deeper understanding of analytical properties of Feynman integrals.



## 8 Differential equations for multiloop integrals

**Author:** Roman Lee [r.n.lee@inp.nsk.su]

The method of differential equations is one of the most powerful methods available for the multiloop calculations. First introduced by Kotikov in Refs. [566–568], and later generalized by Remiddi for the differentiation with respect to kinematic invariants, Ref. [569], this technique relies on the IBP reduction procedure, another powerful technique suggested by Chetyrkin and Tkachov, Refs. [414, 415]. In this contribution we will review the recent advances and the present status of the differential equation method.

### 8.1 Obtaining differential equations

Integration-by-part identities originally relied on the momentum-space representation of the multiloop integral in  $d$  dimensions

$$j(\mathbf{n}) = j(n_1, \dots, n_N) = \int \frac{d^d l_1 \dots d^d l_L}{(i\pi^{d/2})^L D_1^{n_1} \dots D_N^{n_N}}. \quad (\text{E.94})$$

Here the ‘denominators’  $D_\alpha$  depend linearly on the scalar products  $s_{ij} = l_i \cdot q_j$  involving loop momenta  $l_i$  ( $q_j$  is either loop or external momentum). We assume that these denominators constitute a basis in a sense that any scalar product  $s_{ij}$  can be uniquely expressed as a linear combination of  $D_1, \dots, D_N$  and a free term. In particular,  $N = L(L+1)/2 + LE$ , where  $L$  is a number of loops and  $E$  is a number of linearly independent external momenta.

The IBP identities have the form

$$0 = \int \frac{d^d l_1 \dots d^d l_L}{(i\pi^{d/2})^L} \partial_i \cdot q_j D_1^{-n_1} \dots D_N^{-n_N}. \quad (\text{E.95})$$

Performing explicit differentiation, we express the right-hand side in terms of the integrals (E.94) with shifted indices. It is convenient to represent the resulting identities with the help of operators  $A_\alpha$  and  $B_\alpha$ ,

$$\begin{aligned} (A_\alpha f)(\dots, n_\alpha, \dots) &= n_\alpha f(\dots, n_\alpha + 1, \dots) \\ (B_\alpha f)(\dots, n_\alpha, \dots) &= f(\dots, n_\alpha - 1, \dots) \end{aligned} \quad (\text{E.96})$$

Then the IBP identities have the structure

$$0 = \mathcal{O}_{ij} j(\mathbf{n}) = (a_{ij}^{\alpha\beta} A_\alpha B_\beta + b_{ij}^\alpha A_\alpha + d\delta_{ij}) j(\mathbf{n}), \quad (\text{E.97})$$

where the explicit form of the coefficients  $a_{ij}^{\alpha\beta}$  and  $b_{ij}^\alpha$  is determined by that of the functions  $D_\alpha$ . Solving these identities for different  $\mathbf{n}, i, j$  with respect to the most complex integrals, we can collect a database of rules which reduce all integrals (E.94) to a finite set of what is called *master integrals*

$$\mathbf{j} = (j_1, \dots, j_r)^T = (j(\mathbf{n}^{(1)}), \dots, j(\mathbf{n}^{(r)}))^T \quad (\text{E.98})$$

Note that the set of master integrals depends on the chosen criterion of complexity which can vary within certain limits. In the present review we will not discuss several important properties of the IBP reduction, such as the Lie algebra of the IBP operators  $\mathcal{O}_{ij}$ , the proof of finiteness of the set of master integrals, the connection between the number of master integrals and topological invariants of

Feynman and Baikov polynomials, the derivation of IBP identities and differential equations directly in Feynman and Baikov representation using syzygies and other algebraic geometry tools and refer the interested reader to Refs. [570–578].

Although the original idea behind the IBP reduction was to reduce the number of integrals to be calculated, in no way less important is the possibility to use IBP reduction to obtain differential and difference systems for a finite number of master integrals.

Let the integrals depend on some external parameter  $x$ . In particular,  $x$  may be some mass, or kinematic invariant constructed of the external momenta. Then we can express the derivative of the master integrals via the integrals of the same form (E.94). If  $x$  is mass, this is obvious as one may directly differentiate the integrand. If  $x$  is a kinematic invariant, one should take into account that the integrand depends on external momenta but, in general, not on their invariants. One may use the formulas

$$\frac{\partial}{\partial (p_1 \cdot p_2)} j(\mathbf{n}) = \sum [\mathbb{G}^{-1}]_{i2} p_i \cdot \partial_{p_1} j(\mathbf{n}), \quad \frac{\partial}{\partial (p_1^2)} j(\mathbf{n}) = \frac{1}{2} \sum [\mathbb{G}^{-1}]_{i1} p_i \cdot \partial_{p_1} j(\mathbf{n}), \quad (\text{E.99})$$

where  $\mathbb{G} = \{p_i \cdot p_j\}_{i,j=1\dots E}$  is a Gram matrix of the external momenta  $p_i$ . The operators on the right-hand side can act directly on the integrand.

Using IBP reduction, we may reduce the result of differentiation to the same set of master integrals. Thus, we obtain the system of the first-order differential equations which is natural to represent in matrix form

$$\partial_x \mathbf{j} = M \mathbf{j}, \quad (\text{E.100})$$

where  $M$  is an  $r \times r$  matrix with entries being the rational functions of  $x$  and  $d$ .

The idea of differential equation method is that, instead of performing the explicit loop integration in (E.94), one may search the master integrals as solutions of the differential equations (E.100). This method appears to be superior in the majority of applications. Also, many properties of the loop integrals can be easily read-off from the differential system even before solving it. In particular, the branching points of the integrals necessarily coincide with the singular points of the differential system (the poles of  $M$ ).

Let us note that for the cases when the loop integrals depend only on one dimensionful parameter, the differential equations can not help as the system trivializes to a set of decoupled equations of the form  $\partial_x j_k = \nu_k x^{-1} j_k$ , where  $\nu_k$  is the physical dimension of  $j_k$  defined as  $[j_k] = [x^{\nu_k}]$ . In this case, the differential equations may only serve as a check of completeness of the IBP reduction.

It is very instructive to use the differential equations for the cases when there are several dimensionful parameters  $x_1, \dots, x_k$ . Then we have one differential system per each parameter  $x_a$ :

$$\partial_a \mathbf{j} = M_a \mathbf{j}, \quad (\text{E.101})$$

where now each matrix  $M_a$ , in addition to  $d$ , depends, in general, on all variables  $\mathbf{x}$ . There is a nontrivial compatibility condition:

$$\partial_b M_a - \partial_a M_b + [M_a, M_b] = 0, \quad (\text{E.102})$$

which can be thought of as the flatness of the connection  $\partial_a - M_a$ . In the present review we will mostly concentrate on the differential system with respect to one variable and discuss the multivariate case in the end.

## 8.2 $\epsilon$ -expansion of differential equations

Let us assume that  $M$ , as a function of  $x$ , does not have singular points which depend on  $\epsilon$ . Strictly speaking, this might be not the case. Even worse: in the denominators of entries of  $M$  there might appear powers of ugly irreducible polynomials depending simultaneously on  $x$  and  $\epsilon$ . Fortunately, such singularities must be apparent, which can be understood on physical grounds and also strictly proved from the properties of Feynman parametrization (or Baikov representation). Such apparent singularities can be removed in a systematic way which does not require explicit manipulations with roots of these polynomials. In particular, to reduce the powers to at most one, it is instructive to use the algorithm of Ref. [579]. The algorithm of eliminating first powers of irreducible polynomials in the denominators will be presented elsewhere. Thus, from now on, we assume that all singularities of  $M$ , as function of  $x$ , are independent of  $\epsilon$ .

In general, the solution of the differential equations exact in  $d$  can not be found in a close form. Fortunately, we typically need the expansion of the loop integral in  $\epsilon = (4 - d)/2$ . Therefore, the knowledge of the exact in  $\epsilon$  solution is not necessary for physical applications (and may even be not sufficient given the complexity of series expansion of some emerging functions in  $\epsilon$ ). Assuming the solution of Eq. (E.100) can be expanded in Laurent series<sup>3</sup> in  $\epsilon$

$$j = \sum j^{(n)} \epsilon^n \quad (\text{E.103})$$

we can search for the coefficients  $j^{(n)}$  by expanding both sides of Eq. (E.100) in  $\epsilon$ .

This is, of course, valid when we hold  $x$  to be general (i.e. as symbol), but we should be careful when applying boundary conditions in a singular point of the differential equations. If  $x_0$  is a singular point of the matrix  $M$ , one should bear in mind that  $\epsilon$ -expansion, in general, does not commute with the expansion in  $x - x_0$ . In particular, it is not safe to put  $x = x_0$  in the  $d$ -dimensional integral and then expand in  $\epsilon$  to obtain the boundary conditions. The irony is that usually we do need to fix boundary conditions at a singular point of  $M$ . One should, therefore, consider the asymptotics of the integrals when  $x \rightarrow x_0$  and use the expansion by regions method [580] to obtain contributions of different regions.

## 8.3 $\epsilon$ -form of the differential systems

In Ref. [432] a remarkable observation has been made. It appeared that in many cases a suitable choice of the master integrals exists such that the matrix  $M$  in (E.100) is plainly proportional to  $\epsilon$ , i.e. when  $M(x, \epsilon) = \epsilon S(x)$ , so that

$$\partial_x \mathbf{J} = \epsilon S(x) \mathbf{J}, \quad (\text{E.104})$$

Here we intentionally changed notations  $j \rightarrow \mathbf{J}$  in order to have a reference both to generic masters and to the ‘canonical’ masters. This form (we will refer to it as the  $\epsilon$ -form) makes the  $\epsilon$ -expansion of Eq. (E.100) trivial, and one can obtain as many terms of expansion (E.103) as needed by successive integration using

$$\mathbf{J}^{(n)}(x) = \int dx S(x) \mathbf{J}^{(n-1)}(x) \quad (\text{E.105})$$

Immediately after [432] appeared, the  $\epsilon$ -form of the differential equations was used in many practical applications, Refs. [434, 581–583], to mention a few.

<sup>3</sup>Note that the existence of Laurent series does not follow solely from the rationality of  $M$  (consider, e.g.  $\partial_x f = \frac{f}{\epsilon x}$ ), but rather can be safely assumed and checked *a posteriori* for all differential systems which appear in multiloop calculations.

It is instructive to write the general solution of the differential system (E.104) in the form  $\mathbf{J}(x) = F(x, x_0)\mathbf{J}(x_0)$ , where the fundamental matrix  $F(x, x_0)$  is expressed via the path-ordered exponent:

$$F(x, x_0) = \text{Pexp} \left[ \epsilon \int_{x_0}^x dx' M(x') \right]. \quad (\text{E.106})$$

We will refer to  $F(x, x_0)$  as an evolution operator from  $x_0$  to  $x$ . Then, using the well-known form of the perturbative expansion of path-ordered exponent, we obtain

$$F(x, x_0) = \sum_{n=0}^{\infty} \epsilon^n F^{(n)}(x, x_0) = \sum_{n=0}^{\infty} \epsilon^n \int_{x_0 < x_1 \dots < x_n < x} \dots \int dx_n \dots dx_1 S(x_n) \dots S(x_1) \quad (\text{E.107})$$

If the entries of the matrix  $S(x)$  are rational functions, the integrals in the above equation are expressed in terms of multiple polylogarithms, Ref. [584], or equivalent functions  $G$ , see below.

Let us explain how the boundary conditions should be fixed when  $x_0$  tends to a singular point of the differential system. Suppose  $x = 0$  is a singular point of the matrix  $S$  and  $x_0 \rightarrow 0$ . Then, obviously,  $\lim_{x_0 \rightarrow 0} F(x, x_0)$  does not exist as in Eq. (E.107) the integrals over  $x_1$  diverge at the lower limit. We will assume that  $x = 0$  is a simple pole of  $S(x)$ , i.e., that

$$S(x) = \frac{A}{x} + B(x), \quad (\text{E.108})$$

where  $B(x)$  is regular at  $x = 0$ . Then we define a reduced evolution operator

$$\tilde{F}(x, 0) = \lim_{x_0 \rightarrow 0} F(x, x_0) x_0^{\epsilon A}. \quad (\text{E.109})$$

Here and below we assume that we have fixed a path in the complex plane starting from 0 and containing both  $x$  and  $x_0$ , and the limits  $x_0 \rightarrow 0$  or  $x \rightarrow 0$  are understood in a sense that the corresponding variable travels along this path towards zero. Note that if  $x = 0$  is a regular point of the differential system, we have  $A = 0$  and, therefore,  $\tilde{F}(x, 0) = F(x, 0)$ . It can be understood that thus defined function  $\tilde{F}$  has the asymptotics

$$\tilde{F}(x, 0) \xrightarrow{x \rightarrow 0} x^{\epsilon A}. \quad (\text{E.110})$$

The convenience of our definition for  $\tilde{F}$  becomes especially obvious if the matrix  $S(x)$  is rational, decays at infinity and has only simple poles. Then, we have a symbolic identity

$$\tilde{F}^{(n)}(x, 0) = S(x_n) \dots S(x_1) \Big|_{\frac{1}{x_n - a_n} \dots \frac{1}{x_1 - a_1} \rightarrow G(a_n, \dots, a_1 | x)}, \quad (\text{E.111})$$

where  $G$  is defined recursively as [585]

$$\begin{aligned} G(\underbrace{0, \dots, 0}_n | x) &= \frac{\ln^n x}{n!}, \\ G(a_n, \dots, a_1 | x) &= \int_0^x \frac{dx_n}{x_n - a_n} G(a_{n-1}, \dots, a_1 | x_n). \end{aligned} \quad (\text{E.112})$$

In order to fix the boundary conditions, we write the general solution as

$$\mathbf{J}(x) = \tilde{F}(x, 0) \mathbf{J}_0, \quad (\text{E.113})$$

where  $\mathbf{J}_0$  is a column of constants. These constants can be related to the specific coefficients in the asymptotic expansion of  $J(x)$  defined by that of  $\tilde{F}(x, 0)$

$$\tilde{F}(x, 0) = \sum_{\lambda \in \mathcal{S}} \sum_{n=0}^{\infty} \sum_{k=0}^{K_\lambda} \frac{1}{k!} C(n + \lambda, k) x^{n+\lambda} \ln^k x, \quad (\text{E.114})$$

We refer the reader to Ref. [586] for details on how to find this expansion in an algorithmic way. Here we only note that the described method is very economic, in a sense that it allows to determine the minimal set of asymptotic contributions needed to fix the constants  $\mathbf{J}_0$ .

#### 8.4 Reducing differential systems to $\epsilon$ -form

As we have seen in the previous section, casting differential equations in  $\epsilon$ -form is very desirable. It puts a question of how to find the appropriate transformation. One possible approach is to use some additional information which is not contained in the differential systems. Namely, one might try to find the set of master integrals, having the homogeneous transcendentality property, by means of constant leading singularity method. This approach was supported in Ref. [432] and then used in many applications. However, it is very desirable to be able to reduce a given differential system to  $\epsilon$ -form relying only on its form. This is especially required for the complicated cases, in particular, for the massive diagrams where the required transformation is not rational anymore in terms of the original kinematic parameters.

So, we would like to find the transformation matrix  $T$  which connects the initial functions  $\mathbf{j}$  and new functions  $\mathbf{J}$  by

$$\mathbf{j} = T \mathbf{J}, \quad (\text{E.115})$$

such that  $\mathbf{J}$  satisfies Eq. (E.104).

The algorithm of finding the rational transformation  $T$  has been presented in Ref. [587]. There are now two public implementations of the algorithm of Ref. [587] `Fuchsia` [588] and `epsilon` [589]. The algorithm consists of a series of transformations,  $T = T_1 T_2 \dots T_K$ , each ‘improving’ the properties of the system. The process of reduction can be approximately split into three stages:

**I. Fuchsification:** The multiple poles and polynomial part of  $M$  are removed.

**II. Normalization:** The eigenvalues of the matrix residues are normalized to be proportional to  $\epsilon$ .

**III. Factoring out  $\epsilon$ :** A constant transformation depending on  $\epsilon$  is searched for to factor out  $\epsilon$ .

*Fuchsification.*

Reducing the differential system to Fuchsian form is a classical problem of the ODE theory and the algorithms to accomplish this task have been known long before Ref. [587]. In particular, the algorithm of Barkatou and Pflügel, Ref. [590, 591], allows one to get rid of all multiple poles. However, the polynomial part of the matrix, in general, explodes after applying this algorithm. The reason is that each separate step of the Barkatou-Pflügel algorithm can increase the order of polynomial part by one. Possible roots of such an inaccurate treatment of the singularity at infinity is that, in general, it is not possible to get rid of both the multiple poles and the polynomial part. This impossibility is closely related to negative solution of the 21st Hilbert problem<sup>4</sup>, given by Bolibrukh [592].

<sup>4</sup>Formulation of the 21st Hilbert problem: to show that there always exists a linear differential system of the Fuchsian class, with given singular points and monodromic group.

In Ref. [587] the transformations similar to those of Ref. [590, 591] have been used. However, they have been additionally adjusted to conserve, if possible, the properties of the system in the second point (always chosen to be  $\infty$  in Barkatou-Pflügel algorithm). In order to explain one step of the ‘Fuchsification’ stage, let us suppose that  $x_1 \neq \infty$  and  $x_2 \neq \infty$  are singular points of the differential system (E.100). Near these points the matrix  $M$  has the expansions:

$$M(x) = \frac{A_0}{(x - x_1)^{p+1}} + \frac{A_1}{(x - x_1)^p} + O((x - x_1)^{1-p}) , \quad (\text{E.116})$$

$$M(x) = \frac{B_0}{(x - x_2)^{q+1}} + O((x - x_2)^{-q}) , \quad (\text{E.117})$$

where  $p > 0$  and  $q \geq 0$  are the *Poincaré ranks* of the system at  $x = x_1$  and at  $x = x_2$ . The algorithm of Ref. [587] consists in finding the *balance* transformation

$$T = \mathcal{B}(P, x_1, x_2|x) = \bar{P} + \frac{x - x_2}{x - x_1} P , \quad (\text{E.118})$$

where  $P = P^2$  is some projector,  $\bar{P} = 1 - P$ , and the following properties of  $P$  are required. Let

$$U = \text{Im } P = \{\mathbf{u} | \exists \tilde{\mathbf{u}} : \mathbf{u} = P\tilde{\mathbf{u}}\}$$

and

$$V^\top = \text{coIm } P = \{\mathbf{v}^\top | \exists \tilde{\mathbf{v}}^\top : \mathbf{v}^\top = \tilde{\mathbf{v}}^\top P\}$$

be the image and coimage of  $P$ . Then we require

$$\begin{aligned} 1. & A_0 U = 0, \\ 2. & A_1 U \subseteq \text{Im } A_0 + U, \\ 3. & U \cap \text{Im } A_0 > \{0\}, \end{aligned} \quad (\text{E.119})$$

and

$$4. V^\top B_0 \subseteq V^\top . \quad (\text{E.120})$$

The first three conditions concern the image of  $P$  and are basically accounted for in the Barkatou-Pflügel algorithm. The last condition secures that the transformation (E.118) does not increase the Poincaré rank at  $x = x_2$ . More specifically, it is straightforward to check that the transformed matrix  $\tilde{M} = T^{-1} (MT - \partial_x T)$  has the expansions

$$\tilde{M}(x) = \frac{\tilde{A}_0}{(x - x_1)^{p+1}} + O((x - x_1)^{-p}) , \quad (\text{E.121})$$

$$\tilde{M}(x) = \frac{\tilde{B}_0}{(x - x_2)^{q+1}} + O((x - x_2)^{-q}) , \quad (\text{E.122})$$

where

$$\tilde{A}_0 = \bar{P} (A_0 + (x_1 - x_2) A_1 P) . \quad (\text{E.123})$$

The first expansion is valid thanks to condition 1 ( $A_0 U = 0$ ), while the second is due to condition 4. It is easy to show that  $\text{rank } \tilde{A}_0 < \text{rank } A_0$ . Indeed, from condition 2 we have  $\text{Im}(A_0 + (x_1 - x_2) A_1 P) \subseteq$

$\text{Im } A_0 + U$ , and from condition 3 it follows that  $\bar{P}(\text{Im } A_0 + U) \subsetneq \text{Im } A_0$  (strict inclusion). Therefore  $\text{Im } \tilde{A}_0 \subsetneq \text{Im } A_0$  which implies  $\text{rank } \tilde{A}_0 < \text{rank } A_0$ .

In Refs. [587, 590, 591] finding the subspace  $U$  with the properties 1-3 relied on quite technical issues (in particular, Claim 1 and Algorithm 1 of Ref. [587]). Here we will present a much more simple algorithm to find  $U$ . We start from the Moser's necessary criterion of reducibility [593]:

$$x^r \det(A_0/x + A_1 - \lambda)|_{x=0} = 0, \quad (\text{E.124})$$

where  $r = \text{rank } A_0$ . Let us note that this criterion can be reformulated as

$$\dim \ker \begin{pmatrix} A_0 & A_1 - \lambda \\ 0 & A_0 \end{pmatrix} > \dim \ker A_0. \quad (\text{E.125})$$

To understand the equivalence of Eq. (E.124) and Eq. (E.125), it is instructive to rely on the basis where  $A_0$  is in Jordan form. Then, striking out the rows and columns which contain 1s in the upper left and lower right blocks (blocks, corresponding to  $A_0$ ), we can easily identify the matrix  $L(A, \lambda)$  from Ref. [590] standing in the upper right block. The condition (E.125) simply states that the number of null eigenvectors of the matrix  $\mathcal{A} = \begin{pmatrix} A_0 & A_1 - \lambda \\ 0 & A_0 \end{pmatrix}$  should be larger than that of  $A_0$ . Let us note that if  $u$  is a null eigenvector of  $A_0$  then  $\begin{pmatrix} u \\ 0 \end{pmatrix}$  is that of  $\mathcal{A}$ , and *vice versa*. Therefore, the criterion (E.125) states that there must be at least one null eigenvector of  $\mathcal{A}$  of the form  $\begin{pmatrix} u(\lambda) \\ u(\lambda) \end{pmatrix}$  with  $u(\lambda) \neq 0$ . The null eigenvectors can be found routinely and their components are, in general, the rational functions of  $\lambda$ . As one can always get rid of common denominator, we can assume that these components are polynomials in  $\lambda$  and

$$u(\lambda) = u_0 + u_1 \lambda + \dots + u_k \lambda^k \quad (\text{E.126})$$

Now, we can easily check that  $U = \{c_0 u_0 + \dots + c_k u_k \mid c_i \in \mathbb{C}\}$  satisfies conditions 1-3 in (E.119). We leave it as a simple exercise for the reader.

Once we find subspaces  $U$  and  $V^\top$  satisfying (E.119) and (E.120) and having equal dimensionality, it is easy to reconstruct the projector  $P$  with  $\text{Im } P = U$  and  $\text{coIm } P = V^\top$ . To do this, it is convenient to slightly abuse the notation by denoting as  $U$  not the image of  $P$  itself, but the matrix whose columns constitute the basis of the image (NB: in general  $U$  is a rectangular matrix). Equivalently,  $V^\top$  will denote the matrix whose columns constitute the basis of the co-image. Then

$$P = U(V^\top U)^{-1} V^\top \quad (\text{E.127})$$

This form make obvious one possible obstruction to the construction of the projector: the matrix  $V^\top U$  may be singular. If, among many possible choices of  $U$  and  $V$  pairs we did not manage to find one suitable for the construction of the projector, this is a strong indication of the irreducibility to Fuchsian form (so to say, the 'Bolibrukh counterexample').

Repetitive application of the transformations (E.118) with the projector  $P$  satisfying (E.119) reduce the matrix rank of the leading coefficient  $A_0$  to zero (which means that the coefficient itself becomes zero). If, in addition, on each step we manage to find a suitable singular point  $x_2$  such that the condition (E.120) can be fulfilled, we can reduce the Poincaré rank at  $x = x_1$  to zero. Acting in the same way for all singular points, we can eliminate higher-order poles and polynomial terms in  $M$ . The point  $x = \infty$  does not make too much difference as, e.g., it can be mapped to  $y = 0$  by the variable change  $x = y^{-1}$ .

*Normalization of matrix residues and choice of variable.*

Suppose now that we have successfully achieved the global Fuchsian form of the differential system, i.e. the matrix  $M$  has the form

$$M = \sum_{i=1}^k \frac{R_i(\epsilon)}{x - x_i}. \quad (\text{E.128})$$

The next step of the algorithm of Ref. [587] is the normalization of the matrix residues  $R_i(\epsilon)$ . We want to find the rational transformation which makes all eigenvalues of all matrix residues to be proportional to  $\epsilon$ . Since the rational transformations do not change the monodromy group, they can only shift the eigenvalues by integer values. Therefore, if not all eigenvalues have the form

$$n + k\epsilon \quad (\text{E.129})$$

where  $n$  is integer, there is no rational transformation which normalizes the matrix residues. One might try to extend the class of ‘allowed’ transformations by considering those which are rational in a new variable  $y$  connected with  $x$  by

$$x = f(y), \quad (\text{E.130})$$

where  $f(y)$  is some rational function. Indeed, such transformations might help. We stress that this kind of variable change retains Fuchsian form as can be checked explicitly.

Suppose that the eigenvalues of the matrix residue at point  $x = x_1$  have the form (E.129) but with rational  $n$ . Let  $b$  be the common denominator of the eigenvalues at  $\epsilon \rightarrow 0$ . Then the necessary condition is that the function  $f_{y^*}^{-1}(x)$  has the  $B$ -root branching point at  $x = x_1$ , where  $B$  is a multiple of  $b$ . By  $y^*$  we denote a separate preimage of  $x_1$ , so that  $f(y^*) = x_1$ , and  $f_{y^*}^{-1}(x)$  denotes a local inversion of the function  $f$  in the vicinity of  $y^*$ . In Ref. [594] the frequently encountered case  $b = 2$  (below we refer to singular points with  $b = 2$  as *square root branching points*) has been considered in detail. The results of these considerations are the following:

- If there are two square root branching points, one should map them to 0 and  $\infty$  by Moebius transformation and make the canonical<sup>5</sup> variable change  $x = y^2$  (for two finite points  $x_1$  and  $x_2$  this amounts to  $x = \frac{x_2 y^2 - x_1}{y^2 - 1}$ ). Normalization (with rational in  $y$  transformation) is either possible after this, or impossible for any variable change (E.130) at all.
- If there are three square root branching points, one should map them to 0, 1, and  $\infty$  by Moebius transformation and make the canonical variable change  $x = \left(\frac{y^2+1}{2y}\right)^2$  (for three finite points  $x_1$ ,  $x_2$ , and  $x_3$  this amounts to  $x = \frac{x_1(4x_2y^2+x_3(y^2-1)^2)-x_2x_3(y^2+1)^2}{-4x_3y^2+x_1(y^2+1)^2-x_2(y^2-1)^2}$ ). Normalization (with rational in  $y$  transformation) is either possible after this, or impossible for any variable change (E.130) at all.
- If there are four or more square root branching points with  $b = 2$ , there is no suitable variable change. Normalization (and, therefore,  $\epsilon$ -form) is impossible by any transformation rational in  $y$  (connected with  $x$  by rational function  $f$ , Eq. (E.130)).
- If there is one square root branching point, there is no canonical variable change, but rather a wide class of suitable transformations  $x = \frac{p(y)^2}{q(y)}$ , where  $p$  and  $q$  are polynomials.

<sup>5</sup> Here by ‘canonical’ variable change we mean that once this variable change is tried, any other may be spared. This variable change is definitely not unique. E.g. different numeration of the points result in different variable changes.



Apart from rarely encountered latter case, this allows one to unambiguously define the suitable variable, or understand that  $\epsilon$ -form is impossible.

Suppose now that we've managed to find a proper variable in terms of which all eigenvalues of all matrix residues have the form (E.129) with integer  $n$ . Then the prescription of Ref. [587] is to apply transformations of the form (E.118) with the projector

$$P = \frac{uv^\top}{(v^\top u)}, \quad (\text{E.131})$$

where  $u$  and  $v^\top$  are the eigenvectors of  $R_1$  and  $R_2^\top$ , i.e.,

$$R_1 u = \lambda u, \quad v^\top R_2 = \mu v^\top. \quad (\text{E.132})$$

This transformation shifts  $\lambda \rightarrow \lambda + 1$ ,  $\mu \rightarrow \mu - 1$ . Again, there might be an obstruction  $(v^\top u) = 0$  to the construction of such a transformation. Therefore, successive application of such transformations can eliminate integer constants  $n$  in the eigenvalues of the form (E.129).

*Factorizing  $\epsilon$ .*

Suppose now that we have successfully normalized all matrix residues. Then the final stage consists in finding an  $x$ -independent transformation  $T(\epsilon)$  such that the transformed matrix has the form  $\tilde{M}(x, \epsilon) = \epsilon A(x)$ . This step can be reduced to solving the linear system of equations

$$\begin{aligned} \epsilon^{-1} R_1(\epsilon) T &= \mu^{-1} R_1(\mu) T \\ &\vdots \\ \epsilon^{-1} R_k(\epsilon) T &= \mu^{-1} R_k(\mu) T \end{aligned}$$

for sufficiently generic  $\mu$  treating elements of  $T$  as unknowns (see Ref. [587] for details).

*Criterion of (ir)reducibility.*

It is important to have both the effective reduction algorithm and the strict criterion of irreducibility. The latter has been presented in Ref. [594]

A simple but important proposition from Ref. [594] states that the normalization at any given point can not survive the transformation which is singular in this point. This, in particular, means that once we have achieved a global normalized Fuchsian form, we are allowed to make only transformations independent on  $x$ . Now, by examining the steps of the reduction algorithm, one may see that it is always possible to reduce the system to normalized Fuchsian form everywhere, except, maybe, one singular point (called below the *exceptional*) chosen arbitrarily. The recipe of Ref. [594] is to reduce the system to normalized Fuchsian form first choosing the exceptional point to be  $x = \infty$ , and then to be  $x = 0$ <sup>6</sup>. Let  $M$  correspond to the first choice and

$$\tilde{M} = M_U = U^{-1}(MU - \partial_x U) \quad (\text{E.133})$$

correspond to the second. Now we note that, if  $T$  exists, such that  $M_T = T^{-1}(MT - \partial_x T)$  is normalized everywhere, then both  $T$  and  $T^{-1}$  should be polynomial in  $x$ , and  $S = U^{-1}T$  is necessarily

<sup>6</sup>by Möbius transformations, we can always map any two points to  $\infty$  and 0.

polynomial in  $x^{-1}$  with constant determinant. These are direct consequences of the proposition formulated above. Therefore there should exist a decomposition

$$U = T(x)S^{-1}(x^{-1}) \quad (\text{E.134})$$

where both  $T$  and  $S$  are polynomial matrices of their arguments ( $x$  and  $x^{-1}$ , respectively) with the determinants independent of  $x$ . This decomposition explicitly demonstrates that  $\det U$  should be independent of  $x$  and that  $U$  and  $U^{-1}$  are necessarily regular in all points but two:  $x = 0$  and  $x = \infty$ , so, their entries are Laurent polynomials in  $x$ . Let us note that if the decomposition exists, it is unique, up to the transformations  $T(x) \rightarrow T(x)L$ ,  $S(x^{-1}) \rightarrow S(x^{-1})L$ , where  $L$  is constant matrix. We refer the reader to Ref. [594] for an algorithm which finds the decomposition (E.134) or proves that it does not exist.

Let us present a ‘troubleshooting’ table for the reduction to  $\epsilon$ -form:

Case	Explanation
It appears that there are some irreducible denominators depending both on $x$ and $\epsilon$ , which can not be eliminated by means of algorithm of Ref. [579].	The system is obviously irreducible to $\epsilon$ -form by any transformations. Almost definitely the IBP reduction is not complete.
After the reduction to Fuchsian form there are some square root branching points (say, $m$ points), i.e. some matrix residues have eigenvalues of the form $n + \frac{1}{2} + k\epsilon$ .	If $m \leq 3$ , make variable change [594], described above (in particular, for 2 and 3 points try only canonical change). If $m \geq 4$ the system can not be reduced to $\epsilon$ -form.
It seems to be impossible to find a pair $(U, V^\top)$ ( $(u, v^\top)$ ) on the first (second) stage such that $V^\top U$ is invertible ( $v^\top u \neq 0$ ).	Very likely this is an irreducible case. To strictly prove it (or disprove and find the required transformation), follow the algorithm of Ref. [594]
$\epsilon$ -factorization stage does not give invertible matrix $T$ .	Factorization is not possible [594].

Let us comment about irreducible cases (also known as ‘elliptic’). A natural generalization of  $\epsilon$ -form is the linear in  $\epsilon$  form

$$\partial_x \mathbf{J} = [A(x) + \epsilon B(x)] \mathbf{J}. \quad (\text{E.135})$$

If this form is obtained, one can achieve  $\epsilon$ -form by ‘integrating-out’ the  $\epsilon^0$  term [595, 596] i.e., by passing to  $\tilde{\mathbf{J}}$  via  $\mathbf{J} = F_0 \tilde{\mathbf{J}}$ , where  $F_0$  is the solution of the equation

$$\partial_x F_0 = A(x) F_0 \quad (\text{E.136})$$

One has

$$\partial_x \tilde{\mathbf{J}} = \epsilon \tilde{B}(x) \tilde{\mathbf{J}}, \quad (\text{E.137})$$

where  $\tilde{B}(x) = F_0^{-1}(x)B(x)F_0(x)$ . While being natural and, in principle, quite promising, this approach has weakness connected with the necessity to solve Eq. (E.136) on a case-by-case basis and with our poor understanding of the class of functions which may appear in the general solution of Eq. (E.136). We refer the reader to Refs. [597–603] for further information about known elliptic cases. From the practical point of view, there is also a problem of efficient numerical calculation of the iterative integrals  $\int \dots \int_{x_0 < x_1 < \dots < x_n < x} dx_n \dots dx_1 \tilde{B}(x_n) \dots \tilde{B}(x_1)$  which appear in the  $\epsilon$ -expansion of  $\tilde{\mathbf{J}}$ .

In contrast, the problem of finding the transformation to the form (E.135) seems to be quite approachable thanks to the algorithms reviewed here. The reason is that in many cases (in fact, in all

known to the author), it is possible to reduce the ‘elliptic’ systems to  $\epsilon$ -form near an odd dimensionality<sup>7</sup>. This means that we can achieve even more specific form (naturally referred to as  $(\epsilon + 1/2)$ -form)

$$\partial_x \mathbf{J} = (\epsilon + 1/2) B(x) \mathbf{J}. \quad (\text{E.138})$$

Let us briefly discuss the multivariate case. First, we note that for multivariate case the  $\epsilon$ -form of the differential equations is even more profitable than for the case of single variable. Indeed, the condition (E.102) becomes

$$\epsilon (\partial_b S_a - \partial_a S_b) + \epsilon^2 [S_a, S_b] = 0, \quad (\text{E.139})$$

and, therefore, coefficients in front of  $\epsilon$  and  $\epsilon^2$  should vanish separately [432]. The first condition  $\partial_b S_a - \partial_a S_b = 0$  indicates that there should be a matrix  $S$ , such that  $S_a = \partial_a S$  and the systems with respect to different variables can be unified in what is called *d log-form*

$$d\mathbf{J} = \epsilon(dS) \mathbf{J}. \quad (\text{E.140})$$

It is important to realize that the algorithms presented above are sufficient for the multivariate reduction once the variables are fixed. To use them, one should simply make the reduction with respect to each variable in turn. The important consequence of the proposition proved in Ref. [594] (and presented above) is that, after passing to next variable, one should consider only the transformations independent of the variables already processed. We refer the reader to [604] for an alternative approach to multivariate reduction to  $\epsilon$ -form. Unfortunately, the choice of ‘correct’ variables for multivariate setup lacks systematic treatment so far and mostly remains the matter of art and luck.

## Acknowledgements

*R.L.* is grateful to Andrei Pomeransky for constant interest and numerous fruitful discussions.

---

<sup>7</sup>We remark here that once  $\epsilon$ -form exists for  $d = n - 2\epsilon$ , it automatically exists for  $d = n + 2k - 2\epsilon$  where  $k$  is integer. This is a trivial consequence of the dimensional recurrences. However, shifting  $d$  by one is not trivial.



## 9 About Cuts of Feynman integrals and differential equations

**Author:** Costas G. Papadopoulos [Costas.Papadopoulos@cern.ch]

### 9.1 Introduction

It is almost seventy years from the time Feynman Integrals (FI) were first introduced [605–607] and forty-five years since the dimensional regularisation [361] set up the framework for an efficient use of loop integrals in computing scattering matrix elements, and still the frontier of multi-scale multi-loop integral calculations (maximal both in number of scales and number of loops) is determined by the planar five-point two-loop on-shell massless integrals [608, 609], recently computed<sup>8</sup>. On the other hand, in order to keep up with the increasing experimental accuracy as more data is collected at the LHC, more precise theoretical predictions and higher loop calculations are required [610].

In the last years our understanding of the reduction of one-loop amplitudes to a set of Master Integrals (MI), a minimal set of FI that form a basis, either based on unitarity methods [158, 611, 612] or at the integrand level via the OPP method [613, 614], has drastically changed the way one-loop calculations are performed resulting in many fully automated numerical tools (some reviews on the topic are [539, 615, 616]), making the next-to-leading order (NLO) approximation the default precision for theoretical predictions at the LHC. In the recent years, progress has been made also towards the extension of these reduction methods for two-loop amplitudes at the integral [476, 617–625] as well as the integrand [626–631] level. The master equation at the integrand level can be given schematically as follows [630]

$$\frac{N(l_1, l_2; \{p_i\})}{D_1 D_2 \dots D_n} = \sum_{m=1}^{\min(n,8)} \sum_{S_{m;n}} \frac{\Delta_{i_1 i_2 \dots i_m}(l_1, l_2; \{p_i\})}{D_{i_1} D_{i_2} \dots D_{i_m}}. \quad (\text{E.141})$$

where an arbitrary contribution to the two-loop amplitude (left), can be reduced to a sum of terms (right) of all partitions  $S_{m;n}$ , with up to eight denominators;  $l_1, l_2$  are the loop momenta,  $D_i$  are the inverse scalar Feynman propagators,  $N(l_1, l_2; \{p_i\})$  is a general numerator polynomial and  $\Delta_{i_1 i_2 \dots i_m}(l_1, l_2; \{p_i\})$  are the residues of multivariate polynomial division. In addition  $R_2$  terms [614] have to be studied at two loops in order to achieve a complete framework.

Two-loop MI are defined using the *integration by parts* (IBP) identities [414, 415, 423], an indispensable tool beyond one loop. Contrary to the one-loop case, where MI have been known for a long time already [632], a complete library of MI at two-loops is still missing. At the moment this is the main obstacle to obtain a fully automated NNLO calculation framework similar to the one-loop one, that will satisfy the precision requirements at the LHC [610].

Many methods have been introduced in order to compute MI [633]. The overall most successful one, is based on expressing the FI in terms of an integral representation over Feynman parameters, involving the two well-known Symanzik Polynomials  $U$  and  $F$  [464]. The introduction of the sector decomposition [439, 466, 467, 482, 487] method resulted in a powerful computational framework for the numerical evaluation of FI, see for instance SecDec [71]. An alternative is based on Mellin-Barnes representation [436, 437], implemented in [448]<sup>9</sup>. Nevertheless, the most successful method to calculate multi-scale multi-loop FI is, for the time being, the differential equations (DE) approach [525, 566, 569, 634, 635], which has been used in the past two decades to calculate various

<sup>8</sup>Complete results, including physical region kinematics, are presented in [609]. Notice that numerical codes, like for instance SecDec [71], can reproduce analytic results only at Euclidean region kinematics; results for physical region kinematics are not supported due to poor numerical convergence.

<sup>9</sup>See also <https://mbttools.hepforge.org>

MI at two-loops and beyond. Following the work of refs. [584, 636, 637], there has been a building consensus that the so-called *Goncharov Polylogarithms* (GPs) form a functional basis for many MI. The so-called canonical form of DE, introduced by Henn [432], manifestly results in MI expressed in terms of GPs<sup>10</sup>. Nevertheless the reduction of a given DE to a canonical form is by no means fully understood. First of all, despite recent efforts [587, 588, 604], and the existence of *sufficient* conditions that a given MI can be expressed in terms of GPs, no criterion, with practical applicability, that is at the same time *necessary and sufficient* has been introduced so far. Moreover, it is well known that when for instance enough internal masses are introduced, MI are not anymore expressible in terms of GPs, and in fact a new class of functions involving elliptic integrals is needed [477, 639–642].

In this contribution we start in Section 9.2 by briefly reviewing the Simplified Differential Equations approach. In Section 9.3 we present the results of the most advanced calculation achieved nowadays, namely the calculation of planar pentabox MI. The Baikov representation is introduced in Section 9.4. In Section 9.5 we give the definition of the cut [643] of a FI based on Baikov representation [644–649]. Finally in Section 9.6 we discuss possible future directions.

## 9.2 The Simplified Differential Equations Approach

Assume that one is interested in calculating an  $l$ -loop Feynman integral with external momenta  $\{p_j\}$  and internal propagators that are massless. Any  $l$ -loop Feynman integral can be then written as

$$G_{a_1 \dots a_n}(\{p_j\}, \epsilon) = \int \left( \prod_{r=1}^l \frac{d^d k_r}{i\pi^{d/2}} \right) \frac{1}{D_1^{a_1} \dots D_n^{a_n}}, \quad D_i = (c_{ij}k_j + d_{ij}p_j)^2, \quad d = 4 - 2\epsilon \quad (\text{E.142})$$

with matrices  $\{c_{ij}\}$  and  $\{d_{ij}\}$  determined by the topology and the momentum flow of the graph, and the denominators are defined in such a way that all scalar product invariants can be written as a linear combination of them. The exponents  $a_i$  are integers and may be negative in order to accommodate irreducible numerators. Any integral  $G_{a_1 \dots a_n}$  can be written as a linear combination of a finite subset of such integrals, called Master Integrals, with coefficients depending on the independent scalar products,  $s_{ij} = p_i \cdot p_j$ , and space-time dimension  $d$ , by the use of *integration by parts* identities [414, 415].

SDE approach [650] is an attempt not only to simplify, but also to systematize, as much as possible, the derivation of the appropriate system of DE satisfied by the MI. To this end the external incoming momenta are *parametrized* linearly in terms of  $x$  as  $p_i(x) = p_i + (1 - x)q_i$ , where the  $q_i$ 's are a linear combination of the momenta  $\{p_i\}$  such that  $\sum_i q_i = 0$ . If  $p_i^2 = 0$ , the parameter  $x$  captures the off-shell-ness of the external legs. The class of Feynman integrals in (E.142) are now dependent on  $x$  through the external momenta:

$$G_{a_1 \dots a_n}(\{s_{ij}\}, \epsilon; x) = \int \left( \prod_{r=1}^l \frac{d^d k_r}{i\pi^{d/2}} \right) \frac{1}{D_1^{a_1} \dots D_n^{a_n}}, \quad D_i = (c_{ij}k_j + d_{ij}p_j(x))^2. \quad (\text{E.143})$$

By introducing the dimensionless parameter  $x$ , the vector of MI  $\vec{G}^{MI}(\{s_{ij}\}, \epsilon; x)$ , which now depends on  $x$ , satisfies

$$\frac{\partial}{\partial x} \vec{G}^{MI}(\{s_{ij}\}, \epsilon; x) = \mathbf{H}(\{s_{ij}\}, \epsilon; x) \vec{G}^{MI}(\{s_{ij}\}, \epsilon; x) \quad (\text{E.144})$$

a system of differential equations in one independent variable. Experience up to now shows that this simple parametrization can be used universally to deal with up to six kinematical scales involved [609, 650, 651]. The expected benefit is that the integration of the DE naturally captures

<sup>10</sup>For an alternative method in the single scale case see also ref. [638]

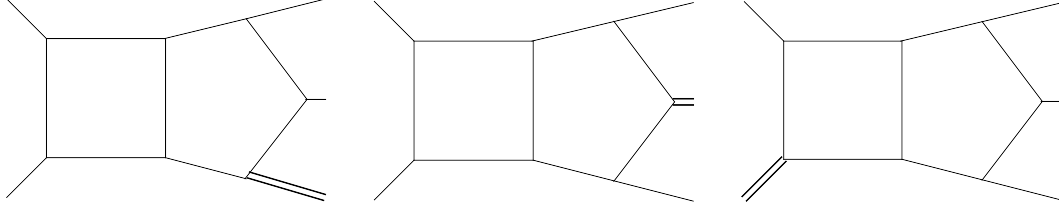


Fig. E.20: The three planar pentaboxes of the families  $P_1$  (left),  $P_2$  (middle) and  $P_3$  (right) with one external massive leg.

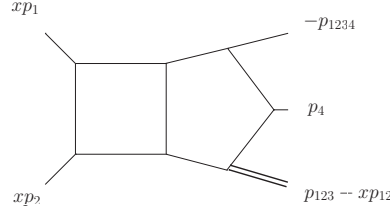


Fig. E.21: The parametrization of external momenta in terms of  $x$  for the planar pentabox of the family  $P_1$ . All external momenta are incoming.

the expressibility of MI in terms of GPs and more importantly makes the problem *independent on the number of kinematical scales* (independent invariants) involved. Note that as  $x \rightarrow 1$ , the original configuration of the loop integrals (E.142) is reproduced, which eventually corresponds to a simpler one with one scale less.

### 9.3 Massless pentabox MI with up to one off-shell leg

For the massless pentabox MI with one off-shell leg, there are in total three families of planar MI whose members with the maximum amount of denominators, namely eight, are graphically shown in Fig.E.20. We have checked that the other five-point integrals with one massive external leg are reducible to MI in one of these eight MI families. In [609] we have recently completed the calculation of the  $P_1$  family (Fig.E.20). In fact by taking the limit  $x \rightarrow 1$  all planar graphs for massless on-shell external momenta have been derived as well. We have used the C++ implementation of the program **FIRE** [421] to perform the IBP reduction to the set of MI in  $P_1$ .

For the family of integrals  $P_1$  the external momenta are parametrized in  $x$  as shown in Fig.E.21. The parametrization is chosen such that the double box MI with two massive external legs that is contained in the family  $P_1$  has exactly the same parametrization as that one chosen in [651], i.e. two massless external momenta  $xp_1$  and  $xp_2$  and two massive external momenta  $p_{123} - xp_{12}$  and  $-p_{123}$ . The MI in the family  $P_1$  are therefore a function of a parameter  $x$  and the following five invariants:  $s_{12} := p_{12}^2, s_{23} := p_{23}^2, s_{34} := p_{34}^2, s_{45} := p_{45}^2 = p_{123}^2, s_{51} := p_{15}^2 = p_{234}^2, p_i^2 = 0$ , where the notation  $p_{i\dots j} = p_i + \dots + p_j$  is used and  $p_5 := -p_{1234}$ . As the parameter  $x \rightarrow 1$ , the external momentum  $q_3 := p_{123} - xp_{12}$  becomes massless, such that our parametrization also captures the on-shell case.

The resulting differential equation in matrix form can be written as

$$\partial_x \mathbf{G} = \mathbf{M}(\{s_{ij}\}, \varepsilon, x) \mathbf{G} \quad (\text{E.145})$$

where  $\mathbf{G}$  stands for the array of the 74 MI involved in the family  $P_1$ . The twenty letters  $l_i$  involved, are given in [609]. Although the DE can be solved starting from , e.g. (E.145), and the result can be expressed as a sum of GPs with argument  $x$  and weights given by the letters  $l_i$ , it is more elegant and easy-to-solve to derive a Fuchsian system of equations [652], where only single poles in the variable

$x$  will appear. A series of transformation described in [609], brings the system into the form

$$\partial_x \mathbf{G} = \left( \varepsilon \sum_{i=1}^{19} \frac{\mathbf{M}_i}{(x - l_i)} \right) \mathbf{G} \quad (\text{E.146})$$

where the residue matrices  $\mathbf{M}_i$  are independent of  $x$  and  $\varepsilon$ . The result can be straightforwardly given as

$$\begin{aligned} \mathbf{G} = & \varepsilon^{-2} \mathbf{b}_0^{(-2)} + \varepsilon^{-1} \left( \sum \mathcal{G}_a \mathbf{M}_a \mathbf{b}_0^{(-2)} + \mathbf{b}_0^{(-1)} \right) + \left( \sum \mathcal{G}_{ab} \mathbf{M}_a \mathbf{M}_b \mathbf{b}_0^{(-2)} + \sum \mathcal{G}_a \mathbf{M}_a \mathbf{b}_0^{(-1)} + \mathbf{b}_0^{(0)} \right) \\ & + \varepsilon \left( \sum \mathcal{G}_{abc} \mathbf{M}_a \mathbf{M}_b \mathbf{M}_c \mathbf{b}_0^{(-2)} + \sum \mathcal{G}_{ab} \mathbf{M}_a \mathbf{M}_b \mathbf{b}_0^{(-1)} + \sum \mathcal{G}_a \mathbf{M}_a \mathbf{b}_0^{(0)} + \mathbf{b}_0^{(1)} \right) \\ & + \varepsilon^2 \left( \sum \mathcal{G}_{abcd} \mathbf{M}_a \mathbf{M}_b \mathbf{M}_c \mathbf{M}_d \mathbf{b}_0^{(-2)} + \sum \mathcal{G}_{abc} \mathbf{M}_a \mathbf{M}_b \mathbf{M}_c \mathbf{b}_0^{(-1)} \right. \\ & \left. + \sum \mathcal{G}_{ab} \mathbf{M}_a \mathbf{M}_b \mathbf{b}_0^{(0)} + \sum \mathcal{G}_a \mathbf{M}_a \mathbf{b}_0^{(1)} + \mathbf{b}_0^{(2)} \right) \end{aligned} \quad (\text{E.147})$$

with the arrays  $\mathbf{b}_0^{(k)}$ ,  $k = -2, \dots, 2$  representing the  $x$ -independent boundary terms in the limit  $x = 0$  at order  $\varepsilon^k$ . The expression is in terms of Goncharov polylogarithms,  $\mathcal{G}_{ab\dots} = \mathcal{G}(l_a, l_b, \dots; x)$ . Details on the calculation of boundary terms and of the  $x \rightarrow 1$  limit can be found in [609]

The solution for all 74 MI contains  $O(3,000)$  GPs which is roughly six times more than the corresponding double-box with two off-shell legs planar MI. We have performed several numerical checks of all our calculations. The numerical results, also included in the ancillary files<sup>11</sup>, have been obtained with the **GiNaC** library [585] and compared with those provided by the numerical code **SecDec** [71,439,440,445] in the Euclidean region for all MI and in the physical region whenever possible (due to CPU time limitations in using **SecDec**) and found perfect agreement. For the physical region we are using the analytic continuation as described in the previous section as well as in [651]. At the present stage we are not setting a fully-fledged numerical implementation, which will be done when all families will be computed. Our experience with double-box computations show that using for instance **HyperInt** [653] to bring all GPs in their range of convergence, *before* evaluating them numerically by **GiNaC**, increases efficiency by two orders of magnitude. Moreover expressing GPs in terms of classical polylogarithms and  $Li_{2,2}$ , could also reduce substantially the CPU time [654]. Based on the above we estimate that a target of  $O(10^2 - 10^3)$  milliseconds can be achieved.

## 9.4 The Baikov representation

An  $L$ -loop Feynman Integral with  $E + 1$  external lines can be written in the form

$$F_{\alpha_1 \dots \alpha_N} = \int \left( \prod_{i=1}^L \frac{d^d k_i}{i\pi^{d/2}} \right) \frac{1}{D_1^{\alpha_1} \dots D_N^{\alpha_N}} \quad (\text{E.148})$$

with  $N = \frac{L(L+1)}{2} + LE$ ,  $\alpha_i$  arbitrary integers, and  $D_a$ ,  $a = 1, \dots, N$ , inverse Feynman propagators,

$$D_a = \sum_{i=1}^L \sum_{j=i}^M A_a^{ij} s_{ij} + f_a = \sum_{i=1}^L \sum_{j=i}^L A_a^{ij} k_i \cdot k_j + \sum_{i=1}^L \sum_{j=L+1}^M A_a^{ij} k_i \cdot p_{j-L} + f_a, \quad a = 1, \dots, N \quad (\text{E.149})$$

where  $q_i = k_i$ , ( $i = 1, \dots, L$ ) the loop momenta and  $q_{L+i} = p_i$ , ( $i = 1, \dots, E$ ), the independent external momenta,  $M = L + E$ ,  $s_{ij} = q_i \cdot q_j$  and  $f_a$  depend on external kinematics and internal masses.  $A_a^{ij}$  can be understood as an  $N \times N$  matrix, with  $a$  running obviously from 1 to  $N$  and with  $(ij)$  taking also  $N$  values as  $i = 1, \dots, L$  and  $j = i, \dots, M$ . The elements of the matrix  $A_a^{ij}$  are integer numbers taken from

<sup>11</sup><https://www.dropbox.com/s/90iiqfcazrhwtso/results.tgz?dl=0>



the set  $\{-2, -1, 0, +1, +2\}$ . This matrix is characteristic of the corresponding Feynman graph and can, in a loose sense, be associated with the ‘topology’ of the graph. Then, by projecting each of the loop momenta  $q_i = k_i$ , ( $i = 1, \dots, L$ ) with respect to the space spanned by the external momenta involved plus a transverse component (for details see [648]), we may write

$$F_{\alpha_1 \dots \alpha_N} = C_N^L (G(p_1, \dots, p_E))^{(-d+E+1)/2} \int \frac{dx_1 \dots dx_N}{x_1^{\alpha_1} \dots x_N^{\alpha_N}} P_N^L(x_1 - f_1, \dots, x_N - f_N)^{(d-M-1)/2} \quad (\text{E.150})$$

with

$$C_N^L = \frac{\pi^{-L(L-1)/4 - LE/2}}{\prod_{i=1}^L \Gamma\left(\frac{d-M+i}{2}\right)} \det(A_{ij}^a) \quad (\text{E.151})$$

and

$$P_N^L(x_1, x_2, \dots, x_N) = G(k_1, \dots, k_L, p_1, \dots, p_E) \Big|_{s_{ij} = \sum_{a=1}^N A_{ij}^a x_a \text{ \& } s_{ji} = s_{ij}}$$

with  $G$  representing the Gram determinant,  $G(q_1, \dots, q_n) = \det(q_i \cdot q_j)$  and  $A_{ij}^a$  is the inverse of the topology matrix  $A_a^{ij}$ . An alternative derivation of the Baikov representation for one- and two-loop FI as well as the *loop-by-loop representation*, can be found in Appendix A of ref. [643]. The derivation of the Baikov representation can easily be implemented in a computer algebra code<sup>12</sup>.

We conclude this section by elaborating on the limits of the  $x_a$ -integrations in Eq. (E.150). In order to simplify the discussion, let us start with a generic one-loop configuration defined by

$$x_1 = k^2 - m_1^2, \quad x_2 = (k + p_1)^2 - m_2^2, \quad \dots, \quad x_N = (k + p_1 + \dots + p_{N-1})^2 - m_N^2$$

Then consider the generic integral ( $\alpha_i \geq 0$ ),

$$F_{\alpha_1 \dots \alpha_N} = C_N^1 G(p_1, \dots, p_{N-1})^{(N-d)/2} \int \frac{dx_1 \dots dx_N}{x_1^{\alpha_1} \dots x_N^{\alpha_N}} P_N^1 (d-N-1)/2 \quad (\text{E.152})$$

$$C_N^1 = \frac{\pi^{-(N-1)/2}}{\Gamma\left(\frac{d-N+1}{2}\right)} \left(\frac{1}{2}\right)^{N-1} \quad (\text{E.153})$$

It is easy to verify that  $P_N^1$  is a polynomial that is quadratic in the variables  $x_a$  [646], and that obviously when  $\alpha_N = 0$ , the external momentum  $p_{N-1}$  decouples, so that

$$\begin{aligned} F_{\alpha_1 \dots \alpha_{N-1} 0} &= C_N^1 G(p_1, \dots, p_{N-1})^{(N-d)/2} \int \frac{dx_1 \dots dx_{N-1}}{x_1^{\alpha_1} \dots x_{N-1}^{\alpha_{N-1}}} \int_{x_N^-}^{x_N^+} dx_N P_N^1 (d-N-1)/2 \\ &= C_{N-1}^1 G(p_1, \dots, p_{N-2})^{(N-1-d)/2} \int \frac{dx_1 \dots dx_{N-1}}{x_1^{\alpha_1} \dots x_{N-1}^{\alpha_{N-1}}} P_{N-1}^1 (d-(N-1)-1)/2 \end{aligned} \quad (\text{E.154})$$

where  $P_N^1(x_N^+) = P_N^1(x_N^-) = 0$  and

$$\begin{aligned} \int_{x_N^-}^{x_N^+} dx_N P_N^1 (d-N-1)/2 &= \frac{2\pi^{1/2} \Gamma\left(\frac{d-N+1}{2}\right)}{\Gamma\left(\frac{d-N+2}{2}\right)} G(p_1, \dots, p_{N-1})^{(d-N)/2} G(p_1, \dots, p_{N-2})^{(N-1-d)/2} \\ &\times P_{N-1}^1 (d-(N-1)-1)/2 \end{aligned}$$

<sup>12</sup>A Mathematica script, Baikov.m, is provided as an attachment in ref. [643]

using  $P_N^1 = \frac{1}{4} G(p_1, \dots, p_{N-2}) (x_N^+ - x_N) (x_N - x_N^-)$  and  $(x_N^+ - x_N^-)^2 = 16 \frac{G(p_1, \dots, p_{N-1})}{G(p_1, \dots, p_{N-2})^2} P_{N-1}^1$ . This can be repeated straightforwardly for all variables except  $x_1 = k^2 - m_1^2$  whose integration limits are simply derived from the  $k$ -modulus integration limits. The generalisation to the two-loop case is straightforward, with the integration at each step performed over the  $x$ -variables involving a given external momentum, and the last ones derived by the corresponding  $k_1$ - and  $k_2$ -modulus integration limits. We have checked both analytically and numerically that the limits, as defined above, reproduce the known results for several examples at one and two loops.

## 9.5 Cutting Feynman Integrals

Cutting FI in the Baikov representation has a very natural definition. Indeed we define an  $n$ -cut as follows

$$F_{\alpha_1 \dots \alpha_N}|_{n \times \text{cut}} \equiv C_N^L(G)^{(-d+E+1)/2} \left( \prod_{a=n+1}^N \int dx_a \right) \left( \prod_{c=1}^n \oint_{x_c=0} dx_c \right) \frac{1}{x_1^{\alpha_1} \dots x_N^{\alpha_N}} P_N^{L(d-M-1)/2} \quad (\text{E.155})$$

where the Baikov variables  $\{x_a : a = 1, \dots, N\}$  have been divided in two subsets, containing  $n$  cut propagators and  $(N - n)$  uncut ones. The cut operation defined above is operational in any space-time dimension  $d$  and for any FI given by Eq. (E.148). Notice that the definition of the cut, Eq. (E.155), is not identical to the traditional unitarity cut, see for instance Section 8.4 of ref. [655], due to the lack of the  $\theta$ -function constraint on the energy, and therefore it is not directly related to the discontinuity of the FI [656, 657].

Let us now consider a set of MI,  $F_i \equiv F_{\alpha_1^{(i)} \dots \alpha_N^{(i)}}$ ,  $i = 1, \dots, I$ , satisfying a system of DE, with respect to variables  $X_j$ ,

$$\frac{\partial}{\partial X_j} F_i = \sum_{l=1}^I M_{il}^{(j)} F_l \quad (\text{E.156})$$

with matrices  $M^{(j)}$  depending on kinematical variables, internal masses, and the space-time dimension,  $d$ . Since the derivation of DE [643] is insensitive to the cut operation, as defined in Eq. (E.155), we may immediately write

$$\frac{\partial}{\partial X_j} F_i|_{n \times \text{cut}} = \sum_{l=1}^I M_{il}^{(j)} F_l|_{n \times \text{cut}} \quad (\text{E.157})$$

with  $F|_{n \times \text{cut}}$  representing an arbitrary  $n$ -cut: in other words, the cut integrals satisfy the same DE as the uncut ones<sup>13</sup>. Of course for a given  $n$ -cut many of the MI that are not supported on the corresponding cut vanish identically. Nevertheless, Eq. (E.157) remains valid. Especially for the maximally cut integrals defined so that  $n$  is equal to the number of propagators (with  $\alpha_i > 0$ ) of the integral, all integrals not supported on the cut vanish and the resulting DE is restricted to its homogeneous part. Evaluating the maximally cut MI provides therefore a solution to the homogeneous equation [602, 652]. Non-maximally cut integrals, on the other hand, can resolve non-homogenous parts of the DE as well [652].

One important implication is that cut and uncut integrals, although very different in many respects, as for instance their structure in  $\epsilon$ -expansion ( $\epsilon \equiv (4 - d)/2$ ), they are expressed in terms of the same class of functions<sup>14</sup>. This is particularly important if we want to know *a priori* if a system of DE can be solved, for instance, in terms of Goncharov Polylogarithms, or if the solution contains a larger class of functions including, for instance Elliptic Integrals.

Several results of maximally cut MI, expressed either in terms of Polylogarithmic functions or in terms of Elliptic Integrals, can be found in the Appendix B of ref. [643] as well as in refs. [660, 661].

<sup>13</sup>See also ref. [574, 658, 659] for related considerations.

<sup>14</sup>See also related discussion in ref. [476], section 3.4.1.

## 9.6 Discussion and Outlook

In this contribution we have presented recent results for the calculation of two-loop five-point Feynman Integrals, based on the simplified differential equations approach. We have also presented the Baikov representation of Feynman integrals. We have shown how to determine the limits of integration and how to obtain DE with respect to external kinematics and internal masses. Then we provided a definition of a cut integral, operational in  $d$  dimensions, and show that a cut integral satisfies the same system of DE as the uncut, original integral.

Based on the fact that cut integrals satisfy the same system of DE as the full, uncut integrals we have verified that their analytic expressions are given in terms of the same class of functions, such as Goncharov Polylogarithms or Elliptic Integrals. We have therefore arrived at the conclusion that in a family of MI satisfying a given system of DE, the study of the maximally cut integrals for all its members can provide a *necessary and sufficient* criterion for the existence of a canonical form of the DE, and in the case when such a canonical form does not exist, it provides solutions of the homogeneous parts of the system of DE (see also ref. [602, 652]).

By completing the calculation of non-planar pentabox integral families we expect that in the near future all five-point massless two-loop Feynman Integrals will be available. The road to complete the full list of two-loop Master Integrals with up to eight denominators and vanishing internal masses, seems a feasible task for the years to come. Nevertheless, the calculation of the full list of two-loop Master Integrals with up to eight denominators and non-vanishing internal masses requires further understanding of the class of functions involved. Combination of analytic and numerical approaches may be the final solution. Once this problem is solved, the efficient computation of arbitrary two-loop scattering amplitudes will be realised, providing the basis of the most precise theoretical predictions for current and future high-energy collider experiments.



## 10 Exploring the function space of Feynman integrals

Authors: Stefan Weinzierl [weinzierl@uni-mainz.de]

### 10.1 Introduction: Precision calculations for the FCC-ee

The physics program of a future circular collider operating in electron-positron annihilation mode will be centred around a detailed study of the heavy particles of the Standard Model: the  $Z$ - and  $W$ -bosons, the Higgs boson and the top quark. Precision studies of these particles are sensitive to contributions from new physics at higher mass scales reaching the order of 100 TeV. However, in order to extract these effects, the experimental precision has to be matched with the same precision in the theoretical calculations. This requires the computation of quantum corrections at the two-loop or three-loop order. There is a class of Feynman integrals, which evaluate to multiple polylogarithm. This class of Feynman integrals is by now quite well understood and captures a significant part of the Feynman integrals occurring in massless quantum field theories. However, for the processes relevant to the FCC-ee we do not want to neglect the masses of the heavy particles of the Standard Model (i.e. the  $Z$ -,  $W$ -,  $H$ - and top masses). With non-zero internal masses we leave already at two loops the function space of multiple polylogarithms. The simplest Feynman integral, which cannot be expressed in terms of multiple polylogarithms is given by the two-loop sunrise integrals with equal non-zero masses. The systematic study of the functions, to which these more complicated Feynman integrals evaluate is now an active field of study. Below, I will summarise the current state-of-the-art, based on [600]. As it is a field under active development, it is likely that this survey will be outdated in a few years. Phrased differently, the need for precision (as imposed by the FCC-ee program) triggers research in this direction and it is not unlikely that we will see substantial progress in the years to come.

### 10.2 Differential equations and multiple polylogarithms

Let us start with a review of differential equations and multiple polylogarithms. The method of differential equations [432, 566, 569, 575, 634, 635, 638, 652, 662, 663] is a powerful tool to tackle Feynman integrals. Let  $t$  be an external invariant (e.g.  $t = (p_i + p_j)^2$ ) or an internal mass and let  $I_i \in \{I_1, \dots, I_N\}$  be a master integral. Carrying out the derivative  $\partial I_i / \partial t$  under the integral sign and using integration-by-parts identities allows us to express the derivative as a linear combination of the master integrals:

$$\frac{\partial}{\partial t} I_i = \sum_{j=1}^N a_{ij} I_j \quad (\text{E.158})$$

More generally, let us denote by  $\vec{I} = (I_1, \dots, I_N)$  the vector of the master integrals, and by  $\vec{x} = (x_1, \dots, x_n)$  the vector of kinematic variables the master integrals depend on. Repeating the above procedure for every master integral and every kinematic variable we obtain a system of differential equations of Fuchsian type

$$d\vec{I} = A\vec{I}, \quad (\text{E.159})$$

where  $A$  is a matrix-valued one-form

$$A = \sum_{i=1}^n A_i dx_i. \quad (\text{E.160})$$

The matrix-valued one-form  $A$  satisfies the integrability condition  $dA - A \wedge A = 0$ .

There is a class of Feynman integrals, which may be expressed in terms of multiple polylogarithms. Multiple polylogarithms are defined by the nested sum [584, 664–666]

$$\text{Li}_{m_1, m_2, \dots, m_k}(x_1, x_2, \dots, x_k) = \sum_{n_1 > n_2 > \dots > n_k > 0} \frac{x_1^{n_1}}{n_1^{m_1}} \cdot \frac{x_2^{n_2}}{n_2^{m_2}} \cdot \dots \cdot \frac{x_k^{n_k}}{n_k^{m_k}}. \quad (\text{E.161})$$

There is an alternative definition based on iterated integrals

$$G(z_1, \dots, z_k; y) = \int_0^y \frac{dt_1}{t_1 - z_1} \int_0^{t_1} \frac{dt_2}{t_2 - z_2} \dots \int_0^{t_{k-1}} \frac{dt_k}{t_k - z_k}. \quad (\text{E.162})$$

The two notations are related by

$$\text{Li}_{m_1, \dots, m_k}(x_1, \dots, x_k) = (-1)^k G_{m_1, \dots, m_k} \left( \frac{1}{x_1}, \frac{1}{x_1 x_2}, \dots, \frac{1}{x_1 \dots x_k}; 1 \right), \quad (\text{E.163})$$

where

$$G_{m_1, \dots, m_k}(z_1, \dots, z_k; y) = G(\underbrace{0, \dots, 0}_{m_1-1}, z_1, \dots, z_{k-1}, \underbrace{0, \dots, 0}_{m_k-1}, z_k; y). \quad (\text{E.164})$$

Let us return to the differential equation (E.159). If we change the basis of the master integrals  $\vec{J} = U\vec{I}$ , where  $U$  is a  $N \times N$ -matrix, whose entries may depend on  $\vec{x}$  and the dimensional regularisation parameter  $\varepsilon$ , the differential equation becomes

$$d\vec{J} = A'\vec{J}, \quad A' = UAU^{-1} - U dU^{-1}. \quad (\text{E.165})$$

Suppose further one finds a transformation matrix  $U$ , such that

$$A' = \varepsilon \sum_j C_j d \ln p_j(\vec{x}), \quad (\text{E.166})$$

where the dimensional regularisation parameter  $\varepsilon$  appears only as prefactor, the  $C_j$  are matrices with constant entries, and where the  $p_j(\vec{x})$  are polynomials in the external variables, then the system of differential equations is easily solved in terms of multiple polylogarithms [432, 652]. In order to obtain the  $\varepsilon$ -form we may perform a transformation of the kinematic variables

$$(x_1, \dots, x_n) \rightarrow (x'_1, \dots, x'_n). \quad (\text{E.167})$$

This corresponds to a change of variables in the base manifold. Quite often, the transformation is rational or algebraic. A change of kinematic variables can be done to absorb square roots for massive integrals. For example, the transformation ( $x = s/m^2$ )

$$\frac{s}{m^2} = -\frac{(1-x')^2}{x'}, \quad (\text{E.168})$$

rationalises the typical square root occurring in two-particle cuts:

$$\frac{ds}{\sqrt{-s(4m^2 - s)}} = \frac{dx'}{x'}. \quad (\text{E.169})$$

In addition, we may change the basis of the master integrals

$$\vec{I} \rightarrow U\vec{I}. \quad (\text{E.170})$$

Quite often  $U$  is rational in the kinematic variables. A transformation of the form as in eq. (E.170) corresponds to a change of basis in the fibre. Methods to find the right transformation have been discussed in [587–589, 594, 595, 604, 667–670].

At the end of the day we would like to evaluate the multiple polylogarithms numerically, taking into account that the multiple polylogarithms  $\text{Li}_{m_1, m_2, \dots, m_k}(x_1, x_2, \dots, x_k)$  have branch cuts as a function of the  $k$  complex variables  $x_1, x_2, \dots, x_k$ . The numerical evaluation can be done as follows: One uses a truncation of the sum representation within the region of convergence. The integral representation is used to map the arguments into the region of convergence. On top of that, acceleration techniques are used to speed up the computation [585].

### 10.3 Beyond multiple polylogarithms: Single scale integrals

Starting from two-loops, there are integrals which cannot be expressed in terms of multiple polylogarithms. The simplest example is given by the two-loop sunrise integral [639, 671–688] with equal masses. A slightly more complicated integral is the two-loop kite integral [596, 598, 599, 689–691], which contains the sunrise integral as a sub-topology. Both integrals depend on a single dimensionless variable  $t/m^2$ . In the following we will change the variable from  $t/m^2$  to the nome  $q$  of an elliptic curve or the parameter  $\tau$ , related to the nome by  $q = e^{i\pi\tau}$ . Before giving a definition of these new variables, let us first see how an elliptic curve emerges. For the sunrise integral there are two possibilities. The first option reads off an elliptic curve from the Feynman graph polynomial

$$E_{\text{graph}} : -x_1 x_2 x_3 t + m^2 (x_1 + x_2 + x_3) (x_1 x_2 + x_2 x_3 + x_3 x_1) = 0, \quad (\text{E.171})$$

the second option obtains an elliptic curve from the maximal cut [476, 618, 643, 644, 660, 661, 692] of the sunrise integral

$$E_{\text{cut}} : y^2 - \left(x - \frac{t}{m^2}\right) \left(x + 4 - \frac{t}{m^2}\right) \left(x^2 + 2x + 1 - 4\frac{t}{m^2}\right) = 0. \quad (\text{E.172})$$

In the following we will consider the elliptic curve of eq. (E.171). The periods  $\psi_1, \psi_2$  of the elliptic curve are solutions of the homogeneous differential equation [683]. In general, the maximal cut of a Feynman integral is a solution of the homogeneous differential equation for this Feynman integral [602]. We define the new variables  $\tau$  and  $q$  by

$$\tau = \frac{\psi_2}{\psi_1}, \quad q = e^{i\pi\tau}. \quad (\text{E.173})$$

Let us now turn to the transcendental functions, in which we may express the sunrise and the kite integral. We remind the reader of the definition of the classical polylogarithms

$$\text{Li}_n(x) = \sum_{j=1}^{\infty} \frac{x^j}{j^n}. \quad (\text{E.174})$$

Starting from this expression, we consider a generalisation with two sums, which are coupled through the variable  $q$ :

$$\text{ELi}_{n;m}(x; y; q) = \sum_{j=1}^{\infty} \sum_{k=1}^{\infty} \frac{x^j}{j^n} \frac{y^k}{k^m} q^{jk}. \quad (\text{E.175})$$

The elliptic dilogarithm is a linear combination of these functions and the classical dilogarithm:

$$\text{E}_{2;0}(x; y; q) = \frac{1}{i} \left[ \frac{1}{2} \text{Li}_2(x) - \frac{1}{2} \text{Li}_2(x^{-1}) + \text{ELi}_{2;0}(x; y; q) - \text{ELi}_{2;0}(x^{-1}; y^{-1}; q) \right]. \quad (\text{E.176})$$

In the mathematical literature there exist various slightly different definitions of elliptic polylogarithms [477, 603, 684, 693–701]. In order to express the sunrise and the kite integral to all orders in  $\varepsilon$  we introduce the functions

$$\begin{aligned} & \text{ELi}_{n_1, \dots, n_l; m_1, \dots, m_l; 2o_1, \dots, 2o_{l-1}}(x_1, \dots, x_l; y_1, \dots, y_l; q) = \\ & = \sum_{j_1=1}^{\infty} \dots \sum_{j_l=1}^{\infty} \sum_{k_1=1}^{\infty} \dots \sum_{k_{l-1}=1}^{\infty} \frac{x_1^{j_1}}{j_1^{n_1}} \dots \frac{x_l^{j_l}}{j_l^{n_l}} \frac{y_1^{k_1}}{k_1^{m_1}} \dots \frac{y_l^{k_l}}{k_l^{m_l}} \frac{q^{j_1 k_1 + \dots + j_l k_l}}{\prod_{i=1}^{l-1} (j_i k_i + \dots + j_l k_l)^{o_i}}. \end{aligned} \quad (\text{E.177})$$

Let us write the Taylor expansion of the sunrise integral around  $D = 2 - 2\varepsilon$  as

$$S = \frac{\psi_1}{\pi} \sum_{j=0}^{\infty} \varepsilon^j E^{(j)}. \quad (\text{E.178})$$

Each term in this  $\varepsilon$ -series is of the form

$$E^{(j)} \sim \text{linear combination of } \text{ELi}_{n_1, \dots, n_l; m_1, \dots, m_l; 2o_1, \dots, 2o_{l-1}} \text{ and } \text{Li}_{n_1, \dots, n_l}. \quad (\text{E.179})$$

Using dimensional-shift relations this translates to the expansion around  $D = 4 - 2\varepsilon$ . Thus we find that the functions of eq. (E.177) together with the multiple polylogarithms are the class of functions to express the equal mass sunrise graph and the kite integral to all orders in  $\varepsilon$  [598, 686].

The functions in eq. (E.177) are defined as multiple sums. We may ask if every term in the  $\varepsilon$ -expansion can be expressed in terms of iterated integrals. For the equal-mass sunrise integral and the kite integral this is indeed the case and relates these Feynman integrals to modular forms [690]. A function  $f(\tau)$  on the complex upper half plane is a modular form of weight  $k$  for  $\text{SL}_2(\mathbb{Z})$  if  $f$  transforms under Möbius transformations as

$$f\left(\frac{a\tau + b}{c\tau + d}\right) = (c\tau + d)^k \cdot f(\tau) \quad \text{for} \quad \begin{pmatrix} a & b \\ c & d \end{pmatrix} \in \text{SL}_2(\mathbb{Z}). \quad (\text{E.180})$$

In addition,  $f$  is required to be holomorphic on the complex upper half plane and at  $\tau = i\infty$ . Furthermore, there are modular forms for congruence subgroups of  $\text{SL}_2(\mathbb{Z})$ . We introduce iterated integrals of modular forms

$$I(f_1, f_2, \dots, f_n; \bar{q}) = (2\pi i)^n \int_{\tau_0}^{\tau} d\tau_1 f_1(\tau_1) \int_{\tau_0}^{\tau_1} d\tau_2 f_2(\tau_2) \dots \int_{\tau_0}^{\tau_{n-1}} d\tau_n f_n(\tau_n), \quad \bar{q} = e^{2\pi i \tau}. \quad (\text{E.181})$$

As base point it is convenient to take  $\tau_0 = i\infty$ . Repeated sequences of letters are abbreviated as in  $\{f_1, f_2\}^3 = f_1, f_2, f_1, f_2, f_1, f_2$ . With the help of the iterated integrals of modular forms one finds a compact all-order expression for the equal-mass sunrise integral around  $D = 2 - 2\varepsilon$  dimensions:

$$S = \frac{\psi_1}{\pi} e^{-\varepsilon I(f_2; q) + 2 \sum_{n=2}^{\infty} \frac{(-1)^n}{n} \zeta_n \varepsilon^n} \left\{ \sum_{j=0}^{\infty} \varepsilon^j \sum_{k=0}^{\lfloor \frac{j}{2} \rfloor} I\left(\{1, f_4\}^k, 1, f_3, \{f_2\}^{j-2k}; q\right) + \left[ \sum_{j=0}^{\infty} \left( \varepsilon^{2j} I\left(\{1, f_4\}^j; q\right) - \frac{1}{2} \varepsilon^{2j+1} I\left(\{1, f_4\}^j, 1; q\right) \right) \right] \sum_{k=0}^{\infty} \varepsilon^k B^{(k)} \right\}, \quad (\text{E.182})$$

where the  $B^{(k)}$ 's are boundary constants. This expression has uniform depth, i.e. at order  $\varepsilon^j$  one has exactly  $(j+2)$  iterated integrations. The alphabet is given by four modular forms  $1, f_2, f_3, f_4$ . To give an example, the modular form  $f_3$  is given by

$$f_3 = -\frac{1}{24} \left( \frac{\psi_1}{\pi} \right)^3 \frac{t(t-m^2)(t-9m^2)}{m^6}. \quad (\text{E.183})$$

The letters  $1, f_2, f_3$  and  $f_4$  may be expressed as a linear combination of generalised Eisenstein series, which makes the property of being a modular form manifest.

Let us now return to question if there is an  $\varepsilon$ -form for the differential equations for the sunrise and kite integrals. It is not possible to obtain an  $\varepsilon$ -form by an algebraic change of variables and/or an algebraic transformation of the basis of master integrals. However by the (non-algebraic) change of variables from  $t$  to



$\tau$  and by factoring off the (non-algebraic) expression  $\psi_1/\pi$  from the master integrals in the sunrise sector one obtains an  $\varepsilon$ -form for the kite/sunrise family [596]:

$$\frac{d}{d\tau} \vec{I} = \varepsilon A(\tau) \vec{I}, \quad (\text{E.184})$$

where  $A(\tau)$  is an  $\varepsilon$ -independent  $8 \times 8$ -matrix whose entries are modular forms.

Let us turn to the numerical evaluation: The complete elliptic integrals entering  $\psi_1$  can be computed efficiently from the arithmetic-geometric mean. The numerical evaluation of the ELi-functions is straightforward in the region where the sum converges: One simply truncates the  $q$ -series at a certain order such that the desired numerical precision is reached. Methods to map the arguments outside the region of convergence into this region have been discussed in [702]. It turns out that for the sunrise integral and the kite integral the  $q$ -series converges for all  $t \in \mathbb{R} \setminus \{m^2, 9m^2, \infty\}$ , in particular there is no need to distinguish the cases  $t < 0$ ,  $0 < t < m^2$ ,  $m^2 < t < 9m^2$  or  $9m^2 < t$  [691]. Our default choice of the periods corresponds to  $q = 0$  for  $t = 0$ . We may use a  $\text{SL}_2(\mathbb{Z})$ -transformation to achieve that  $q$  vanishes at a chosen singular point  $t \in \{0, m^2, 9m^2, \infty\}$  of the differential equation. This gives a convergent  $q$ -series around the chosen singular point, and allows a numerical evaluation for all  $t \in \mathbb{R}$ .

#### 10.4 Towards multi-scale integrals beyond multiple polylogarithms

Let us now turn from single-scale integrals to multi-scale integrals. We are interested in the ones, which are not expressible in terms of multiple polylogarithms [475, 601, 639–642, 685, 703, 704], but are expressible in terms of elliptic generalisations of these functions. Therefore we expect in the differential equation for a given master integral irreducible second-order factors. A system of first-order differential equations is easily converted to a higher-order differential equation for a single master integral. We may work modulo sub-topologies, therefore the order of the differential equation is given by the number of master integrals in this sector. The number of master integrals in a given sector may be larger than 2 and we face the question on how to transform to a suitable basis of master integrals, which decouples the original system of differential equations at order  $\varepsilon^0$  to a system of maximal block size of 2. This can be done by exploiting the factorisation properties of the Picard-Fuchs operator [669]. To this aim one first projects the problem to a single-scale problem by setting  $x_i(\lambda) = \alpha_i \lambda$  with  $\alpha = [\alpha_1 : \dots : \alpha_n] \in \mathbb{CP}^{n-1}$  and by viewing the master integrals as functions of  $\lambda$ . For the derivative with respect to  $\lambda$  we have

$$\frac{d}{d\lambda} \vec{I} = B \vec{I}, \quad B = \sum_{i=1}^n \alpha_i A_i, \quad B = B^{(0)} + \sum_{j>0} \varepsilon^j B^{(j)}. \quad (\text{E.185})$$

In order to find the required transformation we may work modulo  $\varepsilon$ -corrections, i.e. we focus on  $B^{(0)}$ . Let  $I$  be one of the master integrals  $\{I_1, \dots, I_N\}$ . We determine the largest number  $r$ , such that the matrix which expresses  $I, (d/d\lambda)I, \dots, (d/d\lambda)^{r-1}I$  in terms of the original set  $\{I_1, \dots, I_N\}$  has full rank. It follows that  $(d/d\lambda)^r I$  can be written as a linear combination of  $I, \dots, (d/d\lambda)^{r-1}I$ . This defines the Picard-Fuchs operator  $L_r$  for the master integral  $I$  with respect to  $\lambda$ :

$$L_r I = 0, \quad L_r = \sum_{k=0}^r R_k \frac{d^k}{d\lambda^k}. \quad (\text{E.186})$$

$L_r$  is easily found by transforming to a basis which contains  $I, \dots, (d/d\lambda)^{r-1}I$ . We may factor the differential operator into irreducible factors [705].

$$L_r = L_{1,r_1} L_{2,r_2} \dots L_{s,r_s}, \quad (\text{E.187})$$

where  $L_{i,r_i}$  denotes a differential operator of order  $r_i$ . We may then convert the system of differential equations at order  $\varepsilon^0$  into a block triangular form with blocks of size  $r_1, r_2, \dots, r_s$ . A basis for block  $i$  is given by

$$J_{i,j} = \frac{d^{j-1}}{d\lambda^{j-1}} L_{i+1,r_{i+1}} \dots L_{s,r_s} I, \quad 1 \leq j \leq r_i. \quad (\text{E.188})$$

This decouples the original system into sub-systems of size  $r_1, r_2, \dots, r_s$ . Let us write the transformation to the new basis as  $\vec{J} = V(\alpha_1, \dots, \alpha_{n-1}, \lambda) \vec{I}$ . Setting

$$U = V\left(\frac{x_1}{x_n}, \dots, \frac{x_{n-1}}{x_n}, x_n\right) \quad (\text{E.189})$$

gives a transformation in terms of the original variables  $x_1, \dots, x_n$ . Terms in the original matrix  $A$  of the form  $d \ln Z(x_1, \dots, x_n)$ , where  $Z(x_1, \dots, x_n)$  is a rational function in  $(x_1, \dots, x_n)$  and homogeneous of degree zero in  $(x_1, \dots, x_n)$ , map to zero in the matrix  $B$ . These terms are in many cases easily removed by a subsequent transformation. Let us look at an example. For the planar double-box integral for  $t\bar{t}$ -production with a closed top loop one finds in the top sector five master integrals. These may be decoupled as

$$5 = 1 + 2 + 1 + 1. \quad (\text{E.190})$$

Thus we need to solve only two coupled equations, not five.

## 10.5 Conclusions

There is rapid progress on Feynman integrals, which cannot be expressed in terms of multiple polylogarithms. The function space of these Feynman integrals leads to elliptic generalisations of multiple polylogarithms. The simplest examples of these are the Feynman integrals belonging to the families of the equal-mass sunrise integral and the kite integral. By now, we have quite a good understanding of the Feynman integrals from this family: With a non-algebraic change of variables and a non-algebraic basis transformation it is possible to transform the differential equation to an  $\varepsilon$ -form. This allows us to obtain the analytic expression to any order in the dimensional regularisation parameter. At each order  $\varepsilon$ , the solution is either given as a sum representation (ELi-representation) or as an iterated integral representation (iterated integrals of modular forms). There exist fast and efficient methods for the numerical evaluation.

In the future the focus will be on multi-scale integrals beyond multiple polylogarithms. These will be needed for precision calculations within the FCC-ee physics program. We expect that sufficient progress will be made within the coming years.

## 11 Direct calculation of multi-loop integrals in $d = 4$ with FDR

Author: Roberto Pittau [pittau@ugr.es]

In view of the increasing complexity of the perturbative calculations needed to cope with the precision requirements of the future FCC-ee experiments, it is appropriate to investigate new methods to compute radiative corrections. Here we report on the main features of the FDR [706] approach to multi-loop calculus in the presence of UV and IR divergences.

In FDR, the UV subtraction is embedded in a new definition of the loop integration, allowing one to compute renormalized Green's functions directly in four dimensions. Note that this differs from other four-dimensional techniques [707, 708], where Dimensional Regularization (DReg [361]) is implicitly assumed.

The advantage of working in four dimensions is expected to lead to considerable simplifications, especially in connection with numerical techniques. In addition, this approach is attractive also in supersymmetric calculations, where the fermionic and bosonic sectors must share the same number of degrees of freedom.

### 11.1 UV divergent loop integrals

The FDR loop integration over UV divergent integrands is defined in such a way to preserve the fundamental properties of the gauge theories at the quantum level, that is

Shift invariance of the loop integrals; (E.191)

The possibility of simplifying at the integrand level reconstructed propagators and denominators; (E.192)

The possibility of inserting sub-loop expressions in higher loop calculations (sub-integration consistency); (E.193)

The first condition ensures routing invariance, the second requirement maintains the needed gauge cancellations and the third property is essential to keep the theory unitary.<sup>15</sup>

As an illustrative example, we consider the FDR loop integration over the one-loop integrand

$$J^{\mu\nu} = \frac{l^2 g^{\mu\nu} - 4l^\mu l^\nu}{(l^2 - M^2)^3}, \quad (\text{E.194})$$

which is logarithmic divergent by power counting. This integral is responsible for the no-decoupling properties of the  $H \rightarrow \gamma\gamma$  amplitude when  $m_H \rightarrow \infty$ , giving rise to a certain debate in the recent literature [709, 710].

The UV behavior is extracted by making the replacement

$$l^2 \rightarrow \bar{l}^2 \equiv l^2 - \mu^2 \quad (\text{E.195})$$

and expanding

$$\frac{1}{(\bar{l}^2 - M^2)^3} = \frac{1}{\bar{l}^6} + M^2 \left( \frac{1}{(\bar{l}^2 - M^2)^3 \bar{l}^2} + \frac{1}{(\bar{l}^2 - M^2)^2 \bar{l}^4} + \frac{1}{(\bar{l}^2 - M^2)^3 \bar{l}^6} \right). \quad (\text{E.196})$$

This results in

$$J^{\mu\nu} \rightarrow \bar{J}^{\mu\nu} \equiv \frac{\bar{l}^2 g^{\mu\nu} - 4l^\mu l^\nu}{\bar{l}^6} + M^2 (\bar{l}^2 g^{\mu\nu} - 4l^\mu l^\nu) \left( \frac{1}{(\bar{l}^2 - M^2)^3 \bar{l}^2} + \frac{1}{(\bar{l}^2 - M^2)^2 \bar{l}^4} + \frac{1}{(\bar{l}^2 - M^2)^3 \bar{l}^6} \right) \quad (\text{E.197})$$

Only the first term contains UV divergent integrands parametrized in terms of the unphysical scale  $\mu$ . It acts as a natural counterterm cancelling the UV behavior directly at the integrand level. Thus, the FDR integration over  $J^{\mu\nu}$  is *defined* as follows

$$\int [d^4 l] J^{\mu\nu} \equiv \lim_{\mu \rightarrow 0} \int d^4 l \left( \bar{J}^{\mu\nu} - \frac{\bar{l}^2 g^{\mu\nu} - 4l^\mu l^\nu}{\bar{l}^6} \right). \quad (\text{E.198})$$

<sup>15</sup>The unitarity equation  $T - T^\dagger = i T^\dagger T$  mixes different loop orders, so that it is essential that the result of a sub-loop integration stays the same also when embedded in higher loop computations.

Finally, by tensor decomposition one easily computes

$$\int [d^4 l] \bar{J}^{\mu\nu} = g^{\mu\nu} \lim_{\mu \rightarrow 0} \mu^2 \int d^4 l \frac{1}{l^6} = -g^{\mu\nu} \frac{i\pi^2}{2}, \quad (\text{E.199})$$

which implies no decoupling limit of  $H \rightarrow \gamma\gamma$ .

The main properties of the FDR integration are listed below

- Expansions as in Eq. (E.196) can be performed at any loop order. A two-loop example with  $\bar{D}_1 = \bar{l}_1^2 - m_1^2$ ,  $\bar{D}_2 = \bar{l}_2^2 - m_2^2$ ,  $\bar{D}_{12} = \bar{l}_{12}^2 - m_{12}^2$ ,  $l_{12} = l_1 + l_2$  reads

$$\begin{aligned} \frac{1}{\bar{D}_1 \bar{D}_2 \bar{D}_{12}} &= \left[ \frac{1}{\bar{l}_1^2 \bar{l}_2^2 \bar{l}_{12}^2} \right] + m_1^2 \left[ \frac{1}{\bar{l}_1^4 \bar{l}_2^2 \bar{l}_{12}^2} \right] + m_2^2 \left[ \frac{1}{\bar{l}_1^2 \bar{l}_2^4 \bar{l}_{12}^2} \right] + m_{12}^2 \left[ \frac{1}{\bar{l}_1^2 \bar{l}_2^2 \bar{l}_{12}^4} \right] \\ &+ \frac{m_1^4}{(\bar{D}_1 \bar{l}_1^4)} \left[ \frac{1}{\bar{l}_2^4} \right] + \frac{m_2^4}{(\bar{D}_2 \bar{l}_2^4)} \left[ \frac{1}{\bar{l}_1^4} \right] + \frac{m_{12}^4}{(\bar{D}_{12} \bar{l}_{12}^4)} \left[ \frac{1}{\bar{l}_1^4} \right] + J_F(l_1, l_2), \end{aligned} \quad (\text{E.200})$$

where  $J_F(l_1, l_2)$  is UV convergent and UV divergent integrands are written between square brackets. Notice the appearance of factorized sub-divergences beyond one loop. Thus

$$\int [d^4 l_1][d^4 l_2] \frac{1}{\bar{D}_1 \bar{D}_2 \bar{D}_{12}} \equiv \lim_{\mu \rightarrow 0} \int d^4 l_1 d^4 l_2 J_F(l_1, l_2). \quad (\text{E.201})$$

A few more two-loop examples are reported in the Appendix C of [711];

- In general, a logarithmic dependence of  $\mu$  is left after the  $\mu \rightarrow 0$  limit. In that case  $\mu$  is interpreted as the renormalization scale  $\mu_R$ . For instance [706]

$$\int [d^4 l] \frac{1}{(\bar{l}^2 - M^2)^2} = -i\pi^2 \ln \frac{M^2}{\mu_R^2}; \quad (\text{E.202})$$

- In the absence of IR singularities  $\lim_{\mu \rightarrow 0} \int d^4 l \bar{J}^{\mu\nu} = \int d^4 l J^{\mu\nu}$  in Eq. (E.198);
- UV counterterms extracted as in Eq. (E.196) and Eq. (E.200) should always be subtracted from the original integrands. As a consequence, UV divergent integrals coinciding with they own counterterm vanish. They are sometimes refereed as *vacuum integrals*. For instance

$$\int [d^4 l] \frac{1}{l^4} = \int [d^4 l_1][d^4 l_2] \frac{1}{\bar{l}_1^2 \bar{l}_2^2 \bar{l}_{12}^2} = \int [d^4 l_1][d^4 l_2] \frac{1}{\bar{l}_1^4 \bar{l}_2^2 \bar{l}_{12}^2} = 0; \quad (\text{E.203})$$

- In UV convergent integrals the subtraction term is zero, so that FDR and ordinary integration coincide, as should be;
- This definition fulfills (E.191) because the same UV counterterm is shared by the shifted and the unshifted version of any loop integral;
- To keep (E.192), the replacement of Eq. (E.195) should be performed also in the numerator when  $l^2$  comes from Feynman rules. We dub this *global prescription*;
- The replacement of Eq. (E.195) *should not* be performed in the numerator when  $l^2$  is generated by tensor decomposition<sup>16</sup>. This difference is parametrized by the introduction of Extra Integrals (EI) of the kind

$$\int [d^4 l] \frac{l^2 - \bar{l}^2}{(\bar{l}^2 - M^2)^3} = \int [d^4 l] \frac{\mu^2}{(\bar{l}^2 - M^2)^3}, \quad (\text{E.204})$$

<sup>16</sup>UV divergent tensors are defined by subtracting their corresponding UV counterterms, such as  $\frac{l^\mu l^\nu}{l^6}$  in Eq. (E.198). Replacing  $l^2$  with  $\bar{l}^2$  when reducing them would change this definition. In practice this means that the replacement of Eq. (E.195) should be performed before tensor reduction.

where the same UV subtraction should be performed as if  $\mu^2 = l^2$ . Using Eq. (E.196) gives the constant

$$\int [d^4l] \frac{\mu^2}{(\bar{l}^2 - M^2)^3} = -\lim_{\mu \rightarrow 0} \mu^2 \int d^4l \frac{1}{\bar{l}^6} = \frac{i\pi^2}{2}, \quad (\text{E.205})$$

which causes a non zero value in the r.h.s. of Eq. (E.199);

- It is possible to use integrand manipulations, tensor reduction and integration-by-parts [712] directly on FDR integrals *before* using their explicit definition.

## 11.2 Keeping unitarity

With more than one loop the requirement in (E.192) may clash with the sub-integration consistency of (E.193). In fact, the global prescription at the level of a multi-loop diagram may be incompatible with the global prescription needed in each of its UV divergent sub-loops. This is cured by adding additional FDR integrals (called EEIs), which restore the correct behavior. Such integrals can be inferred by directly considering the multi-loop diagram and do not require the introduction of counterterms in the Lagrangian. This strategy has been proved to work at two loops in QCD [713].

It is intriguing the fact that the EEIs also provide a fix to two-loop “naive” FDH in DReg [713]. By dubbing  $G^{(2\text{-loop})}$  a generic two-loop QCD correlator, one finds that the replacement

$$G_{\text{bare, DReg}}^{(2\text{-loop})}|_{n_s=4} \rightarrow G_{\text{bare, DReg}}^{(2\text{-loop})}|_{n_s=4} + \sum_{\text{Diag}} \text{EEI}_b|_{n_s=4} \quad (\text{E.206})$$

produces correlators with the right behavior under renormalization. In Eq. (E.206)  $n_s = \gamma_\mu \gamma^\mu = g_{\mu\nu} g^{\mu\nu}$  is the number of spin degrees of freedom and the  $\text{EEI}_b$ s are DReg integrals obtained from the EEIs by dropping the subtraction term, such as

$$\text{EEI} = \int [d^4l] \frac{1}{(\bar{l}^2 - M^2)^2} \rightarrow \int d^4l \frac{1}{(l^2 - M^2)^2} = \text{EEI}_b. \quad (\text{E.207})$$

Differently stated, the  $\text{EEI}_b$ s reproduce the effect of the evanescent operators needed in FDH and dimensional reduction to restore renormalizability, at least off-shell. A two-loop study of the  $\gamma^* \rightarrow q\bar{q}$  and  $H \rightarrow q\bar{q}$  QCD vertices indicates that the same pattern is observed on-shell [714].

## 11.3 Infrared singularities

In massless calculations IR divergences are present both in loop and phase-space integrals. The replacement of Eq. (E.195) in the loop propagators regulates soft and collinear virtual singularities. For instance, the massless one-loop triangle is defined as [715]

$$\int [d^4l] \frac{1}{\bar{l}^2 \bar{D}_{p_1} \bar{D}_{p_2}} \equiv \lim_{\mu \rightarrow 0} \int d^4l \frac{1}{\bar{l}^2 \bar{D}_{p_1} \bar{D}_{p_2}} = \frac{i\pi^2}{2s} \ln^2 \left( \frac{\mu^2}{-s - i0} \right), \quad (\text{E.208})$$

where  $\bar{D}_{p_i} = (l + p_i)^2 - \mu^2$ ,  $p_i^2 = 0$  and  $s = (p_1 - p_2)^2 = -2(p_1 \cdot p_2)$ . Thus, the IR behavior is parametrized in terms of logarithms of  $\mu$ . They have to be compensated by the phase-space integration over the real radiation.<sup>17</sup> The underlying mechanism for this cancellation is provided by the cutting rule

$$\frac{i}{\bar{l}^2 + i0^+} \rightarrow (2\pi) \delta_+(\bar{l}^2) \quad (\text{E.209})$$

depicted in Fig. E.22. Uncut thick lines represent virtual propagators replaced according to Eq. (E.195), while thick cut lines refer to external particles with  $\bar{k}_{i,j}^2 = \mu^2$  dubbed “ $\mu$ -massive” particles. For instance, Eq. (E.208)

<sup>17</sup>Or are absorbed in the initial state parton densities.

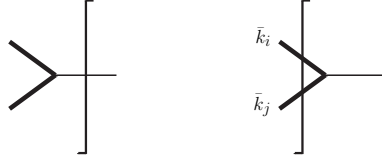


Fig. E.22: IR divergent splitting regulated by  $\mu$ -massive (thick) unobserved particles. The cut on the left represents the virtual part. The two-particle cut on the right contributes to the real radiation. The sum of the two is free of IR divergences.

can be rewritten as an eikonal integrated over a  $\mu$ -massive three-body phase-space  $\bar{\Phi}_3$

$$\int_{\Phi_2} \Re e \left( \int [d^4 l] \frac{1}{l^2 \bar{D}_{p_1} \bar{D}_{p_2}} \right) = \lim_{\mu \rightarrow 0} \int_{\bar{\Phi}_3} \frac{1}{\bar{s}_{13} \bar{s}_{23}} \left\{ \begin{array}{l} \bar{s}_{ij} = (\bar{k}_i + \bar{k}_j)^2 \\ \bar{k}_{i,j}^2 = \mu^2 \end{array} \right. , \quad (\text{E.210})$$

which acts as a counterterm for the real radiation.

To keep gauge invariance, numerator/denominator cancellations should be maintained when replacing

$$k_i \rightarrow \bar{k}_i \quad (\text{E.211})$$

in the real matrix element before integrating it over the  $\mu$ -massive phase-space. This can be achieved by performing the massless calculation and then replacing everywhere

$$s_{i\dots j} = (k_i + \dots + k_j)^2 \rightarrow \bar{s}_{i\dots j} = (\bar{k}_i + \dots + \bar{k}_j)^2. \quad (\text{E.212})$$

As in the loop case, tensor reduction should be performed *after* the replacement of Eq. (E.211). This is usually immaterial in NLO computations but relevant at NNLO. Take for instance

$$\gamma^*(P) \rightarrow q(k_1) \bar{q}(k_2) q'(k_3) \bar{q}'(k_4) \quad (\text{E.213})$$

considered as a NNLO QCD correction to  $\gamma^* \rightarrow 2$  jets. A massless calculation generates the irreducible tensor

$$\frac{k_3^\mu k_3^\nu}{s_{134} s_{234} s_{34}^2}. \quad (\text{E.214})$$

The phase-space integral

$$R^{\mu\nu} \equiv \int d\Phi_4(P \rightarrow k_1 + k_2 + k_3 + k_4) \frac{k_3^\mu k_3^\nu}{s_{134} s_{234} s_{34}^2} \quad (\text{E.215})$$

is IR divergent, so that one has to consider

$$\bar{R}^{\mu\nu} \equiv \lim_{\mu \rightarrow 0} \int d\bar{\Phi}_4(P \rightarrow \bar{k}_1 + \bar{k}_2 + \bar{k}_3 + \bar{k}_4) \frac{\bar{k}_3^\mu \bar{k}_3^\nu}{\bar{s}_{134} \bar{s}_{234} \bar{s}_{34}^2}. \quad (\text{E.216})$$

Only after the integral is defined as in Eq. (E.216), tensor reduction is allowed. Splitting the four-body phase-space gives

$$\bar{R}^{\mu\nu} = \lim_{\mu \rightarrow 0} \int_{4\mu^2}^{(\sqrt{s}-2\mu)^2} d\bar{s}_{34} \int d\bar{\Phi}_3(P \rightarrow \bar{k}_1 + \bar{k}_2 + \bar{k}_{34}) \frac{1}{\bar{s}_{134} \bar{s}_{234} \bar{s}_{34}^2} \int d\bar{\Phi}_2(\bar{k}_{34} \rightarrow \bar{k}_3 + \bar{k}_4) \bar{k}_3^\mu \bar{k}_3^\nu, \quad (\text{E.217})$$

and Lorentz invariance dictates

$$\int d\bar{\Phi}_2(\bar{k}_{34} \rightarrow \bar{k}_3 + \bar{k}_4) \bar{k}_3^\mu \bar{k}_3^\nu = \left[ -g^{\mu\nu} \frac{\bar{s}_{34}}{12} \left( 1 - 4 \frac{\mu^2}{\bar{s}_{34}} \right) + \frac{\bar{k}_{34}^\mu \bar{k}_{34}^\nu}{3} \left( 1 - \frac{\mu^2}{\bar{s}_{34}} \right) \right] \int d\bar{\Phi}_2(\bar{k}_{34} \rightarrow \bar{k}_3 + \bar{k}_4) \quad (\text{E.218})$$

Despite the  $\mu \rightarrow 0$  limit, the  $\frac{\mu^2}{\bar{s}_{34}}$  terms in Eq. (E.218) produce a non vanishing  $\mu^2/\mu^2$  contribution when inserted in Eq. (E.217). Such terms are missed if one first reduces Eq. (E.215) and then uses Eq. (E.211).

### 11.4 Scaleless integrals

As in DReg, scaleless FDR integrals which are both UV and logarithmically IR divergent vanish. This is a direct consequence of their definition. For example, if  $p^2 = 0$

$$\int [d^4 l] \frac{1}{\bar{l}^2(\bar{l}^2 + 2(l \cdot p))} = \int [d^4 l] \left( \frac{1}{\bar{l}^4} - \frac{2(l \cdot p)}{\bar{l}^4(\bar{l}^2 + 2(l \cdot p))} \right) = 0, \quad (\text{E.219})$$

because the first term in the r.h.s. is a vacuum integral and the last contribution gives zero by tensor decomposition. Analogously, when  $p_1^2 = p_2^2 = 0$

$$\int [d^4 l_1][d^4 l_2] \frac{(l_2 \cdot p_1)(l_2 \cdot p_2)}{\bar{l}_1^4(\bar{l}_1^2 + 2(l_1 \cdot p_1))\bar{l}_2^2((l_1 + l_2)^2 - \mu^2)} = 0. \quad (\text{E.220})$$

This facilitates the computation since the wave function renormalization of massless external states never contributes.

### 11.5 Renormalization

Unlike in the customary approach [466, 716, 717], no order-by-order renormalization is necessary in FDR. The reason is that UV sub-divergences are already subtracted by the definition of FDR integration, as in Eq. (E.200). This means that no UV counterterms need to be introduced in the Lagrangian  $\mathcal{L}(p_i, \dots, p_m)$ . The bare parameters  $p_i$  in  $\mathcal{L}(p_i, \dots, p_m)$  are directly linked to physical observables by means of  $m$  measurements

$$\mathcal{O}_i^{\text{EXP}} = \mathcal{O}_i^{\text{TH}, \ell\text{-loop}}(p_i, \dots, p_m), \quad (\text{E.221})$$

which determine them globally in terms of measured observables  $\mathcal{O}_i^{\text{EXP}}$  and corrections computed at the perturbative level  $\ell$  one is working. Inverting Eq. (E.221) gives

$$p_i^{\ell\text{-loop}}(\mathcal{O}_i^{\text{EXP}}, \dots, \mathcal{O}_m^{\text{EXP}}) \equiv \hat{p}_i, \quad (\text{E.222})$$

where the  $\hat{p}_i$  do not have to be calculated iteratively in the perturbative expansion. Note that  $p_i$  and  $\hat{p}_i$  are both finite, so that we refer to Eq. (E.222) as a global finite renormalization.

In the presence of IR divergences, one has to disentangle logarithms of  $\mu$  of IR origin from logs of the renormalization scale  $\mu_R$  (see e.g. Eq. (E.202)). The former compensate the divergent real radiation contribution, or are absorbed in the parton densities. The latter contribute to the running of the  $\hat{p}_i$ .

As an example, in massless QCD the only parameter to be fixed is the strong coupling constant, which can be determined by means of  $e^+e^- \rightarrow \text{hadrons}$  computed at the scale  $Q^2$ . In this case, Eq. (E.222) reads at one loop

$$\hat{p}_1 \equiv \alpha_S^{1\text{-loop}}(\alpha_S^{\text{FDR}}(Q^2)) = \frac{\alpha_S^{\text{FDR}}(Q^2)}{1 + \frac{\alpha_S^{\text{FDR}}(Q^2)}{4\pi} (11 - 2N_f/3) \ln \frac{\mu_R^2}{Q^2}}. \quad (\text{E.223})$$

As for the numerical value of strong coupling constant, the shift between  $\alpha_S^{\text{FDR}}$  and  $\alpha_S^{\overline{\text{MS}}}$  is known up to two loops [713]

$$\frac{\alpha_S^{\text{FDR}}}{\alpha_S^{\overline{\text{MS}}}} = 1 + \left( \frac{\alpha_S^{\overline{\text{MS}}}}{4\pi} \right) \frac{N_c}{3} + \left( \frac{\alpha_S^{\overline{\text{MS}}}}{4\pi} \right)^2 \left\{ \frac{89}{18} N_c^2 + 8 N_c^2 f + N_f \left[ N_c - \frac{3}{2} C_F - f \left( \frac{2}{3} N_c + \frac{4}{3} C_F \right) \right] \right\} \quad (\text{E.224})$$

where

$$f = \int_0^1 \frac{\ln(x)}{1 - x(1 - x)} = -\frac{2}{\sqrt{3}} \text{Cl}_2 \left( \frac{\pi}{3} \right). \quad (\text{E.225})$$

Note that  $\alpha_S^{\text{FDR}} = \alpha_S^{\text{FDH}}$  at one loop. In massive QCD, the quark mass shift reads [713]

$$\frac{m_q^{\text{FDR}}}{m_q^{\overline{\text{MS}}}} = 1 - C_F \left( \frac{\alpha_S^{\overline{\text{MS}}}}{4\pi} \right) + C_F \left( \frac{\alpha_S^{\overline{\text{MS}}}}{4\pi} \right)^2 \left\{ \frac{77}{24} N_c - \frac{5}{8} C_F + f \left( 9N_c + \frac{11}{3} C_F \right) + N_f \left( \frac{1}{4} - \frac{2}{3} f \right) \right\} \quad (\text{E.226})$$

Eqs. (E.224) and (E.226) provide the transition rules from IR finite QCD quantities computed in FDR and their analogue in  $\overline{\text{MS}}$ .

## 11.6 Making contact with other methods

FDR is a four-dimensional renormalization approach independent of DReg. This is in contrast to other four-dimensional methods [707, 708], where DReg is implicitly assumed but convenient subtractions are performed in order to directly set  $d \rightarrow 4$  in particular combinations of integrals. It is also peculiar to FDR the mechanism of avoiding an order-by-order renormalization by means of the EEIs described in [713]. To our knowledge, this represents a new approach to renormalization [718]. Nevertheless, a one-to-one correspondence exists at NLO between DReg and FDR integrals [360]. As for one-loop integrals, one finds

$$\Gamma(1 - \epsilon) \pi^\epsilon \int \frac{d^n l}{\mu_R^{-2\epsilon}} F(l^2, l) \Big|_{\mu_R = \mu \text{ and } \frac{1}{\epsilon^i} = 0} = \int [d^4 l] F(\bar{l}^2, l), \quad (\text{E.227})$$

while the connection between real radiation integrals reads

$$\begin{aligned} & \left( \frac{\mu_R^2}{s} \right)^\epsilon \int_{\phi_3} dx dy dz (\dots) F(x, y, z) \delta(1 - x - y - z) (xyz)^{-\epsilon} \Big|_{\mu_R = \mu \text{ and } \frac{1}{\epsilon^i} = 0} \\ &= \int_{\bar{\phi}_3} d\bar{x} d\bar{y} d\bar{z} F(\bar{x}, \bar{y}, \bar{z}) \delta(1 - \bar{x} - \bar{y} - \bar{z} + 3\mu^2/s), \end{aligned} \quad (\text{E.228})$$

where  $\phi_3$  and  $\bar{\phi}_3$  are massless and  $\mu$ -massive three-body phase spaces, and  $\bar{x} = \bar{s}_{12}/s$ ,  $\bar{y} = \bar{s}_{13}/s$ ,  $\bar{z} = \bar{s}_{23}/s$ .

To our knowledge, a direct correspondence between FDR and DReg integrals cannot be found beyond one loop. This is probably due to the absence of counterterms in the FDR approach. The equivalence between DReg and FDR is restored only once all parts of the calculation are collected together to produce physical predictions.

## 11.7 Results

In this section we present a few selected results obtained in the framework of FDR.

### Internal consistency

The consistency of the FDR approach up to NNLO has been proven by using off-shell QCD as a test case [713]. An explicit calculation of the correlators in Fig. E.23 shows that the FDR results can be mimicked by a particular choice of renormalization scheme in DReg. So that FDR produces the same physical predictions of DReg. The necessary shifts between the two schemes have been presented in Eqs. (E.224) and (E.226).

It is also interesting to study how the correct value of the ABJ anomaly is produced in FDR [706]. The contributing diagrams are given in Fig. E.24. In the massless case a convenient way of implementing the global prescription is replacing the fermion propagators as follows

$$\frac{1}{l} \rightarrow \frac{1}{l - \mu}, \quad \frac{1}{p_1 + l} \rightarrow \frac{1}{p_1 + l - \mu}, \quad \frac{1}{p_2 + l} \rightarrow \frac{1}{p_2 + l - \mu}. \quad (\text{E.229})$$



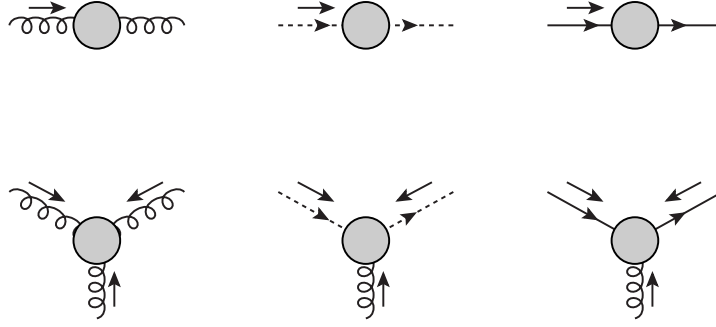


Fig. E.23: Irreducible QCD Green's functions. The gray blobs denote the sum of all possible two-loop Feynman diagrams.

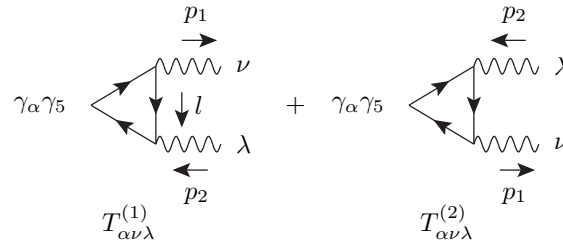


Fig. E.24: The two diagrams generating the ABJ anomaly.

Contracting with  $p = p_1 - p_2$  gives a result completely proportional to a FDR Extra Integral

$$p^\alpha \left( T_{\alpha\nu\lambda}^{(1)} + T_{\alpha\nu\lambda}^{(2)} \right) = -i \frac{e^2}{4\pi^4} \text{Tr}[\gamma_5 \not{p}_2 \gamma_\lambda \gamma_\nu \not{p}_1] \int [d^4 l] \mu^2 \frac{1}{\bar{l}^2 ((l + p_1)^2 - \mu^2) ((l + p_2)^2 - \mu^2)}. \quad (\text{E.230})$$

Computing this as in Eq. (E.205) leads to the right answer. Note that before performing the shift of Eq. (E.229),  $\gamma_5$  should be put in the vertex in which the current is not conserved.

#### Gluonic NLO corrections to $H \rightarrow gg$ in the large top mass limit

The well-known fully inclusive result

$$\Gamma(H \rightarrow gg) = \Gamma^{(0)}(\alpha_S(M_H^2)) \left[ 1 + \frac{95}{4} \frac{\alpha_S}{\pi} \right] \quad (\text{E.231})$$

has been re-derived in [715]. The calculation of the diagrams in Fig. E.25 involves all key ingredients of QCD, namely ultraviolet, infrared and collinear divergences, besides  $\alpha_S$  renormalization, showing that FDR can be successfully used in massless NLO computations.

#### $H \rightarrow \gamma\gamma$ at two loops

The leading QCD corrections to the amplitude  $\mathcal{M}^{2\text{-loop}}(H \rightarrow \gamma\gamma)$  have been computed in [711] by considering the  $m_{\text{top}} \rightarrow \infty$  limit of the two-loop diagrams depicted in Fig. E.26. The known result

$$\mathcal{M}^{2\text{-loop}} = \mathcal{M}^{1\text{-loop}} \left( 1 - \frac{\alpha_S}{\pi} \right) + \mathcal{O} \left( \frac{m_H^2}{m_{\text{top}}^2} \right) \quad (\text{E.232})$$

is reproduced. It is worth to mention that there is no need of renormalizing at one loop the top mass and the Yukawa coupling. In fact, when  $m_{\text{top}} \rightarrow \infty$  no parameter is left to be fixed by means of Eq. (E.222), so

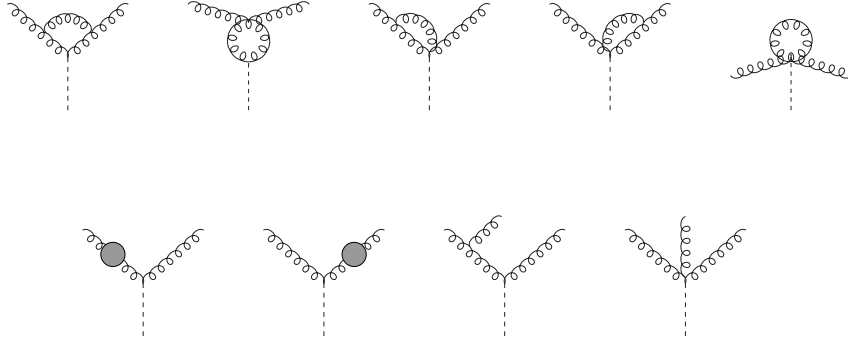


Fig. E.25: Virtual and real diagrams contributing to  $H \rightarrow gg(g)$  at  $\mathcal{O}(\alpha_s^3)$ .

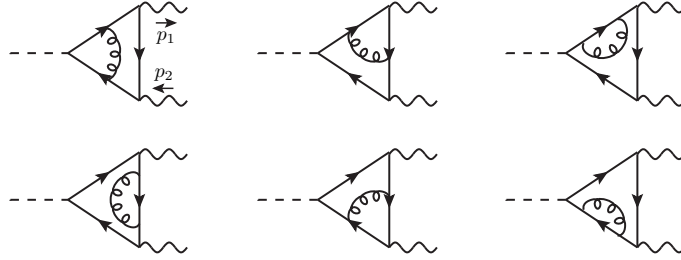


Fig. E.26: Feynman diagrams contributing to the QCD corrections of the top-loop-mediated Higgs decay into two photons. The same diagrams with the electric charge flowing counterclockwise also contribute.

that the UV finite result in Eq. (E.232) directly follows from the two-loop computation. In contrast, one-loop renormalization is necessary in DReg to subtract the sub-divergences in the diagrams of Fig. E.26.

### The three-loop beta function

By considering the difference between  $\alpha_s^{\overline{\text{MS}}}$  and  $\alpha_s^{\text{FDR}}$  it is possible to extract the three-loop beta function in FDR

$$\beta^{\text{FDR}} = \mu \frac{d}{d\mu} \frac{\alpha_s^{\text{FDR}}}{4\pi} = \left( \frac{\alpha_s^{\text{FDR}}}{4\pi} \right)^2 \left[ b_0^{\text{FDR}} + b_1^{\text{FDR}} \left( \frac{\alpha_s^{\text{FDR}}}{4\pi} \right) + b_2^{\text{FDR}} \left( \frac{\alpha_s^{\text{FDR}}}{4\pi} \right)^2 + \mathcal{O} \left( \frac{\alpha_s^{\text{FDR}}}{4\pi} \right)^3 \right]. \quad (\text{E.233})$$

One finds [713]

$$\begin{aligned} b_2^{\text{FDR}} = & N_c^3 \left( -\frac{3610}{27} - \frac{176}{3} f \right) + N_f^2 \left( -\frac{40}{9} C_F - \frac{43}{27} N_c + f \left( -\frac{16}{9} C_F - \frac{8}{9} N_c \right) \right) \\ & + N_f \left( \frac{1331}{27} N_c^2 + \frac{292}{9} N_c C_F - 2 C_F^2 + f \left( \frac{140}{9} N_c^2 + \frac{88}{9} N_c C_F \right) \right), \end{aligned} \quad (\text{E.234})$$

with  $f$  given in Eq. (E.225).

### Numerical evaluation of two-loop FDR integrals

The  $\mathcal{O}(G_F \alpha_s)$  corrections to the  $\rho$  parameter in the  $m_{\text{top}} \rightarrow \infty$  limit have been determined numerically by Tom Zirke [719] by analytically extracting the logarithmic  $\mu$  dependence from the two-loop integrals presented in Fig. E.27. The comparison with the  $\overline{\text{MS}}$  result requires the use of Eq. (E.226) at one loop.

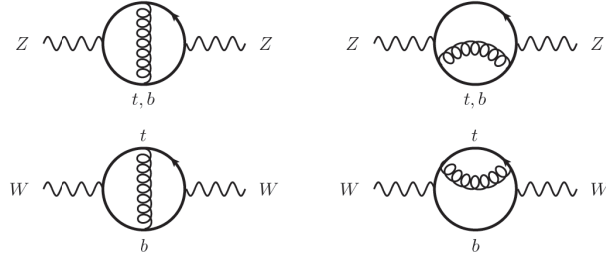


Fig. E.27: Heavy-quark corrections to the  $W$  and  $Z$  propagator contributing to the  $\rho$  parameter at  $\mathcal{O}(G_F\alpha_S)$  (from [719]).

Finally, the result in Eq. (E.232) is reproduced by means of numerical techniques.

### Local IR subtraction at one loop

It is possible to set up a local FDR subtraction of the final-state IR infinities by rewriting the virtual logarithms as counterterms to be added to the real radiation [360], in the same spirit of Eq. (E.210). Schematically

$$\begin{aligned} \sigma_{\text{NLO}} &= \int_{\Phi_2} \left( |M|_{\text{Born}}^2 + \underbrace{|M|_{\text{Virt}}^2}_{\text{devoid of logs of } \mu} \right) F_J^{(2)}(k_1, k_2) \\ &+ \underbrace{\int_{\Phi_3}}_{\mu \rightarrow 0 \text{ here}} \left( |M|_{\text{Real}}^2 F_J^{(3)}(k_1, k_2, k_3) - |M|_{\text{CT}}^2 F_J^{(2)}(\underbrace{\hat{k}_1, \hat{k}_2}_{\text{mapped kinematics}}) \right), \end{aligned} \quad (\text{E.235})$$

where  $F_J$  are jet functions. For instance, in the case of  $e^+e^- \rightarrow \gamma^* \rightarrow q\bar{q}(g)$ , the explicit form of the local counterterm is

$$|M|_{\text{CT}}^2 = \frac{16\pi\alpha_s}{s} C_F |M|_{\text{Born}}^2(\hat{k}_1, \hat{k}_2) \left( \frac{s^2}{s_{13}s_{23}} - \frac{s}{s_{13}} - \frac{s}{s_{23}} + \frac{s_{13}}{2s_{23}} + \frac{s_{23}}{2s_{13}} - \frac{17}{2} \right), \quad (\text{E.236})$$

and the mapping reads

$$\hat{k}_1^\alpha = \kappa \Lambda_\beta^\alpha k_1^\beta \left( 1 + \frac{s_{23}}{s_{12}} \right), \quad \hat{k}_2^\alpha = \kappa \Lambda_\beta^\alpha k_2^\beta \left( 1 + \frac{s_{13}}{s_{12}} \right), \quad (\text{E.237})$$

where  $\kappa = \sqrt{\frac{ss_{12}}{(s_{12}+s_{13})(s_{12}+s_{23})}}$  and  $\Lambda_\beta^\alpha$  is the boost that brings the sum of  $\hat{k}_1$  and  $\hat{k}_2$  back to the center of mass frame:  $\hat{k}_1 + \hat{k}_2 = (\sqrt{s}, 0, 0, 0)$ .

The inclusive  $\sigma_{\text{NLO}} = \sigma_0 \left( 1 + C_F \frac{3}{4} \frac{\alpha_s}{\pi} \right)$  cross section is reproduced by a numerical implementation of Eq. (E.235). In addition, successful comparisons [720] with MadGraph5\_aMC@NLO [721] interfaced with FastJet [722] have been attained for realistic jet observables.

## 11.8 Outlook

The results collected so far show that FDR is turning to a competitive tool to compute radiative corrections. The UV subtraction is incorporated in the definition of the loop integration. As a consequence, one directly deals with four dimensional integrals and avoids the customary order-by-order insertion of UV counterterms in the Lagrangian. This has been proven to be a workable alternative to DReg up to two loops for off-shell quantities.

The FDR regularization of the IR divergences is well understood at NLO, and a completely local subtraction of final-state IR infinities has been worked out for two-jet cross sections. Initial state IR singularities

have not been studied yet. However, the one-to-one correspondence in Eq. (E.228) makes it plausible that it should not be difficult to accommodate them in FDR, at least at NLO.

Going on-shell at two-loops looks feasible. A complete NNLO FDR calculation of the processes  $\gamma^*, H \rightarrow q\bar{q}(q'\bar{q}')$  is ongoing. In particular, it is interesting to study the correspondence in Eq. (E.209) beyond one loop. Ideally, one would like to exploit it to establish a general way to extract the NNLO IR behavior directly from the virtual integrals, to be rewritten in the form of local counterterms for the real radiation without the need of computing them, as in Eq. (E.210). If possible, this would pave the way for a completely numerical approach, considerably simplifying the computation of radiative corrections beyond NLO.

## 12 Subtractions versus unsubtractions

**Author:** German Rodrigo [german.rodrigo@csic.es]

One of the main difficulties in perturbative calculations at higher orders in Quantum Field Theory (QFT) is the requirement to cancel the unphysical soft and collinear singularities. Those singularities are the consequence of treating the quantum state with  $N$  external partons as different from the quantum state with emission of extra massless particles at zero energy, such as photons and gluons, and the possibility to emit particles at exactly the same direction. Moreover, loops in QFT implicitly extrapolate the validity of the Standard Model (SM) to infinite energies, much above the Planck scale.

The traditional approach to solve this problem and extract physical predictions from the theory consists in altering the dimensions of the space-time to e.g.  $d = 4 - 2\epsilon$ . In Dimensional Regularization (DREG) [361, 723–726], the singularities appear as explicit poles in  $1/\epsilon$  through integration of the loop momenta and the phase-space of real radiation. After renormalisation of the ultraviolet (UV) singularities, virtual and real quantum corrections contribute with poles in  $1/\epsilon$  of opposite sign such that the total result is finite. Although this procedure efficiently transforms the theory into a calculable and well-defined mathematical framework, a big effort needs to be invested in evaluating loop integrals in higher space-time dimensions, and to adequately subtract the singularities of the real radiation contributions, particularly at higher perturbative orders.

The general idea of subtraction consists of introducing counter-terms which mimic the local IR behaviour of the real components and that can easily be integrated analytically in  $d$ -dimensions. In this way, the integrated form is combined with the virtual component whilst the unintegrated counter-term cancels the IR poles originated from the phase-space integration of the real-radiation contribution. Part of the success of the so called NLO revolution, which led to the automation of radiative corrections at second order in Monte Carlo event generators, was due, besides to a better understanding of the mathematical beauty of scattering amplitudes, to the existence of general purpose subtraction algorithms at NLO [727–730].

In the last two years, there has been also a quite stunning progress at NNLO, with lots of new calculations of  $2 \rightarrow 2$  LHC processes. This progress has been possible thanks to the effort of many different groups, each one having developing different working subtraction methods at NNLO [731–739]. Unfortunately, there is not yet a general working method, as at NLO, able to overpass the current frontier for  $2 \rightarrow 3$  processes at NNLO.

An alternative approach is introduced by the Four-Dimensional Unsubtraction (FDU) [707, 740–743], which is based in the loop-tree duality (LTD) [744–748]. The idea behind FDU is to exploit a suitable mapping of momenta between the virtual and real kinematics in such a way that the summation over the degenerate soft and collinear quantum states is performed locally at integrand level without the necessity to introduce infrared (IR) subtractions. Suitable counter-terms are used to cancel, also locally, the UV singularities, in such a way that calculations can be performed without altering the dimensions of the space-time. The method should improve the efficiency of Monte Carlo event generators because it is meant for integrating simultaneously real and virtual contributions. The LTD formalism or a similar framework has also been used to derive causality and unitarity constraints [749], and to integrate numerically subtraction terms [708], and can be related to the forward limit of scattering amplitudes [744, 750]. It has also been used in the framework of the color-kinematics duality [751].

Also, there has been lot of effort in the community to define perturbative methods directly in  $d = 4$  space-time dimensions in order to avoid the complexity of working in a non-physical multidimensional space. Examples of those methods are the four-dimensional formulation (FDF) [372] of the four-dimensional helicity scheme, the six-dimensional formalism (SDF) [752], implicit regularisation (IREG) [753], and four-dimensional regularisation/ renormalisation (FDR) [711], see section E.12. For a review of all these methods see e.g. Ref. [360].

LTD [744–746] transforms any loop integral or loop scattering amplitude into a sum of tree-level like objects that are constructed by setting on-shell a number of internal loop propagators equal to the number of loops. Explicitly, LTD is realised by modifying the  $i0$  prescription of the Feynman propagators that remain

off-shell

$$G_F(q_j) = \frac{1}{q_j^2 - m_j^2 + i0} \quad \rightarrow \quad G_D(q_i; q_j) = \frac{1}{q_j^2 - m_j^2 - i0 \eta k_{ji}} \Big|_{G_F(q_i) \text{ on-shell}}, \quad (\text{E.238})$$

with  $k_{ji} = q_j - q_i$ , and  $\eta^\mu$  an arbitrary future-like vector. The most convenient choice, however, is  $\eta^\mu = (1, 0)$ , which is equivalent to integrate out the loop energy components of the loop momenta through the Cauchy residue theorem. The left-over integration is then restricted to the Euclidean space of the loop three-momenta. The dual prescription can hence be  $+i0$  for some dual propagators, and  $-i0$  for others, and encodes in a compact and elegant way the contribution of the multiple cuts that are introduced by the Feynman tree theorem [754]. The on-shell condition is given by  $\tilde{\delta}(q_i) = i 2\pi \theta(q_{i,0}) \delta(q_i^2 - m_i^2)$ , and determines that the loop integration is restricted to the positive energy modes of the on-shell hyperboloids (light-cones for massless particles).

It is interesting to note that although the on-shell loop three-momenta are unrestricted, after analysing the singular behaviour of the loop integrand one realises that thanks to a partial cancellation of singularities among different dual components, all the physical threshold and IR singularities are restricted to a compact region of the loop three-momentum [747]. This relevant fact allows to construct the mappings between the virtual and real kinematics based on the factorisation properties of QCD and then the summation over degenerate soft and collinear states.

As usual, the NLO cross-section is constructed in FDU from the one-loop virtual correction with  $N$  external partons and the exclusive real cross-section with  $N + 1$  partons

$$\sigma^{\text{NLO}} = \int_N d\sigma_V^{(1,\text{R})} + \int_{N+1} d\sigma_R^{(1)}, \quad (\text{E.239})$$

integrated over the corresponding phase-space,  $\int_N$  and  $\int_{N+1}$ . The virtual contribution is obtained from its LTD representation

$$\int_N d\sigma_V^{(1,\text{R})} = \int_N \int_{\vec{\ell}_1} 2 \text{Re} \langle \mathcal{M}_N^{(0)} | \left( \sum_i \mathcal{M}_N^{(1)}(\tilde{\delta}(q_i)) \right) - \mathcal{M}_{\text{UV}}^{(1)}(\tilde{\delta}(q_{\text{UV}})) \rangle \hat{\mathcal{O}}(\{p_k\}_N). \quad (\text{E.240})$$

In Eq. (E.240),  $\mathcal{M}_N^{(0)}$  is the  $N$ -leg scattering amplitude at LO, and  $\mathcal{M}_N^{(1)}(\tilde{\delta}(q_i))$  is the dual representation of the unrenormalised one-loop scattering amplitude with the internal momentum  $q_i$  set on-shell. The integral is weighted with the function  $\hat{\mathcal{O}}(\{p_k\}_N)$  that defines a given observable, for example the jet cross-section in the  $k_T$ -algorithm. The expression includes appropriate counter-terms that implement renormalization by subtracting the UV singularities locally, as discussed in Ref. [707, 743], including UV singularities of degree higher than logarithmic that integrate to zero.

By means of an appropriate mapping between the real and virtual kinematics [707, 741]:

$$\{p'_j\}_{N+1} \rightarrow (q_i, \{p_k\}_N), \quad (\text{E.241})$$

the real phase-space is rewritten in terms of the virtual phase-space and the loop three-momentum

$$\int_{N+1} = \int_N \int_{\vec{\ell}_1} \sum_i \mathcal{J}_i(q_i) \mathcal{R}_i(\{p'_j\}_{N+1}), \quad (\text{E.242})$$

where  $\mathcal{J}_i(q_i)$  is the Jacobian of the transformation with  $q_i$  on-shell, and  $\mathcal{R}_i(\{p'_j\}_{N+1})$  defines a complete partition of the real phase-space

$$\sum_i \mathcal{R}_i(\{p'_j\}_{N+1}) = 1. \quad (\text{E.243})$$

In this way, the NLO cross-section can be cast into a single integral in the Born/virtual phase-space and the loop three momentum

$$\sigma^{\text{NLO}} = \int_N \int_{\vec{\ell}_1} \left[ 2 \text{Re} \langle \mathcal{M}_N^{(0)} | \left( \sum_i \mathcal{M}_N^{(1)}(\tilde{\delta}(q_i)) \right) - \mathcal{M}_{\text{UV}}^{(1)}(\tilde{\delta}(q_{\text{UV}})) \rangle \hat{\mathcal{O}}(\{p_k\}_N) \right]$$

$$+ \sum_i \mathcal{J}_i(q_i) \mathcal{R}_i(\{p'_j\}_{N+1}) |\mathcal{M}_{N+1}^{(0)}(\{p'_j\}_{N+1})|^2 \hat{\mathcal{O}}(\{p'_j\}_{N+1}) \Big] , \quad (\text{E.244})$$

The NLO cross-section defined in Eq. (E.244) has a smooth four-dimensional limit and can be evaluated directly in four space-time dimensions. DREG is only necessary to fix the UV renormalisation counter-terms in order to define the cross-section in e.g. the  $\overline{MS}$  scheme, the rest of the calculation is feasible directly at  $d = 4$ . The Eq. (E.244) exhibits also an smooth massless limit for massive partons if the mapping in Eq. (E.241) maps conveniently the quasicollinear configurations [707]. This is another advantage of the formalism because it allows to describe with a single implementation the same process with either massless or massive partons.

In order to extend LTD to higher orders [745], we need to introduce the following functions

$$G_F(\alpha_k) = \prod_{i \in \alpha_k} G_F(q_i) , \quad G_D(\alpha_k) = \sum_{i \in \alpha_k} \tilde{\delta}(q_i) \prod_{j \in \alpha_k, j \neq i} G_D(q_i; q_j) , \quad (\text{E.245})$$

where  $\alpha_k$  labels all the internal propagators, Feynman or dual, of a given subset. An interesting identity fulfilled by these function is the following

$$G_D(\alpha_i \cup \alpha_j) = G_D(\alpha_i) G_D(\alpha_j) + G_D(\alpha_i) G_F(\alpha_j) + G_F(\alpha_i) G_D(\alpha_j) , \quad (\text{E.246})$$

involving the union of two subsets  $\alpha_i$  and  $\alpha_j$ . These are all the ingredients necessary to iteratively extend LTD to two loops and beyond. For example, a one loop scattering amplitude with  $N$  external partons gets the form

$$\mathcal{A}_N^{(1)} = \int_{\ell_1} \mathcal{N}(\ell_1, \{p_k\}_N) G_F(\alpha_1) = - \int_{\ell_1} \mathcal{N}(\ell_1, \{p_k\}_N) G_D(\alpha_1) , \quad (\text{E.247})$$

where  $\mathcal{N}(\ell_1, \{p_k\}_N)$  is the numerator.

At two loops all the internal propagators can be classified into three different subsets. Starting from the Feynman representation of a two loop scattering amplitude

$$\mathcal{A}_N^{(2)} = \int_{\ell_1} \int_{\ell_2} \mathcal{N}(\ell_1, \ell_2, \{p_k\}_N) G_F(\alpha_1 \cup \alpha_2 \cup \alpha_3) , \quad (\text{E.248})$$

we obtain in a first step by applying LTD to one of the loops (Eq. (E.247)):

$$\mathcal{A}_N^{(2)} = - \int_{\ell_1} \int_{\ell_2} \mathcal{N}(\ell_1, \ell_2, \{p_k\}_N) G_F(\alpha_1) G_D(\alpha_2 \cup \alpha_3) . \quad (\text{E.249})$$

Before applying LTD to the second loop, it is necessary to use Eq. (E.246) to express the dual function  $G_D(\alpha_2 \cup \alpha_3)$  in a suitable form where dual integrand is split into a first term that contains two dual functions, and therefore two internal lines on-shell, and two more terms with the dual function of one of the subsets and Feynman propagators of the other, to which we can again apply LTD. The final dual representation of the two-loop amplitude in Eq. (E.248) is

$$\begin{aligned} \mathcal{A}_N^{(2)} &= \int_{\ell_1} \int_{\ell_2} \mathcal{N}(\ell_1, \ell_2, \{p_k\}_N) \otimes \left\{ G_D(\alpha_2) G_D(\alpha_1 \cup \alpha_3) \right. \\ &\quad \left. + G_D(-\alpha_2 \cup \alpha_1) G_D(\alpha_3) - G_F(\alpha_1) G_D(\alpha_2) G_D(\alpha_3) \right\} . \end{aligned} \quad (\text{E.250})$$

In Eq. (E.250), it is necessary to take into account that the momentum flow in the loop formed by the union of  $\alpha_1$  and  $\alpha_2$  occurs in opposite directions. Therefore, it is necessary to change the direction of the momentum flow in one of the two sets. This is represented by adding a sign in front of e.g.  $\alpha_2$ , namely, we have written

$$\int_{\ell_1} \int_{\ell_2} G_F(\alpha_1 \cup \alpha_2) = - \int_{\ell_1} \int_{\ell_2} G_D(-\alpha_2 \cup \alpha_1) . \quad (\text{E.251})$$

Changing the momentum flow is equivalent to select the negative energy modes. For the internal momenta in the set  $\alpha_2$  this means

$$\tilde{\delta}(-q_j) = \frac{i\pi}{q_{j,0}^{(+)}} \delta(q_{j,0} + q_{j,0}^{(+)}), \quad j \in \alpha_2. \quad (\text{E.252})$$

The dual representation of Eq. (E.250) assumes that there are only single powers of the Feynman propagators. This restriction cannot be avoided anymore at two-loops where, for example, selfenergy insertions in internal lines lead automatically to double powers of one propagator. However, all the double poles can be included with a clever labelling of the internal momenta in the set  $\alpha_1$ , exclusively, which is not integrated in the first instance. Therefore, the numerator will not be affected by the first application of LTD, and Eq. (E.246) will be still valid regardless of the numerator. The calculation of the residues of double poles to obtain the LTD representation requires the participation of the numerator. This is represented in Eq. (E.250) by  $\mathcal{N}(\ell_1, \ell_2, \{p_i\}_N) \otimes G_D(\pm\alpha_i \cup \alpha_1)$ . A similar iterative procedure would extend LTD to higher orders.

Once we have obtained the dual representation of the two-loop scattering amplitude, we can outline how to extend FDU at NNLO or higher orders. Analogously to the NLO case, at NNLO, the total cross-section consists of three contributions

$$\sigma^{\text{NNLO}} = \int_N d\sigma_{\text{VV}}^{(2)} + \int_{N+1} d\sigma_{\text{VR}}^{(2)} + \int_{N+2} d\sigma_{\text{RR}}^{(2)}, \quad (\text{E.253})$$

where the double virtual cross-section  $d\sigma_{\text{VV}}^{(2)}$  receives contributions from the interference of the two-loop with the Born scattering amplitudes, and the square of the one-loop scattering amplitude with  $N$  external partons, the virtual-real cross-section  $d\sigma_{\text{VR}}^{(2)}$  includes the contributions from the interference of one-loop and tree-level scattering amplitudes with one extra external particle, and the double real cross-section  $d\sigma_{\text{RR}}^{(2)}$  are tree-level contributions with emission of two extra particles. The LTD representation of the two-loop scattering amplitude is obtained by setting two internal lines on-shell [745]. It leads to the two-loop dual components  $\langle \mathcal{M}_N^{(0)} | \mathcal{M}_N^{(2)}(\tilde{\delta}(q_i, q_j)) \rangle$ , while the two-loop momenta of the squared one-loop amplitude are independent and generate dual contributions of the type  $\langle \mathcal{M}_N^{(1)}(\tilde{\delta}(q_i)) | \mathcal{M}_N^{(1)}(\tilde{\delta}(q_j)) \rangle$ . In both cases, there are two independent loop three-momenta and  $N$  external momenta, from where we can reconstruct the kinematics of the tree-level corrections entering  $d\sigma_{\text{RR}}^{(2)}$  and the one-loop corrections in  $d\sigma_{\text{VR}}^{(2)}$ :

$$\{p_r''\}_{N+2} \rightarrow (q_i, q_j, \{p_k\}_N), \quad (q'_l, \{p'_s\}_{N+1}) \rightarrow (q_i, q_j, \{p_k\}_N), \quad (\text{E.254})$$

In summary, the bottleneck in higher order perturbative calculations is not only the evaluation of multi-loop Feynman diagrams, but also the gathering of all the quantum corrections from different loop orders (and thus different number of final-state partons). In order to match the expected experimental accuracy at the LHC, particularly in the high luminosity phase, and at future colliders new theoretical efforts are still needed to overcome the current precision frontier.



## 13 Numerical Integration with the Cuba Library

Author: Thomas Hahn [hahn@mpp.mpg.de]

### 13.1 Overview

Concepts and implementation of the Cuba library for multidimensional numerical integration are elucidated, with special emphasis on the parallelization features.

The Cuba library [156, 450, 492, 493] offers four algorithms for multidimensional numerical integration. All four can integrate vector integrands and they have interfaces for Fortran, C/C++, and Mathematica. Third-party interfaces exist for Maple [755], R [756], REDUCE [757], Python [758], and Julia [759], though none of these use Cuba's parallel features.

Routine	Basic integration method	Type	Variance reduction
Vegas	Sobol sample or Mersenne Twister sample or Ranlux sample	quasi-Monte Carlo pseudo-Monte Carlo pseudo-Monte Carlo	importance sampling
Suave	Sobol sample or Mersenne Twister sample or Ranlux sample	quasi-Monte Carlo pseudo-Monte Carlo pseudo-Monte Carlo	globally adaptive subdivision + importance sampling
Divonne	Korobov sample or Sobol sample or Mersenne Twister sample or Ranlux sample or cubature rules	lattice method quasi-Monte Carlo pseudo-Monte Carlo pseudo-Monte Carlo deterministic	stratified sampling, aided by methods from numerical optimization
Cuhre	cubature rules	deterministic	globally adaptive subdivision

The terms in this table are explained in the following sections on Concepts and Algorithms. Theoretical understanding is of limited use in picking the optimal integration routine in most practical applications, however. Performance depends highly on the integrand and there are always cases, and not just academic ones, in which one routine outperforms the others, or conversely, in which one routine simply gives wrong results. This, of course, is the main reason why there are four independent and easily interchangeable algorithms in the Cuba library.

Numerical integration is a fairly obvious candidate for distributed computing. Indeed, in Fortran and C/C++ the Cuba routines by default automatically parallelize the sampling. The details (and caveats) are discussed in the section on Parallelization.

### 13.2 Concepts

#### 13.2.1 Deterministic vs. Monte Carlo

Cuba contains both deterministic and Monte Carlo integration methods. The deterministic approach is based on *cubature rules*,

$$\mathbf{I}f \approx \mathbf{C}_n f := \sum_{i=1}^n w_i f(\vec{x}_i) \quad (\text{E.255})$$

with specially chosen *nodes*  $\vec{x}_i$  and *weights*  $w_i$ . Error estimation is done e.g., by null rules  $\mathbf{N}_m$  ( $m < n$ ) which are constructed to give zero for functions integrated exactly by  $\mathbf{C}_n$  and thus measure errors due to “higher terms.”

The Monte Carlo estimate, although quite similar in form,

$$\mathbf{I}f \approx \mathbf{M}_n f := \frac{1}{n} \sum_{i=1}^n f(\vec{x}_i), \quad (\text{E.256})$$

is conceptually very different as this formula denotes the *statistical average* over independent and identically distributed random samples  $\vec{x}_i$ . In this case the standard deviation furnishes a probabilistic estimate of the integration error:

$$\sigma(\mathbf{M}_n f) = \sqrt{\mathbf{M}_n f^2 - \mathbf{M}_n^2 f}. \quad (\text{E.257})$$

### Construction of Cubature Rules

Starting from an orthogonal basis of functions  $\{b_1, \dots, b_m\}$  – usually monomials – with which most  $f$  can (hopefully) be approximated sufficiently well one imposes that each  $b_i$  be integrated exactly by  $\mathbf{C}_n$ :  $\mathbf{I} b_i \stackrel{!}{=} \mathbf{C}_n b_i$ . These are  $m$  moment equations

$$\sum_{k=1}^n w_k b_i(\vec{x}_k) = \int_0^1 d^d x b_i(\vec{x}) \quad (\text{E.258})$$

for  $nd + n$  unknowns  $\vec{x}_i$  and  $w_i$ . They pose a formidable, in general nonlinear, system of equations. Additional assumptions, e.g., symmetries, are usually necessary to solve this system. Cuba employs the Genz–Malik rules [760] constructed from a symmetric monomial basis.

### Globally Adaptive Subdivision

Once an error estimate for the integral is available, global adaptiveness is easy to implement:

1. Integrate the entire region:  $I_{\text{tot}} \pm E_{\text{tot}}$ .
2. while  $E_{\text{tot}} > \max(\varepsilon_{\text{rel}} I_{\text{tot}}, \varepsilon_{\text{abs}})$
3. Find the region  $r$  with the largest error.
4. Bisect (or otherwise cut up)  $r$ .
5. Integrate each subregion of  $r$  separately.
6.  $I_{\text{tot}} = \sum I_i$ ,  $E_{\text{tot}} = \sqrt{\sum E_i^2}$ .
7. end while

A remark is in order here about the two precisions,  $\varepsilon_{\text{rel}}$  and  $\varepsilon_{\text{abs}}$ . Naively what one imposes is the relative precision: the result is supposed to be accurate to, say, one part in a thousand, i.e.,  $\varepsilon_{\text{rel}} = 10^{-3}$ . For integral values approaching zero, however, this goal becomes harder and harder to reach, and so as not to spend inordinate amounts of time in such cases, an absolute precision  $\varepsilon_{\text{abs}}$  can be prescribed, where typically  $\varepsilon_{\text{abs}} \ll \varepsilon_{\text{rel}}$ .

### Importance Sampling

Importance sampling introduces a weight function into the integral:

$$\mathbf{I}f = \int_0^1 d^d x w(\vec{x}) \frac{f(\vec{x})}{w(\vec{x})}, \quad w(\vec{x}) > 0, \quad \mathbf{I}w = 1, \quad (\text{E.259})$$

with two requirements: a) one must be able to sample from the distribution  $w(\vec{x})$ , b)  $f/w$  should be “smooth” in the sense that  $\sigma_w(f/w) < \sigma(f)$ , e.g.,  $w$  and  $f$  should have the same peak structure. The ideal choice is known to be  $w(\vec{x}) = |f(\vec{x})|/\mathbf{I}f$  which has  $\sigma_w(f/w) = 0$ , but is of little use as it requires a-priori knowledge of the integral value.

### Stratified Sampling

Stratified sampling works by sampling subregions. Consider a total of  $n$  points sampled in a region  $r = r_a + r_b$  vs.  $n/2$  points sampled in  $r_a$  and  $n/2$  in  $r_b$ . In the latter case the variance is

$$\frac{1}{4} \left( \frac{\sigma_a^2 f}{n/2} + \frac{\sigma_b^2 f}{n/2} \right) = \frac{\sigma_a^2 f + \sigma_b^2 f}{2n} \quad (\text{E.260})$$

whereas in the former case it can be written as

$$\frac{\sigma^2 f}{n} = \frac{\sigma_a^2 f + \sigma_b^2 f}{2n} + \frac{(\mathbf{I}_a f - \mathbf{I}_b f)^2}{4n}. \quad (\text{E.261})$$

Even in this simple example the latter variance is at best equal to the former one, and only if the integral values are identical. The optimal reduction of variance can be shown to occur for  $n_a/n_b = \sigma_a f / \sigma_b f$  [761]. The recipe is thus to split up the integration region into parts with equal variance, and then sample all parts with same number of points.

### Quasi-Monte Carlo Methods

Quasi-Monte Carlo methods are based on the Koksma–Hlawka inequality which gives an upper bound on the error of a cubature formula  $\mathbf{C}_n f = \frac{1}{n} \sum_{i=1}^n f(\vec{x}_i)$ ,

$$|\mathbf{C}_n f - \mathbf{I}f| \leq V(f) D^*(\vec{x}_1, \dots, \vec{x}_n). \quad (\text{E.262})$$

Apart from choosing a different integrand there is little one can do about  $V(f)$ , the “variation in the sense of Hardy and Krause.” The *discrepancy*  $D^*$  of a sequence  $\vec{x}_1, \dots, \vec{x}_n$  is defined as

$$D^* = \sup_{r \in [0,1]^d} \left| \frac{\nu(r)}{n} - \text{Vol } r \right|, \quad (\text{E.263})$$

where  $\nu(r)$  counts the  $\vec{x}_i$  that fall into  $r$ . For an equidistributed sequence,  $\nu(r)$  should be proportional to  $\text{Vol } r$ . Quasi-random sequences can be constructed with a substantially lower discrepancy than (pseudo-)random numbers. A Monte Carlo algorithm based on these sequences typically achieves convergence rates of  $\mathcal{O}(\log^{d-1} n/n)$  rather than the usual  $\mathcal{O}(1/\sqrt{n})$ .

Cuba offers a choice of quasi-random Sobol sequences [762], or pseudo-random Mersenne Twister [763] or Ranlux [764, 765] sequences for all Monte Carlo algorithms. Figure E.28 shows that quasi-random numbers cover the plane much more homogeneously than pseudo-random numbers.

### Lattice Methods

Lattice methods require a periodic integrand, usually obtained by applying a *periodizing transformation* (Cuba’s Divonne uses  $x \rightarrow |2x-1|$ ). Sampling is done on an *integration lattice*  $L$  spanned by a carefully selected integer vector  $\vec{z}$ :

$$\mathbf{C}_n f = \frac{1}{n} \sum_{i=0}^{n-1} f\left(\left\{\frac{i}{n} \vec{z}\right\}\right), \quad \{x\} = \text{fractional part of } x. \quad (\text{E.264})$$

$\vec{z}$  is chosen (by extensive computer searches) to knock out as many low-order “Bragg reflections” as possible in the error term (see e.g., [766]):

$$\mathbf{C}_n f - \mathbf{I}f = \sum_{\vec{k} \in \mathbb{Z}^d} \tilde{f}(\vec{k}) \mathbf{C}_n \Re e^{2\pi i \vec{k} \cdot \vec{x}} - \tilde{f}(\vec{0}) = \sum_{\vec{k} \in L^\perp, \vec{k} \neq \vec{0}} \tilde{f}(\vec{k}), \quad (\text{E.265})$$

where  $L^\perp = \{\vec{k} \in \mathbb{Z}^d : \vec{k} \cdot \vec{z} = 0 \pmod{n}\}$  is the reciprocal lattice.

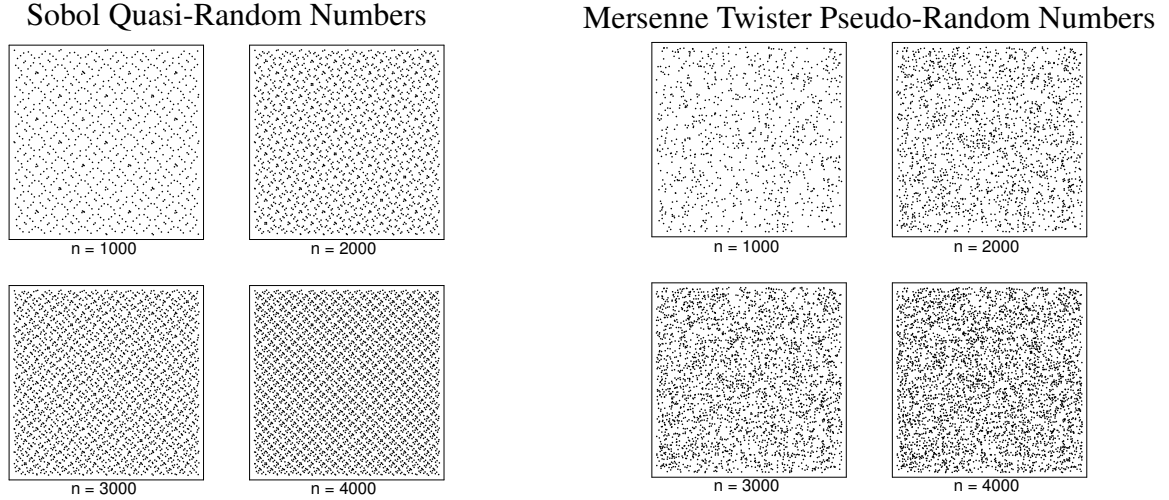


Fig. E.28: Comparison of sequences.

### 13.3 Algorithms

#### 13.3.1 Vegas

Vegas is Lepage's classic Monte Carlo algorithm [767, 768]. It uses importance sampling for variance reduction for which it iteratively builds up a piecewise constant weight function, represented on a rectangular grid. Each iteration consists of a sampling step followed by a refinement of the grid.

In Cuba's implementation Vegas can memorize its grid for subsequent invocations and it can save its internal state to a file from which it can be used in a different integration.

#### 13.3.2 Suave

Suave is a cross-breed of Vegas and Miser [769], a Monte Carlo algorithm which combines Vegas-style importance sampling with globally adaptive subdivision.

The algorithm works as follows: Until the requested accuracy is reached, bisect the region with the largest error along the axis in which the fluctuations of the integrand are reduced most. Prorate the number of new samples in each half for its fluctuation.

The Vegas grid is kept across divisions, i.e., a region which is the result of  $n - 1$  subdivisions has had  $n$  Vegas iterations performed on it. On the downside, Suave is somewhat memory hungry, as it needs to retain samples for later use.

#### 13.3.3 Divonne

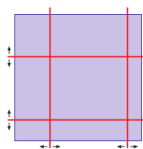
Divonne is a significantly extended version of CERNlib's Algorithm D151 [770, 771]. It is essentially a Monte Carlo algorithm but has cubature rules built in for comparison, too. Variance reduction is by stratified sampling, which is aided by methods from numerical optimization. Divonne has a three-phase algorithm:

##### Phase 1: Partitioning

The integration region is split into subregions of (approximately) equal spread  $s$ , defined as

$$s(r) = \frac{\text{Vol } r}{2} \left( \max_{\vec{x} \in r} f(\vec{x}) - \min_{\vec{x} \in r} f(\vec{x}) \right). \quad (\text{E.266})$$

Minimum and maximum of each subregion are sought using methods from numerical optimization (basically a quasi-Newton search). Then, 'dividers' are moved around (see picture) to find the optimal splitting. This latter procedure can cleverly be translated into the solution of a linear system and is hence quite fast (for details see [771]).



### Phase 2: Sampling

The subregions determined in Phase 1 are independently sampled with the same number of points each. The latter is extrapolated from the results of Phase 1.

### Phase 3: Refinement

Regions whose results from Phase 1 and 2 do not agree within their errors are subdivided or sampled again. This phase is an addition to the original algorithm since it was found that often enough the error estimate, or even the integral value, was off because characteristics of the integrand had not been found in Phase 1.

Two important features have been added in the Cuba implementation:

- The user can point out extrema for tricky integrands.
- For integrands which cannot be sampled too close to the border, a ‘safety distance’ can be prescribed in which values will be extrapolated from two points in the interior.

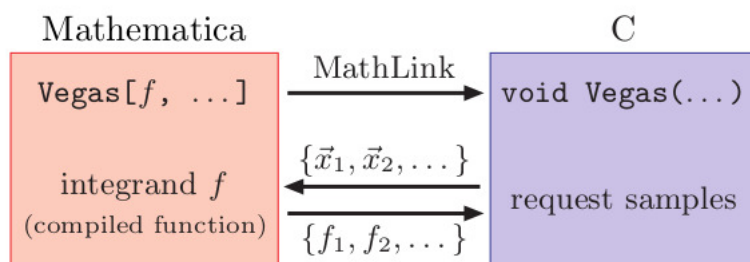
### 13.3.4 Cuhre

Cuhre is a deterministic algorithm. It uses the Genz–Malik cubature rules [760] in a globally adaptive subdivision scheme. The algorithm is thus: Until the requested accuracy is reached, bisect the region with the largest error along the axis with the largest fourth difference.

Cuhre has been re-implemented in Cuba mostly for a consistent interface, it is the same as the original DCUHRE subroutine [772].

## 13.4 Mathematica interface

The Mathematica interface deserves a special mention, as it is not a library in the proper sense. It is rather four executables which communicate with Mathematica via the MathLink API:



After loading the appropriate MathLink executable, e.g., with `Install["Vegas"]`, the corresponding routine can be used almost like Mathematica’s native `NIntegrate`. The integrand is evaluated completely in Mathematica, which means that one can do things like

```
Cuhre[Zeta[x y], {x, 2, 3}, {y, 4, 5}]
```

## 13.5 Parallelization

Numerical integration is particularly suited for parallelization, which can significantly speed up the computation as it generally incurs only a small overhead. The following design considerations were relevant for the parallelization of the Cuba routines.

1. No additional software shall be needed: Parallelization thus proceeds through operating-system functions only; no external message-passing interface is used. This of course fills the internal cores (typically 4–8) only, i.e., parallelization across the network is not possible. On the other hand, the speed-ups cannot be expected to increase linearly, so utilizing many more cores is more of a theoretical option anyway.

2. Parallelization shall work for any integrand: The programmer shall not need to rewrite the integrand function for parallel execution, which means in particular that reentrancy cannot be taken for granted. Cuba uses `fork/wait` rather than the `pthread*` functions since the former create a completely independent copy of the running process and thus work for any integrand.

3. Parallelization shall work ‘automatically’: The number of cores to use is determined through an environment variable and hence requires no re-compile. More importantly, its default value is set automatically to the number of idle cores on the present machine, so a program using Cuba will automatically take advantage of the system’s capabilities.

4. Parallelization shall be available on all platforms: The POSIX functions `fork` and `wait` are unavailable on native Windows, but Cygwin provides a suitably licensed (GPL) emulation. The emulated `fork` is rather slow, however, so Cuba keeps the `fork` calls at a minimum.

### 13.5.1 Parallelization model

Cuba operates in a master–worker model. The master process orchestrates the parallelization but does not count towards the number of cores, e.g., `CUBACORES = 4` means four workers and one master. Very importantly, the samples are generated by the master process only and distributed to the workers, such that random numbers are never used more than once.

The parallelization of Cuba centers on the main sampling routine `DoSample`, which in principle parallelizes straightforwardly on  $N$  cores:

<i>Serial version:</i>	<i>Parallel version:</i>
sample $n$ points.	sample $n/N$ points on core 1,
	$\vdots$
	sample $n/N$ points on core $N$ .

The actual distribution strategy is somewhat more involved and is described in Sect. 13.5.5 below.

Speed-ups measured with Divonne by parallelizing `DoSample` alone were generally unsatisfactory and significantly below those of the other integrators, e.g.,  $\lesssim 1.5$  on four cores. It turned out that the Partitioning Phase (see Sect. 13.3.3) was crucial for attaining reasonable speed-ups and needed special treatment. Firstly, the original partitioning algorithm divided the regions recursively (and with a minimum recursion depth, too) and had to be ‘un-recursed’, mainly by better bookkeeping of the subregions. Secondly, the Partitioning Phase was modified such that each core receives an entire region to subdivide, not just a list of points (as `DoSample` does). In particular the minimum/maximum search, during which only one point at a time is sampled, is distributed much more efficiently this way. The other two phases were not so critical precisely because they sample more points per region.

### 13.5.2 Parallelization in Mathematica

The parallelization procedure is rather different in Fortran/C/C++ and in Mathematica, and much of this has to do with the way the MathLink protocol works: As all MathLink programs, Cuba’s run independently of

Mathematica, so all parallelization must be done by Mathematica means. (A clever way, too, of preventing the user from acquiring more licenses than paid for.)

Sampling in Mathematica is handled through a function `MapSample` which by default is identical to `Map`, i.e., the serial version. To parallelize sampling one merely needs to redefine `MapSample = ParallelMap` (after loading Cuba). If the integrand depends on user-defined symbols or functions, their definitions must be distributed to the workers beforehand using `DistributeDefinitions` and likewise required packages must be loaded with `ParallelNeeds` instead of `Needs`. This is standard procedure, however, and is explained in detail in the Mathematica manual.

### 13.5.3 Parallelization in Fortran and C/C++

In Fortran and C/C++ the Cuba library can (and usually does) automatically parallelize the sampling of the integrand. It parallelizes through `fork` and `wait` which, though slightly less performant than `pthread`s, do not require reentrant code. (Reentrancy may not even be under full control of the programmer, for example Fortran's I/O is usually non-reentrant.) Worker processes are started and shut down only as few times as possible, however, so the performance penalty is really quite minor even for non-native `fork` implementations such as Cygwin's. Parallelization is not available on native Windows for lack of the `fork` function.

The communication of samples to and from the workers is done through IPC shared memory (`shmget` etc.), or if that is not available, through a `socketpair` (two-way pipe). The control information is always transferred via `socketpair` since this elegantly and portably solves the synchronization issues. Remarkably, shared memory's anticipated performance advantage turned out to be hardly perceptible. Possibly there are cache-coherence issues introduced by several workers writing simultaneously to the same shared-memory area.

### 13.5.4 Starting and stopping the workers

The workers are usually started and stopped automatically by Cuba's integration routines, but the user may choose to start them manually or keep them running after one integration and shut them down later, e.g., at the end of the program, which can be slightly more efficient. The latter mode is referred to as 'Spinning Cores' and must be employed with certain care, for running workers will not 'see' subsequent changes in the main program's data (e.g., global variables, common blocks) or code (e.g., via `dlsym`) unless special arrangements are made (e.g., shared memory).

### 13.5.5 Accelerators and Cores

Based on the strategy used to distribute samples, Cuba distinguishes two kinds of workers.

Workers of the first kind are referred to as 'Accelerators' even though Cuba does not actually send anything to a GPU or Accelerator in the system by itself – this can only be done by the integrand routine. The assumption behind this strategy is that the integrand evaluation is running on a device so highly parallel that the sampling time is more or less independent of the number of points, up to the number of threads  $p_{\text{accel}}$  available in hardware. Cuba tries to send exactly  $p_{\text{accel}}$  points to each core – never more, less only for the last batch. To sample e.g., 2400 points on three accelerators with  $p_{\text{accel}} = 1000$ , Cuba sends batches of 1000/1000/400 and not, for example, 800/800/800 or 1200/1200.

CPU-bound workers are just called 'Cores'. Their distribution strategy is different in that all available cores are used and points are distributed evenly. In the example above, the batches would be 800/800/800 thus. Each core receives at least 10 points, or else fewer cores are used. If no more than 10 points are requested in total, Cuba uses no workers at all but lets the master sample those few points. This happens during the partitioning phase of Divonne, for instance, where only single points are evaluated in the minimum/maximum search. Conversely, if the division of points by cores does not come out even, the remaining few points ( $< n_{\text{cores}}$ ) are simply added to the existing batches, to avoid an extra batch because of rounding. Sampling 2001 points on two cores with  $p_{\text{cores}} = 1000$  will hence give two batches 1001/1000 and not three batches 1000/1000/1.

### 13.5.6 Concurrency issues

By creating a new process image, `fork` circumvents all memory concurrency, to wit: each worker modifies only its own copy of the parent's memory and never overwrites any other's data. The programmer should be aware of a few potential problems nevertheless:

- Communicating back results other than the intended output from the integrand to the main program or exchanging data between workers is not straightforward because, by the same token, each worker modifies only its own memory space.
- `fork` does not guard against competing use of other common resources. For example, if the integrand function writes to a file (debug output, say), there is no telling in which order the lines will end up in the file, or even if they will end up as complete lines at all.
- Fortran users should flush (or close) open files before calling Cuba, i.e., call `flush(unit)`, for the workers inherit all file buffers, and *each* will write out the buffer content at exit.

### 13.5.7 Vectorization

Vectorization means evaluating the integrand function for several points at once. This is different from ordinary parallelization where independent threads are executed concurrently. Vector instructions are commonly available in hardware and it is usually possible to employ vectorization on top of parallelization.

Cuba cannot automatically vectorize the integrand function, of course, but it does pass (up to) `nvec` points per integrand call. This value need not correspond to the hardware vector length – computing several points in one call can also make sense e.g., if the computations have significant intermediate results in common. The actual number of points passed is indicated through the corresponding `nvec` argument of the integrand.

## 13.6 Summary

Cuba is a library for multidimensional numerical integration written in C. It contains four independent algorithms: Vegas, Suave, Divonne, and Cuhre, which have similar invocations and can be exchanged easily for comparison. All routines can integrate vector integrands and have a Fortran, C/C++, and Mathematica interface.

Concurrent sampling achieves significant speed-ups and is turned on by default for Fortran and C/C++ (but can be controlled through API calls or the environment). No extra software needs to be installed since only operating-system functions are used. No reentrancy is required for the integrand function since `fork/wait` is applied.

Cuba is available from <http://feynarts.de/cuba>, is licensed under the LGPL, and easy to build (autoconf). The download includes a manual which gives full details on installation and usage.



# Acknowledgements

The work of *T.R.* was supported in part by an Alexander von Humboldt Polish Honorary Research Fellowship. The work of *I.D.* was supported by a research grant of Deutscher Akademischer Austauschdienst (DAAD) and by Deutsches Elektronensynchrotron DESY.

The work of *W.F.* and *J.G.* was supported by the Polish National Science Centre (NCN) under the Grant Agreement 2017/25/B/ST2/01987.

The work of *A.F.* was supported in part by the National Science Foundation under grant no. PHY-1519175.

The work of *R.P.* was supported by the MECD project FPA2016-78220-C3-3-P.

The work of *M.P.* was supported by BMBF contract 05H15PACC1.

The work of *G.R.* was supported by the Spanish Government and ERDF funds from the European Commission (Grants No. FPA2014-53631-C2-1-P and SEV-2014-0398), Generalitat Valenciana under Grant No. PROMETEO/2017/053, and Consejo Superior de Investigaciones Científicas (Grant No. PIE-201750E021).

The work of *R.L.* was supported by the ‘Basis’ foundation for theoretical physics and mathematics.

The work of *R.B.* was supported by the German Science Foundation (DFG) within the Collaborative Research Center 676 “Particles, Strings and the Early Universe”.

The work of *S.B.* was supported by the ERC Starting Grant “MathAm” (39568).

*G.Y.* was supported in part by the Chinese Academy of Sciences (CAS) Hundred-Talent Program, by the Key Research Program of Frontier Sciences of CAS, and by Project 11747601 supported by National Natural Science Foundation of China (NSFC).

The work of *J.U.* has received funding from the European Research Council (ERC) under the European Union’s Horizon 2020 research and innovation programme under grant agreement No 647356 (CutLoops). It was also supported by Graduiertenkolleg 1504 “Masse, Spektrum, Symmetrie” of Deutsche Forschungsgemeinschaft (DFG).

The work of *S.J.* was partly supported by the Polish National Science Center grant 2016/23/B/ST2/03927.

The report was partly supported by COST (European Cooperation in Science and Technology) Action CA16201 PARTICLEFACE.



# Bibliography

- [1] European Strategy for Particle Physics by the European Strategy Group for Particle Physics, CERN's white paper for the 15th European Strategy Session of the Council, <https://council.web.cern.ch/en/content/european-strategy-particle-physics>.
- [2] FCC – Future Circular Collider Project, CERN, <https://fcc.web.cern.ch>.
- [3] M. Bicer, et al., First Look at the Physics Case of TLEP, JHEP 01 (2014) 164, in: Proceedings of the 2013 Community Summer Study on the Future of U.S. Particle Physics: Snowmass on the Mississippi (CSS2013): Minneapolis, MN, USA, July 29-August 6, 2013. arXiv:1308.6176, doi:10.1007/JHEP01(2014)164.
- [4] A. Arbey, et al., Physics at the  $e^+e^-$  Linear Collider, Eur. Phys. J. C75 (8) (2015) 371. arXiv:1504.01726, doi:10.1140/epjc/s10052-015-3511-9.
- [5] CLIC – Compact Linear International Collider Project, CERN, <http://clicstudy.web.cern.ch/>.
- [6] CEPC – Circular Electron Positron Collider Project, China, <http://cepc.ihep.ac.cn/>.
- [7] K. Abe, et al., Measurement of the branching ratio of the  $Z^0$  into heavy quarks, Phys. Rev. D71 (2005) 112004. arXiv:hep-ex/0503005, doi:10.1103/PhysRevD.71.112004.
- [8] A. Blondel, J. Gluza, P. Janot (org.), Mini workshop: *Precision EW and QCD calculations for the FCC studies: methods and tools*, 12-13 January 2018, CERN, Geneva, Switzerland, webpage <https://indico.cern.ch/event/669224/>.
- [9] M. Awramik, M. Czakon, A. Freitas, Bosonic corrections to the effective weak mixing angle at  $O(\alpha^2)$ , Phys. Lett. B642 (2006) 563–566. arXiv:hep-ph/0605339, doi:10.1016/j.physletb.2006.07.035.
- [10] M. Awramik, M. Czakon, A. Freitas, Electroweak two-loop corrections to the effective weak mixing angle, JHEP 0611 (2006) 048. arXiv:hep-ph/0608099, doi:10.1088/1126-6708/2006/11/048.
- [11] ALEPH collab., DELPHI collab., L3 collab., OPAL collab., SLD collab., LEP Electroweak Working Group, SLD Electroweak Group, SLD Heavy Flavour Group, S. Schael, et al., Precision electroweak measurements on the  $Z$  resonance, Phys. Rept. 427 (2006) 257–454. arXiv:hep-ex/0509008, doi:10.1016/j.physrep.2005.12.006.
- [12] The ATLAS Collaboration, Measurement of the effective leptonic weak mixing angle using electron and muon pairs from  $Z$ -boson decay in the ATLAS experiment at  $\sqrt{s} = 8$  TeV, note ATL-CONF-2018-037 (11 July 2018), <https://cds.cern.ch/record/2630340/files/ATLAS-CONF-2018-037.pdf>.
- [13] H. Baer, T. Barklow, K. Fujii, Y. Gao, A. Hoang, S. Kanemura, J. List, H. E. Logan, A. Nomerotski, M. Perelstein, et al., The International Linear Collider Technical Design Report - Volume 2: Physics arXiv:1306.6352.
- [14] J. Erler, S. Heinemeyer, W. Hollik, G. Weiglein, P. M. Zerwas, Physics impact of GigaZ, Phys. Lett. B486 (2000) 125–133, [1389(2000)]. arXiv:hep-ph/0005024, doi:10.1016/S0370-2693(00)00749-8.
- [15] I. Dubovyk, A. Freitas, J. Gluza, T. Riemann, J. Usovitsch, The two-loop electroweak bosonic corrections to  $\sin^2 \theta_{\text{eff}}^b$ , Phys. Lett. B762 (2016) 184–189. arXiv:1607.08375, doi:10.1016/j.physletb.2016.09.012.
- [16] I. Dubovyk, A. Freitas, J. Gluza, T. Riemann, J. Usovitsch, Complete electroweak two-loop corrections to  $Z$  boson production and decay, Phys. Lett. B783 (2018) 86–94. arXiv:1804.10236, doi:10.1016/j.physletb.2018.06.037.

- [17] I. Dubovyk, J. Gluza, A. Freitas, T. Riemann, J. Usovitsch, "Theory - status", talk held by J. Gluza at [8], [https://indico.cern.ch/event/669224/contributions/2805413/attachments/1581532/2499590/FCC\\_gluza\\_TheoryStatus.pdf](https://indico.cern.ch/event/669224/contributions/2805413/attachments/1581532/2499590/FCC_gluza_TheoryStatus.pdf).
- [18] I. Dubovyk, J. Gluza, A. Freitas, W. Grzanka, S. Jadach, T. Riemann, J. Usovitsch, Precision calculations for FCC, poster presented by S. Jadach at the FCC weak 2018, 9-13 April 2018, Amsterdam. 2AMSP38-Poster-FCCee-PhyExp-Jadach\_et\_al.pdf.
- [19] I. Dubovyk, J. Gluza, A. Freitas, T. Riemann, J. Usovitsch, The Z boson resonance at 2 loops. Talk held by J. Gluza at LL2018, April 29 to May 4, 2018, St. Goar, Germany. <https://indico.desy.de/indico/event/16613/session/4/contribution/22/material/slides/0.pdf>.
- [20] M. Czakon, J. Gluza, F. Jegerlehner, M. Zralek, Confronting electroweak precision measurements with new physics models, Eur. Phys. J. C13 (2000) 275–281. arXiv:hep-ph/9909242, doi:10.1007/s100520000278.
- [21] B. Grzadkowski, M. Iskrzynski, M. Misiak, J. Rosiek, Dimension-six terms in the Standard Model lagrangian, JHEP 10 (2010) 085. arXiv:1008.4884, doi:10.1007/JHEP10(2010)085.
- [22] G. F. Giudice, C. Grojean, A. Pomarol, R. Rattazzi, The Strongly-Interacting Light Higgs, JHEP 06 (2007) 045. arXiv:hep-ph/0703164, doi:10.1088/1126-6708/2007/06/045.
- [23] R. Contino, M. Ghezzi, C. Grojean, M. Muhlleitner, M. Spira, Effective Lagrangian for a light Higgs-like scalar, JHEP 07 (2013) 035. arXiv:1303.3876, doi:10.1007/JHEP07(2013)035.
- [24] S. Das Bakshi, J. Chakraborty, S. K. Patra, CoDEx: Wilson coefficient calculator connecting SMEFT to UV theory. arXiv:1808.04403.
- [25] S. Dawson, A. Ismail, SMEFT Corrections to Z Boson Decays. arXiv:1808.05948.
- [26] J. de Blas, M. Ciuchini, E. Franco, S. Mishima, M. Pierini, L. Reina, L. Silvestrini, The Global Electroweak and Higgs Fits in the LHC era, PoS EPS-HEP2017 (2017) 467. arXiv:1710.05402, doi:10.22323/1.314.0467.
- [27] D. Bardin, M. Bilenky, P. Christova, M. Jack, L. Kalinovskaya, A. Olchevski, S. Riemann, T. Riemann, ZFITTER 6.21: A semi-analytical program for fermion pair production in  $e^+e^-$  annihilation, Comput. Phys. Commun. 133 (2001) 229–395. arXiv:hep-ph/9908433, doi:10.1016/S0010-4655(00)00152-1.
- [28] G. J. H. Burgers, On the Two Loop QED Vertex Correction in the High-energy Limit, Phys. Lett. 164B (1985) 167–169. doi:10.1016/0370-2693(85)90053-X.
- [29] S. Jadach, B. F. L. Ward, Z. Was, The Precision Monte Carlo event generator KK for two fermion final states in  $e^+e^-$  collisions, Comput. Phys. Commun. 130 (2000) 260–325, up to date source available from <http://home.cern.ch/jadach/>. arXiv:hep-ph/9912214, doi:10.1016/S0010-4655(00)00048-5.
- [30] D. Y. Bardin, M. S. Bilenky, T. Riemann, M. Sachwitz, H. Vogt, P. C. Christova, DIZET: A program package for the calculation of electroweak one loop corrections for the process  $e^+e^- \rightarrow f^+f^-$  around the  $Z^0$  peak, Comput. Phys. Commun. 59 (1990) 303–312. doi:10.1016/0010-4655(90)90179-5.
- [31] A. Leike, T. Riemann, J. Rose, S-matrix approach to the Z line shape, Phys. Lett. B273 (1991) 513–518. arXiv:hep-ph/9508390, doi:10.1016/0370-2693(91)90307-C.
- [32] T. Riemann, Cross-section asymmetries around the Z peak, Phys. Lett. B293 (1992) 451–456. arXiv:hep-ph/9506382, doi:10.1016/0370-2693(92)90911-M.
- [33] M. Misiak, M. Steinhauser, Large- $m_c$  Asymptotic Behaviour of  $O(\alpha_s^2)$  Corrections to  $B \rightarrow X_s \gamma$ , Nucl. Phys. B840 (2010) 271–283. arXiv:1005.1173, doi:10.1016/j.nuclphysb.2010.07.009.
- [34] M. Misiak, A. Rehman, M. Steinhauser, NNLO QCD counterterm contributions to  $\bar{B} \rightarrow X_s \gamma$  for the physical value of  $m_c$ , Phys. Lett. B770 (2017) 431–439. arXiv:1702.07674, doi:10.1016/j.

- physletb.2017.05.008.
- [35] J. Gluza, A. Freitas, T. Riemann, et al., The Z boson line shape - from 1.5 loops at LEP to 2.5 loops in future. Talk held by T. Riemann at [8], <https://indico.cern.ch/event/669224/contributions/2805418/attachments/1581648/2504620/riemann-FCCeeminiCERN-short.pdf>.
  - [36] A. Arbuzov, M. Awramik, M. Czakon, A. Freitas, M. Grünewald, K. Mönig, S. Riemann, T. Riemann, ZFITTER: A Semi-analytical program for fermion pair production in  $e^+e^-$  annihilation, from version 6.21 to version 6.42, *Comput. Phys. Commun.* 174 (2006) 728–758. [arXiv:hep-ph/0507146](#), doi:10.1016/j.cpc.2005.12.009.
  - [37] K. G. Chetyrkin, J. H. Kuhn, A. Kwiatkowski, QCD corrections to the  $e^+e^-$  cross-section and the Z boson decay rate, CERN 95-03. See also: QCD corrections to the  $e^+e^-$  cross-section and the Z boson decay rate: Concepts and results, LBL-36678-REV and *Phys. Rept.* 277 (1996) 189-281. [arXiv:hep-ph/9503396](#), doi:10.1016/S0370-1573(96)00012-9.
  - [38] M. Awramik, M. Czakon, A. Freitas, B. Kniehl, Two-loop electroweak fermionic corrections to  $\sin^2 \theta_{\text{eff}}^{\text{bb}}$ , *Nucl. Phys. B* 813 (2009) 174–187. [arXiv:0811.1364](#), doi:10.1016/j.nuclphysb.2008.12.031.
  - [39] A. Freitas, Higher-order electroweak corrections to the partial widths and branching ratios of the Z boson, *JHEP* 1404 (2014) 070. [arXiv:1401.2447](#), doi:10.1007/JHEP04(2014)070.
  - [40] "Motivation: Experimental capabilities and requirements", talk held by A. Blondel at [8], [https://indico.cern.ch/event/669224/contributions/2805398/attachments/1581811/2499870/Blondel-FCC-ee-physics\\_case\\_and\\_theory\\_errors-v2.pdf](https://indico.cern.ch/event/669224/contributions/2805398/attachments/1581811/2499870/Blondel-FCC-ee-physics_case_and_theory_errors-v2.pdf).
  - [41] A. Akhundov, D. Bardin, T. Riemann, Electroweak one loop corrections to the decay of the neutral vector boson, *Nucl. Phys. B* 276 (1986) 1, Dubna preprint JINR-E2-85-617 (Aug 1985). doi:10.1016/0550-3213(86)90014-3.
  - [42] C. Patrignani, et al., Review of Particle Physics, *Chin. Phys. C* 40 (10) (2016) 100001. doi:10.1088/1674-1137/40/10/100001.
  - [43] M. Steinhauser, Leptonic contribution to the effective electromagnetic coupling constant up to three loops, *Phys. Lett. B* 429 (1998) 158–161. [arXiv:hep-ph/9803313](#), doi:10.1016/S0370-2693(98)00503-6.
  - [44] M. Davier, A. Hoecker, B. Malaescu, Z. Zhang, Reevaluation of the Hadronic Contributions to the Muon g-2 and to  $\alpha(\text{MZ})$ , *Eur. Phys. J. C* 71 (2011) 1515, [Erratum: *Eur. Phys. J. C* 72,1874(2012)]. [arXiv:1010.4180](#), doi:10.1140/epjc/s10052-012-1874-8, 10.1140/epjc/s10052-010-1515-z.
  - [45] R. Barbieri, M. Beccaria, P. Ciafaloni, G. Curci, A. Vicere, Radiative correction effects of a very heavy top, *Phys. Lett. B* 288 (1992) 95–98, [Erratum: *Phys. Lett. B* 312,511(1993)]. [arXiv:hep-ph/9205238](#), doi:10.1016/0370-2693(93)90990-Y, 10.1016/0370-2693(92)91960-H.
  - [46] R. Barbieri, M. Beccaria, P. Ciafaloni, G. Curci, A. Vicere, Two loop heavy top effects in the Standard Model, *Nucl. Phys. B* 409 (1993) 105–127, doi:10.1016/0550-3213(93)90448-X. doi:10.1016/0550-3213(93)90448-X.
  - [47] J. Fleischer, O. V. Tarasov, F. Jegerlehner, Two loop heavy top corrections to the rho parameter: A Simple formula valid for arbitrary Higgs mass, *Phys. Lett. B* 319 (1993) 249–256. doi:10.1016/0370-2693(93)90810-5.
  - [48] J. Fleischer, O. V. Tarasov, F. Jegerlehner, Two loop large top mass corrections to electroweak parameters: Analytic results valid for arbitrary Higgs mass, *Phys. Rev. D* 51 (1995) 3820–3837. doi:10.1103/PhysRevD.51.3820.
  - [49] A. Djouadi, C. Verzegnassi, Virtual very heavy top effects in LEP/SLC precision measurements, *Phys. Lett. B* 195 (1987) 265.

- [50] A. Djouadi,  $O(\alpha\alpha_s)$  Vacuum Polarization Functions of the Standard Model Gauge Bosons, *Nuovo Cim. A100* (1988) 357. doi:10.1007/BF02812964.
- [51] B. A. Kniehl, Two loop corrections to the vacuum polarizations in perturbative QCD, *Nucl. Phys. B347* (1990) 86–104. doi:10.1016/0550-3213(90)90552-0.
- [52] B. A. Kniehl, A. Sirlin, Dispersion relations for vacuum polarization functions in electroweak physics, *Nucl. Phys. B371* (1992) 141–148. doi:10.1016/0550-3213(92)90232-Z.
- [53] A. Djouadi, P. Gambino, Electroweak gauge bosons selfenergies: Complete QCD corrections, *Phys. Rev. D49* (1994) 3499–3511, Erratum: *Phys. Rev. D53* (1996) 4111. arXiv:hep-ph/9309298, doi:10.1103/PhysRevD.49.3499, 10.1103/PhysRevD.53.4111.
- [54] L. Avdeev, J. Fleischer, S. Mikhailov, O. Tarasov,  $O(\alpha\alpha_s^2)$  correction to the electroweak  $\rho$  parameter, *Phys. Lett. B336* (1994) 560–566, doi:10.1016/0370-2693(94)90573-8, Erratum-ibid. B349 (1995) 597–598, hep-ph/9406363v2. doi:10.1016/0370-2693(94)90573-8.
- [55] K. Chetyrkin, J. H. Kühn, M. Steinhauser, Corrections of order  $O(G_F M_t^2 \alpha_s^2)$  to the  $\rho$  parameter, *Phys. Lett. B351* (1995) 331–338, doi:10.1016/0370-2693(95)00380-4. arXiv:hep-ph/9502291, doi:10.1016/0370-2693(95)00380-4.
- [56] J. J. van der Bij, K. G. Chetyrkin, M. Faisst, G. Jikia, T. Seidensticker, Three loop leading top mass contributions to the  $\rho$  parameter, *Phys. Lett. B498* (2001) 156–162. arXiv:hep-ph/0011373, doi:10.1016/S0370-2693(01)00002-8.
- [57] M. Faisst, J. H. Kühn, T. Seidensticker, O. Veretin, Three loop top quark contributions to the  $\rho$  parameter, *Nucl. Phys. B665* (2003) 649–662. arXiv:hep-ph/0302275, doi:10.1016/S0550-3213(03)00450-4.
- [58] Y. Schröder, M. Steinhauser, Four-loop singlet contribution to the  $\rho$  parameter, *Phys. Lett. B622* (2005) 124–130. arXiv:hep-ph/0504055, doi:10.1016/j.physletb.2005.06.085.
- [59] K. G. Chetyrkin, M. Faisst, J. H. Kühn, P. Maierhofer, C. Sturm, Four-loop QCD corrections to the rho parameter, *Phys. Rev. Lett. 97* (2006) 102003. arXiv:hep-ph/0605201, doi:10.1103/PhysRevLett.97.102003.
- [60] R. Boughezal, M. Czakon, Single scale tadpoles and  $O(G_F m_t^2 \alpha(s)^3)$  corrections to the  $\rho$  parameter, *Nucl. Phys. B755* (2006) 221–238. arXiv:hep-ph/0606232, doi:10.1016/j.nuclphysb.2006.08.007.
- [61] A. Czarnecki, J. H. Kühn, Nonfactorizable QCD and electroweak corrections to the hadronic  $Z$  boson decay rate, *Phys. Rev. Lett. 77* (1996) 3955–3958. arXiv:hep-ph/9608366.
- [62] R. Harlander, T. Seidensticker, M. Steinhauser, Complete corrections of order  $O(\alpha\alpha_s)$  to the decay of the  $Z$  boson into bottom quarks, *Phys. Lett. B426* (1998) 125–132. arXiv:hep-ph/9712228, doi:10.1016/S0370-2693(98)00220-2.
- [63] J. Fleischer, O. V. Tarasov, F. Jegerlehner, P. Raczka, Two loop  $O(\alpha_s G_\mu m_t^2)$  corrections to the partial decay width of the  $Z^0$  into  $b\bar{b}$  final states in the large top mass limit, *Phys. Lett. B293* (1992) 437–444. doi:10.1016/0370-2693(92)90909-N.
- [64] G. Buchalla, A. J. Buras, QCD corrections to the  $\bar{s}dZ$  vertex for arbitrary top quark mass, *Nucl. Phys. B398* (1993) 285–300. doi:10.1016/0550-3213(93)90110-B.
- [65] G. Degrandi, Current algebra approach to heavy top effects in  $Z \rightarrow b + \bar{b}$ , *Nucl. Phys. B407* (1993) 271–289. arXiv:hep-ph/9302288, doi:10.1016/0550-3213(93)90058-W.
- [66] K. Chetyrkin, A. Kwiatkowski, M. Steinhauser, Leading top mass corrections of order  $O(\alpha\alpha_s m_t^2/M_W^2)$  to partial decay rate  $\Gamma(Z \rightarrow b\bar{b})$ , *Mod. Phys. Lett. A8* (1993) 2785–2792, doi:10.1142/S0217732393003172. doi:10.1142/S0217732393003172.
- [67] I. Dubovyk, J. Gluza, T. Riemann, J. Usovitsch, "MB-suite 1: AMBRE news: non-planar 3-loop vertices", talk held by I. Dubovyk at [8], <https://indico.cern.ch/event/669224/overview>.
- [68] S. Borowka, "pySecDec for phenomenological predictions", talk held at [8], <https://indico.cern.ch/event/669224/overview>.

- [//indico.cern.ch/event/669224/contributions/2805456/attachments/1582115/2500426/miniWS2018\\_sophia.pdf](https://indico.cern.ch/event/669224/contributions/2805456/attachments/1582115/2500426/miniWS2018_sophia.pdf).
- [69] A. Freitas, Numerical multi-loop integrals and applications, *Prog. Part. Nucl. Phys.* 90 (2016) 201–240. [arXiv:1604.00406](https://arxiv.org/abs/1604.00406), [doi:10.1016/j.pnpnp.2016.06.004](https://doi.org/10.1016/j.pnpnp.2016.06.004).
- [70] A. V. Smirnov, FIESTA 3: cluster-parallelizable multiloop numerical calculations in physical regions, *Comput. Phys. Commun.* 185 (2014) 2090–2100. [arXiv:1312.3186](https://arxiv.org/abs/1312.3186), [doi:10.1016/j.cpc.2014.03.015](https://doi.org/10.1016/j.cpc.2014.03.015).
- [71] S. Borowka, G. Heinrich, S. P. Jones, M. Kerner, J. Schlenk, T. Zirke, SecDec-3.0: numerical evaluation of multi-scale integrals beyond one loop, *Comput. Phys. Commun.* 196 (2015) 470–491. [arXiv:1502.06595](https://arxiv.org/abs/1502.06595), [doi:10.1016/j.cpc.2015.05.022](https://doi.org/10.1016/j.cpc.2015.05.022).
- [72] J. Gluza, K. Kajda, T. Riemann, AMBRE - a Mathematica package for the construction of Mellin-Barnes representations for Feynman integrals, *Comput. Phys. Commun.* 177 (2007) 879–893. [arXiv:0704.2423](https://arxiv.org/abs/0704.2423), [doi:10.1016/j.cpc.2007.07.001](https://doi.org/10.1016/j.cpc.2007.07.001).
- [73] J. Gluza, K. Kajda, T. Riemann, V. Yundin, Numerical Evaluation of Tensor Feynman Integrals in Euclidean Kinematics, *Eur. Phys. J. C* 71 (2011) 1516. [arXiv:1010.1667](https://arxiv.org/abs/1010.1667), [doi:10.1140/epjc/s10052-010-1516-y](https://doi.org/10.1140/epjc/s10052-010-1516-y).
- [74] K. Bielas, I. Dubovyk, J. Gluza, T. Riemann, Some Remarks on Non-planar Feynman Diagrams, *Acta Phys. Polon. B* 44 (11) (2013) 2249–2255. [arXiv:1312.5603](https://arxiv.org/abs/1312.5603), [doi:10.5506/APhysPolB.44.2249](https://doi.org/10.5506/APhysPolB.44.2249).
- [75] I. Dubovyk, J. Gluza, T. Riemann, Non-planar Feynman diagrams and Mellin-Barnes representations with AMBRE 3.0, *J. Phys. Conf. Ser.* 608 (1) (2015) 012070. [doi:10.1088/1742-6596/608/1/012070](https://doi.org/10.1088/1742-6596/608/1/012070).
- [76] I. Dubovyk, J. Gluza, T. Riemann, J. Usovitsch, Numerical integration of massive two-loop Mellin-Barnes integrals in Minkowskian regions, *PoS LL2016* (2016) 034, <https://pos.sissa.it/260/034/pdf>. [arXiv:1607.07538](https://arxiv.org/abs/1607.07538).
- [77] I. Dubovyk, J. Gluza, T. Jelinski, T. Riemann, J. Usovitsch, New prospects for the numerical calculation of Mellin-Barnes integrals in Minkowskian kinematics, *Acta Phys. Polon. B* 48 (2017) 995. [arXiv:1704.02288](https://arxiv.org/abs/1704.02288), [doi:10.5506/APhysPolB.48.995](https://doi.org/10.5506/APhysPolB.48.995).
- [78] S. Jadach, "How to calculate QED higher orders in a form useful for MC event generators with soft photon and/or collinear resummation?", talk held at [8], <https://indico.cern.ch/event/669224/overview>.
- [79] D. Y. Bardin, A. Leike, T. Riemann, M. Sachwitz, Energy Dependent Width Effects in  $e^+e^-$  Annihilation Near the  $Z$  Boson Pole, *Phys. Lett. B* 206 (1988) 539–542. [doi:10.1016/0370-2693\(88\)91625-5](https://doi.org/10.1016/0370-2693(88)91625-5).
- [80] D. Y. Bardin, M. S. Bilenky, A. Chizhov, A. Sazonov, Y. Sedykh, T. Riemann, M. Sachwitz, The convolution integral for the forward - backward asymmetry in  $e^+e^-$  annihilation, *Phys. Lett. B* 229 (1989) 405, <http://cds.cern.ch/record/198110/files/198906505.pdf?version=1>. [doi:10.1016/0370-2693\(89\)90428-0](https://doi.org/10.1016/0370-2693(89)90428-0).
- [81] D. Bardin, M. Bilenky, G. Mitselmakher, T. Riemann, M. Sachwitz, A Realistic Approach to the Standard  $Z$  Peak, *Z. Phys. C* 44 (1989) 493, <https://lib-extopc.kek.jp/preprints/PDF/1989/8906/8906215.pdf>. [doi:10.1007/BF01415565](https://doi.org/10.1007/BF01415565).
- [82] D. Y. Bardin, M. S. Bilenky, A. Chizhov, A. Sazonov, O. Fedorenko, T. Riemann, M. Sachwitz, Analytic approach to the complete set of QED corrections to fermion pair production in  $e^+e^-$  annihilation, *Nucl. Phys. B* 351 (1991) 1–48. [arXiv:hep-ph/9801208](https://arxiv.org/abs/hep-ph/9801208), [doi:10.1016/0550-3213\(91\)90080-H](https://doi.org/10.1016/0550-3213(91)90080-H).
- [83] D. Bardin, M. Bilenky, A. Sazonov, Y. Sedykh, T. Riemann, M. Sachwitz, QED corrections with partial angular integration to fermion pair production in  $e^+e^-$  annihilation, *Phys. Lett. B* 255 (1991) 290–296. [arXiv:hep-ph/9801209](https://arxiv.org/abs/hep-ph/9801209), [doi:10.1016/0370-2693\(91\)90250-T](https://doi.org/10.1016/0370-2693(91)90250-T).

- [84] D. Bardin, M. Bilenky, A. Chizhov, O. Fedorenko, S. Ganguli, A. Gurtu, M. Lokajicek, G. Mitselmakher, A. Olshevsky, J. Ridky, S. Riemann, T. Riemann, M. Sachwitz, A. Sazonov, A. Schaile, Y. Sedykh, I. Sheer, L. Vertogradov, ZFITTER: An analytical program for fermion pair production in  $e^+e^-$  annihilation, <http://cds.cern.ch/record/265101/files/th-6443-92.ps.gz?version=1> (1992, preprint CERN/TH. 6443). arXiv:hep-ph/9412201.
- [85] P. C. Christova, M. Jack, T. Riemann, Hard photon emission in  $e^+e^- \rightarrow \bar{f}f$  with realistic cuts, Phys. Lett. B456 (1999) 264–269. arXiv:hep-ph/9902408, doi:10.1016/S0370-2693(99)00528-6.
- [86] A. Akhundov, A. Arbuzov, S. Riemann, T. Riemann, The ZFITTER project, Phys. Part. Nucl. 45 (3) (2014) 529–549. arXiv:1302.1395, doi:10.1134/S1063779614030022.
- [87] The ZFITTER homepage, <http://sanc.jinr.ru/users/zfitter>.
- [88] ALEPH collab., DELPHI collab., L3 collab., OPAL collab., LEP Electroweak Working Group, S. Schael, et al., Electroweak Measurements in Electron-Positron Collisions at W-Boson-Pair Energies at LEP, Phys. Rept. 532 (2013) 119–244. arXiv:1302.3415, doi:10.1016/j.physrep.2013.07.004.
- [89] C. Patrignani, et al., Review of Particle Physics, Chin. Phys. C40 (10) (2016) 100001, update by M. Grünewald and A. Gurtu, *The Z boson* (1 Oct 2016, 19:58), <http://pdg.lbl.gov/2016/reviews/rpp2016-rev-z-boson.pdf>. doi:10.1088/1674-1137/40/10/100001.
- [90] R. Tenchini, "EW measurements at FCC", talk held at the FCC weak 2018, 9-13 April 2018, Amsterdam. [https://indico.cern.ch/event/656491/contributions/2945302/attachments/1630715/2599367/FCC-EWK\\_Amsterdam2018.pdf](https://indico.cern.ch/event/656491/contributions/2945302/attachments/1630715/2599367/FCC-EWK_Amsterdam2018.pdf).
- [91] M. Greco, G. Pancheri-Srivastava, Y. Srivastava, Radiative corrections for colliding beam resonances, Nucl. Phys. B101 (1975) 234–262. doi:10.1016/0550-3213(75)90304-1.
- [92] G. Bonneau, F. Martin, Hard photon emission in  $e^+e^-$  reactions, Nucl. Phys. B27 (1971) 381–397. doi:10.1016/0550-3213(71)90102-7.
- [93] G. Montagna, F. Piccinini, O. Nicrosini, G. Passarino, R. Pittau, TOPAZ0: A Program for computing observables and for fitting cross-sections and forward - backward asymmetries around the  $Z^0$  peak, Comput. Phys. Commun. 76 (1993) 328–360. doi:10.1016/0010-4655(93)90060-P.
- [94] G. Montagna, O. Nicrosini, G. Passarino, F. Piccinini, TOPAZO 2.0: A Program for computing deconvoluted and realistic observables around the  $Z^0$  peak, Comput. Phys. Commun. 93 (1996) 120–126. arXiv:hep-ph/9506329, doi:10.1016/0010-4655(95)00127-1.
- [95] G. Montagna, O. Nicrosini, F. Piccinini, G. Passarino, TOPAZO 4.0: A new version of a computer program for evaluation of deconvoluted and realistic observables at LEP-1 and LEP-2, Comput. Phys. Commun. 117 (1999) 278–289. arXiv:hep-ph/9804211, doi:10.1016/S0010-4655(98)00080-0.
- [96] M. Bilenky, A. Sazonov, QED corrections at  $Z^0$  pole with realistic kinematical cuts, unpublished JINR preprint E2-89-792 (1989). <https://lib-extopc.kek.jp/preprints/PDF/1990/9003/9003360.pdf>.
- [97] M. A. Jack, Semianalytical calculation of QED radiative corrections to  $e^+e^- \rightarrow \bar{f}f$  with special emphasis on kinematical cuts to the final state. DESY-THESIS-2000-030. arXiv:hep-ph/0009068.
- [98] J. Fleischer, A. Leike, T. Riemann, A. Werthenbach, Electroweak one loop corrections for  $e^+e^-$  annihilation into  $t\bar{t}$  including hard bremsstrahlung, Eur. Phys. J. C31 (2003) 37. arXiv:hep-ph/0302259, doi:10.1140/epjc/s2003-01263-8.
- [99] D. Y. Bardin, L. Kalinovskaya, G. Nanava, An electroweak library for the calculation of EWRC to  $e^+e^- \rightarrow f\bar{f}$  within the tofit project. arXiv:hep-ph/0012080.
- [100] J. Fleischer, J. Fujimoto, T. Ishikawa, A. Leike, T. Riemann, Y. Shimizu, A. Werthenbach, One loop corrections to the process  $e^+e^- \rightarrow t\bar{t}$  including hard bremsstrahlung, in: Y. Kurihara (ed.), Second



- Symposium on Computational Particle Physics (CPP, Tokyo, 28–30 Nov 2001), KEK Proceedings 2002-11 (2002), p. 153. [arXiv:hep-ph/0203220](#).
- [101] J. Fleischer, A. Leike, T. Riemann, A. Werthenbach, fortran program `topfit.F` 0.91 (06 March 2002), <https://www-zeuthen.desy.de/~riemann/doc/topfit/topfit.html>.
- [102] J. Fleischer, A. Leike, A. Lorca, T. Riemann, A. Werthenbach, fortran program `topfit.F` 0.92 (01 July 2003), <https://www-zeuthen.desy.de/~riemann/doc/topfit/topfit.html>.
- [103] T. Hahn, W. Hollik, A. Lorca, T. Riemann, A. Werthenbach,  $O(\alpha)$  electroweak corrections to the processes  $e^+e^- \rightarrow \tau^-\tau^+$ ,  $c\bar{c}$ ,  $b\bar{b}$ ,  $t\bar{t}$ : A comparison. <http://www-flc.desy.de/lcnotes/notes/LC-TH-2003-083.pdf>. [arXiv:hep-ph/0307132](#).
- [104] J. Gluza, A. Lorca, T. Riemann, Automated use of DIANA for two-fermion production at colliders, Nucl. Instrum. Meth. A534 (2004) 289–292. [arXiv:hep-ph/0409011](#), doi:10.1016/j.nima.2004.07.103.
- [105] A. Lorca, T. Riemann, Automated calculations for massive fermion production with aiTALC, Nucl. Phys. Proc. Suppl. 135 (2004) 328. [arXiv:hep-ph/0407149](#).
- [106] A. Lorca, T. Riemann, An Integrated tool for loop calculations: aiTALC, Comput. Phys. Commun. 174 (2006) 71–82. [arXiv:hep-ph/0412047](#), doi:10.1016/j.cpc.2005.09.003.
- [107] J. Fleischer, J. Gluza, A. Lorca, T. Riemann, First order radiative corrections to Bhabha scattering in d dimensions, Eur. J. Phys. 48 (2006) 35–52. [arXiv:hep-ph/0606210](#), doi:10.1140/epjc/s10052-006-0008-6.
- [108] A. Sirlin, Radiative Corrections in the  $SU(2)_L \times U(1)$  Theory: A Simple Renormalization Framework, Phys. Rev. D22 (1980) 971–981. doi:10.1103/PhysRevD.22.971.
- [109] D. Yu. Bardin, M. Grünewald, G. Passarino, Precision calculation project report. [arXiv:hep-ph/9902452](#).
- [110] W. J. Marciano, A. Sirlin, Radiative Corrections to Neutrino Induced Neutral Current Phenomena in the  $SU(2)_L \times U(1)$  Theory, Phys. Rev. D22 (1980) 2695. doi:10.1103/PhysRevD.22.2695.
- [111] T. Teubner, K. Hagiwara, R. Liao, A. Martin, D. Nomura,  $g-2$  and  $\alpha(M_Z^2)$ : Status of the standard model predictions, Nucl. Phys. Proc. Suppl. 225-227 (2012) 282–287. doi:10.1016/j.nuclphysbps.2012.02.059.
- [112] M. Davier, A. Hoecker, B. Malaescu, Z. Zhang, Reevaluation of the hadronic vacuum polarisation contributions to the Standard Model predictions of the muon  $g-2$  and  $\alpha(m_Z^2)$  using newest hadronic cross-section data, Eur. Phys. J. C77 (12) (2017) 827. [arXiv:1706.09436](#), doi:10.1140/epjc/s10052-017-5161-6.
- [113] F. Jegerlehner, Variations on Photon Vacuum Polarization [arXiv:1711.06089](#).
- [114] A. Keshavarzi, D. Nomura, T. Teubner, The muon  $g-2$  and  $\alpha(M_Z^2)$ : a new data-based analysis, Phys. Rev. D97 (11) (2018) 114025. [arXiv:1802.02995](#), doi:10.1103/PhysRevD.97.114025.
- [115] D. Bardin, C. Burdik, P. Khristova, T. Riemann, Electroweak radiative corrections to deep inelastic scattering at HERA. Neutral current scattering, Z. Phys. C42 (1989) 679, <https://lib-extopc.kek.jp/preprints/PDF/1989/8904/8904210.pdf>. doi:10.1007/BF01557676.
- [116] D. Y. Bardin, P. K. Khristova, O. Fedorenko, On the Lowest Order Electroweak Corrections to Spin 1/2 Fermion Scattering. 2. The One Loop Amplitudes, Nucl. Phys. B197 (1982) 1. doi:10.1016/0550-3213(82)90152-3.
- [117] D. Bardin, P. Khristova, O. Fedorenko, On the lowest order electroweak corrections to spin 1/2 fermion scattering. 1. The one loop diagrammar, Nucl. Phys. B175 (1980) 435. doi:10.1016/0550-3213(80)90021-8.
- [118] A. Borrelli, M. Consoli, L. Maiani, R. Sisto, Model independent analysis of the  $Z$  line shape in  $e^+e^-$  annihilation, Nucl. Phys. B333 (1990) 357. doi:10.1016/0550-3213(90)90042-C.
- [119] R. G. Stuart, Gauge invariance, analyticity and physical observables at the  $Z^0$  resonance, Phys. Lett.

- B262 (1991) 113–119. doi:10.1016/0370-2693(91)90653-8.
- [120] R. G. Stuart, General renormalization of the gauge invariant perturbation expansion near the  $Z^0$  resonance, Phys. Lett. B272 (1991) 353–358. doi:10.1016/0370-2693(91)91842-J.
  - [121] S. Kirsch, T. Riemann, SMATASY: A program for the model independent description of the  $Z$  resonance, Comput. Phys. Commun. 88 (1995) 89–108. arXiv:hep-ph/9408365, doi:10.1016/0010-4655(95)00016-9.
  - [122] T. Riemann, S-matrix Approach to the  $Z$  Resonance, Acta Phys. Polon. B46 (11) (2015) 2235. arXiv:1610.04501, doi:10.5506/APhysPolB.46.2235.
  - [123] S. Willenbrock, G. Valencia, On the definition of the  $Z$  boson mass, Phys. Lett. B259 (1991) 373–376. doi:10.1016/0370-2693(91)90843-F.
  - [124] A. Sirlin, Theoretical considerations concerning the  $Z^0$  mass, Phys. Rev. Lett. 67 (1991) 2127–2130. doi:10.1103/PhysRevLett.67.2127.
  - [125] H. G. J. Veltman, Mass and width of unstable gauge bosons, Z. Phys. C62 (1994) 35–52. doi:10.1007/BF01559523.
  - [126] M. Passera, A. Sirlin, Radiative corrections to  $W$  and quark propagators in the resonance region, Phys. Rev. D58 (1998) 113010. arXiv:hep-ph/9804309, doi:10.1103/PhysRevD.58.113010.
  - [127] P. Gambino, P. A. Grassi, The Nielsen identities of the SM and the definition of mass, Phys. Rev. D62 (2000) 076002. arXiv:hep-ph/9907254, doi:10.1103/PhysRevD.62.076002.
  - [128] A. R. Böhm, N. L. Harshman, On the mass and width of the  $Z$  boson and other relativistic quasistable particles, Nucl. Phys. B581 (2000) 91–115. arXiv:hep-ph/0001206, doi:10.1016/S0550-3213(00)00249-2.
  - [129] M. Grünewald, S. Kirsch, T. Riemann, Fortran package SMATASY 6.42 (2 June 2005). [http://www.cern.ch/Martin.Grunewald/afs/public/smatasy/smata6\\_42.fortran](http://www.cern.ch/Martin.Grunewald/afs/public/smatasy/smata6_42.fortran).
  - [130] R. N. Cahn, Analytic forms for the  $e^+e^-$  annihilation cross-section near the  $Z$  including initial state radiation, Phys. Rev. D36 (1987) 2666, [Erratum: Phys. Rev.D40,922(1989)]. doi:10.1103/PhysRevD.36.2666, 10.1103/PhysRevD.40.922.
  - [131] G. Alexander, et al., A precise measurement of the tau polarization and its forward - backward asymmetry at LEP, Z. Phys. C72 (1996) 365–375. doi:10.1007/s002880050257.
  - [132] S. Riemann, Precision electroweak physics at high energies, Rept. Prog. Phys. 73 (2010) 126201. doi:10.1088/0034-4885/73/12/126201.
  - [133] A. Freitas, Two-loop fermionic electroweak corrections to the  $Z$ -boson width and production rate, Phys. Lett. B730 (2014) 50–52. arXiv:1310.2256, doi:10.1016/j.physletb.2014.01.017.
  - [134] F. Jegerlehner, Precision tests of electroweak interaction parameters, In: R. Manka, M. Zralek (eds.), proceedings of the 11th Int. School of Theoretical Physics, Testing the standard model, Szczyrk, Poland, Sep 18-22, 1987 (Singapore, World Scientific, 1988), pp. 33-108, Bielefeld preprint BI-TP-87/16, <https://lib-extopc.kek.jp/preprints/PDF/1988/8801/8801263.pdf>.
  - [135] J. Bernabeu, A. Pich, A. Santamaria,  $\Gamma(Z \rightarrow b\bar{b})$ : A signature of hard mass terms for a heavy top, Phys. Lett. B200 (1988) 569–574. doi:10.1016/0370-2693(88)90173-6.
  - [136] W. Beenakker, W. Hollik, The width of the  $Z$  Boson, Z. Phys. C40 (1988) 141. doi:10.1007/BF01559728.
  - [137] M. Awramik, M. Czakon, A. Freitas, G. Weiglein, Complete two-loop electroweak fermionic corrections to  $\sin^2\theta_{\text{eff}}^{\text{lept}}$  and indirect determination of the Higgs boson mass, Phys. Rev. Lett. 93 (2004) 201805. arXiv:hep-ph/0407317, doi:10.1103/PhysRevLett.93.201805.
  - [138] A. Freitas, Y.-C. Huang, Electroweak two-loop corrections to  $\sin^2\theta_{\text{eff}}^{b\bar{b}}$  and  $R_b$  using numerical Mellin-Barnes integrals, JHEP 1208 (2012) 050. arXiv:1205.0299, doi:10.1007/JHEP08(2012)050.
  - [139] A. R. Böhm, Y. Sato, Relativistic resonances: Their masses, widths, lifetimes, superposition, and

- causal evolution, Phys. Rev. D71 (2005) 085018. arXiv:hep-ph/0412106, doi:10.1103/PhysRevD.71.085018.
- [140] A. A. Penin, Two-loop corrections to Bhabha scattering, Phys. Rev. Lett. 95 (2005) 010408. arXiv:hep-ph/0501120, doi:10.1103/PhysRevLett.95.010408.
- [141] A. Penin, Two-loop photonic corrections to massive Bhabha scattering, Nucl. Phys. B734 (2006) 185–202. arXiv:hep-ph/0508127, doi:10.1016/j.nuclphysb.2005.11.016.
- [142] J. H. Kühn, S. Moch, A. A. Penin, V. A. Smirnov, Next-to-next-to-leading logarithms in four-fermion electroweak processes at high energy, Nucl. Phys. B616 (2001) 286–306. arXiv:hep-ph/0106298, doi:10.1016/S0550-3213(01)00454-0.
- [143] S. Jadach, B. F. L. Ward, Z. Was, Coherent exclusive exponentiation CEEX: The Case of the resonant  $e^+e^-$  collision, Phys. Lett. B449 (1999) 97–108. arXiv:hep-ph/9905453, doi:10.1016/S0370-2693(99)00038-6.
- [144] S. Jadach, B. Ward, Z. Was, Coherent exclusive exponentiation for precision Monte Carlo calculations, Phys. Rev. D63 (2001) 113009. arXiv:hep-ph/0006359, doi:10.1103/PhysRevD.63.113009.
- [145] M. Greco, G. Pancheri-Srivastava, Y. Srivastava, Radiative Effects for Resonances with Applications to Colliding Beam Processes, Phys. Lett. B56 (1975) 367–372. doi:10.1016/0370-2693(75)90321-4.
- [146] M. Greco, A. F. Grillo, Radiative asymmetry in  $e^+e^- \rightarrow \mu^+\mu^-$  near a narrow resonance with polarized beams, Lett. Nuovo Cim. 15 (1976) 174. doi:10.1007/BF02727477.
- [147] M. Greco, G. Pancheri-Srivastava, Y. Srivastava, Radiative corrections to  $e^+e^- \rightarrow \mu^+\mu^-$  around the  $Z^0$ , Nucl. Phys. B171 (1980) 118, [Erratum: Nucl. Phys. B197,543(1982)]. doi:10.1016/0550-3213(82)90458-8, 10.1016/0550-3213(80)90363-6.
- [148] M. Consoli, M. Greco, S. Lo Presti, Bhabha scattering around the  $Z^0$  pole, Phys. Lett. 113B (1982) 415. doi:10.1016/0370-2693(82)90776-6.
- [149] M. Greco, Bhabha scattering near the  $Z^{(0)}$ , Phys. Lett. B177 (1986) 97–105. doi:10.1016/0370-2693(86)90023-7.
- [150] O. Nicrosini, L. Trentadue, Soft photons and second order radiative corrections to  $e^+e^- \rightarrow Z^0$ , Phys. Lett. B196 (1987) 551. doi:10.1016/0370-2693(87)90819-7.
- [151] O. Nicrosini, L. Trentadue, Second order electromagnetic radiative corrections to  $e^+e^- \rightarrow \gamma^*, Z^0 \rightarrow \mu^+\mu^-$ , Z. Phys. C39 (1988) 479. doi:10.1007/BF01555976.
- [152] F. Aversa, M. Greco, Hard photon corrections to Bhabha scattering near the  $Z^0$ , Phys. Lett. B271 (1991) 435–439. doi:10.1016/0370-2693(91)90114-6.
- [153] V. S. Fadin, E. A. Kuraev, L. N. Lipatov, N. P. Merenkov, L. Trentadue, Small angle Bhabha scattering: Two loop approximation, JINR-E2-92-577.
- [154] V. S. Fadin, E. A. Kuraev, L. Lipatov, N. P. Merenkov, L. Trentadue, Forward per mille Bhabha scattering. Prepared for Tennessee International Symposium on Radiative Corrections: Status and Outlook, Gatlinburg, TN, 27 Jun - 1 Jul 1994.
- [155] T. Hahn, Generating Feynman diagrams and amplitudes with FeynArts 3, Comput. Phys. Commun. 140 (2001) 418–431. arXiv:hep-ph/0012260.
- [156] B. Chokoufe Nejad, T. Hahn, J. N. Lang, E. Mirabella, FormCalc 8: Better Algebra and Vectorization, J. Phys. Conf. Ser. 523 (2014) 012050. arXiv:1310.0274, doi:10.1088/1742-6596/523/1/012050.
- [157] G. Ossola, C. G. Papadopoulos, R. Pittau, CutTools: A Program implementing the OPP reduction method to compute one-loop amplitudes, JHEP 03 (2008) 042. arXiv:0711.3596, doi:10.1088/1126-6708/2008/03/042.
- [158] C. F. Berger, Z. Bern, L. J. Dixon, F. Febres Cordero, D. Forde, H. Ita, D. A. Kosower, D. Maitre,

- An Automated Implementation of On-Shell Methods for One-Loop Amplitudes, *Phys. Rev. D* **78** (2008) 036003. [arXiv:0803.4180](#), [doi:10.1103/PhysRevD.78.036003](#).
- [159] A. Kanaki, C. G. Papadopoulos, HELAC: A Package to compute electroweak helicity amplitudes, *Comput. Phys. Commun.* **132** (2000) 306–315. [arXiv:hep-ph/0002082](#), [doi:10.1016/S0010-4655\(00\)00151-X](#).
  - [160] A. van Hameren, C. G. Papadopoulos, R. Pittau, Automated one-loop calculations: A Proof of concept, *JHEP* **09** (2009) 106. [arXiv:0903.4665](#), [doi:10.1088/1126-6708/2009/09/106](#).
  - [161] P. Mastrolia, G. Ossola, T. Reiter, F. Tramontano, Scattering AMplitudes from Unitarity-based Reduction Algorithm at the Integrand-level, *JHEP* **08** (2010) 080. [arXiv:1006.0710](#), [doi:10.1007/JHEP08\(2010\)080](#).
  - [162] V. Hirschi, R. Frederix, S. Frixione, M. V. Garzelli, F. Maltoni, R. Pittau, Automation of one-loop QCD corrections, *JHEP* **05** (2011) 044. [arXiv:1103.0621](#), [doi:10.1007/JHEP05\(2011\)044](#).
  - [163] G. Cullen, N. Greiner, G. Heinrich, G. Luisoni, P. Mastrolia, G. Ossola, T. Reiter, F. Tramontano, Automated One-Loop Calculations with GoSam, *Eur. Phys. J. C* **72** (2012) 1889. [arXiv:1111.2034](#), [doi:10.1140/epjc/s10052-012-1889-1](#).
  - [164] F. Cascioli, P. Maierhofer, S. Pozzorini, Scattering Amplitudes with Open Loops, *Phys. Rev. Lett.* **108** (2012) 111601. [arXiv:1111.5206](#), [doi:10.1103/PhysRevLett.108.111601](#).
  - [165] S. Actis, A. Denner, L. Hofer, J.-N. Lang, A. Scharf, S. Uccirati, RECOLA: REcursive Computation of One-Loop Amplitudes, *Comput. Phys. Commun.* **214** (2017) 140–173. [arXiv:1605.01090](#), [doi:10.1016/j.cpc.2017.01.004](#).
  - [166] J. Fleischer, J. Gluza, K. Kajda, T. Riemann, Pentagon diagrams of Bhabha scattering, *Acta Phys. Polon. B* **38** (2007) 3529–3536, [http://www.actaphys.uj.edu.pl/\\_cur/store/vol38/pdf/v38p3529.pdf](http://www.actaphys.uj.edu.pl/_cur/store/vol38/pdf/v38p3529.pdf). [arXiv:0710.5100](#).
  - [167] T. Diakonidis, J. Fleischer, J. Gluza, K. Kajda, T. Riemann, J. B. Tausk, A Complete reduction of one-loop tensor 5 and 6-point integrals, *Phys. Rev. D* **80** (2009) 036003. [arXiv:0812.2134](#), [doi:10.1103/PhysRevD.80.036003](#).
  - [168] J. Fleischer, T. Riemann, A Complete algebraic reduction of one-loop tensor Feynman integrals, *Phys. Rev. D* **83** (2011) 073004. [arXiv:1009.4436](#), [doi:10.1103/PhysRevD.83.073004](#).
  - [169] J. Fleischer, T. Riemann, V. Yundin, New developments in PJFry, *PoS LL2012* (2012) 020, [http://pos.sissa.it/...151/020/LL2012\\_020.pdf](http://pos.sissa.it/...151/020/LL2012_020.pdf). [arXiv:1210.4095](#).
  - [170] J. Fleischer, T. Riemann, V. Yundin, PJFry: A C++ package for tensor reduction of one-loop Feynman integrals. In: [539], preprint DESY 11-252 (2011). <http://www-library.desy.de/cgi-bin/showprep.pl?desy11-252>.
  - [171] V. Yundin, C++ package PJFry. Available at <https://github.com/Vayu/PJFry/>.
  - [172] A. Denner, S. Dittmaier, L. Hofer, Collier: a fortran-based Complex One-Loop Library in Extended Regularizations, *Comput. Phys. Commun.* **212** (2017) 220–238. [arXiv:1604.06792](#), [doi:10.1016/j.cpc.2016.10.013](#).
  - [173] J. A. Maestre, S. Alioli, J. Andersen, R. Ball, A. Buckley, et al., The SM and NLO Multileg and SM MC Working Groups: Summary Report. [arXiv:1203.6803](#).
  - [174] S. Actis, et al., Quest for precision in hadronic cross sections at low energy: Monte Carlo tools vs. experimental data, *Eur. Phys. J. C* **66** (2010) 585–686. [arXiv:0912.0749](#), [doi:10.1140/epjc/s10052-010-1251-4](#).
  - [175] C. Carloni Calame, H. Czyz, J. Gluza, M. Gunia, G. Montagna, O. Nicrosini, F. Piccinini, T. Riemann, M. Worek, NNLO leptonic and hadronic corrections to Bhabha scattering and luminosity monitoring at meson factories, *JHEP* **07** (2011) 126. [arXiv:1106.3178](#), [doi:10.1007/JHEP07\(2011\)126](#).
  - [176] C. M. Carloni Calame, H. Czyz, J. Gluza, M. Gunia, G. Montagna, O. Nicrosini, F. Piccinini,

- T. Riemann, M. Worek, NNLO massive corrections to Bhabha scattering and theoretical precision of BabaYaga@NLO, Nucl. Phys. Proc. Suppl. 225-227 (2012) 293–297. arXiv:1112.2851, doi:10.1016/j.nuclphysbps.2012.02.061.
- [177] F. Campanario, H. Czyż, J. Gluza, M. Gunia, T. Riemann, G. Rodrigo, V. Yundin, Complete QED NLO contributions to the reaction  $e^+e^- \rightarrow \mu^+\mu^-\gamma$  and their implementation in the event generator PHOKHARA, JHEP 1402 (2014) 114. arXiv:1312.3610, doi:10.1007/JHEP02(2014)114.
- [178] J. Gluza, M. Gunia, T. Riemann, M. Worek, Theoretical Improvements for Luminosity Monitoring at Low Energies[PoSRADCOR2011,034(2011)]. arXiv:1201.0968.
- [179] T. Becher, K. Melnikov, Two-loop QED corrections to Bhabha scattering, JHEP 06 (2007) 084. arXiv:0704.3582[hep-ph].
- [180] R. Bonciani, A. Ferroglia, P. Mastrolia, E. Remiddi, J. van der Bij, Two-loop  $N_f = 1$  QED Bhabha scattering differential cross section, Nucl. Phys. B701 (2004) 121–179. arXiv:hep-ph/0405275.
- [181] S. Actis, M. Czakon, J. Gluza, T. Riemann, Two-Loop Fermionic Corrections to Massive Bhabha Scattering, Nucl. Phys. B786 (2007) 26–51. arXiv:0704.2400v2, doi:10.1016/j.nuclphysb.2007.06.023.
- [182] S. Actis, M. Czakon, J. Gluza, T. Riemann, Fermionic NNLO contributions to Bhabha scattering, Acta Phys. Polon. B38 (2007) 3517–3528, <http://www.actaphys.uj.edu.pl/.vol38/.v38p3517.pdf>. arXiv:0710.5111[hep-ph].
- [183] S. Actis, M. Czakon, J. Gluza, T. Riemann, Virtual hadronic and leptonic contributions to Bhabha scattering, Phys. Rev. Lett. 100 (2008) 131602. arXiv:0711.3847, doi:10.1103/PhysRevLett.100.131602.
- [184] R. Bonciani, Electroweak corrections to Higgs production and decay, J. Phys. Conf. Ser. 110 (2008) 042004. doi:10.1088/1742-6596/110/4/042004.
- [185] R. Bonciani, A. Ferroglia, A. Penin, Calculation of the Two-Loop Heavy-Flavor Contribution to Bhabha Scattering, JHEP 0802 (2008) 080. arXiv:0802.2215, doi:10.1088/1126-6708/2008/02/080.
- [186] S. Actis, M. Czakon, J. Gluza, T. Riemann, Virtual Hadronic and Heavy-Fermion  $O(\alpha^2)$  Corrections to Bhabha Scattering, Phys. Rev. D78 (2008) 085019. arXiv:0807.4691, doi:10.1103/PhysRevD.78.085019.
- [187] J. H. Kühn, S. Uccirati, Two-loop QED hadronic corrections to Bhabha scattering, Nucl. Phys. B806 (2009) 300–326. arXiv:0807.1284, doi:10.1016/j.nuclphysb.2008.08.002.
- [188] S. Jadach, M. Skrzypek, M. Martinez, Light pair corrections to the Z line shape parameters, Phys. Lett. B280 (1992) 129–136.
- [189] S. Jadach, S. Yost, QED interference in charge asymmetry near the Z resonance at future electron-positron collidersPreprint IFJPAN-IV-2017-11. arXiv:1801.08611.
- [190] S. Jadach, B. Pietrzyk, E. Tournefier, B. F. L. Ward, Z. Was, Initial final state interference in the Z line shape, Phys. Lett. B465 (1999) 254–259. arXiv:hep-ph/9907547, doi:10.1016/S0370-2693(99)01047-3.
- [191] S. Jadach, B. F. L. Ward, Z. Was, Coherent exclusive exponentiation (ceex) the case of resonant  $e^+e^-$  annihilation, Phys. Lett. B449 (1999) 97–108. arXiv:hep-ph/9905453.
- [192] D. R. Yennie, S. C. Frautschi, H. Suura, The infrared divergence phenomena and high-energy processes, Ann. Phys. 13 (1961) 379–452.
- [193] A. Akhundov, A. Arbuzov, S. Riemann, T. Riemann, The ZFITTER project, Phys. Part. Nucl. 45 (2014) 529–549. arXiv:1302.1395, doi:10.1134/S1063779614030022.
- [194] Former ZFITTER homepage (20 June 2013 till March 2014), documentation, <http://zfitter.com>.
- [195] The ZFITTER homepage (since 5 April 2014), <http://zfitter.education>.
- [196] Conference CALC2018, JINR, Dubna, Russia, August 2018, <https://indico.jinr.ru/>

- conferenceDisplay.py?ovw=True&confId=418.
- [197] T. Riemann, *A legacy of Dima Bardin: ZFITTER and the future*, talk held at the conference CALC2018, JINR, Dubna, Russia, August 2018, <https://indico.jinr.ru/getFile.py/access?contribId=19&sessionId=0&resId=0&materialId=slides&confId=418>.
  - [198] D. Y. Bardin, P. K. Khristova, O. M. Fedorenko, On the lowest order electroweak corrections to spin 1/2 fermion scattering. 2. the one loop amplitudes, Nucl. Phys. B197 (1982) 1.
  - [199] D. Bardin, S. Riemann, T. Riemann, Electroweak one loop corrections to the decay of the charged vector boson, Z. Phys. C32 (1986) 121, <https://lib-extopc.kek.jp/preprints/PDF/1986/8607/8607019.pdf>. doi:10.1007/BF01441360.
  - [200] H. Dosch, C. Scherf, webpage “DESY - Fall Zfitter/Gfitter- Stellungnahme DESY Direktorium zum Fall ZFITTER/GFitter” (22 March 2014, in German, <http://zfitter-gfitter.desy.de>). The ZFITTER authors do not share all statements of the webpage. The website’s copyright does not allow to publish an English translation (DESY, private communication, 6 July 2014).
  - [201] D. Bardin, et al., ZFITTER 6.21: A semi-analytical program for fermion pair production in  $e^+e^-$  annihilation, Comput. Phys. Commun. 133 (2001) 229–395. arXiv:hep-ph/9908433.
  - [202] T. Aushev, W. Bartel, A. Bondar, J. Brodzicka, T. Browder, et al., Physics at Super B Factory. <http://belle2.kek.jp/physics.html>. arXiv:1002.5012.
  - [203] T. Ferber, Towards First Physics at Belle II. Talk at Spring Conference of DPG, 9-13 March 2015, Wuppertal, Germany. [http://www.staff.uni-giessen.de/~gd1472/belle/dpg2015\\_torbenferber.pdf](http://www.staff.uni-giessen.de/~gd1472/belle/dpg2015_torbenferber.pdf).
  - [204] J. van der Bij, H. Czyż, S. Eidelman, G. Fedotovitch, T. Ferber, et al., Mini-Proceedings, 15th meeting of the Working Group on Rad. Corrections and MC Generators for Low Energies. arXiv:1406.4639.
  - [205] O. Fedorenko, T. Riemann, Analytic bremsstrahlung integration for the process  $e^+e^- \rightarrow \mu^+\mu^-\gamma$  in QED, Acta Phys. Polon. B18 (1987) 761, [http://www.actaphys.uj.edu.pl/\\_old/vol18/pdf/v18p0761.pdf](http://www.actaphys.uj.edu.pl/_old/vol18/pdf/v18p0761.pdf).
  - [206] R. G. Stuart, Gauge invariant perturbation theory near a gauge resonance, in: Workshop on High-energy Phenomenology (CINVESTAV) Mexico City, Mexico, July 1-10, 1991, 1991, pp. 0331–341, <https://lib-extopc.kek.jp/preprints/PDF/1992/9201/9201503.pdf>.
  - [207] R. G. Stuart, The Structure of the  $Z^0$  resonance and the physical properties of the  $Z^0$  boson, Phys. Rev. Lett. 70 (1993) 3193–3196. doi:10.1103/PhysRevLett.70.3193.
  - [208] R. G. Stuart, Production cross-sections for unstable particles, Nucl. Phys. B498 (1997) 28–38. arXiv:hep-ph/9504215, doi:10.1016/S0550-3213(97)00276-9.
  - [209] O. Adriani, et al., An S matrix analysis of the Z resonance, Phys. Lett. B315 (1993) 494–502. doi:10.1016/0370-2693(93)91646-5.
  - [210] ALEPH collab., D. Buskulic, et al., Measurement of hadron and lepton pair production from  $e^+e^-$  annihilation at center-of-mass energies of 130 GeV and 136 GeV, Phys. Lett. B378 (1996) 373–384. doi:10.1016/0370-2693(96)00504-7.
  - [211] OPAL collab., G. Abbiendi, et al., Precise determination of the Z resonance parameters at LEP: ‘Zedometry’, Eur. Phys. J. C19 (2001) 587–651. arXiv:hep-ex/0012018, doi:10.1007/s100520100627.
  - [212] K. Sachs, Standard model at LEP II, Proc. of XXXVIII Rencontres de Moriond: Electroweak Interactions and Unified Theories, Les Arcs, March 15-22, 2003. arXiv:hep-ex/0307009.
  - [213] P. Holt, Fermion pair production above the  $Z^0$  resonance, PoS HEP2001 (2001) 115. [http://pos.sissa.it/archive/conferences/007/115/hep2001\\_115.pdf](http://pos.sissa.it/archive/conferences/007/115/hep2001_115.pdf).
  - [214] VENUS collab., K. Yusa, et al., Precise measurement of the total hadronic cross-section in  $e^+e^-$  annihilation at  $\sqrt{s} = 57.77$  GeV, Phys. Lett. B447 (1999) 167–177. doi:10.1016/S0370-2693(98)

01560-3.

- [215] TOPAZ collab., K. Miyabayashi, et al., Measurement of the total hadronic cross-section and determination of  $\gamma Z$  interference in  $e^+e^-$  annihilation, Phys. Lett. B347 (1995) 171-178. doi:10.1016/0370-2693(95)00038-M.
- [216] A. Leike, S. Riemann, T. Riemann,  $Z Z'$  mixing and radiative corrections at LEP-1, Phys. Lett. B291 (1992) 187-194. arXiv:hep-ph/9507436, doi:10.1016/0370-2693(92)90142-Q.
- [217] D. Bardin, O. Fedorenko, T. Riemann, The electromagnetic  $\alpha^3$  contributions to  $e^+e^-$  annihilation into fermions in the electroweak theory: Total cross-section  $\sigma_T$  and integrated asymmetry  $A_{FB}$ . Unpublished JINR preprint E2-87-663 (1988). <https://lib-extopc.kek.jp/preprints/PDF/1988/8801/8801179.pdf>.
- [218] D. Bardin, M. Bilenky, O. Fedorenko, T. Riemann, The electromagnetic  $\alpha^3$  contributions to  $e^+e^-$  annihilation into fermions in the electroweak theory: Total cross-section  $\sigma_T$  and integrated asymmetry  $A_{FB}$ . Unpublished JINR preprint E2-88-324 (1988). <https://lib-extopc.kek.jp/preprints/PDF/1988/8808/8808103.pdf>.
- [219] F. A. Berends, R. Kleiss, S. Jadach, Radiative corrections to muon pair and quark pair production in electron-positron collisions in the  $Z^0$  region, Nucl. Phys. B202 (1982) 63-88. doi:10.1016/0550-3213(82)90221-8.
- [220] F. A. Berends, R. Kleiss, S. Jadach, Monte Carlo Simulation of Radiative Corrections to the Processes  $e^+e^- \rightarrow \mu^+\mu^-$  and  $e^+e^- \rightarrow \bar{q}q$  in the  $Z^0$  Region, Comput. Phys. Commun. 29 (1983) 185-200, 10.1016/0010-4655(83)90073-5. doi:10.1016/0010-4655(83)90073-5.
- [221] T. Riemann, M. Sachwitz, D. Bardin, The Z boson line shape at LEP, contribution to XI Warsaw symposium on elementary particle physics: New theories in physics, 23-27 May 1988, Kazimierz, Poland; proceedings edited by Z. Ajduk, S. Pokorski, A. Trautman (Teaneck, N.J., World Scientific, 1988), p. 238-246. <https://lib-extopc.kek.jp/preprints/PDF/1989/8901/8901077.pdf>.
- [222] A. Leike, T. Riemann, M. Sachwitz, QED corrected extra Z boson effects at  $e^+e^-$  colliders, Phys. Lett. B241 (1990) 267, <http://streaming.ictp.it/preprints/P/89/380.pdf>. doi:10.1016/0370-2693(90)91291-I.
- [223] G. Passarino, Hard bremsstrahlung corrections for the process  $e^+e^- \rightarrow \mu^+\mu^-$ , Nucl. Phys. B204 (1982) 237-266, doi:10.1016/0550-3213(82)90147-X. doi:10.1016/0550-3213(82)90147-X.
- [224] D. Bardin, N. Shumeiko, An Exact Calculation of the Lowest Order Electromagnetic Correction to the Elastic Scattering, Nucl. Phys. B127 (1977) 242, doi:10.1016/0550-3213(77)90213-9. doi:10.1016/0550-3213(77)90213-9.
- [225] A. Akhundov, D. Bardin, O. Fedorenko, T. Riemann, Some integrals for exact calculation of QED bremsstrahlung, Dubna preprint JINR-E2-84-777, unpublished, <https://lib-extopc.kek.jp/preprints/PDF/1985/8504/8504203.pdf>.
- [226] D. Yu. Bardin, O. M. Fedorenko, T. Riemann, Some integrals for analytic bremsstrahlung calculation. photon and  $Z^0$  boson exchange in the ultrarelativistic limit, JINR-E2-87-664, <https://lib-extopc.kek.jp/preprints/PDF/1988/8801/8801180.pdf>.
- [227] C. M. Carloni Calame, C. Lunardini, G. Montagna, O. Nicrosini, F. Piccinini, Large-angle Bhabha scattering and luminosity at flavour factories, Nucl. Phys. B584 (2000) 459-479. arXiv:hep-ph/0003268, doi:10.1016/S0550-3213(00)00356-4.
- [228] C. M. Carloni Calame, An improved parton shower algorithm in QED, Phys. Lett. B520 (2001) 16-24. arXiv:hep-ph/0103117, doi:10.1016/S0370-2693(01)01108-X.
- [229] C. M. Carloni Calame, G. Montagna, O. Nicrosini, F. Piccinini, The BABAYAGA event generator, Nucl. Phys. Proc. Suppl. 131 (2004) 48-55. arXiv:hep-ph/0312014, doi:10.1016/j.nuclphysbps.2004.02.008.
- [230] G. Balossini, C. M. Carloni Calame, G. Montagna, O. Nicrosini, F. Piccinini, Matching perturbative and

- parton shower corrections to Bhabha process at flavour factories, Nucl. Phys. B758 (2006) 227–253. arXiv:hep-ph/0607181, doi:10.1016/j.nuclphysb.2006.09.022.
- [231] G. Balossini, C. Bignamini, C. M. C. Calame, G. Montagna, O. Nicrosini, F. Piccinini, Photon pair production at flavour factories with per mille accuracy, Phys. Lett. B663 (2008) 209–213. arXiv:0801.3360, doi:10.1016/j.physletb.2008.04.007.
- [232] S. Jadach, W. Placzek, B. F. L. Ward, BHWIDE 1.00: O( $\alpha$ ) YFS exponentiated Monte Carlo for Bhabha scattering at wide angles for LEP1/SLC and LEP2, Phys. Lett. B390 (1997) 298–308. arXiv:hep-ph/9608412, doi:10.1016/S0370-2693(96)01382-2.
- [233] A. B. Arbuzov, G. V. Fedotov, F. V. Ignatov, E. A. Kuraev, A. L. Sibidanov, Monte-Carlo generator for  $e^+e^-$  annihilation into lepton and hadron pairs with precise radiative corrections, Eur. Phys. J. C46 (2006) 689–703. arXiv:hep-ph/0504233.
- [234] F. Berends, R. Kleiss, Distributions in the process  $e^+e^- \rightarrow e^+e^- (\gamma)$ , Nucl. Phys. B228 (1983) 537. doi:10.1016/0550-3213(83)90558-8.
- [235] F. A. Berends, R. Kleiss, Distributions for electron-Positron Annihilation Into Two and Three Photons, Nucl. Phys. B186 (1981) 22–34. doi:10.1016/0550-3213(81)90090-0.
- [236] R. Bonciani, A. Ferroglia, P. Mastrolia, E. Remiddi, J. van der Bij, Two-loop  $N_f = 1$  QED Bhabha scattering: Soft emission and numerical evaluation of the differential cross-section, Nucl. Phys. B716 (2005) 280–302. arXiv:hep-ph/0411321v2.
- [237] R. Bonciani, A. Ferroglia, P. Mastrolia, E. Remiddi, J. van der Bij, Planar box diagram for the ( $N(F) = 1$ ) two loop QED virtual corrections to Bhabha scattering, Nucl. Phys. B681 (2004) 261–291. arXiv:hep-ph/0310333, doi:10.1016/j.nuclphysb.2004.08.003; 10.1016/j.nuclphysb.2004.08.003.
- [238] R. Bonciani, P. Mastrolia, E. Remiddi, QED vertex form factors at two loops, Nucl. Phys. B676 (2004) 399–452. arXiv:hep-ph/0307295.
- [239] R. Bonciani, P. Mastrolia, E. Remiddi, Vertex diagrams for the QED form factors at the 2-loop level, Nucl. Phys. B661 (2003) 289–343. arXiv:hep-ph/0301170.
- [240] R. Bonciani, A. Ferroglia, Two-loop Bhabha scattering in QED, Phys. Rev. D72 (2005) 056004. arXiv:hep-ph/0507047.
- [241] M. Czakon, J. Gluza, T. Riemann, The planar four-point master integrals for massive two-loop Bhabha scattering, Nucl. Phys. B751 (2006) 1–17. arXiv:hep-ph/0604101, doi:10.1016/j.nuclphysb.2006.05.033.
- [242] M. Czakon, J. Gluza, T. Riemann, Master integrals for massive two-loop Bhabha scattering in QED, Phys. Rev. D71 (2005) 073009. arXiv:hep-ph/0412164, doi:10.1103/PhysRevD.71.073009.
- [243] L. Barze, G. Balossini, C. Bignamini, C. M. C. Calame, G. Montagna, O. Nicrosini, F. Piccinini, Radiative Events as a Probe of Dark Forces at GeV-Scale  $e^+e^-$  Colliders, Eur. Phys. J. C71 (2011) 1680. arXiv:1007.4984, doi:10.1140/epjc/s10052-011-1680-8.
- [244] A. Anastasi, et al., Limit on the production of a low-mass vector boson in  $e^+e^- \rightarrow U\gamma$ ,  $U \rightarrow e^+e^-$  with the KLOE experiment, Phys. Lett. B750 (2015) 633–637. arXiv:1509.00740, doi:10.1016/j.physletb.2015.10.003.
- [245] D. Babusci, et al., Search for light vector boson production in  $e^+e^- \rightarrow \mu^+\mu^-\gamma$  interactions with the KLOE experiment, Phys. Lett. B736 (2014) 459–464. arXiv:1404.7772, doi:10.1016/j.physletb.2014.08.005.
- [246] G. Abbiendi, et al., Measuring the leading hadronic contribution to the muon  $g-2$  via  $\mu e$  scattering, Eur. Phys. J. C77 (3) (2017) 139. arXiv:1609.08987, doi:10.1140/epjc/s10052-017-4633-z.
- [247] C. M. Carloni Calame, M. Passera, L. Trentadue, G. Venanzoni, A new approach to evaluate the leading



- hadronic corrections to the muon  $g-2$ , Phys. Lett. B746 (2015) 325–329. arXiv:1504.02228, doi:10.1016/j.physletb.2015.05.020.
- [248] S. Eidelman, F. Jegerlehner, Hadronic contributions to  $g - 2$  of the leptons and to the effective fine structure constant  $\alpha(M_Z^2)$ , Z. Phys. C67 (1995) 585–602, doi:10.1007/BF01553984. arXiv:hep-ph/9502298, doi:10.1007/BF01553984.
- [249] F. Jegerlehner, The running fine structure constant  $\alpha(E)$  via the Adler function, Nucl. Phys. Proc. Suppl. 181-182 (2008) 135–140. arXiv:0807.4206, doi:10.1016/j.nuclphysbps.2008.09.010.
- [250] M. Dam, Luminosity measurement with diphoton: plan , talk at the *FCC-ee physics coordination meeting*, January 25<sup>th</sup> 2018, CERN (2018).
- [251] M. Dam, LumiCal for FCC-ee and beam-background impact , talk at the *FCC-Week*, 9-13 April 2018, Amsterdam (2018).
- [252] M. Bicer, et al., First Look at the Physics Case of TLEP, JHEP 01 (2014) 164. arXiv:1308.6176, doi:10.1007/JHEP01(2014)164.
- [253] S. Jadach, E. Richter-Was, B. F. L. Ward, Z. Was, Monte Carlo program BHLUMI-2.01 for Bhabha scattering at low angles with Yennie-Frautschi-Suura exponentiation, Comput. Phys. Commun. 70 (1992) 305–344. doi:10.1016/0010-4655(92)90196-6.
- [254] S. Jadach, W. Placzek, E. Richter-Was, B. F. L. Ward, Z. Was, Upgrade of the Monte Carlo program BHLUMI for Bhabha scattering at low angles to version 4.04, Comput. Phys. Commun. 102 (1997) 229–251. doi:10.1016/S0010-4655(96)00156-7.
- [255] S. Jadach, M. Melles, B. F. L. Ward, S. A. Yost, Exact results on O( $\alpha$ ) corrections to the single hard bremsstrahlung process in low angle Bhabha scattering in the SLC / LEP energy regime, Phys. Lett. B377 (1996) 168–176. arXiv:hep-ph/9603248, doi:10.1016/0370-2693(96)00354-1.
- [256] S. Jadach, M. Melles, B. F. L. Ward, S. A. Yost, New results on the precision of the LEP luminosity, Acta Phys. Polon. B30 (1999) 1745–1750.
- [257] S. Jadach, B. F. L. Ward, Missing third order leading log corrections in the small angle Bhabha calculation, Phys. Lett. B389 (1996) 129–136. doi:10.1016/S0370-2693(96)01242-7.
- [258] H. Burkhardt, B. Pietrzyk, Update of the hadronic contribution to the QED vacuum polarization, Phys. Lett. B356 (1995) 398–403. doi:10.1016/0370-2693(95)00820-B.
- [259] S. Jadach, M. Skrzypek, B. F. L. Ward, Analytical results for low angle Bhabha scattering with pair production, Phys. Rev. D47 (1993) 3733–3741. doi:10.1103/PhysRevD.47.3733.
- [260] S. Jadach, M. Skrzypek, B. F. L. Ward, Soft pairs corrections to low angle Bhabha scattering: YFS Monte Carlo approach, Phys. Rev. D55 (1997) 1206–1215. doi:10.1103/PhysRevD.55.1206.
- [261] S. Jadach, W. Placzek, B. F. L. Ward, Precision calculation of the gamma - Z interference effect in the SLC / LEP luminosity process, Phys. Lett. B353 (1995) 349–361. doi:10.1016/0370-2693(95)00576-7.
- [262] A. Arbuzov, et al., The Present theoretical error on the Bhabha scattering cross-section in the luminometry region at LEP, Phys. Lett. B383 (1996) 238–242. arXiv:hep-ph/9605239, doi:10.1016/0370-2693(96)00733-2.
- [263] B. F. L. Ward, S. Jadach, M. Melles, S. A. Yost, New results on the theoretical precision of the LEP / SLC luminosity, Phys. Lett. B450 (1999) 262–266. arXiv:hep-ph/9811245, doi:10.1016/S0370-2693(99)00104-5.
- [264] S. Jadach, E. Richter-Was, B. F. L. Ward, Z. Was, QED multi - photon corrections to Bhabha scattering at low angles: Monte Carlo solution, Phys. Lett. B268 (1991) 253–262. doi:10.1016/0370-2693(91)90813-6.
- [265] S. Jadach, E. Richter-Was, B. F. L. Ward, Z. Was, Higher order radiative corrections to low angle Bhabha scattering: The YFS Monte Carlo approach, Phys. Lett. B353 (1995) 362–372, [Er-

- ratum: Phys. Lett.B384,488(1996)]. doi:10.1016/0370-2693(95)00577-8, 10.1016/0370-2693(96)00923-9.
- [266] G. Abbiendi, et al., Precision luminosity for Z0 line shape measurements with a silicon tungsten calorimeter, Eur. Phys. J. C14 (2000) 373–425. arXiv:hep-ex/9910066, doi:10.1007/s100520000353.
  - [267] G. Montagna, M. Moretti, O. Nicrosini, A. Pallavicini, F. Piccinini, Light pair correction to Bhabha scattering at small angle, Nucl. Phys. B547 (1999) 39–59. arXiv:hep-ph/9811436.
  - [268] G. Montagna, M. Moretti, O. Nicrosini, A. Pallavicini, F. Piccinini, Light-pair corrections to small-angle Bhabha scattering in a realistic set-up at LEP, Phys. Lett. B459 (1999) 649–652. arXiv:hep-ph/9905235.
  - [269] C. M. Carloni Calame, G. Montagna, O. Nicrosini, F. Piccinini, High-precision Luminosity at  $e^+e^-$  Colliders: Theory Status and Challenges, Acta Phys. Polon. B46 (11) (2015) 2227. doi:10.5506/APhysPolB.46.2227.
  - [270] S. Jadach, QED calculations for Bhabha Luminometer - summary of LEP and lessons for the future, FCAL workshop at IFJ PAN, [http://nz42.ifj.edu.pl/\\_media/user/jadach/](http://nz42.ifj.edu.pl/_media/user/jadach/).
  - [271] C. Carloni Calame, The (theoretical) challenge of precise luminosity measurement, FCC-ee Physics Workshop (TLEP9), SNS Pisa.
  - [272] F. Jegerlehner, alphaQED(MZ) and future prospects with low energy  $e + e$  collider data, FCC-ee Mini-Workshop, "Physics Behind Precision" <https://indico.cern.ch/event/469561/>.
  - [273] S. Jadach, E. Richter-Was, B. F. L. Ward, Z. Was, Analytical  $O(\alpha)$  distributions for Bhabha scattering at low angles, Phys. Lett. B253 (1991) 469–477. doi:10.1016/0370-2693(91)91754-J.
  - [274] S. Jadach, et al., Event Generators for Bhabha Scattering (1996). arXiv:hep-ph/9602393.
  - [275] S. Jadach, MC tools for extracting luminosity spectra, Seminar at SLAC, [http://nz42.ifj.edu.pl/\\_media/user/jadach/](http://nz42.ifj.edu.pl/_media/user/jadach/).
  - [276] M. Czakon, J. Gluza, T. Riemann, On the massive two-loop corrections to Bhabha scattering, Acta Phys. Polon. B36 (2005) 3319–3326, <http://www.actaphys.uj.edu.pl/fulltext?series=Reg&vol=36&page=3319>. arXiv:hep-ph/0511187.
  - [277] R. Kleiss, W. J. Stirling, Spinor Techniques for Calculating  $p$  anti- $p \rightarrow W^{+-} / Z0 + \text{Jets}$ , Nucl. Phys. B262 (1985) 235–262. doi:10.1016/0550-3213(85)90285-8.
  - [278] F. A. Berends, P. De Causmaecker, R. Gastmans, R. Kleiss, W. Troost, T. T. Wu, Multiple Bremsstrahlung in Gauge Theories at High-energies. 6. The Process  $e^+e^- \rightarrow e^+e^-\gamma\gamma$ , Nucl. Phys. B264 (1986) 265–276. doi:10.1016/0550-3213(86)90482-7.
  - [279] S. Jadach, B. F. L. Ward, S. A. Yost, Exact results on  $e^+e^- \rightarrow e^+e^- 2 \text{ gamma}$  at SLC / LEP energies, Phys. Rev. D47 (1993) 2682–2689. arXiv:hep-ph/9211252, doi:10.1103/PhysRevD.47.2682.
  - [280] S. Jadach, B. F. L. Ward, S. A. Yost, Comparisons of exact results for the virtual photon contribution to single hard bremsstrahlung in radiative return for electron-positron annihilation, Phys. Rev. D73 (2006) 073001. arXiv:hep-ph/0602197, doi:10.1103/PhysRevD.73.073001.
  - [281] S. Actis, P. Mastrolia, G. Ossola, NLO QED Corrections to Hard-Bremsstrahlung Emission in Bhabha Scattering, Phys. Lett. B682 (2010) 419–427. arXiv:0909.1750, doi:10.1016/j.physletb.2009.11.035.
  - [282] F. A. Berends, W. L. van Neerven, G. J. H. Burgers, Higher Order Radiative Corrections at LEP Energies, Nucl. Phys. B297 (1988) 429, [Erratum: Nucl. Phys.B304,921(1988)]. doi:10.1016/0550-3213(88)90313-6, 10.1016/0550-3213(88)90662-1.
  - [283] Z. Bern, L. Dixon, A. Ghinculov, Two-loop correction to Bhabha scattering, Phys. Rev. D63 (2001) 053007. arXiv:hep-ph/0010075.
  - [284] R. Bonciani, A. Ferroglia, A. Penin, Heavy-flavor contribution to Bhabha scattering, Phys. Rev. Lett. 100 (2008) 131601. arXiv:0710.4775, doi:10.1103/PhysRevLett.100.131601.

- [285] S. Jadach, B. F. L. Ward, Semianalytical third order calculations of the small angle Bhabha cross-sections, *Acta Phys. Polon.* B28 (1997) 1907–1979.
- [286] F. Jegerlehner, Precision measurements of  $\sigma_{had}$  for  $\alpha_{eff}(e)$  at ilc energies and  $(g-2)(\mu)$ , *Nucl. Phys. Proc. Suppl.* 162 (2006) 22–32. [arXiv:hep-ph/0608329](#).
- [287] F. Jegerlehner, The Anomalous Magnetic Moment of the Muon, *Springer Tracts Mod. Phys.* 274 (2017) pp.1–693. doi:10.1007/978-3-319-63577-4.
- [288] S. Eidelman, F. Jegerlehner, A. L. Kataev, O. Veretin, Testing nonperturbative strong interaction effects via the Adler function, *Phys. Lett.* B454 (1999) 369–380. [arXiv:hep-ph/9812521](#), doi:10.1016/S0370-2693(99)00389-5.
- [289] P. Janot, Direct measurement of  $\alpha_{QED}(m_Z^2)$  at the FCC-ee, *JHEP* 02 (2016) 053, [Erratum: *JHEP*11,164(2017)]. [arXiv:1512.05544](#), doi:10.1007/JHEP02(2016)053, 10.1007/JHEP11(2017)164.
- [290] A. B. Arbuzov, et al., Small-angle Bhabha scattering at LEP1: Analytical results for wide-narrow angular acceptance, *Phys. Lett.* B399 (1997) 312–320. [arXiv:hep-ph/9612201](#), doi:10.1016/S0370-2693(97)00307-9.
- [291] A. Arbuzov, et al., Small-angle electron positron scattering with a per mille accuracy, *Nucl. Phys.* B485 (1997) 457–502. [arXiv:hep-ph/9512344](#).
- [292] A. B. Arbuzov, E. A. Kuraev, N. P. Merenkov, L. Trentadue, Pair production in small angle Bhabha scattering, *J. Exp. Theor. Phys.* 81 (1995) 638–646, [*Zh. Eksp. Teor. Fiz.*108,1164(1995)]. [arXiv:hep-ph/9509405](#).
- [293] A. Arbuzov, et al., Small-angle electron positron scattering, *Phys. Lett.* B394 (1997) 218–224. [arXiv:hep-ph/9606425](#).
- [294] N. P. Merenkov, et al., Analytical calculation of small angle Bhabha cross-section at LEP-1, *Acta Phys. Polon.* B28 (1997) 491–507.
- [295] F. Caravaglios, M. Moretti, An algorithm to compute Born scattering amplitudes without Feynman graphs, *Phys. Lett.* B358 (1995) 332–338. [arXiv:hep-ph/9507237](#).
- [296] R. Barbieri, J. A. Mignaco, E. Remiddi, Electron form-factors up to fourth order. 1., *Nuovo Cim.* A11 (1972) 824–864. doi:10.1007/BF02728545.
- [297] R. Barbieri, J. A. Mignaco, E. Remiddi, Electron form factors up to fourth order. 2., *Nuovo Cim.* A11 (1972) 865–916. doi:10.1007/BF02728546.
- [298] S. Jadach, M. Skrzypek, B. F. L. Ward, Soft pairs real and virtual infrared functions in QED, *Phys. Rev.* D49 (1994) 1178–1182. doi:10.1103/PhysRevD.49.1178.
- [299] S. Jadach, W. Placzek, M. Skrzypek, B. F. L. Ward, Z. Was, Monte Carlo program KoralW 1.42 for all four-fermion final states in  $e^+e^-$  collisions, *Comput. Phys. Commun.* 119 (1999) 272–311. [arXiv:hep-ph/9906277](#), doi:10.1016/S0010-4655(99)00219-2.
- [300] S. Jadach, W. Placzek, M. Skrzypek, B. F. L. Ward, Z. Was, Electric charge screening effect in single W production with the KoralW Monte Carlo, *Eur. Phys. J.* C27 (2003) 19–32. [arXiv:hep-ph/0209268](#), doi:10.1140/epjc/s2002-01085-2.
- [301] A. Denner, S. Dittmaier, M. Roth, D. Wackerth, RACOONWW1.3: A Monte Carlo program for four fermion production at  $e^+e^-$  colliders, *Comput. Phys. Commun.* 153 (2003) 462–507. [arXiv:hep-ph/0209330](#), doi:10.1016/S0010-4655(03)00205-4.
- [302] F. A. Berends, R. Kleiss, W. Hollik, Radiative Corrections to Bhabha Scattering at High-Energies. 2. Hard Photon Corrections and Monte Carlo Treatment, *Nucl. Phys.* B304 (1988) 712–748. doi:10.1016/0550-3213(88)90651-7.
- [303] W. Beenakker, F. A. Berends, S. C. van der Marck, Large angle Bhabha scattering, *Nucl. Phys.* B349 (1991) 323–368. doi:10.1016/0550-3213(91)90328-U.
- [304] W. Beenakker, F. A. Berends, S. C. van der Marck, Small angle Bhabha scattering, *Nucl. Phys.* B355

- (1991) 281–294. doi:10.1016/0550-3213(91)90114-D.
- [305] M. Battaglia, S. Jadach, D. Bardin, Luminosity determination at CLIC, eConf C010630 (2001) E3015.
- [306] S. Frixione, B. R. Webber, Matching NLO QCD computations and parton shower simulations, JHEP 06 (2002) 029. arXiv:hep-ph/0204244.
- [307] P. Nason, A new method for combining NLO QCD with shower Monte Carlo algorithms, JHEP 11 (2004) 040. arXiv:hep-ph/0409146.
- [308] S. Jadach, W. Placzek, S. Sapeta, A. Siodmok, M. Skrzypek, Matching NLO QCD with parton shower in Monte Carlo scheme - the KrkNLO method, JHEP 10 (2015) 052. arXiv:1503.06849, doi:10.1007/JHEP10(2015)052.
- [309] A. Arbuzov, D. Y. Bardin, J. Blümlein, L. Kalinovskaya, T. Riemann, Hector 1.00: A Program for the calculation of QED, QCD and electroweak corrections to  $e p$  and lepton+- N deep inelastic neutral and charged current scattering, Comput. Phys. Commun. 94 (1996) 128–184. arXiv:hep-ph/9511434, doi:10.1016/0010-4655(96)00005-7.
- [310] A. Andonov, A. Arbuzov, D. Bardin, S. Bondarenko, P. Christova, L. Kalinovskaya, G. Nanava, W. von Schlippe, SANCscope - v.1.00, Comput. Phys. Commun. 174 (2006) 481–517, [Erratum: Comput. Phys. Commun. 177,623(2007)]. arXiv:hep-ph/0411186, doi:10.1016/j.cpc.2005.12.006, 10.1016/j.cpc.2007.06.010.
- [311] A. Arbuzov, D. Bardin, S. Bondarenko, P. Christova, L. Kalinovskaya, U. Klein, V. Kolesnikov, L. Rumyantsev, R. Sadykov, A. Saproinov, Update of the MCSANC Monte Carlo integrator, v. 1.20, JETP Lett. 103 (2) (2016) 131–136. arXiv:1509.03052, doi:10.1134/S0021364016020041.
- [312] P. Richardson, R. R. Sadykov, A. A. Saproinov, M. H. Seymour, P. Z. Skands, QCD parton showers and NLO EW corrections to Drell-Yan, JHEP 06 (2012) 090. arXiv:1011.5444, doi:10.1007/JHEP06(2012)090.
- [313] G. Moortgat-Pick, et al., The Role of polarized positrons and electrons in revealing fundamental interactions at the linear collider, Phys. Rept. 460 (2008) 131–243. arXiv:hep-ph/0507011, doi:10.1016/j.physrep.2007.12.003.
- [314] R. Vega, J. Wudka, A Covariant method for calculating helicity amplitudes, Phys. Rev. D53 (1996) 5286–5292, [Erratum: Phys. Rev.D56,6037(1997)]. arXiv:hep-ph/9511318, doi:10.1103/PhysRevD.53.5286, 10.1103/PhysRevD.56.6037.
- [315] B. Ruijl, T. Ueda, J. Vermaseren, FORM version 4.2, arXiv:1707.06453.
- [316] T. Hahn, Loop calculations with FeynArts, FormCalc, and LoopTools, Acta Phys. Polon. B30 (1999) 3469–3475. arXiv:hep-ph/9910227.
- [317] G. Belanger, F. Boudjema, J. Fujimoto, T. Ishikawa, T. Kaneko, et al., Automatic calculations in high energy physics and Grace at one-loop, Phys. Rept. 430 (2006) 117–209. arXiv:hep-ph/0308080, doi:10.1016/j.physrep.2006.02.001.
- [318] D. Bardin, A. Arbuzov, S. Bondarenko, Y. Dydyshka, L. Kalinovskaya, L. Rumyantsev, R. Sadykov, One-loop electroweak radiative corrections to polarized Bhabha scattering arXiv:1801.00125.
- [319] W. Hollik, A. Zepeda, Polarized Bhabha Scattering in Multiboson Electroweak Gauge Models, Z. Phys. C12 (1982) 67. doi:10.1007/BF01475733.
- [320] W. Hollik, Higher order qed contributions to polarized bhabha scattering, Phys. Lett. 123B (1983) 259–264. doi:10.1016/0370-2693(83)90434-3.
- [321] A. Arbuzov, D. Y. Bardin, A. Leike, Analytic final state corrections with cut for  $e^+e^- \rightarrow$  massive fermions, Mod. Phys. Lett. A7 (1992) 2029–2038, E: A9 (1994) 1515, scan: KEK, doi:10.1142/S0217732392001762. doi:10.1142/S0217732392001762.
- [322] A. Djouadi, B. Lampe, P. M. Zerwas, A Note on the QCD corrections to forward - backward asymmetries of heavy quark jets in Z decays, Z. Phys. C67 (1995) 123–128. arXiv:hep-ph/9411386, doi:10.1007/BF01564827.

- [323] W. Bernreuther, et al., Two-loop QCD corrections to the heavy quark form factors: Axial vector contributions, Nucl. Phys. B712 (2005) 229–286. [arXiv:hep-ph/0412259](#), doi:10.1016/j.nuclphysb.2005.01.035.
- [324] W. Bernreuther, et al., Two-loop QCD corrections to the heavy quark form factors: Anomaly contributions, Nucl. Phys. B723 (2005) 91–116. [arXiv:hep-ph/0504190](#), doi:10.1016/j.nuclphysb.2005.06.025.
- [325] W. Bernreuther, R. Bonciani, T. Gehrmann, R. Heinesch, P. Mastrolia, E. Remiddi, Decays of scalar and pseudoscalar Higgs bosons into fermions: Two-loop QCD corrections to the Higgs-quark-antiquark amplitude, Phys. Rev. D72 (2005) 096002. [arXiv:hep-ph/0508254](#), doi:10.1103/PhysRevD.72.096002.
- [326] W. Bernreuther, R. Bonciani, T. Gehrmann, R. Heinesch, T. Leineweber, P. Mastrolia, E. Remiddi, Two-loop QCD corrections to the heavy quark form factors: The vector contributions, Nucl. Phys. B706 (2005) 245–324. [arXiv:hep-ph/0406046](#), doi:10.1016/j.nuclphysb.2004.10.059.
- [327] W. Bernreuther, R. Bonciani, T. Gehrmann, R. Heinesch, T. Leineweber, P. Mastrolia, E. Remiddi, QCD corrections to static heavy quark form-factors, Phys. Rev. Lett. 95 (2005) 261802. [arXiv:hep-ph/0509341](#), doi:10.1103/PhysRevLett.95.261802.
- [328] J. Gluza, A. Mitov, S. Moch, T. Riemann, The QCD form factor of heavy quarks at NNLO, JHEP 07 (2009) 001. [arXiv:0905.1137](#), doi:10.1088/1126-6708/2009/07/001.
- [329] J. Ablinger, A. Behring, J. Blumlein, G. Falcioni, A. De Freitas, P. Marquard, N. Rana, C. Schneider, The Heavy Quark Form Factors at Two Loops [arXiv:1712.09889](#).
- [330] R. N. Lee, A. V. Smirnov, V. A. Smirnov, M. Steinhauser, Three-loop massive form factors: complete light-fermion corrections for the vector current, JHEP 03 (2018) 136. [arXiv:1801.08151](#), doi:10.1007/JHEP03(2018)136.
- [331] R. N. Lee, A. V. Smirnov, V. A. Smirnov, M. Steinhauser, Three-loop massive form factors: complete light-fermion and large- $N_c$  corrections for vector, axial-vector, scalar and pseudo-scalar currents [arXiv:1804.07310](#).
- [332] J. Henn, A. V. Smirnov, V. A. Smirnov, M. Steinhauser, Massive three-loop form factor in the planar limit, JHEP 01 (2017) 074. [arXiv:1611.07535](#), doi:10.1007/JHEP01(2017)074.
- [333] J. Ablinger, J. Blumlein, P. Marquard, N. Rana, C. Schneider, Heavy Quark Form Factors at Three Loops in the Planar Limit [arXiv:1804.07313](#).
- [334] J. M. Henn, A. V. Smirnov, V. A. Smirnov, Analytic results for planar three-loop integrals for massive form factors, JHEP 12 (2016) 144. [arXiv:1611.06523](#), doi:10.1007/JHEP12(2016)144.
- [335] J. Blumlein, C. Schneider, Analytic computing methods for precision calculations in quantum field theory, Int. J. Mod. Phys. A33 (17) (2018) 1830015. doi:10.1142/S0217751X18300156.
- [336] A. Grozin, J. M. Henn, G. P. Korchemsky, P. Marquard, The three-loop cusp anomalous dimension in QCD and its supersymmetric extensions, JHEP 01 (2016) 140. [arXiv:1510.07803](#), doi:10.1007/JHEP01(2016)140.
- [337] A. Grozin, J. M. Henn, G. P. Korchemsky, P. Marquard, Three Loop Cusp Anomalous Dimension in QCD, Phys. Rev. Lett. 114 (6) (2015) 062006. [arXiv:1409.0023](#), doi:10.1103/PhysRevLett.114.062006.
- [338] A. Mitov, S. Moch, The singular behavior of massive QCD amplitudes, JHEP 05 (2007) 001. [arXiv:hep-ph/0612149](#).
- [339] T. Becher, M. Neubert, Infrared singularities of QCD amplitudes with massive partons, Phys. Rev. D79 (2009) 125004, [Erratum: Phys. Rev.D80,109901(2009)]. [arXiv:0904.1021](#), doi:10.1103/PhysRevD.79.125004, 10.1103/PhysRevD.80.109901.
- [340] G. Kramer, B. Lampe, Two Jet Cross-Section in  $e^+ e^-$  Annihilation, Z. Phys. C34 (1987) 497, [Erratum: Z. Phys.C42,504(1989)]. doi:10.1007/BF01679868.

- [341] T. Matsuura, S. C. van der Marck, W. L. van Neerven, The Calculation of the Second Order Soft and Virtual Contributions to the Drell-Yan Cross-Section, Nucl. Phys. B319 (1989) 570–622. doi:10.1016/0550-3213(89)90620-2.
- [342] T. Matsuura, W. L. van Neerven, Second Order Logarithmic Corrections to the Drell-Yan Cross-section, Z. Phys. C38 (1988) 623. doi:10.1007/BF01624369.
- [343] R. V. Harlander, Virtual corrections to  $g g \rightarrow H$  to two loops in the heavy top limit, Phys. Lett. B492 (2000) 74–80. arXiv:hep-ph/0007289, doi:10.1016/S0370-2693(00)01042-X.
- [344] V. Ravindran, J. Smith, W. L. van Neerven, Two-loop corrections to Higgs boson production, Nucl. Phys. B704 (2005) 332–348. arXiv:hep-ph/0408315, doi:10.1016/j.nuclphysb.2004.10.039.
- [345] T. Gehrmann, T. Huber, D. Maitre, Two-loop quark and gluon form factors in dimensional regularisation, Phys. Lett. B622 (2005) 295–302. arXiv:hep-ph/0507061, doi:10.1016/j.physletb.2005.07.019.
- [346] P. A. Baikov, K. G. Chetyrkin, A. V. Smirnov, V. A. Smirnov, M. Steinhauser, Quark and gluon form factors to three loops. arXiv:0902.3519.
- [347] T. Gehrmann, E. W. N. Glover, T. Huber, N. Ikizlerli, C. Studerus, Calculation of the quark and gluon form factors to three loops in QCD, JHEP 06 (2010) 094. arXiv:1004.3653, doi:10.1007/JHEP06(2010)094.
- [348] T. Gehrmann, E. W. N. Glover, T. Huber, N. Ikizlerli, C. Studerus, The quark and gluon form factors to three loops in QCD through to  $O(\epsilon^2)$ , JHEP 11 (2010) 102. arXiv:1010.4478, doi:10.1007/JHEP11(2010)102.
- [349] G. Heinrich, T. Huber, D. A. Kosower, V. A. Smirnov, Nine-Propagator Master Integrals for Massless Three-Loop Form Factors. arXiv:0902.3512.
- [350] T. Gehrmann, G. Heinrich, T. Huber, C. Studerus, Master integrals for massless three-loop form-factors: One-loop and two-loop insertions, Phys. Lett. B640 (2006) 252–259. arXiv:hep-ph/0607185, doi:10.1016/j.physletb.2006.08.008.
- [351] G. Heinrich, T. Huber, D. Maitre, Master integrals for fermionic contributions to massless three-loop form-factors, Phys. Lett. B662 (2008) 344–352. arXiv:0711.3590, doi:10.1016/j.physletb.2008.03.028.
- [352] S. Catani, The singular behaviour of QCD amplitudes at two-loop order, Phys. Lett. B427 (1998) 161–171. arXiv:hep-ph/9802439, doi:10.1016/S0370-2693(98)00332-3.
- [353] G. Sterman, M. E. Tejeda-Yeomans, Multi-loop amplitudes and resummation, Phys. Lett. B552 (2003) 48–56. arXiv:hep-ph/0210130.
- [354] T. Becher, M. Neubert, Infrared singularities of scattering amplitudes in perturbative QCD. arXiv:0901.0722.
- [355] E. Gardi, L. Magnea, Factorization constraints for soft anomalous dimensions in QCD scattering amplitudes, JHEP 03 (2009) 079. arXiv:0901.1091, doi:10.1088/1126-6708/2009/03/079.
- [356] J. M. Henn, A. V. Smirnov, V. A. Smirnov, M. Steinhauser, A planar four-loop form factor and cusp anomalous dimension in QCD, JHEP 05 (2016) 066. arXiv:1604.03126, doi:10.1007/JHEP05(2016)066.
- [357] J. Henn, A. V. Smirnov, V. A. Smirnov, M. Steinhauser, R. N. Lee, Four-loop photon quark form factor and cusp anomalous dimension in the large- $N_c$  limit of QCD, JHEP 03 (2017) 139. arXiv:1612.04389, doi:10.1007/JHEP03(2017)139.
- [358] R. N. Lee, A. V. Smirnov, V. A. Smirnov, M. Steinhauser, The  $n_f^2$  contributions to fermionic four-loop form factors, Phys. Rev. D96 (1) (2017) 014008. arXiv:1705.06862, doi:10.1103/PhysRevD.96.014008.
- [359] A. von Manteuffel, R. M. Schabinger, Quark and gluon form factors to four-loop order in QCD:

- the  $N_f^3$  contributions, Phys. Rev. D95 (3) (2017) 034030. arXiv:1611.00795, doi:10.1103/PhysRevD.95.034030.
- [360] C. Gnendiger, et al., To  $d$ , or not to  $d$ : recent developments and comparisons of regularization schemes, Eur. Phys. J. C77 (7) (2017) 471. arXiv:1705.01827, doi:10.1140/epjc/s10052-017-5023-2.
- [361] G. 't Hooft, M. J. G. Veltman, Regularization and Renormalization of Gauge Fields, Nucl. Phys. B44 (1972) 189–213. doi:10.1016/0550-3213(72)90279-9.
- [362] P. Breitenlohner, D. Maison, Dimensional Renormalization and the Action Principle, Commun. Math. Phys. 52 (1977) 11–38. doi:10.1007/BF01609069.
- [363] S. A. Larin, The Renormalization of the axial anomaly in dimensional regularization, Phys. Lett. B303 (1993) 113–118. arXiv:hep-ph/9302240, doi:10.1016/0370-2693(93)90053-K.
- [364] C. Gnendiger, A. Signer,  $\gamma_5$  in the four-dimensional helicity scheme, Phys. Rev. D97 (9) (2018) 096006. arXiv:1710.09231, doi:10.1103/PhysRevD.97.096006.
- [365] S. Heinemeyer, D. Stockinger, G. Weiglein, Electroweak and supersymmetric two-loop corrections to  $(g-2)(\mu)$ , Nucl. Phys. B699 (2004) 103–123. arXiv:hep-ph/0405255, doi:10.1016/j.nuclphysb.2004.08.014.
- [366] A. Freitas, W. Hollik, W. Walter, G. Weiglein, Electroweak two loop corrections to the  $M_W - M_Z$  mass correlation in the Standard Model, Nucl. Phys. B632 (2002) 189–218, E: B666 (2003) 305–307, hep-ph/0202131v4. doi:10.1016/S0550-3213(02)00243-2.
- [367] A. V. Bednyakov, A. F. Pikelnr, Four-loop strong coupling beta-function in the Standard Model, Phys. Lett. B762 (2016) 151–156. arXiv:1508.02680, doi:10.1016/j.physletb.2016.09.007.
- [368] M. F. Zoller, Top-Yukawa effects on the  $\beta$ -function of the strong coupling in the SM at four-loop level, JHEP 02 (2016) 095. arXiv:1508.03624, doi:10.1007/JHEP02(2016)095.
- [369] J. G. Korner, D. Kreimer, K. Schilcher, A Practicable  $\gamma_5$  scheme in dimensional regularization, Z. Phys. C54 (1992) 503–512. doi:10.1007/BF01559471.
- [370] F. Jegerlehner, Facts of life with  $\gamma_5$ , Eur. Phys. J. C18 (2001) 673–679. arXiv:hep-th/0005255, doi:10.1007/s100520100573.
- [371] A. M. Bruque, A. L. Cherchiglia, M. Perez-Victoria, Dimensional regularization vs methods in fixed dimension with and without  $\gamma_5$  arXiv:1803.09764.
- [372] R. A. Fazio, P. Mastrolia, E. Mirabella, W. J. Torres Bobadilla, On the Four-Dimensional Formulation of Dimensionally Regulated Amplitudes, Eur. Phys. J. C74 (12) (2014) 3197. arXiv:1404.4783, doi:10.1140/epjc/s10052-014-3197-4.
- [373] C. P. Martin, D. Sanchez-Ruiz, The one loop UV divergent structure of U(1) Yang-Mills theory on noncommutative  $R^{**4}$ , Phys. Rev. Lett. 83 (1999) 476–479. arXiv:hep-th/9903077, doi:10.1103/PhysRevLett.83.476.
- [374] P. A. Grassi, T. Hurth, M. Steinhauser, The algebraic method, Nucl. Phys. B610 (2001) 215–250. arXiv:hep-ph/0102005.
- [375] J. M. Maldacena, The Large N limit of superconformal field theories and supergravity, Int. J. Theor. Phys. 38 (1999) 1113–1133, [Adv. Theor. Math. Phys.2,231(1998)]. arXiv:hep-th/9711200, doi:10.1023/A:1026654312961, 10.4310/ATMP.1998.v2.n2.a1.
- [376] R. H. Boels, T. Huber, G. Yang, Four-Loop Nonplanar Cusp Anomalous Dimension in N=4 Supersymmetric Yang-Mills Theory, Phys. Rev. Lett. 119 (20) (2017) 201601. arXiv:1705.03444, doi:10.1103/PhysRevLett.119.201601.
- [377] R. H. Boels, T. Huber, G. Yang, The Sudakov form factor at four loops in maximal super Yang-Mills theory, JHEP 01 (2018) 153. arXiv:1711.08449, doi:10.1007/JHEP01(2018)153.
- [378] R. H. Boels, B. A. Kniehl, O. V. Tarasov, G. Yang, Color-kinematic Duality for Form Factors, JHEP 02

- (2013) 063. [arXiv:1211.7028](#), [doi:10.1007/JHEP02\(2013\)063](#).
- [379] G. 't Hooft, A Planar Diagram Theory for Strong Interactions, *Nucl. Phys. B* 72 (1974) 461, [,337(1973)]. [doi:10.1016/0550-3213\(74\)90154-0](#).
- [380] Z. Bern, L. J. Dixon, V. A. Smirnov, Iteration of planar amplitudes in maximally supersymmetric Yang-Mills theory at three loops and beyond, *Phys. Rev. D* 72 (2005) 085001. [arXiv:hep-th/0505205](#), [doi:10.1103/PhysRevD.72.085001](#).
- [381] A. H. Mueller, On the Asymptotic Behavior of the Sudakov Form-factor, *Phys. Rev. D* 20 (1979) 2037. [doi:10.1103/PhysRevD.20.2037](#).
- [382] J. C. Collins, Algorithm to compute corrections to the sudakov form-factor, *Phys. Rev. D* 22 (1980) 1478. [doi:10.1103/PhysRevD.22.1478](#).
- [383] A. Sen, Asymptotic Behavior of the Sudakov Form-Factor in QCD, *Phys. Rev. D* 24 (1981) 3281. [doi:10.1103/PhysRevD.24.3281](#).
- [384] L. Magnea, G. Sterman, Analytic continuation of the Sudakov form-factor in QCD, *Phys. Rev. D* 42 (1990) 4222–4227. [doi:10.1103/PhysRevD.42.4222](#).
- [385] G. P. Korchemsky, Asymptotics of the Altarelli-Parisi-Lipatov Evolution Kernels of Parton Distributions, *Mod. Phys. Lett. A* 4 (1989) 1257–1276. [doi:10.1142/S0217732389001453](#).
- [386] A. V. Kotikov, L. N. Lipatov, NLO corrections to the BFKL equation in QCD and in supersymmetric gauge theories, *Nucl. Phys. B* 582 (2000) 19–43. [arXiv:hep-ph/0004008](#), [doi:10.1016/S0550-3213\(00\)00329-1](#).
- [387] S. S. Gubser, I. R. Klebanov, A. M. Polyakov, A Semiclassical limit of the gauge / string correspondence, *Nucl. Phys. B* 636 (2002) 99–114. [arXiv:hep-th/0204051](#), [doi:10.1016/S0550-3213\(02\)00373-5](#).
- [388] N. Beisert, et al., Review of AdS/CFT Integrability: An Overview, *Lett. Math. Phys.* 99 (2012) 3–32. [arXiv:1012.3982](#), [doi:10.1007/s11005-011-0529-2](#).
- [389] Z. Bern, M. Czakon, L. Dixon, D. Kosower, V. Smirnov, The four-loop planar amplitude and cusp anomalous dimension in maximally supersymmetric Yang-Mills theory, *Phys. Rev. D* 75 (2007) 085010. [arXiv:hep-th/0610248](#).
- [390] F. Cachazo, M. Spradlin, A. Volovich, Four-loop cusp anomalous dimension from obstructions, *Phys. Rev. D* 75 (2007) 105011. [arXiv:hep-th/0612309](#), [doi:10.1103/PhysRevD.75.105011](#).
- [391] J. M. Henn, T. Huber, The four-loop cusp anomalous dimension in  $\mathcal{N} = 4$  super Yang-Mills and analytic integration techniques for Wilson line integrals, *JHEP* 09 (2013) 147. [arXiv:1304.6418](#), [doi:10.1007/JHEP09\(2013\)147](#).
- [392] A. Grozin, J. Henn, M. Stahlhofen, On the Casimir scaling violation in the cusp anomalous dimension at small angle, *JHEP* 10 (2017) 052. [arXiv:1708.01221](#), [doi:10.1007/JHEP10\(2017\)052](#).
- [393] S. Moch, B. Ruijl, T. Ueda, J. A. M. Vermaseren, A. Vogt, Four-Loop Non-Singlet Splitting Functions in the Planar Limit and Beyond, *JHEP* 10 (2017) 041. [arXiv:1707.08315](#), [doi:10.1007/JHEP10\(2017\)041](#).
- [394] S. Moch, B. Ruijl, T. Ueda, J. A. M. Vermaseren, A. Vogt, On quartic colour factors in splitting functions and the gluon cusp anomalous dimension, *Phys. Lett. B* 782 (2018) 627–632. [arXiv:1805.09638](#), [doi:10.1016/j.physletb.2018.06.017](#).
- [395] R. Bruser, A. G. Grozin, J. M. Henn, M. Stahlhofen, Four-loop results for the cusp anomalous dimension, in: 14th DESY Workshop on Elementary Particle Physics: Loops and Legs in Quantum Field Theory 2018 (LL2018) St Goar, Germany, April 29-May 4, 2018, 2018. [arXiv:1807.05145](#).
- [396] A. Vogt, F. Herzog, S. Moch, B. Ruijl, T. Ueda, J. A. M. Vermaseren, Anomalous dimensions and splitting functions beyond the next-to-next-to-leading order, 2018. [arXiv:1808.08981](#).
- [397] W. L. van Neerven, Infrared Behavior of On-shell Form-factors in a  $N = 4$  Supersymmetric Yang-Mills Field Theory, *Z. Phys. C* 30 (1986) 595. [doi:10.1007/BF01571808](#).



- [398] R. N. Lee, A. V. Smirnov, V. A. Smirnov, Analytic Results for Massless Three-Loop Form Factors, JHEP 04 (2010) 020. [arXiv:1001.2887](#), [doi:10.1007/JHEP04\(2010\)020](#).
- [399] A. von Manteuffel, E. Panzer, R. M. Schabinger, On the Computation of Form Factors in Massless QCD with Finite Master Integrals, Phys. Rev. D93 (12) (2016) 125014. [arXiv:1510.06758](#), [doi:10.1103/PhysRevD.93.125014](#).
- [400] T. Ahmed, J. M. Henn, M. Steinhauser, High energy behaviour of form factors, JHEP 06 (2017) 125. [arXiv:1704.07846](#), [doi:10.1007/JHEP06\(2017\)125](#).
- [401] J. Davies, A. Vogt, B. Ruijl, T. Ueda, J. A. M. Vermaseren, Large- $n_f$  contributions to the four-loop splitting functions in QCD, Nucl. Phys. B915 (2017) 335–362. [arXiv:1610.07477](#), [doi:10.1016/j.nuclphysb.2016.12.012](#).
- [402] L. J. Dixon, The Principle of Maximal Transcendentality and the Four-Loop Collinear Anomalous Dimension, JHEP 01 (2018) 075. [arXiv:1712.07274](#), [doi:10.1007/JHEP01\(2018\)075](#).
- [403] A. Grozin, Four-loop cusp anomalous dimension in QED, JHEP 06 (2018) 073. [arXiv:1805.05050](#), [doi:10.1007/JHEP06\(2018\)073](#).
- [404] T. Becher, M. Neubert, On the Structure of Infrared Singularities of Gauge-Theory Amplitudes, JHEP 06 (2009) 081, [Erratum: JHEP11,024(2013)]. [arXiv:0903.1126](#), [doi:10.1088/1126-6708/2009/06/081](#), [doi:10.1007/JHEP11\(2013\)024](#).
- [405] C. Anzai, Y. Kiyo, Y. Sumino, Violation of Casimir Scaling for Static QCD Potential at Three-loop Order, Nucl. Phys. B838 (2010) 28–46, [Erratum: Nucl. Phys. B890,569(2015)]. [arXiv:1004.1562](#), [doi:10.1016/j.nuclphysb.2010.05.012](#), [doi:10.1016/j.nuclphysb.2014.11.025](#).
- [406] L. J. Dixon, Matter Dependence of the Three-Loop Soft Anomalous Dimension Matrix, Phys. Rev. D79 (2009) 091501. [arXiv:0901.3414](#), [doi:10.1103/PhysRevD.79.091501](#).
- [407] L. J. Dixon, E. Gardi, L. Magnea, On soft singularities at three loops and beyond, JHEP 02 (2010) 081. [arXiv:0910.3653](#), [doi:10.1007/JHEP02\(2010\)081](#).
- [408] V. Ahrens, M. Neubert, L. Vernazza, Structure of Infrared Singularities of Gauge-Theory Amplitudes at Three and Four Loops, JHEP 09 (2012) 138. [arXiv:1208.4847](#), [doi:10.1007/JHEP09\(2012\)138](#).
- [409] G. P. Korchemsky, Instanton effects in correlation functions on the light-cone, JHEP 12 (2017) 093. [arXiv:1704.00448](#), [doi:10.1007/JHEP12\(2017\)093](#).
- [410] Z. Bern, J. J. M. Carrasco, H. Johansson, New Relations for Gauge-Theory Amplitudes, Phys. Rev. D78 (2008) 085011. [arXiv:0805.3993](#), [doi:10.1103/PhysRevD.78.085011](#).
- [411] Z. Bern, J. J. M. Carrasco, H. Johansson, Perturbative Quantum Gravity as a Double Copy of Gauge Theory, Phys. Rev. Lett. 105 (2010) 061602. [arXiv:1004.0476](#), [doi:10.1103/PhysRevLett.105.061602](#).
- [412] J. J. M. Carrasco, Gauge and Gravity Amplitude Relations, in: Proceedings, Theoretical Advanced Study Institute in Elementary Particle Physics: Journeys Through the Precision Frontier: Amplitudes for Colliders (TASI 2014): Boulder, Colorado, June 2-27, 2014, WSP, WSP, 2015, pp. 477–557. [arXiv:1506.00974](#), [doi:10.1142/9789814678766\\_0011](#).  
URL <https://inspirehep.net/record/1374212/files/arXiv:1506.00974.pdf>
- [413] G. Yang, Color-kinematics duality and Sudakov form factor at five loops for  $N=4$  supersymmetric Yang-Mills theory, Phys. Rev. Lett. 117 (27) (2016) 271602. [arXiv:1610.02394](#), [doi:10.1103/PhysRevLett.117.271602](#).
- [414] K. Chetyrkin, F. Tkachov, Integration by parts: The algorithm to calculate  $\beta$  functions in 4 loops, Nucl. Phys. B192 (1981) 159–204. [doi:10.1016/0550-3213\(81\)90199-1](#).
- [415] F. V. Tkachov, A Theorem on Analytical Calculability of Four Loop Renormalization Group Functions, Phys. Lett. 100B (1981) 65–68. [doi:10.1016/0370-2693\(81\)90288-4](#).
- [416] R. Boels, B. A. Kniehl, G. Yang, Master integrals for the four-loop Sudakov form factor, Nucl. Phys.

- B902 (2016) 387–414. [arXiv:1508.03717](#), [doi:10.1016/j.nuclphysb.2015.11.016](#).
- [417] A. von Manteuffel, C. Studerus, Reduze 2 - Distributed Feynman Integral Reduction, [arXiv:1201.4330](#).
- [418] C. Anastasiou, A. Lazopoulos, Automatic integral reduction for higher order perturbative calculations, JHEP 07 (2004) 046. [arXiv:hep-ph/0404258](#).
- [419] A. V. Smirnov, Algorithm FIRE – Feynman Integral REduction, JHEP 10 (2008) 107. [arXiv:0807.3243](#), [doi:10.1088/1126-6708/2008/10/107](#).
- [420] A. V. Smirnov, V. A. Smirnov, FIRE4, LiteRed and accompanying tools to solve integration by parts relations, Comput. Phys. Commun. 184 (2013) 2820–2827. [arXiv:1302.5885](#), [doi:10.1016/j.cpc.2013.06.016](#).
- [421] A. V. Smirnov, FIRE5: a C++ implementation of Feynman Integral REduction, Comput. Phys. Commun. 189 (2015) 182–191. [arXiv:1408.2372](#), [doi:10.1016/j.cpc.2014.11.024](#).
- [422] C. Studerus, Reduze - Feynman integral reduction in C++, Computer Physics Communications 181 (2010) 1293–1300. [arXiv:0912.2546](#), [doi:10.1016/j.cpc.2010.03.012](#).
- [423] S. Laporta, High-precision calculation of multi-loop Feynman integrals by difference equations, Int. J. Mod. Phys. A15 (2000) 5087–5159. [arXiv:hep-ph/0102033](#), [doi:10.1016/S0217-751X\(00\)00215-7](#).
- [424] R. N. Lee, Presenting LiteRed: a tool for the Loop InTEgrals REDuction, [arXiv:1212.2685](#).
- [425] R. N. Lee, LiteRed 1.4: a powerful tool for reduction of multiloop integrals, J. Phys. Conf. Ser. 523 (2014) 012059. [arXiv:1310.1145](#), [doi:10.1088/1742-6596/523/1/012059](#).
- [426] J. Blumlein, D. J. Broadhurst, J. A. M. Vermaseren, The Multiple Zeta Value Data Mine, Comput. Phys. Commun. 181 (2010) 582–625. [arXiv:0907.2557](#), [doi:10.1016/j.cpc.2009.11.007](#).
- [427] A. V. Kotikov, L. N. Lipatov, DGLAP and BFKL equations in the  $N = 4$  supersymmetric gauge theory, Nucl. Phys. B661 (2003) 19–61, [Erratum: Nucl. Phys. B685,405(2004)]. [arXiv:hep-ph/0208220](#), [doi:10.1016/S0550-3213\(03\)00264-5](#), [doi:10.1016/j.nuclphysb.2004.02.032](#).
- [428] A. V. Kotikov, L. N. Lipatov, A. I. Onishchenko, V. N. Velizhanin, Three loop universal anomalous dimension of the Wilson operators in  $N = 4$  SUSY Yang-Mills model, Phys. Lett. B595 (2004) 521–529, [Erratum: Phys. Lett. B632,754(2006)]. [arXiv:hep-th/0404092](#), [doi:10.1016/j.physletb.2004.05.078](#), [doi:10.1016/j.physletb.2005.11.002](#).
- [429] T. Gehrmann, J. M. Henn, T. Huber, The three-loop form factor in  $N=4$  super Yang-Mills, JHEP 03 (2012) 101. [arXiv:1112.4524](#), [doi:10.1007/JHEP03\(2012\)101](#).
- [430] N. Arkani-Hamed, J. L. Bourjaily, F. Cachazo, J. Trnka, Singularity Structure of Maximally Supersymmetric Scattering Amplitudes, Phys. Rev. Lett. 113 (26) (2014) 261603. [arXiv:1410.0354](#), [doi:10.1103/PhysRevLett.113.261603](#).
- [431] Z. Bern, E. Herrmann, S. Litsey, J. Stankowicz, J. Trnka, Logarithmic Singularities and Maximally Supersymmetric Amplitudes, JHEP 06 (2015) 202. [arXiv:1412.8584](#), [doi:10.1007/JHEP06\(2015\)202](#).
- [432] J. M. Henn, Multiloop integrals in dimensional regularization made simple, Phys. Rev. Lett. 110 (25) (2013) 251601. [arXiv:1304.1806](#), [doi:10.1103/PhysRevLett.110.251601](#).
- [433] Z. Bern, E. Herrmann, S. Litsey, J. Stankowicz, J. Trnka, Evidence for a Nonplanar Amplituhedron, JHEP 06 (2016) 098. [arXiv:1512.08591](#), [doi:10.1007/JHEP06\(2016\)098](#).
- [434] J. M. Henn, A. V. Smirnov, V. A. Smirnov, Evaluating single-scale and/or non-planar diagrams by differential equations, JHEP 03 (2014) 088. [arXiv:1312.2588](#), [doi:10.1007/JHEP03\(2014\)088](#).
- [435] R. H. Boels, B. A. Kniehl, G. Yang, On a four-loop form factor in  $N=4$ , PoS LL2016 (2016) 039. [arXiv:1607.00172](#).
- [436] V. A. Smirnov, Analytical result for dimensionally regularized massless on shell double box, Phys. Lett. B460 (1999) 397–404. [arXiv:hep-ph/9905323](#), [doi:10.1016/S0370-2693\(99\)](#)

00777–7.

- [437] J. Tausk, Nonplanar massless two loop Feynman diagrams with four on-shell legs, *Phys. Lett. B* 469 (1999) 225–234. [arXiv:hep-ph/9909506](#), [doi:10.1016/S0370-2693\(99\)01277-0](#).
- [438] C. Anastasiou, A. Daleo, Numerical evaluation of loop integrals, *JHEP* 0610 (2006) 031. [arXiv:hep-ph/0511176](#), [doi:10.1088/1126-6708/2006/10/031](#).
- [439] T. Binoth, G. Heinrich, An automatized algorithm to compute infrared divergent multi-loop integrals, *Nucl. Phys. B* 585 (2000) 741–759. [arXiv:hep-ph/0004013v.2](#).
- [440] G. Heinrich, Sector Decomposition, *Int. J. Mod. Phys. A* 23 (2008) 1457–1486. [arXiv:0803.4177](#), [doi:10.1142/S0217751X08040263](#).
- [441] A. V. Smirnov, M. N. Tentyukov, Feynman Integral Evaluation by a Sector decomposition Approach (FIESTA), *Comput. Phys. Commun.* 180 (2009) 735–746. [arXiv:0807.4129](#), [doi:10.1016/j.cpc.2008.11.006](#).
- [442] A. V. Smirnov, V. A. Smirnov, M. Tentyukov, FIESTA 2: Parallelizeable multiloop numerical calculations, *Comput. Phys. Commun.* 182 (2011) 790–803. [arXiv:0912.0158](#), [doi:10.1016/j.cpc.2010.11.025](#).
- [443] A. V. Smirnov, FIESTA 4: optimized Feynman integral calculations with GPU support [arXiv:1511.03614](#).
- [444] J. Carter, G. Heinrich, SecDec: A general program for sector decomposition, *Comput. Phys. Commun.* 182 (2011) 1566–1581. [arXiv:1011.5493](#), [doi:10.1016/j.cpc.2011.03.026](#).
- [445] S. Borowka, J. Carter, G. Heinrich, Numerical Evaluation of Multi-Loop Integrals for Arbitrary Kinematics with SecDec 2.0, *Comput. Phys. Commun.* 184 (2013) 396–408. [arXiv:1204.4152](#), [doi:10.1016/j.cpc.2012.09.020](#).
- [446] V. Smirnov, Evaluating Feynman integrals, *Springer Tracts Mod. Phys.* 211 (2004) 1–244.
- [447] V. A. Smirnov, *Feynman integral calculus* Berlin, Germany: Springer (2006) 283 p.
- [448] M. Czakon, Automatized analytic continuation of Mellin-Barnes integrals, *Comput. Phys. Commun.* 175 (2006) 559–571. [arXiv:hep-ph/0511200](#), [doi:10.1016/j.cpc.2006.07.002](#).
- [449] A. Smirnov, V. Smirnov, On the Resolution of Singularities of Multiple Mellin-Barnes Integrals, *Eur. Phys. J. C* 62 (2009) 445–449. [arXiv:0901.0386](#), [doi:10.1140/epjc/s10052-009-1039-6](#).
- [450] T. Hahn, CUBA: A Library for multidimensional numerical integration, *Comput. Phys. Commun.* 168 (2005) 78–95. [arXiv:hep-ph/0404043](#), [doi:10.1016/j.cpc.2005.01.010](#).
- [451] P. Marquard, A. V. Smirnov, V. A. Smirnov, M. Steinhauser, D. Wellmann,  $\overline{\text{MS}}$ -on-shell quark mass relation up to four loops in QCD and a general  $\text{SU}(N)$  gauge group, *Phys. Rev. D* 94 (7) (2016) 074025. [arXiv:1606.06754](#), [doi:10.1103/PhysRevD.94.074025](#).
- [452] H. R. P. Ferguson, D. H. Bailey, S. Arno, Analysis of pslq, an integer relation finding algorithm, *Math. Comput.* 68 (225) (1999) 351–369. [doi:10.1090/S0025-5718-99-00995-3](#).  
URL <http://dx.doi.org/10.1090/S0025-5718-99-00995-3>
- [453] R. M. Schabinger, Constructing multi-loop scattering amplitudes with manifest singularity structure [arXiv:1806.05682](#).
- [454] J. Henn, "Bootstrapping pentagon functions", talk held [8], [https://indico.cern.ch/event/669224/contributions/2805490/attachments/1582262/2500779/henn\\_cern\\_jan\\_2018.pdf](https://indico.cern.ch/event/669224/contributions/2805490/attachments/1582262/2500779/henn_cern_jan_2018.pdf).
- [455] J. M. Borwein, D. H. Bailey, R. Girgensohn, *Experimentation in Mathematics: Computational Paths to Discovery*, CRC Press, 2004.
- [456] D. H. Bailey, J. M. Borwein, High-precision arithmetic in mathematical physics, *Mathematics* 3 (2) (2015) 337–367. [doi:10.3390/math3020337](#).  
URL <http://www.mdpi.com/2227-7390/3/2/337>

- [457] H. Ita, "Expectations from Current Multi-loop Computations with the Unitarity Method", talk held at [8], [https://indico.cern.ch/event/669224/contributions/2805502/attachments/1582263/2500780/Ita\\_FCC\\_ee\\_QCD.pdf](https://indico.cern.ch/event/669224/contributions/2805502/attachments/1582263/2500780/Ita_FCC_ee_QCD.pdf).
- [458] V. Smirnov, "A mini review of methods of evaluating Feynman integrals. Solving differential equations for Feynman integrals by expansions near singular points", talk held at [8], <https://indico.cern.ch/event/669224/contributions/2805433/attachments/1581916/2500083/smirnov.pdf>.
- [459] O. Gituliar, "Fuchsia and differential equations for multi-scale master integrals", talk held at [8], [https://indico.cern.ch/event/669224/contributions/2805514/attachments/1582273/2500797/gituliar\\_fcc.pdf](https://indico.cern.ch/event/669224/contributions/2805514/attachments/1582273/2500797/gituliar_fcc.pdf).
- [460] J. Blümlein, P. Marquard, Loops and Legs in Quantum Field Theory, April 29, 2018 to May 4, 2018, St. Goar, Germany, <https://indico.desy.de/indico/event/16613/>.
- [461] J. Huston, A. von Manteuffel, R. Schabinger, B. Wenzlick, LoopFest 2018 16-20 Jul 2018, <https://web.pa.msu.edu/people/huston/LoopFest2018/>.
- [462] V. Smirnov, "Evaluating Feynman Integrals" (Springer Verlag, Berlin, 2004).
- [463] V. Smirnov, "Feynman integral calculus" (Springer Verlag, Berlin, 2006).
- [464] C. Bogner, S. Weinzierl, Feynman graph polynomials, *Int. J. Mod. Phys. A* **25** (2010) 2585–2618. arXiv:1002.3458, doi:10.1142/S0217751X10049438.
- [465] G. Heinrich, V. Smirnov, Analytical evaluation of dimensionally regularized massive on-shell double boxes, *Phys. Lett. B* **598** (2004) 55–66. arXiv:hep-ph/0406053.
- [466] K. Hepp, Proof of the Bogolyubov-Parasiuk theorem on renormalization, *Commun. Math. Phys.* **2** (1966) 301–326, <http://www.projecteuclid.org/euclid.cmp/1103815087>. doi:10.1007/BF01773358.
- [467] T. Binoth, G. Heinrich, Numerical evaluation of multiloop integrals by sector decomposition, *Nucl. Phys. B* **680** (2004) 375–388. arXiv:hep-ph/0305234, doi:10.1016/j.nuclphysb.2003.12.023.
- [468] T. Binoth, G. Heinrich, Numerical evaluation of phase space integrals by sector decomposition, *Nucl. Phys. B* **693** (2004) 134–148. arXiv:hep-ph/0402265, doi:10.1016/j.nuclphysb.2004.06.005.
- [469] A. Denner, S. Pozzorini, An Algorithm for the high-energy expansion of multi-loop diagrams to next-to-leading logarithmic accuracy, *Nucl. Phys. B* **717** (2005) 48–85. arXiv:hep-ph/0408068, doi:10.1016/j.nuclphysb.2005.03.036.
- [470] S. Borowka, N. Greiner, G. Heinrich, S. Jones, M. Kerner, J. Schlenk, U. Schubert, T. Zirke, Higgs Boson Pair Production in Gluon Fusion at Next-to-Leading Order with Full Top-Quark Mass Dependence, *Phys. Rev. Lett.* **117** (1) (2016) 012001, [Erratum: *Phys. Rev. Lett.* **117**, no. 7, 079901 (2016)]. arXiv:1604.06447, doi:10.1103/PhysRevLett.117.079901, 10.1103/PhysRevLett.117.012001.
- [471] S. Borowka, N. Greiner, G. Heinrich, S. P. Jones, M. Kerner, J. Schlenk, T. Zirke, Full top quark mass dependence in Higgs boson pair production at NLO, *JHEP* **10** (2016) 107. arXiv:1608.04798, doi:10.1007/JHEP10(2016)107.
- [472] R. Grober, A. Maier, T. Rauh, Reconstruction of top-quark mass effects in Higgs pair production and other gluon-fusion processes, *JHEP* **03** (2018) 020. arXiv:1709.07799, doi:10.1007/JHEP03(2018)020.
- [473] A. Sabry, Fourth order spectral functions for the electron propagator, *Nuclear Physics* **33** (1962) 401 – 430. doi:[https://doi.org/10.1016/0029-5582\(62\)90535-7](https://doi.org/10.1016/0029-5582(62)90535-7).  
URL <http://www.sciencedirect.com/science/article/pii/0029558262905357>
- [474] U. Aglietti, R. Bonciani, L. Grassi, E. Remiddi, The Two loop crossed ladder vertex diagram with

- two massive exchanges, Nucl. Phys. B789 (2008) 45–83. [arXiv:0705.2616](#), [doi:10.1016/j.nuclphysb.2007.07.019](#).
- [475] A. von Manteuffel, L. Tancredi, A non-planar two-loop three-point function beyond multiple polylogarithms, JHEP 06 (2017) 127. [arXiv:1701.05905](#), [doi:10.1007/JHEP06\(2017\)127](#).
- [476] S. Caron-Huot, K. J. Larsen, Uniqueness of two-loop master contours, JHEP 10 (2012) 026. [arXiv:1205.0801](#), [doi:10.1007/JHEP10\(2012\)026](#).
- [477] J. Broedel, C. Duhr, F. Dulat, L. Tancredi, Elliptic polylogarithms and iterated integrals on elliptic curves I: general formalism [arXiv:1712.07089](#).
- [478] S. Borowka, G. Heinrich, Massive non-planar two-loop four-point integrals with SecDec 2.1, Comput. Phys. Commun. 184 (2013) 2552–2561. [arXiv:1303.1157](#), [doi:10.1016/j.cpc.2013.05.022](#).
- [479] S. Borowka, G. Heinrich, S. Jahn, S. P. Jones, M. Kerner, J. Schlenk, T. Zirke, pySecDec: a toolbox for the numerical evaluation of multi-scale integrals, Comput. Phys. Commun. 222 (2018) 313–326. [arXiv:1703.09692](#), [doi:10.1016/j.cpc.2017.09.015](#).
- [480] S. Borowka, T. Gehrmann, D. Hulme, Systematic approximation of multi-scale Feynman integrals, JHEP 08 (2018) 111. [arXiv:1804.06824](#), [doi:10.1007/JHEP08\(2018\)111](#).
- [481] C. Bogner, S. Borowka, T. Hahn, G. Heinrich, S. P. Jones, M. Kerner, A. von Manteuffel, M. Michel, E. Panzer, V. Papara, Loopedia, a Database for Loop Integrals, Comput. Phys. Commun. 225 (2018) 1–9. [arXiv:1709.01266](#), [doi:10.1016/j.cpc.2017.12.017](#).
- [482] M. Roth, A. Denner, High-energy approximation of one loop Feynman integrals, Nucl. Phys. B479 (1996) 495–514. [arXiv:hep-ph/9605420](#), [doi:10.1016/0550-3213\(96\)00435-X](#).
- [483] H. Cheng, T. Wu, Expanding Protons: Scattering at High Energies, The MIT Press, 1987.
- [484] T. Kaneko, T. Ueda, A Geometric method of sector decomposition, Comput. Phys. Commun. 181 (2010) 1352–1361. [arXiv:0908.2897](#), [doi:10.1016/j.cpc.2010.04.001](#).
- [485] T. Kaneko, T. Ueda, Sector Decomposition Via Computational Geometry, PoS ACAT2010 (2010) 082. [arXiv:1004.5490](#).
- [486] J. Schlenk, Techniques for higher order corrections and their application to LHC phenomenology, Ph.D. thesis, Technical University Munich (2016).
- [487] C. Bogner, S. Weinzierl, Resolution of singularities for multi-loop integrals, Comput. Phys. Commun. 178 (2008) 596–610. [arXiv:0709.4092](#), [doi:10.1016/j.cpc.2007.11.012](#).
- [488] C. Bogner, S. Weinzierl, Blowing up Feynman integrals, Nucl. Phys. Proc. Suppl. 183 (2008) 256–261. [arXiv:0806.4307](#), [doi:10.1016/j.nuclphysbps.2008.09.113](#).
- [489] A. Smirnov, V. Smirnov, Hepp and Speer Sectors within Modern Strategies of Sector Decomposition, JHEP 0905 (2009) 004. [arXiv:0812.4700](#), [doi:10.1088/1126-6708/2009/05/004](#).
- [490] J. Vermaseren, New features of FORM. [arXiv:math-ph/0010025](#).
- [491] J. Kuipers, T. Ueda, J. A. M. Vermaseren, Code Optimization in FORM, Comput. Phys. Commun. 189 (2015) 1–19. [arXiv:1310.7007](#), [doi:10.1016/j.cpc.2014.08.008](#).
- [492] S. Agrawal, T. Hahn, E. Mirabella, FormCalc 7, J. Phys. Conf. Ser. 368 (2012) 012054. [arXiv:1112.0124](#), [doi:10.1088/1742-6596/368/1/012054](#).
- [493] T. Hahn, Concurrent Cuba [arXiv:1408.6373](#).
- [494] M. Galassi, al., GNU Scientific Library Reference Manual - Third Edition, 3rd Edition, Network Theory Ltd., 2009.
- [495] B. D. McKay, A. Piperno, Practical graph isomorphism, II, ArXiv e-prints [arXiv:1301.1493](#).
- [496] <http://www.graphviz.org>.
- [497] S. Borowka, G. Heinrich, S. Jahn, S. P. Jones, M. Kerner, J. Schlenk, Numerical evaluation of two-loop integrals with pySecDec, in: The Final HiggsTools Meeting Durham, UK, September 11-15, 2017, 2017.

- arXiv:1712.05755.  
URL <https://inspirehep.net/record/1643669/files/arXiv:1712.05755.pdf>
- [498] E. Panzer, On hyperlogarithms and Feynman integrals with divergences and many scales, JHEP 03 (2014) 071. arXiv:1401.4361, doi:10.1007/JHEP03(2014)071.
  - [499] A. von Manteuffel, E. Panzer, R. M. Schabinger, A quasi-finite basis for multi-loop Feynman integrals, JHEP 02 (2015) 120. arXiv:1411.7392, doi:10.1007/JHEP02(2015)120.
  - [500] C. Bauer, A. Frink, R. Kreckel, Introduction to the GiNaC Framework for Symbolic Computation within the C++ Programming Language, J. Symbolic Computation 33 (2002) 1. arXiv:cs.sc/0004015.
  - [501] S. Wolfram, the Mathematica book, Wolfram media/Cambridge University Press, 2003.
  - [502] AMBRE webpage: <http://prac.us.edu.pl/~gluza/ambre>.
  - [503] J. Gluza, F. Haas, K. Kajda, T. Riemann, Automatizing the application of Mellin-Barnes representations for Feynman integrals, PoS ACAT2007 (2007) 081, <https://cds.cern.ch/record/1048613/files/ACAT-081.pdf>. arXiv:0707.3567.
  - [504] J. Gluza, K. Kajda, T. Riemann, V. Yundin, New results for loop integrals: AMBRE, CSectors, hexagon, PoS ACAT08 (2008) 124, <https://pos.sissa.it/070/124/pdf>. arXiv:0902.4830.
  - [505] J. Gluza, K. Kajda, T. Riemann, V. Yundin, News on Ambre and CSectors, Nucl. Phys. Proc. Suppl. 205-206 (2010) 147–151. arXiv:1006.4728, doi:10.1016/j.nuclphysbps.2010.08.034.
  - [506] I. Dubovyk, A. Freitas, J. Gluza, T. Riemann, J. Usovitsch, 30 years, some 700 integrals, and 1 dessert, or: Electroweak two-loop corrections to the  $Z\bar{b}b$  vertex, PoS LL2016 (2016) 075, [https://pos.sissa.it/archive/conferences/260/034/LL2016\\_075.pdf](https://pos.sissa.it/archive/conferences/260/034/LL2016_075.pdf). arXiv:1610.07059.
  - [507] M. Czakon, A. Mitov, S. Moch, Heavy-quark production in gluon fusion at two loops in QCD, Nucl. Phys. B798 (2008) 210–250. arXiv:0707.4139, doi:10.1016/j.nuclphysb.2008.02.001.
  - [508] K. Kajda, I. Dubovyk, AMBRE 2.2 (12 Sep 2015), a Mathematica package representing Feynman integrals by Mellin-Barnes integrals, available at <http://prac.us.edu.pl/~gluza/ambre/>, [73].
  - [509] I. Dubovyk, AMBRE 3.0 (1 Sep 2015), a Mathematica package representing Feynman integrals by Mellin-Barnes integrals, available at <http://prac.us.edu.pl/~gluza/ambre/>, [73, 75].
  - [510] D. Kosower, Mathematica program barnesroutines.m version 1.1.1 (July 23, 2009), available at the MB Tools webpage, <http://projects.hepforge.org/mbtools/>.
  - [511] J. Usovitsch, I. Dubovyk, T. Riemann, Numerical calculation of multiple MB-integral representations for Feynman integrals. J. Usovitsch, MBnumerics, a Mathematica/Fortran package, to be made available at <http://prac.us.edu.pl/~gluza/ambre/>.
  - [512] MBtools webpage, <http://projects.hepforge.org/mbtools/>.
  - [513] J. Blümlein, K. H. Phan, T. Riemann, Scalar one-loop vertex integrals as meromorphic functions of space-time dimension  $d$ , Acta Phys. Polon. B48 (2017) 2313. arXiv:1711.05510, doi:10.5506/APhysPolB.48.2313.
  - [514] T. Riemann, et al., Scalar one-loop Feynman integrals in arbitrary space-time dimension. Talk held at LL2018, April 29 to May 4, 2018, St. Goar, Germany. <https://indico.desy.de/indico/event/16613/session/12/contribution/24/material/slides/0.pdf>.
  - [515] P. Cvitanovic, T. Kinoshita, Feynman-Dyson rules in parametric space, Phys. Rev. D10 (1974) 3978–3991. doi:10.1103/PhysRevD.10.3978.
  - [516] V. Smirnov, “Applied Asymptotic Expansions in Momenta and Masses” (Springer Verlag, Berlin, 2002).
  - [517] J. Blümlein, I. Dubovyk, J. Gluza, M. Ochman, C. G. Raab, T. Riemann, C. Schneider, Non-planar Feynman integrals, Mellin-Barnes representations, multiple sums, PoS LL2014 (2014) 052. arXiv:1407.7832.
  - [518] M. Prausa, Mellin-Barnes meets Method of Brackets: a novel approach to Mellin-Barnes representations of Feynman integrals, Eur. Phys. J. C77 (9) (2017) 594. arXiv:1706.09852, doi:10.1140/

- epjc/s10052-017-5150-9.
- [519] M. Czakon, MBasymptotics.m, <https://mbtools.hepforge.org>.
  - [520] M. Ochman, T. Riemann, MBsums - a Mathematica package for the representation of Mellin-Barnes integrals by multiple sums, *Acta Phys. Polon. B* 46 (11) (2015) 2117. arXiv:1511.01323, doi: 10.5506/APhysPolB.46.2117.
  - [521] I. Gonzalez, I. Schmidt, Optimized negative dimensional integration method (NDIM) and multiloop Feynman diagram calculation, *Nucl. Phys. B* 769 (2007) 124–173. arXiv:hep-th/0702218, doi: 10.1016/j.nuclphysb.2007.01.031.
  - [522] I. Gonzalez, V. H. Moll, Definite integrals by the method of brackets. Part 1, *Advances in Applied Mathematics* 45 (1) (2010) 50 – 73. arXiv:0812.3356, doi:http://dx.doi.org/10.1016/j.aam.2009.11.003.
  - [523] I. Gonzalez, Method of Brackets and Feynman diagrams evaluation, *Nucl. Phys. Proc. Suppl.* 205-206 (2010) 141–146. arXiv:1008.2148, doi:10.1016/j.nuclphysbps.2010.08.033.
  - [524] J. Fleischer, F. Jegerlehner, O. Tarasov, A New hypergeometric representation of one loop scalar integrals in d dimensions, *Nucl. Phys. B* 672 (2003) 303–328. arXiv:hep-ph/0307113, doi:10.1016/j.nuclphysb.2003.09.004.
  - [525] Z. Bern, L. J. Dixon, D. A. Kosower, Dimensionally regulated one loop integrals, *Phys. Lett. B* 302 (1993) 299–308, [Erratum: *Phys. Lett. B* 318, 649 (1993)]. arXiv:hep-ph/9212308, doi:10.1016/0370-2693(93)90469-X, 10.1016/0370-2693(93)90400-C.
  - [526] O. Tarasov, Connection between Feynman integrals having different values of the space-time dimension, *Phys. Rev. D* 54 (1996) 6479–6490. arXiv:hep-th/9606018, doi:10.1103/PhysRevD.54.6479.
  - [527] J. Usovitsch, et al., MBnumerics: Numerical integration of Mellin-Barnes integrals in physical regions. Talk held by J. Usovitsch at LL2018, April 29 to May 4, 2018, St. Goar, Germany. <https://indico.desy.de/indico/event/16613/session/4/contribution/22/material/slides/0.pdf>.
  - [528] A. I. Davydychev, A simple formula for reducing Feynman diagrams to scalar integrals, *Phys. Lett. B* 263 (1991) 107–111. doi:10.1016/0370-2693(91)91715-8.
  - [529] J. Fleischer, F. Jegerlehner, O. Tarasov, Algebraic reduction of one-loop Feynman graph amplitudes, *Nucl. Phys. B* 566 (2000) 423–440. arXiv:hep-ph/9907327, doi:10.1016/S0550-3213(99)00678-1.
  - [530] P. Maierhoefer, J. Usovitsch, P. Uwer, Kira - a Feynman integral reduction program arXiv:1705.05610, doi:10.1016/j.cpc.2018.04.012.
  - [531] D. B. Melrose, Reduction of Feynman diagrams, *Nuovo Cim.* 40 (1965) 181–213. doi:10.1007/BF028329.
  - [532] J. Usovitsch, I. Dubovyk, T. Riemann, "MB-suite 2: MBnumerics news", talk held by J. Usovitsch at [8], <https://indico.cern.ch/event/669224/contributions/2805454/attachments/1581984/2500208/Usovitsch.pdf>.
  - [533] E. W. Barnes, A new development of the theory of the hypergeometric functions, *Proc. Lond. Math. Soc.* (2) 6 (1908) 141–177. doi:10.1112/plms/s2-6.1.141.
  - [534] A. Freitas, Y.-C. Huang, On the Numerical Evaluation of Loop Integrals With Mellin-Barnes Representations, *JHEP* 04 (2010) 074. arXiv:1001.3243, doi:10.1007/JHEP04(2010)074.
  - [535] I. Bernshtein, Modules over a ring of differential operators. Moscow State University, translated from *Funktsional'nyi Analiz i Ego Prilozheniya*, Vol. 5, pp. 1-16, April 1971. Available at [http://www.math1.tau.ac.il/~bernstei/Publication\\_list/publication\\_texts/bernstein-mod-dif-FAN.pdf](http://www.math1.tau.ac.il/~bernstei/Publication_list/publication_texts/bernstein-mod-dif-FAN.pdf). doi:10.1007/BF01076413.
  - [536] V.A. Golubeva and V.Z. Enol'skii, The differential equations for the Feynman amplitude of a single-

- loop graph with four vertices, Mathematical Notes of the Academy of Sciences of the USSR 23 (1978) 63. doi:10.1007/BF01104888, available at <http://www.mathnet.ru/links/c4b9d8a15c8714d3d8478d1d7b17609b/mzm8124.pdf>.
- [537] G. Devaraj, R. G. Stuart, Reduction of one-loop tensor form-factors to scalar integrals: A general scheme, Nucl. Phys. B519 (1998) 483–513. arXiv:hep-ph/9704308, doi:10.1016/S0550-3213(98)00035-2.
- [538] G. Passarino, M. Veltman, One loop corrections for  $e^+e^-$  annihilation into  $\mu^+\mu^-$  in the Weinberg model, Nucl. Phys. B160 (1979) 151. doi:10.1016/0550-3213(79)90234-7.
- [539] J. Alcaraz Maestre, T. Riemann, V. Yundin, et al., The SM and NLO Multileg and SM MC Working Groups: Summary Report. arXiv:1203.6803.
- [540] J. Fleischer, T. Riemann, V. Yundin, One-Loop Tensor Feynman Integral Reduction with Signed Minors, J. Phys. Conf. Ser. 368 (2012) 012057. arXiv:1112.0500, doi:10.1088/1742-6596/368/1/012057.
- [541] V. Yundin, Massive loop corrections for collider physics, Ph.D thesis, Humboldt-Universität zu Berlin, 2012, <http://edoc.hu-berlin.de/dissertationen/yundin-valery-2012-02-01/PDF/yundin.pdf>.
- [542] T. Hahn, M. Perez-Victoria, Automatized one loop calculations in four-dimensions and D-dimensions, Comput. Phys. Commun. 118 (1999) 153–165. arXiv:hep-ph/9807565, doi:10.1016/S0010-4655(98)00173-8.
- [543] K. Bielas, I. Dubovyk, planarityTest.m, a Mathematica package for testing the planarity of Feynman diagrams: <http://us.edu.pl/~gluza/ambre/planarity/>.
- [544] M. Czakon (MB, MBasymptotics), D. Kosower (barnesroutines), A. Smirnov, V. Smirnov (MBresolve), K. Bielas, I. Dubovyk, J. Gluza, K. Kajda, T. Riemann (AMBRE, PlanarityTest), Mbtools webpage [hepforge.org/.https://mbtools](http://hepforge.org/.https://mbtools).
- [545] Wong, R., *Asymptotic Approximations of Integrals: Classics in Applied Mathematics*, Society for Industrial and Applied Mathematics, 2001.
- [546] Temme, N.M., *Asymptotic Methods for Integrals*, World Scientific, 2014.
- [547] J. Gluza, T. Jelinski, D. A. Kosower, Efficient Evaluation of Massive Mellin-Barnes Integrals, Phys. Rev. D95 (7) (2017) 076016. arXiv:1609.09111, doi:10.1103/PhysRevD.95.076016.
- [548] A. V. Sidorov, V. I. Lashkevich, O. P. Solovtsova, Asymptotics of the contour of the stationary phase and efficient evaluation of the Mellin-Barnes integral for the  $F_3$  structure function, Phys. Rev. D97 (7) (2018) 076009. arXiv:1712.05601, doi:10.1103/PhysRevD.97.076009.
- [549] Axler, S. and Bourdon, P. and Wade, R., *Harmonic Function Theory*, Springer, 2001.
- [550] D. Kaminski, Exponentially improved stationary phase approximations for double integrals, Methods and Applications of Analysis, 01 (1994) 44–56.
- [551] F. Pham, Vanishing homologies and the n variable saddlepoint method, Proc. Sympos. Pure Math. 40, 40 (1983) 319–333.
- [552] F. Pham, La descente des cols par les onglets de lefschetz, avec vues sur Gauss-Manin, Systèmes Différentiels et Singularités (Luminy, 1983) (Astérisque) 130 (1985) 11–47.
- [553] E. Delabaere, C. J. Howls, Global asymptotics for multiple integrals with boundaries, Duke Math. J 112 (2) (2002) 199–264.
- [554] D. A. Kosower, Evolution of parton distributions, Nucl. Phys. B506 (1997) 439–467. arXiv:hep-ph/9706213, doi:10.1016/S0550-3213(97)00526-9.
- [555] E. Witten, A New Look At The Path Integral Of Quantum Mechanics. arXiv:1009.6032.
- [556] E. Witten, Analytic Continuation Of Chern-Simons Theory, AMS/IP Stud. Adv. Math. 50 (2011) 347–446. arXiv:1001.2933.
- [557] M. Cristoforetti, F. Di Renzo, L. Scorzato, New approach to the sign problem in quantum field theories: High density QCD on a Lefschetz thimble, Phys. Rev. D86 (2012) 074506. arXiv:1205.3996,



- doi:10.1103/PhysRevD.86.074506.
- [558] H. Fujii, D. Honda, M. Kato, Y. Kikukawa, S. Komatsu, T. Sano, Hybrid Monte Carlo on Lefschetz thimbles - A study of the residual sign problem, JHEP 10 (2013) 147. arXiv:1309.4371, doi:10.1007/JHEP10(2013)147.
  - [559] A. Alexandru, G. Basar, P. Bedaque, Monte Carlo algorithm for simulating fermions on Lefschetz thimbles, Phys. Rev. D93 (1) (2016) 014504. arXiv:1510.03258, doi:10.1103/PhysRevD.93.014504.
  - [560] A. Alexandru, G. Basar, P. F. Bedaque, G. W. Ridgway, N. C. Warrington, Sign problem and Monte Carlo calculations beyond Lefschetz thimbles, JHEP 05 (2016) 053. arXiv:1512.08764, doi:10.1007/JHEP05(2016)053.
  - [561] Y. Tanizaki, H. Nishimura, J. J. M. Verbaarschot, Gradient flows without blow-up for Lefschetz thimbles, JHEP 10 (2017) 100. arXiv:1706.03822, doi:10.1007/JHEP10(2017)100.
  - [562] A. Alexandru, P. F. Bedaque, H. Lamm, S. Lawrence, Deep Learning Beyond Lefschetz Thimbles, Phys. Rev. D96 (9) (2017) 094505. arXiv:1709.01971, doi:10.1103/PhysRevD.96.094505.
  - [563] S. Bluecher, J. M. Pawłowski, M. Scherzer, M. Schlosser, I.-O. Stamatescu, S. Syrkowski, F. P. G. Ziegler, Reweighting Lefschetz Thimbles. arXiv:1803.08418.
  - [564] L. Nicolaescu, *An Invitation to Morse Theory*, Springer, 2007.
  - [565] A. Alexandru, G. Basar, P. F. Bedaque, G. W. Ridgway, N. C. Warrington, Monte Carlo calculations of the finite density Thirring model, Phys. Rev. D95 (1) (2017) 014502. arXiv:1609.01730, doi:10.1103/PhysRevD.95.014502.
  - [566] A. Kotikov, Differential equations method: New technique for massive Feynman diagrams calculation, Phys. Lett. B254 (1991) 158–164. doi:10.1016/0370-2693(91)90413-K.
  - [567] A. V. Kotikov, Differential equations method: The Calculation of vertex type Feynman diagrams, Phys. Lett. B259 (1991) 314–322. doi:10.1016/0370-2693(91)90834-D.
  - [568] A. V. Kotikov, Differential equation method: The Calculation of N point Feynman diagrams, Phys. Lett. B267 (1991) 123–127, [Erratum: Phys. Lett.B295,409(1992)]. doi:10.1016/0370-2693(91)90536-Y.
  - [569] E. Remiddi, Differential equations for Feynman graph amplitudes, Nuovo Cim. A110 (1997) 1435–1452. arXiv:hep-th/9711188.
  - [570] R. N. Lee, Group structure of the integration-by-part identities and its application to the reduction of multiloop integrals, J. High Energy Phys. 07 (2008) 031.
  - [571] A. V. Smirnov, A. V. Petukhov, The Number of Master Integrals is Finite, Lett. Math. Phys. 97 (2011) 37–44. arXiv:1004.4199, doi:10.1007/s11005-010-0450-0.
  - [572] R. N. Lee, A. A. Pomeransky, Critical points and number of master integrals, J. High Energy Phys. 1311 (2013) 165. arXiv:1308.6676, doi:10.1007/JHEP11(2013)165.
  - [573] R. N. Lee, Modern techniques of multiloop calculations, in: E. Auge, J. Dumarchez (Eds.), Proceedings, 49th Rencontres de Moriond on QCD and High Energy Interactions, Moriond, Moriond, Paris, France, 2014, pp. 297–300. arXiv:1405.5616.
  - [574] K. J. Larsen, Y. Zhang, Integration-by-parts reductions from unitarity cuts and algebraic geometry, Phys. Rev. D93 (4) (2016) 041701. arXiv:1511.01071, doi:10.1103/PhysRevD.93.041701.
  - [575] J. Bosma, K. J. Larsen, Y. Zhang, Differential equations for loop integrals in Baikov representation, Phys. Rev. D97 (10) (2018) 105014. arXiv:1712.03760, doi:10.1103/PhysRevD.97.105014.
  - [576] J. Böhm, A. Georgoudis, K. J. Larsen, M. Schulze, Y. Zhang, Complete sets of logarithmic vector fields for integration-by-parts identities of Feynman integrals, Phys. Rev. D98 (2) (2018) 025023. arXiv:1712.09737, doi:10.1103/PhysRevD.98.025023.
  - [577] T. Bitoun, C. Bogner, R. P. Klausen, E. Panzer, Feynman integral relations from parametric annihilators, arXiv:1712.09215.

- [578] J. Boehm, A. Georgoudis, K. J. Larsen, H. Schoenemann, Y. Zhang, Complete integration-by-parts reductions of the non-planar hexagon-box via module intersections [arXiv:1805.01873](#).
- [579] A. Barkatou, A rational version of moser's algorithm, in: Proceedings of the 1995 international symposium on Symbolic and Algebraic computation, ACM, 1995, pp. 297–302.
- [580] M. Beneke, V. A. Smirnov, Asymptotic expansion of feynman integrals near threshold, Nucl. Phys. B 522 (1998) 321–344. [arXiv:hep-ph/9711391](#), doi:10.1016/S0550-3213(98)00138-2.
- [581] J. M. Henn, V. A. Smirnov, Analytic results for two-loop master integrals for Bhabha scattering I, JHEP 1311 (2013) 041. [arXiv:1307.4083](#), doi:10.1007/JHEP11(2013)041.
- [582] J. M. Henn, A. V. Smirnov, V. A. Smirnov, Analytic results for planar three-loop four-point integrals from a Knizhnik-Zamolodchikov equation, JHEP 1307 (2013) 128. [arXiv:1306.2799](#), doi:10.1007/JHEP07(2013)128.
- [583] J. M. Henn, K. Melnikov, V. A. Smirnov, Two-loop planar master integrals for the production of off-shell vector bosons in hadron collisions, JHEP 1405 (2014) 090. [arXiv:1402.7078](#), doi:10.1007/JHEP05(2014)090.
- [584] A. B. Goncharov, Multiple polylogarithms, cyclotomy and modular complexes, Math. Res. Lett. 5 (1998) 497–516. [arXiv:1105.2076](#), doi:10.4310/MRL.1998.v5.n4.a7.
- [585] J. Vollinga, S. Weinzierl, Numerical evaluation of multiple polylogarithms, Comput. Phys. Commun. 167 (2005) 177. [arXiv:hep-ph/0410259](#), doi:10.1016/j.cpc.2004.12.009.
- [586] R. N. Lee, A. V. Smirnov, V. A. Smirnov, Solving differential equations for Feynman integrals by expansions near singular points, JHEP 03 (2018) 008. [arXiv:1709.07525](#), doi:10.1007/jhep03(2018)008.
- [587] R. N. Lee, Reducing differential equations for multiloop master integrals, JHEP 04 (2015) 108. [arXiv:1411.0911](#), doi:10.1007/JHEP04(2015)108.
- [588] O. Gituliar, V. Magerya, Fuchsia: a tool for reducing differential equations for Feynman master integrals to epsilon form, Comput. Phys. Commun. 219 (2017) 329–338. [arXiv:1701.04269](#), doi:10.1016/j.cpc.2017.05.004.
- [589] M. Prausa, epsilon: A tool to find a canonical basis of master integrals, Comput. Phys. Commun. 219 (2017) 361–376. [arXiv:1701.00725](#), doi:10.1016/j.cpc.2017.05.026.
- [590] M. A. Barkatou, E. Pflügel, Computing super-irreducible forms of systems of linear differential equations via moser-reduction: A new approach, in: Proceedings of the 2007 International Symposium on Symbolic and Algebraic Computation, ISSAC '07, ACM, New York, NY, USA, 2007, pp. 1–8. doi:10.1145/1277548.1277550.  
URL <http://doi.acm.org/10.1145/1277548.1277550>
- [591] M. A. Barkatou, E. Pflügel, On the moser-and super-reduction algorithms of systems of linear differential equations and their complexity, Journal of Symbolic Computation 44 (8) (2009) 1017–1036.
- [592] A. A. Bolibrukh, The riemann-hilbert problem on the complex projective line, Matematicheskije Zametki 46 (3) (1989) 118–120.
- [593] J. Moser, The order of a singularity in fuchs' theory, Mathematische Zeitschrift 72 (1) (1959) 379–398.
- [594] R. N. Lee, A. A. Pomeransky, Normalized Fuchsian form on Riemann sphere and differential equations for multiloop integrals [arXiv:1707.07856](#).
- [595] M. Argeri, S. Di Vita, P. Mastrolia, E. Mirabella, J. Schlenk, et al., Magnus and Dyson Series for Master Integrals, JHEP 1403 (2014) 082. [arXiv:1401.2979](#), doi:10.1007/JHEP03(2014)082.
- [596] L. Adams, S. Weinzierl, The  $\varepsilon$ -form of the differential equations for Feynman integrals in the elliptic case [arXiv:1802.05020](#), doi:10.1016/j.physletb.2018.04.002.
- [597] L. Adams, C. Bogner, S. Weinzierl, The sunrise integral around two and four space-time dimensions in terms of elliptic polylogarithms, Acta Phys. Polon. B46 (11) (2015) 2131. [arXiv:1510.02048](#), doi:10.5506/APhysPolB.46.2131.

- [598] L. Adams, C. Bogner, A. Schweitzer, S. Weinzierl, The kite integral to all orders in terms of elliptic polylogarithms, *J. Math. Phys.* 57 (12) (2016) 122302. [arXiv:1607.01571](#), [doi:10.1063/1.4969060](#).
- [599] E. Remiddi, L. Tancredi, Differential equations and dispersion relations for Feynman amplitudes. The two-loop massive sunrise and the kite integral, *Nucl. Phys. B* 907 (2016) 400–444. [arXiv:1602.01481](#), [doi:10.1016/j.nuclphysb.2016.04.013](#).
- [600] L. Adams, C. Bogner, E. Chaubey, A. Schweitzer, S. Weinzierl, Differential equations for Feynman integrals beyond multiple polylogarithms, in: 13th International Symposium on Radiative Corrections: Application of Quantum Field Theory to Phenomenology (RADCOR 2017) St. Gilgen, Austria, September 24–29, 2017, 2017. [arXiv:1712.03532](#).  
URL <http://inspirehep.net/record/1642456/files/arXiv:1712.03532.pdf>
- [601] A. Primo, L. Tancredi, Maximal cuts and differential equations for Feynman integrals. An application to the three-loop massive banana graph, *Nucl. Phys. B* 921 (2017) 316–356. [arXiv:1704.05465](#), [doi:10.1016/j.nuclphysb.2017.05.018](#).
- [602] A. Primo, L. Tancredi, On the maximal cut of Feynman integrals and the solution of their differential equations, *Nucl. Phys. B* 916 (2017) 94–116. [arXiv:1610.08397](#), [doi:10.1016/j.nuclphysb.2016.12.021](#).
- [603] E. Remiddi, L. Tancredi, An Elliptic Generalization of Multiple Polylogarithms, *Nucl. Phys. B* 925 (2017) 212–251. [arXiv:1709.03622](#), [doi:10.1016/j.nuclphysb.2017.10.007](#).
- [604] C. Meyer, Algorithmic transformation of multi-loop master integrals to a canonical basis with CANON-ICA, *Comput. Phys. Commun.* 222 (2018) 295–312. [arXiv:1705.06252](#), [doi:10.1016/j.cpc.2017.09.014](#).
- [605] R. P. Feynman, Space - time approach to quantum electrodynamics, *Phys. Rev.* 76 (1949) 769–789. [doi:10.1103/PhysRev.76.769](#).
- [606] F. J. Dyson, The Radiation theories of Tomonaga, Schwinger, and Feynman, *Phys. Rev.* 75 (1949) 486–502. [doi:10.1103/PhysRev.75.486](#).
- [607] F. J. Dyson, The S matrix in quantum electrodynamics, *Phys. Rev.* 75 (1949) 1736–1755. [doi:10.1103/PhysRev.75.1736](#).
- [608] T. Gehrmann, J. M. Henn, N. A. Lo Presti, Analytic form of the two-loop planar five-gluon all-plus-helicity amplitude in QCD, *Phys. Rev. Lett.* 116 (6) (2016) 062001, [Erratum: *Phys. Rev. Lett.* 116, no. 18, 189903 (2016)]. [arXiv:1511.05409](#), [doi:10.1103/PhysRevLett.116.189903](#), [10.1103/PhysRevLett.116.062001](#).
- [609] C. G. Papadopoulos, D. Tommasini, C. Wever, The Pentabox Master Integrals with the Simplified Differential Equations approach, *JHEP* 04 (2016) 078. [arXiv:1511.09404](#), [doi:10.1007/JHEP04\(2016\)078](#).
- [610] J. R. Andersen, et al., Les Houches 2013: Physics at TeV Colliders: Standard Model Working Group Report [arXiv:1405.1067](#).
- [611] Z. Bern, L. J. Dixon, D. C. Dunbar, D. A. Kosower, Fusing gauge theory tree amplitudes into loop amplitudes, *Nucl. Phys. B* 435 (1995) 59–101. [arXiv:hep-ph/9409265](#), [doi:10.1016/0550-3213\(94\)00488-Z](#).
- [612] Z. Bern, L. J. Dixon, D. C. Dunbar, D. A. Kosower, One-Loop n-Point Gauge Theory Amplitudes, Unitarity and Collinear Limits, *Nucl. Phys. B* 425 (1994) 217–260. [arXiv:hep-ph/9403226](#), [doi:10.1016/0550-3213\(94\)90179-1](#).
- [613] G. Ossola, C. Papadopoulos, R. Pittau, Reducing full one-loop amplitudes to scalar integrals at the integrand level, *Nucl. Phys. B* 763 (2007) 147–169. [arXiv:hep-ph/0609007](#), [doi:10.1016/j.nuclphysb.2006.11.012](#).
- [614] G. Ossola, C. G. Papadopoulos, R. Pittau, On the Rational Terms of the one-loop amplitudes, *JHEP* 0805

- (2008) 004. arXiv:0802.1876, doi:10.1088/1126-6708/2008/05/004.
- [615] R. K. Ellis, Z. Kunszt, K. Melnikov, G. Zanderighi, One-loop calculations in quantum field theory: from Feynman diagrams to unitarity cuts, *Phys. Rept.* 518 (2012) 141–250. arXiv:1105.4319, doi:10.1016/j.physrep.2012.01.008.
  - [616] H. van Deurzen, G. Luisoni, P. Mastrolia, G. Ossola, Z. Zhang, Automated Computation of Scattering Amplitudes from Integrand Reduction to Monte Carlo tools, *Nucl. Part. Phys. Proc.* 267-269 (2015) 140–149. doi:10.1016/j.nuclphysbps.2015.10.094.
  - [617] J. Gluza, K. Kajda, D. A. Kosower, Towards a Basis for Planar Two-Loop Integrals. arXiv:1009.0472.
  - [618] D. A. Kosower, K. J. Larsen, Maximal Unitarity at Two Loops, *Phys.Rev. D* 85 (2012) 045017. arXiv:1108.1180, doi:10.1103/PhysRevD.85.045017.
  - [619] H. Johansson, D. A. Kosower, K. J. Larsen, Two-Loop Maximal Unitarity with External Masses, *Phys. Rev. D* 87 (2) (2013) 025030. arXiv:1208.1754, doi:10.1103/PhysRevD.87.025030.
  - [620] H. Johansson, D. A. Kosower, K. J. Larsen, An Overview of Maximal Unitarity at Two Loops, *PoS LL2012* (2012) 066, [PoSLL2012,066(2012)]. arXiv:1212.2132.
  - [621] H. Johansson, D. A. Kosower, K. J. Larsen, Maximal Unitarity for the Four-Mass Double Box, *Phys. Rev. D* 89 (12) (2014) 125010. arXiv:1308.4632, doi:10.1103/PhysRevD.89.125010.
  - [622] M. S gaard, Y. Zhang, Multivariate Residues and Maximal Unitarity, *JHEP* 12 (2013) 008. arXiv:1310.6006, doi:10.1007/JHEP12(2013)008.
  - [623] H. Ita, Two-loop Integrand Decomposition into Master Integrals and Surface Terms, *Phys. Rev. D* 94 (11) (2016) 116015. arXiv:1510.05626, doi:10.1103/PhysRevD.94.116015.
  - [624] H. Johansson, D. A. Kosower, K. J. Larsen, M. S gaard, Cross-Order Integral Relations from Maximal Cuts, *Phys. Rev. D* 92 (2) (2015) 025015. arXiv:1503.06711, doi:10.1103/PhysRevD.92.025015.
  - [625] P. Mastrolia, T. Peraro, A. Primo, Adaptive Integrand Decomposition in parallel and orthogonal space, *JHEP* 08 (2016) 164. arXiv:1605.03157, doi:10.1007/JHEP08(2016)164.
  - [626] P. Mastrolia, G. Ossola, On the Integrand-Reduction Method for Two-Loop Scattering Amplitudes, *JHEP* 1111 (2011) 014. arXiv:1107.6041, doi:10.1007/JHEP11(2011)014.
  - [627] S. Badger, H. Frellesvig, Y. Zhang, Hepta-Cuts of Two-Loop Scattering Amplitudes, *JHEP* 1204 (2012) 055. arXiv:1202.2019, doi:10.1007/JHEP04(2012)055.
  - [628] P. Mastrolia, E. Mirabella, G. Ossola, T. Peraro, Integrand-Reduction for Two-Loop Scattering Amplitudes through Multivariate Polynomial Division, *Phys. Rev. D* 87 (8) (2013) 085026. arXiv:1209.4319, doi:10.1103/PhysRevD.87.085026.
  - [629] S. Badger, H. Frellesvig, Y. Zhang, A Two-Loop Five-Gluon Helicity Amplitude in QCD, *JHEP* 1312 (2013) 045. arXiv:1310.1051, doi:10.1007/JHEP12(2013)045.
  - [630] C. Papadopoulos, R. Kleiss, I. Malamos, Reduction at the integrand level beyond NLO, *PoS Corfu2012* (2013) 019.
  - [631] S. Badger, G. Mogull, A. Ochirov, D. O’Connell, A Complete Two-Loop, Five-Gluon Helicity Amplitude in Yang-Mills Theory, *JHEP* 10 (2015) 064. arXiv:1507.08797, doi:10.1007/JHEP10(2015)064.
  - [632] G. ’t Hooft, M. Veltman, Scalar One Loop Integrals, *Nucl. Phys. B* 153 (1979) 365–401. doi:10.1016/0550-3213(79)90605-9.
  - [633] V. A. Smirnov, Analytic tools for Feynman integrals, *Springer Tracts Mod. Phys.* 250 (2012) 1–296. doi:10.1007/978-3-642-34886-0.
  - [634] A. V. Kotikov, Differential equation method: The Calculation of N point Feynman diagrams, *Phys. Lett. B* 267 (1991) 123–127.
  - [635] T. Gehrmann, E. Remiddi, Differential equations for two-loop four-point functions, *Nucl. Phys. B* 580

- (2000) 485–518. [arXiv:hep-ph/9912329](#).
- [636] E. Remiddi, J. Vermaseren, Harmonic polylogarithms, *Int. J. Mod. Phys. A* 15 (2000) 725–754. [arXiv:hep-ph/9905237](#), doi:10.1142/S0217751X00000367.
- [637] A. Goncharov, Multiple polylogarithms and mixed Tate motives [arXiv:math/0103059](#).
- [638] J. Ablinger, A. Behring, J. Blumlein, A. De Freitas, A. von Manteuffel, C. Schneider, Calculating Three Loop Ladder and V-Topologies for Massive Operator Matrix Elements by Computer Algebra, *Comput. Phys. Commun.* 202 (2016) 33–112. [arXiv:1509.08324](#), doi:10.1016/j.cpc.2016.01.002.
- [639] L. Adams, C. Bogner, S. Weinzierl, The two-loop sunrise integral around four space-time dimensions and generalisations of the Clausen and Glaisher functions towards the elliptic case, *J. Math. Phys.* 56 (7) (2015) 072303. [arXiv:1504.03255](#), doi:10.1063/1.4926985.
- [640] R. Bonciani, V. Del Duca, H. Frellesvig, J. M. Henn, F. Moriello, V. A. Smirnov, Two-loop planar master integrals for  $Higgs \rightarrow 3$  partons with full heavy-quark mass dependence, *JHEP* 12 (2016) 096. [arXiv:1609.06685](#), doi:10.1007/JHEP12(2016)096.
- [641] J. Ablinger, J. Blümlein, M. De Freitas, A. an Hoeij, E. Imamoglu, C. G. Raab, C. Radu, C. Schneider, Iterated Elliptic and Hypergeometric Integrals for Feynman Diagrams, *J. Math. Phys.* 59 (6) (2018) 062305. [arXiv:1706.01299](#), doi:10.1063/1.4986417.
- [642] J. L. Bourjaily, A. J. McLeod, M. Spradlin, M. von Hippel, M. Wilhelm, The Elliptic Double-Box Integral: Massless Amplitudes Beyond Polylogarithms [arXiv:1712.02785](#).
- [643] H. Frellesvig, C. G. Papadopoulos, Cuts of Feynman Integrals in Baikov representation, *JHEP* 04 (2017) 083. [arXiv:1701.07356](#), doi:10.1007/JHEP04(2017)083.
- [644] P. A. Baikov, Explicit solutions of the multiloop integral recurrence relations and its application, *Nucl. Instrum. Meth. A* 389 (1997) 347–349. [arXiv:hep-ph/9611449](#), doi:10.1016/S0168-9002(97)00126-5.
- [645] P. A. Baikov, Explicit solutions of the three loop vacuum integral recurrence relations, *Phys. Lett. B* 385 (1996) 404–410. [arXiv:hep-ph/9603267](#), doi:10.1016/0370-2693(96)00835-0.
- [646] V. A. Smirnov, M. Steinhauser, Solving recurrence relations for multiloop Feynman integrals, *Nucl. Phys. B* 672 (2003) 199–221. [arXiv:hep-ph/0307088](#), doi:10.1016/j.nuclphysb.2003.09.003.
- [647] R. N. Lee, Calculating multiloop integrals using dimensional recurrence relation and  $D$ -analyticity, *Nucl. Phys. Proc. Suppl.* 205-206 (2010) 135–140. [arXiv:1007.2256](#), doi:10.1016/j.nuclphysbps.2010.08.032.
- [648] A. G. Grozin, Integration by parts: An Introduction, *Int. J. Mod. Phys. A* 26 (2011) 2807–2854. [arXiv:1104.3993](#), doi:10.1142/S0217751X11053687.
- [649] R. N. Lee, A. A. Pomeransky, Critical points and number of master integrals, *JHEP* 11 (2013) 165. [arXiv:1308.6676](#), doi:10.1007/JHEP11(2013)165.
- [650] C. G. Papadopoulos, Simplified differential equations approach for Master Integrals, *JHEP* 1407 (2014) 088. [arXiv:1401.6057](#), doi:10.1007/JHEP07(2014)088.
- [651] C. G. Papadopoulos, D. Tommasini, C. Wever, Two-loop Master Integrals with the Simplified Differential Equations approach, *JHEP* 01 (2015) 072. [arXiv:1409.6114](#), doi:10.1007/JHEP01(2015)072.
- [652] J. M. Henn, Lectures on differential equations for Feynman integrals, *J. Phys. A* 48 (2015) 153001. [arXiv:1412.2296](#), doi:10.1088/1751-8113/48/15/153001.
- [653] E. Panzer, Algorithms for the symbolic integration of hyperlogarithms with applications to Feynman integrals, *Comput. Phys. Commun.* 188 (2014) 148–166. [arXiv:1403.3385](#), doi:10.1016/j.cpc.2014.10.019.
- [654] T. Gehrmann, A. von Manteuffel, L. Tancredi, The two-loop helicity amplitudes for  $q\bar{q}' \rightarrow V_1 V_2 \rightarrow 4$

- leptons, JHEP 09 (2015) 128. [arXiv:1503.04812](#), [doi:10.1007/JHEP09\(2015\)128](#).
- [655] M. J. G. Veltman, *Diagrammatica: The Path to Feynman Rules*. Cambridge, UK: Univ. Pr. (1994) 284 p. (Cambridge lecture notes in physics, 4).
- [656] S. Abreu, R. Britto, C. Duhr, E. Gardi, From multiple unitarity cuts to the coproduct of Feynman integrals, JHEP 10 (2014) 125. [arXiv:1401.3546](#), [doi:10.1007/JHEP10\(2014\)125](#).
- [657] S. Abreu, R. Britto, H. Grönqvist, Cuts and coproducts of massive triangle diagrams, JHEP 07 (2015) 111. [arXiv:1504.00206](#), [doi:10.1007/JHEP07\(2015\)111](#).
- [658] C. Anastasiou, K. Melnikov, Higgs boson production at hadron colliders in NNLO QCD [arXiv:hep-ph/0207004](#).
- [659] R. N. Lee, V. A. Smirnov, The Dimensional Recurrence and Analyticity Method for Multicomponent Master Integrals: Using Unitarity Cuts to Construct Homogeneous Solutions, JHEP 12 (2012) 104. [arXiv:1209.0339](#), [doi:10.1007/JHEP12\(2012\)104](#).
- [660] J. Bosma, M. Søgaard, Y. Zhang, Maximal Cuts in Arbitrary Dimension, JHEP 08 (2017) 051. [arXiv:1704.04255](#), [doi:10.1007/JHEP08\(2017\)051](#).
- [661] M. Harley, F. Moriello, R. M. Schabinger, Baikov-Lee Representations Of Cut Feynman Integrals, JHEP 06 (2017) 049. [arXiv:1705.03478](#), [doi:10.1007/JHEP06\(2017\)049](#).
- [662] M. Argeri, P. Mastrolia, Feynman Diagrams and Differential Equations, *Int. J. Mod. Phys. A* 22 (2007) 4375–4436. [arXiv:0707.4037](#), [doi:10.1142/S0217751X07037147](#).
- [663] S. Müller-Stach, S. Weinzierl, R. Zayadeh, Picard-Fuchs equations for Feynman integrals, *Commun.Math.Phys.* 326 (2014) 237–249. [arXiv:1212.4389](#), [doi:10.1007/s00220-013-1838-3](#).
- [664] A. B. Goncharov, Multiple polylogarithms and mixed tate motives [arXiv:math.AG/0103059](#).
- [665] J. M. Borwein, D. M. Bradley, D. J. Broadhurst, P. Lisonek, Special values of multiple polylogarithms, *Trans. Amer. Math. Soc.* 353:3 (2001) 907. [arXiv:math.CA/9910045](#).
- [666] S. Moch, P. Uwer, S. Weinzierl, Nested sums, expansion of transcendental functions and multi-scale multi-loop integrals, *J. Math. Phys.* 43 (2002) 3363–3386. [arXiv:hep-ph/0110083](#).
- [667] T. Gehrmann, A. von Manteuffel, L. Tancredi, E. Weihs, The two-loop master integrals for  $q\bar{q} \rightarrow VV$ , JHEP 06 (2014) 032. [arXiv:1404.4853](#), [doi:10.1007/JHEP06\(2014\)032](#).
- [668] C. Meyer, Transforming differential equations of multi-loop Feynman integrals into canonical form [arXiv:1611.01087](#).
- [669] L. Adams, E. Chaubey, S. Weinzierl, Simplifying differential equations for multi-scale Feynman integrals beyond multiple polylogarithms, *Phys. Rev. Lett.* 118 (14) (2017) 141602. [arXiv:1702.04279](#), [doi:10.1103/PhysRevLett.118.141602](#).
- [670] M. Becchetti, R. Bonciani, Two-Loop Master Integrals for the Planar QCD Massive Corrections to Diphoton and Di-jet Hadro-production, JHEP 01 (2018) 048. [arXiv:1712.02537](#), [doi:10.1007/JHEP01\(2018\)048](#).
- [671] D. Broadhurst, J. Fleischer, O. Tarasov, Two loop two point functions with masses: Asymptotic expansions and Taylor series, in any dimension, *Z. Phys.* C60 (1993) 287–302. [arXiv:hep-ph/9304303](#).
- [672] F. A. Berends, M. Buza, M. Böhm, R. Scharf, Closed expressions for specific massive multiloop self-energy integrals, *Z.Phys.* C63 (1994) 227–234. [doi:10.1007/BF01411014](#).
- [673] S. Bauberger, M. Böhm, G. Weiglein, F. A. Berends, M. Buza, Calculation of two loop selfenergies in the electroweak standard model, *Nucl. Phys. Proc. Suppl.* 37B (1994) 95–114. [arXiv:hep-ph/9406404](#).
- [674] S. Bauberger, F. A. Berends, M. Böhm, M. Buza, Analytical and numerical methods for massive two loop selfenergy diagrams, *Nucl.Phys.* B434 (1995) 383–407. [arXiv:hep-ph/9409388](#), [doi:10.1016/0550-3213\(94\)00475-T](#).
- [675] S. Bauberger, M. Böhm, Simple one-dimensional integral representations for two loop selfenergies:

- The Master diagram, Nucl.Phys. B445 (1995) 25–48. [arXiv:hep-ph/9501201](#), [doi:10.1016/0550-3213\(95\)00199-3](#).
- [676] M. Caffo, H. Czyz, S. Laporta, E. Remiddi, The master differential equations for the 2-loop sunrise selfmass amplitudes, Nuovo Cim. A111 (1998) 365–389, ex tr. [arXiv:hep-th/9805118](#).
  - [677] S. Laporta, E. Remiddi, Analytic treatment of the two loop equal mass sunrise graph [arXiv:hep-ph/0406160](#).
  - [678] B. A. Kniehl, A. V. Kotikov, A. Onishchenko, O. Veretin, Two-loop sunset diagrams with three massive lines, Nucl. Phys. B738 (2006) 306–316. [arXiv:hep-ph/0510235](#), [doi:10.1016/j.nuclphysb.2006.01.013](#).
  - [679] S. Groote, J. G. Körner, A. A. Pivovarov, On the evaluation of a certain class of Feynman diagrams in x-space: Sunrise-type topologies at any loop order, Annals Phys. 322 (2007) 2374–2445. [arXiv:hep-ph/0506286](#), [doi:10.1016/j.aop.2006.11.001](#).
  - [680] S. Groote, J. Körner, A. Pivovarov, A numerical test of differential equations for one- and two-loop sunrise diagrams using configuration space techniques, Eur.Phys.J. C72 (2012) 2085. [arXiv:1204.0694](#), [doi:10.1140/epjc/s10052-012-2085-z](#).
  - [681] D. H. Bailey, J. M. Borwein, D. Broadhurst, M. L. Glasser, Elliptic integral evaluations of Bessel moments, J. Phys. A41 (2008) 205203. [arXiv:0801.0891](#), [doi:10.1088/1751-8113/41/20/205203](#).
  - [682] S. Müller-Stach, S. Weinzierl, R. Zayadeh, A second-order differential equation for the two-loop sunrise graph with arbitrary masses, Commun. Num. Theor. Phys. 6 (2012) 203–222. [arXiv:1112.4360](#).
  - [683] L. Adams, C. Bogner, S. Weinzierl, The two-loop sunrise graph with arbitrary masses, J. Math. Phys. 54 (2013) 052303. [arXiv:1302.7004](#).
  - [684] S. Bloch, P. Vanhove, The elliptic dilogarithm for the sunset graph, J. Numb. Theor. 148 (2015) 328–364. [arXiv:1309.5865](#).
  - [685] L. Adams, C. Bogner, S. Weinzierl, The two-loop sunrise graph in two space-time dimensions with arbitrary masses in terms of elliptic dilogarithms, J. Math. Phys. 55 (2014) 102301. [arXiv:1405.5640](#).
  - [686] L. Adams, C. Bogner, S. Weinzierl, The iterated structure of the all-order result for the two-loop sunrise integral, J. Math. Phys. 57 (3) (2016) 032304. [arXiv:1512.05630](#), [doi:10.1063/1.4944722](#).
  - [687] E. Remiddi, L. Tancredi, Schouten identities for Feynman graph amplitudes; The Master Integrals for the two-loop massive sunrise graph, Nucl.Phys. B880 (2014) 343–377. [arXiv:1311.3342](#), [doi:10.1016/j.nuclphysb.2014.01.009](#).
  - [688] S. Bloch, M. Kerr, P. Vanhove, Local mirror symmetry and the sunset Feynman integral, Adv. Theor. Math. Phys. 21 (2017) 1373–1453. [arXiv:1601.08181](#), [doi:10.4310/ATMP.2017.v21.n6.a1](#).
  - [689] A. Sabry, Fourth order spectral functions for the electron propagator, Nucl. Phys. 33 (1962) 401–430.
  - [690] L. Adams, S. Weinzierl, Feynman integrals and iterated integrals of modular forms, Commun. Num. Theor. Phys. 12 (2018) 193–251. [arXiv:1704.08895](#), [doi:10.4310/CNTP.2018.v12.n2.a1](#).
  - [691] C. Bogner, A. Schweitzer, S. Weinzierl, Analytic continuation and numerical evaluation of the kite integral and the equal mass sunrise integral, Nucl. Phys. B922 (2017) 528–550. [arXiv:1705.08952](#), [doi:10.1016/j.nuclphysb.2017.07.008](#).
  - [692] R. N. Lee, Space-time dimensionality  $D$  as complex variable: calculating loop integrals using dimensional recurrence relation and analytical properties with respect to  $D$ , Nucl. Phys. B830 (2010) 474–492. [arXiv:0911.0252](#), [doi:10.1016/j.nuclphysb.2009.12.025](#).
  - [693] A. Beilinson, A. Levin, The elliptic polylogarithm In *Motives*, ed. U. Jannsen, S. Kleiman, J.-P. Serre, Proc. of Symp. in Pure Mathematics **55**, Part 2, AMS, 1994, 97-121.

- [694] A. Levin, Elliptic polylogarithms: an analytic theory, *Comp. Math.* 106 (1997) 267.
- [695] A. Levin, G. Racinet, Towards multiple elliptic polylogarithms [arXiv:math/0703237](#).
- [696] B. Enriquez, Elliptic associators, *Selecta Math.* 20 (2014) 491–584. [arXiv:1003.1012](#).
- [697] F. Brown, A. Levin, Multiple elliptic polylogarithms [arXiv:1110.6917](#).
- [698] J. Wildeshaus, Realizations of polylogarithms *Lect. Notes Math.* **1650**, Springer, (1997).
- [699] S. Bloch, M. Kerr, P. Vanhove, A Feynman integral via higher normal functions, *Compos. Math.* 151 (2015) 2329–2375. [arXiv:1406.2664](#), [doi:10.1112/S0010437X15007472](#).
- [700] J. Broedel, C. Duhr, F. Dulat, L. Tancredi, Elliptic polylogarithms and iterated integrals on elliptic curves II: an application to the sunrise integral [arXiv:1712.07095](#).
- [701] J. Broedel, C. Duhr, F. Dulat, B. Penante, L. Tancredi, Elliptic symbol calculus: from elliptic polylogarithms to iterated integrals of Eisenstein series [arXiv:1803.10256](#).
- [702] G. Passarino, Elliptic polylogarithms and basic hypergeometric functions, *European Physical Journal C* 77 (2017) 77. [arXiv:1610.06207](#), [doi:10.1140/epjc/s10052-017-4623-1](#).
- [703] M. Sogaard, Y. Zhang, Elliptic Functions and Maximal Unitarity, *Phys. Rev. D* 91 (8) (2015) 081701. [arXiv:1412.5577](#), [doi:10.1103/PhysRevD.91.081701](#).
- [704] M. Hidding, F. Moriello, All orders structure and efficient computation of linearly reducible elliptic Feynman integrals [arXiv:1712.04441](#).
- [705] M. van Hoeij, Factorization of Differential Operators with Rational Functions Coefficients, *J. Symbolic Computation* 24 (1997) 537–561.
- [706] R. Pittau, A four-dimensional approach to quantum field theories, *JHEP* 11 (2012) 151. [arXiv:1208.5457](#), [doi:10.1007/JHEP11\(2012\)151](#).
- [707] G. F. R. Sborlini, F. Driencourt-Mangin, R. Hernandez-Pinto, G. Rodrigo, Four-dimensional unsubtraction from the loop-tree duality, *JHEP* 08 (2016) 160. [arXiv:1604.06699](#), [doi:10.1007/JHEP08\(2016\)160](#).
- [708] S. Seth, S. Weinzierl, Numerical integration of subtraction terms, *Phys. Rev. D* 93 (11) (2016) 114031. [arXiv:1605.06646](#), [doi:10.1103/PhysRevD.93.114031](#).
- [709] R. Gastmans, S. L. Wu, T. T. Wu, Higgs Decay into Two Photons, Revisited [arXiv:1108.5872](#).
- [710] K. Melnikov, A. Vainshtein, Higgs boson decay to two photons and dispersion relations, *Phys. Rev. D* 93 (5) (2016) 053015. [arXiv:1601.00406](#), [doi:10.1103/PhysRevD.93.053015](#).
- [711] A. M. Donati, R. Pittau, FDR, an easier way to NNLO calculations: a two-loop case study, *Eur. Phys. J. C* 74 (2014) 2864. [arXiv:1311.3551](#), [doi:10.1140/epjc/s10052-014-2864-9](#).
- [712] R. Pittau, Integration-by-parts identities in FDR, *Fortsch. Phys.* 63 (2015) 601–608. [arXiv:1408.5345](#), [doi:10.1002/prop.201500040](#).
- [713] B. Page, R. Pittau, Two-loop off-shell QCD amplitudes in FDR, *JHEP* 11 (2015) 183. [arXiv:1506.09093](#), [doi:10.1007/JHEP11\(2015\)183](#).
- [714] C. Gnendiger, A. Signer, Private communication.
- [715] R. Pittau, QCD corrections to  $H \rightarrow gg$  in FDR, *Eur. Phys. J. C* 74 (1) (2014) 2686. [arXiv:1307.0705](#), [doi:10.1140/epjc/s10052-013-2686-1](#).
- [716] N. N. Bogoliubov, O. S. Parasiuk, On the Multiplication of the causal function in the quantum theory of fields, *Acta Math.* 97 (1957) 227–266. [doi:10.1007/BF02392399](#).
- [717] W. Zimmermann, Convergence of Bogolyubov’s method of renormalization in momentum space, *Commun. Math. Phys.* 15 (1969) 208–234, [*Lect. Notes Phys.* 558, 217(2000)]. [doi:10.1007/BF01645676](#).
- [718] R. Pittau, On the predictivity of the non-renormalizable quantum field theories, *Fortsch. Phys.* 63 (2015) 132–141. [arXiv:1305.0419](#), [doi:10.1002/prop.201400079](#).
- [719] T. J. E. Zirke, Numerical Evaluation of Two-Loop Integrals in FDR, *JHEP* 02 (2016) 029. [arXiv:](#)



- 1512.04920, doi:10.1007/JHEP02(2016)029.
- [720] M. Moretti, R. Pittau, In preparation.
  - [721] J. Alwall, R. Frederix, S. Frixione, V. Hirschi, F. Maltoni, O. Mattelaer, H. S. Shao, T. Stelzer, P. Torrielli, M. Zaro, The automated computation of tree-level and next-to-leading order differential cross sections, and their matching to parton shower simulations, *JHEP* 07 (2014) 079. arXiv:1405.0301, doi:10.1007/JHEP07(2014)079.
  - [722] M. Cacciari, G. P. Salam, G. Soyez, FastJet User Manual, *Eur. Phys. J. C* 72 (2012) 1896. arXiv:1111.6097, doi:10.1140/epjc/s10052-012-1896-2.
  - [723] C. G. Bollini, J. J. Giambiagi, Dimensional Renormalization: The Number of Dimensions as a Regularizing Parameter, *Nuovo Cim. B* 12 (1972) 20–26. doi:10.1007/BF02895558.
  - [724] G. M. Cicuta, E. Montaldi, Analytic renormalization via continuous space dimension, *Lett. Nuovo Cim.* 4 (1972) 329–332. doi:10.1007/BF02756527.
  - [725] J. F. Ashmore, A Method of Gauge Invariant Regularization, *Lett. Nuovo Cim.* 4 (1972) 289–290. doi:10.1007/BF02824407.
  - [726] K. G. Wilson, Quantum field theory models in less than four-dimensions, *Phys. Rev. D* 7 (1973) 2911–2926. doi:10.1103/PhysRevD.7.2911.
  - [727] Z. Kunszt, D. E. Soper, Calculation of jet cross-sections in hadron collisions at order  $\alpha_s^3$ , *Phys. Rev. D* 46 (1992) 192–221. doi:10.1103/PhysRevD.46.192.
  - [728] S. Frixione, Z. Kunszt, A. Signer, Three jet cross-sections to next-to-leading order, *Nucl. Phys. B* 467 (1996) 399–442. arXiv:hep-ph/9512328, doi:10.1016/0550-3213(96)00110-1.
  - [729] S. Catani, M. H. Seymour, The Dipole Formalism for the Calculation of QCD Jet Cross Sections at Next-to-Leading Order, *Phys. Lett. B* 378 (1996) 287–301. arXiv:hep-ph/9602277.
  - [730] S. Catani, M. H. Seymour, A General algorithm for calculating jet cross-sections in NLO QCD, *Nucl. Phys. B* 485 (1997) 291–419, [Erratum: *Nucl. Phys. B* 510, 503 (1998)]. arXiv:hep-ph/9605323, doi:10.1016/S0550-3213(96)00589-5, 10.1016/S0550-3213(98)81022-5.
  - [731] A. Gehrmann-De Ridder, T. Gehrmann, E. W. N. Glover, Antenna subtraction at NNLO, *JHEP* 09 (2005) 056. arXiv:hep-ph/0505111, doi:10.1088/1126-6708/2005/09/056.
  - [732] S. Catani, M. Grazzini, An NNLO subtraction formalism in hadron collisions and its application to Higgs boson production at the LHC, *Phys. Rev. Lett.* 98 (2007) 222002. arXiv:hep-ph/0703012, doi:10.1103/PhysRevLett.98.222002.
  - [733] M. Czakon, A novel subtraction scheme for double-real radiation at NNLO, *Phys. Lett. B* 693 (2010) 259–268. arXiv:1005.0274, doi:10.1016/j.physletb.2010.08.036.
  - [734] P. Bolzoni, G. Somogyi, Z. Trocsanyi, A subtraction scheme for computing QCD jet cross sections at NNLO: integrating the iterated singly-unresolved subtraction terms, *JHEP* 01 (2011) 059. arXiv:1011.1909, doi:10.1007/JHEP01(2011)059.
  - [735] R. Boughezal, C. Focke, X. Liu, F. Petriello,  $W$ -boson production in association with a jet at next-to-next-to-leading order in perturbative QCD, *Phys. Rev. Lett.* 115 (6) (2015) 062002. arXiv:1504.02131, doi:10.1103/PhysRevLett.115.062002.
  - [736] J. Gaunt, M. Stahlhofen, F. J. Tackmann, J. R. Walsh, N-jettiness Subtractions for NNLO QCD Calculations, *JHEP* 09 (2015) 058. arXiv:1505.04794, doi:10.1007/JHEP09(2015)058.
  - [737] V. Del Duca, C. Duhr, A. Kardos, G. Somogyi, Z. Szor, Z. Trocsanyi, Z. Tulipant, Jet production in the CoLoRFulNNLO method: event shapes in electron-positron collisions, *Phys. Rev. D* 94 (7) (2016) 074019. arXiv:1606.03453, doi:10.1103/PhysRevD.94.074019.
  - [738] F. Caola, K. Melnikov, R. Rötsch, Nested soft-collinear subtractions in NNLO QCD computations, *Eur. Phys. J. C* 77 (4) (2017) 248. arXiv:1702.01352, doi:10.1140/epjc/s10052-017-4774-0.
  - [739] L. Magnea, E. Maina, G. Pelliccioli, C. Signorile-Signorile, P. Torrielli, S. Uccirati, Local Analytic

Sector Subtraction at NNLO [arXiv:1806.09570](https://arxiv.org/abs/1806.09570).

- [740] R. J. Hernandez-Pinto, G. F. R. Sborlini, G. Rodrigo, Towards gauge theories in four dimensions, JHEP 02 (2016) 044. [arXiv:1506.04617](https://arxiv.org/abs/1506.04617), doi:10.1007/JHEP02(2016)044.
- [741] G. F. R. Sborlini, F. Driencourt-Mangin, G. Rodrigo, Four-dimensional unsubtraction with massive particles, JHEP 10 (2016) 162. [arXiv:1608.01584](https://arxiv.org/abs/1608.01584), doi:10.1007/JHEP10(2016)162.
- [742] F. Driencourt-Mangin, G. Rodrigo, G. F. R. Sborlini, Universal dual amplitudes and asymptotic expansions for  $gg \rightarrow H$  and  $H \rightarrow \gamma\gamma$  in four dimensions, Eur. Phys. J. C78 (3) (2018) 231. [arXiv:1702.07581](https://arxiv.org/abs/1702.07581), doi:10.1140/epjc/s10052-018-5692-5.
- [743] N. Selomit Ramirez-Urbe, R. J. Hernandez-Pinto, G. Rodrigo, QED and QCD self-energy corrections through the loop-tree duality, J. Phys. Conf. Ser. 912 (1) (2017) 012013. [arXiv:1709.07802](https://arxiv.org/abs/1709.07802), doi:10.1088/1742-6596/912/1/012013.
- [744] S. Catani, T. Gleisberg, F. Krauss, G. Rodrigo, J.-C. Winter, From loops to trees by-passing Feynman's theorem, JHEP 09 (2008) 065. [arXiv:0804.3170](https://arxiv.org/abs/0804.3170), doi:10.1088/1126-6708/2008/09/065.
- [745] I. Bierenbaum, S. Catani, P. Draggiotis, G. Rodrigo, A Tree-Loop Duality Relation at Two Loops and Beyond, JHEP 10 (2010) 073. [arXiv:1007.0194](https://arxiv.org/abs/1007.0194), doi:10.1007/JHEP10(2010)073.
- [746] I. Bierenbaum, S. Buchta, P. Draggiotis, I. Malamos, G. Rodrigo, Tree-Loop Duality Relation beyond simple poles, JHEP 03 (2013) 025. [arXiv:1211.5048](https://arxiv.org/abs/1211.5048), doi:10.1007/JHEP03(2013)025.
- [747] S. Buchta, G. Chachamis, P. Draggiotis, I. Malamos, G. Rodrigo, On the singular behaviour of scattering amplitudes in quantum field theory, JHEP 11 (2014) 014. [arXiv:1405.7850](https://arxiv.org/abs/1405.7850), doi:10.1007/JHEP11(2014)014.
- [748] S. Buchta, G. Chachamis, P. Draggiotis, G. Rodrigo, Numerical implementation of the loop-tree duality method, Eur. Phys. J. C77 (5) (2017) 274. [arXiv:1510.00187](https://arxiv.org/abs/1510.00187), doi:10.1140/epjc/s10052-017-4833-6.
- [749] E. T. Tomboulis, Causality and Unitarity via the Tree-Loop Duality Relation, JHEP 05 (2017) 148. [arXiv:1701.07052](https://arxiv.org/abs/1701.07052), doi:10.1007/JHEP05(2017)148.
- [750] S. Caron-Huot, Loops and trees, JHEP 05 (2011) 080. [arXiv:1007.3224](https://arxiv.org/abs/1007.3224), doi:10.1007/JHEP05(2011)080.
- [751] J. L. Jurado, G. Rodrigo, W. J. Torres Bobadilla, From Jacobi off-shell currents to integral relations, JHEP 12 (2017) 122. [arXiv:1710.11010](https://arxiv.org/abs/1710.11010), doi:10.1007/JHEP12(2017)122.
- [752] Z. Bern, A. De Freitas, L. Dixon, H. L. Wong, Supersymmetric regularization, two-loop QCD amplitudes and coupling shifts [arXiv:hep-ph/0202271](https://arxiv.org/abs/hep-ph/0202271).
- [753] O. A. Battistel, A. L. Mota, M. C. Nemes, Consistency conditions for 4-D regularizations, Mod. Phys. Lett. A13 (1998) 1597–1610. doi:10.1142/S0217732398001686.
- [754] R. P. Feynman, Quantum theory of gravitation, Acta Phys. Polon. 24 (1963) 697–722, [272(1963)].
- [755] Maplesoft, Maple 18+.  
URL <https://www.maplesoft.com/support/help/AddOns/view.aspx?path=evalf/Int/cuba>
- [756] A. Bouvier, K. Ki  u, R2Cuba.  
URL <https://cran.r-project.org/package=R2Cuba>
- [757] K. Oikonomou, Cuba Interface to REDUCE.  
URL <https://sourceforge.net/projects/reduce-algebra>
- [758] J. Buchner, pyCuba.  
URL <https://johannesbuchner.github.io/PyMultiNest/pycuba.html>
- [759] M. Giordano, Cuba.jl.  
URL <https://github.com/giordano/Cuba.jl>
- [760] A. Genz, A. Malik, An imbedded family of fully symmetric numerical integration rules, SIAM J. Numer.

- Anal. 20 (3) (1983) 580–588. doi:10.1137/0720038.  
URL <https://doi.org/10.1137/0720038>
- [761] W. H. Press, S. A. Teukolsky, W. T. Vetterling, B. P. Flannery, Numerical Recipes in FORTRAN: The Art of Scientific Computing.
- [762] P. Bratley, B. L. Fox, Algorithm 659: Implementing sobol’s quasirandom sequence generator, ACM Trans. Math. Softw. 14 (1) (1988) 88–100. doi:10.1145/42288.214372.  
URL <http://doi.acm.org/10.1145/42288.214372>
- [763] M. Matsumoto, T. Nishimura, Mersenne twister: A 623-dimensionally equidistributed uniform pseudo-random number generator, ACM Trans. Model. Comput. Simul. 8 (1) (1998) 3–30. doi:10.1145/272991.272995.  
URL <http://doi.acm.org/10.1145/272991.272995>
- [764] M. Luscher, A Portable high quality random number generator for lattice field theory simulations, Comput. Phys. Commun. 79 (1994) 100–110. arXiv:hep-lat/9309020, doi:10.1016/0010-4655(94)90232-1.
- [765] F. James, RANLUX: A FORTRAN implementation of the high quality pseudorandom number generator of Lüscher, Comput. Phys. Commun. 79 (1994) 111–114, [Erratum: Comput. Phys. Commun. 97,357(1996)]. doi:10.1016/0010-4655(94)90233-X.
- [766] H. Keng, W. Yuan, Applications of number theory to numerical analysis, Springer-Verlag Berlin Heidelberg, 1981.
- [767] G. P. Lepage, VEGAS: An adaptive multidimensional integration program.  
URL <https://lib-extopc.kek.jp/preprints/PDF/1980/8006/8006210.pdf>
- [768] G. P. Lepage, A New Algorithm for Adaptive Multidimensional Integration, J. Comput. Phys. 27 (1978) 192. doi:10.1016/0021-9991(78)90004-9.
- [769] W. H. Press, G. R. Farrar, Recursive stratified sampling for multidimensional Monte Carlo integration, Computers in Physics 4, 190 (1990).doi:10.1063/1.4822899.
- [770] J. H. Friedman, M. H. Wright, DIVONNE4: A program for multiple integration and adaptive importance sampling.
- [771] J. H. Friedman, M. H. Wright, A nested partitioning procedure for numerical multiple integration, ACM Trans. Math. Softw. 7 (1) (1981) 76–92. doi:10.1145/355934.355939.  
URL <http://doi.acm.org/10.1145/355934.355939>
- [772] J. Berntsen, T. O. Espelid, A. Genz, Algorithm 698: Dcuhre: An adaptive multidemensional integration routine for a vector of integrals, ACM Trans. Math. Softw. 17 (4) (1991) 452–456. doi:10.1145/210232.210234.  
URL <http://doi.acm.org/10.1145/210232.210234>